IDENTIFICATION AND CHARACTERIZATION OF THE MOLECULAR MACHINERY OF AUXIN-DEPENDENT CANALIZATION DURING VASCULATURE FORMATION AND REGENERATION

by

JAKUB HAJNÝ

July, 2020

A thesis presented to the
Graduate School
of the
Institute of Science and Technology Austria, Klosterneuburg, Austria
in partial fulfillment of the requirements
for the degree of
Doctor of Philosophy

The dissertation of Jakub Hajný, titled *Identification and characterization of the molecular machinery of auxin-dependent canalization during vasculature formation and regeneration*, is approved by:

Supervisor: Jiří Friml, IST Austria, Klosterneuburg, Austria

Signature: _____

Committee Member: Eva Benková, IST Austria, Klosterneuburg, Austria

Signature: _____

Committee Member: Youssef Belkhadir, GMI, Wien, Austria

Signature: _____

Exam Chair: Florian Schur, IST Austria, Klosterneuburg, Austria

Signature: _____

Signed page is on the file.

IST Austria Thesis, ISSN: 2663-337X

I hereby declare that this dissertation is my own work and that it does not contain other people's work without this being so stated; this thesis does not contain my previous work without this being stated, and the bibliography contains all the literature that I used in writing the dissertation.

I declare that this is a true copy of my thesis, including any final revisions, as approved by my thesis committee, and that this thesis has not been submitted for a higher degree to any other university or institution.

I certify that any republication of materials presented in this thesis has been approved by the relevant publishers and co-authors.

Signature: _____

Jakub Hajný

December 1, 2020

Signed page is on the file.

Abstract

Self-organization is a hallmark of plant development manifested e.g. by intricate leaf vein patterns, flexible formation of vasculature during organogenesis or its regeneration following wounding. Spontaneously arising channels transporting the phytohormone auxin, created by coordinated polar localizations of *PIN-FORMED 1 (PIN1)* auxin exporter, provide positional cues for these as well as other plant patterning processes. To find regulators acting downstream of auxin and the TIR1/AFB auxin signaling pathway essential for PIN1 coordinated polarization during auxin canalization, we performed microarray experiments. Besides the known components of general PIN polarity maintenance, such as PID and PIP5K kinases, we identified and characterized a new regulator of auxin canalization, the transcription factor *WRKY DNA-BINDING PROTEIN 23 (WRKY23).*

Next, we designed a subsequent microarray experiment to further uncover other molecular players, downstream of auxin-TIR1/AFB-WRKY23 involved in the regulation of auxin-mediated PIN repolarization. We identified a novel and crucial part of the molecular machinery underlying auxin canalization. The auxin-regulated malectin-type receptor-like kinase CAMEL and the associated leucine-rich repeat receptor-like kinase CANAR target and directly phosphorylate PIN auxin transporters. *camel* and *canar* mutants are impaired in PIN1 subcellular trafficking and auxin-mediated repolarization leading to defects in auxin transport, ultimately to leaf venation and vasculature regeneration defects. Our results describe the CAMEL-CANAR receptor complex, which is required for auxin feed-back on its own transport and thus for coordinated tissue polarization during auxin canalization.

Acknowledgments

I would like to first acknowledge my supervisor Jiří Friml who was brave enough to give a chance to a naïve chemist with perhaps big dreams but without a proper biology background. I appreciate that you gave me autonomy and let me pursue directions I believed in, Jiří. I remember when you sent me in your lab for the first time with the words: “Don’t worry, just look what others do, keep asking questions and you will know everything you need”. And I have been asking questions ever since. I really enjoyed my time in the lab since people were rather family than just colleagues, each of them teaching me how to master different kinds of experiments and patiently answering all my stupid questions. My special thanks belongs to Lesia, a Ukrainian lady with Spanish spirits. Lesia adopted me from the very beginning, teaching me all the biology knowledge I was missing and guided me through most of the methodology necessary for completing my PhD. Thank you Lesia, I am happy you never gave up on me and it was an honor to be in the same team with you. Another important person during my PhD was Juan Carlos, my Spanish hermano, always setting a mirror to me whenever I behaved like an idiot. Carlos, we have been through a lot, you helped me to remove my tunnel vision in life and evolved me into a better person. I will never forget.

I would also like to thank to my young brother Michael, the most important person in my life. In my eyes you are just a boy, but truth is you are a man who already has something to teach me. I would like to dedicate this work to you since you are my ultimate motivation to never give up.

About the Author

Jakub Hajný finished his Bachelor's degree in Biochemistry and Master's degree in Analytical chemistry at Palacký University Olomouc. He worked for 4 months as a gass chromatography specialist at quality control department in Teva Pharmaceutical Industries. Next, he joined the Friml group at IST Austria for an internship from which he continued his PhD studies with focus on auxin signaling and transport during vasculature formation and regeneration.

List of Publications Appearing in Thesis

1. P. Grones, M. Abas, **J. Hajný**, A. Jones, S. Waidmann, J. Kleine-Vehn, J. Friml. PID/WAG-mediated phosphorylation of the Arabidopsis PIN3 auxin transporter mediates polarity switches during gravitropism. *Sci. Rep.* **8**, 10279 (2018).

2. T. Prát*, **J. Hajný***, W. Grunewald, M. Vasileva, G. Molnár, R. Tejos, M. Schmid, M. Sauer, J. Friml. WRKY23 is a component of the transcriptional network mediating auxin feedback on PIN polarity. *PLOS Genet.* **14**, e1007177 (2018).

3. A. Oochi, **J. Hajný**, K. Fukui, Y. Nakao, M. Gallei, M. Quareshy, K. Takahashi, T. Kinoshita, S. Harborough, S. Kepinski, H. Kasahara, R. Napier, J. Friml, K. Hayashi. Pinstatic acid promotes auxin transport by inhibiting PIN internalization. *Plant Physiology*. **180**, 2 (2019).

4. S. Tan, M. Abas, I. Verstraeten, M. Glanc, G. Molnár, **J. Hajný**, P. Lasák, I. Petřík, E. Russinova, J. Petrášek, O. Novák, J. Pospíšil, J. Friml. Salicylic Acid Targets Protein Phosphatase 2A to Attenuate Growth in Plants. *Curr. Biol.* **30**, 381-395.e8 (2020).

5. E. Mazur, I. Kulik, **J. Hajný**, J. Friml. Auxin canalization and vascular tissue formation by TIR1/AFB-mediated auxin signaling in Arabidopsis. *New Phytol.* **n/a**, doi:10.1111/nph.16446 (2020).

6. **J. Hajný**, T. Prát, N. Rydza, L. Rodriguez, S. Tan, I. Verstraeten, D. Domjan, E. Smakowska-Luzan, W. Smet, E. Mor, J. Nolf, W. Grunewald, G. Molnár, Y. Belkhadir, B. de Rybel, J. Friml. Receptor kinase module targets PIN-dependent auxin transport during canalization. *Science.* **370**, 550-557 (2020).

7. Z. Gelová, M. Gallei, M. Pernisová, G. Brunoud, X. Zhang, M. Glanc, L. Li, J. Michalko, Z. Pavlovičová, I. Verstraeten, H. Han, **J. Hajný,** R. Hauschild, M. Čovanová, M. Zwiewka, L. Hoermayer, M. Frendrych, T. Xu, J. Friml. Developmental roles of Auxin Binding Protein 1 in *Arabidopsis thaliana*. *Plant Science*. **303**, 110750 (2020).

8. H. Han, I. Verstraeten, M. Roosjen, **J. Hajný**, E. Mazur, N. Rydza, D. Weijers, J. Friml. Myosin XI protein dependent PIN polarity regulation in *Arabidopsis thaliana*. *Manuscript in preparation.*

9. L. Rodriguez, **J. Hajný**, I. Verstraeten, S. Tan, J. Michalko, Z. Gelová, L. Hörmayer, L. Li, M. Marques-Bueno, A. Monzer, T. Xu, Y. Jaillais and J. Friml. TMK1 cell surface auxin signaling targets PIN2-mediated auxin fluxes during root gravitropism. *Manuscript in preparation.*

10. **J. Hajný***, Z. Gelová*, L. Rodriguez*, S. Tan, I. Verstraeten, E. Mazur, N. Rydza, B. de Rybel and J. Friml. Convergence of auxin and peptide signaling mediates auxin canalization. *Manuscript in preparation.*

11. **J.Hajný**[*], Jiří Friml. Molecular mechanism of auxin canalization and tissue polarization in plants. *Review in preparation.*

Table of Contents

List of Figures

List of Tables

List of Symbols/Abbreviations

CAMEL	Canalization-related Auxin-dependent malectin-type RLK
CANAR	Canalization-related Receptor-like kinase
DEX	Dexamethasone
DEX/GR	Dexamethasone-glucocorticoid
DMSO	Dimethyl sulfoxide
GFP	Green fluorescent protein
HS	Heat-shock
IAA	Indole-3-acetic acid
LRR-RLK	Leucine-rich repeat receptor-like protein kinase
NAA	1-Naphthalene-acetic acid
PIN	PIN-FORMED
PIP5K	Phosphatydilinositol 4-phosphate 5-kinase
qRT-PCR	Quantitative real-time PCR
RFP	Red fluorescent protein
SAM	Shoot apical meristem
TF	Transcription factor
TUB2	TUBULIN BETA CHAIN 2
WRKY23	WRKY DNA-BINDING PROTEIN 23

1 Introduction

Formatted for Review:

J. Hajný, S. Tan, J. Friml. Molecular mechanism of auxin canalization and tissue polarization in plants.

Vascular plants have evolved specialized vascular tissue for conducting water, minerals and photosynthetic products throughout the plant body. The plant vascular tissue forms highly ordered and complex patterns, which secure coherent nutrient and water supply to all the organs of the plant. For decades, researches have been puzzled how the vascular pattern is reproducibly organized across plant tissues. Early experiments showed that the phytohormone auxin (indole-3-acetic acid, IAA) alone is sufficient to cause vascular differentiation in a variety of systems (Jacobs, 1952; Sachs, 1969; Snow, 1935; Wangermann, 1967). External auxin application induced a continuous vascular strand, which was attracted towards the existing vasculature. This was prevented by chemical inhibition of auxin transport. Continuity of auxin-induced vascular strands indicates that auxin serves as a positional cue guiding vasculature emergence and that the auxin signal needs to be propagated across the plant tissues. Further experiments with radio-labelled auxin showed auxin transport through differentiating vascular channels and concluded auxin transport to be an early stage of vasculature differentiation (Sachs, 1975). These observations led Tsvi Sachs to formulate the canalization hypothesis in which auxin transport through an initially homogeneous tissue follows a self-organizing pattern canalizing auxin from an initially broad field of auxin-transporting cells gradually to narrow channels with high auxin-transporting capacity (Fig 1A). Auxin is canalized from its source towards its sink and this flux can both polarize cells and maintain their polarity (Sachs, 1981).

Auxin acts as a polarizing cue by means of its directional intercellular flow, facilitated by plasma membrane-resident importers and exporters, including PIN-FORMED (PIN) auxin efflux carriers (Petrášek et al., 2006; Wiśniewska et al., 2006). PINs are gradually polarized from the auxin source into narrow channels which precede all cases of vasculature formation (Balla et al., 2011; Benková et al., 2003; Mazur et al., n.d.; Verna et al., 2019), supporting Tsvi Sachs observations. Furthermore, auxin has the unique ability to direct subcellular localization

of PINs to determine the directionality of its own cell-to-cell transport (Mazur et al., n.d.; Prát et al., 2018). This positive feedback loop appears to be a crucial mechanism driving the self-organizing manner of auxin canalization, and multiple novel molecular components have been identified.

1.1 *Classical CANALIZATION-DEPENDENT PROCESSES in development*

1.1.1 Vasculature formation

Complex leaf venation patterns are a remarkable manifestation of self-organizing properties of auxin transport (Fig 1.1B). Prior to procambium specification, PIN1-expressing channels are formed and their subcellular coordinated polarities guides auxin transport toward pre-existing vasculature (Scarpella et al., 2006a). Thus, PIN polarity represents the polarization of previously homogenous tissue by auxin. Convergence of auxin flow to narrow channels constituting a complex pattern suggests that cell polarity is stable as long as the flux continues, therefore auxin both induces and maintains the polarity.

Critical roles of PIN-mediated auxin transport are revealed by pharmacological treatment by the auxin transport inhibitor NPA, and in the *pin1* mutant. Interestingly, auxin-induced vein formation can still occur, albeit abnormal, in the absence of PIN proteins or any other intercellular auxin transporter (Verna et al., 2019), suggesting either additional components beyond PINs or the existence of so far unknown auxin-derived signal driving canalization (Ravichandran et al., n.d.).

1.1.2 Vasculature regeneration after wounding

Wounding-induced disrupted vasculature results in local accumulation of auxin which triggers polarization of PIN1 in neighbouring cells, transporting auxin in a progressively narrower channel circumventing the wound and ultimately reconnecting to the pre-existing vasculature. After reconnection, the auxin channel differentiates into a continuous vascular strand uniting vasculature above and below the wound once more (Fig 1.1C) (Mazur et al., n.d.; Sauer et al., 2006a). Experimental work demonstrated that auxin transport, auxin signaling and PIN1 activity are indispensable for vasculature regeneration after wounding (Mazur et al., n.d.). Classical studies on auxin canalization were based on local auxin

application onto the tissues of different plant species (Sachs, 1981, 1975) including *Pisum sativum* (Sauer et al., 2006a) and *Arabidopsis thaliana* (Mazur et al., 2016). Local auxin application after wounding offers several advantages over the wounding approach without application mentioned above, such as excluding potential other wounding-related factors, control of auxin exposure dosage and duration, and the possibility to test various auxin analogues and inhibitors. In this setup, auxin-transporting channels arise from the application site placed close to the wound and gradually develop into continuous vascular strands connecting it to the pre-existing vasculature (Fig 1.1D), which indicates the self-organized nature of auxin canalization and confirms that auxin polar transport is a sufficient signal to polarize a tissue and to induce vein formation. Auxin canalization is *TIR1/AFB*-dependent and in mutants of auxin transcriptional signaling, PIN1 cannot co-ordinately repolarize to create a continuous auxin transporting channel (Mazur et al., n.d.; Prát et al., 2018). This suggest that auxin can control subcellular PIN1 polarity, and thus its own cell-to-cell flow, via auxin transcriptional TIR1/AFB signaling.

1.1.3 Maintaining of apical dominance and shoot branching

Apical dominance is a process where formation of side branches is inhibited in presence of a dominant shoot apex, which serves as the auxin source to repress the vascular development of lateral buds. Upon apex removal, auxin can then mediate emergence of vasculature connecting lateral buds to pre-existing stem vasculature according to the canalization hypothesis (Sachs, 1981, 1975). This was supported by Balla et al., 2011 where the authors showed that after decapitation, activated axillary buds rapidly polarize PIN1 facing away from the source and mediate directional auxin transport from the bud, demarcating the position of future vascular connections between the activated bud (or site of auxin application) and the stem vasculature (Fig 1.1E). Intriguingly, recent studies show that the branching hormone, strigolactone, regulates shoot architecture via modulating PIN recycling and polarity (Shinohara et al., 2013; Bennett et al., 2016; Zhang et al., 2020).

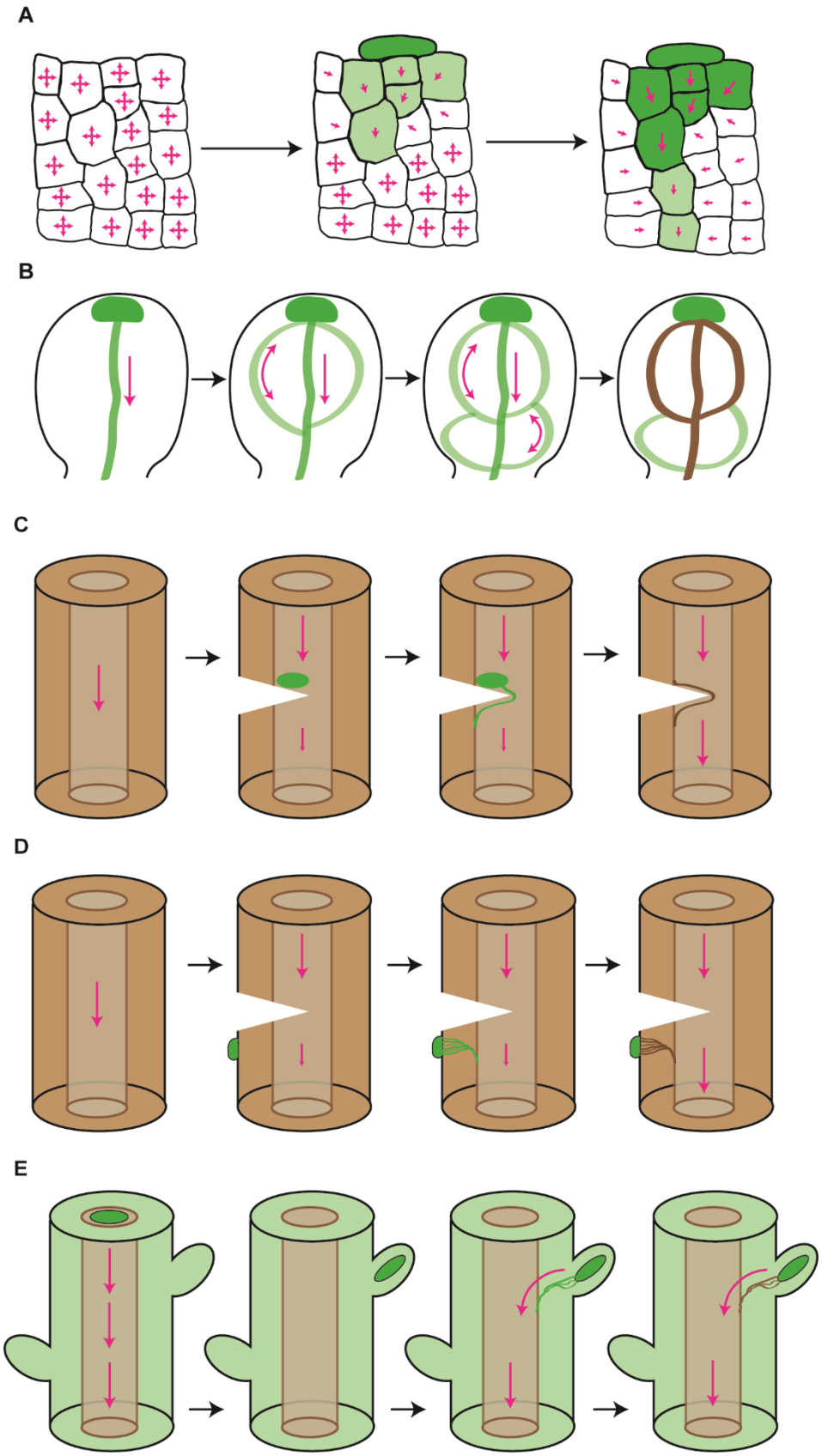

Figure 1. 1 Central dogma of canalization and related patterning processes

(A) Auxin source (represented in dark green) polarizes originally homogenous cells to create directional transport of auxin (marked by the magenta arrow) away from its source. The self-organizing property of auxin transport allows to canalize auxin from an initially broad domain into a narrow channel with high auxin-transporting capacity. (B) The auxin maximum in the leaf tip drives the induction of auxin-transporting channels, demarcating future positions of vasculature. (C) Wounding of stem vasculature results in auxin accumulation. Auxin is canalized around the wound to reconnect the vasculature above and below the wound. (D) External application of auxin below the wound triggers vascular strand formation connecting the auxin source with the pre-existing vasculature. (E) The shoot apex is a well-known source of auxin which keeps lateral buds inhibited. Once the apex is removed, the closest lateral bud is released from inhibition and becomes a new dominant auxin source. Auxin canalization initiates vasculature formation, connecting the lateral bud to the pre-existing stem vasculature.

1.2 *Molecular mechanisms underlying canalization*

The feedback regulation of its own intercellular polar transport by auxin has been reported to underlie many patterning processes. Here we summarize recent advances in uncovering the molecular mechanism of auxin feedback on PIN subcellular localization and thus on its own transport. Specifically, we focus on two key questions: (i) how auxin can mechanistically change subcellular localization of PINs and (ii) how this effect is propagated across cells to coordinately repolarize PINs into a continuous channel. Notably, the developmental processes described above also involve other molecular components, beyond the auxin-PIN feedback loop. For instance, during post-wounding regeneration, genes required for vascular development also play an essential role, however, that is out of the scope of this chapter.

1.2.1 Canonical TIR1/AFBs-mediated auxin feedback on PIN polarity

Auxin induced repolarization of PINs was firstly demonstrated in the *Arabidopsis thaliana* root meristem where 4h 10 µM NAA (synthetic auxin) treatment leads to PIN1 relocalization from the basal to the inner-lateral side of endodermal/pericycle cells and PIN2 relocalization from the basal to the outer-lateral side of cortex cells (Fig 1.2A) (Sauer et al., 2006a). The biological relevance of PIN1/2 repolarization in the root meristem is not yet clear, but mutants defective in this process (Fig 1.2A) exhibit auxin transport-related phenotypes such as abnormal vasculature venation in leaves (Prát et al., 2018, p. 23; Hajný et al., 2020), the lack of vasculature regeneration after wounding (Han et al., 2020; Mazur et al., 2020, n.d.; Hajný et al., 2020), problems with the termination of gravitropic hypocotyl bending (Han et al., 2020)

or defects during embryogenesis (Grunewald et al., 2013; Tejos et al., 2018). This proves that the *Arabidopsis thaliana* root meristem is a suitable tool for testing auxin feedback on PIN polarity. Prolonged auxin treatment indicates the involvement of a whole transcriptional cascade. Indeed, the TIR1/AFB auxin transcriptional pathway is indispensable for auxin feedback on PIN polarity in roots (Prát et al., 2018, p. 23), leaves (Mazur et al., n.d.; Prát et al., 2018, p. 23; Verna et al., 2019) and shoots (Han et al., 2020; Mazur et al., n.d.). Auxin can also control the transcription of several PIN genes via TIR1/AFB (Prát et al., 2018, p. 23) in a tissue-specific manner (Vieten et al., 2005) and *de novo* PIN protein synthesis is required for re-establishment of PIN2 polarity in the epidermis after cell division (Glanc et al., 2018). Notably, after inhibition of protein synthesis by cycloheximide (CHX), auxin-mediated PIN1 repolarization from the basal-to-inner lateral side in endodermis is abolished and PIN1 localization stretches from basal to both outer- and inner-lateral sides, resulting in U-shaped localization (Sauer et al., 2006a). This indicates that TIR1/AFB is not only needed for *de novo* synthesis of PIN proteins, but also for synthesis of PIN polarity regulators. A high throughout transcriptional profiling identified multiple molecular players, downstream of the auxin and TIR1/AFBs-IAA17(AXR3) signaling cascade (Prát et al., 2018, p. 23), among which a transcription factor WRKY DNA-BINDING PROTEIN 23 (WRKY23) came out as a central regulator. WRKY23 is required for the auxin feedback on PIN polarity in roots, leaves (Prát et al., 2018, p. 23), shoots (Hajný et al., 2020) and during embryogenesis (Grunewald et al., 2013, p. 23). From this study, multiple previously known genes involved in PIN polarity regulation have been identified, including *PINOID* (Friml et al., 2004), *PATELLINs* (Tejos et al., 2018), and *PIP5K1* (Ischebeck et al., 2013).

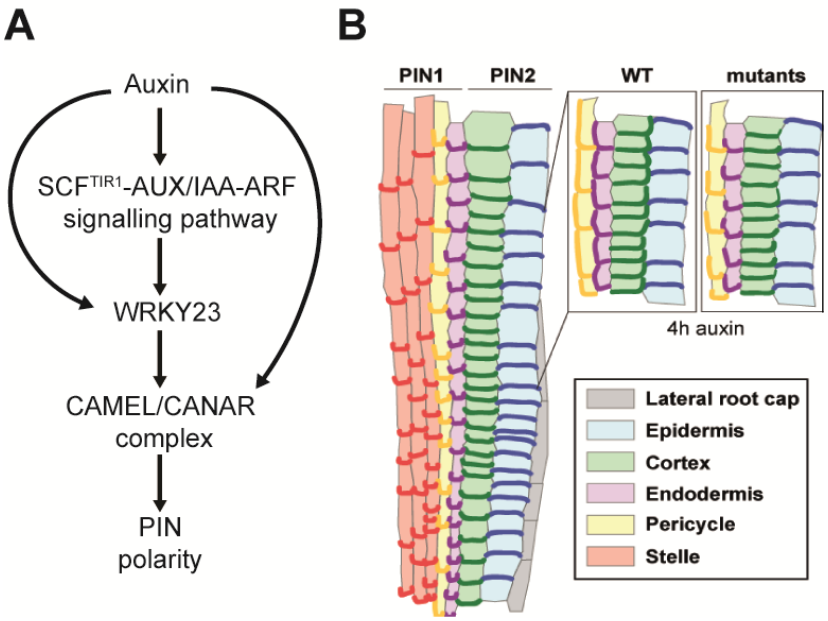

Figure 1. 2 Tissue-specific effect of auxin on PIN subcellular localization

(A) Molecular pathway underlying the auxin feedback on PIN polarity. (B) Prolonged auxin treatment repolarizes PIN1 in the pericycle/endodermis from the basal to inner lateral side of the cells, whereas PIN2 in cortex undergoes a basal to outer-lateral polarity shift. In mutants with defective auxin feedback on PIN polarity, PIN1/2's ability to repolarize after auxin treatment is reduced.

1.2.2 Emerging role of TMK1 as an essential auxin signaling module at the PM

The *TRANSMEMBRANE KINASE 1 (TMK1*) was firstly described to form a complex with AUXIN BINDING PROTEIN 1 (ABP1). However, the role for the latter protein in auxin signaling and plant development has been questioned as wrong mutant alleles were used in the past (Gao et al., 2015). Despite this, the *tmk1 tmk4* double mutant exhibits severe growth and developmental defects (Dai et al., 2013), some of which seems to be caused by defective auxin signaling, such as embryogenesis and lateral root organogenesis (Dai et al., 2013; Xu et al., 2014). Auxin (NAA) was recently proposed to impact the lipid distribution in the PM, thus regulating the property of lipid nanodomains and clustering of ROP GTPase, ROP6 (Platre et al., 2019). This auxin-induced stabilization of ROP6 at a local nanodomain dramatically affects endocytosis of PIN2 protein. Intriguingly, TMK1 exhibits a similar auxin-induced clustering phenomenon, which is required for further ROP6 responses (Pan et al., 2019). Moreover, TMK1-mediated phosphorylation of PIN2 is important for auxin feedback on its asymmetric distribution during gravistimulation (Rodriguez, unpublished). These studies together propose a TMK1-mediated signaling perceiving extracellular auxin levels, and activated TMK1 could either inhibit the ROP6 pathway to suppress PIN2 endocytosis, or directly phosphorylate PIN2 to govern its stability. However, how TMK1 perceives auxin and whether this occurs directly or not, requires further investigation.

1.2.3 Endomembrane trafficking as a key modulator for auxin-mediated repolarization of PINs

PINs are dynamically cycling between their polar domain at the plasma membrane and endosomal compartments. The recycling (and partially endocytosis as well) of PIN1 is mediated by ADP-ribosylation factor guanine-nucleotide exchange factors (ARF-GEFs) (Zhang et al., 2020). These molecular players are important for the formation of coated vesicles facilitating numerous trafficking events in the endomembrane system. The fungal toxin brefeldin A (BFA) inhibits PIN trafficking by targeting ARF-GEFs and triggers the accumulation of PINs into "BFA bodies". This effect is fully reversible after BFA washout (Paciorek et al., 2005). The ARF-GEF *gnom* mutant exhibites impaired PIN polarity coordination in embryogenesis, leading to severe defects in apical-basal patterning (Steinmann et al., 1999) and this mutant failed to form continuous PIN1-positive channels in leaves where PIN1 was localized ubiquitously resulting in disorganized vasculature (Verna et al., 2019).

Auxin can inhibit PIN clathrin-mediated endocytosis and thus increases PINs abundance at the plasma membrane to promote the efflux of auxin from the cells. This can be visualized by reduced FM dye internalization after auxin treatment and by reduced BFA-induced internalization of PIN1/2 if pretreated with auxin (Paciorek et al., 2005). Nevertheless, BFA experiments should be interpreted with caution as was pointed out in (Jásik et al., 2016) by using a PIN2-Dendra2 photo-convertible line. These authors observed that the majority of PIN2 in BFA aggregations is newly synthetized protein and only a minor fraction of PIN2 comes from endocytic pools. The importance of endocytosis on PIN polarity establishment can be visualized during cell division. Immediately after cytokinesis, PIN2 trafficking is redirected to the cell plate, which creates a situation where the lower daughter cell has the correct apically localized PIN2, but the upper daughter cell has ectopically basally localized PIN2. By the removal of basal PIN2 via endocytosis, solely apical PIN2 polar localization can be re-established (Glanc et al., 2018). Recent work (Mazur et al., 2020) expands previous observations and experimentally proves that the PIN subcellular dynamics, PIN internalization by clathrin-mediated trafficking and the actin/myosin cytoskeleton are indispensable for the auxin feedback on PIN polarity, auxin canalization during *de novo* vasculature formation and vasculature regeneration after wounding.

1.2.4 Coordination of PIN polarities for tissue patterning

Despite recent advances in understanding the molecular aspects of auxin feedback on PIN polarity, the main question still remains open: How do the cells know the tissue context to form defined auxin-transporting channels? To channel auxin by coordinated PIN polarization, the cells need to have some information about auxin levels in all neighboring cells. This cell communication should be rapid because as the canalization progresses, the neighboring cells need to synthetize new PIN proteins and PIN polarity regulators to polarize PINs at the proper side to maintain the auxin flow (Hajný et al., 2020; Mazur et al., n.d.; Prát et al., 2018; Sauer et al., 2006a). A good candidate for such a rapid signal is Ca^{2+} since transient changes of cytoplasmic calcium ion concentration are essential for PIN1 polarity changes during SAM development (Li et al., 2019). Ca^{2+} signal could advance to the neighboring cell through the cytoplasm using plasmodesmata. Indeed, there is evidence that auxin triggers Ca^{2+} signals, which are propagated as long-distance waves between root cells. Interestingly, this response requires auxin transport mediated by the auxin importer AUX1 and the TIR1/AFB transcriptional pathway (Dindas et al., 2018).

1.3 *Other developmental processes requiring auxin feed-back on PIN polarity*

There are other developmental processes, which do not require presence of auxin channels *per se,* but which are dependent on the formation of auxin gradients across tissues.

1.3.1 Establishment of the embryonic apical-basal axis

The embryonic apical-basal body axis emerges at early stages after fertilization (Jeong et al., 2011). Firstly, *YUCCA* (YUC) auxin biosynthetic genes are expressed at the base of the young embryo and this basal source of auxin causes polarization of PIN7 towards the apical end of the embryonic axis to form the auxin maxima required for proembryo specification (Friml et al., 2003). Later at the globular stage, *TAA1/YUC*-dependent auxin production is shifted to the apex from where PIN1 is polarized to the embryo base and this leads to the formation of a new auxin maximum that is important for the specification of the future root

pole (Robert et al., 2013). Thus, the spatiotemporal auxin biosynthesis and auxin feedback on polar auxin transport specify the establishment of the embryonic apical-basal axis. This is supported by theoretical modeling of young embryos (Wabnik et al., 2013), where the postulation of dynamic auxin sources combined with an auxin feedback on PIN polarity were sufficient to reproduce the PIN polarity and auxin asymmetric distribution during embryogenesis.

1.3.2 Organogenesis

Whereas the most body organization of animals is established during embryogenesis, the architecture of an adult plant is determined by post-embryonic development. Newly formed organs are initiated from organ primordia. Auxin accumulation marks the position of these future primordia and at the later stages a PIN-mediated auxin gradient is progressively established with its maximum at the primordium tip, which drives subsequent organ development (Benková et al., 2003). PIN polarity can be very dynamic, while during the foundation of a shoot apical meristem (SAM), PIN1 in the outer layers polarizes apically to accumulate auxin in the primordium tip. Later auxin is drained through the primordium's interior by basally localized PIN1 to develop vasculature reconnecting the newly forming organ to the main vasculature network (Benková et al., 2003). Likely, the auxin feedback on PIN polarity is required to create the auxin gradient determining the growth axis of the newly developing organ.

1.3.3 Termination of shoot bending responses

Plants align their growth according to gravity. Gravity stimulation of hypocotyl induces polarization of PIN3 to the bottom sides of endodermal cells, which correlates with increased auxin accumulation at the lower side of hypocotyl, resulting in induction of cell elongation and organ bending (Rakusová et al., 2016). To avoid hypocotyl overbending, approximately after 16h, auxin-dependent PIN3 polarization to the upper endodermal cells restores PIN3 symmetry, equalizing auxin levels between upper and lower sides, and terminating the hypocotyl bending response (Rakusová et al., 2016).

1.4 *Concluding remarks*

The auxin canalization is a fascinating self-organizing process which requires a cooperation of a specific subset of cells to create a directional auxin transport. An understanding of the molecular mechanism of the coordinated auxin-mediated repolarization of PINs can help to elucidate how generally the cell polarity is established and maintained, and how cells communicate among themselves to follow self-organizing patterns.

1.5 *References*

1. Wm. P. Jacobs, The Role of Auxin in Differentiation of Xylem Around a Wound. *American Journal of Botany*. **39**, 301–309 (1952).

2. T. Sachs, Polarity and the Induction of Organized Vascular Tissues. *Ann Bot*. **33**, 263–275 (1969).

3. R. Snow, Activation of Cambial Growth by Pure Hormones. *New Phytologist*. **34**, 347–360 (1935).

4. E. Wangermann, The Effect of the Leaf on Differentiation of Primary Xylem in the Internode of Coleus Blumei Benth. *New Phytologist*. **66**, 747–754 (1967).

5. T. Sachs, The induction of transport channels by auxin. *Planta*. **127**, 201–206 (1975).

6. T. Sachs, in *Advances in Botanical Research*, H. W. Woolhouse, Ed. (Academic Press, 1981; http://www.sciencedirect.com/science/article/pii/S0065229608603511), vol. 9, pp. 151–262.

7. J. Petrášek, J. Mravec, R. Bouchard, J. J. Blakeslee, M. Abas, D. Seifertová, J. Wiśniewska, Z. Tadele, M. Kubeš, M. Čovanová, P. Dhonukshe, P. Skůpa, E. Benková, L. Perry, P. Křeček, O. R. Lee, G. R. Fink, M. Geisler, A. S. Murphy, C. Luschnig, E. Zažímalová, J. Friml, PIN Proteins Perform a Rate-Limiting Function in Cellular Auxin Efflux. *Science*. **312**, 914–918 (2006).

8. J. Wiśniewska, J. Xu, D. Seifertová, P. B. Brewer, K. Růžička, I. Blilou, D. Rouquié, E. Benková, B. Scheres, J. Friml, Polar PIN Localization Directs Auxin Flow in Plants. *Science*. **312**, 883–883 (2006).

9. J. Balla, P. Kalousek, V. Reinöhl, J. Friml, S. Procházka, Competitive canalization of PIN-dependent auxin flow from axillary buds controls pea bud outgrowth. *The Plant Journal*. **65**, 571–577 (2011).

10. E. Benková, M. Michniewicz, M. Sauer, T. Teichmann, D. Seifertová, G. Jürgens, J. Friml, Local, Efflux-Dependent Auxin Gradients as a Common Module for Plant Organ Formation. *Cell*. **115**, 591–602 (2003).

11. E. Mazur, I. Kulik, J. Hajný, J. Friml, Auxin canalization and vascular tissue formation by TIR1/AFB-mediated auxin signaling in Arabidopsis. *New Phytologist*. **n/a**, doi:10.1111/nph.16446.

12. C. Verna, S. J. Ravichandran, M. G. Sawchuk, N. M. Linh, E. Scarpella, Coordination of tissue cell polarity by auxin transport and signaling. *eLife*. **8**, e51061 (2019).

13. T. Prát, J. Hajný, W. Grunewald, M. Vasileva, G. Molnár, R. Tejos, M. Schmid, M. Sauer, J. Friml, WRKY23 is a component of the transcriptional network mediating auxin feedback on PIN polarity. *PLOS Genetics*. **14**, e1007177 (2018).

14. E. Scarpella, D. Marcos, J. Friml, T. Berleth, Control of leaf vascular patterning by polar auxin transport. *Genes Dev.* **20**, 1015–1027 (2006).

15. S. J. Ravichandran, N. M. Linh, E. Scarpella, The Canalization Hypothesis — Challenges and Alternatives. *New Phytologist*. **n/a**, doi:10.1111/nph.16605.

16. M. Sauer, J. Balla, C. Luschnig, J. Wiśniewska, V. Reinöhl, J. Friml, E. Benková, Canalization of auxin flow by Aux/IAA-ARF-dependent feedback regulation of PIN polarity. *Genes Dev.* **20**, 2902–2911 (2006).

17. E. Mazur, E. Benková, J. Friml, Vascular cambium regeneration and vessel formation in wounded inflorescence stems of Arabidopsis. *Sci Rep*. **6** (2016), doi:10.1038/srep33754.

18. H. Han, H. Rakusova, I. Verstraeten, Y. Zhang, J. Friml, SCFTIR1/AFB auxin signaling for bending termination during shoot gravitropism. *Plant Physiology* (2020), doi:10.1104/pp.20.00212.

19. E. Mazur, M. Gallei, M. Adamowski, H. Han, H. S. Robert, J. Friml, Clathrin-mediated trafficking and PIN trafficking are required for auxin canalization and vascular tissue formation in Arabidopsis. *Plant Science*. **293**, 110414 (2020).

20. W. Grunewald, I. De Smet, B. De Rybel, H. S. Robert, B. van de Cotte, V. Willemsen, G. Gheysen, D. Weijers, J. Friml, T. Beeckman, Tightly controlled *WRKY23* expression mediates Arabidopsis embryo development. *EMBO reports*. **14**, 1136–1142 (2013).

21. R. Tejos, C. Rodriguez-Furlán, M. Adamowski, M. Sauer, L. Norambuena, J. Friml, PATELLINS are regulators of auxin-mediated PIN1 relocation and plant development in Arabidopsis thaliana. *J Cell Sci*. **131** (2018), doi:10.1242/jcs.204198.

22. A. Vieten, S. Vanneste, J. Wisniewska, E. Benkova, R. Benjamins, T. Beeckman, C. Luschnig, J. Friml, Functional redundancy of PIN proteins is accompanied by auxin-dependentcross-regulation of PIN expression. *Development*. **132**, 4521–4531 (2005).

23. M. Glanc, M. Fendrych, J. Friml, Mechanistic framework for cell-intrinsic re-establishment of PIN2 polarity after cell division. *Nature Plants*. **4**, 1082–1088 (2018).

24. J. Friml, X. Yang, M. Michniewicz, D. Weijers, A. Quint, O. Tietz, R. Benjamins, P. B. F. Ouwerkerk, K. Ljung, G. Sandberg, P. J. J. Hooykaas, K. Palme, R. Offringa, A PINOID-Dependent Binary Switch in Apical-Basal PIN Polar Targeting Directs Auxin Efflux. *Science*. **306**, 862–865 (2004).

25. T. Ischebeck, S. Werner, P. Krishnamoorthy, J. Lerche, M. Meijón, I. Stenzel, C. Löfke, T. Wiessner, Y. J. Im, I. Y. Perera, T. Iven, I. Feussner, W. Busch, W. F. Boss, T. Teichmann, B. Hause, S. Persson, I. Heilmann, Phosphatidylinositol 4,5-bisphosphate influences PIN polarization by controlling clathrin-mediated membrane trafficking in Arabidopsis. *Plant Cell*. **25**, 4894–4911 (2013).

26. Y. Gao, Y. Zhang, D. Zhang, X. Dai, M. Estelle, Y. Zhao, Auxin binding protein 1 (ABP1) is not required for either auxin signaling or Arabidopsis development. *PNAS*. **112**, 2275–2280 (2015).

27. N. Dai, W. Wang, S. E. Patterson, A. B. Bleecker, The TMK Subfamily of Receptor-Like Kinases in Arabidopsis Display an Essential Role in Growth and a Reduced Sensitivity to Auxin. *PLoS One*. **8** (2013), doi:10.1371/journal.pone.0060990.

28. T. Xu, N. Dai, J. Chen, S. Nagawa, M. Cao, H. Li, Z. Zhou, X. Chen, R. D. Rycke, H. Rakusová, W. Wang, A. M. Jones, J. Friml, S. E. Patterson, A. B. Bleecker, Z. Yang, Cell Surface ABP1-TMK Auxin-Sensing Complex Activates ROP GTPase Signaling. *Science*. **343**, 1025–1028 (2014).

29. M. P. Platre, V. Bayle, L. Armengot, J. Bareille, M. del M. Marquès-Bueno, A. Creff, L. Maneta-Peyret, J.-B. Fiche, M. Nollmann, C. Miège, P. Moreau, A. Martinière, Y. Jaillais, Developmental control of plant Rho GTPase nano-organization by the lipid phosphatidylserine. *Science*. **364**, 57–62 (2019).

30. X. Pan, L. Fang, J. Liu, B. Senay-Aras, W. Lin, S. Zheng, T. Zhang, U. Manor, W. Chen, Z. Yang, Auxin-induced nanoclustering of membrane signaling complexes underlies cell polarity establishment in Arabidopsis. *bioRxiv*, 734665 (2019).

31. X. Zhang, M. Adamowski, P. Marhava, S. Tan, Y. Zhang, L. Rodriguez, M. Zwiewka, V. Pukyšová, A. S. Sánchez, V. K. Raxwal, C. S. Hardtke, T. Nodzyński, J. Friml, Arabidopsis Flippases Cooperate with ARF GTPase Exchange Factors to Regulate the Trafficking and Polarity of PIN Auxin Transporters. *The Plant Cell*. **32**, 1644–1664 (2020).

32. T. Paciorek, E. Zazímalová, N. Ruthardt, J. Petrásek, Y.-D. Stierhof, J. Kleine-Vehn, D. A. Morris, N. Emans, G. Jürgens, N. Geldner, J. Friml, Auxin inhibits endocytosis and promotes its own efflux from cells. *Nature*. **435**, 1251–1256 (2005).

33. T. Steinmann, N. Geldner, M. Grebe, S. Mangold, C. L. Jackson, S. Paris, L. Gälweiler, K. Palme, G. Jürgens, Coordinated Polar Localization of Auxin Efflux Carrier PIN1 by GNOM ARF GEF. *Science*. **286**, 316–318 (1999).

34. J. Jásik, B. Bokor, S. Stuchlík, K. Mičieta, J. Turňa, E. Schmelzer, Effects of Auxins on PIN-FORMED2 (PIN2) Dynamics Are Not Mediated by Inhibiting PIN2 Endocytosis. *Plant Physiology*. **172**, 1019–1031 (2016).

35. T. Li, A. Yan, N. Bhatia, A. Altinok, E. Afik, P. Durand-Smet, P. T. Tarr, J. I. Schroeder, M. G. Heisler, E. M. Meyerowitz, Calcium signals are necessary to establish auxin transporter polarity in a plant stem cell niche. *Nature Communications*. **10**, 726 (2019).

36. J. Dindas, S. Scherzer, M. R. G. Roelfsema, K. Meyer, H. M. Müller, K. a. S. Al-Rasheid, K. Palme, P. Dietrich, D. Becker, M. J. Bennett, R. Hedrich, AUX1-mediated root hair auxin influx governs SCF TIR1/AFB -type Ca 2+ signaling. *Nature Communications*. **9**, 1174 (2018).

37. S. Jeong, M. Bayer, W. Lukowitz, Taking the very first steps: from polarity to axial domains in the early Arabidopsis embryo. *J Exp Bot*. **62**, 1687–1697 (2011).

38. J. Friml, A. Vieten, M. Sauer, D. Weijers, H. Schwarz, T. Hamann, R. Offringa, G. Jürgens, Efflux-dependent auxin gradients establish the apical–basal axis of Arabidopsis. *Nature*. **426**, 147–153 (2003).

39. H. S. Robert, P. Grones, A. N. Stepanova, L. M. Robles, A. S. Lokerse, J. M. Alonso, D. Weijers, J. Friml, Local Auxin Sources Orient the Apical-Basal Axis in Arabidopsis Embryos. *Current Biology*. **23**, 2506–2512 (2013).

40. K. Wabnik, H. S. Robert, R. S. Smith, J. Friml, Modeling Framework for the Establishment of the Apical-Basal Embryonic Axis in Plants. *Current Biology*. **23**, 2513–2518 (2013).

41. H. Rakusová, M. Abbas, H. Han, S. Song, H. S. Robert, J. Friml, Termination of Shoot Gravitropic Responses by Auxin Feedback on PIN3 Polarity. *Current Biology*. **26**, 3026–3032 (2016).

42. J. Hajný, T. Prát, N. Rydza, L. Rodriguez, S. Tan, I. Verstraeten, D. Domjan, E. Mazur, E. Smakowska-Luzan, W. Smet, E. Mor, J. Nolf, B. Yang, W. Grunewald, G. Molnár, Y. Belkhadir, B.D. Rybel, J. Friml, Receptor kinase module targets PIN-dependent auxin transport during canalization. *Science.* **370**, 550-557 (2020).

2 WRKY23 is a component of the transcriptional network mediating auxin feedback on PIN polarity

Adapted and modified from

T. Prát*, **J. Hajný***, W. Grunewald, M. Vasileva, G. Molnár, R. Tejos, M. Schmid, M. Sauer, J. Friml. WRKY23 is a component of the transcriptional network mediating auxin feedback on PIN polarity. *PLOS Genet.* **14**, e1007177 (2018)

2.1 *Introduction*

The phytohormone auxin plays a key role in many aspects of the plant's life cycle. A unique attribute of auxin is its polarized, intercellular movement that depends, among other components, on the polarly localized PIN-FORMED (PIN) auxin exporters (Adamowski and Friml, 2015; Petrášek et al., 2006; Wiśniewska et al., 2006). The so-called canalization hypothesis proposes that auxin acts also as a cue in the establishment of new polarity axes during the polarization of tissues by the formation of self-organizing patterns due to the formation of narrow auxin transport channels driven by the polarized auxin carriers from an initially broad domain of auxin-transporting cells (Bennett et al., 2014; Sachs, 1986, 1975). Canalization has been implied to mediate multiple key plant developmental processes, including formation of new vasculature (Berleth and Sachs, 2001), regeneration after wounding (Mazur et al., 2016; Sauer et al., 2006a), and competitive control of apical dominance (Balla et al., 2011; Bennett et al., 2016; Booker et al., 2003). Whereas the molecular details of canalization are largely unknown, the key constituents are *(i)* feedback regulation of the auxin transport directionality by auxin and *(ii)* gradual concentrating and narrowing of auxin channels (Sachs, 1975). Auxin feedback on the transport directionality can be realized by the auxin impact on PIN polarity (Sauer et al., 2006a) and might be related to an auxin effect on clathrin-mediated internalization of PIN proteins (Paciorek et al., 2005; Robert et al., 2010), but the connection is still unclear (Wabnik et al., 2010). Presumably, this feedback regulation of the PIN repolarization also plays a role in the establishment of the embryonic apical-basal axis (Robert et al., 2013; Wabnik et al., 2013b), during organogenesis (Benková et al., 2003), and termination of shoot bending responses (Rakusová et al., 2016).

Auxin feedback on the PIN polarity can be experimentally approximated by PIN polarity rearrangements after auxin treatment of *Arabidopsis thaliana* roots. Under standard conditions, PIN1 is localized at the basal (root-ward) sides of endodermal and pericycle cells and cells of the vascular tissue (Jiří Friml et al., 2002), whereas PIN2 exhibits a basal polarity in the young cortex cells, but an apical (shoot-ward) polarity in epidermal cells (Kleine-Vehn et al., 2008b; Müller et al., 1998, p. 2). After treatment with auxin, PIN1 changes from predominantly basal to also inner-lateral in endodermal and pericycle cells, whereas PIN2 undergoes a localization shift from the basal to also outer-lateral side of cortex cells (Sauer et al., 2006a). The exact molecular mechanism and biological significance of this effect is unclear, but it has so far successfully served as easy, experimentally tractable proxy for auxin feedback on PIN polarity (Sauer et al., 2006a). It depends on the transcriptional SCF^{TIR1}-Aux/IAA-ARF auxin signaling pathway (Chapman and Estelle, 2009). In brief, upon auxin binding to the TIR1/AFB receptor family, transcriptional repressors and co-receptors of the Aux/IAA class are degraded, in turn releasing auxin response transcription activators of the ARF family (Salehin et al., 2015).

In a heat-shock (HS)-inducible *HS::axr3-1* line expressing a mutated, non-degradable version of the IAA17 transcriptional repressor (Knox et al., 2003; Salehin et al., 2015), as well as in the *arf7 arf19* double mutant defective for these two functionally redundant transcriptional activators expressed in primary roots (Wilmoth et al., 2005), auxin is no longer effective in mediating PIN polarity rearrangements in the root meristem (Sauer et al., 2006a). These results suggest that transcriptional auxin signaling regulates the cellular abundance of so far unknown regulators, which, in turn, modify subcellular sorting or trafficking pathways and other polarity determinants, ultimately leading to changes in the polar PIN distribution.

In this work, we carried out an expression profiling experiment in *Arabidopsis* roots to identify potential regulators of the PIN polarity that are transcriptionally regulated by auxin signaling. We identified several novel regulators and characterized in more detail the transcription factor WRKY23 and its role in auxin-mediated PIN polarization, thus providing initial insights into a molecular mechanism of the auxin feedback on the directional auxin flow – one of the key prerequisites of canalization.

2.2 *Results*

2.2.1 Microarray-based identification of components mediating auxin impact on PIN polarity

The rationale behind the microarray approach was to search for genes that were (*i*) regulated by auxin in roots under conditions when auxin changes PIN polarity and (*ii*) their auxin regulation is mediated by the IAA17 (AXR3) transcriptional repressor. First, to look for auxin-induced genes, we matched data from NAA-treated and untreated heat-shocked wild type (WT) Columbia-0 (Col-0) control seedlings and found 523 auxin-induced genes, with a minimum of two-fold difference. As in the *HS::axr3-1* line under the same conditions auxin fails to induce PIN polarity changes (Fig 2.1A and B) (Sauer et al., 2006a), we compared heat-shocked and auxin-treated Col-0 seedlings to similarly handled *HS::axr3-1* seedlings, expressing the auxin-resistant version of IAA17 (AXR3) and we identified 667 genes (Fig 2.1C). The overlap of this set with the 523 auxin-induced genes yielded 245 genes induced by auxin and regulated downstream of IAA17 (Appendix Tab S2.1), including *PATELLIN2* and *PATELLIN6* that encode phosphatidylinositol transfer proteins, concomitantly characterized to be crucial for the regulation of embryo and seedling patterning in *Arabidopsis* (Tejos et al., 2018). Further comparison with published microarray data on *arf7 arf19* mutant seedlings (Okushima et al., 2005), which are also ineffective in rearranging the PIN polarity (Sauer et al., 2006a), yielded a final list of 125 genes (Appendix Tab S2.2), of which some had previously been found to be involved in a general PIN polarity regulation, including the AGC3 kinase PINOID (PID) and its homologs WAG1 and WAG2 which are known to phosphorylate PIN proteins (Michniewicz et al., 2007), contributing to the control of their polar distribution (Friml et al., 2004; Zhang et al., 2010). Nevertheless, overexpression of PID was shown to be dominant over the auxin-induced PIN lateralization (Sauer et al., 2006a). Another identified candidate with a known role in the PIN polar distribution was the phosphatidylinositol-4-phosphate 5 kinase PIP5K1. This protein, together with its close homolog PIP5K2, is enriched on basal and apical membrane domains and they are required for PIN trafficking (Mei et al., 2012; Ugalde et al., 2016) and localization (Ischebeck et al., 2013; Tejos et al., 2014). Other candidates for polarity determinants include several previously known players in auxin-mediated plant development, such as RUL1, a leucine-rich repeat receptor-like kinase regulating cambium formation, a process linked to PIN polarity control (Agusti et al., 2011).

Auxin-dependent PIN lateralization in the root meristem requires a rather prolonged auxin treatment (Sauer et al., 2006a), hinting at the involvement of a whole cascade of transcriptional processes. Therefore, we looked for additional auxin-induced transcription factor (TF) genes, which, based on their analogous behavior in similar experiments and on their known functions, would be potential candidates for having a role in auxin-mediated development. The list of candidates contains *e.g. MINI ZINC FINGER1 (MIF1*), affecting auxin responses during ectopic meristem formation (Hu et al., 2011), but also *WRKY23*. *WRKY* genes belong to a plant-specific family of 72 TFs in *Arabidopsis*, typically associated with plant defense processes and plant-pathogen interactions (Eulgem and Somssich, 2007). These genes were named by a shared sequence motif of 60 amino acids containing a conserved domain of seven invariant amino acids (WRKYGQK) (Eulgem et al., 2000). The WRKYGQK motif provides a high binding preference and contacts a 6-bp DNA sequence element – the W-box (/TTGACT/C) contained in target gene promoters (Eulgem and Somssich, 2007; Ülker and Somssich, 2004). Distinct WRKY TFs have distinct selective binding preferences to certain W-box variants (Ciolkowski et al., 2008). The role of WRKY23 has been established in plant defense processes during plant-nematode interactions, but also in auxin transport regulation by flavonol biosynthesis that affects root and embryo development. In *Arabidopsis* embryos, the *WRKY23* expression attenuates both auxin-dependent and auxin-independent signaling pathways toward stem cell specification (Grunewald et al., 2013, 2012, 2008). In addition, *WRKY23* is unique within its gene family, because none of the other *WRKY* genes in these experimental conditions was responsive to auxin and, thus, present in the gene selection (Appendix Tab S2.2). In this work, we focused on one of the transcription factors fulfilling our selection criteria, and investigated the role of WRKY23-dependent transcriptional regulation in auxin-dependent PIN repolarization.

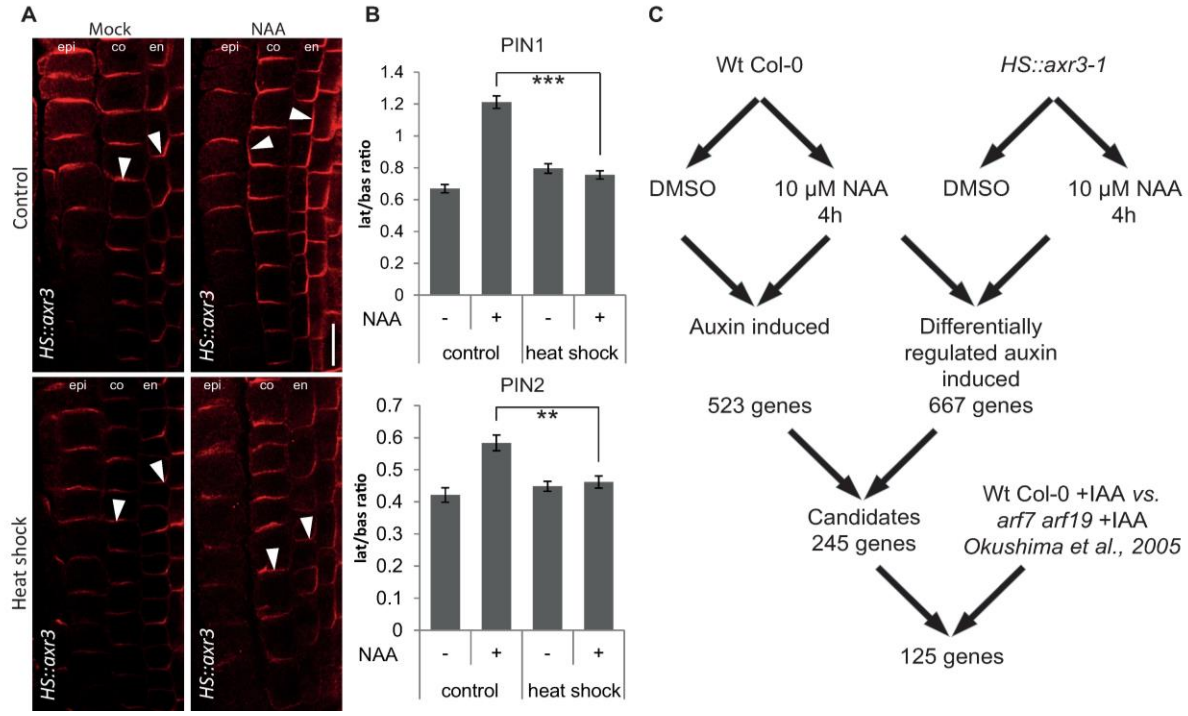

Figure 2. 1 Putative transcriptional components of the auxin-mediated PIN polarization

(A) Simultaneous immunolocalization of PIN1 and PIN2 in *HS::axr3-1* plants. Heat shock-induced overexpression of *axr3-1* abolishes lateral PIN relocation after auxin (4 h, 10 µM NAA) treatment, confirming dependence on the SCF^{TIR1}-Aux/IAA-ARF signaling pathway. Arrowheads highlight representative examples of PIN localization in the respective tissues and treatments (PIN1 in endodermis and PIN2 in cortex). Bar = 10 µm. epi, epidermis; co, cortex; en, endodermis. (B) Quantitative evaluation of (A), confirming reduced auxin-dependent relocation of PIN1 (top) and PIN2 (bottom) in the induced *HS::axr3-1* line. Graph shows mean ratio of lateral-to-basal signal intensity of PIN1 in endodermal and PIN2 in cortex cells. Error bars indicate standard error. A One-Way ANOVA test compared marked sets of data. (** p<0.01; *** p<0.0001; n>35 cells corresponding to a minimum of 10 roots per treatment and experiment were imaged under comparable conditions). Experiments were carried out at least 3 times; one representative experiment is presented. (C) Scheme of the microarray experiment and analysis strategy.

2.2.2 *WRKY23* expression is regulated by auxin signaling

First, we confirmed and analysed the auxin regulation of *WRKY23* expression. Promoters of auxin-inducible genes typically contain tandem-localized auxin response elements (AuxREs) that are recognised by auxin response factors (ARFs) (Boer et al., 2014; Ulmasov et al., 1997, p. 1). ARFs dimerize to act as molecular calipers and provide specificity to the auxin-dependent gene regulation by measuring the distance of AuxREs in the element pair at the promoter (Boer et al., 2014). The length of the intergenic region between the 3'-UTR of the previous gene *UPBEAT* (*UPB*; *At2g47270*) and the 5'-UTR of *WRKY23* (*At2g47260*) is 4.5 kbp. The predicted 2.4-kbp *WRKY23* promoter by the AGRIS tool (Yilmaz et al., 2011) contains 10

AuxRE and AuxRE-like sites and the extended promoter of 3.2 kbp used for the native promoter fusion construct (Grunewald et al., 2008) contains two additional AuxRE sites (Fig 2.2A). Such a density of auxin-regulatory sequences in the promoter makes direct regulation by ARF-dependent auxin signaling a plausible scenario.

In accordance with these results, we found that *WRKY23* is auxin-inducible in a dose- and time-dependent manner. When we treated *Arabidopsis* seedlings with 100 nM NAA for 4 h, the *WRKY23* transcription increased 2-fold, and 1 µM NAA led to a 6-fold increase (Fig 2.2B). Time response experiments at the consensus concentration of 10 µM NAA used in PIN lateralization experiments (Sauer et al., 2006a) revealed that the *WRKY23* transcription starts to increase approximately after 1.5 h of auxin treatment with a stronger increase after between 2 and 4 h (Fig 2.2C). This relatively slow auxin-mediated transcriptional regulation of *WRKY23* is well within the time frame for the auxin-mediated PIN lateralization that also occurs strongly only after 4 h (Sauer et al., 2006a). The dependence on the auxin signaling was further supported by the compromised *WRKY23* auxin inducibility in the *HS::axr3-1* and *arf7 arf19* mutants (Fig 2.2D and E). These results show that the *WRKY23* transcription depends on the SCF^{TIR1}-Aux/IAA-ARF auxin signaling pathway and confirm *WRKY23* as a candidate regulator of auxin-mediated PIN polarization.

A transgenic line harbouring the *uidA* reporter gene (or GUS-coding gene) under the control of a 3.2-kb upstream sequence from *WRKY23* (*WRKY23::GUS*), whose expression pattern has previously been confirmed by *in situ* hybridization (Grunewald et al., 2012, 2008), revealed that auxin induces the ectopic expression of *WRKY23* in root tissues, partly overlapping with root regions, in which PIN lateralization can be observed (Fig S2.1G and H). Without auxin treatment, the expression pattern of *WRKY23* partially overlaps with the *DR5* auxin response reporter (Fig S2.1G and I) and auxin distribution as revealed by anti-IAA immunolocalization (Friml et al., 2003; Grunewald et al., 2012, 2008). Previously, *WRKY23* has been shown to be expressed in all apical cells of an octant stage embryo and at heart stage to be detected in both the root and the shoot stem cell niches (Fig S2.1D and E) (Grunewald et al., 2013), possibly indicating that *WRKY23* has -besides its role in root development- also a function in shoot development. We found *WRKY23::GUS* expression in pollen grains (Fig S2.1C), the shoot apical meristem (SAM) (Fig S2.1A and Fig 2.2F), as well as at the hydathodes of cotyledons (Fig S2.1F), coinciding with known auxin response maxima (Scarpella et al., 2006a). Sectioning the SAM revealed specific *WRKY23* expression in the L1, L2, and L3 layers

(Fig S2.1A). *WRKY23* promoter activity was prominently associated with the vascular tissues of flowers, cotyledons, and leaves (Fig S2.1B, F and Fig 2.2G). Notably, the *WRKY23* expression mirrored the pattern of developing leave vasculature with the highest expression in cells adjacent to the differentiated xylem (Fig 2.2G) and were detected in a venation-like pattern even before any morphological changes typical for the differentiated vasculature were visible (Fig 2.2F and 2.2G). In the previous, external auxin source-mediated canalization experiments in pea stems, the PIN channels were preceding the formation of vasculature and later the differentiated xylem formed adjacent to the PIN channels (Balla et al., 2011). Thus, the WRKY23 expression pattern in Arabidopsis largely overlaps with presumptive PIN channels being consistent with a role of WRKY23 in venation patterning of leaves – a process regulated by the polarized auxin transport (Mattsson et al., 2003; Scarpella et al., 2006a).

In summary, the presence of auxin-responsive elements in the promoter, the auxin-inducibility of the *WRKY23* expression together with its dependence on AXR3*,* ARF7 and ARF19 activities indicate that the *WRKY23* transcription is regulated by Aux/IAA- and ARF-dependent auxin signaling. In addition, the association of the *WRKY23* expression with developing vasculature is consistent with a possible involvement of WRKY23 in the auxin-mediated PIN polarization process.

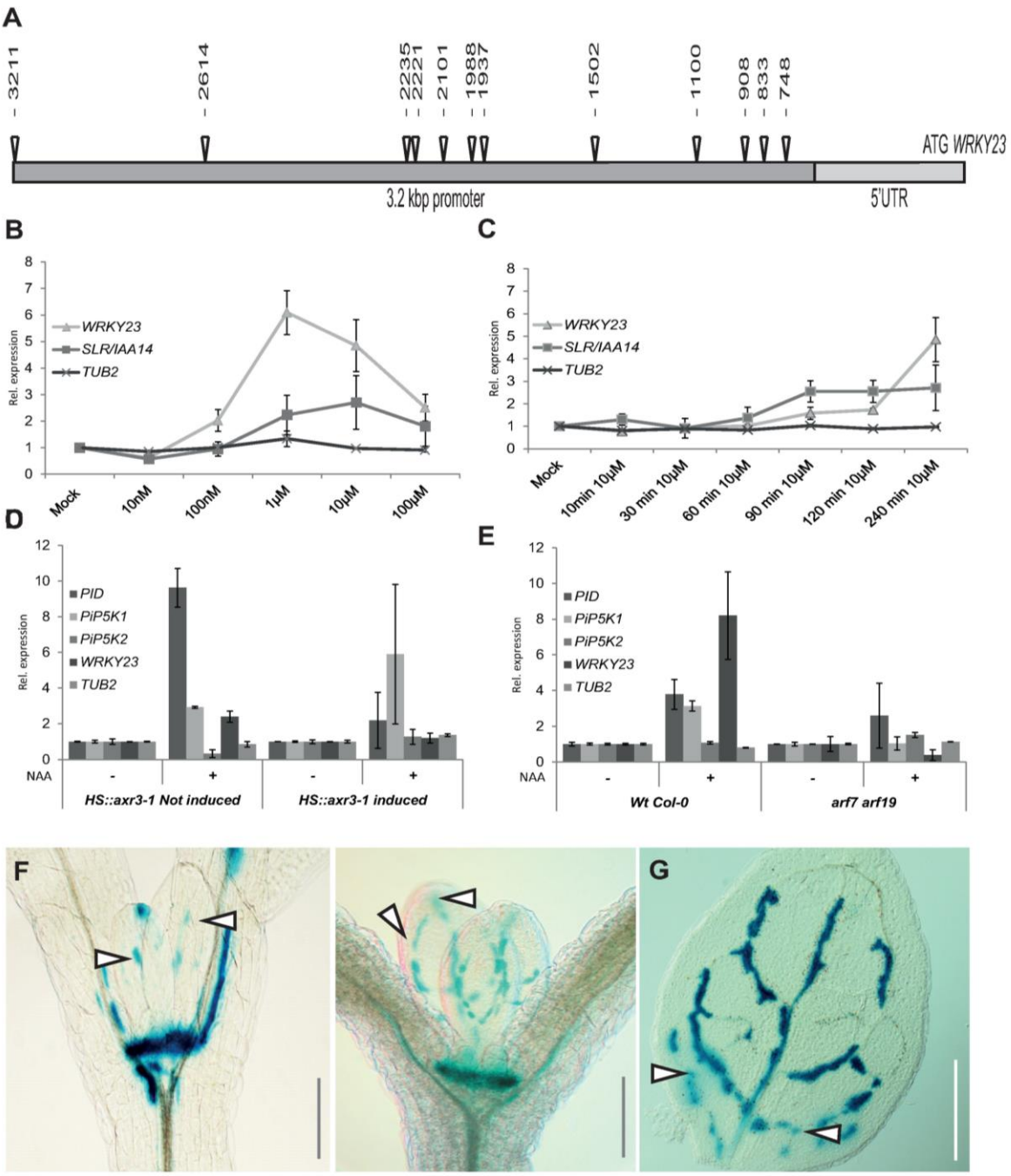

Figure 2. 2 WRKY23 acts downstream of the Aux/IAA-ARF auxin pathway and marks developing vasculature.

(A) Schematic depiction of WRKY23 promoter; AuxRE and AuxRE-like response elements are shown as triangles (B and C) *WRKY23* transcript levels depend on auxin dose and treatment time. qRT-PCR analysis of *WRKY23* expression after a 4 h treatment with different concentrations of NAA (B) and after different treatment times with 10 µM NAA (C). *TUB2* and *SLR/IAA14* are shown as negative and positive controls, respectively. Values represent relative fold change of expression. Error bars represent standard deviation (see Materials and Methods for detailed description). (D and E) *WRKY23* expression depends on the SCF^{TIR1}-Aux/IAA-ARF signaling pathway. qRT-PCR confirmation of the microarray experiment showing the expression of *WRKY23* and genes previously connected to PIN

polarity in *HS::arx3-1* (D), and in *arf7 arf19* double mutant plants (E). Values represent relative fold change. Error bars indicate standard deviation (see Materials and Methods for detailed description). (F, G) Expression of *WRKY23::GUS* in the shoot apical meristem (SAM) and in the presumptive leaf vasculature (G). Besides strong activity in the SAM, GUS staining overlaps with, and partly precedes, the appearance of differentiating vascular strands in young leaves. Two representative plants in consecutive developmental stages are shown. Patchy expression of *WRKY23::GUS* in the vasculature of young developing true leaves (G). Arrowheads in F and G depict areas with GUS activity presumably coinciding with future vascular strands that are not morphologically discernible yet.

2.2.3 WRKY23 gain-of-function leads to PIN1 and PIN2 lateralization

Next, we tested whether altered *WRKY23* expression or activity affected the auxin regulation of the PIN1 and PIN2 protein localization. A strong constitutive overexpression of *WRKY23* was obtained by means of a GAL4-VP16-*UAS* transactivation system (*RPS5A>>WRKY23*) (Aida et al., 2004; Grunewald et al., 2013, 2012). The *35S* promoter-driven WRKY23 line (*35S::WRKY23*) as well as also *35S* promoter-driven dexamethasone-glucocorticoid (DEX/GR) receptor system (*35S::WRKY23-GR*) were used for constitutive overexpression, eventually, with inducible nuclear localization (Grunewald et al., 2013, 2012). Constitutive overexpression of *WRKY23* had an impact on the PIN2 but not PIN1 polarity. It caused PIN2 lateralization in root cortex cells, to some extent mimicking the application of auxin (Fig 2.3A and B). Subsequent treatment with NAA further increased lateralization of PIN2 in cortex cells and caused increased lateralization of PIN1 as compared to wild type (Fig 2.3A, B and Fig S2.2C, D). An inducible *WRKY23* gain-of-function line had a similar effect: seedlings of a *35S::WRKY23-GR* line treated with DEX to induce WRKY23-GR translocation to the nucleus, resulted in PIN2, but not PIN1 lateralization in the cortex cells. Again, additional NAA treatment had an additive effect on PIN2 lateralization and caused a stronger PIN1 lateralization than as seen in the wild type (Fig S2.3C, D and Fig S2.2C, D).

Thus, both constitutive and inducible *WRKY23* gain-of-function consistently led to PIN2 lateralization and increased the auxin-mediated PIN1 and PIN2 lateralization.

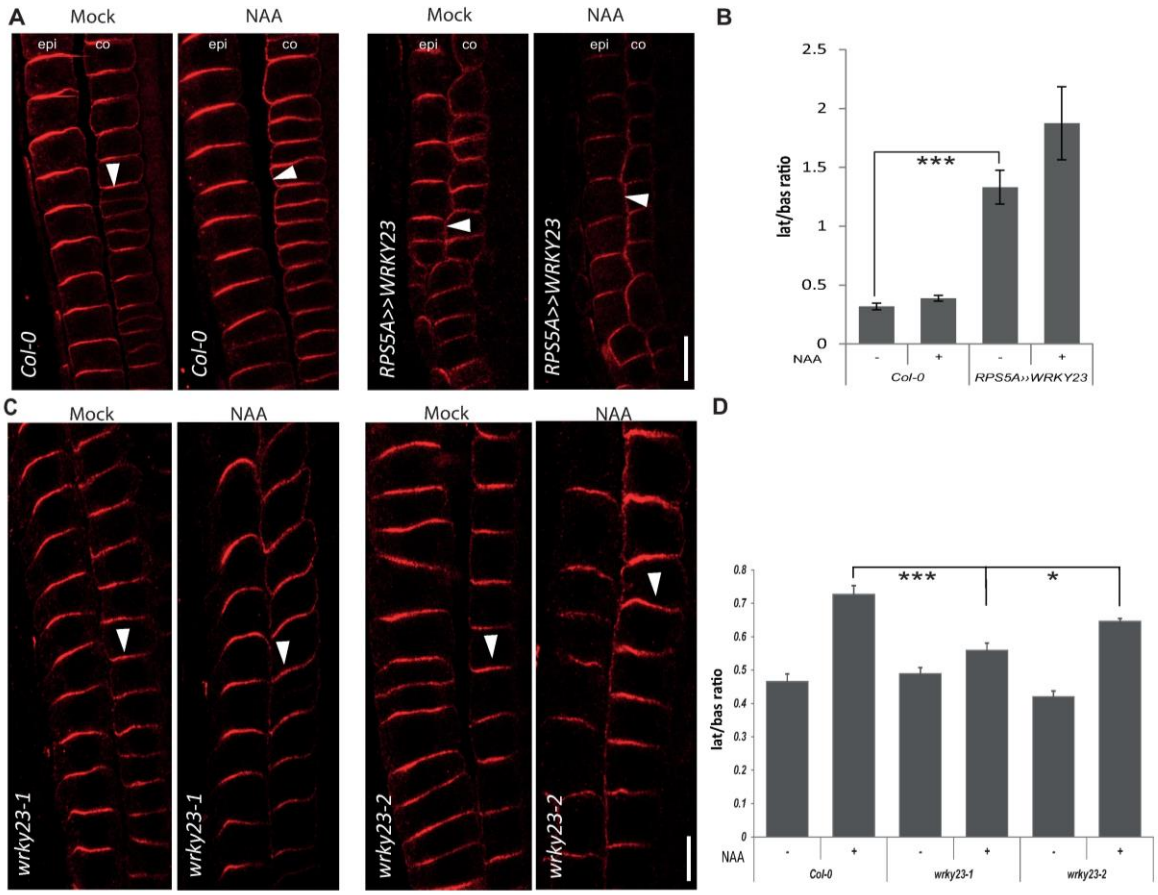

Figure 2. 3 WRKY23 is required for auxin-mediated PIN lateralization in the root.

(A) Immunolocalization analysis of PIN2 without or after NAA (4 h, 10 µM) treatment in WT Col-0 and *RPS5A>>WRKY23*. Arrowheads highlight PIN2 polarity. epi, epidermis; co, cortex. (B) Quantitative evaluation of (A) showing mean ratio of PIN2 lateral-to-basal signal intensity in cortex cells. Note that PIN2 lateralization in *RPS5A>>WRKY23* roots is increased even without auxin that still remains effective. Error bars indicate standard error. A One-Way ANOVA test compared marked sets of data (*** p<0.0001; n>35 cells corresponding to a minimum of 10 roots per treatment and experiment were imaged under comparable conditions). (C) Immunolocalization analysis of PIN2 without or with NAA treatment in WT Col-0 and *wrky23* mutants. Arrowheads highlight representative examples of PIN2 polarity in the. epi, epidermis; co, cortex. (D) Quantitative evaluation of the experiment in (C) showing mean ratio of PIN2 lateral-to-basal signal intensity in epidermis. Error bars indicate standard error. A One-Way ANOVA test compared marked sets of data (* p<0.05; *** p<0.001; n>100 cells corresponding to a minimum of 10 roots per treatment and experiment were imaged under comparable conditions). Experiments were carried out 3 times; one representative experiment is presented)

2.2.4 Repression of WRKY23 activity abolishes the auxin effect on the PIN2 polarization

In complementary experiments, we tested the downregulation effect of the WRKY23 function. The large WRKY family of homologous proteins has an extensive functional redundancy among individual members (Schluttenhofer and Yuan, 2015). As the functional compensation of *wrky23* loss-of-function by other members was likely, given the large size of the *WRKY* gene family, we used a dominant-negative approach with the chimeric repressor silencing technology (Hiratsu et al., 2003). This technology is based on a translational fusion of an activating TF with the repressor domain SRDX, thus inhibiting the expression of target genes. The transactivation activity of WRKY23 had previously been verified in a tobacco transient expression assay, in which the activating or repressing potential of the TF fused to GAL4 had been checked in the presence of a *UAS::Luciferase* construct (Grunewald et al., 2012).

Plants expressing *WRKY23-SRDX* under both the native and constitutive promoters showed a clear auxin insensitivity in PIN2 lateralization, namely the auxin treatment did not lead to lateralization when compared to the controls (Fig S2.3A and B). Notably, PIN1 lateralization did not change visibly after NAA treatment (Fig S2.2C and D).

2.2.5 *wrky23* partial loss-of-function mutants are defective in auxin impact on the PIN polarity

To investigate intrafamily redundancy and to assess specifically the role of WRKY23 on the auxin effect on the PIN polarity, we isolated two T-DNA insertional mutants in the *WRKY23* locus, designated *wrky23-1* and *wrky23-2* (Fig 2.4A). The reverse transcription-polymerase chain reaction (RT-PCR) analysis revealed that both alleles are knock-downs, *wrky23-1* having more downregulated expression (Fig 2.4B).

Similarly to the *WRKY23-SRDX* lines, both *wrky23* mutant alleles showed a reduced PIN2 lateralization response to auxin treatment and, additionally, also reduced PIN1 lateralization. Specifically, following the NAA treatment, the PIN1 and PIN2 lateralization in root cells was diminished in the *wrky23-2* weaker knock-down and, even more so, in the stronger *wrky23-1* allele (Fig S2.2A, B and Fig 2.3C, D). The observed opposite effects of WRKY23 gain- and loss-

of-function on the PIN lateralization suggested that WRKY23 plays an important role in the auxin-mediated PIN polarity rearrangements.

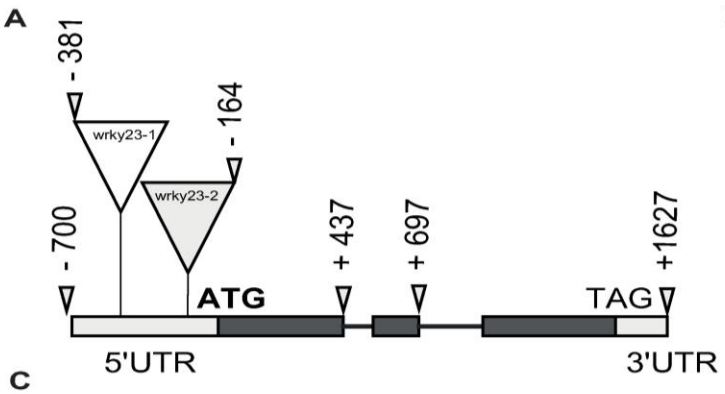

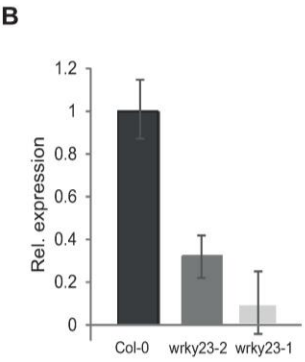

C

[%]	BD	UD	EL	LL	HS
Col-0	49	1.9	0	11.7	0
WRKY23-SRDX	69*	3	3	13.6	4.5
35S::WRKY23-SRDX	56.3	2.8	7*	0	14.1**
wrky23-1	53.8	7.7	1.9	26.9*	0
wrky23-2	55.6	6.7	0	15.5	2.2

BD-bottom disconnectivity *LL-less loops*
UD-upper disconnectivity *HS-higher structure*
EL-extra loops

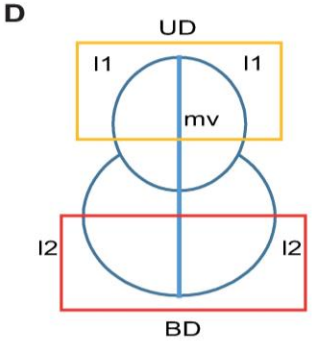

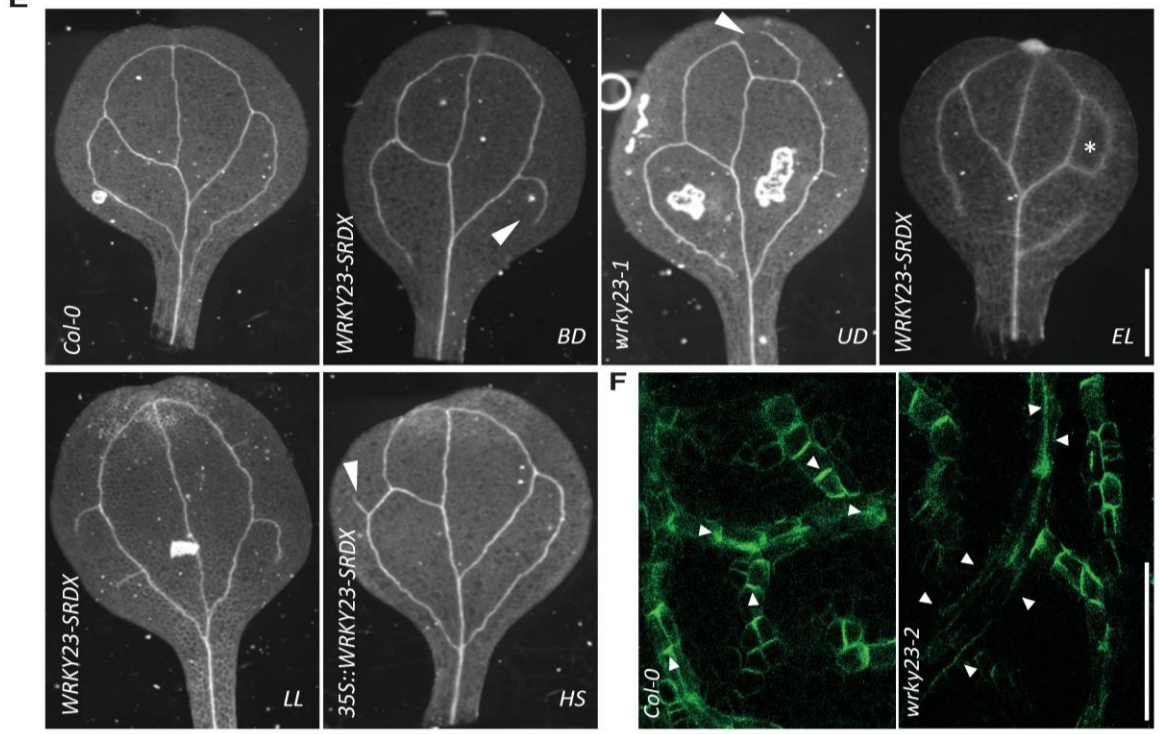

Figure 2. 4 Isolation and characterization of* wrky23 *mutants.

(A) Schematic representation of the *WRKY23* locus. Exons are represented by boxes, while introns are shown as lines. Coding regions are filled with dark grey. Exact locations of the T-DNA insertions are depicted. (B) qRT-PCR analysis of *WRKY23* expression in the isolated mutant lines. Relative expression values are normalized to the level detected in WT Col-0. See Materials and Methods for more details. (C) Evaluation of cotyledon vasculature defects in *WRKY23-SRDX*, *35S::WRKY23-SRDX* and *wrky23* mutants. A One-Way ANOVA test compared marked sets of data (* $p<0.05$; *** $p<0.001$; $n>50$ cotyledons). (D) Schematic representation of cotyledon vasculature pattern. l1, first loop; l2, second loop; mv, midvein. Yellow and red box delineate UD and BD zone of evaluating. (E) Representative images of analysed vasculature defects (F) Representative images of immunolocalization analysis of PIN1 in developing young first leaves. In the WT, PIN1 shows typical polarization, whereas in *wrky23-2* mutant this polarization is abolished. At least 50 leaves per genotype were analysed.

2.2.6 WRKY23 plays a role in PIN polarization during venation patterning

The importance of tight PIN polarity regulation for directional auxin fluxes and plant growth and development has been demonstrated previously (Adamowski and Friml, 2015; Wiśniewska et al., 2006). Therefore, we analysed the phenotypes related to PIN polarity or auxin transport in transgenic lines with an altered expression or activity of *WRKY23*. *35S::WRKY23* overexpressing plants show growth retardation and root meristem patterning defects (Grunewald et al., 2012). Also, dominant-negative lines showed severe defects in lateral root organogenesis (Grunewald et al., 2012). Both *WRKY23-SRDX* and *35S::WRKY23* lines had shorter roots than those of Col-0 (Fig S2.4A) and *WRKY23-SRDX* showed defects in gravitropism, similar to those observed in the auxin transport mutant *pin2/eir1* (Baster et al., 2013; Luschnig et al., 1998, p. 1). Notably, native promoter-driven *WRKY23-SRDX* displayed a significant increase in lateral root density (Fig S2.4B). None of these phenotypical defects, including root meristem disorganization, root growth inhibition and lateral root development alteration were observed in the *wrky23* mutant alleles (Fig S2.4A and B), suggesting that these more pleiotropic defects are not related to the WRKY23 action specifically, but they could reflect a broader role of the *WRKY* gene family in plant development.

The canalization hypothesis proposed that the leaf venation pattern depends on the auxin feedback on the PIN polarity (Sawchuk and Scarpella, 2013). We analysed several features of vascular defects in cotyledons. – bottom disconnectivity of l2 vein loops (BD), upper disconnectivity of l1 vein loops (UD), extra loops (EL), less loops (LL) and appearance of higher order structures (HS) (Fig 2.4C-E). In plants expressing *WRKY23::WRKY23-SRDX* and

35S::WRKY23-SRDX, we observed vasculature patterning defects manifested by increased incidence in BD, HS and EL. On the other hand, both *wrky23-1* and *wrky23-2* mutant alleles showed more defects in UD and LL (Fig 2.4C).

Next, we tested the PIN1 polarity during vascular tissue development by means of anti-PIN1 antibody staining on young first leaves. In the WT leaves, the staining revealed a pronounced PIN1 polarization along the basipetal (rootward) direction (Fig S2.4C). In the *35S::WRKY23* and *WRKY23-SRDX* lines, the typical PIN1 polarity was partly or completely abolished in some veins or their parts (Fig S2.4C). Similar PIN1 polarity defects were also found in *wrky23-1* and *wrky23-2* lines (Fig 2.4F and S2.4 C). The venation defects might be interpreted in terms of defective canalization (as suggested by the PIN1 polarity defects), although the venation defects differ somewhat from defects induced by auxin transport inhibition (Mattsson et al., 2003; Scarpella et al., 2006a). This observation indicates that interference with the PIN polarization does not have the same consequence as inhibition of PIN auxin transport activity.

In summary, our genetic analysis revealed that from the numerous functions of the WRKY family in the regulation of plant development (Bakshi and Oelmüller, 2014; Grunewald et al., 2013, 2012; Guan et al., 2014), WRKY23 is more specifically involved in auxin-mediated PIN polarity rearrangements and leaf venation patterning.

2.3 *Discussion*

Classical experiments have led to the formulation of the so-called canalization hypothesis that proposes an auxin feedback on the auxin transport and consequent formation of auxin channels as a central element of multiple self-organizing developmental processes; in particular formation and regeneration of vasculature (Berleth and Sachs, 2001). In canalization, the auxin transport through an initially homogeneous tissue follows a self-organizing pattern, leading from initially broad fields of auxin-transporting cells to eventually a narrow transport channel, consequently establishing the position of future vascular veins (Bennett et al., 2014). This hypothesis (Sachs, 1986, 1975) is further supported by successful modelling efforts based on the concerted cellular polarization via a feedback mechanism, by which auxin influences the directionality of its own flow by polarity rearrangement of auxin carriers (Bennett et al., 2014; Cieslak et al., 2015; Smith et al., 2006; Wabnik et al., 2011,

2010). Most of these models rely on hypothetical propositions, such as auxin flux sensors or direct cell-to-cell communication, giving testimony of our lack of understanding how canalization works mechanistically. However, the auxin impact on the PIN polarization has been experimentally demonstrated in different contexts and this effect has been shown to rely on the transcriptional gene expression activation through auxin signaling (Balla et al., 2011; Mazur et al., 2016; Rakusová et al., 2016; Sauer et al., 2006a).

Our transcriptional profiling experiments on auxin-dependent PIN rearrangements in *Arabidopsis* roots provide insight into the transcriptional reprogramming during auxin-mediated PIN polarity rearrangements and identify potential downstream molecular components in this process, including established PIN polarity regulators, such as PID, PIP5K, and PATELLINS (Michniewicz et al., 2007; Stenzel et al., 2008; Tejos et al., 2018, 2014), validating the soundness of the experimental concept. Among a number of novel components awaiting further characterization, we also found the transcriptional activator *WRKY23*.

WRKY23 is an auxin-responsive gene. The local upregulation of the *WRKY23* expression following the auxin application is consistent with a possible involvement in the PIN repolarization process. The *WRKY23* transcription is induced by auxin in a dose- and time-dependent manner and it is reminiscent of the expression pattern of the *DR5rev* auxin signaling reporter. Notably, *WRKY* genes are traditionally known to be involved in defensive processes in plants. More and more, this limited functional spectrum has been broadened by studies uncovering the involvement of these TFs in developmental and physiological processes other than plant defense (Bakshi and Oelmüller, 2014; Grunewald et al., 2013, 2012; Guan et al., 2014). In the case of *WRKY23*, besides a role in plant-nematode interaction with subsequent activation of auxin responses, participation in auxin transport through flavonol synthesis in the root as well as a function in a *mp/bdl*-dependent pathway in embryo development have been demonstrated (Grunewald et al., 2013, 2012, 2008).

We show that *WRKY23* is a crucial factor required for auxin-mediated PIN polarity rearrangements, because gain-of-function and dominant-negative *WRKY23* lines as well as *wrky23* mutants were strongly affected in this process. These defects at the cellular level revealed by the exogenous auxin application appears to be developmentally relevant, because *wrky23* mutants are defective also in the PIN1 polarization process during vascular tissue formation of leaf venation and consequently in vascular tissue formation. Notably, increased PIN2 but not PIN1 lateralization in the *WRKY23* overexpression lines and PIN2 but

not PIN1 insensitivity to auxin treatment in *WRKY23-SRDX* lines indicate a partly diverging mechanism controlling PIN1 and PIN2 relocation. This is consistent with reported differences in PIN1 and PIN2 trafficking mechanisms (Kleine-Vehn et al., 2008a).

Our results also suggest that *WRKY23* is a critical player in auxin feedback on PIN polar localization. As a TF, *WRKY23* is probably not directly involved in regulating localization of transmembrane proteins, such as PIN proteins. Instead, this work opens avenues for future studies revealing the *WRKY23*-dependent transcriptional network. The identification of WRKY23 and its role in the auxin feedback on the PIN polarity along with other established PIN polarity regulators proves that our transcriptomics dataset can be mined in the future to identify additional regulators. Ultimately, it will provide insights into the molecular mechanism of this key aspect of the canalization-dependent regulation of plant development.

2.4 *Materials and Methods*

Plant material and growth conditions

All *Arabidopsis thaliana* (L.) Heynh. lines were in Columbia-0 (Col-0) background. The insertional mutants *wrky23-1* (SALK_003943) and *wrky23-2* (SALK_38289) were obtained from NASC and genotyped with the primers listed in Table S1.3. The *arf7 arf19* double mutant and the *HS::axr3-1* transgenic line have been described previously (Knox et al., 2003, p. 3; Okushima et al., 2005) as well as the *DR5::GUS* (Benková et al., 2003) and *PIN1-GFP* (Xu et al., 2006). For *RPS5A>>WRKY23* analyses, the F1 generation of a *RPS5A::GAL4VP16* (Aida et al., 2004) × *UAS::WRKY23* (Grunewald et al., 2012) cross was analysed and compared with the F1 generations from the *UAS::WRKY23* × WT Col-0 and *RPS5A::GAL4VP16* × WT Col-0 crosses. *WRKY23::GUS*, *35S::WRKY23-GR,35S::WRKY23*, *WRKY23::WRKY23-SRDX,* and *35S::WRKY23-SRDX* have been described previously (Grunewald et al., 2012, 2008). Seeds were surface-sterilized overnight by chlorine gas, sown on solid *Arabidopsis* medium (AM+; half-strength MS basal salts, 1% [w/v] sucrose, and 0.8% [w/v] phytoagar, pH 5.7), and stratified at 4°C for at least 2 days prior to transfer to a growth room with a 16-h light/8-h dark regime at 21°C. The seedlings were grown vertically for 4 or 6 days, depending on the assay.

Arabidopsis seedlings were treated with auxin or chemicals in liquid AM+ at 21°C in a growth room with the following concentrations and times: for NAA (Sigma-Aldrich) at 10 µM

for 4 h; dexamethasone (DEX; Sigma-Aldrich) 10 µM for 24 h. Mock treatments were done with equivalent amounts of DMSO.

Microarray analysis

Wild type Col-0 and *HS::axr3-1* seeds were grown vertically on AM+ plates for 5 days. We applied a 40 min heat shock at 37°C to the seedlings, followed by a 1.5-h recovery at normal growth temperature. Subsequently, the seedlings were transferred to liquid AM+ and treated with 10 µM NAA or DMSO for 4 h. Afterward, the lower third of 100-130 roots from each treatment was cut off, frozen in liquid N_2. RNA was extracted with the RNAeasy mini kit (Qiagen). Probes were prepared and hybridized to the *Arabidopsis* ATH1–121501 gene expression array (Affymetrix) as described (Benschop et al., 2007). Expression data for Col-0, *HS::axr3-1*, both NAA and mock treated, had been deposited under the ArrayExpress number E-MEXP-3283. Expression profiling data for *arf7 arf19* (ArrayExpress: E-GEOD-627) have been published previously (Okushima et al., 2005). Raw data were pairwise analysed with the logit-t algorithm (Lemon et al., 2003) with a cutoff of p=0.05.

RNA extraction, cDNA synthesis, and quantitative RT-PCR and analysis

RNA extraction, cDNA synthesis, and quantitative (q)RT-PCR were done as described (Tejos et al., 2014). Selected candidate gene transcript levels were quantified with qRT-PCR with specific primer pairs, designed with Primer-BLAST (http://www.ncbi.nlm.nih.gov/tools/primer-blast/). Transcript levels were normalized to *GAMMA-TUBULIN 2* (*TUB2*; *AT5G05620*), which was constitutively expressed and auxin independent across samples. All PCRs were run in three biological replicates per three technical repeats. The data were processed with a qRT-PCR analysis software (Frederik Coppens, Ghent University-VIB, Ghent, Belgium). Primers used in this study are listed in the Table S1.3.

Whole-mount *in situ* immunolocalization, microscopy, and quantitative PIN relocalization analysis

PIN immunolocalizations of primary roots and young leaves were carried out as described (Sauer and Friml, 2010). The antibodies were used as follows: anti-PIN1, 1:1000 (Paciorek et al., 2005) and anti-PIN2, 1:1000 (Abas et al., 2006). For primary roots, the secondary goat anti-

rabbit antibody coupled to Cy3 (Sigma-Aldrich) was diluted 1:600. For young leaves, the secondary goat anti-rabbit antibody coupled to Alexa Fluor 488 (Sigma-Aldrich) was diluted 1:600. For confocal microscopy, a Zeiss LSM 700 confocal microscope was used. The PIN relocalization was quantitative analysed as described (Sauer et al., 2006a), at least 3 experiments were performed for each observation. Note that the absolute levels of the PIN lateralization index may vary between individual experiments (depending on the anti-PIN signal strength), but the relative differences are always consistent.

Phenotypic analysis

All measurements were done with ImageJ (http://rsb.info.nih.gov/ij). For the root length analysis 6-day-old seedlings were scanned and root lengths were measured. For the lateral roots analysis 10-day-old seedlings were scanned and lateral root density was calculated from ratio number of LR/root length.

Histological analyses and microscopy

To detect β-glucuronidase (GUS) activity, seedlings were incubated in reaction buffer containing 0.1 M sodium phosphate buffer (pH 7), 1 mM ferricyanide, 1 mM ferrocyanide, 0.1% Triton X-100, and 1 mg/ml X-Gluc for 2 h in the dark at 37 °C. Afterward, chlorophyll was removed by destaining in 70% ethanol and seedlings were cleared.

Tissues (seedlings and cotyledons) were cleared in a solution containing 4% HCl and 20% methanol for 15 min at 65°C, followed by a 15-min incubation in 7% NaOH and 70% ethanol at room temperature. Next, seedlings were rehydrated by successive incubations in 70%, 50%, 25%, and 10% ethanol for 5 min, followed by incubation in a solution containing 25% glycerol and 5% ethanol. Finally, seedlings were mounted in 50% glycerol and monitored by differential interference contrast microscopy DIC (Olympus BX53) or a stereomicroscope (Olympus SZX16).

2.5 *Acknowledgements*

We thank D. Weigel for support with microarray analysis; F. Coppens for assistance with the qRT-PCR analysis and M. De Cock and M. Abas for help in preparing the manuscript. We gratefully acknowledge the Nottingham Arabidopsis Stock Center (NASC) for providing

mutant lines. This work was supported by the European Research Council (project ERC-2011-StG 20101109-PSDP).

2.6 *Author Contributions*

Jakub Hajný:

- Expression analysis of *pWRKY23::GUS* (Fig 2.2F and G; Fig S2.1F-J)
- Isolation of *wrky23-1* /*-2* mutant lines - qRT-PCR (Fig 2.4A and B)
- Fenotypic analysis of venation pattern in cotyledons (Fig 2.4C and E)
- Fenotypic analysis of root length and lateral root density (Fig S2.4A and B)
- Immunolocalization of PIN1 in root meristem (Fig 2.3 C and D; Fig S2.2A-D)
- Immunolocalization of PIN1 in young developing leaves (Fig 2.4F; S2.4C and D)

2.7 *Supporting information*

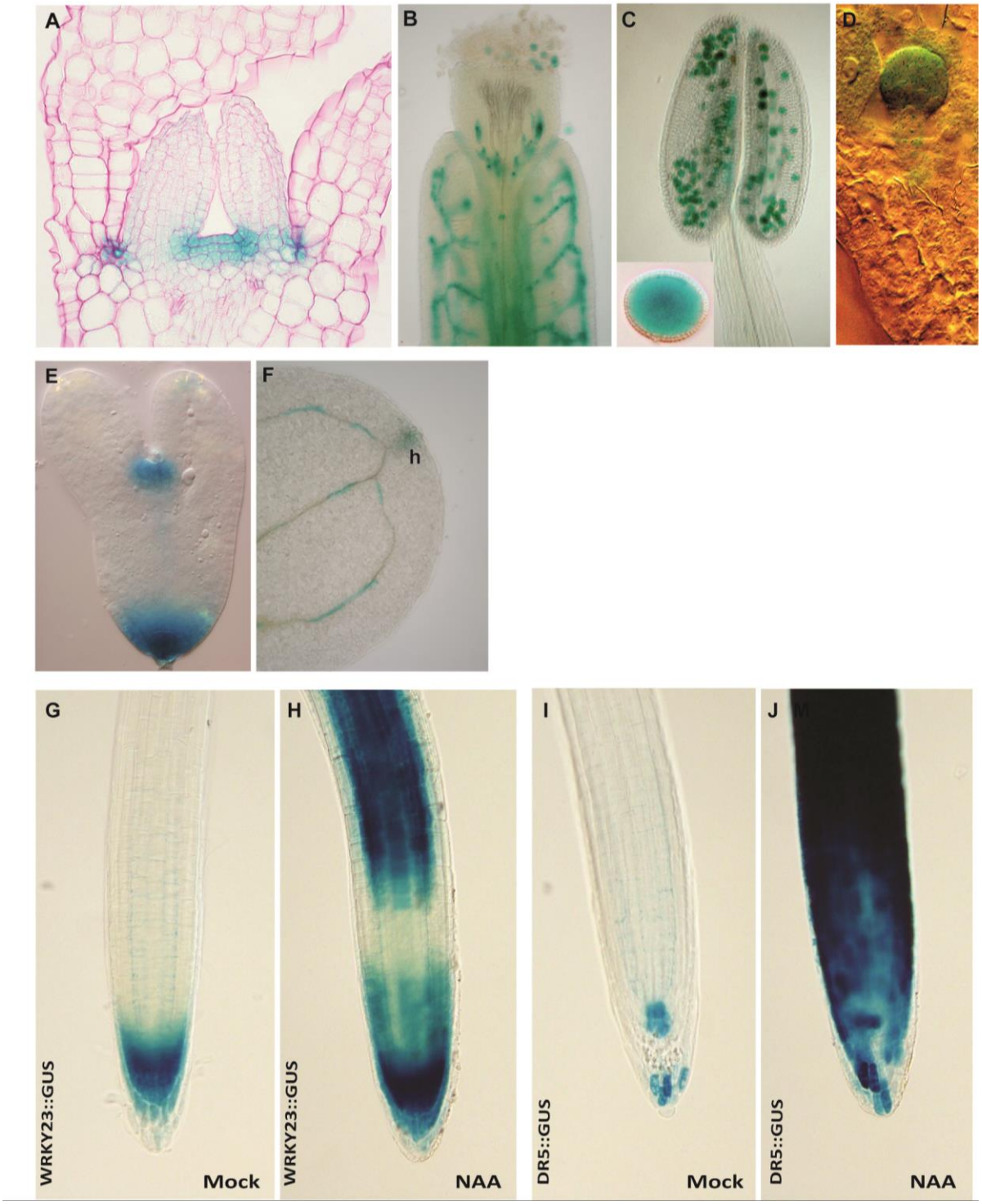

***Figure S2. 1* Pattern of GUS expression in WRKY23::GUS plants.**

(A) SAM section showing specific *WRKY23* expression in the L1, L2, and L3 layers. (B) *WRKY23* expression in the pistil vasculature. (C) Another showing *WRKY23::GUS* activity in pollen (inset). (D) GUS staining of *WRKY23::GUS* embryos showing promoter activity in all apical cells of an early globular embryo. (E) GUS activity in the SAM and RAM of an early torpedo stage embryo. (F) Cotyledon showing GUS staining at the hydathode (h) and in the vasculature. (G-J) *WRKY23* promoter activation by auxin treatment. G and H: Expression pattern of *WRKY23::GUS* in the root changes following 6 h of auxin treatment. GUS staining becomes generally stronger and additionally expressed in the meristematic and transition zones of the root tip). (I) and (J): *DR5::GUS* activity under the same experimental conditions as in (G-H).

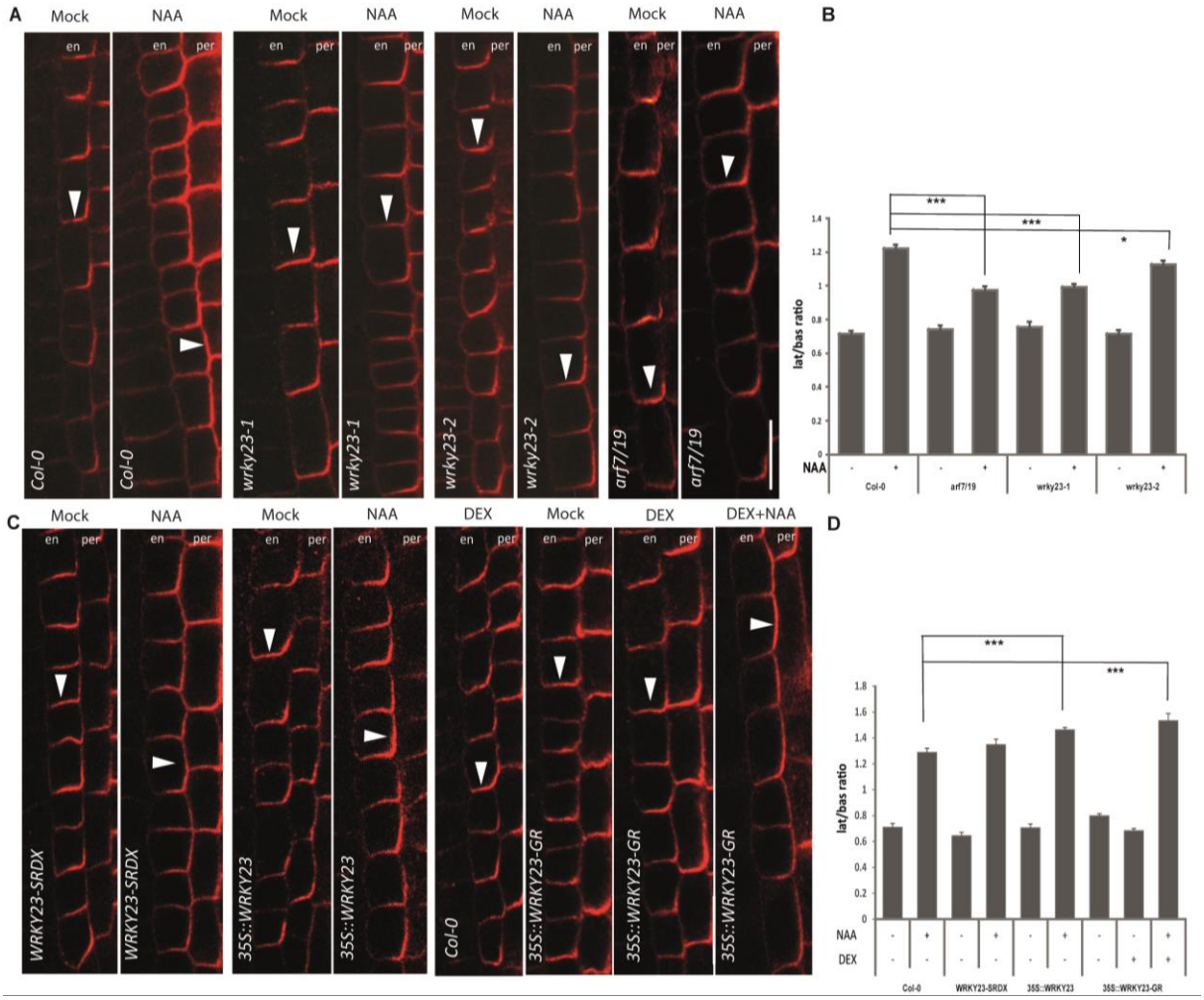

Figure S2. 2 Polarity of PIN1 in WRKY23 transgenic lines.

(A and B) Immunolocalization of PIN1 in *wrky23* mutants and *arf7/19* lines revealing reduced lateralization of PIN1. Arrowheads highlight PIN1 polarity. en, endodermis; per, pericycle. Graph shows mean ratio of lateral-to-basal signal intensity of PIN1 in endodermal cells. Error bars indicate standard error. A One-Way ANOVA test compared marked sets of data (*** p<0.0001; n>60 cells corresponding to a minimum of 10 roots per treatment and per experiment imaged under comparable

conditions). Experiments were carried out at least 3 times; one representative experiment is shown. (C) Immunolocalization of PIN1 in dominant-negative *WRKY23-SRDX* plants driven by native promoter and overexpression lines - *35S::WRKY23*, *35S::WRKY23-GR*. WT Col-0 was used as a control. Arrowheads highlight PIN1 polarity in endodermal cells. en, endodermis; per, pericycle. Bar = 10 µm. (D) Quantitative evaluation of (C) showing mean ratio of lateral-to-basal signal intensity of PIN1 in endodermis cells. Error bars indicate standard error. A One-Way ANOVA test compared marked sets of data (*** p<0.0001; n>60 cells corresponding to a minimum of 10 roots per treatment and per experiment were imaged under comparable conditions). Experiments were carried out at least 3 times; one representative experiment is shown.

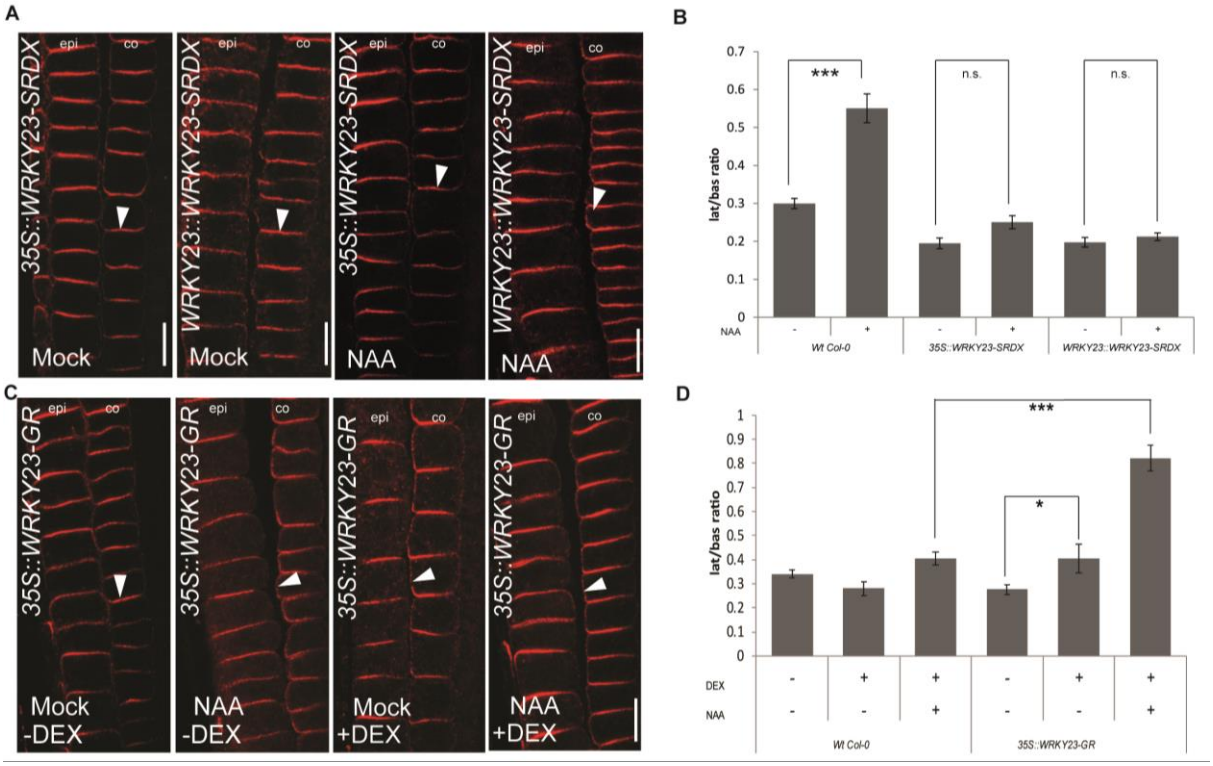

Figure S2. 3 Polarity of PIN2 in WRKY23 transgenic lines.

(A) Immunolocalization of PIN2 in dominant-negative *WRKY23-SRDX* plants driven by native and constitutive promoter. WT Col-0 was used as a control (see Fig. 1.3 A and quantification in S 1.3 B). Arrowheads highlight PIN2 polarity in cortex cells. epi, epidermis; co, cortex. Bar = 10 µm. (B) Quantitative evaluation of (A) showing mean ratio of lateral-to-basal signal intensity of PIN2 in cortex cells. Error bars indicate standard error. A One-Way ANOVA test compared marked sets of data (*** p<0.0001; n>70 cells corresponding to a minimum of 10 roots per treatment and per experiment were imaged under comparable conditions). Experiments were carried out at least 3 times; one representative experiment is shown.

(C) Immunolocalization of PIN2 in DEX-inducible *35S::WRKY23-GR* plants treated with DEX and/or NAA. WT Col-0 was used as control (see quantification in S1.3 D). Arrowheads highlight PIN2 polarity in cortex cells. epi, epidermis; co, cortex. Bar = 10 µm. (D) Graph showing mean ratio of lateral-to-basal signal intensity of PIN2 in cortex cells. Induced *35S::WRKY23-GR* roots show slightly more PIN2 lateralization without auxin that is apparently more effective to increase PIN2 lateralization in this line

than the controls. Error bars indicate standard error. A One-Way ANOVA test compared marked sets of data (*** p<0.0001, * p<0.05; n>35 cells corresponding to a minimum of 10 roots per treatment and per experiment were imaged under comparable conditions). Experiments were carried out at least 3 times; one representative experiment is shown.

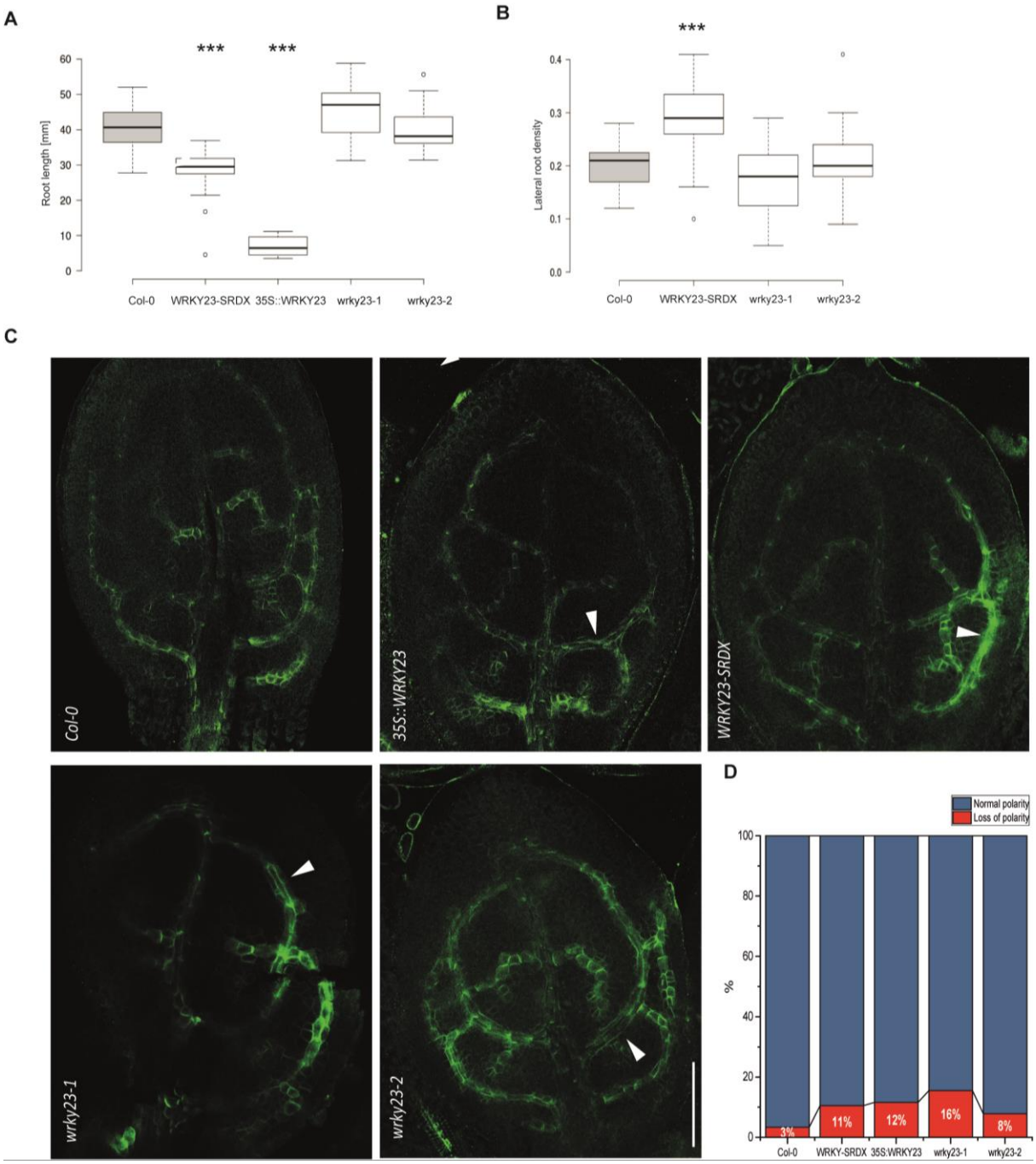

Figure S2. 4 **Phenotype defects in WRKY23 transgenic lines and wrky23 mutants.**

(A) Primary root length of 6-day-old transgenic lines and *wrky23* mutants. Central lines show median values; box limits indicate the 25th and 75th percentiles as determined by the R software; whiskers extend 1.5 times the interquartile range from the 25th and 75th percentiles. Significance was

determined by two-tailed equal T-test between Col-0 and other lines; (*** p<0.001); n>60 roots per line. (B) Lateral root density in plants with impaired WRKY23 function. WRKY-SRDX denotes *WRKY23::WRKY23-SRDX*. Box plot properties and statistical analysis are as in (A). n>80 roots per line. (C) Immunolocalization analysis of PIN1 in developing true leaves. In the WT, PIN1 shows typical polarization towards the leaf base, whereas in WRKY23 transgenic lines and *wrky23* mutants this polarization of some branches is abolished. Arrowheads highlights defective PIN1 polarization in vasculature. At least 50 leaves per genotype were analysed. (D) Quantitative evaluation of (C) showing percentage of abolished PIN1 polarity. At least 50 branches per genotype were analysed.

Primer	Sequence	Reference
PID_FOR	5 -TGCCGACTCTTTACGCTGAG-3	This study
PID_REV	5 -CTTCGGCGGCATAAAATCTGG-3	This study
WRKY23_FOR	5 -AGTCTCGGTAATGGTTGCTTTGG-3	Grunewald et al., 2013
WRKY23_REV	5 -TGTTGCTGCTGTTGGTGATGG-3	Grunewald et al., 2013
SALK_003943_FOR	5 -CGGTGGGTTTATCAACAAATG-3	This study
SALK_003943_REV	5 -TGTTGCTGCTGTTGGTGATGG-3	This study
SALK_38289_FOR	5 -CGATCACATTTTTCTTTTCGC-3	This study
SALK_38289_REV	5 -CGGTGGGTTTATCAACAAATG-3	This study
TUB-2_FOR	5 -ACTCGTTGGGAGGAGGAACT-3	Grunewald et al., 2013
TUB-2_REV	5 -ACACCAGACATAGTAGCAGAAATCAAG-3	Grunewald et al., 2013
IAA14_FOR	5 -CCTTCTAAGCCTCCTGCTAAAGC-3	Shkolnik-Inbar and Bar-Zvi, 2010
IAA14_REV	5 -CCGCTCTTCTGATTAGCCATAAC-3	Tejos et al., 2014
PIP5K1_FOR	5 -GGAACATTGTGAATCGAGGACTG-3	Tejos et al., 2014
PIP5K1_REV	5 -CCGTCTCGTCTCTCTACTTCTT-3	Tejos et al., 2014
PIP5K2_FOR	5 -ATGATGCGTGAACCGCTTG-3	Tejos et al., 2014
PIP5K2_REV	5 -TTCCATGCTGCAGGTTGAGCA-3	Tejos et al., 2014

Table S2. 1 List of PCR primers used.

2.8 *References*

1. M. Adamowski, J. Friml, PIN-Dependent Auxin Transport: Action, Regulation, and Evolution. *The Plant Cell Online*. **27**, 20–32 (2015).

2. J. Petrášek, J. Mravec, R. Bouchard, J. J. Blakeslee, M. Abas, D. Seifertová, J. Wiśniewska, Z. Tadele, M. Kubeš, M. Čovanová, P. Dhonukshe, P. Skůpa, E. Benková, L. Perry, P. Křeček, O. R. Lee, G. R. Fink, M. Geisler, A. S. Murphy, C. Luschnig, E. Zažímalová, J. Friml, PIN Proteins Perform a Rate-Limiting Function in Cellular Auxin Efflux. *Science*. **312**, 914–918 (2006).

3. J. Wiśniewska, J. Xu, D. Seifertová, P. B. Brewer, K. Růžička, I. Blilou, D. Rouquié, E. Benková, B. Scheres, J. Friml, Polar PIN Localization Directs Auxin Flow in Plants. *Science*. **312**, 883–883 (2006).

4. T. Bennett, G. Hines, O. Leyser, Canalization: what the flux? *Trends in Genetics*. **30**, 41–48 (2014).

5. T. Sachs, Cellular interactions in tissue and organ development. *Symp. Soc. Exp. Biol.* **40**, 181–210 (1986).

6. T. Sachs, The induction of transport channels by auxin. *Planta*. **127**, 201–206 (1975).

7. T. Berleth, T. Sachs, Plant morphogenesis: long-distance coordination and local patterning. *Current Opinion in Plant Biology*. **4**, 57–62 (2001).

8. E. Mazur, E. Benková, J. Friml, Vascular cambium regeneration and vessel formation in wounded inflorescence stems of Arabidopsis. *Sci Rep*. **6** (2016), doi:10.1038/srep33754.

9. M. Sauer, J. Balla, C. Luschnig, J. Wiśniewska, V. Reinöhl, J. Friml, E. Benková, Canalization of auxin flow by Aux/IAA-ARF-dependent feedback regulation of PIN polarity. *Genes Dev.* **20**, 2902–2911 (2006).

10. J. Balla, P. Kalousek, V. Reinöhl, J. Friml, S. Procházka, Competitive canalization of PIN-dependent auxin flow from axillary buds controls pea bud outgrowth. *The Plant Journal*. **65**, 571–577 (2011).

11. T. Bennett, G. Hines, M. van Rongen, T. Waldie, M. G. Sawchuk, E. Scarpella, K. Ljung, O. Leyser, Connective Auxin Transport in the Shoot Facilitates Communication between Shoot Apices. *PLOS Biology*. **14**, e1002446 (2016).

12. J. Booker, S. Chatfield, O. Leyser, Auxin Acts in Xylem-Associated or Medullary Cells to Mediate Apical Dominance. *The Plant Cell*. **15**, 495–507 (2003).

13. T. Paciorek, E. Zazímalová, N. Ruthardt, J. Petrásek, Y.-D. Stierhof, J. Kleine-Vehn, D. A. Morris, N. Emans, G. Jürgens, N. Geldner, J. Friml, Auxin inhibits endocytosis and promotes its own efflux from cells. *Nature*. **435**, 1251–1256 (2005).

14. S. Robert, J. Kleine-Vehn, E. Barbez, M. Sauer, T. Paciorek, P. Baster, S. Vanneste, J. Zhang, S. Simon, M. Čovanová, K. Hayashi, P. Dhonukshe, Z. Yang, S. Y. Bednarek, A. M. Jones, C. Luschnig, F. Aniento, E. Zažímalová, J. Friml, ABP1 Mediates Auxin Inhibition of Clathrin-Dependent Endocytosis in Arabidopsis. *Cell*. **143**, 111–121 (2010).

15. K. Wabnik, J. Kleine-Vehn, J. Balla, M. Sauer, S. Naramoto, V. Reinöhl, R. M. H. Merks, W. Govaerts, J. Friml, Emergence of tissue polarization from synergy of intracellular and extracellular auxin signaling. *Molecular Systems Biology*. **6**, 447 (2010).

16. H. S. Robert, P. Grones, A. N. Stepanova, L. M. Robles, A. S. Lokerse, J. M. Alonso, D. Weijers, J. Friml, Local Auxin Sources Orient the Apical-Basal Axis in Arabidopsis Embryos. *Current Biology*. **23**, 2506–2512 (2013).

17. K. Wabnik, H. S. Robert, R. S. Smith, J. Friml, Modeling framework for the establishment of the apical-basal embryonic axis in plants. *Curr. Biol.* **23**, 2513–2518 (2013).

18. E. Benková, M. Michniewicz, M. Sauer, T. Teichmann, D. Seifertová, G. Jürgens, J. Friml, Local, Efflux-Dependent Auxin Gradients as a Common Module for Plant Organ Formation. *Cell*. **115**, 591–602 (2003).

19. H. Rakusová, M. Abbas, H. Han, S. Song, H. S. Robert, J. Friml, Termination of Shoot Gravitropic Responses by Auxin Feedback on PIN3 Polarity. *Current Biology*. **26**, 3026–3032 (2016).

20. J. Friml, E. Benková, I. Blilou, J. Wisniewska, T. Hamann, K. Ljung, S. Woody, G. Sandberg, B. Scheres, G. Jürgens, K. Palme, AtPIN4 Mediates Sink-Driven Auxin Gradients and Root Patterning in Arabidopsis. *Cell*. **108**, 661–673 (2002).

21. J. Kleine-Vehn, J. Leitner, M. Zwiewka, M. Sauer, L. Abas, C. Luschnig, J. Friml, Differential degradation of PIN2 auxin efflux carrier by retromer-dependent vacuolar targeting. *PNAS*. **105**, 17812–17817 (2008).

22. A. Müller, C. Guan, L. Gälweiler, P. Tänzler, P. Huijser, A. Marchant, G. Parry, M. Bennett, E. Wisman, K. Palme, AtPIN2 defines a locus of Arabidopsis for root gravitropism control. *EMBO J*. **17**, 6903–6911 (1998).

23. E. J. Chapman, M. Estelle, Mechanism of Auxin-Regulated Gene Expression in Plants. *Annu. Rev. Genet.* **43**, 265–285 (2009).

24. M. Salehin, R. Bagchi, M. Estelle, SCF $^{TIR1/AFB}$ -Based Auxin Perception: Mechanism and Role in Plant Growth and Development. *The Plant Cell Online*. **27**, 9–19 (2015).

25. K. Knox, C. S. Grierson, O. Leyser, AXR3 and SHY2 interact to regulate root hair development. *Development*. **130**, 5769–5777 (2003).

26. J. C. Wilmoth, S. Wang, S. B. Tiwari, A. D. Joshi, G. Hagen, T. J. Guilfoyle, J. M. Alonso, J. R. Ecker, J. W. Reed, NPH4/ARF7 and ARF19 promote leaf expansion and auxin-induced lateral root formation. *The Plant Journal*. **43**, 118–130 (2005).

27. R. Tejos, C. Rodriguez-Furlán, M. Adamowski, M. Sauer, L. Norambuena, J. Friml, PATELLINS are regulators of auxin-mediated PIN1 relocation and plant development in Arabidopsis thaliana. *J Cell Sci*. **131** (2018), doi:10.1242/jcs.204198.

28. Y. Okushima, P. J. Overvoorde, K. Arima, J. M. Alonso, A. Chan, C. Chang, J. R. Ecker, B. Hughes, A. Lui, D. Nguyen, C. Onodera, H. Quach, A. Smith, G. Yu, A. Theologis,

Functional Genomic Analysis of the *AUXIN RESPONSE FACTOR* Gene Family Members in *Arabidopsis thaliana* : Unique and Overlapping Functions of *ARF7* and *ARF19*. *The Plant Cell*. **17**, 444–463 (2005).

29. M. Michniewicz, M. K. Zago, L. Abas, D. Weijers, A. Schweighofer, I. Meskiene, M. G. Heisler, C. Ohno, J. Zhang, F. Huang, R. Schwab, D. Weigel, E. M. Meyerowitz, C. Luschnig, R. Offringa, J. Friml, Antagonistic Regulation of PIN Phosphorylation by PP2A and PINOID Directs Auxin Flux. *Cell*. **130**, 1044–1056 (2007).

30. J. Friml, X. Yang, M. Michniewicz, D. Weijers, A. Quint, O. Tietz, R. Benjamins, P. B. F. Ouwerkerk, K. Ljung, G. Sandberg, P. J. J. Hooykaas, K. Palme, R. Offringa, A PINOID-Dependent Binary Switch in Apical-Basal PIN Polar Targeting Directs Auxin Efflux. *Science*. **306**, 862–865 (2004).

31. J. Zhang, T. Nodzyński, A. Pěnčík, J. Rolčík, J. Friml, PIN phosphorylation is sufficient to mediate PIN polarity and direct auxin transport. *Proc Natl Acad Sci U S A*. **107**, 918–922 (2010).

32. Y. Mei, W.-J. Jia, Y.-J. Chu, H.-W. Xue, Arabidopsis phosphatidylinositol monophosphate 5-kinase 2 is involved in root gravitropism through regulation of polar auxin transport by affecting the cycling of PIN proteins. *Cell Research*. **22**, 581–597 (2012).

33. J.-M. Ugalde, C. Rodriguez-Furlán, R. D. Rycke, L. Norambuena, J. Friml, G. León, R. Tejos, Phosphatidylinositol 4-phosphate 5-kinases 1 and 2 are involved in the regulation of vacuole morphology during Arabidopsis thaliana pollen development. *Plant Science*. **250**, 10–19 (2016).

34. T. Ischebeck, S. Werner, P. Krishnamoorthy, J. Lerche, M. Meijón, I. Stenzel, C. Löfke, T. Wiessner, Y. J. Im, I. Y. Perera, T. Iven, I. Feussner, W. Busch, W. F. Boss, T. Teichmann, B. Hause, S. Persson, I. Heilmann, Phosphatidylinositol 4,5-bisphosphate influences PIN polarization by controlling clathrin-mediated membrane trafficking in Arabidopsis. *Plant Cell*. **25**, 4894–4911 (2013).

35. R. Tejos, M. Sauer, S. Vanneste, M. Palacios-Gomez, H. Li, M. Heilmann, R. van Wijk, J. E. M. Vermeer, I. Heilmann, T. Munnik, J. Friml, Bipolar Plasma Membrane Distribution of Phosphoinositides and Their Requirement for Auxin-Mediated Cell Polarity and Patterning in Arabidopsis. *The Plant Cell*. **26**, 2114–2128 (2014).

36. J. Agusti, R. Lichtenberger, M. Schwarz, L. Nehlin, T. Greb, Characterization of transcriptome remodeling during cambium formation identifies MOL1 and RUL1 as opposing regulators of secondary growth. *PLoS Genet.* **7**, e1001312 (2011).

37. W. Hu, B. Feng, H. Ma, Ectopic expression of the Arabidopsis MINI ZINC FINGER1 and MIF3 genes induces shoot meristems on leaf margins. *Plant Mol. Biol.* **76**, 57–68 (2011).

38. T. Eulgem, I. E. Somssich, Networks of WRKY transcription factors in defense signaling. *Current Opinion in Plant Biology*. **10**, 366–371 (2007).

39. T. Eulgem, P. J. Rushton, S. Robatzek, I. E. Somssich, The WRKY superfamily of plant transcription factors. *Trends in Plant Science*. **5**, 199–206 (2000).

40. B. Ülker, I. E. Somssich, WRKY transcription factors: from DNA binding towards biological function. *Current Opinion in Plant Biology*. **7**, 491–498 (2004).

41. I. Ciolkowski, D. Wanke, R. P. Birkenbihl, I. E. Somssich, Studies on DNA-binding selectivity of WRKY transcription factors lend structural clues into WRKY-domain function. *Plant Mol Biol*. **68**, 81–92 (2008).

42. W. Grunewald, I. De Smet, B. De Rybel, H. S. Robert, B. van de Cotte, V. Willemsen, G. Gheysen, D. Weijers, J. Friml, T. Beeckman, Tightly controlled *WRKY23* expression mediates Arabidopsis embryo development. *EMBO reports*. **14**, 1136–1142 (2013).

43. W. Grunewald, I. De Smet, D. R. Lewis, C. Löfke, L. Jansen, G. Goeminne, R. V. Bossche, M. Karimi, B. De Rybel, B. Vanholme, Transcription factor WRKY23 assists auxin distribution patterns during Arabidopsis root development through local control on flavonol biosynthesis. *Proceedings of the National Academy of Sciences*. **109**, 1554–1559 (2012).

44. W. Grunewald, M. Karimi, K. Wieczorek, E. Van de Cappelle, E. Wischnitzki, F. Grundler, D. Inze, T. Beeckman, G. Gheysen, A Role for AtWRKY23 in Feeding Site Establishment of Plant-Parasitic Nematodes. *PLANT PHYSIOLOGY*. **148**, 358–368 (2008).

45. D. R. Boer, A. Freire-Rios, W. A. M. van den Berg, T. Saaki, I. W. Manfield, S. Kepinski, I. López-Vidrieo, J. M. Franco-Zorrilla, S. C. de Vries, R. Solano, D. Weijers, M. Coll, Structural Basis for DNA Binding Specificity by the Auxin-Dependent ARF Transcription Factors. *Cell*. **156**, 577–589 (2014).

46. T. Ulmasov, G. Hagen, T. J. Guilfoyle, ARF1, a Transcription Factor That Binds to Auxin Response Elements. *Science*. **276**, 1865–1868 (1997).

47. A. Yilmaz, M. K. Mejia-Guerra, K. Kurz, X. Liang, L. Welch, E. Grotewold, AGRIS: the Arabidopsis Gene Regulatory Information Server, an update. *Nucleic Acids Res.* **39**, D1118-1122 (2011).

48. J. Friml, A. Vieten, M. Sauer, D. Weijers, H. Schwarz, T. Hamann, R. Offringa, G. Jürgens, Efflux-dependent auxin gradients establish the apical–basal axis of Arabidopsis. *Nature*. **426**, 147–153 (2003).

49. E. Scarpella, D. Marcos, J. Friml, T. Berleth, Control of leaf vascular patterning by polar auxin transport. *Genes Dev.* **20**, 1015–1027 (2006).

50. J. Mattsson, W. Ckurshumova, T. Berleth, Auxin Signaling in Arabidopsis Leaf Vascular Development. *Plant Physiology*. **131**, 1327–1339 (2003).

51. M. Aida, D. Beis, R. Heidstra, V. Willemsen, I. Blilou, C. Galinha, L. Nussaume, Y.-S. Noh, R. Amasino, B. Scheres, The PLETHORA Genes Mediate Patterning of the Arabidopsis Root Stem Cell Niche. *Cell*. **119**, 109–120 (2004).

52. C. Schluttenhofer, L. Yuan, Regulation of Specialized Metabolism by WRKY Transcription Factors. *Plant Physiology*. **167**, 295–306 (2015).

53. K. Hiratsu, K. Matsui, T. Koyama, M. Ohme-Takagi, Dominant repression of target genes by chimeric repressors that include the EAR motif, a repression domain, in Arabidopsis. *The Plant Journal*. **34**, 733–739 (2003).

54. P. Baster, S. Robert, J. Kleine-Vehn, S. Vanneste, U. Kania, W. Grunewald, B. De Rybel, T. Beeckman, J. Friml, SCFTIR1/AFB-auxin signalling regulates PIN vacuolar trafficking and auxin fluxes during root gravitropism. *The EMBO Journal*. **32**, 260–274 (2013).

55. C. Luschnig, R. A. Gaxiola, P. Grisafi, G. R. Fink, EIR1, a root-specific protein involved in auxin transport, is required for gravitropism in Arabidopsis thaliana. *Genes Dev*. **12**, 2175–2187 (1998).

56. M. G. Sawchuk, E. Scarpella, Polarity, Continuity, and Alignment in Plant Vascular Strands. *Journal of Integrative Plant Biology*. **55**, 824–834 (2013).

57. M. Bakshi, R. Oelmüller, WRKY transcription factors. *Plant Signaling & Behavior*. **9**, e27700 (2014).

58. Y. Guan, X. Meng, R. Khanna, E. LaMontagne, Y. Liu, S. Zhang, Phosphorylation of a WRKY Transcription Factor by MAPKs Is Required for Pollen Development and Function in Arabidopsis. *PLOS Genetics*. **10**, e1004384 (2014).

59. M. Cieslak, A. Runions, P. Prusinkiewicz, Auxin-driven patterning with unidirectional fluxes. *Journal of Experimental Botany*. **66**, 5083–5102 (2015).

60. R. S. Smith, S. Guyomarc'h, T. Mandel, D. Reinhardt, C. Kuhlemeier, P. Prusinkiewicz, A plausible model of phyllotaxis. *PNAS*. **103**, 1301–1306 (2006).

61. K. Wabnik, J. Kleine-Vehn, W. Govaerts, J. Friml, Prototype cell-to-cell auxin transport mechanism by intracellular auxin compartmentalization. *Trends in Plant Science*. **16**, 468–475 (2011).

62. I. Stenzel, T. Ischebeck, S. König, A. Hołubowska, M. Sporysz, B. Hause, I. Heilmann, The Type B Phosphatidylinositol-4-Phosphate 5-Kinase 3 Is Essential for Root Hair Formation in Arabidopsis thaliana. *Plant Cell*. **20**, 124–141 (2008).

63. J. Kleine-Vehn, Ł. Łangowski, J. Wiśniewska, P. Dhonukshe, P. B. Brewer, J. Friml, Cellular and Molecular Requirements for Polar PIN Targeting and Transcytosis in Plants. *Molecular Plant*. **1**, 1056–1066 (2008).

64. J. Xu, H. Hofhuis, R. Heidstra, M. Sauer, J. Friml, B. Scheres, A Molecular Framework for Plant Regeneration. *Science*. **311**, 385–388 (2006).

65. J. J. Benschop, S. Mohammed, M. O'Flaherty, A. J. R. Heck, M. Slijper, F. L. H. Menke, Quantitative Phosphoproteomics of Early Elicitor Signaling in Arabidopsis. *Mol Cell Proteomics*. **6**, 1198–1214 (2007).

66. W. J. Lemon, S. Liyanarachchi, M. You, A high performance test of differential gene expression for oligonucleotide arrays. *Genome Biology*. **4**, R67 (2003).

67. M. Sauer, J. Friml, in *Plant Developmental Biology: Methods and Protocols*, L. Hennig, C. Köhler, Eds. (Humana Press, Totowa, NJ, 2010; https://doi.org/10.1007/978-1-60761-765-5_17), *Methods in Molecular Biology*, pp. 253–263.

68. L. Abas, R. Benjamins, N. Malenica, T. Paciorek, J. Wišniewska, J. C. Moulinier–Anzola, T. Sieberer, J. Friml, C. Luschnig, Intracellular trafficking and proteolysis of the Arabidopsis auxin-efflux facilitator PIN2 are involved in root gravitropism. *Nature Cell Biology*. **8**, 249–256 (2006).

69. M. Sauer, J. Balla, C. Luschnig, J. Wiśniewska, V. Reinöhl, J. Friml, E. Benková, Canalization of auxin flow by Aux/IAA-ARF-dependent feedback regulation of PIN polarity. *Genes Dev.* **20**, 2902–2911 (2006).

3 CAMEL-CANAR receptor kinase module targets PIN-dependent transport during auxin canalization

Adapted and modified from

J. Hajný, T. Prát, N. Rydza, L. Rodriguez, S. Tan, I. Verstraeten, D. Domjan, E. Mazur, E. Smakowska-Luzan, W. Smet, E. Mor, J. Nolf, B. Yang, W. Grunewald, G. Molnár, Y. Belkhadir, B.D. Rybel, J. Friml, Receptor kinase module targets PIN-dependent auxin transport during canalization. *Science.* **370**, 550-557 (2020).

3.1 *Introduction*

Plant development flexibly adapts the plant's architecture and physiology to an ever-changing environment. Much of this adaptive development is characterized by self-organization of patterning processes, such as the integration of new organs with the pre-existing vascular network, rise of complex leaf venation patterns and flexible vasculature regeneration around a wound.

Formation of organized vasculature from originally uniform tissues involves coordinated polarization of individual cells. The canalization hypothesis proposes that the plant hormone auxin acts as a polarizing cue by means of its directional intercellular flow and feed-back between auxin signaling and transport (Berleth and Sachs, 2001). Auxin transport is mediated by polarly localized PIN auxin transport proteins (Adamowski and Friml, 2015) and thus auxin signaling coordinating the repolarization of PINs in individual cells can generate auxin transport channels demarcating the future position of forming vasculature. The emergence of PIN-expressing auxin channels preceding vasculature formation has been observed in different plant species connecting newly formed organs (Benková et al., 2003) or lateral shoot branches (Balla et al., 2011) with pre-existing vasculature network, also during leaf venation (Scarpella et al., 2006), in embryogenesis (Robert et al., 2013) and during regeneration after wounding (Mazur et al., 2016; Sauer et al., 2006). Similar PIN-expressing auxin channels arise from an artificial local auxin source revealing that auxin is the necessary and sufficient signal for channel formation (Balla et al., 2011; Sauer et al., 2006).

It remains enigmatic how such auxin feed-back on subcellular PIN localization leading to coordinated tissue polarization can integrate directional and positional cues. Auxin

transcriptionally regulates *PIN* expression (Vieten et al., 2005) and inhibits PIN endocytic recycling (Paciorek et al., 2005), which may explain auxin-mediated PIN repolarization by *de novo* secretion and by a differential endocytosis rate of PIN proteins from the plasma membrane leading to the establishment of polarity (Glanc et al., 2018). A mechanistic model of auxin canalization (Wabnik et al., 2010) predicts that PIN polarization away from the auxin source can arise from a combination of intracellular, transcriptional auxin signaling regulating PIN abundance and cell surface auxin signaling regulating the PIN internalization rate (Paciorek et al., 2005) and thereby stabilizing PINs at the given cell side. This mechanism would sense an auxin gradient throughout the tissue and translate it into tissue polarization. Additionally, a so far elusive short-range signaling mechanism would mediate coordination between individual cells during this process.

Here, we identified the CAMEL-CANAR cell surface receptor complex, acting downstream of the canonical TIR1/AFB-WRKY23 auxin signaling, which is required for the auxin effect on PIN trafficking and polarity in individual cells as well as for coordinated tissue polarization during vascular formation and regeneration.

3.2 *Results*

3.2.1 Identification of potential auxin canalization regulators downstream of WRKY23

To understand the molecular regulation of PIN polarity, we designed a microarray experiment to find genes downstream of the transcription factor that regulates auxin-mediated PIN repolarization - *WRKY DNA-BINDING Protein 23* (*WRKY23)* (Prát et al., 2018) (Fig S3.1A) by using lines where *WRKY23* is either targeted to the nucleus in an inducible way (*35S::WRKY23-GR*) or engineered into a transcriptional repressor (*35S::WRKY23-SRDX*) (Grunewald et al., 2012, 2008). First, by comparing *35S::WRKY23-GR* seedling roots with and without induction by dexamethasone (Dex), we obtained a set of 110 genes, which were up-regulated in the dexamethasone-treated seedlings, as potential WRKY23 targets. Next, we identified 950 genes, which were auxin-inducible in Col-0 wild type (Wt), but lost this auxin-responsiveness in dominant-negative *35S::WRKY23-SRDX* roots. The overlap between the two datasets

yielded a list of 61 genes (Fig S3.1B). This list was compared with previously published microarray data on auxin-treated seedlings of *solitary root1* (*slr-1*) mutant (Vanneste, 2005) because *WRKY23* acts downstream of the *SLR/IAA14* transcriptional repressor (Grunewald et al., 2008). The overlap yielded 14 genes, which were up-regulated in Col-0 but not in *slr-1* seedlings after auxin treatment and were at the same time auxin-inducible, potential targets of WRKY23 (Fig 3.1A; Tab 3.1A).

We used previously described or isolated T-DNA insertional loss-of-function mutants (see Materials and Methods) of candidate genes and analysed their phenotypes to identify regulators of PIN polarity and canalization processes. As a proxy for a role in canalization, we used the formation of vasculature during cotyledon development as this is a classical process requiring auxin feedback on PIN-dependent auxin transport (Scarpella et al., 2006b). Typically, Wt cotyledons form a conserved pattern of four loops and loss-of-function mutants in most of the candidate genes had no or only minor defects with low frequency deviating from this pattern with exception of mutants in AT5G40780 and AT1G05700, in which we observed frequent, strong venation defects: (Fig S3.1D; AT5G40780/*lht1-1*: 41% and AT1G05700/*camel-1*: 45% of the cotyledons had any type of abnormality deviating from the typical four loops pattern).

Thus, we identified AT5G40780 and AT1G05700 required for canalization-based processes such as leaf venation and they probably would act as potential targets of WRKY23 downstream of auxin signaling.

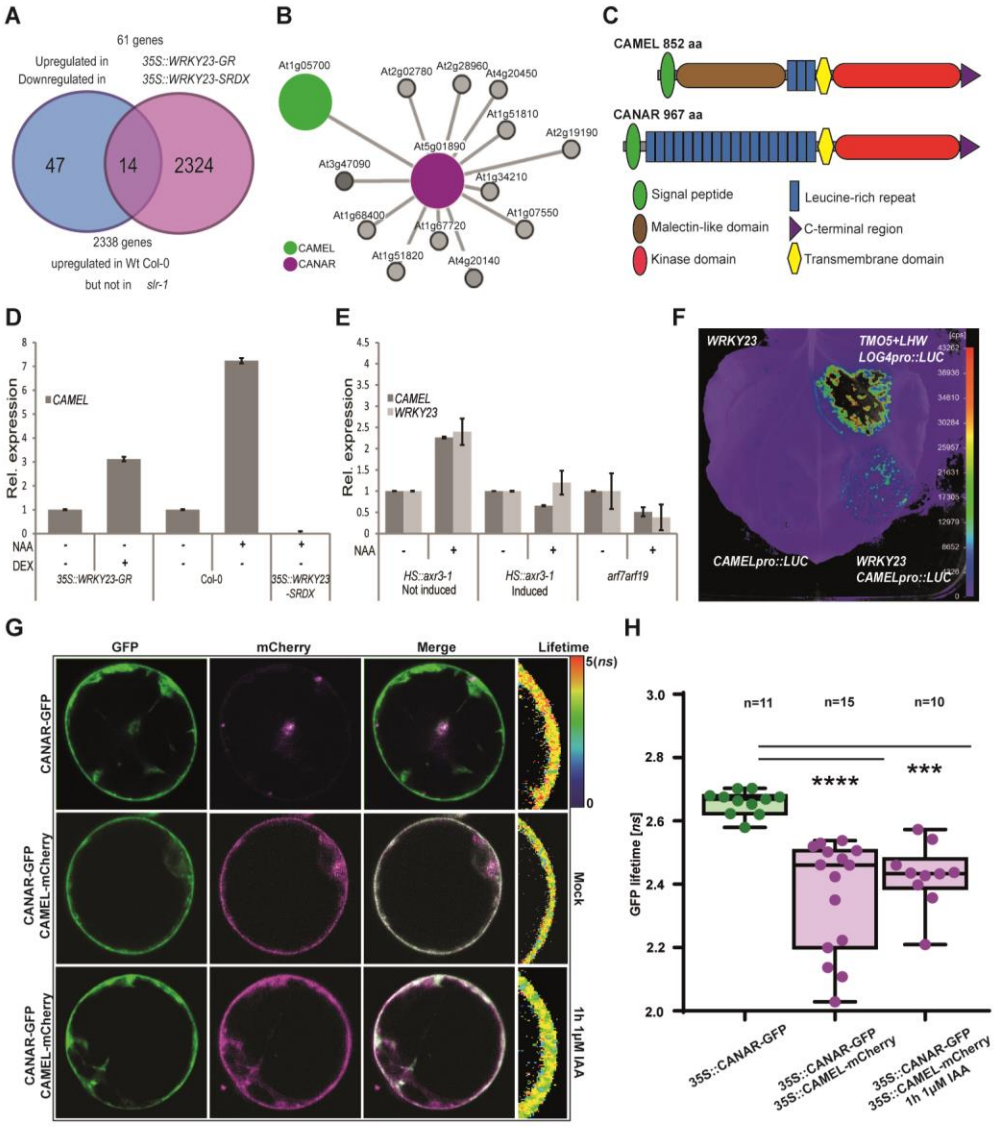

Figure 3. 1 CAMEL expression is regulated by WRKY23 and depends on the TIR1/AFB-WRKY23 pathway.

(A) Scheme of the microarray experimental setup to identify auxin-regulated genes downstream of the TIR1/AFB-WRKY23 signaling module. (B) Map of physical interactions between extracellular domains of putative interactors of CANAR from a previous study (Smakowska-Luzan et al., 2018) with CAMEL being one of high confidence interactors, illustrated with the BAR interaction viewer. (C) Schematic representation of the domain organization of CAMEL and CANAR. (D and E) RT-qPCR experiments showing that (D) *CAMEL* expression depends on WRKY23 and (E) auxin-mediated upregulation of *CAMEL* requires the TIR1/AFB activity. (F) Luciferase assay in *Nicotiana benthamiana: 35S::WRKY23* co-expressed with *CAMELpro:LUC* and negative control of *35S:WRKY23* or *CAMEL:LUC*. (G and H) FRET-FLIM analysis of transiently expressed *35S::CANAR-GFP* and *35S::CAMEL-mCherry* in protoplasts. The GFP fluorescence lifetime was calculated as described in the Methods section and the heat map represents the fluorescent lifetime values. A One-Way ANOVA test compared marked sets of data (***, p<0.001; ****, p<0.0001). *n* denotes the number of scored protoplasts.

A

Locus	Gene name	*35S::WRKY23-GR* DEX vs. *35S::WRKY23-GR* Mock		*35S::WRKY23-SRDX* NAA vs. WT Col-0 NAA		Vanneste *et al.*, 2005 Log FC	
		Log FC	P.Value	Log FC	P.Value	Wt Col-0 NAA 6h/0h	*slr* NAA 6h/0h
AT1G05700	Leucine-rich repeat transmembrane protein kinase protein	3.45	9.08E-06	-19.27	2.57E-10	3.47	-1.72
AT1G28400	Unknown	2.97	1.23E-04	-1.76	3.67E-03	2.39	1.46
AT1G53070	Legume lectin family protein	3.26	3.45E-07	-1.98	4.33E-06	1.49	1.25
AT2G26440	Plant invertase/pectin methylesterase inhibitor superfamily	4.77	9.08E-06	-1.93	1.77E-03	3.99	2.29
AT3G07540	Actin-binding FH2 (formin homology 2) family protein	2.37	1.85E-05	-3.51	5.25E-08	29.34	1.12
AT3G50010	Cysteine/Histidine-rich C1 domain family protein	2.94	2.04E-06	-2.95	1.63E-07	1.50	-2.49
AT4G12470	Azelaic acid induced 1	1.42	3.42E-02	-70.25	2.26E-12	2.61	-1.36
AT4G12480	Early Arabidopsis aluminium induced 1	1.38	2.26E-01	-25.66	7.67E-10	2.93	-1.35
AT4G12490	Azelaic acid induced 3	4.41	2.21E-07	-49.12	2.26E-12	11.07	1.42
AT4G12500	Azelaic acid induced 4	6.45	1.39E-05	-34.12	3.65E-09	6.01	1.08
AT4G38210	Expansin A20	3.39	1.01E-07	-1.61	3.15E-05	7.15	1.62
AT5G40590	Cysteine/Histidine-rich C1 domain family protein	3.83	2.86E-05	-8.10	4.41E-08	2.37	-3.11
AT5G40780	Lysine histidine transporter 1	2.01	2.83E-04	-2.98	5.45E-07	4.55	-1.00
AT5G51550	EXORDIUM like 3	2.70	1.59E-07	-3.02	3.78E-09	6.16	-1.05

Table 3. 1 Statistically significant candidates obtained from the microarray designed to find PIN polarity regulators downstream of TIR1/AFB-WRKY23.

3.2.2 Malectin-type LRR Receptor-like kinase CAMEL downstream of auxin signaling

AT1G05700 encodes a previously uncharacterized member of the Leucine-Rich Repeat (LRR) receptor-like kinase (RLK) family from subfamily I and its extracellular domain consists of a large Malectin-like domain and three LRR repeats (Fig. 3.1C; Fig. S3.1D). We named AT1G05700 CAMEL (Canalization-related Auxin-dependent Malectin-like RLK).

qRT-PCR on lines where *WRKY23* is either targeted inducibly to the nucleus (*35S::WRKY23-GR*) or engineered into a transcriptional repressor (*35S::WRKY23-SRDX*) (Grunewald et al., 2012) confirmed that *CAMEL* mRNA levels increased after activation of WRKY23 and decreased upon its repression (Fig. 3.1D). The JASPAR database of transcription factors (TFs) (Khan et al., 2018) also predicted WRKY23 among the top candidates binding to a 2000bp *CAMEL* promoter (Tab. S3.2). We confirmed activation of *CAMELpro* by WRKY23 using a luciferase-based reporter system in *Nicotiana benthamiana*. Co-expression of *35S::WRKY23* and *CAMELpro::LUC* led to activation of luciferase activity (Fig. 3.1F). This supports that *CAMEL* is a downstream gene of WRKY23.

As shown previously, the TIR1/AFB auxin pathway is required for auxin-mediated PIN polarity re-arrangements and canalization-based development (Balla et al., 2011; Sauer et al., 2006) and this goes in part through *WRKY23* (Prát et al., 2018, p. 23). Consistently with this, *CAMEL* transcription, similar to *WRKY23,* is induced by auxin in a time- and dose-dependent manner (Fig. S3.1E,F) and this auxin effect is not observed in *35S::WRKY23-SRDX* or in mutants defective in transcriptional auxin signaling (*HS::axr3-1* and *arf7arf19*) (Fig. 3.1D,E). Furthermore, *CAMELpro* contains 6 auxin responsive elements (Fig. S3.1G), suggesting additional auxin regulation, possibly directly by ARFs, also supported by fast upregulation of *CAMEL* by auxin (Fig. S3.1F).

Thus, *CAMEL* is transcriptionally regulated by WRKY23 downstream of the TIR1/AFB-ARF signaling module.

3.2.3 CAMEL and CANAR form a signaling complex at the cell surface

LRR-RLKs typically act in complexes with other RLKs (Chinchilla et al., 2007; Nam and Li, 2002). Generally, these complexes consist of a big receptor and smaller co-receptor and ligand-induced heterodimerization of ligand/receptor/co-receptor activates the cytoplasmic signaling cascade, which translates external signals into intercellular responses (Santiago et al., 2013; Sun et al., 2013). We used a map of physical interactions between extracellular domains of *Arabidopsis* LRR-RLKs to identify proteins that might interact with CAMEL (Smakowska-Luzan et al., 2018). Only one protein was retrieved as a high-confidence interactor, a large class VII LRR-RLK (Fig 3.1B and C). This was previously annotated *PXC2* (*PXY/TDR CORRELATED 2*; At5g01890) based on *in silico* co-expression clustering analyses (Mott et al., 2019). Given its association with CAMEL in canalization processes, we named this LRR-RLK, CANAR (Canalization-related Receptor-like kinase).

To determine whether CAMEL and CANAR interact *in vivo* as full-length proteins we used three approaches. Firstly, we generated a *35S::CANAR-eGFP* transgenic line, immunoprecipitated CANAR-GFP using anti-GFP antibodies and performed tandem mass spectrometry (MS/MS) to identify proteins co-immunoprecipitated with our bait. We obtained a list with possible interacting partners including CAMEL among the top 10 interactors (Appendix Tab S3.4). Next, we tested the CAMEL-CANAR interaction using bimolecular fluorescence complementation (BiFC) in *Nicotiana benthamiana* leaves. Co-

infiltration of *CAMEL* and *CANAR* resulted in a signal in both combinations (35S::CAMEL-(C)CFP + 35S::CANAR-(N)CFP and *vice versa*). Co-expression of 35S::CAMEL(C)CFP + 35S::CAMEL(N)CFP also gave a signal, demonstrating that CAMEL homodimerizes. Another LRR-RLK *TMK2,* (At1g24650) was used as a negative control and co-transfected leaves with 35S::TMK2(C)CFP + 35S::CANAR(N)CFP did not show a signal (Fig S3.1E).

To test the CAMEL-CANAR interaction more quantitatively, we used Förster resonance energy transfer combined with fluorescence lifetime imaging microscopy (FRET-FLIM) (Wallrabe and Periasamy, 2005). We co-expressed *35S::CANAR-eGFP* and *35S::CAMEL-mCherry* in *Arabidopsis* root protoplasts and detected a reduction in the fluorescence life time for eGFP as compared to *35S::CANAR-eGFP* expressed alone (Fig 3.1G,H). Auxin treatment had no additional effect on the eGFP life time in this experimental set-up, implying that CAMEL-CANAR interaction is insensitive to increased concentration of auxin. Spatial resolution of FRET-FLIM experiments suggested that both proteins are localized and form complexes at the cell surface (Fig 3.1G).

Thus, we showed auxin-insensitive, interaction between the two LRR-RLKs CAMEL and CANAR.

3.2.4 CAMEL and CANAR play roles in leaf venation

Next, we tested genetically an involvement of the CAMEL-CANAR complex in auxin-mediated canalization. We isolated publicly available T-DNA insertional loss-of-function mutants in both genes: *camel-1/-2* and *canar-1/-2* (Fig. S3.2A-D), and generated gain-of-function transgenic lines overexpressing *CAMEL* and *CANAR* under the constitutive *RPS5A* and *35S* promoters, respectively (Fig. S3.2E,F).

The *camel-1/-2* mutants showed abnormal vascular patterning with disconnected upper loops, extra branches and extra or missing loops. Two independent overexpression lines also exhibited vasculature defects, albeit with lesser frequency (Fig. 3.2A,B). Both *canar-1/-2* mutant alleles showed similar, even more pronounced vasculature abnormalities whereas *35S::CANAR-GFP* exhibited overall less frequent defects (Fig. 3.2C,D). The double mutant *camel-1xcanar-1* exhibited largely rescued venation, implying a possible antagonistic action of CAMEL and CANAR (Fig. 3.2A,C; S3.2G). CAMEL/CANAR function appears to be rather

specific to vasculature formation as no other obvious growth defects were observed (Fig. S3.2H-P).

Next, we tested if these venation defects are linked to altered auxin distribution and auxin transport. We analyzed the expression of the auxin-responsive reporter *DR5rev::GFP*, which can be correlated with auxin distribution (Friml et al., 2003). In both *camel-1* and *canar-1* mutants DR5 activity was decreased compared to the control (Fig. 3.2E,F). When analysing the basipetal (rootward) auxin transport in hypocotyls, we observed that both *camel-1* and *canar-1* mutants have reduced auxin flow (Fig. S3.2Q). Given that formation of PIN1-expressing, polarized channels has been linked to vein formation (Scarpella et al., 2006), we examined PIN1 polarity in young first leaves by means of anti-PIN1 antibody staining. In Wt leaves, coordinated PIN1 polarity defining an auxin-transporting channel was observed with rare PIN1 polarity abnormalities in primary and secondary branches. In contrast, both *camel-1* and *canar-1* mutants showed higher incidence of PIN1 polarity defects (marked by red arrows) in primary and *canar-1* also in secondary branches (Fig. 3.2G,H), whereas no defects were observed in the midvein for any of the tested genotypes (Fig. S3.2R).

These observations show that CAMEL and CANAR mediate vasculature development during leaf venation and coordinate PIN1 polarities during this process.

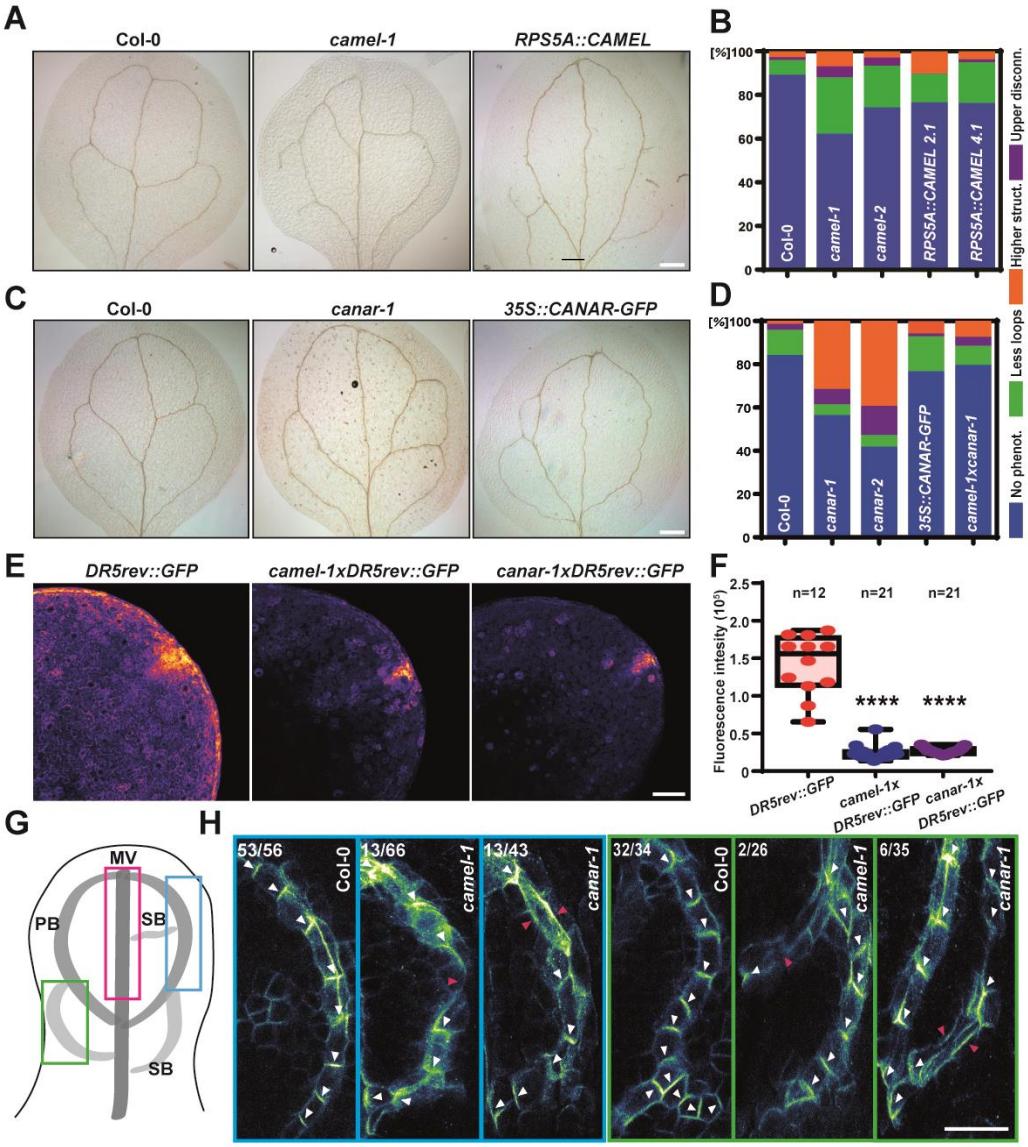

Figure 3. 2 camel-1 and canar-1 show abnormal vascular development suggesting a defect in auxin feedback on auxin transport.

(A and C) Representative images of venation patterning defects in cotyledons of *camel-1* (A) or *canar-1* (C), respectively. Scale bar: 100 µm. (B and D) Quantification of venation defects in *camel* and *canar* mutants (n>75 for each genotype). Scored categories: No phenotype, less loops, higher structure (including extra loops or branches) and upper disconnections.
(E and F) DR5rev::GFP signal distribution and (F) intensity in cotyledons of *camel-1*/*canar-1* mutants. (n>12 for each genotype). Scale bar: 100 µm. (G and H) Coordinated PIN1 polarity in Col-0 and defective PIN1 polarity in *camel-1*/*canar-1* mutants. Colored boxes in (G) illustrate positions of close-ups in (H). (H) Representative images of PIN1 immunolocalization in first leaves. The number in the left top corner indicates the incidence of observed PIN1 defective polarity in a total amount of analyzed leaves. White arrows show typical PIN1 polar localization. Red arrows mark defective PIN1 polarity. Evaluation criteria are described in the Materials and Method section. Scale bar: 10 µm

3.2.5 CAMEL and CANAR are required for vasculature regeneration after wounding

Another classical example of a canalization-mediated process is vasculature regeneration after wounding when new vasculature is generated circumventing the wound (Mazur et al., 2016; Sauer et al., 2006).

We interrupted the vasculature in *Arabidopsis thaliana* inflorescence stems by a horizontal cut (Fig. 3.3A) and analyzed *GUS* expression at 1-7 days after wounding (DAW). Both *CAMEL* and *CANAR,* as well as their upstream regulator *WRKY23* showed promoter activities during the regeneration (Fig. 3.3B; S3.3A). Next, we analyzed the extent of vasculature regeneration in loss-of-function mutants and overexpressing lines visualized by toluidine blue staining (TBO) of regenerated vasculature. In Wt vasculature was fully developed and both newly regenerated vessel cells (white asterisk) and lignified parenchyma cells (red asterisk) stained in blue were visible. All tested mutants showed defective regeneration caused by inability to form a continuous strand of regenerated cells. *RPS5A::CAMEL* showed less frequent defects and *35S::CANAR-GFP* exhibited even improved regeneration over Wt (Fig. 3.3C,D; S3.3B,C). Similar defects were observed also for flexible formation of auxin transport channels. In *PIN1*-GFP, but not in *canar-1xPIN1-GFP*, a PIN1-GFP expressing channel (marked by yellow arrow) circumventing the wound was formed (Fig. S3.3D). In contrast to leaf venation, *camel-1xcanar-1* double mutant showed regeneration defects comparable to the individual mutants (Fig. S3.3B,C).

To analyze more directly auxin-mediated formation of auxin transport channels, we used external, local auxin application (Mazur et al., 2020). Application of an IAA droplet on the stem side below the wound (marked in magenta) led to formation of a PIN1-expressing channel connecting with the pre-existing vasculature already 2 DAW in Wt, which was not observed in *canar-1* even after 4 DAW (Fig. S3.3E). Accordingly, the similar, newly formed vascular strands (shown by TBO staining) could only be observed in Wt (Fig. S3.3F).

These results revealed a role for CAMEL and CANAR, as well as their upstream regulator WRKY23 in the flexible regeneration of vasculature following wounding.

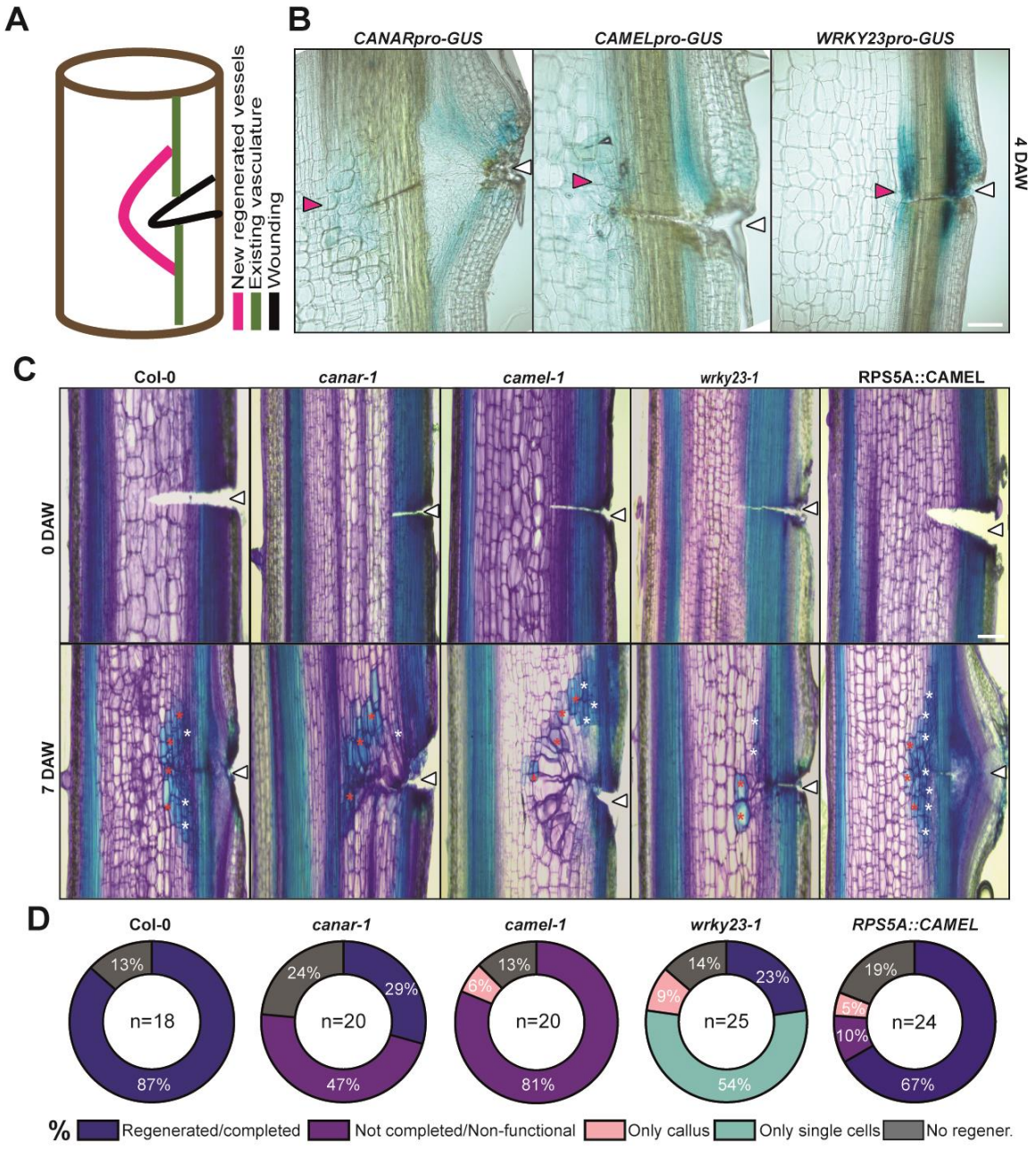

Figure 3. 3 Defective vasculature regeneration after wounding of mutant lines canar-1, camel-1, wrky23-1 and RPS5A::CAMEL overexpressing line.

(A) Schematic representation of the experiment to analyse vasculature regeneration after wounding. (B) Expression of *CANARpro::GUS, CAMELpro::GUS* and *WRKY23pro::GUS* 4 days after wounding (DAW). GUS expression can be seen above/below the wound in previously existing vasculature and in the adjacent area of the wound, where newly regenerating vasculature is formed (red arrowhead). The wound site is marked by a white arrowhead. Scale bar: 100 µm. (C) Wounded stems at 0 and 7DAW. Stems are stained by toluidine blue to visualize newly regenerated blue-vessel cells (white asterisks) and lignified parenchyma cells (red asterisks). The wound site is marked by a white arrowhead. *canar-1, camel-1, wrky23-1, RPS5A::CAMEL* lines exhibit defects in vasculature

regeneration compared to Col-0. Scale bar: 100 µm. (D) Quantification of regeneration defects for the mutant lines mentioned above. *n* denotes the number of evaluated plants.

3.2.6 CAMEL and CANAR regulate polarity and trafficking of PIN auxin transporters

Since auxin feed-back on PIN polarity is one of the main features of canalization and PIN polar localization is linked to its constitutive endocytic recycling (Glanc et al., 2018; Wabnik et al., 2010) we tested whether CAMEL and CANAR are involved in this process. PIN endocytic recycling can be indirectly visualized by PIN intracellular aggregation in response to treatment with the trafficking inhibitor Brefeldin A (BFA) (Geldner et al., 2001). Anti-PIN1 immunostaining in roots showed that following BFA treatment, PIN1 intracellular aggregation was reduced in *camel-1* and *canar-1* mutants (Fig. 3.4A,B). The same phenomenon was observed for *camel-1xPIN2-GFP* and *canar-1xPIN2-GFP* crosses (Fig. S3.4A,B) indicating a defect in PIN endocytic recycling.

The auxin effect on PIN polarity can be approximated by repolarization of PIN1 from the basal to the inner lateral side in the root endodermis cells (Sauer et al., 2006). Anti-PIN1 immunolocalization revealed that following auxin treatment, PIN1 repolarization was reduced in *camel* and *canar* mutants (Fig. 3.4C,D; S3.4C-E).

These results imply that the CAMEL-CANAR complex not only plays a role in the canalization-related development at the level of organs and tissues, but also targets PIN1 in individual cells, regulating its subcellular trafficking and auxin feed-back on PIN polarity.

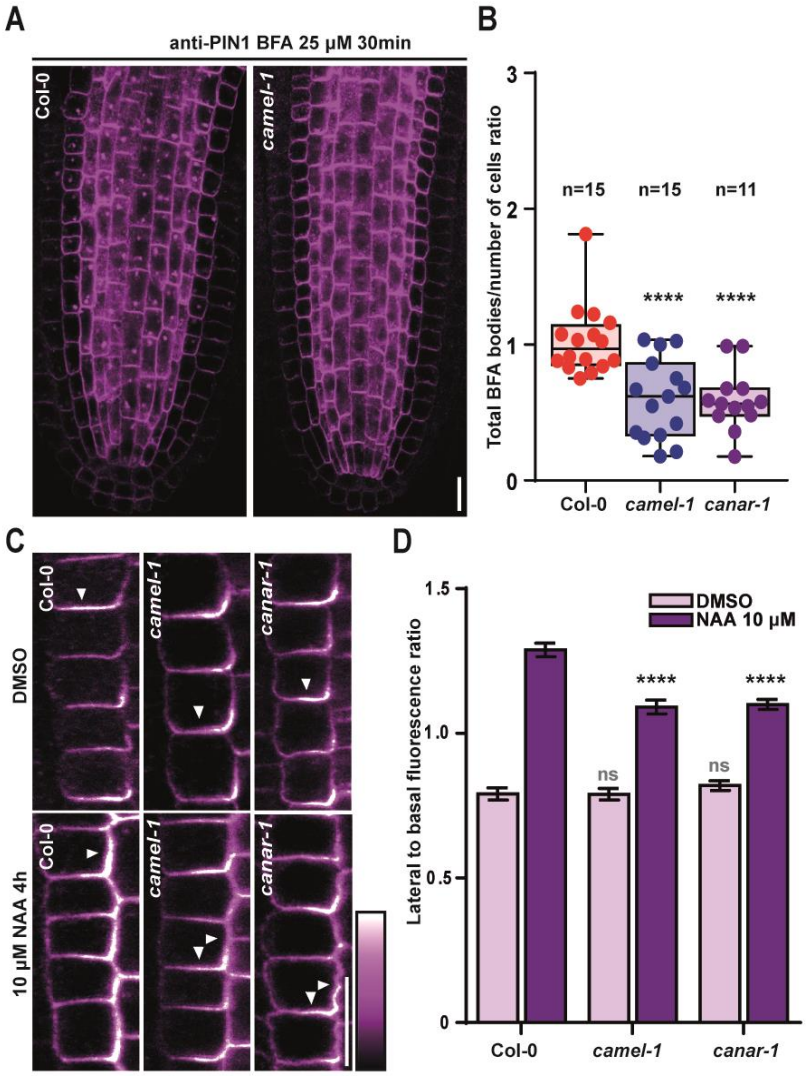

Figure 3. 4 Subcellular trafficking and auxin feed-back on PIN polarity is compromised in camel-1 and canar-1 mutants.

(A) Representative confocal images of primary root stele cells after immunostaining PIN1 in Wt*, camel-1* and *canar-1*. Seedlings were BFA-treated (25 µM) for 30min. Scale bar: 10 µm. (B) Quantitative evaluation of (A) shows the ratio of the total number of BFA bodies/total number of evaluated cells per root. *n* denotes the number of evaluated seedlings (****p<0.0001). (C) Immunolocalization of PIN1 in endodermis of root meristem after 4h NAA (10 µM) treatment. Scale bar: 10 µm. (D) Quantitative evaluation of (C) shows mean PIN1 lateral-to-basal signal intensity ratio in endodermal cells. Error bars indicate standard error. The experiment was carried out three times, one representative experiment is presented. A One-Way ANOVA test compared the marked datasets (****p<0.0001; n>80 cells corresponding to a minimum of 10 roots per treatment and the experiments were imaged using comparable settings).

3.2.7 CAMEL-CANAR receptor complex targets and phosphorylates PIN auxin transporters

To get insight into the mechanism of CAMEL-CANAR action and downstream processes, we immunoprecipitated CAMEL-GFP from seedlings to identify the interactome of CAMEL. Co-immunoprecipitated proteins were analyzed using mass spectrometry (Tab. S3.4). Among the list of putative interactors multiple PIN proteins were found.

To confirm the interaction with PIN1, we transiently co-expressed *35S::CAMEL-GFP+35S::PIN1-mRFP* and *35S::CANAR-GFP+35S::PIN1-mRFP* in *Arabidopsis* root protoplasts. PIN1-mRFP co-immunoprecipitated with both CANAR-GFP and CAMEL-GFP (Fig. 3.5A). Furthermore, we performed FRET-FLIM in root protoplasts expressing *35S::CAMEL-GFP* or *35S::CANAR-GFP*. The lifetime of CAMEL-GFP and CANAR-GFP was reduced after co-expression with *35S::PIN1^{HL}-mCherry* (HL=hydrophilic loop) further confirming an interaction between CAMEL/CANAR and PIN1 (Fig. 3.5B,C).

Since CAMEL and CANAR are expected to act as kinases and PIN phosphorylation is a well-established mode of regulation of PIN activity and polar localization (Adamowski and Friml, 2015), we tested the ability of CAMEL and CANAR to phosphorylate PINs. We therefore performed an *in vitro* kinase assay by incubating purified PIN1^{HL}, PIN2^{HL} or PIN3^{HL} with purified cytoplasmic kinase domains of CAMEL and CANAR with radiolabeled ATP. We detected phosphorylation of PIN loops by CAMEL with PIN1^{HL} being the best substrate (Fig. 3.5D). However, CANAR did not show kinase activity (Fig. S3.5A). This lack of kinase activity can be explained by losing an aspartic acid from the conserved HRD motif in the catalytic core similarly to other known pseudokinases: BIR2, GHR1, PRK5 (Fig. S3.5B).

Considering the lack of CANAR kinase activity, constitutive CAMEL-CANAR interaction and complementation of leaf vasculature defects in *camel-1xcanar-1* double mutants, we hypothesize that CANAR might be a negative regulator of CAMEL. This is further supported by the ability of CANAR kinase domains to reduce the auto-phosphorylation of CAMEL and its kinase activity towards PIN1 (Fig. S3.5C).

To test the relevance of CAMEL-mediated PIN1 phosphorylation, we analysed the products of an *in vitro* kinase reaction using mass spectrometry and identified five mostly conserved putative phosphosites in PIN1^{HL} (Fig. S3.5D; 3.6A-C). These sites seem unique since they are not shared by any previously reported kinase phosphorylating PIN loops, such as

PID/WAGs, D6PK or MPKs (Fig. S3.5D) and when mutated, they decreased the ability of CAMEL kinase to phosphorylate PIN1^{HL} (Fig. S3.6A,B).

We generated phosphodead *PIN1-GFP^{T3AS2A}* and phosphomimic *PIN1-GFP^{T3ES2E}* constructs by substitution of three threonine and two serine to alanine or glutamic acid, respectively, placed them under control of the native *PIN1* promoter and introduced these constructs into Wt plants. Positive, GFP-expressing transformants for both constructs showed already in the first generation naked inflorescence stems (7/20 for *PIN1-GFP^{T3AS2A}* and 3/18 for *PIN1-GFP^{T3ES2E}*) strongly reminiscent of *pin1* loss-of-function (Fig. 3.6B). Other positive plants did not show strong phenotypes and produced seeds allowing analysis in the next generation. Venation in cotyledons of both *PIN1-GFP^{T3AS2A}* and *PIN1-GFP^{T3ES2E}* lines exhibited increased incidences of vascular abnormalities (Fig. 3.6D,E; S3.6C). All positive transformants in the first generation for *PIN1^{T3AS2A}* (4/4) and *PIN1^{T3ES2E}* (2/2) showing naked inflorescence stems exhibited no vasculature regeneration after wounding characterized by fragmented vessel cells, non-functional parenchyma cell connections or extensive callus formation in the wound (Fig. S3.6E). To test the role of the identified phosphosites in canalization, we tested the effect of auxin on the mutated PIN1 variants. While PIN1-GFP in root endodermal cells is localized predominantly basally, both PIN1-GFP^{T3AS2A} and PIN1-GFP^{T3ES2E} showed more apolar localization already without any treatments (Fig. 3.6C; S3.6D). When immunolocalized with anti-GFP antibody, both PIN1-GFP^{T3AS2A} and PIN1-GFP^{T3ES2E} already partially polarized to the inner-lateral side in the mock situation and did not show any further polarity changes following auxin application (Fig. 3.6F; S3.6D).

In conclusion, the CAMEL-CANAR complex interacts with PINs and CAMEL is capable of phosphorylating PIN cytosolic loops. Defects in phosphomimic and phosphodead mutations in the PIN1 loop support the relevance of these phosphorylations for auxin transport and auxin canalization. The stronger defects in lines carrying PIN1 with mutated CAMEL-targeted phosphorylation sites as compared to the *camel/canar* mutants suggest that these phosphosites are shared by other kinases controlling auxin transport in a different developmental context.

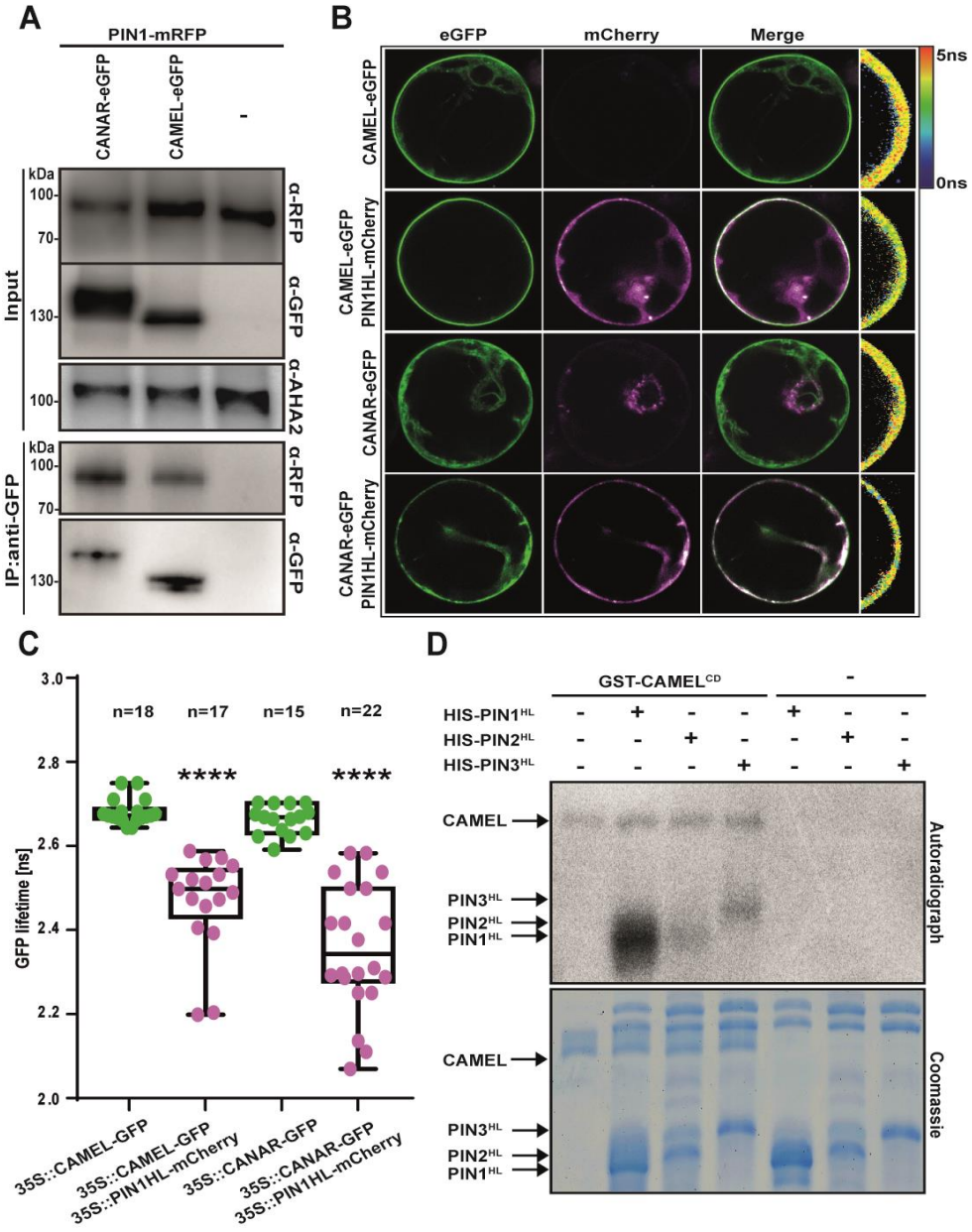

Figure 3. 5 The CAMEL-CANAR signaling module directly targets PIN1.

(A) The interaction of CAMEL-CANAR with PIN1 was determined by co-immunoprecipitation (Co-IP) from *Arabidopsis* root protoplasts. The protein complex of CAMEL-PIN1 and CANAR-PIN1 was co-immunoprecipitated by anti-GFP beads. Anti-AHA2 was used as the loading control. The experiment was carried out three times. (B) and (C) FRET-FLIM analysis of transiently expressed *35S::CAMEL-eGFP* and *35S::CANAR-eGFP* with *35S::PIN1HL-mCherry* (HL-hydrophilic loop) in protoplasts. The eGFP fluorescence lifetime was calculated as described in the Methods section and the heat map indicates the fluorescent lifetime values. After co-expression of *CANAR/CAMEL-eGFP* with *PIN1HL-mCherry*, the eGFP lifetime was decreased, suggesting interaction between the proteins. A One-Way ANOVA test compared the marked data sets (****, $p<0.0001$). *n* denotes the number of scored protoplasts.
(D) Autoradiograph of an *in vitro* kinase phosphorylation assay of PIN1/2/3HL by CAMEL^{CD} (CD-cytoplasmic domain). Aliquots of the samples were separated by SDS-PAGE and exposed to

autoradiography. Coomassie blue staining was used as loading control and presence of the respective recombinant proteins. The blots shown are representative for tree biological replicates.

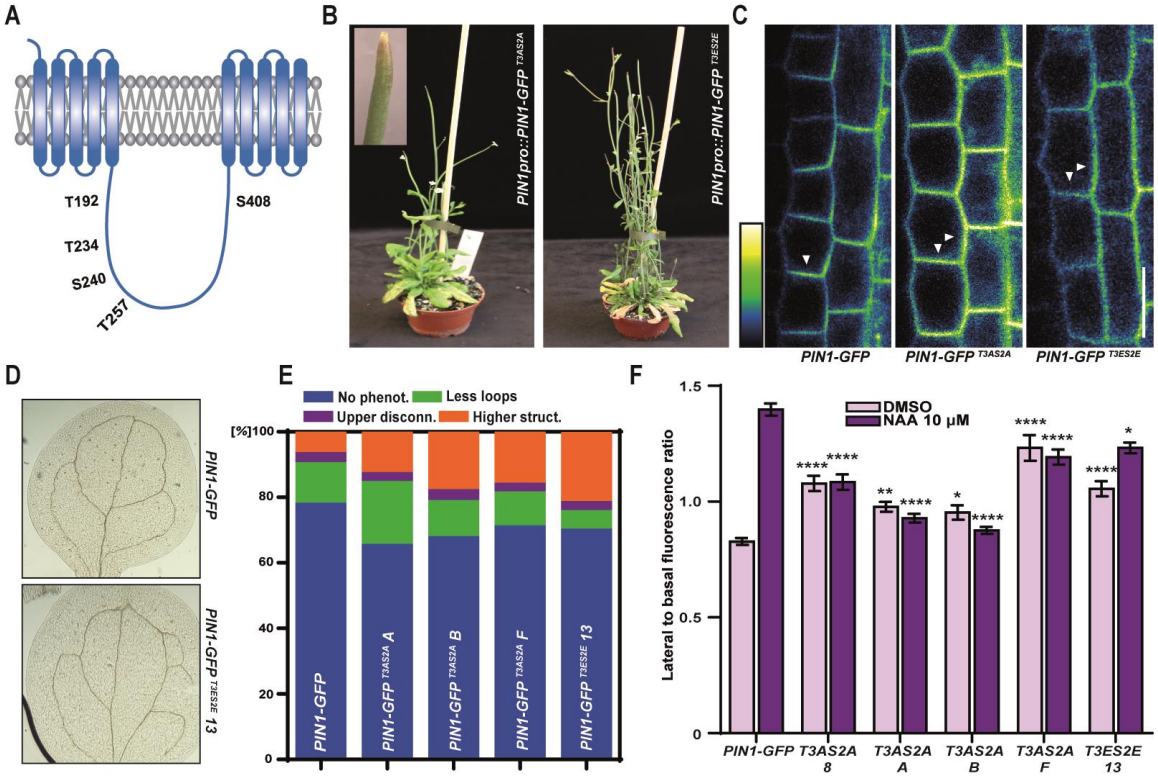

Figure 3. 6 CAMEL-targeted phosphosites in the PIN1 cytoplasmic loop are important for PIN polarity and venation.

(A) Schematic representation of PIN1 in the plasma membrane with the phosphosites targeted by CAMEL marked in the cytoplasmic loop. (B) Phenotypes of *PIN1pro::PIN1-GFP*^{T3AS2A} and *PIN1pro::PIN1-GFP*^{T3ES2E}. 35 days old plants. (C) Subcellular localization of PIN1-GFP, PIN1-GFP^{T3AS2A} and PIN1-GFP^{T3ES2E} in root meristem endodermal cells. White arrows mark the predominant subcellular localization. (D) Representative images of vasculature defects in cotyledons of *PIN1pro::PIN1-GFP*, *PIN1pro::PIN1-GFP*^{T3ES2E} (line13). Scale bar: 100 µm. (E) Quantification of vasculature defects in *PIN1pro::PIN1-GFP*, *PIN1pro::PIN1-GFP*^{T3AS2A} (lines A, B, F) and *PIN1pro::PIN1-GFP*^{T3ES2E} (line 13) (n>68 for each genotype). Scored categories: normal vasculature, less loops, higher structure (including extra loops or branches) and upper disconnections. (F) Quantitative evaluation of (Fig. S6D) shows the mean lateral-to-basal ratio of PIN1-GFP signal in endodermal cells. Error bars indicate standard errors. The experiment was carried out three times, one representative experiment is presented. A One-Way ANOVA test was performed to compare marked datasets (*p<0.05,**p<0.01,***p<0.001,****p<0.0001; n>40 cells corresponding to a minimum of 8 roots per treatment and experiments were imaged using comparable settings).

3.3 *Discussion*

In this study, we provided mechanistic insight into how auxin controls its own directional cell-to-cell transport and we identified molecular components of the so-called auxin canalization

mechanism underlying flexible and self-organizing formation of auxin channels guiding vasculature formation. Identification of the CAMEL-CANAR complex downstream of transcriptional auxin TIR1/AFB-WRKY23 signaling module and its direct regulation of PIN-dependent auxin transport provides a potential means how to integrate global auxin signals with a so far hypothetical short range signaling for coordinating cell polarities during plant adaptive development.

The CAMEL-CANAR interaction appears insensitive to auxin. CANAR is a pseudokinase, which likely is a negative regulator of CAMEL kinase activity. While in *camel-1xcanar-1* double mutant cotyledons the vascular defects are largely rescued, in stem vasculature regeneration after wounding is still impaired, suggesting a tissue specific function of the CAMEL-CANAR complex during auxin canalization.

Whereas *camel/canar* mutants have specific phenotypes in vasculature development and regeneration, mutation of CAMEL-targeted phosphosites led to, in addition to defective vasculature formation and regeneration, a severe flower phenotype resulting in either sterile flowers or naked inflorescence stem. This observation proposes that these phosphosites are most likely shared by another kinases and CAMEL-induced phosphorylation occurs specifically only during vasculature development and regeneration.

CAMEL-induced phosphorylation of the PIN1 loop is essential for general polarity and auxin-mediated repolarization of PIN1. In Glanc et al., 2018, the authors show that establishment of PIN2 polarity requires *de novo* protein synthesis and endocytosis. They hypothesize that initially, newly secreted PIN is send to all sides of the cell and then differential endocytosis rates creates a defined PIN polar domain. In line with this observation, the apolar localization of our phospho-mutated PIN1 constructs indicates that these phosphosites might be part of the machinery deciding which PIN stays and which one will be removed from the plasma membrane.

We believe that we are still missing an important piece of the machinery: a ligand. The ligand would be providing cells with information about the immediate tissues context. In this view, the CAMEL-CANAR receptor complex would integrate the long-distance auxin (or auxin-derived ligand) input with a short-range tissue signaling to coordinate the behavior of cells allowing concerted tissue repolarization necessary for flexible, self-organized plant development.

3.4 *Materials and Methods*

Plant material and growth conditions

All *Arabidopsis thaliana* lines were in the Columbia-0 background. T-DNA mutants were acquired from the Nottingham *Arabidopsis* Stock Centre (NASC; http://www.arabidopsis.info). T-DNA mutants used in this study are SALK_025603C (*camel-1*), SALK_048526 (*camel-2*), SALK_055351C (*canar-1*), SALK_018730C (*canar-2*), SALK_003943 (*wrky23-1*), SALK_062169 (*exp20-1*), SALK_124968 (*exl3-1*), SALK_048655 (*pmei1-1*), SALK_092291 (*chr1-1*), SAIL_761_D09 (*chr2-1*) and SALK_034566 (*lht1-1*). Primers used for genotyping are listed in Supplemental Tab. 2.2. The *arf7 arf19* double mutant (Okushima et al., 2007), *HS::axr3-1* (Knox et al., 2003), *DR5rev-GFP* (Jirí Friml et al., 2002)*, Co-0::EARLI1 RNAi* [1-1] (Cecchini et al., 2015), 35S*::WRKY23-GR* (Grunewald et al., 2012, 2008), *35S::WRKY23-SRDX* (Grunewald et al., 2012, 2008), DR5-GUS (Benková et al., 2003), pPIN2::PIN2-GFP (Xu and Scheres, 2005), *WRKY23pro::GUS* (Grunewald et al., 2012, 2008), *CANARpro::GUS and CAMELpro::GUS* (Wu et al., 2016), have been described previously. Seeds were sterilized overnight by chlorine gas, sown on solid *Arabidopsis* medium (AM+: half-strength MS basal salts, 1% sucrose, and 0.8% phyto-agar, pH 5.7), and stratified at 4°C for at least 2 days prior to transfer to a growth room with a 16-h-light/8-h-dark light cycle at 21°C. Seedlings were grown vertically for 4 or 6 days, depending on the assay.

Microarray analysis

Roots of 5-day-old *35S::WRKY23-GR* were treated with 10 µM DEX for 6 hours or DMSO, respectively. Wt Col-0 and *35S::WRKY23-SRDX* plants were treated with 10 µM NAA or DMSO for 6 hours. The roots were subsequently collected for RNA isolation. All points were sampled in three independent experiments. Total RNA (200 µg per array) was used to hybridize ATH1 Affymetrix *Arabidopsis* arrays in accordance with standard procedures at VIB Nucleomics Core. Data files containing the probe level intensities (.cel files) were used for background correction and normalization using the log2 scale RMA procedure (Irizarry *et al.*, 2003) with R (http://www.r-project.org) and the Bioconductor package affylmGUI (http://bioinf.wehi.edu.au/affylmGUI/). Genes with the same or contrasting *WRKY23* expression profiles were selected by Pavlidis template matching in TMeV 4.0 (TIGR) (Saeed

et al., 2003). Finally, genes with a significant P value (< 0.001), denoting expression above background, with minimum 2-fold change compared to the respective control, were retained for further analysis.

Construction of transgenic lines

DNA constructs were created with the Gateway cloning technology (Invitrogen), using published destination vectors (Karimi et al., 2007). Primers used for cloning are summarized in Supplemental Tab. 2.3. For the *RPS5A::CAMEL* construct, the genomic sequence of *CAMEL* was introduced into pDONR221 and then recombined by LR MultiSite reaction with the pDONRP4P1R entry clone containing the *RPS5A* promoter into binary destination gateway vector pB7m24GW,3. To create *35S::CAMEL-GFP* construct, the pDONR P221 entry clone containing genomic sequence of *CAMEL* without STOP codon (stop codon was substituted by a three amino acid linker sequence Trp; Asp; Pro) was combined into binary vector pB7FWG2.0. Similarly, *35S:CANAR-GFP* was generated by recombination of pDONR P221 entry clone containing the genomic sequence of the *CANAR* without STOP codon into destination vector pB7FWG2.0. *CAMELpro(500bp)::CAMEL-GFP and CAMELpro(1500bp)::CAMEL-mRUBY* were cloned by recombination of a genomic fragment *CAMEL* in pDONR221, GFP/mRUBY in pDONRP2rP3 and 500bp/1500bp promoter in pDONRP4P1R. The obtained vectors were introduced into the *Agrobacterium tumefaciens* strain C58C1 (pMP90) and transformed into appropriate *Arabidopsis thaliana* genotypes using floral dip transformation. At least two independent, single insertional, homozygous transgenic lines were isolated and examined. Overexpression of these lines was confirmed by qRT-PCR or fluorescence microscopy.

Preparation of recombinant proteins

To express the cytoplasmic domain of CANAR ($CANAR^{CD}$; residues from 631 to 967) and CAMEL ($CAMEL^{CD}$; residues from 532 to 852), the coding sequences were amplified with primers (Supplemental Tab. 3) and cloned into the pGEX-4T-1 vector (GE Healthcare Life Science). The hydrophilic loops of PIN1/2/3 (PIN HL) were amplified with primers described previously (Tan et al., 2019) and cloned into the pET-28a vector (GE Healthcare Life Science). The constructs were transformed into *E.Coli* BL21 cells and induced at OD600 of 0.6 with 0.5mM IPTG at 16°C overnight. Proteins were purified using Glutathione Agarose (Thermo

Scientific) for GST-CANAR^{CD}, GST-CAMEL^{CD} and Ni-NTA His binding resin (Thermo Scientific) for HIS-PIN1/2/3^{HL} according to the manufacturer's instructions. The recombinant proteins were analysed by SDS-PAGE visualized by Coomassie briliant blue staining (Biof-Safe Coomassie Stain, Bio-Rad).

***In vitro* protein kinase assay**

The *in vitro* protein kinase assay was carried out according to a previous report with minor modifications (Jia et al., 2016). The recombinant GST-CAMEL^{CD} (5µg) or GST-CANAR^{CD} (5µg) were incubated with the HIS-tagged hydrophilic loop of PIN1/2/3 (HIS-PIN1/2/3^{HL}) (10µg) in 25µL kinase reaction buffer (50mM Tris-HCl pH 7.5, 10mM $MgCl_2$, 1mM DTT, 0.1mM ATP, 5 µCi [γ-32P] ATP) at room temperature for 1 hour. The reactions were stopped by addition of SDS-loading buffer. Phosphorylation was visualized by autoradiography after being resolved in a 10% SDS-polyacrylamide gel.

Proteomic analysis

a) Sample Preparation

Samples were lysed in 4% SDS, 100 mM tris pH 7.4, 150 mM NaCl, 100 mM TCEP, heated at 95°C for 10 min, sonicated, cleared by centrifugation (10 min, 17,000 g), then digested into tryptic peptides using a variant of the FASP (Filter-Aided Sample Preparation) method: briefly, Vivacon 30,000 Da MWCO filters (Sartorius) were pre-wetted in 8 M urea, 100 mM TCEP ("UT" buffer), then samples were loaded and buffer exchanged to UT buffer, alkylated for 30 min in the dark with 50 mM N-Ethylmaleimide, washed in UT buffer, exchanged to 100 mM TCEP then digested overnight at 37°C with MS-grade trypsin (Promega); peptides were eluted sequentially with 100 mM TCEP, then 500 mM NaCl, acidified with 1/10th volume 10 mM Trifluoroacetic Acid,de-salted on tC18 SepPak plates (Waters) according to manufacturer's instructions, vacuum-dried then re-disolved in 5% Formic Acid (FA) for LC-MS analysis.

b) LC-MS/MS analysis

Peptide samples were analysed by nanoLC-MS/MS on a Q-Exactive HF Orbitrap mass spectrometer with online Ultimate 3000 nanoLC system (Thermo Scientific). Peptides were

loaded onto an Acclaim PepMap C18 nano-trap column (Thermo Scientific) then resolved on a 500 mm x 75 µm, 2 µm C18 particles EasySpray column (ES803A, Thermo Scientific) using a gradient starting at 5 min into the run at 2% B, ramping up linearly to 31% B (165 min), then to 44% B (185 min), and followed by a 5 min plateau at 90% B. Solvents A and B were 100% water + 0.1% FA, and 80% Acetonitrile in water + 0.08% FA, respectively. Peptides were ionized by electrospray ionization at 1.8 kV at a capillary temperature of 275°C. The Q-Exactive HF mass spectrometer was operated in Positive mode, using a Data-Dependent Acquisition method. MS1 spectra were collected in profile mode from 350 to 1,500 m/z at a resolution of 120,000, with an automatic gain control (AGC) target of 3e6 and a max injection time of 50 ms. Precursor were filtered for fragmentation using an intensity threshold of 50,000, accepting charge states 2 to 7, and with a 60 s dynamic exclusion window. Up to 20 precursors per cycle were sequentially selected using an 1.4 m/z isolation window and fragmented by HCD at 28% NCE. MS2 spectra were acquired in centroided mode, with an AGC target of 5e4.

c) Data Analysis

Acquired raw files were searched in MaxQuant (1.6.8.0) against an Arabidopsis thaliana fasta database (UniProtKB). Fixed modification was set to NEM (+). Variable modifications were Oxidation (M), Acetyl (Protein N-term), Deamidation (NQ), Gln->pyro-Glu and Phospho (STY). Second Peptides, Dependent Peptides and Match Between Runs were activated. All false discovery rates were set to 1%. Some minor reprocessing of the MaxQuant output was done in R using in-house scripts.

Identification of interacting proteins using IP/MS-MS

Immunoprecipitation (IP) experiments were performed in three biological replicates as described previously (De Rybel et al., 2013) using 1 g of 5-day-old seedlings from the *35S::CANAR-eGFP* and 3 g of 5-day-old seedlings from the *35S::CAMEL-eGFP* transgenic lines. Interacting proteins were isolated by applying total protein extracts to anti-GFP coupled magnetic beads (Miltenyi Biotech). Three replicates of *35S::CANAR-eGFP* (Appendix Supplemental Tab. S4) or *35S::CAMEL-eGFP* (Appendix Supplemental Tab. S5) were compared to three replicates of Col-0 Wt controls. Tandem mass spectrometry (MS) and statistical

analysis using MaxQuant and Perseus software was performed as described previously (Wendrich et al., 2017).

RNA extraction, cDNA synthesis, and quantitative RT-PCR and analysis

RNA extraction, cDNA synthesis, and quantitative RT-PCR were performed as described previously (Tejos et al., 2014). Targets were quantified with specific primer pairs designed with Primer-BLAST (http://www.ncbi.nlm.nih.gov/tools/primer-blast/). The expression levels were normalized to *GAMMA-TUBULIN 2* (*TUB2*; *At5g05620*), which was constitutively expressed across the samples. All qPCRs were run in three technical repeats and the data were processed with the qRT PCR analysis software (Frederik Coppens; Applied Bioinformatics & Biostatistics group; PSB VIB, Belgium). Primers used in the study are listed in Supplemental Tab. 2.

Whole-mount *in situ* immunolocalization, microscopy and quantitative analysis of PIN repolarization

PIN immunolocalizations in primary root were performed as described (Sauer and Friml, 2010). The anti-PIN1 antibody was used in the 1:1000 dilution. The secondary goat anti-rabbit antibody coupled to Cy3 (Sigma-Aldrich) was diluted 1:600. Confocal microscopy was performed using a Zeiss LSM 700 confocal microscope. Quantitative analysis of PIN relocalization was performed as described (Sauer et al., 2006b). PIN1 immunolocalizations in young leaves were performed as described (Sauer and Friml, 2010) with additional steps after fication:

1. Washing 2x 10min with PBS
2. Clearing of tissue with: 2x 10min methanol (37°C), 2x 10min ethanol/xylene (1:1, 37°C), 2x 10min xylene (37°C), 2x 10min ethanol/xylene (1:1, RT) 2x 10min 100% ethanol (RT), 1x 10min 90% ethanol (RT), 1x 10min 75% ethanol (RT), 1x 10min 50% ethanol (RT), 1x 10min 25% ethanol (RT), 1x 10min 10% ethanol (RT), 1x 10min water

The secondary goat anti-rabbit antibody coupled to Alexa Fluor 488 (Sigma-Aldrich) was diluted 1:600.

Förster Resonance Energy Transfer with Fluorescence Lifetime Imaging Microscopy (FRET-FLIM)

Protoplasts were isolated from the root cell suspension as described before(Grones et al., 2015). The genomic sequence of *CAMEL, CANAR* and *PIN1HL* were cloned into pDONOR P221 and recombined into protoplast vectors containing GFP (p2GWF7,0) or RFP (p2GWCh7,0). Protoplasts were transfected with 12 µg of a plasmid DNA of the appropriate gateway vector. Protoplasts were overnight dark incubated at room temperature in glucose-mannitol (GM) medium. FRET-FLIM experiments were performed using a TriM Scope II inverted 2-photon microscope equipped with a FLIM X16 TCSPC Detector for time correlated single photon counting (LaVision BioTec). Fluorescence lifetime image stacks (150 slices, with 0,082ns time interval) were acquired, and a threshold mask was created from the sum projection of each stack in FIJI(Schindelin et al., 2012) to segment the apical PM domains. All pixels within the masked area were then pooled and averaged at each time point of the FLIM stack. The intensity at t=0 was normalized and a simple exponential decay with offset was fitted to the data.

Co-immunoprecipitation assay

Co-immunoprecipitation assay was performed in the *Arabidopsis* root protoplasts. Transfected protoplasts were lysed with 500 µL of lysis buffer (50mM Tris-HCl pH 7.4, 150mM NaCl, 0.5mM EDTA, 1x protease inhibitor cocktail (cOmplete Tablets, Roche), 1x phosphatase inhibitor cocktail (PhosStop, Roche) and then the membrane fraction was isolated: flash freeze in liquid nitrogen, thawing on ice, centrifuging 16250g at 4°C for 15min, removing supernatant, resuspending in lysis buffer with an addition of 0.5% of Triton X-100 and NP-40 detergents, flash freeze in liquid nitrogen, thawing on ice, centrifuging 12000g at 4°C for 15min and taking the supernatant. For co-immunoprecipitation, the membrane fraction of protein extracts were incubated with anti-GFP beads (Chromotek) for 2 hours at 4°C. The immunoprecipitated proteins were then washed 4 times with washing buffer 1 (150mM NaCl, 1% Igepal CA-630, 0.5% sodium deoxycholate, 0.1% SDS, 50mM Tris HCl pH 8.0) and 1 time with washing buffer 2 (20mN Tris HCl pH 7.5). Elution of the beads was done with 95°C elution buffer (50mM Tris HCl pH 6.8, 50mM DTT, 1% SDS, 1mM EDTA, 0.005% bromphenol blue, 10% glycerol) followed by SDS-PAGE separation, western blotting and detection with the respective primary antibodies (α-RFP, α-GFP and α-AHA2) (Miltenyi Biotec).

Bimolecular fluorescence complementation (BiFC) assay

For a generation of BiFC constructs, the genomic sequence of *CANAR, CAMEL* and *TMK2* was amplified with M13 primers (Supplemental Tab. 3) from the pDONR P221 entry vectors containing individual genes and recombined into BiFC binary vectors pSCYNE(R) and pSCYCE (Gehl et al., 2009). BiFC was performed in transiently transformed *Nicotiana benthamiana* leaf epidermis cells (Schütze et al., 2009). Presence of fluorescence was observed two days after infiltration using Confocal Laser Scanning Microscopy (CLSM).

Basipetal auxin transport assay in *Arabidopsis* hypocotyls

For shoot basipetal transport, cotyledons of 6-day-old *Col-0* etiolated seedlings were removed to prevent endogenous auxin biosynthesis. Droplets of 1.25% agar with ^{3}H-IAA were applied onto the apical part of hypocotyls. After 6h, all roots were removed and the hypocotyls were collected and homogenized using liquid nitrogen and grinder. Homogenized tissue was mixed with Opti-Fluor scintillation solution (Perkin Elmer) and incubated overnight. The amount of ^{3}H-IAA was measured in a scintillation counter (Hidex 300SL) for 300s. As a control, seedlings were pre-incubated with 10µM NPA during 6h incubation with ^{3}H-IAA droplets.

Vasculature regeneration assay after wounding

The regeneration experiment was performed as described previously (Mazur et al., 2016). Stem segments were cut by an automated vibratome (Leica VT1200 S, Leica Microsystems Ltd., Wetzlar, Germany) and 80µm-thick native sections were prepared. The native sections were stained with a 0.025 % Toluidine Blue O aqueous solution (Sigma-Aldrich) and regeneration was analysed in stems using a bright field microscope (Zeiss Axioscope.A1) and pictures of vasculature were taken with a camera (Axiocam 506) at 10x magnification. For observation of GUS activity after wounding, the same technique of plant preparation was used as described previously for regeneration analysis. Stem segments were incubated with 1 mg/ml X-Gluc solution at 37°C, overnight, and fixed with a 70% ethanol solution at room temperature. The samples with positive GUS reaction were cut by an automated vibratome and 80µm-thick native sections were prepared. The native sections were cleared in a solution containing 4% HCl and 20% methanol for 15 min at 65°C, followed by a 15-min incubation in 7% NaOH and 70% ethanol at room temperature. Seedlings were rehydrated by successive incubations in 70%, 50%, 25%, and 10% ethanol for 10 min at room temperature, followed by incubation in a solution containing 25% glycerol and 5% ethanol for 10 min at room

temperature. Finally, seedlings were mounted in 50% glycerol and observed using a bright field microscope. Pictures of GUS activity were taken with a camera at 10x magnification.

Cotyledon vasculature analysis

12-day-old seedlings were left in 70% ethanol overnight to remove chlorophyll and seedlings were cleared according to the protocol described in the vasculature regeneration assay after wounding section. Finally, seedlings were mounted in 50% glycerol and monitored by differential interference contrast microscopy (Olympus BX53) or stereomicroscope (Olympus SZX16).

Homology analysis

CAMEL and *CANAR* genes were translated into protein sequences and aligned with ClustalX (Thompson et al., 1997). Neighbor-joining (NJ) phylogenetic analysis was conducted in MEGA 7 (Kumar et al., 2016). NJ analysis was performed using the protein Poisson distances and the pairwise deletion of gap sites. To evaluate the reliability of the phylogenetic tree, 1000 bootstrap replicates were performed.

3.5 *Acknowledgements*

We would like to acknowledge M. Glanc and Y. Zhang for providing entry clones; Vienna Biocenter Core Facilities (VBCF) for recombinant protein production and purification; Vienna Biocenter Mass spectrometry Facility, Bioimaging and Life Science Facilities at IST Austria and Proteomics Core Facility CEITEC for a great assistance. **Funding:** This project received funding from the European Research Council (ERC) under the European Union's Horizon 2020 research and innovation program (grant agreement No 742985) and Austrian Science Fund (FWF): I 3630-B25 to J.F and by grants from the Austrian Academy of Science through the Gregor Mendel Institute (Y.B.); the Austrian Agency for International Cooperation in Education & Research to D.D.; W.S. was funded by the Netherlands Organization for Scientific Research (NWO; VIDI-864.13.001); the Research Foundation - Flanders (FWO; Odysseus II G0D0515N) and a European Research Council grant (ERC; StG TORPEDO; 714055) to B.D.R., B.Y. and E.M.; the Hertha Firnberg Programme post-doctoral fellowship (T-947) from the FWF Austrian Science Fund to E.S.-L.. J.H. is Recipient of a DOC Fellowship of the Austrian Academy

of Sciences at IST Austria. **Author contributions:** J.F. and W.G. conceived and designed the experiments. J.H. and J.F. wrote the paper with help of B.R. and Y.B. J.H., T.P., L.R., S.T., I.V., D.D., N.R., E.M., E.S.L., W.S., E.M., B.Y., B.D.R., Y.B., J.N. conducted experiments and contributed to the study design. G.M., J.H. and I.V., analyzed the data. **Competing interests:** The authors declare that they have no competing interests. **Data and materials availability:** All data is available in the main text or the supplementary materials. Raw microarray data from this article can be found in the EMBL ArrayExpress repository under accession number: E-MTAB-9563.

3.6 *Author contribution*

Jakub Hajný:

- FRET-FLIM interaction assays (Fig 3.1G, H; Fig 3.1B, C)
- BiFC interaction assays (Fig S3.1E)
- Fenotypic analysis of venation pattern in cotyledons (Fig 3.2A-D; Fig S3.2E)
- Confocal analysis of $DR5_{rev}$-GFP distribution (Fig 3.2E, F)
- Confocal analysis of PIN2-GFP BFA sensitivity (Fig S3.4A)
- Immunolocalization of PIN1 in root meristem (Fig 3.4A-D; Fig S3.4B-E)
- Immunolocalization of PIN1 in young developing leaves (Fig 3.2G and H)
- Construction of phylogenetic trees (Fig S3.1F and G)
- Confocal imaging of 35S::CANAR-GFP (Fig S3.2C)
- qRT-PCR (Fig S3.2D and E)
- Auxin transport assay in hypocotyls (Fig S3.3C)
- *In vitro* kinase assay (Fig 3.5D; Fig S3.5A)
- Protein sequences alignment (Fig S3.5B and C)
- Cloning and crossing of all required material

3.7 *Supporting information*

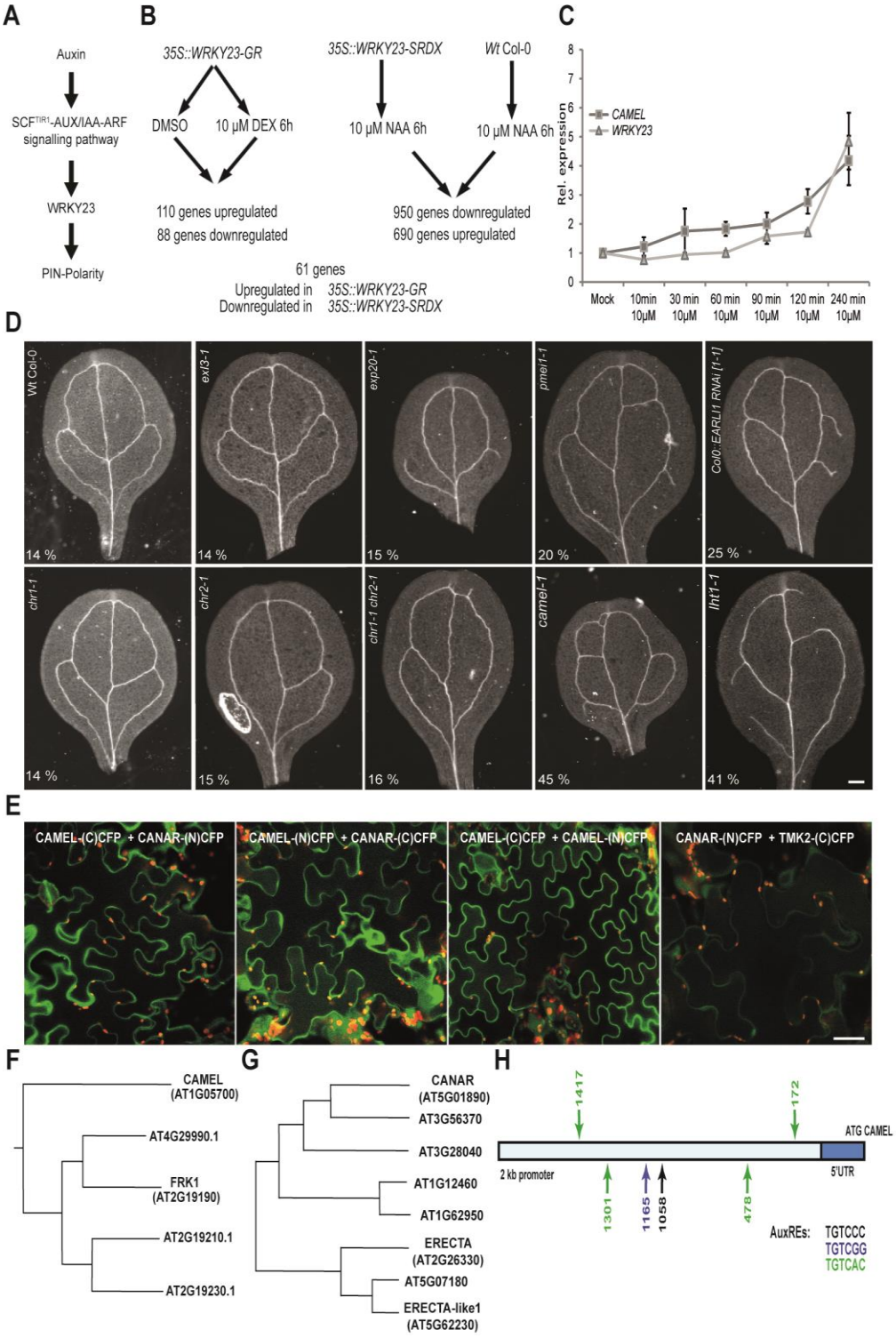

Figure S3. 1 CAMEL is a putative regulator of PIN polarity. CANAR is a plasma membrane interactor of CAMEL.

(A) Scheme of signaling pathway regulating PIN polarity based on (Prát et al., 2018). (B) The microarray experimental setup to identify auxin-regulated genes downstream of *TIR1/AFB/WRKY23* signaling module. (C) Time-dependent up-regulation of *CAMEL* and *WRKY23* expression by 10 µM NAA. Points represent relative fold change of expression normalized to *TUB2*. Error bars represent standard

deviation. For each experiment, three biological replicates were used. (D) Representative images of vascular venation of candidate mutant lines based on the microarray experiment. Scale bar: 100 µm. (E) Bimolecular fluorescence complementation (BiFC) of CAMEL-CANAR interaction in *Nicotiana benthamiana* leaves. TMK2 was used as a negative control. The experiment was carried out three times. Scale bar: 25 µm. (F) and (G) visualize a phylogenetic tree of (F) CAMEL and (G) CANAR closest *Arabidopsis* paralogues based on the protein sequence (see Materials and Methods section). (H) Schematic depiction of the CAMEL promoter; AuxRE and AuxRE-like response elements are shown as arrows.

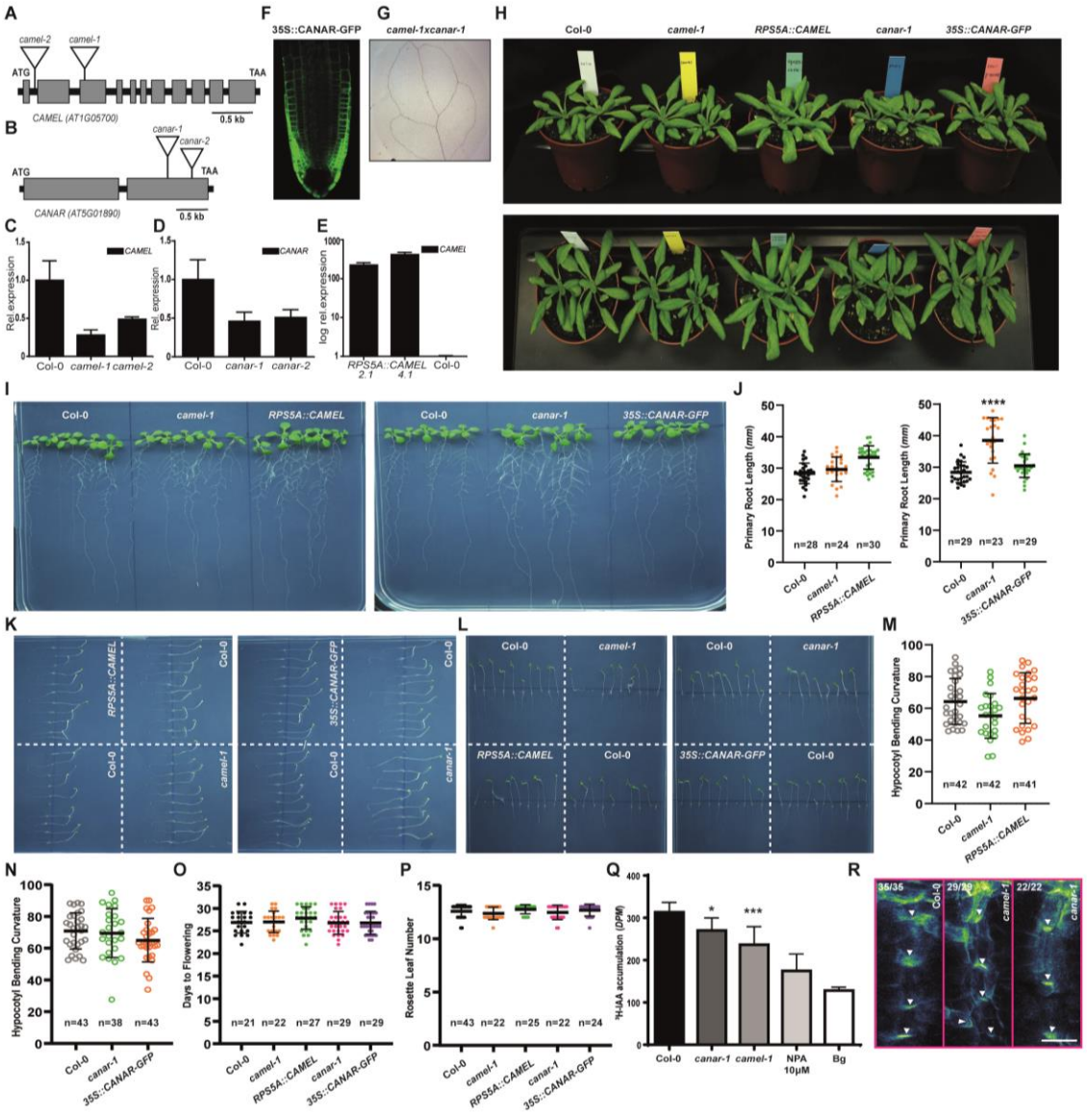

Figure S3. 2 Expression of CAMEL and CANAR in mutant and overexpression lines.

(A and B) T-DNA insertion sites for *camel-1/2* (A) and *canar-1/2* (B) in Col-0 background. (C and D) RT-qPCR analysis of *CAMEL* (C) and *CANAR* (D) expression in the isolated mutant lines. (E) RT-qPCR analysis in *CAMEL* gain-of-function lines. Relative expression values are normalized to Col-0 expression and *TUB2* was used as housekeeping gene. Error bars represent ± SD. For each experiment, three biological replicates were considered. One representative experiment is presented. (F) Confocal image of a 5-d-

old root tip of 35S::CANAR-GFP in Col-0 background. (G) Representative picture of the *camel-1xcanar-1* double mutant vasculature phenotype. (H) Rosette size of *camel-1, canar-1, RPS5A::CAMEL* and *35S::CANAR-GFP.* (I and J) Primary root length in *camel-1, canar-1, RPS5A::CAMEL* and *35S::CANAR-GFP* (10 days old seedlings). (K to N) Gravitropic and phototropic responses of *camel-1, canar-1, RPS5A::CAMEL* and *35S::CANAR-GFP.* (O) Flowering time of *camel-1, canar-1, RPS5A::CAMEL* and *35S::CANAR-GFP.* (P) Rosette leaf number of *camel-1, canar-1, RPS5A::CAMEL* and *35S::CANAR-GFP.* (Q) Basipetal transport of radiolabeled ^{3}H-IAA in hypocotyls. The auxin transport inhibitor NPA was used as a negative control. Bg stands for background signal. Results are means ± SD. The experiment was repeated three times, one representative repetition is presented. One-Way ANOVA compared the datasets (*p<0.05,***p<0.001). (R) Representative images of PIN1 immunolocalization in the midvein of young leaves. The number in the left top corner indicates the incidence of the observed phenotype. The white arrows shows the typical PIN1 polar localization. Scale bar: 10 µm

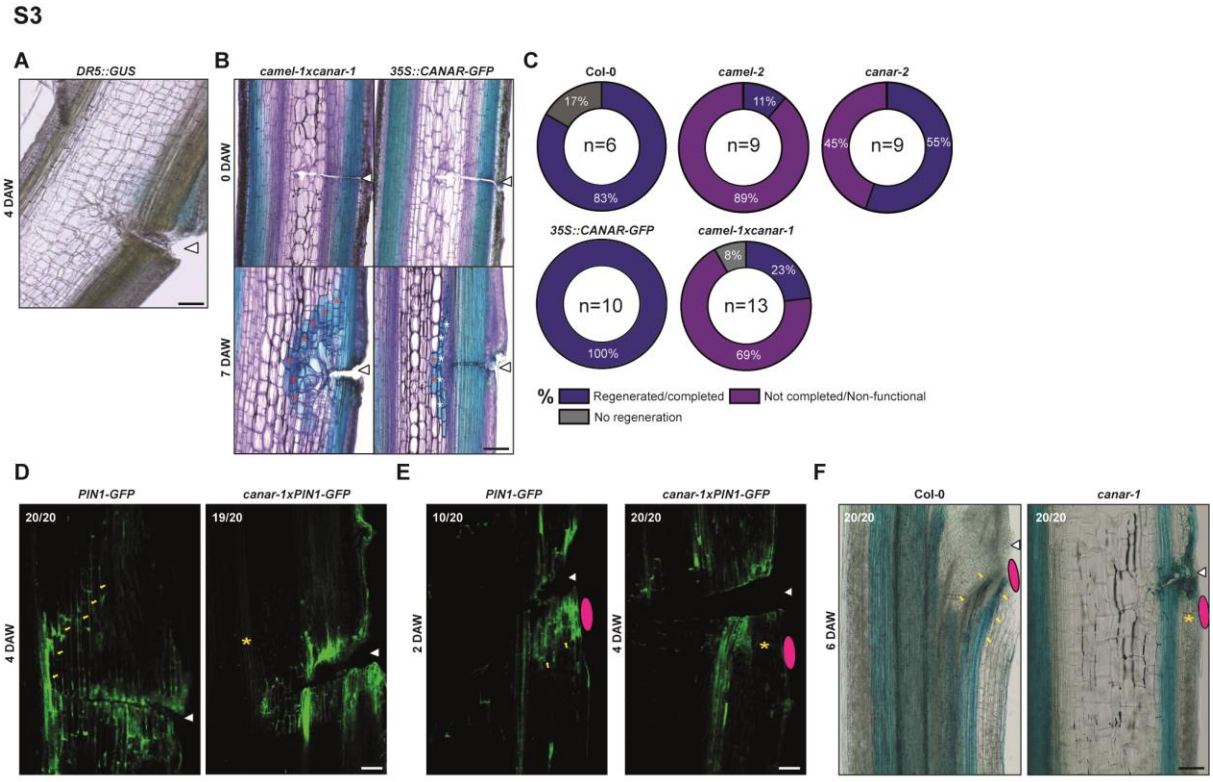

Figure S3. 3 Defective vasculature regeneration after wounding of mutant lines canar-2 and camel-2.

(A) Expression of *DR5::GUS* 4 days after wounding (DAW). The wound site is marked by an arrowhead. (B and C) Regeneration defects for *camel-2*, *canar-2, camel-1xcanar-1* and *35S::CANAR-GFP*. *n* denotes the number of tested plants. (D) Formation of PIN1-expressing channels (marked by yellow arrows) 4 DAW (marked by the white arrowhead) in control *PIN1-GFP* and mutant *canar-1xPIN1-GFP* lines. The yellow asterisk marks the absence of a PIN1-expressing channel. The number in the left top corner indicates the incidence of the observed phenotype. (E) Formation of PIN1-expressing channels originating from an IAA application site (marked in magenta) in *PIN1-GFP* and failing channel in *canar-1xPIN1-GFP* lines. (F) Toluidine blue staining to visualize the formation of vascular channels (marked by yellow arrows) originating from an IAA application site below a cut site in Col-0 and not in *canar-1* lines (indicated by yellow asterisk) (D-F) Scale bar: 100 µm. The number in left top corner indicates the incidence of the observed phenotype.

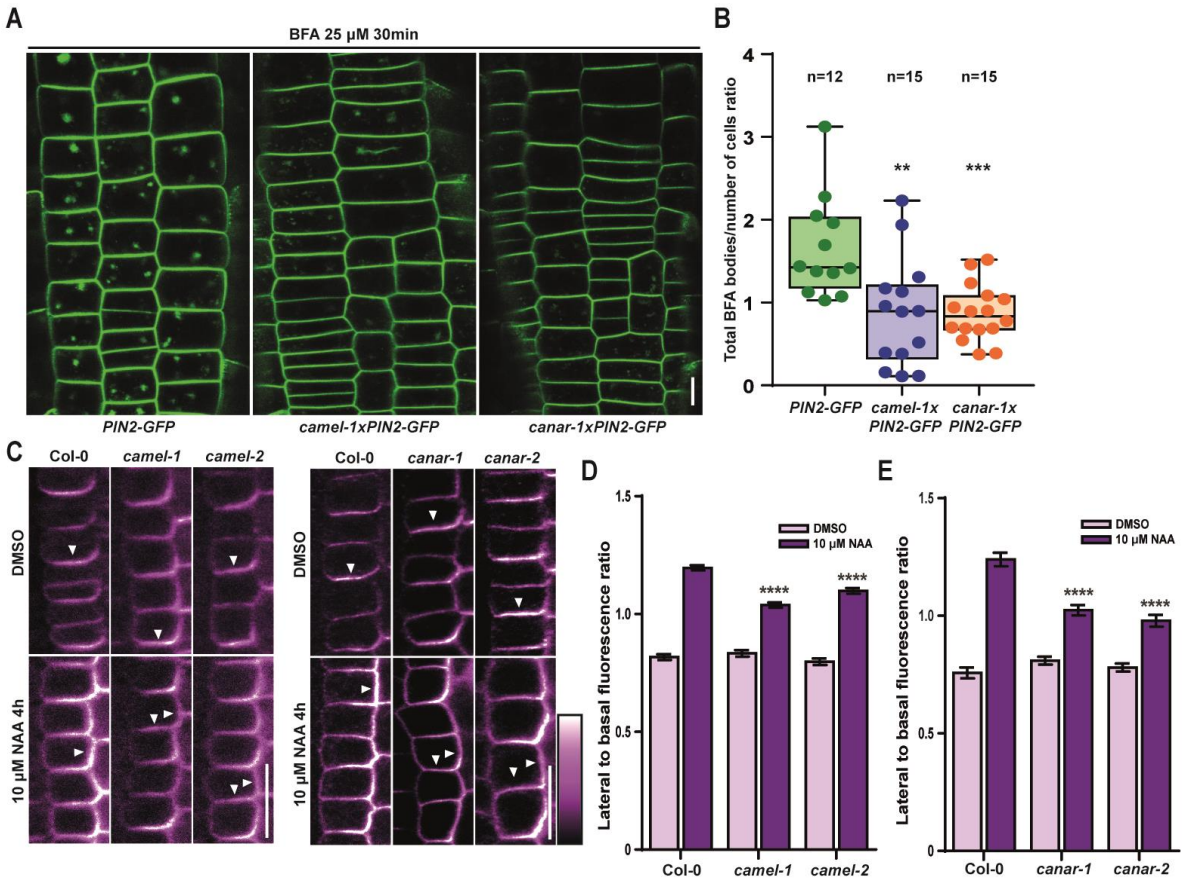

Figure S3. 4 Subcellular trafficking and auxin feed-back on PIN polarity is compromised in camel and canar mutants

(A) Representative confocal images of primary root epidermal cells of *PIN2-GFP, camel-1xPIN2-GFP* and *canar-1xPIN2-GFP* after BFA (25 µM) treatment for 30min. Scale bar: 10 µm. (B) Quantitative evaluation of (A) showing the ratio of total number of BFA bodies/total number of cells per root. *n* denotes the number of evaluated seedlings (**p<0.01, ***p<0.001). (C) Immunolocalization of PIN1 in endodermal cells of root meristem of *camel-1*, *camel-2,* canar-*1, canar-2* after 4h of 10 µM NAA treatment. White arrows mark the predominant subcellular localization. (D and E) Quantitative evaluation of (C) showing the mean PIN1 lateral-to-basal signal intensity ratio in endodermis cells. Error bars indicate SEM. The experiment was carried out three times, one representative experiment is presented. One-Way ANOVA was used to compare the datasets (****p<0.0001; n>80 cells corresponding to a minimum of 10 roots per treatment and experiments were imaged under comparable conditions). Scale bar: 10 µm.

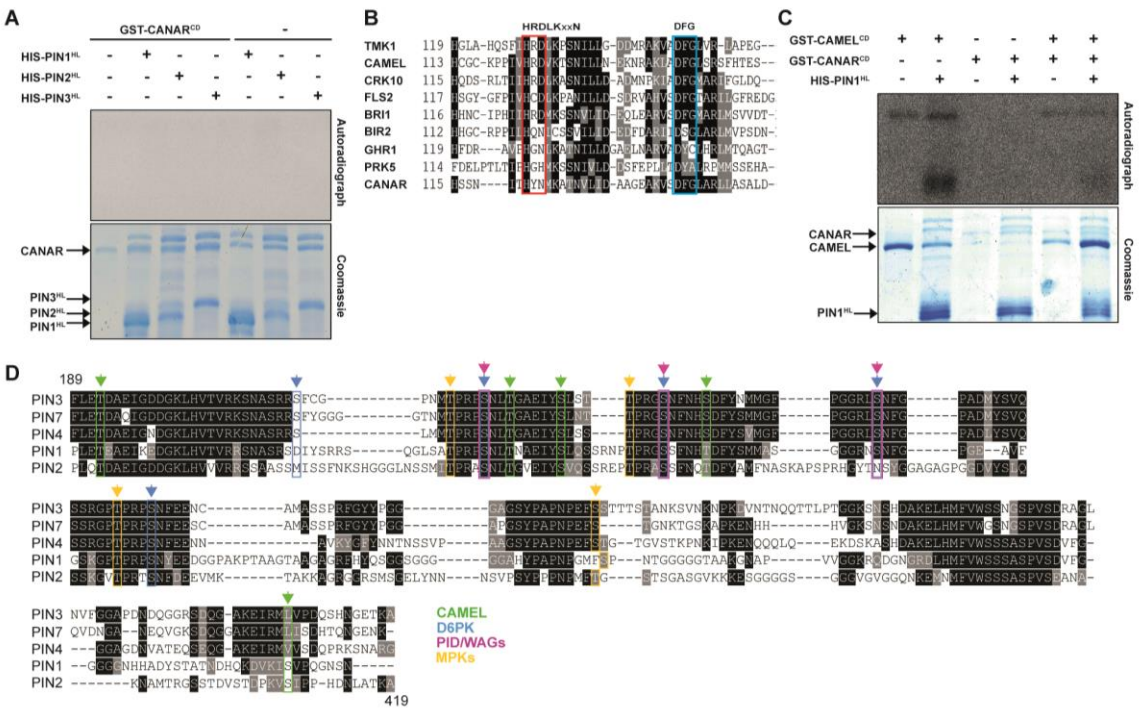

Figure S3. 5 Kinase activity of CANAR and putative phosphosites in PIN1 hydrophilic loop targeted by CAMEL

(A) Autoradiograph of *in vitro* kinase phosphorylation assay of PIN1/2/3^{HL} by CANAR^{CD}. CANAR^{CD} lacks *in vitro* kinase activity. Samples were separated by SDS-PAGE and exposed to autoradiography. Coomassie brilliant blue staining was used to compare protein loading. The experiment was repeated three times. (B) Catalytic core protein sequence alignment of active and inactive receptor-like kinases (Sierla et al., 2018). Residues HRD and DFG, marked with red and blue boxes respectively, are considered indispensable for kinase activity (Langeberg and Scott, 2015). (C) Autoradiograph of *in vitro* kinase phosphorylation assay of PIN1^{HL} by CANAR^{CD} and CAMEL^{CD}. CAMEL^{CD} has decreased kinase activity upon incubation with CANAR^{CD}. Samples were separated by SDS-PAGE and exposed to autoradiography. Coomassie brilliant blue staining was used to compare protein loading. The experiment was repeated three times. (D) Protein sequence alignment of cytoplasmic loops of long PINs. Colored boxes with arrows mark phosphosites targeted by different kinases.

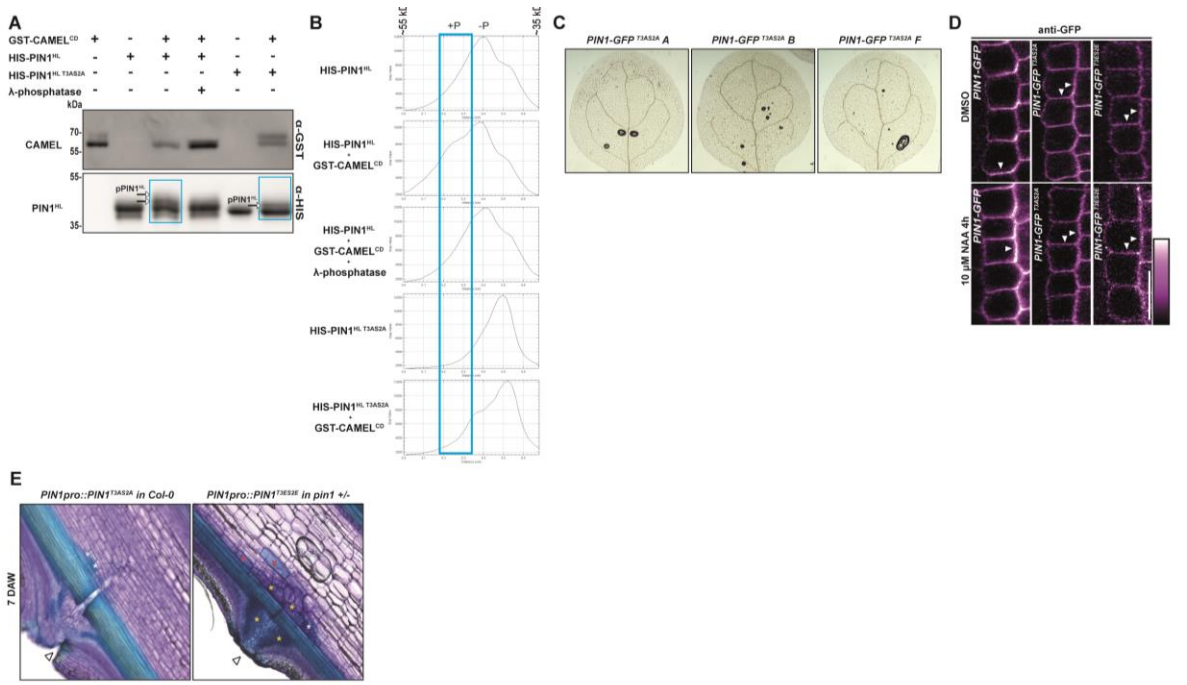

Figure S3. 6 Biochemical confirmation of PIN1 phosphosites targeted by CAMEL and phenotypic analyses of transformants harboring the corresponding PIN1 variants

(A to B) *In vitro* kinase assay confirmed reduced phosphorylation of PIN1$^{HL\ T3AS2A}$ by CAMEL. Samples were run on SDS-PAGE and followed by Western blot (A). The shifted bands (marked by arrows) correspond to phosphorylated PIN1^{HL}, which is confirmed by λ-phosphatase treatment where they do not occur. Upper lane, anti-GST antibody; bottom, anti-HIS antibody. (B) Plots showing band intensities of PIN1^{HL} and pPIN1^{HL} bands. The position of the phosphorylated PIN1^{HL} peak is indicated. (C) Representative images of vasculature defects in cotyledons of *PIN1pro::PIN1-GFP*, *PIN1pro::PIN1-GFP* ^{T3AS2A} (lines A, B and F). Scale bar: 100 µm. See quantification in (Fig. 6E). (D) Immunolocalization of *PIN1pro::PIN1-GFP*, *PIN1pro::PIN1-GFP* ^{T3AS2A} (lines 8, A, B, F) independent lines and *PIN1pro::PIN1-GFP* ^{T3ES2E} (line 13) in root meristem endodermis after 4h NAA (10 µM) treatment. White arrows mark the predominant subcellular localization. Scale bar: 10 µm. See quantification in (Fig. 6F). (E) Wounded stems of *PIN1pro::PIN1* ^{T3AS2A} and *PIN1pro::PIN1* ^{T3ES2E} at 7DAW. Stems are stained by toluidine blue to visualize newly regenerated channels (white asterisks), lignified parenchyma cells (red asterisks) and callus (yellow asterisks). The wound site is marked by a white arrowhead.

Matrix ID	Name	Score	Relative score	Sequence	Start	End	Strand	Predicted sequence
MA1309.1	WRKY3	17.7658	1.000000016	pCAMEL	1777	1787	-	aaaagtcaacg
MA0129.1	TGA1A	10.5435	1.000000015	pCAMEL	1881	1887	+	tacgtca
MA1302.1	WRKY65	18.1099	1.000000012	pCAMEL	1777	1787	-	aaaagtcaacg
MA1071.1	DOF5.3	7.38855	1.000000009	pCAMEL	1968	1974	-	gaaaaag
MA1201.1	AGL42	12.3116	1.000000009	pCAMEL	1529	1535	+	catcatc
MA1089.1	WRKY57	12.917	1.000000008	pCAMEL	1777	1786	-	aaagtcaacg
MA1202.1	AGL55	11.2098	1.000000006	pCAMEL	2	7	+	tcacca
MA1202.1	AGL55	11.2098	1.000000006	pCAMEL	231	236	-	tcacCA
MA1202.1	AGL55	11.2098	1.000000006	pCAMEL	319	324	+	TCACCA
MA1202.1	AGL55	11.2098	1.000000006	pCAMEL	1790	1795	-	tcacca
MA1202.1	AGL55	11.2098	1.000000006	pCAMEL	1811	1816	+	tcacca
MA0096.1	bZIP910	11.6944	1.000000004	pCAMEL	1882	1888	-	ctgacgt
MA0951.1	ATHB-16	14.1743	1	pCAMEL	1749	1756	+	taataatt
MA1316.1	WRKY71	18.5349	1	pCAMEL	1777	1787	-	aaaagtcaacg
MA1301.1	WRKY33	17.543	0.999999999	pCAMEL	1777	1787	-	aaaagtcaacg
MA0008.1	HAT5	12.8077	0.999999997	pCAMEL	1750	1757	-	caattatt
MA1080.1	WRKY23	14.4475	0.999999997	pCAMEL	1777	1784	-	agtcaacg
MA1026.1	ATHB-15	12.4353	0.999999996	pCAMEL	1889	1896	-	taattatt
MA1026.1	ATHB-15	12.4353	0.999999996	pCAMEL	1891	1898	+	taattatt

Table S3. 1 Predicted transcription factors (TFs) binding to the 2000bp of CAMEL promoter.

Primer	Sequence
SALK025603C_FOR	ATATATGACCCGTTAACCCGC
SALK025603C_REV	CTTAGGTTTCTCGGGAACGAC
SALK048526C_FOR	ATACATGCCGAGTCGTGATTC
SALK048526C_REV	CTTCTTTGGAAACAATGCTCG
SALK055351C_FOR	CAATCTCTCGGGAAGTCTTCC
SALK055351C_REV	CCTTCTCTCACCGTCTCACAC
SALK018730_FOR	TGGACCCTTTGTGACTTTCAC
SALK018730_REV	GCGGAAGCTTGTACAGACATC
SALK003943_FOR	CGGTGGGTTTATCAACAAATG
SALK003943_REV	ATTCTTGATCACGATTCACGG
SALK062169C_FOR	AAGACAAAGATGAGCCACTCG
SALK062169C_REV	GTCAGAGCAATCTTTTGTCGC
SALK124968C_FOR	GCAATCATTAGGCAAAAGCTG
SALK124968C_REV	TCAGCCGTTGGATCTAAACAC
SALK048655_FOR	TACTTGCTCCAAGCCTTCAAC
SALK048655_REV	TGCCCCAAACTATACCACTTG
SALK092291C_FOR	TGCGTTGTTGTTTTTGTTTTC
SALK092291C_REV	ACAAACATCGCATTTGGAAAC
SALK034566_FOR	CTGTACATCCCCAAAAATCATG
SALK034566_REV	ACCTGAGAGACATAACGGCAG
SAIL_761_D09_FOR	ATAATCTCCACGAAACATGCG
SAIL_761_D09_REV	CTCCCTCCGGTTTCTTAAAAG
CAMEL_FOR	TCAAACCAGTCCAATGGCGA
CAMEL_REV	TCCTTTGCCGAGGACTTGAC
CANAR_FOR	TGTTCGGCTTTAAACACAATAAATC
CANAR_REV	GTTGCTCAGACTGCCAATGC
WRKY23_FOR	AGTCTCGGTAATGGTTGCTTTGG
WRKY23_REV	TGTTGCTGCTGTTGGTGATGG
TUB-2_FOR	ACTCGTTGGGAGGAGGAACT
TUB-2_REV	ACACCAGACATAGTAGCAGAAATCAAG
LHT1_FOR	GCCATCTACAAACCCAAGAAATAC
LHT1_REV	TGCTTGAATAACGATTGTCCTTAG
AZI1_FOR	ACCCTTACAACACCGAATATAAC
AZI1_REV	GTGGAGGAGGACATTGGAC
EARLI1_FOR	GTGATGCCCGTGCACAAATA
EARLI1_REV	AGTCTCACTCTCACACATTGGT
AZI3_FOR	ACACATACGACGCACACAGT
AZI3_REV	TGCGCGGAAAAAGATAACGC
AZI4_FOR	CTTAACCACTGCTACTGATTGTC
AZI4_REV	GGACCGAAGGACTTGGAATC
EXP20_FOR	AAGTGGTTGGTGTGAAAG
EXP20_REV	TTCCTTGGTATGTCATTCC

Table S3. 2 List of primers used in this study for genotyping and qRT-PCR

Primer	Sequence
CAMEL_attB1_Fw	5 - GGGGACAAGTTTGTACAAAAAAGCAGGCTTCATGGAAGAGTTTCGTTTTCTC - 3
CAMEL_attB2_Rv	5 - GGGGACCACTTTGTACAAGAAAGCTGGGTTTCAATAGTTCTTGTTACTCT-CTTC - 3
CAMEL_NS_attB2_Rv	5 - GGGGACCACTTTGTACAAGAAAGCTGGGTTTGGTTCCCAATAGTTCTTGTTACTCTCTTC - 3
CANAR_attB1_Fw	5 - GGGGACAAGTTTGTACAAAAAAGCAGGCTGAAAAAGTATTAAAGTAGTA - 3
CANAR_NS_attB2_Rv	5 - GGGGACCACTTTGTACAAGAAAGCTGGGTAACTCACGAGAAAAACTTCT - 3
CAMEL_CD_(EcoRI)	5 - GGAATTCTGGAGAATCAGAAACCGGAGAAAC - 3
CAMEL_CD_(XhoI)	5 - CCGCTCGAGATAGTTCTTGTTACTCTCTTCTCT - 3
CANAR_CD_(EcoRI)	5 - GGAATTCAACGTGCACGCCCGATCTAGTGTTTC - 3
CANAR_CD_(XhoI)	5 - CCGCTCGAGCTCTAAGTCATGAGAGGGACATTG - 3
M13 F	5 - TGTAAAACGACGGCCAGT - 3
M13 R	5 - CAGGAAACAGCTATGACC - 3

Table S3. 3 List of primers used in this study for cloning.

3.8 *References*

1. T. Berleth, T. Sachs, Plant morphogenesis: long-distance coordination and local patterning. *Curr. Opin. Plant Biol.* **4**, 57–62 (2001).

2. M. Adamowski, J. Friml, PIN-Dependent Auxin Transport: Action, Regulation, and Evolution. *Plant Cell Online*. **27**, 20–32 (2015).

3. E. Benková, M. Michniewicz, M. Sauer, T. Teichmann, D. Seifertová, G. Jürgens, J. Friml, Local, Efflux-Dependent Auxin Gradients as a Common Module for Plant Organ Formation. *Cell*. **115**, 591–602 (2003).

4. J. Balla, P. Kalousek, V. Reinöhl, J. Friml, S. Procházka, Competitive canalization of PIN-dependent auxin flow from axillary buds controls pea bud outgrowth. *Plant J.* **65**, 571–577 (2011).

5. E. Scarpella, D. Marcos, J. Friml, T. Berleth, Control of leaf vascular patterning by polar auxin transport. *Genes Dev.* **20**, 1015–1027 (2006).

6. H. S. Robert, P. Grones, A. N. Stepanova, L. M. Robles, A. S. Lokerse, J. M. Alonso, D. Weijers, J. Friml, Local auxin sources orient the apical-basal axis in Arabidopsis embryos. *Curr. Biol. CB*. **23**, 2506–2512 (2013).

7. E. Mazur, E. Benková, J. Friml, Vascular cambium regeneration and vessel formation in wounded inflorescence stems of Arabidopsis. *Sci. Rep.* **6** (2016), doi:10.1038/srep33754.

8. M. Sauer, J. Balla, C. Luschnig, J. Wiśniewska, V. Reinöhl, J. Friml, E. Benková, Canalization of auxin flow by Aux/IAA-ARF-dependent feedback regulation of PIN polarity. *Genes Dev.* **20**, 2902–2911 (2006).

9. A. Vieten, S. Vanneste, J. Wisniewska, E. Benkova, R. Benjamins, T. Beeckman, C. Luschnig, J. Friml, Functional redundancy of PIN proteins is accompanied by auxin-dependentcross-regulation of PIN expression. *Development*. **132**, 4521–4531 (2005).

10. T. Paciorek, E. Zazímalová, N. Ruthardt, J. Petrásek, Y.-D. Stierhof, J. Kleine-Vehn, D. A. Morris, N. Emans, G. Jürgens, N. Geldner, J. Friml, Auxin inhibits endocytosis and promotes its own efflux from cells. *Nature*. **435**, 1251–1256 (2005).

11. M. Glanc, M. Fendrych, J. Friml, Mechanistic framework for cell-intrinsic re-establishment of PIN2 polarity after cell division. *Nat. Plants*. **4**, 1082–1088 (2018).

12. K. Wabnik, J. Kleine-Vehn, J. Balla, M. Sauer, S. Naramoto, V. Reinöhl, R. M. H. Merks, W. Govaerts, J. Friml, Emergence of tissue polarization from synergy of intracellular and extracellular auxin signaling. *Mol. Syst. Biol.* **6** (2010), doi:10.1038/msb.2010.103.

13. T. Prát, J. Hajný, W. Grunewald, M. Vasileva, G. Molnár, R. Tejos, M. Schmid, M. Sauer, J. Friml, WRKY23 is a component of the transcriptional network mediating auxin feedback on PIN polarity. *PLOS Genet.* **14**, e1007177 (2018).

14. W. Grunewald, M. Karimi, K. Wieczorek, E. Van de Cappelle, E. Wischnitzki, F. Grundler, D. Inze, T. Beeckman, G. Gheysen, A Role for AtWRKY23 in Feeding Site Establishment of Plant-Parasitic Nematodes. *PLANT Physiol.* **148**, 358–368 (2008).

15. W. Grunewald, I. De Smet, D. R. Lewis, C. Löfke, L. Jansen, G. Goeminne, R. V. Bossche, M. Karimi, B. De Rybel, B. Vanholme, Transcription factor WRKY23 assists auxin distribution patterns during Arabidopsis root development through local control on flavonol biosynthesis. *Proc. Natl. Acad. Sci.* **109**, 1554–1559 (2012).

16. S. Vanneste, Cell Cycle Progression in the Pericycle Is Not Sufficient for SOLITARY ROOT/IAA14-Mediated Lateral Root Initiation in Arabidopsis thaliana. *PLANT CELL ONLINE*. **17**, 3035–3050 (2005).

17. E. Smakowska-Luzan, G. A. Mott, K. Parys, M. Stegmann, T. C. Howton, M. Layeghifard, J. Neuhold, A. Lehner, J. Kong, K. Grünwald, N. Weinberger, S. B. Satbhai, D. Mayer, W. Busch, M. Madalinski, P. Stolt-Bergner, N. J. Provart, M. S. Mukhtar, C. Zipfel, D. Desveaux, D. S. Guttman, Y. Belkhadir, An extracellular network of *Arabidopsis* leucine-rich repeat receptor kinases. *Nature*. **553**, 342 (2018).

18. A. Khan, O. Fornes, A. Stigliani, M. Gheorghe, J. A. Castro-Mondragon, R. van der Lee, A. Bessy, J. Chèneby, S. R. Kulkarni, G. Tan, D. Baranasic, D. J. Arenillas, A. Sandelin, K. Vandepoele, B. Lenhard, B. Ballester, W. W. Wasserman, F. Parcy, A. Mathelier, JASPAR 2018: update of the open-access database of transcription factor binding profiles and its web framework. *Nucleic Acids Res.* **46**, D260–D266 (2018).

19. D. Chinchilla, C. Zipfel, S. Robatzek, B. Kemmerling, T. Nürnberger, J. D. G. Jones, G. Felix, T. Boller, A flagellin-induced complex of the receptor FLS2 and BAK1 initiates plant defence. *Nature*. **448**, 497–500 (2007).

20. K. H. Nam, J. Li, BRI1/BAK1, a Receptor Kinase Pair Mediating Brassinosteroid Signaling. *Cell*. **110**, 203–212 (2002).

21. J. Santiago, C. Henzler, M. Hothorn, Molecular Mechanism for Plant Steroid Receptor Activation by Somatic Embryogenesis Co-Receptor Kinases. *Science*. **341**, 889–892 (2013).

22. Y. Sun, L. Li, A. P. Macho, Z. Han, Z. Hu, C. Zipfel, J.-M. Zhou, J. Chai, Structural Basis for flg22-Induced Activation of the Arabidopsis FLS2-BAK1 Immune Complex. *Science*. **342**, 624–628 (2013).

23. G. A. Mott, E. Smakowska-Luzan, A. Pasha, K. Parys, T. C. Howton, J. Neuhold, A. Lehner, K. Grünwald, P. Stolt-Bergner, N. J. Provart, M. S. Mukhtar, D. Desveaux, D. S. Guttman, Y. Belkhadir, Map of physical interactions between extracellular domains of Arabidopsis leucine-rich repeat receptor kinases. *Sci. Data*. **6**, 190025 (2019).

24. H. Wallrabe, A. Periasamy, Imaging protein molecules using FRET and FLIM microscopy. *Curr. Opin. Biotechnol.* **16**, 19–27 (2005).

25. J. Friml, A. Vieten, M. Sauer, D. Weijers, H. Schwarz, T. Hamann, R. Offringa, G. Jürgens, Efflux-dependent auxin gradients establish the apical–basal axis of Arabidopsis. *Nature*. **426**, 147–153 (2003).

26. E. Mazur, I. Kulik, J. Hajný, J. Friml, Auxin canalization and vascular tissue formation by TIR1/AFB-mediated auxin signaling in Arabidopsis. *New Phytol.* **226**, 1375–1383 (2020).

27. N. Geldner, J. Friml, Y.-D. Stierhof, G. Jürgens, K. Palme, Auxin transport inhibitors block PIN1 cycling and vesicle trafficking. *Nature*. **413**, 425–428 (2001).

4 Convergence of auxin and peptide signaling mediates auxin canalization

4.1 *Introduction*

To get more mechanistic insight into the CAMEL/CANAR complex dynamics, we sought to identify putative ligand/s which may influence CAMEL/CANAR complex stability or CAMEL/CANAR-PIN1 interaction. Previous testing of auxin effect on the CAMEL/CANAR interaction disproved auxin to be a potential ligand (Fig 3.1G and H). Since the CAMEL/CANAR complex is important for vasculature formation and regeneration, obvious suspects were *CLAVATA3/EMBRYO SURROUNDING REGION (CLE)* peptide ligands, which were implicated in the regulation of vasculature development (Hazak et al., 2017, p.; Hirakawa et al., 2008; Whitford et al., 2008). Moreover, *CLE41/44* was found together with *WRKY23* in our first microarray designed to find downstream players of auxin TIR1/AFB signaling (Appendix Tab S2.1).

To date, CLE peptides were also reported to regulate other processes such as seed development, lateral root establishment, stem cell homeostasis in the shoot apical meristem (SAM) and the root apical meristem (RAM) (Czyzewicz et al., 2013; Ingram and Gutierrez-Marcos, 2015). CLE genes are present in many plant species and some plant parasitic nematodes. In *Arabidopsis*, the CLE family encompasses 32 members encoding 27 distinct CLE peptides. CLE precursor proteins consist of an N-terminal signal peptide and 12-14 conserved C-terminal amino acids, called the CLE domain from which, after post-translational modifications such as glycosylation and hydroxylation (Matsubayashi, 2011) a mature peptide is produced through proteolytic cleavage (Fukuda and Hardtke, 2020; Wang et al., 2016). The CLE peptides can be divided into two functional classes: *(i)* A-type CLE peptides (CLV3, CLE1-27, CLE40 and CLE45), which have the ability to arrest primary root growth by suppression of protopholem sieve element differentiation (Rodriguez-Villalon et al., 2014) and *(ii)* B-type CLE peptides (CLE41-CLE44), which suppress differentiation in vasculature tracheary elements (Whitford et al., 2008). CLEs peptides are perceived by leucine-rich repeat receptor-like kinases LRR-RLKs, which translate CLE input into intracellular signaling (Betsuyaku et al., 2011; Murphy et al., 2012). Despite a vast number of LRR-RLKs in *Arabidopsis*, only limited amount of CLE receptors were identified (Zhang et al., 2016a).

Here, we provide preliminary observation indicating that CAMEL and CANAR kinases may be new receptors for CLE25, CLE26 and CLE27 peptides. Based on defective auxin-mediated PIN1 repolarization after CLE25, CLE26, CLE27 treatments and in respective mutants, on *canar-1* partial resistance to the inhibitory effect of CLE25, CLE26 and CLE27 on root growth and based on *in vitro* binding of CLE peptides to the extracellular domain of CAMEL and CANAR, we presume that binding of CLEs to the CAMEL-CANAR complex might cause dissociation of the complex, which releases CAMEL from the inhibitory effect of CANAR and promotes CAMEL's kinase activity.

4.2 *Results*

4.2.1 CLE25, CLE26 and CLE27 are important for auxin feedback on PIN polarity

Given the fact that auxin is a main driving force of canalization (Sachs, 1975), we presumed that putative CAMEL/CANAR ligand/s should be auxin-regulated. Hence, we focused on three CLEs: (i) CLE26 which was reported to be auxin regulated in seedling roots, altered auxin distribution in roots and decreased the abundance of pPIN1::PIN1-GFP (Nathan Czyzewicz et al., 2015) and (ii) CLE27 and CLE41/44, which were auxin up-regulated in a microarray performed by Nathan Czyzewicz et al. (2015).

Since overexpression of some CLE genes resulted in similar root growth inhibitory phenotypes (Strabala et al., 2006) and mutants of CLEs did not display strong phenotypes (Gregory et al., 2018), a high degree of redundancy among CLEs is expected, which prompted us to test CLE26, CLE27 and CLE41/44 and also the relevant closest paralogs such as CLE25, CLE42 with CLE46 (Ito et al., 2006).

To mimic overexpression of CLE genes, we used a synthetic version of secreted CLE peptides and tested their effect on auxin-mediated PIN1 repolarization. Normally, PIN1 is localized basally in root endodermal cells and after prolonged auxin treatment (NAA, 4h, 10 µM) PIN1 repolarizes to the inner lateral side of these cells (Sauer et al., 2006b). After 6h treatment of 10 µM CLE41/44, CLE42, CLE46, CLE25, CLE26 and CLE27, no changes in PIN1 basal polarity were observed (Fig 4.1A and B). Interestingly, 2h pretreatment of 10 µM CLEs with subsequent co-incubation of 10 µM NAA/CLEs showed reduced auxin-mediated repolarization of PIN1 for CLE25, CLE26 and CLE27. Next, we evaluated PIN1 polar localization

in roots in available CLE mutants (provided by prof. Takashi Ishida). No change of PIN1 localization was observed for any of the tested genotypes: *cle41/44, cle42, cle25, cle26, cle25/26, cle1/2/3/4/5/6/7/19/25/27/41/46* (hereafter referred to as *cle duodecuple).* After auxin treatment (NAA, 4h, 10 µM), only *cle25, cle26, cle25/26, cle27* and *cle duodecuple* mutant lines exhibited decreased auxin-mediated repolarization of PIN1 in endodermis, similar to CLE25/26/27 synthetic peptide treatment, suggesting a fine-tuning mechanism of CLEs on auxin feedback on PIN polarity.

Then, we tested a manifestation of auxin feedback on its own cell-to-cell transport – vasculature formation (Scarpella et al., 2006b). We analyzed the venation pattern in cotyledons of *cle* mutant lines, which exhibited reduced auxin-mediated PIN1 repolarization in the previous PIN1 experiments (Fig 4.1C-D), namely *cle25, cle26, cle25/26, cle27* and *cle duodecuple.* All tested mutants showed more frequent abnormal patterning of the vasculature compared to wild type cotyledons. The higher order mutants exhibited the highest incidence of defects, indicating functional redundancy of CLEs (Fig 4.1E and F).

Altogether, these results show that CLE25, CLE26 and CLE27 play a role in auxin feedback on PIN1 polarity and during vasculature development.

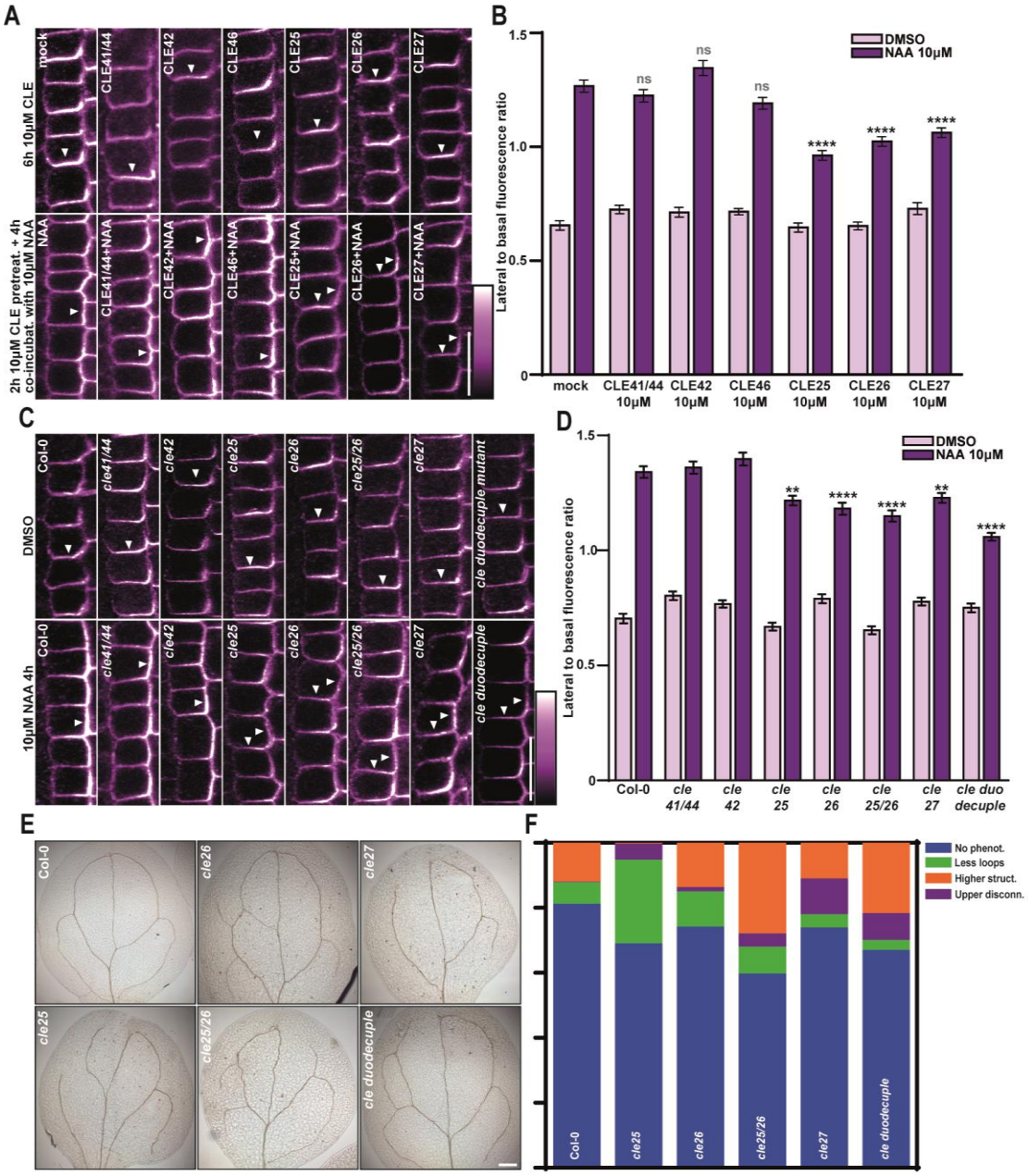

Figure 4. 1 CLE25, CLE26 and CLE27 regulate auxin-mediated PIN1 repolarization and vasculature formation.

(A) and (C) Representative images of immunolocalization of PIN1 in endodermis of root meristem after 4h 10 µM NAA treatment. Auxin-mediated repolarization is reduced in *cle25, cle26, cle25/26, cle27 and cle1/2/3/4/5/6/7/19/25/27/41/46* mutants and after 2h 10 µM pretreatment of CLE25, CLE26, CLE27 with subsequent co-incubation of 10 µM CLEs/NAA for 4h (white arrowheads). Scale bar: 10 µm. (B) and (D) Quantitative evaluation of (A) and (C), respectively, showing the mean PIN1 lateral-to-basal signal intensity ratio in endodermis cells. Error bars indicate SEM. The experiment was carried out three times, one representative experiment is presented. A One-Way ANOVA test compared marked datasets (**<p0.01, ****p<0.0001; n>50 cells corresponding to a minimum of 10 roots per

treatment and experiments were imaged using comparable settings). (E) Representative images of vasculature defects in cotyledons of *cle25, cle26, cle25/26, cle27* and *cle1/2/3/4/5/6/7/19/25/27/41/46* mutants. All tested mutants showed an increase in frequency of vasculature defects. The scored categories were: No phenotype, less loops, higher structure (including extra loops or branches) and upper disconnectivity. Scale bar: 100 µm. (F) Quantification of vasculature defects in (E) (n>65 for each genotype).

4.2.2 CLE25, CLE26 and CLE27 are putative ligands for CAMEL/CANAR complex.

Since receptors and co-receptors involved in CLE signaling, such as CLV1, BAM3, CLERK and CRN, exhibit resistance to root growth inhibition by A-type CLEs (Anne et al., 2018), we germinated *camel-1*/*canar-1* mutants on medium containing 10 nM CLE25, 10 nM CLE26 or 100 nM CLE27 peptide and analysed the extent of primary root inhibition to verify involvement of CAMEL or CANAR in CLE signaling. Interestingly, only the *canar-1* mutant showed partial resistance to the root inhibitory effect of the tested CLEs (Fig 4.2A), meaning that CANAR is important for fully sensing CLE25, CLE26 and CLE27 in the root.

To test if these CLEs can bind to CAMEL or CANAR and serve as putative ligands, we performed MicroScale Thermophoresis (MST) binding assay. This technique can quantify biomolecular interactions based on the directed movement of molecules through a temperature gradient -thermophoresis-, using either covalently attached or intrinsic fluorophores. Thermophoresis strongly depends on molecular properties such as size, charge and conformation (Jerabek-Willemsen et al., 2014). All MST experiments were carried out with purified extracellular domain of CAMEL and CANAR from BESV cell cultures. Firstly, we validated and optimized the method by testing CAMEL-CANAR interaction. Indeed, CAMEL-CANAR showed a strong interaction represented by a Kd of 174 nM (Fig 4.2B). With this optimized MST protocol, we tested binding of CLEs to CAMEL and CANAR. CAMEL showed binding to CLE25 (Kd=27,8 µM), CLE26 (Kd=3,3 µM) and to CLE27 (Kd=16,3 µM) (Fig 4.2C, D and E), which is surprising given the fact that *camel-1* mutant had no resistance to the inhibitory effect of these peptides (Fig 4.2A). CANAR exhibited binding to CLE27 (Kd=36,5 µM) (Fig 4.2F), which is in line with the partial resistance of *canar-1* to CLE27 in the root growth inhibition assay. Binding of CLE25 and CLE26 to CANAR still remains to be tested. As a negative control we used CLE46, which did not show any interference with auxin-mediated PIN1 repolarization (Fig 4.1A and B). CLE46 did only weakly bind to CANAR, as evidenced by a high

Kd=262 µM and because of the non-sigmoidal profile of measured values this Kd value might even be an overestimation (Fig 4.2G).

Overall, CAMEL and CANAR might be receptors for CLE25, CLE26 and CLE27, although, the CLE binding needs to be confirmed by other independent binding assays. Importantly, the influence of CLE25, CLE26 and CLE27 binding on the stability of the CAMEL/CANAR complex *in vivo* and the activation of downstream signaling should be addressed in the future.

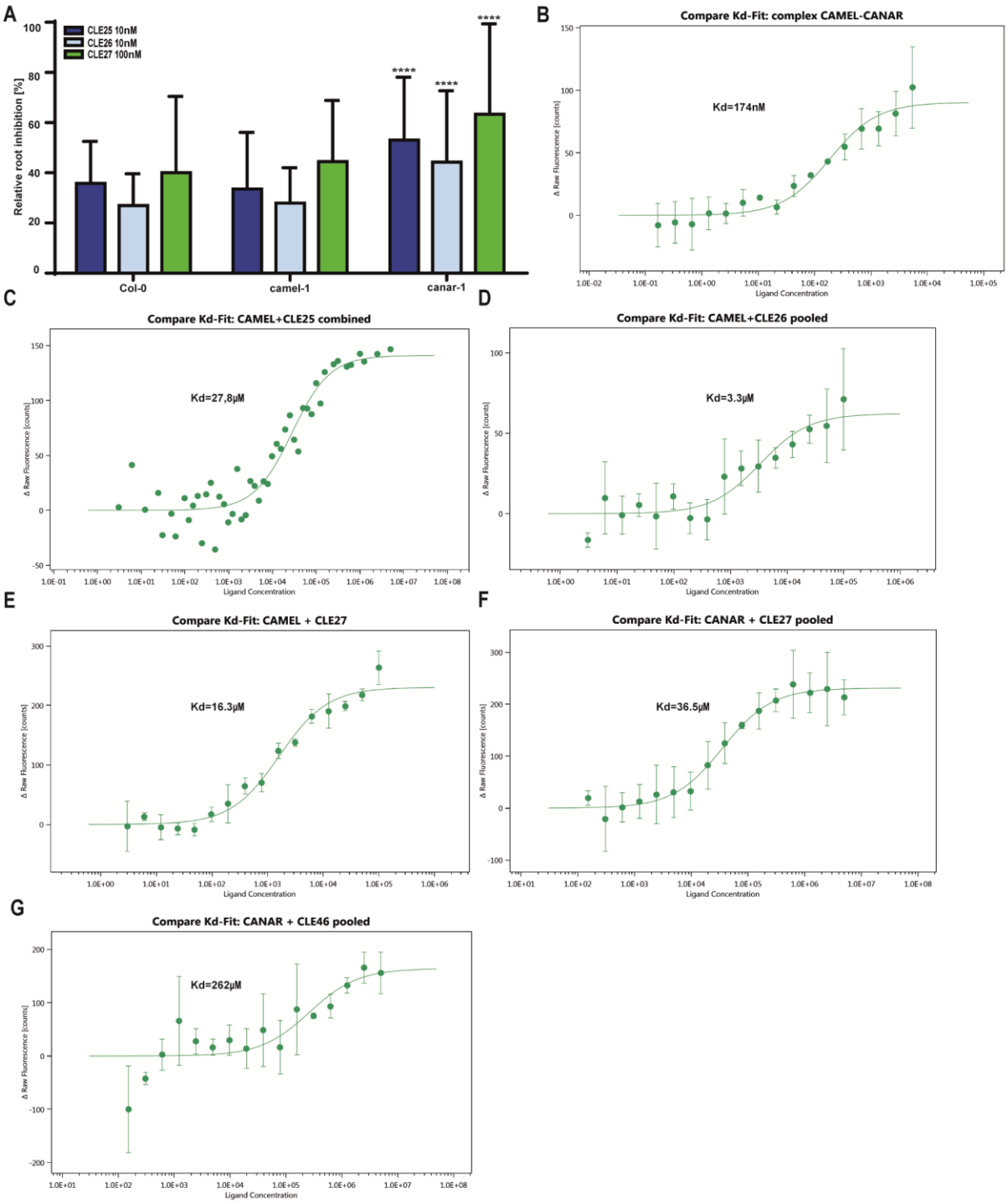

Figure 4. 2 Binding assays of CLE25, CLE26, CLE27 and CLE46 to CAMEL and CANAR

(A) Relative root growth of *camel-1* and *canar-1* mutants 6 days after germination on 10 nM CLE25, 10 nM CLE26 and 100 nM CLE27. Error bars indicate standard deviation. (B-G) MST binding experiments of CAMEL and CANAR. Ligand concentrations are in nM. Error bars represent standard deviation. All experiment were performed three times.

4.3 *Discussion*

Our results revealed that CLE25, CLE26 and CLE27 peptide application interfered with auxin-mediated PIN1 repolarization. Akin outcome was observed with using *cle25, cle26, cle27, cle25/26* and *cle1/2/3/4/5/6/7/19/25/27/41/46* mutants. Similar results of CLE overexpression and CLE mutants imply that CLE25, CLE26 and CLE27 play a role in fine-tuning the auxin feedback on PIN polarity. Increased vasculature abnormalities in *cle25, cle26, cle27, cle25/26* and *cle1/2/3/4/5/6/7/19/25/27/41/46* mutants extends the CLE effect to the whole auxin canalization process, however, more auxin canalization-related phenotypes such as vasculature regeneration in wounded stems and PIN1-positive auxin channels formation after local auxin application need to be analysed.

The extracellular domain of both CAMEL and CANAR can bind CLEs *in vitro*, however, only *canar-1* is partially resistant to the root inhibition of CLE25/26/27. This proposes that CANAR is a new player in CLE signaling. On the other hand, binding of CAMEL to CLE25/26/27 while lacking resistance for their root inhibitory effects makes it less likely that CAMEL plays a role in CLE signaling. Alternatively a scenario where CLE peptides regulate a CAMEL CLE signaling-independent interactome could exist. In our hypothesis, constitutive CAMEL/CANAR interaction can be disrupted by auxin-regulated CLE25/26/27 thereby releasing CAMEL from the inhibiton of the pseudokinase CANAR and resulting in phosphorylation of PINs and ultimately to their repolarization.

Recent observations in leaves suggest that inhibition of auxin transport by auxin transport inhibitors or by genetical removal of all auxin transporters still allows auxin to induce, albeit abnormally, vacular strands formation (Verna et al., 2019). The explanation herefor can be either the existence of other, so far unknown auxin transporters, which are insenstitive to the applied auxin transport inhibitors, or that there is another auxin-derived signal, which drives auxin canalization. Based on the fact that CLE25 was reported a long-distance signaling molecule transported from the root to the shoot to induce stomatal closure

via abscisic acid accumulation during dehydration stress (Takahashi et al., 2018) and based on the evidence we provided here, we believe that the CLE gradient, possibly in conjuction with an auxin gradient provides cells with spatiotemporal information for coordinated PIN repolarization to induce auxin canalization.

Moreover, CLE25 and CLE26 are important for phloem development in *Arabidopsis thaliana* (Anne et al., 2018, p. 25; Ren et al., 2019). This offers a plausible scenario in which CLEs act as a link between auxin canalization secured by CAMEL/CANAR complex, to mark the positions of future vascular strands, and initiation of actual vasculature formation provided by the CLE25/26/27 signaling pathway. We hypothetize that CANAR, due to its partial resistance to CLE25/CLE26/CLE27, might be the mediator between auxin and CLE signaling.

4.4 *Material and methods*

Plant material and growth conditions

All *Arabidopsis thaliana* lines were in the Columbia-0 background. T-DNA mutants were acquired from the Nottingham *Arabidopsis* Stock Centre (NASC; http://www.arabidopsis.info). T-DNA mutants used in this study are SALK_025603C (*camel-1*), SALK_055351C (*canar-1*). Primers used for genotyping are listed in Supplemental Tab. 2.2. The *cle25, cle26, cle27, cle25/26, cle1/2/3/4/5/6/7/19/25/27/41/46* mutants were kindly provided by prof. Takashi Ishida. Seeds were sterilized overnight by chlorine gas, sown on solid *Arabidopsis* medium (AM+: half-strength MS basal salts, 1% sucrose, and 0.8% phyto-agar, pH 5.7), and stratified at 4°C for at least 2 days prior to transfer to a growth room with a 16-h-light/8-h-dark light cycle at 21°C. Seedlings were grown vertically for 4 or 6 days, depending on the assay.

Fluorescent Labeling for Microscale Thermophoresis Studies

Both recombinant proteins were labeled with fluorescent Dye RED-NHS 2nd Generation (NanoTemper Technologies) using Monolith Protein Labeling Kit RED-NHS 2nd Generation (NanoTemper Technologies) according to manual. Both proteins were labelled in 20mM NaH_2PO_4/Na_2HPO_4 pH 7,5 buffer containing 200 mM NaCl and were eluted using the same buffer with addition of 0.01% (w/v) TWEEN®20.

Quantitative Interaction Studies by Microscale Thermophoresis

Protein-protein and protein-peptide interactions were analyzed by microscale thermophoresis (MST) (Duhr and Braun, 2006; Jerabek-Willemsen et al., 2011). Experiments were performed on a Monolith NT.115 Blue/Green (NanoTemper Technologies). Measurements were performed in premium glass capillaries (NanoTemper Technologies). All measurement were carried in 20mM NaH_2PO_4/Na_2HPO_4 pH 7,5, 200 mM NaCl, 0.01% (w/v) TWEEN®20 buffer.For binding studies of CAMEL to CANAR, proteins were used as follows: 25 nM of labeled CAMEL, 5,5 µM as the highest, and 0,168 nM as the lowest CANAR concentration. Measurements were performed at 40% MST power with excitation power 100%. The experiment was performed in 2 independent replicates.For binding studies of CANAR to CLE27, protein and peptide were used as follows: 100 nM of labeled CANAR, 5 mM as the highest, and 153 nM as the lowest CLE27 concentration. Measurements were performed at 60% MST power with excitation power 60%. The experiment was performed in 3 independent replicates. For binding studies of CANAR to CLE46, protein and peptide were used as follows: 100 nM of labeled CANAR, 5 mM as the highest, and 153 nM as the lowest CLE46 concentration. Measurements were performed at 60% MST power with excitation power 60%. The experiment was performed in 3 independent replicates. For binding studies of CAMEL to CLE27, protein and peptide were used as follows: 100 nM of labeled CAMEL, 1 mM as the highest, and 3,05 nM as the lowest CLE27 concentration. Measurements were performed at 40% MST power with excitation power 80%. The experiment was performed in 3 independent replicates. For binding studies of CAMEL to CLE26, protein and peptide were used as follows: 100 nM of labeled CAMEL, 1 mM as the highest, and 3,05 nM as the lowest CLE26 concentration. Measurements were performed at 40% MST power with excitation power 80%. The experiment was performed in 2 independent replicates. For binding studies of CAMEL to CLE25, protein and peptide were used as follows: 100 nM of labeled CAMEL, 5 mM as the highest, and 3,05 nM as the lowest CLE26 concentration. Measurement was performed at 40% MST power with excitation power 80%. The experiment was performed once. For binding studies of CAMEL to CLE44/41, protein and peptide were used as follows: 100 nM of labeled CAMEL, 1 mM as the highest, and 3,05 nM as the lowest CLE44/41 concentration. Measurement was performed at 40% MST power with excitation power 80%. The experiment was performed once. Results were analyzed in MO.Affinity Analysis software (NanoTemper Technologies). The biding affinities were calculated from Δ Raw fluorescence.

All dissociation constants (Kd) were calculated to a binding model assuming a 1:1 stoichiometry per binding partner.

Whole-mount *in situ* immunolocalization, microscopy and quantitative analysis of PIN repolarization

PIN immunolocalizations in primary root were performed as described (Sauer and Friml, 2010). The anti-PIN1 antibody was used in the 1:1000 dilution. The secondary goat anti-rabbit antibody coupled to Cy3 (Sigma-Aldrich) was diluted 1:600. Confocal microscopy was performed using a Zeiss LSM 700 confocal microscope. Quantitative analysis of PIN relocalization was performed as described (Sauer et al., 2006b).

Cotyledon vasculature analysis

12-day-old seedlings were left in 70% ethanol overnight to remove chlorophyll and seedlings were cleared according to the protocol described in the vasculature regeneration assay after wounding section. Finally, seedlings were mounted in 50% glycerol and monitored by differential interference contrast microscopy (Olympus BX53) or stereomicroscope (Olympus SZX16).

4.5 *Acknowledgements*

We thank the Bioimaging and Plant Facility at IST Austria for providing a great service and assistance. We would also like to thank Vienna Biocenter Core Facilities (VBCF) for recombinant protein cloning, production and purification. This project has received funding from the European Research Council (ERC) under the European Union's Horizon 2020 research and innovation program (grant agreement No 742985) and Austrian Science Fund (FWF): I 3630-B25 to J.Friml. J.Hajný is recipient of a DOC Fellowship of the Austrian Academy of Sciences at the Institute of Science and Technology.

4.6 *Author contribution*

Jakub Hajný:

- Immunolocalization of PIN1 (Fig 4.1A-D)
- Fenotypic analysis of venation pattern in cotyledons (Fig 4.1E and F)

- Fenotypic analysis of root inhibition after CLEs treatment (Fig 4.2A)

4.7 *References*

1. O. Hazak, B. Brandt, P. Cattaneo, J. Santiago, A. Rodriguez-Villalon, M. Hothorn, C. S. Hardtke, Perception of root-active CLE peptides requires CORYNE function in the phloem vasculature. *EMBO Rep.* **18**, 1367–1381 (2017).

2. Y. Hirakawa, H. Shinohara, Y. Kondo, A. Inoue, I. Nakanomyo, M. Ogawa, S. Sawa, K. Ohashi-Ito, Y. Matsubayashi, H. Fukuda, Non-cell-autonomous control of vascular stem cell fate by a CLE peptide/receptor system. *Proc. Natl. Acad. Sci.* **105**, 15208–15213 (2008).

3. R. Whitford, A. Fernandez, R. D. Groodt, E. Ortega, P. Hilson, Plant CLE peptides from two distinct functional classes synergistically induce division of vascular cells. *Proc. Natl. Acad. Sci.* **105**, 18625–18630 (2008).

4. N. Czyzewicz, K. Yue, T. Beeckman, I. D. Smet, Message in a bottle: small signalling peptide outputs during growth and development. *J. Exp. Bot.* **64**, 5281–5296 (2013).
5. G. Ingram, J. Gutierrez-Marcos, Peptide signalling during angiosperm seed development. *J. Exp. Bot.* **66**, 5151–5159 (2015).

6. Y. Matsubayashi, Small Post-Translationally Modified Peptide Signals in Arabidopsis. *Arab. Book Am. Soc. Plant Biol.* **9** (2011), doi:10.1199/tab.0150.

7. H. Fukuda, C. S. Hardtke, Peptide Signaling Pathways in Vascular Differentiation. *Plant Physiol.* **182**, 1636–1644 (2020).

8. G. Wang, G. Zhang, M. Wu, CLE Peptide Signaling and Crosstalk with Phytohormones and Environmental Stimuli. *Front. Plant Sci.* **6** (2016), doi:10.3389/fpls.2015.01211.

9. A. Rodriguez-Villalon, B. Gujas, Y. H. Kang, A. S. Breda, P. Cattaneo, S. Depuydt, C. S. Hardtke, Molecular genetic framework for protophloem formation. *Proc. Natl. Acad. Sci.* **111**, 11551–11556 (2014).

10. S. Betsuyaku, S. Sawa, M. Yamada, The Function of the CLE Peptides in Plant Development and Plant-Microbe Interactions. *Arab. Book Am. Soc. Plant Biol.* **9** (2011), doi:10.1199/tab.0149.

11. E. Murphy, S. Smith, I. De Smet, Small Signaling Peptides in Arabidopsis Development: How Cells Communicate Over a Short Distance. *Plant Cell*. **24**, 3198–3217 (2012).

12. H. Zhang, X. Lin, Z. Han, L.-J. Qu, J. Chai, Crystal structure of PXY-TDIF complex reveals a conserved recognition mechanism among CLE peptide-receptor pairs. *Cell Res.* **26**, 543–555 (2016).

13. T. Sachs, The induction of transport channels by auxin. *Planta*. **127**, 201–206 (1975).

14. Nathan Czyzewicz, C.-L. Shi, L. D. Vu, B. Van De Cotte, C. Hodgman, M. A. Butenko, Modulation of *Arabidopsis* and monocot root architecture by CLAVATA3/EMBRYO SURROUNDING REGION 26 peptide. *J. Exp. Bot.* **66**, 5229–5243 (2015).

15. T. J. Strabala, P. J. O'Donnell, A.-M. Smit, C. Ampomah-Dwamena, E. J. Martin, N. Netzler, N. J. Nieuwenhuizen, B. D. Quinn, H. C. C. Foote, K. R. Hudson, Gain-of-Function Phenotypes of Many CLAVATA3/ESR Genes, Including Four New Family Members, Correlate with Tandem Variations in the Conserved CLAVATA3/ESR Domain. *Plant Physiol.* **140**, 1331–1344 (2006).

16. E. F. Gregory, T. Q. Dao, M. A. Alexander, M. J. Miller, J. C. Fletcher, The signaling peptide-encoding genes CLE16, CLE17 and CLE27 are dispensable for Arabidopsis shoot apical meristem activity. *PloS One*. **13**, e0202595 (2018).

17. Y. Ito, I. Nakanomyo, H. Motose, K. Iwamoto, S. Sawa, N. Dohmae, H. Fukuda, Dodeca-CLE Peptides as Suppressors of Plant Stem Cell Differentiation. *Science*. **313**, 842–845 (2006).

18. M. Sauer, J. Balla, C. Luschnig, J. Wiśniewska, V. Reinöhl, J. Friml, E. Benková, Canalization of auxin flow by Aux/IAA-ARF-dependent feedback regulation of PIN polarity. *Genes Dev.* **20**, 2902–2911 (2006).

19. E. Scarpella, D. Marcos, J. Friml, T. Berleth, Control of leaf vascular patterning by polar auxin transport. *Genes Dev.* **20**, 1015–1027 (2006).

20. P. Anne, A. Amiguet-Vercher, B. Brandt, L. Kalmbach, N. Geldner, M. Hothorn, C. S. Hardtke, CLERK is a novel receptor kinase required for sensing of root-active CLE peptides in *Arabidopsis*. *Development*. **145**, dev162354 (2018).

21. M. Jerabek-Willemsen, T. André, R. Wanner, H. M. Roth, S. Duhr, P. Baaske, D. Breitsprecher, MicroScale Thermophoresis: Interaction analysis and beyond. *J. Mol. Struct.* **1077**, 101–113 (2014).

22. C. Verna, S. J. Ravichandran, M. G. Sawchuk, N. M. Linh, E. Scarpella, Coordination of tissue cell polarity by auxin transport and signaling. *eLife*. **8**, e51061 (2019).

23. F. Takahashi, T. Suzuki, Y. Osakabe, S. Betsuyaku, Y. Kondo, N. Dohmae, H. Fukuda, K. Yamaguchi-Shinozaki, K. Shinozaki, A small peptide modulates stomatal control via abscisic acid in long-distance signalling. *Nature*. **556**, 235 (2018).

24. S.-C. Ren, X.-F. Song, W.-Q. Chen, R. Lu, W. J. Lucas, C.-M. Liu, CLE25 peptide regulates phloem initiation in Arabidopsis through a CLERK-CLV2 receptor complex. *J. Integr. Plant Biol.* **61**, 1043–1061 (2019).

25. M. Sauer, J. Friml, in *Plant Developmental Biology: Methods and Protocols*, L. Hennig, C. Köhler, Eds. (Humana Press, Totowa, NJ, 2010; https://doi.org/10.1007/978-1-60761-765-5_17), *Methods in Molecular Biology*, pp. 253–263.

5 Appendix

5.1 *WRKY23 is a component of the transcriptional network mediating auxin feedback on PIN polarity*

Table S2. 2 Candidate genes from the microarray experiment.

(A) Venn diagram representing gene overlay of microarray experiments. Dataset of auxin-regulated genes in WT Col-0 seedlings was overlaid with a second set of genes acquired from the comparison of auxin-treated WT Col-0 and heat-shock-induced auxin-treated *HS::axr3-1* lines. Overlap of these genes yielded a list of 245. (B) List of the 245 genes. Gene model descriptions are depicted as they appear in the TAIR database.

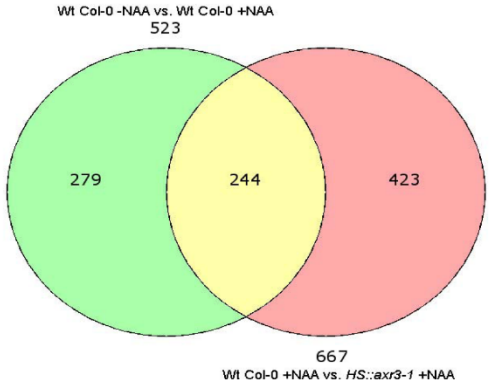

B

Lists contain 946 unique elements

Locus identifier	Primary Gene Symbol	Gene Model Description
AT1G02400	GIBBERELLIN 2-OXIDASE 6 (GA2OX6)	Encodes a gibberellin 2-oxidase that acts on C19 gibberellins but not C20 gibberellins.
AT1G02850	BETA GLUCOSIDASE 11 (BGLU11)	beta glucosidase 11 (BGLU11)
AT1G03820		unknown protein
AT1G03870	FASCICLIN-LIKE ARABINOOGALACTAN 9 (FLA9)	fasciclin-like arabinogalactan-protein 9 (Fla9)
AT1G04040		HAD superfamily, subfamily IIIB acid phosphatase
AT1G05530	UDP-GLUCOSYL TRANSFERASE 75B2 (UGT75B2)	Encodes a protein with glucosyltransferase activity with high sequence homology to UGT1 (AT1G05560). It belongs to an UGT subfamily that binds UDP-glucose but not UDP-glucuronate, UDP-galactose, or UDP-rhamnose as the glycosyl donor. UGT2 was shown to be able to use abscisic acid as glycosylation substrate in the presence of UDP-glucose.
AT1G08500	EARLY NODULIN-LIKE PROTEIN 18 (ENODL18)	early nodulin-like protein 18 (ENODL18); FUNCTIONS IN: electron carrier activity, copper ion binding; LOCATED IN: anchored to membrane;
AT1G14350	FOUR LIPS (FLP)	Encodes a putative MYB transcription factor involved in stomata development, loss of FLP activity results in a failure of guard mother cells (GMCs) to adopt the guard cell fate, thus they continue to divide resulting in abnormal stomata consisting of clusters of numerous guard cell-like cells. This phenotype is enhanced in double mutants with MYB88.
AT1G14540		Peroxidase superfamily protein
AT1G15210	ATP-BINDING CASSETTE G35 (ABCG35)	pleiotropic drug resistance 7 (PDR7)
AT1G15580	INDOLE-3-ACETIC ACID INDUCIBLE 5 (IAA5)	auxin induced protein
AT1G19220	AUXIN RESPONSE FACTOR 19 (ARF19)	Encodes an auxin response factor that contains the conserved VP1-B3 DNA-binding domain at its N-terminus and the Aux/IAA-like domains III and IV present in most ARFs at its C-terminus. The protein interacts with IAA1 (yeast two hybrid) and other auxin response elements such as ER7 and ER9 (yeast one hybrid). ARF19 protein can complement many aspects of the arf7 mutant phenotype and , together with ARF7, is involved in the response to ethylene. In the arf7 arf19 double mutant, several auxin- responsive genes (e.g. IAA5, LBD16, LBD29 and LBD33) are no longer upregulated by auxin.
AT1G21980	PHOSPHATIDYLINOSITO L-4-PHOSPHATE 5-KINASE 1 (PIP5K1)	Type I phosphatidylinositol-4-phosphate 5-kinase. Preferentially phosphorylates PtdIns4P. Induced by water stress and abscisic acid in Arabidopsis thaliana. Expressed in procambial cells of leaves, flowers and roots. A N-terminal Membrane Occupation and Recognition Nexus (MORN) affects enzyme activity and distribution.
AT1G22330		RNA-binding (RRM/RBD/RNP motifs) family protein
AT1G22530	PATELLIN 2 (PATL2)	PATELLIN 2 (PATL2
AT1G23080	PIN-FORMED 7 (PIN7)	Encodes a novel component of auxin efflux that is located apically in the basal cell and is involved during embryogenesis in setting up the apical-basal axis in the embryo. It is also involved in pattern specification during root development. In roots, it is expressed at lateral and basal membranes of provascular cells in the meristem and elongation zone, whereas in the columella cells it coincides with the PIN3 domain. Plasma membrane-localized PIN proteins mediate a saturable efflux of auxin. PINs mediate auxin efflux from mammalian and yeast cells without needing additional plant-specific factors. The action of PINs in auxin efflux is distinct from PGPs, rate-limiting, specific to auxins and sensitive to auxin transport inhibitors. PINs are directly involved of in catalyzing cellular auxin efflux.
AT1G25230		Calcineurin-like metallo-phosphoesterase superfamily protein;
AT1G25450	3-KETOACYL-COA SYNTHASE 5 (KCS5)	Encodes KCS5, a member of the 3-ketoacyl-CoA synthase family involved in the biosynthesis of VLCFA (very long chain fatty acids).
AT1G28370	ERF DOMAIN PROTEIN 11 (ERF11)	encodes a member of the ERF (ethylene response factor) subfamily B-1 of ERF/AP2 transcription factor family. The protein contains one AP2 domain. There are 15 members in this subfamily including ATERF-3, ATERF-4, ATERF-7, and leafy petiole.
AT1G28380	NECROTIC SPOTTED LESIONS 1 (NSL1)	This gene is predicted to encode a protein involved in negatively regulating salicylic acid-related defense responses and cell death programs.
AT1G28680		HXXXD-type acyl-transferase family protein
AT1G29500		SAUR-like auxin-responsive protein family
AT1G29510	SMALL AUXIN UPREGULATED 68 (SAUR68)	SMALL AUXIN UPREGULATED 68 (SAUR68);
AT1G33590		Leucine-rich repeat (LRR) family protein
AT1G33790		jacalin lectin family protein;
AT1G50660		unknown protein;
AT1G52050		Mannose-binding lectin superfamily protein;
AT1G52830	INDOLE-3-ACETIC ACID 6 (IAA6)	An extragenic dominant suppressor of the hy2 mutant phenotype. Also exhibits aspects of constitutive photomorphogenetic phenotype in the absence of hy2. Mutants have dominant leaf curling phenotype shortened hypocotyls and reduced apical hook. Induced by indole-3-acetic acid.
AT1G55330	ARABINOGALACTAN PROTEIN 21 (AGP21)	Encodes a putative arabinogalactan-protein (AGP21).

Locus identifier	Primary Gene Symbol	Gene Model Description
AT2G35980	YELLOW-LEAF-SPECIFIC GENE 9 (YLS9)	Encodes a protein whose sequence is similar to tobacco hairpin-induced gene (HIN1) and Arabidopsis non-race specific disease resistance gene (NDR1). Expression of this gene is induced by cucumber mosaic virus, spermine and during senescence. The gene product is localized to the chloroplast.
AT2G36220		unknown protein
AT2G39350	ATP-BINDING CASSETTE G1 (ABCG1)	ABC-2 type transporter family protein
AT2G39370		unknown protein;
AT2G39700	EXPANSIN A4 (EXPA4)	putative expansin.
AT2G40540	POTASSIUM TRANSPORTER 2 (KT2)	putative potassium transporter AtKT2p (AtKT2) mRNA,
AT2G41100	TOUCH 3 (TCH3)	encodes a calmodulin-like protein, with six potential calcium binding domains. Calcium binding shown by Ca(2+)-specific shift in electrophoretic mobility. Expression induced by touch and darkness. Expression may also be developmentally controlled. Expression in growing regions of roots, vascular tissue, root/shoot junctions, trichomes, branch points of the shoot, and regions of siliques and flowers.
AT2G41380		S-adenosyl-L-methionine-dependent methyltransferases superfamily protein;
AT2G41810		_ unknown
AT2G42430	LATERAL ORGAN BOUNDARIES-DOMAIN 16 (LBD16)	LOB-domain protein gene LBD16. This gene contains one auxin-responsive element (AuxRE).
AT2G42440		Lateral organ boundaries (LOB) domain family protein; CONTAINS InterPro DOMAIN/s: Lateral organ boundaries, LOB (InterPro:IPR004883)
AT2G42570	TRICHOME BIREFRINGENCE-LIKE 39 (TBL39)	Encodes a member of the TBL (TRICHOME BIREFRINGENCE-LIKE) gene family containing a plant-specific DUF231 (domain of unknown function) domain. TBL gene family has 46 members, two of which (TBR/AT5G06700 and TBL3/AT5G01360) have been shown to be involved in the synthesis and deposition of secondary wall cellulose, presumably by influencing the esterification state of pectic polymers. A nomenclature for this gene family has been proposed (Volker Bischoff & Wolf Scheible, 2010, personal communication).
AT2G42870	PHY RAPIDLY REGULATED 1 (PAR1)	Encodes PHYTOCHROME RAPIDLY REGULATED1 (PAR1), an atypical basic helix-loop-helix (bHLP) protein. Closely related to PAR2 (At3g58850). Up regulated after simulated shade perception. Acts in the nucleus to control plant development and as a negative regulator of shade avoidance response. Functions as transcriptional repressor of auxin-responsive genes SAUR15 (AT4G38850) and SAUR68 (AT1G29510).
AT2G43290	MULTICOPY SUPPRESSORS OF SNF4 DEFICIENCY IN YEAST 3 (MSS3)	Encodes calmodulin-like MSS3.
AT2G43590		Chitinase family protein
AT2G43880		Pectin lyase-like superfamily protein;
AT2G45400	(BEN1)	involved in the regulation of brassinosteroid metabolic pathway
AT2G45420	LOB DOMAIN-CONTAINING PROTEIN 18 (LBD18)	LOB domain-containing protein 18 (LBD18)
AT2G47130		NAD(P)-binding Rossmann-fold superfamily protein
AT2G47140		NAD(P)-binding Rossmann-fold superfamily protein
AT2G47260	WRKY DNA-BINDING PROTEIN 23 (WRKY23)	Encodes a member of WRKY Transcription Factor; Group I. Involved in nematode feeding site establishment.
AT2G47440		Tetratricopeptide repeat (TPR)-like superfamily protein Eukaryotes - 33 (source: NCBI BLink).
AT3G01190		Peroxidase superfamily protein
AT3G02850	STELAR K+ OUTWARD RECTIFIER (SKOR)	Encodes SKOR, a member of Shaker family potassium ion (K+) channel. This family includes five groups based on phylogenetic analysis (FEBS Letters (2007) 581: 2357): I (inward rectifying channel): AKT1 (AT2G26650), AKT5 (AT4G32500) and SPIK (also known as AKT6, AT2G25600); II (inward rectifying channel): KAT1 (AT5G46240) and KAT2 (AT4G18290); III (weakly inward rectifying channel): AKT2 (AT4G22200); IV (regulatory subunit involved in inwardly rectifying conductance formation): KAT3 (also known as AtKC1, AT4G32650); V (outward rectifying channel): SKOR (AT3G02850) and GORK (AT5G37500). Mediates the delivery of K+ from stelar cells to the xylem in the roots towards the shoot. mRNA accumulation is modulated by abscisic acid. K+ gating activity is modulated by external and internal K+.
AT3G02885	GAST1 PROTEIN HOMOLOG 5 (GASA5)	GAST1 protein homolog 5 (GASA5); INVOLVED IN: response to gibberellin stimulus;
AT3G06460		GNS1/SUR4 membrane protein family;
AT3G07010		Pectin lyase-like superfamily protein
AT3G07390	AUXIN-INDUCED IN ROOT CULTURES 12 (AIR12)	isolated from differential screening of a cDNA library from auxin-treated root culture. sequence does not show homology to any known proteins and is predicted to be extracellular.
AT3G09280		unknown protein
AT3G12700		Eukaryotic aspartyl protease family protein;
AT3G13380	BRI1-LIKE 3 (BRL3)	Similar to BRI, brassinosteroid receptor protein.
AT3G14690	CYTOCHROME P450, FAMILY 72, SUBFAMILY A, POLYPEPTIDE 15 (CYP72A15)	putative cytochrome P450
AT3G15540	INDOLE-3-ACETIC ACID INDUCIBLE 19 (IAA19)	Primary auxin-responsive gene. Involved in the regulation stamen filaments development.
AT3G16180		Major facilitator superfamily protein
AT3G16570	RAPID ALKALINIZATION FACTOR 23 (RALF23)	Encodes RALF23, a member of a diversely expressed predicted peptide family showing sequence similarity to tobacco Rapid Alkalinization Factor (RALF), and is believed to play an essential role in the physiology of Arabidopsis. Consists of a single exon and is characterized by a conserved C-terminal motif and N-terminal signal peptide. RALF23 is significantly downregulated by brassinolide treatment of seedlings. Overexpression of AtRALF23 impairs brassinolide-induced hypocotyls elongation, and mature overexpressing plants are shorter and bushier. RALF23 overexpression produces slower growing seedlings with roots that have reduced capacity to acidify the rhizosphere.
AT3G18280		Bifunctional inhibitor/lipid-transfer protein/seed storage 2S albumin superfamily protein;
AT3G18560		unknown protein;
AT3G19200		unknown protein;
AT3G19320		Leucine-rich repeat (LRR) family protein
AT3G20015		Eukaryotic aspartyl protease family protein
AT3G20830		AGC (cAMP-dependent, cGMP-dependent and protein kinase C) kinase family protein;
AT3G21250	ATP-BINDING CASSETTE C8 (ABCC8)	member of MRP subfamily
AT3G21700	(SGP2)	Monomeric G protein. Expressed in root epidermal cells that are destined to become atrichoblasts. Also expressed during pollen development and in the pollen tube tip.
AT3G23030	INDOLE-3-ACETIC ACID INDUCIBLE 2 (IAA2)	auxin inducible gene expressed in the nucleus
AT3G23730	XYLOGLUCAN ENDOTRANSGLUCOSYLASE/HYDROLASE 16 (XTH16)	xyloglucan endotransglucosylase/hydrolase 16 (XTH16); FUNCTIONS IN: hydrolase activity, acting on glycosyl bonds, hydrolase activity, hydrolyzing O-glycosyl compounds, xyloglucan:xyloglucosyl transferase activity; INVOLVED IN: carbohydrate metabolic process, cellular glucan metabolic process
AT3G24750		unknown protein
AT3G26610		Pectin lyase-like superfamily protein

Locus identifier	Primary Gene Symbol	Gene Model Description
AT3G26760		NAD(P)-binding Rossmann-fold superfamily protein
AT3G28850		Glutaredoxin family protein
AT3G42800		unknown protein
AT3G43800	GLUTATHIONE S- TRANSFERASE TAU 27 (GSTU27)	Encodes glutathione transferase belonging to the tau class of GSTs. Naming convention according to Wagner et al. (2002).
AT3G44990	XYLOGLUCAN ENDO-TRANSGLYCOSYLASE- RELATED 8 (XTR8)	xyloglucan endo-transglycosylase
AT3G48520	CYTOCHROME P450, FAMILY 94, SUBFAMILY B, POLYPEPTIDE 3 (CYP94B3)	CYP94B3 is a jasmonoyl-isoleucine-12-hydroxylase that catalyzes the formation of 12-OH-JA-Ile from JA-Ile. By reducing the levels of this the biologically active phytohormone, CYP94B3 attenuates the jasmonic acid signaling cascade. CYP94B3 transcript levels rise in response to wounding.
AT3G49350		Ypt/Rab-GAP domain of gyp1p superfamily protein
AT3G49360	6-PHOSPHOGLUCONOLACTO NASE 2 (PGL2)	6-phosphogluconolactonase 2 (PGL2)
AT3G49700	1-AMINOCYCLOPROPANE-1-CARBOXYLATE SYNTHASE 9 (ACS9)	encodes a a member of the 1-aminocyclopropane-1-carboxylate (ACC) synthase (S-adenosyl-L-methionine methylthioadenosine- lyase, EC 4.4.1.14) gene family. Mutants produce elevated levels of ethylene as etiolated seedlings.
AT3G50660	DWARF 4 (DWF4)	Encodes a 22α hydroxylase whose reaction is a rate-limiting step in brassinosteroid biosynthetic pathway. The protein is a member of CYP90B gene family. CLM is an epi-allele with small, compressed rosette, reduced internode length, and reduced fertility, appears in selfed ddm mutant plants possibly due to loss of cytosine methylation. Transcripts accumulate in actively growing tissues, and GUS expression is negatively regulated by brassinosteroids. Localized in the endoplasmic reticulum. The in vitro expressed protein can perform the C-22 hydroxylation of a variety of C27-, C28- and C29-sterols. Cholesterol was the best substrate, followed by campesterol. Sitosterol was a poor substrate.
AT3G51410		Arabidopsis protein of unknown function (DUF241)
AT3G51670	PATL6	SEC14 cytosolic factor family protein / phosphoglyceride transfer family protein
AT3G54000		Uncharacterised conserved protein UCP022260
AT3G54770		RNA-binding (RRM/RBD/RNP motifs) family protein
AT3G54950	PATATIN-RELATED PHOSPHOLIPASE IIIBETA (pPLAIIIbeta)	Encodes pPLAIIIbeta, a member of the Group 3 patatin-related phospholipases. pPLAIIIbeta hydrolyzes phospholipids and galactolipids and additionally has acyl-CoA thioesterase activity. Alterations of pPLAIIIβ result in changes in lipid levels and composition.
AT3G55690		unknown protein;
AT3G55720		Protein of unknown function (DUF620)
AT3G56230		BTB/POZ domain-containing protein
AT3G56880		VQ motif-containing protein
AT3G58190	LATERAL ORGAN BOUNDARIES-DOMAIN 29 (LBD29)	This gene contains two auxin-responsive element (AuxRE).
AT3G60550	CYCLIN P3;2 (CYCP3;2)	cyclin p3;2 (CYCP3;2);
AT3G60630	HAIRY MERISTEM 2 (HAM2)	Belongs to one of the LOM (LOST MERISTEMS) genes: AT2G45160 (LOM1), AT3G60630 (LOM2) and AT4G00150 (LOM3). LOM1 and LOM2 promote cell differentiation at the periphery of shoot meristems and help to maintain their polar organization.
AT3G60640	AUTOPHAGY 8G (ATG8G)	AUTOPHAGY 8G (ATG8G)
AT3G61490		Pectin lyase-like superfamily protein;
AT3G62100	INDOLE-3-ACETIC ACID INDUCIBLE 30 (IAA30)	Encodes a member of the Aux/IAA family of proteins implicated in auxin signaling. IAA30 lacks the conserved degron (domain II) found in many family members. IAA30 transcripts are induced by auxin treatment and accumulate preferentially in the quiescent center cells of the root meristem. Overexpression of IAA30 leads to defects in gravitropism, root development, root meristem maintenance, and cotyledon vascular development. Target of LEC2 and AGL15. Promotes somatyic embryogenesis.
AT3G63440	CYTOKININ OXIDASE/DEHYDROGENAS E 6 (CKX6)	This gene used to be called AtCKX7. It encodes a protein whose sequence is similar to cytokinin oxidase/dehydrogenase, which catalyzes the degradation of cytokinins.
AT4G00080	UNFERTILIZED EMBRYO SAC 11 (UNE11)	unfertilized embryo sac 11 (UNE11)
AT4G01870		tolB protein-related
AT4G03820		Protein of unknown function (DUF3537)
AT4G08040	1-AMINOCYCLOPROPANE-1-CARBOXYLATE SYNTHASE 11 (ACS11)	encodes an aminotransferase that belongs to ACC synthase gene family structurally
AT4G09570	CALCIUM-DEPENDENT PROTEIN KINASE 4 (CPK4)	Encodes a member of Calcium Dependent Protein Kinase (CDPK) gene family.Positive regulator of ABA signaling. Phosphorylates ABA responsive transcription factors ABF1 and ABF4.
AT4G11280	1-AMINOCYCLOPROPANE-1-CARBOXYLIC ACID (ACC) SYNTHASE 6 (ACS6)	encodes a a member of the 1-aminocyclopropane-1-carboxylate (ACC) synthase (S-adenosyl-L-methionine methylthioadenosine- lyase, EC 4.4.1.14) gene family
AT4G12110	STEROL-4ALPHA-METHYL OXIDASE 1-1 (SMO1-1)	Encodes a member of the SMO1 family of sterol 4alpha-methyl oxidases. More specifically functions as a 4,4-dimethyl-9beta,19-cyclopropylsterol-4alpha- methyl oxidase.
AT4G12410		SAUR-like auxin-responsive protein family ; CONTAINS InterPro DOMAIN/s: Auxin responsive SAUR protein (InterPro:IPR003676); BEST Arabidopsis thaliana protein match is: SAUR-like auxin-responsive protein family (TAIR:AT4G22620.1); Has 1137 Blast hits to 1128 proteins in 26 species: Archae - 0; Bacteria - 0; Metazoa - 0; Fungi - 0; Plants - 1136; Viruses - 0; Other Eukaryotes - 1 (source: NCBI BLink).
AT4G12720	(NUDT7)	Encodes a protein with ADP-ribose hydrolase activity. Negatively regulates EDS1-conditioned plant defense and programmed cell death.
AT4G12730	FASCICLIN-LIKE ARABINOGALACTAN 2 (FLA2)	AF333971 Arabidopsis thaliana fasciclin-like arabinogalactan-protein 2 (Fla2) mRNA, complete cds
AT4G12880	EARLY NODULIN-LIKE PROTEIN 19 (ENODL19)	early nodulin-like protein 19 (ENODL19)
AT4G13180		NAD(P)-binding Rossmann-fold superfamily protein).
AT4G13195	CLAVATA3/ESR-RELATED 44 (CLE44)	Belongs to a large gene family, called CLE for CLAVATA3/ESR-related, encoding small peptides with conserved carboxyl termini. The C-terminal 12 amino acid sequence of CLE44 is identical to that of a dodeca peptide (TDIF, tracheary element differentiation inhibitory factor) isolated from Arabidopsis and functions as a suppressor of plant stem cell differentiation. TDIF sequence is also identical to the C-terminal 12 amino acids of CLE41 (At3g24770).
AT4G14130	XYLOGLUCAN ENDOTRANSGLUCOSYLAS E/HYDROLASE 15 (XTH15)	xyloglucan endotransglycosylase-related protein (XTR7)
AT4G14560	INDOLE-3-ACETIC ACID INDUCIBLE (IAA1)	auxin (indole-3-acetic acid) induced gene (IAA1) encoding a short-lived nuclear-localized transcriptional regulator protein.

Locus identifier	Primary Gene Symbol	Gene Model Description
AT4G14750	IQ-DOMAIN 19 (IQD19)	IQ-domain 19 (IQD19); CONTAINS InterPro DOMAIN/s: IQ calmodulin-binding region (InterPro:IPR000048)
AT4G17350		DOMAIN/s: Pleckstrin-like, plant (InterPro:IPR013666), Protein of unknown function DUF828 (InterPro:IPR008546), Pleckstrin homology (InterPro:IPR001849
AT4G17490	ETHYLENE RESPONSIVE ELEMENT BINDING FACTOR 6 (ERF6)	Encodes a member of the ERF (ethylene response factor) subfamily B-3 of ERF/AP2 transcription factor family (ATERF-6). The protein contains one AP2 domain. There are 18 members in this subfamily including ATERF-1, ATERF-2, AND ATERF-5.
AT4G17870	PYRABACTIN RESISTANCE 1 (PYR1)	Encodes a member of the PYR (pyrabactin resistance)/PYL(PYR1-like)/RCAR (regulatory components of ABA receptor) family proteins with 14 members. PYR/PYL/RCAR family proteins function as abscisic acid sensors. Mediate ABA-dependent regulation of protein phosphatase 2Cs ABI1 and ABI2.
AT4G20460		NAD(P)-binding Rossmann-fold superfamily protein
AT4G21200	GIBBERELLIN 2-OXIDASE 8 (GA2OX8)	Encodes a protein with gibberellin 2-oxidase activity which acts specifically on C-20 gibberellins.
AT4G21850	METHIONINE SULFOXIDE REDUCTASE B9 (MSRB9)	methionine sulfoxide reductase B9 (MSRB9);
AT4G21870		HSP20-like chaperones superfamily protein
AT4G22530		S-adenosyl-L-methionine-dependent methyltransferases superfamily protein
AT4G22620		SAUR-like auxin-responsive protein family
AT4G22780	ACT DOMAIN REPEAT 7 (ACR7)	Member of a family of ACT domain containing proteins . ACT domains are involved in amino acid binding .
AT4G24160		Encodes a soluble lysophosphatidic acid acyltransferase with additional triacylglycerol lipase and phosphatidylcholine hydrolyzing enzymatic activities. Plays a pivotal role in maintaining the lipid homeostasis by regulating both phospholipid and neutral lipid levels.
AT4G25250		Plant invertase/pectin methylesterase inhibitor superfamily protein
AT4G26320	ARABINOGALACTAN PROTEIN 13 (AGP13)	arabinogalactan protein 13 (AGP13);
AT4G27260	(WES1)	encodes an IAA-amido synthase that conjugates Asp and other amino acids to auxin in vitro. Lines carrying insertions in this gene are hypersensitive to auxin.
AT4G27280		Calcium-binding EF-hand family protein;
AT4G27290		S-locus lectin protein kinase family protein
AT4G28640	INDOLE-3-ACETIC ACID INDUCIBLE 11 (IAA11)	Auxin induced gene, IAA11 (IAA11).
AT4G29900	AUTOINHIBITED CA(2+)-ATPASE 10 (ACA10)	one of the type IIB calcium pump isoforms. encodes an autoinhibited Ca(2+)-ATPase that contains an N-terminal calmodulin binding autoinhibitory domain.
AT4G30170		Peroxidase family protein
AT4G30420		nodulin MtN21 /EamA-like transporter family protein
AT4G30450		glycine-rich protein
AT4G31320		SAUR-like auxin-responsive protein family
AT4G31910		HXXXD-type acyl-transferase family protein
AT4G32280	INDOLE-3-ACETIC ACID INDUCIBLE 29 (IAA29)	Auxin inducible protein.
AT4G34150		Calcium-dependent lipid-binding (CaLB domain) family protein;
AT4G34710	ARGININE DECARBOXYLASE 2 (ADC2)	encodes a arginine decarboxylase (ADC), a rate-limiting enzyme that catalyzes the first step of polyamine (PA) biosynthesis via ADC pathway in Arabidopsis thaliana. Arabidopsis genome has two ADC paralogs, ADC1 and ADC2. ADC2 is stress-inducible (osmotic stress). Double mutant analysis showed that ADC genes are essential for the production of PA, and are required for normal seed development. Overexpression causes phenotypes similar to GA-deficient plants and these plants show reduced levels of GA due to lower expression levels of AtGA20ox1, AtGA3ox3 and AtGA3ox1.
AT4G35210		Arabidopsis protein of unknown function (DUF241);
AT4G35320		unknown protein
AT4G37290		unknown protein
AT4G37295		unknown protein
AT4G37590	NAKED PINS IN YUC MUTANTS 5 (NPY5)	A member of the NPY gene family (NPY1/AT4G31820, NPY2/AT2G14820, NPY3/AT5G67440, NPY4/AT2G23050, NPY5/AT4G37590). Involved in auxin-mediated organogenesis.
AT5G01750		Protein of unknown function (DUF567)
AT5G01840	OVATE FAMILY PROTEIN 1 (OFP1)	Encodes a member of the plant specific ovate protein family. Members of this family have been shown to bind to KNOX and BELL-like TALE class homeodomain proteins. This interaction may mediate relocalization of the TALE homeodomain from the nucleus to the cytoplasm. Functions as a transcriptional repressor that suppresses cell elongation.
AT5G02760		Protein phosphatase 2C family protein
AT5G03960	IQ-DOMAIN 12 (IQD12)	IQ-domain 12 (IQD12)
AT5G04980		DNAse I-like superfamily protein
AT5G05160	REDUCED IN LATERAL GROWTH1 (RUL1)	Encodes a receptor-like kinase that activates secondary growth, the production of secondary vascular tissues.
AT5G06080	LOB DOMAIN-CONTAINING PROTEIN 33 (LBD33)	LOB domain-containing protein 33 (LBD33)
AT5G10210		C2 calcium-dependent membrane targeting
AT5G10430	ARABINOGALACTAN PROTEIN 4 (AGP4)	Encodes arabinogalactan-protein (AGP4).
AT5G12050		unknown protein;
AT5G13910	LEAFY PETIOLE (LEP)	Encodes a member of the ERF (ethylene response factor) subfamily B-1 of ERF/AP2 transcription factor family (LEAFY PETIOLE). The protein contains one AP2 domain. There are 15 members in this subfamily including ATERF-3, ATERF-4, ATERF-7, and LEAFY PETIOLE. Acts as a positive regulator of gibberellic acid-induced germination.
AT5G15890	TRICHOME BIREFRINGENCE-LIKE 21 (TBL21)	Encodes a member of the TBL (TRICHOME BIREFRINGENCE-LIKE) gene family containing a plant-specific DUF231 (domain of unknown function) domain. TBL gene family has 46 members, two of which (TBR/AT5G06700 and TBL3/AT5G01360) have been shown to be involved in the synthesis and deposition of secondary wall cellulose, presumably by influencing the esterification state of pectic polymers. A nomenclature for this gene family has been proposed (Volker Bischoff & Wolf Scheible, 2010, personal communication).
AT5G16110		unknown protein
AT5G16120		alpha/beta-Hydrolases superfamily protein
AT5G17340		Putative membrane lipoprotein
AT5G18560	(PUCHI)	Encodes PUCHI, a member of the ERF (ethylene response factor) subfamily B-1 of ERF/AP2 transcription factor family. The protein contains one AP2 domain. There are 15 members in this subfamily including ATERF-3, ATERF-4, ATERF-7, and leafy petiole. PUCHI is required for morphogenesis in the early lateral root primordium of Arabidopsis. Expressed in early floral meristem (stage 1 to 2). Required for early floral meristem growth and for bract suppression. Triple mutant with bop1 and bop2 displays a strong defect in the determination of floral meristem identity with reduced LFY expression and the lack of AP1 expression.
AT5G19530	ACAULIS 5 (ACL5)	Encodes a spermine synthase. Required for internode elongation and vascular development, specifically in the mechanism that defines the boundaries between veins and nonvein regions. This mechanism may be mediated by polar auxin transport. Though ACL5 has been shown to function as a spermine synthase in E. coli, an ACL5 knockout has no effect on the endogenous levels of free and conjugated polyamines in Arabidopsis, suggesting that ACL5 may have a very specific or altogether different in vivo function.

Locus identifier	Primary Gene Symbol	Gene Model Description
AT1G55740	SEED IMBIBITION 1 (SIP1)	seed imbibition 1 (SIP1
AT1G56020		unknown protein
AT1G60000		RNA-binding (RRM/RBD/RNP motifs) family protein
AT1G60010		unknown protein
AT1G62770		Plant invertase/pectin methylesterase inhibitor superfamily protein
AT1G63830		PLAC8 family protein;
AT1G64390	GLYCOSYL HYDROLASE 9C2 (GH9C2)	glycosyl hydrolase 9C2 (GH9C2)
AT1G64405		unknown protein
AT1G69530	EXPANSIN A1 (EXPA1)	Member of Alpha-Expansin Gene Family. Naming convention from the Expansin Working Group (Kende et al, Plant Mol Bio). Involved in the formation of nematode-induced syncytia in roots of Arabidopsis thaliana.
AT1G70230	TRICHOME BIREFRINGENCE-LIKE 27 (TBL27)	Encodes a member of the TBL (TRICHOME BIREFRINGENCE-LIKE) gene family containing a plant-specific DUF231 (domain of unknown function) domain. TBL gene family has 46 members, two of which (TBR/AT5G06700 and TBL3/AT5G01360) have been shown to be involved in the synthesis and deposition of secondary wall cellulose, presumably by influencing the esterification state of pectic polymers. A nomenclature for this gene family has been proposed (Volker Bischoff & Wolf Scheible, 2010, personal communication).
AT1G70560	TRYPTOPHAN AMINOTRANSFERASE OF ARABIDOPSIS 1 (TAA1)	TAA1 is involved in the shade-induced production of indole-3-pyruvate (IPA), a precursor to IAA, a biologically active auxin. It is also involved in regulating many aspects of plant growth and development from embryogenesis to flower formation and plays a role in ethylene-mediated signaling. This enzyme can catalyze the formation of IPA from L-tryptophan. Though L-Trp is expected to be the preferred substrate in vivo, TAA1 also acts as an aminotransferase using L-Phe, L-Tyr, L-Leu, L-Ala, L-Met, and L-Gln.
AT1G70940	PIN-FORMED 3 (PIN3)	A regulator of auxin efflux and involved in differential growth. PIN3 is expressed in gravity-sensing tissues, with PIN3 protein accumulating predominantly at the lateral cell surface. PIN3 localizes to the plasma membrane and to vesicles. In roots, PIN3 is expressed without pronounced polarity in tiers two and three of the columella cells, at the basal side of vascular cells, and to the lateral side of pericycle cells of the elongation zone. PIN3 overexpression inhibits root cell growth. Protein phosphorylation plays a role in PIN3 trafficking to the plasma membrane.
AT1G72900		Toll-Interleukin-Resistance (TIR) domain-containing protein;
AT1G73590	PIN-FORMED 1 (PIN1)	Encodes an auxin efflux carrier involved in shoot and root development. It is involved in the maintenance of embryonic auxin gradients. Loss of function severely affects organ initiation, pin1 mutants are characterised by an inflorescence meristem that does not initiate any flowers, resulting in the formation of a naked inflorescence stem. PIN1 is involved in the determination of leaf shape by actively promoting development of leaf margin serrations. In roots, the protein mainly resides at the basal end of the vascular cells, but weak signals can be detected in the epidermis and the cortex. Expression levels and polarity of this auxin efflux carrier change during primordium development suggesting that cycles of auxin build-up and depletion accompany, and may direct, differentstages of primordium development. PIN1 action on plant development does not strictly require function of PGP1 and PGP19 proteins.
AT1G73620		Pathogenesis-related thaumatin superfamily protein
AT1G73780		Bifunctional inhibitor/lipid-transfer protein/seed storage 2S albumin superfamily protein;
AT1G74660	MINI ZINC FINGER 1 (MIF1)	Encodes MINI ZINC FINGER 1 (MIF1) which has a zinc finger domain but lacks other protein motifs normally present in transcription factors. MIF1 physically interact with a group of zinc finger-homeodomain (ZHD) transcription factors, such as ZHD5 (AT1G75240), that regulate floral architecture and leaf development. Gel mobility shift assays revealed that MIF1 blocks the DNA binding activity of ZHD5 homodimers by competitively forming MIF1-ZHD5 heterodimers. Constitutive overexpression of MIF1 caused dramatic developmental defects, seedlings were non-responsive to gibberellin (GA) for cell elongation, hypersensitive to the GA synthesis inhibitor paclobutrazol (PAC) and abscisic acid (ABA), and hyposensitive to auxin, brassinosteroid and cytokinin, but normally responsive to ethylene.
AT1G74790		catalytics
AT1G75500	WALLS ARE THIN 1 (WAT1)	An Arabidopsis thaliana homolog of Medicago truncatula NODULIN21 (MtN21). The gene encodes a plant-specific, predicted integral membrane protein and is a member of the Plant-Drug/Metabolite Exporter (P-DME) family (Transporter Classification number: TC 2.A.7.3).
AT1G77280		Protein kinase protein with adenine nucleotide alpha hydrolases-like domain
AT1G78100		F-box family protein;
AT1G78420		RING/U-box superfamily protein
AT2G01430	HOMEOBOX-LEUCINE ZIPPER PROTEIN 17 (HB17)	homeobox-leucine zipper protein 17 (HB17);
AT2G01910	(ATMAP65-6)	Binds microtubules. Induces a crisscross mesh of microtubules, not bundles. Not involved in microtubule polymerization nor nucleation. Localizes to mitochondria.
AT2G02620		Cysteine/Histidine-rich C1 domain family protein
AT2G03730	ACT DOMAIN REPEAT 5 (ACR5)	Member of a small family of ACT domain containing proteins. ACT domains are thought to be involved in amino acid binding.
AT2G03830	ROOT MERISTEM GROWTH FACTOR 8 (RGF8)	Encodes a root meristem growth factor (RGF). Belongs to a family of functionally redundant homologous peptides that are secreted, tyrosine-sulfated, and expressed mainly in the stem cell area and the innermost layer of central columella cells. RGFs are required for maintenance of the root stem cell niche and transit amplifying cell proliferation. Members of this family include: At5g60810 (RGF1), At1g13620 (RGF2), At2g04025 (RGF3), At3g30350 (RGF4), At5g51451 (RGF5), At4g16515 (RGF6), At3g02240 (RGF7), At2g03830 (RGF8) and At5g64770 (RGF9).
AT2G05940		Protein kinase superfamily protein;
AT2G14960	(GH3.1)	encodes a protein similar to IAA-amido synthases. Lines carrying an insertion in this gene are hypersensitive to auxin.
AT2G18690		unknown protein;
AT2G18800	XYLOGLUCAN ENDOTRANSGLUCOSYLASE/HYDROLASE 21 (XTH21)	xyloglucan endotransglucosylase/hydrolase 21 (XTH21);
AT2G18980		Peroxidase superfamily protein
AT2G22500	UNCOUPLING PROTEIN 5 (UCP5)	Encodes one of the mitochondrial dicarboxylate carriers (DIC): DIC1 (AT2G22500), DIC2 (AT4G24570), DIC3 (AT5G09470).
AT2G23170	(GH3.3)	encodes an IAA-amido synthase that conjugates Asp and other amino acids to auxin in vitro.
AT2G25790		Leucine-rich receptor-like protein kinase family protein;
AT2G28400		Protein of unknown function, DUF584;
AT2G29460	GLUTATHIONE S-TRANSFERASE TAU 4 (GSTU4)	Encodes glutathione transferase belonging to the tau class of GSTs. Naming convention according to Wagner et al. (2002).
AT2G30040	MITOGEN-ACTIVATED PROTEIN KINASE KINASE KINASE 14 (MAPKKK14)	member of MEKK subfamily
AT2G30140		UDP-Glycosyltransferase superfamily protein
AT2G30930		unknown protein
AT2G33310	AUXIN-INDUCED PROTEIN 13 (IAA13)	Auxin induced gene, IAA13 (IAA13).
AT2G34650	PINOID (PID)	Encodes a protein serine/threonine kinase that may act as a positive regulator of cellular auxin efflux, as a a binary switch for PIN polarity, and as a negative regulator of auxin signaling. Recessive mutants exhibit similar phenotypes as pin-formed mutants in flowers and inflorescence but distinct phenotypes in cotyledons and leaves. Expressed in the vascular tissue proximal to root and shoot meristems, shoot apex, and embryos. Expression is induced by auxin. Overexpression of the gene results in phenotypes in the root and shoot similar to those found in auxin-insensitive mutants. The protein physically interacts with TCH3 (TOUCH3) and PID-BINDING PROTEIN 1 (PBP1), a previously uncharacterized protein containing putative EF-hand calcium-binding motifs. Acts together with ENP (ENHANCER OF PINOID) to instruct precursor cells to elaborate cotyledons in the transition stage embryo. Interacts with PDK1. PID autophosphorylation is required for the ability of PID to phosphorylate an exogenous substrate. PID activation loop is required for PDK1-dependent PID phosphorylation and requires the PIF domain. Negative regulator of root hair growth. PID kinase activity is critical for the inhibition of root hair growth and for maintaining the proper subcellular localization of PID.
AT2G35930	PLANT U-BOX 23 (PUB23)	Encodes a cytoplasmically localized U-box domain containing E3 ubiquitin ligase that is involved in the response to water stress and acts as a negative regulator of PAMP-triggered immunity.

Locus identifier	Primary Gene Symbol	Gene Model Description
AT5G20230	BLUE COPPER-BINDING PROTEIN (BCB)	Al-stress-induced gene
AT5G24100		Leucine-rich repeat protein kinase family protein
AT5G26930	GATA TRANSCRIPTION FACTOR 23 (GATA23)	Encodes a member of the GATA factor family of zinc finger transcription factors. Controls lateral root founder cell specification.
AT5G27000	KINESIN 4 (ATK4)	Encodes a kinesin-like protein that binds microtubules in an ATP-dependent manner.
AT5G39670		Calcium-binding EF-hand family protein.
AT5G40540		Protein kinase superfamily protein
AT5G42050		DCD (Development and Cell Death) domain protein
AT5G43700	AUXIN INDUCIBLE 2-11 (ATAUX2-11)	Auxin inducible protein similar to transcription factors.
AT5G47250		LRR and NB-ARC domains-containing disease resistance protein.
AT5G47370	(HAT2)	homeobox-leucine zipper genes induced by auxin, but not by other phytohormones. Plays opposite roles in the shoot and root tissues in regulating auxin-mediated morphogenesis.
AT5G47440		Conserved hypothetical protein (InterPro:IPR013666); Protein of unknown function DUF828 (InterPro:IPR008546); Phosphatidylinositol-4-phosphate 5-kinase (InterPro:IPR002498)
AT5G48150	PHYTOCHROME A SIGNAL TRANSDUCTION 1 (PAT1)	Member of GRAS gene family. Semi-dominant mutant has a reduced response to far-red light and appears to act early in the phytochrome A signaling pathway.
AT5G49360	BETA-XYLOSIDASE 1 (BXL1)	Encodes a bifunctional {beta}-D-xylosidase/{alpha}-L-arabinofuranosidase required for pectic arabinan modification. Located in the extracellular matrix. Gene is expressed specifically in tissues undergoing secondary wall thickening. This is a member of glycosyl hydrolase family 3 and has six other closely related members.
AT5G49450	BASIC LEUCINE-ZIPPER 1 (bZIP1)	basic leucine-zipper 1 (bZIP1)
AT5G51670		Protein of unknown function (DUF668)
AT5G52450		MATE efflux family protein
AT5G52900		unknown protein
AT5G53250	ARABINOGALACTAN PROTEIN 22 (AGP22)	arabinogalactan protein 22 (AGP22)
AT5G54130		Calcium-binding endonuclease/exonuclease/phosphatase family
AT5G54380	THESEUS1 (THE1)	Encodes THESEUS1 (THE1), a receptor kinase regulated by Brassinosteroids and required for cell elongation during vegetative growth.
AT5G54490	PINOID-BINDING PROTEIN 1 (PBP1)	Encodes a PINOID (PID)-binding protein containing putative EF-hand calcium-binding motifs. The interaction is dependent on the presence of calcium. mRNA expression is up-regulated by auxin. Not a phosphorylation target of PID, likely acts upstream of PID to regulate the activity of this protein in response to changes in calcium levels.
AT5G54500	FLAVODOXIN-LIKE QUINONE REDUCTASE 1 (FQR1)	Encodes a flavin mononucleotide-binding flavodoxin-like quinone reductase that is a primary auxin-response gene.
AT5G54510	DWARF IN LIGHT 1 (DFL1)	Encodes an IAA-amido synthase that conjugates Ala, Asp, Phe, and Trp to auxin. Lines overexpressing this gene accumulate IAA-ASP and are hypersensitive to several auxins. Identified as a dominant mutation that displays shorter hypocotyls in light grown plants when compared to wild type siblings. Protein is similar to auxin inducible gene from pea (GH3).
AT5G57100		Nucleotide/sugar transporter family protein
AT5G57520	ZINC FINGER PROTEIN 2 (ZFP2)	Encodes a zinc finger protein containing only a single zinc finger.
AT5G60450	AUXIN RESPONSE FACTOR 4 (ARF4)	Encodes a member of the ARF family of transcription factors which mediate auxin responses. ARF4 appears to have redundant function with ETT(ARF3) in specifying abaxial cell identity.
AT5G60520		Late embryogenesis abundant (LEA) protein-related;
AT5G60660	PLASMA MEMBRANE INTRINSIC PROTEIN 2;4 (PIP2;4)	A member of the plasma membrane intrinsic protein subfamily PIP2. When expressed in yeast cells can conduct hydrogen peroxide into those cells. Mutants exhibit longer root hairs.
AT5G62280		Protein of unknown function (DUF1442)
AT5G64250		Aldolase-type TIM barrel family protein
AT5G65390	ARABINOGALACTAN PROTEIN 7 (AGP7)	arabinogalactan protein 7 (AGP7)
AT5G65670	INDOLE-3-ACETIC ACID INDUCIBLE 9 (IAA9)	auxin (indole-3-acetic acid) induced gene
AT5G67430		Acyl-CoA N-acyltransferases (NAT) superfamily protein

Table S2. 3 Narrowed-down list of candidate genes from the microarray experiments.

(A) Venn diagram representing gene overlay of microarray experiments. Datasets of genes differentially regulated in *HS::axr3-1* compared to auxin-regulated genes in WT Col-0 were overlaid with a third set of genes that are no longer auxin regulated in the *arf7 arf19* background (Okushima et al., 2005). Overlap of all three microarrays gave 125 genes. (B) List of the 125 overlapping genes

containing putative polarity regulators. Gene model descriptions are depicted as they appear in the TAIR database.

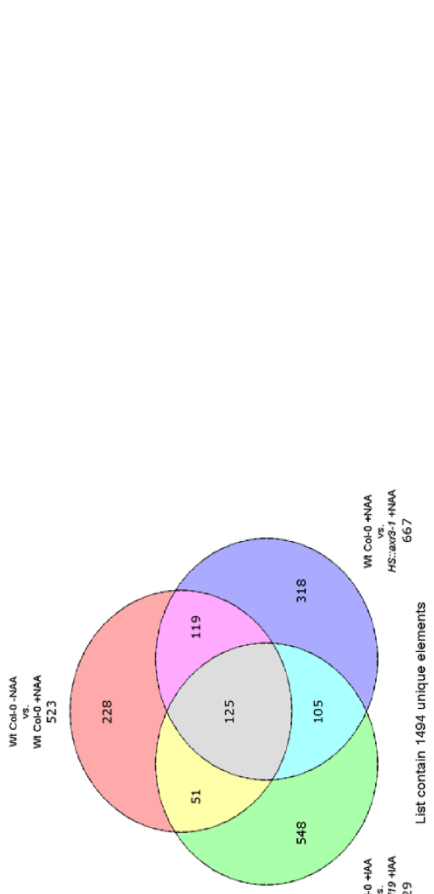

B

Locus Identifier	Primary Gene Symbol	Gene Model Description
AT1G02400	GIBBERELLIN 2-OXIDASE 6 (GA2OX6)	Encodes a gibberellin 2-oxidase that acts on C19 gibberellins but not C20 gibberellins.
AT1G03870	FASCICLIN-LIKEARABINOGALACTAN 9 (FLA9)	fasciclin-like arabinogalactan-protein 9 (fla9)
AT1G08500	EARLY NODULIN-LIKEPROTEIN 18 (ENOD18)	early nodulin-like protein 18 (ENOD18); FUNCTIONS IN: electron carrier activity, copper ion binding; LOCATED IN: anchored to membrane
AT1G15580	INDOLE-3-ACETIC ACIDINDUCIBLE 5 (IAA5)	auxin induced protein
AT1G19220	AUXIN RESPONSE FACTOR19 (ARF19)	Encodes an auxin response factor that contains the conserved VP1 B3 DNA-binding domain at its N-terminus and the Aux/IAA like domains III and IV present in most ARFs at its C-terminus. The protein interacts with IAA1 (yeast two hybrid) and other auxin response elements such as ER7 and ER9 (yeast one hybrid). ARF19 protein can complement many aspects of the arf7 mutant phenotype and, together with ARF7, is involved in the response to ethylene. In the arf7 arf19 double mutant, several auxin- responsive genes (e.g. IAA5, IBD16, LBD29 and LBD33) are no longer upregulated by auxin.
AT1G21980	PHOSPHATIDYLINOSITO L-4-PHOSPHATE 5- KINASE 1 (PIP5K1)	**Type I phosphatidylinositol-4 phosphate 5-kinase. Preferentially phosphorylates PtdIns4P. Induced by water stress and abscisic acid in Arabidopsis thaliana. Expressed in procambial cells of leaves, flowers and roots. A N-terminal Membrane Occupation and Recognition Nexus (MORN) affects enzyme activity and distribution.**
AT1G23080	PIN-FORMED 7 (PIN7)	Encodes a novel component of auxin efflux that is located apically in the basal cell and is involved during embryogenesis in setting up the apical-basal axis in the embryo. It is also involved in pattern specification during root development. In roots, it is expressed at lateral and basal membranes of provascular cells in the meristem and elongation zone, whereas in the columella cells it coincides with the PIN3 domain. Plasma membrane-localized PIN proteins mediate a saturable efflux of auxin. PINs mediate auxin efflux from mammalian and yeast cells without needing additional plant-specific factors. The action of PINs in auxin efflux is distinct from PGPs, rate-limiting, specific to auxins and sensitive to auxin transport inhibitors. PINs are directly involved of in catalyzing cellular auxin efflux.
AT1G28370	ERF DOMAIN PROTEIN 11 (ERF11)	encodes a member of the ERF (ethylene response factor) subfamily B-1 of ERF/AP2 transcription factor family. The protein contains one AP2 domain. There are 15 members in this subfamily including ATERF-3, ATERF-4, ATERF-7, and leafy petiole.
AT1G28680		HOXXD-type acyl-transferase family protein
AT1G29500		SAUR-like auxin-responsive protein family
AT1G29510	SMALL AUXIN UPREGULATED 68(SAUR68)	SMALL AUXIN UPREGULATED 68 (SAUR68);
AT1G33790		jacalin lectin family protein;
AT1G50660		unknown protein;
AT1G52830	INDOLE-3-ACETIC ACID 6 (IAA6)	An extragenic dominant suppressor of the hy2 mutant phenotype. Also exhibits aspects of constitutive photomorphogenetic phenotype in the absence of hy2. Mutants have dominant leaf curling phenotype shortened hypocotyls and reduced apical hook. Induced by indole-3-acetic acid.
AT1G60010		unknown protein
AT1G62770		Plant invertase/pectin methylesterase inhibitor superfamily protein
AT1G64405		unknown protein
AT1G69530	EXPANSIN A1 (EXPA1)	Member of Alpha-Expansin Gene Family. Naming convention from the Expansin Working Group (Kende et al, Plant Mol Bio). Involved in the formation of nematode-induced syncytia in roots of Arabidopsis thaliana.
AT1G70560	TRYPTOPHAN AMINOTRANSFERASE OF ARABIDOPSIS 1 (TAA1)	TAA1 is involved in the shade-induced production of indole-3-pyruvate (IPA), a precursor to IAA, a biologically active auxin. It is also involved in regulating many aspects of plant growth and development from embryogenesis to flower formation and plays a role in ethylene-mediated signaling. This enzyme can catalyze the formation of IPA from L-tryptophan. Though L-Trp is expected to be the preferred substrate in vivo, TAA1 also acts as an aminotransferase using L-Phe, L-Tyr, L-Leu, L-Ala, L-Met, and L-Gln.
AT1G70940	PIN-FORMED 3 (PIN3)	A regulator of auxin efflux and involved in differential growth. PIN3 is expressed in gravity-sensing tissues, with PIN3 protein accumulating predominantly at the lateral cell surface. PIN3 localizes to the plasma membrane and to vesicles. In roots, PIN3 is expressed without pronounced polarity in tiers two and three of the columella cells, at the basal side of vascular cells, and to the lateral side of pericycle cells of the elongation zone. PIN3 overexpression inhibits root cell growth. Protein phosphorylation plays a role in PIN3 trafficking to the plasma membrane.

Locus identifier	Primary Gene Symbol	Gene Model Description
AT1G73590	PIN-FORMED 1 (PIN1)	Encodes an auxin efflux carrier involved in shoot and root development. It is involved in the maintenance of embryonic auxin gradients. Loss of function severely affects organ initiation, pin1 mutants are characterised by an inflorescence meristem that does not initiate any flowers, resulting in the formation of a naked inflorescence stem. PIN1 is involved in the determination of leaf shape by actively promoting development of leaf margin serrations. In roots, the protein mainly resides at the basal end of the vascular cells, but weak signals can be detected in the epidermis and the cortex. Expression levels and polarity of this auxin efflux carrier change during primordium development suggesting that cycles of auxin build-up and depletion accompany, and may direct, different stages of primordium development. PIN1 action on plant development does not strictly require function of PGP1 and PGP19 proteins.
AT1G74660	MINI ZINC FINGER 1 (MIF1)	Encodes MINI ZINC FINGER 1 (MIF1) which has a zinc finger domain but lacks other protein motifs normally present in transcription factors. MIF1 physically interact with a group of zinc finger-homeodomain (ZHD) transcription factors, such as ZHD5 (AT1G75240), that regulate floral architecture and leaf development. Gel mobility shift assays revealed that MIF1 blocks the DNA binding activity of ZHD5 homodimers by competitively forming MIF1-ZHD5 heterodimers. Constitutive overexpression of MIF1 caused dramatic developmental defects, seedlings were non-responsive to gibberellin (GA) for cell elongation, hypersensitive to the GA synthesis inhibitor paclobutrazol (PAC) and abscisic acid (ABA), and hyposensitive to auxin, brassinosteroid and cytokinin, but normally responsive to ethylene.
AT1G77280		Protein kinase protein with adenine nucleotide alpha hydrolases-like domain
AT1G78100		F-box family protein;
AT2G03730	ACT DOMAIN REPEAT 5 (ACR5)	Member of a small family of ACT domain containing proteins. ACT domains are thought to be involved in amino acid binding.
AT2G14960	(GH3.1)	encodes a protein similar to IAA-amido synthases. Lines carrying an insertion in this gene are hypersensitive to auxin.
AT2G18690		unknown protein;
AT2G18980	Peroxidase 16	Peroxidase superfamily protein
AT2G23170	(GH3.3)	encodes an IAA-amido synthase that conjugates Asp and other amino acids to auxin in vitro.
AT2G25790		Leucine-rich receptor-like protein kinase family protein;
AT2G30040	MITOGEN-ACTIVATEDPROTEIN KINASE KINASE KINASE 14 (MAPKKK14)	member of MEKK subfamily
AT2G33310	AUXIN-INDUCED PROTEIN13 (IAA13)	Auxin induced gene, IAA13 (IAA13).
AT2G34650	**PINOID (PID)**	**Encodes a protein serine/threonine kinase that may act as a positive regulator of cellular auxin efflux, as a a binary switch for PIN polarity, and as a negative regulator of auxin signaling. Recessive mutants exhibit similar phenotypes as pin-formed mutants in flowers and inflorescence but distinct phenotypes in cotyledons and leaves. Expressed in the vascular tissue proximal to root and shoot meristems, shoot apex, and embryos. Expression is induced by auxin. Overexpression of the gene results in phenotypes in the root and shoot similar to those found in auxin-insensitive mutants. The protein physically interacts with TCH3 (TOUCH3) and PID-BINDING PROTEIN 1 (PBP1), a previously uncharacterized protein containing putative EF-hand calcium-binding motifs. Acts together with ENP (ENHANCER OF PINOID) to instruct precursor cells to elaborate cotyledons in the transition stage embryo. Interacts with PDK1. PID autophosphorylation is required for the ability of PID to phosphorylate an exogenous substrate. PID activation loop is required for PDK1-dependent PID phosphorylation and requires the PIF domain. Negative regulator of root hair growth. PID kinase activity is critical for the inhibition of root hair growth and for maintaining the proper subcellular localization of PID.**
AT2G35930	PLANT U-BOX 23 (PUB23)	Encodes a cytoplasmically localized U-box domain containing E3 ubiquitin ligase that is involved in the response to water stress and acts as a negative regulator of PAMP-triggered immunity.
AT2G35980	YELLOW-LEAF-SPECIFIC GENE 9 (YLS9)	Encodes a protein whose sequence is similar to tobacco hairpin-induced gene (HIN1) and Arabidopsis non-race specific disease resistance gene (NDR1). Expression of this gene is induced by cucumber mosaic virus, spermine and during senescence. The gene product is localized to the chloroplast.
AT2G36220		unknown protein
AT2G39370		unknown protein;
AT2G39700	EXPANSIN A4 (EXPA4)	putative expansin.
AT2G40540	POTASSIUMTRANSPORTER 2 (KT2)	putative potassium transporter AtKT2p (AtKT2) mRNA,
AT2G41100	TOUCH 3 (TCH3)	encodes a calmodulin-like protein, with six potential calcium binding domains. Calcium binding shown by Ca(2+)-specific shift in electrophoretic mobility. Expression induced by touch and darkness. Expression may also be developmentally controlled. Expression in growing regions of roots, vascular tissue, root/shoot junctions, trichomes, branch points of the shoot, and regions of siliques and flowers.
AT2G41380		S-adenosyl-L-methionine-dependent methyltransferases superfamily protein;
AT2G42430	LATERAL ORGANBOUNDARIES-DOMAIN 16 (LBD16)	LOB-domain protein gene LBD16. This gene contains one auxin-responsive element (AuxRE).
AT2G42440		Lateral organ boundaries (LOB) domain family protein; CONTAINS InterPro DOMAIN/s: Lateral organ boundaries, LOB (InterPro:IPR004883)
AT2G42870	PHY RAPIDLY REGULATED1 (PAR1)	Encodes PHYTOCHROME RAPIDLY REGULATED1 (PAR1), an atypical basic helix-loop-helix (bHLP) protein. Closely related to PAR2 (At3g58850). Up regulated after simulated shade perception. Acts in the nucleus to control plant development and as a negative regulator of shade avoidance response. Functions as transcriptional repressor of auxin-responsive genes SAUR15 (AT4G38850) and SAUR68 (AT1G29510).
AT2G43590		Chitinase family protein
AT2G45400	(BEN1)	involved in the regulation of brassinosteroid metabolic pathway
AT2G45420	LOB DOMAIN-CONTAINING PROTEIN 18 (LBD18)	LOB domain-containing protein 18 (LBD18)
AT2G47130		NAD(P)-binding Rossmann-fold superfamily protein
AT2G47140		NAD(P)-binding Rossmann-fold superfamily protein
AT2G47260	**WRKY DNA-BINDING PROTEIN 23 (WRKY23)**	**Encodes a member of WRKY Transcription Factor; Group I. Involved in nematode feeding site establishment.**
AT3G02885	GAST1 PROTEINHOMOLOG 5 (GASA5)	GAST1 protein homolog 5 (GASA5); INVOLVED IN: response to gibberellin stimulus;
AT3G07010	Probable pectate lyase 8	Pectin lyase-like superfamily protein
AT3G07390	AUXIN-INDUCED IN ROOTCULTURES 12 (AIR12)	isolated from differential screening of a cDNA library from auxin-treated root culture. sequence does not show homology to any known proteins and is predicted to be extracellular.
AT3G09280		unknown protein
AT3G13380	Serine/threonine-protein kinase BRI1-like 3	Similar to BRI, brassinosteroid receptor protein.
AT3G15540	INDOLE-3-ACETIC ACIDINDUCIBLE 19 (IAA19)	Primary auxin-responsive gene. Involved in the regulation stamen filaments development.
AT3G16420	AT3G16420; AT5G54490 PINOID-BINDING PROTEIN 1 (PBP1)	Encodes a PINOID (PID)-binding protein containing putative EF-hand calcium-binding motifs. The interaction is dependent on the presence of calcium. mRNA expression is up-regulated by auxin. Not a phosphorylation target of PID, likely acts upstream of PID to regulate the activity of this protein in response to changes in calcium levels.
AT3G18560		unknown protein;
AT3G19200		unknown protein;
AT3G20830		AGC (cAMP-dependent, cGMP-dependent and protein kinase C) kinase family protein;
AT3G21700	(SGP2)	Monomeric G protein. Expressed in root epidermal cells that are destined to become atrichoblasts. Also expressed during pollen development and in the pollen tube tip.
AT3G23030	INDOLE-3-ACETIC ACID INDUCIBLE 2 (IAA2)	auxin inducible gene expressed in the nucleus
AT3G26760		NAD(P)-binding Rossmann-fold superfamily protein
AT3G28850		Glutaredoxin family protein

Locus identifier	Primary Gene Symbol	Gene Model Description
AT3G42800		unknown protein
AT3G49700	1-AMINOCYCLOPROPANE-1-CARBOXYLATE SYNTHASE 9 (ACS9)	encodes a a member of the 1-aminocyclopropane-1-carboxylate (ACC) synthase (S-adenosyl-L-methionine methylthioadenosine- lyase, EC 4.4.1.14) gene family. Mutants produce elevated levels of ethylene as etiolated seedlings.
AT3G50660	DWARF 4 (DWF4)	Encodes a 22α hydroxylase whose reaction is a rate-limiting step in brassinosteroid biosynthetic pathway. The protein is a member of CYP90B gene family. CLM is an epi-allele with small, compressed rosette, reduced internode length, and reduced fertility, appears in selfed ddm mutant plants possibly due to loss of cytosine methylation. Transcripts accumulate in actively growing tissues, and GUS expression is negatively regulated by brassinosteroids. Localized in the endoplasmic reticulum. The in vitro expressed protein can perform the C-22 hydroxylation of a variety of C27-, C28- and C29-sterols. Cholesterol was the best substrate, followed by campesterol. Sitosterol was a poor substrate.
AT3G51410		Arabidopsis protein of unknown function (DUF241)
AT3G54000		Uncharacterised conserved protein UCP022260
AT3G54950	PATATIN-RELATED PHOSPHOLIPASE IIIBETA (pPLAIIIbeta)	Encodes pPLAIIIbeta, a member of the Group 3 patatin-related phospholipases. pPLAIIIbeta hydrolyzes phospholipids and galactolipids and additionally has acyl-CoA thioesterase activity. Alterations of pPLAIIIβ result in changes in lipid levels and composition.
AT3G55690		unknown protein;
AT3G55720		Protein of unknown function (DUF620)
AT3G58190	LATERAL ORGANBOUNDARIES-DOMAIN 29 (LBD29)	This gene contains two auxin-responsive element (AuxRE).
AT3G60550	CYCLIN P3;2 (CYCP3;2)	cyclin p3;2 (CYCP3;2);
AT3G60630	HAIRY MERISTEM 2(HAM2)	Belongs to one of the LOM (LOST MERISTEMS) genes: AT2G45160 (LOM1), AT3G60630 (LOM2) and AT4G00150 (LOM3). LOM1 and LOM2 promote cell differentiation at the periphery of shoot meristems and help to maintain their polar organization.
AT3G60640	AUTOPHAGY 8G (ATG8G)	AUTOPHAGY 8G (ATG8G)
AT3G62100	INDOLE-3-ACETIC ACID INDUCIBLE 30 (IAA30)	Encodes a member of the Aux/IAA family of proteins implicated in auxin signaling. IAA30 lacks the conserved degron (domain II) found in many family members. IAA30 transcripts are induced by auxin treatment and accumulate preferentially in the quiescent center cells of the root meristem. Overexpression of IAA30 leads to defects in gravitropism, root development, root meristem maintenance, and cotyledon vascular development. Target of LEC2 and AGL15. Promotes somatyic embryogenesis.
AT3G63440	CYTOKININOXIDASE/DEHYDROGENAS E 6 (CKX6)	This gene used to be called AtCKX7. It encodes a protein whose sequence is similar to cytokinin oxidase/dehydrogenase, which catalyzes the degradation of cytokinins.
AT4G00080	UNFERTILIZED EMBRYOSAC 11 (UNE11)	unfertilized embryo sac 11 (UNE11)
AT4G01870		tolB protein-related
AT4G11280	1-AMINOCYCLOPROPANE-1-CARBOXYLIC ACID (ACC) SYNTHASE 6 (ACS6)	encodes a a member of the 1-aminocyclopropane-1-carboxylate (ACC) synthase (S-adenosyl-L-methionine methylthioadenosine- lyase, EC 4.4.1.14) gene family
AT4G12410		SAUR-like auxin-responsive protein family ; CONTAINS InterPro DOMAIN/s: Auxin responsive SAUR protein (InterPro:IPR003676); BEST Arabidopsis thaliana protein match is: SAUR-like auxin-responsive protein family (TAIR:AT4G22620.1); Has 1137 Blast hits to 1128 proteins in 26 species: Archae - 0; Bacteria - 0; Metazoa - 0; Fungi - 0; Plants - 1136; Viruses - 0; Other Eukaryotes - 1 (source: NCBI BLink).
AT4G12720	Nudix hydrolase 7 (NUDT7)	Encodes a protein with ADP-ribose hydrolase activity. Negatively regulates EDS1-conditioned plant defense and programmed cell death.
AT4G13180		NAD(P)-binding Rossmann-fold superfamily protein).
AT4G13195	CLAVATA3/ESR-RELATED44 (CLE44)	Belongs to a large gene family, called CLE for CLAVATA3/ESR-related, encoding small peptides with conserved carboxyl termini. The C-terminal 12 amino acid sequence of CLE44 is identical to that of a dodeca peptide (TDIF, tracheary element differentiation inhibitory factor) isolated from Arabidopsis and functions as a suppressor of plant stem cell differentiation. TDIF sequence is also identical to the C-terminal 12 amino acids of CLE41 (At3g24770).
AT4G14130	XYLOGLUCANENDOTRANSGLUCOSYLAS E/HYDROLASE 15 (XTH15)	xyloglucan endotransglycosylase-related protein (XTR7)
AT4G14560	INDOLE-3-ACETIC ACIDINDUCIBLE (IAA1)	auxin (indole-3-acetic acid) induced gene (IAA1) encoding a short-lived nuclear-localized transcriptional regulator protein.
AT4G17350		DOMAIN/s: Pleckstrin-like, plant (InterPro:IPR013666), Protein of unknown function DUF828 (InterPro:IPR008546), Pleckstrin homology (InterPro:IPR001849
AT4G22530		S-adenosyl-L-methionine-dependent methyltransferases superfamily protein
AT4G22620		SAUR-like auxin-responsive protein family
AT4G22780	ACT DOMAIN REPEAT 7(ACR7)	Member of a family of ACT domain containing proteins . ACT domains are involved in amino acid binding .
AT4G27260	(WES1)	encodes an IAA-amido synthase that conjugates Asp and other amino acids to auxin in vitro. Lines carrying insertions in this gene are hypersensitive to auxin.
AT4G27280		Calcium-binding EF-hand family protein;
AT4G28640	INDOLE-3-ACETIC ACIDINDUCIBLE 11 (IAA11)	Auxin induced gene, IAA11 (IAA11).
AT4G30420		nodulin MtN21 /EamA-like transporter family protein
AT4G31910		HXXXD-type acyl-transferase family protein
AT4G32280	INDOLE-3-ACETIC ACIDINDUCIBLE 29 (IAA29)	Auxin inducible protein.
AT4G37290		unknown protein
AT4G37295		unknown protein
AT4G37590	NAKED PINS IN YUCMUTANTS 5 (NPY5)	A member of the NPY gene family (NPY1/AT4G31820, NPY2/AT2G14820, NPY3/AT5G67440, NPY4/AT2G23050, NPY5/AT4G37590). Involved in auxin-mediated organogenesis.
AT5G01840	OVATE FAMILY PROTEIN 1 (OFP1)	Encodes a member of the plant specific ovate protein family. Members of this family have been shown to bind to KNOX and BELL-like TALE class homeodomain proteins. This interaction may mediate relocalization of the TALE homeodomain from the nucleus to the cytoplasm. Functions as a transcriptional repressor that suppresses cell elongation.
AT5G02760		Protein phosphatase 2C family protein
AT5G04980		DNAse I-like superfamily protein
AT5G05160	REDUCED IN LATERAL GROWTH1 (RUL1)	Encodes a receptor-like kinase that activates secondary growth, the production of secondary vascular tissues.
AT5G06080	LOB DOMAIN-CONTAINING PROTEIN 33 (LBD33)	LOB domain-containing protein 33 (LBD33)
AT5G12050		unknown protein;
AT5G16110		unknown protein
AT5G17340		Putative membrane lipoprotein
AT5G18560	(PUCHI)	Encodes PUCHI, a member of the ERF (ethylene response factor) subfamily B-1 of ERF/AP2 transcription factor family. The protein contains one AP2 domain. There are 15 members in this subfamily including ATERF-3, ATERF-4, ATERF-7, and leafy petiole. PUCHI is required for morphogenesis in the early lateral root primordium of Arabidopsis. Expressed in early floral meristem (stage 1 to 2). Required for early floral meristem growth and for bract suppression. Triple mutant with bop1 and bop2 displays a strong defect in the determination of floral meristem identity with reduced LFY expression and the lack of AP1 expression.
AT5G26930	GATA TRANSCRIPTIONFACTOR 23 (GATA23)	Encodes a member of the GATA factor family of zinc finger transcription factors. Controls lateral root founder cell specification.
AT5G40540		Protein kinase superfamily protein

Locus identifier	Primary Gene Symbol	Gene Model Description
AT5G43700	AUXIN INDUCIBLE 3-11(ATAUX2-11)	Auxin inducible protein similar to transcription factors.
AT5G47370	(HAT2)	Homeobox-leucine zipper protein; induced by auxin, but not by other phytohormones. Plays opposite roles in the shoot and root tissues in regulating auxin-mediated morphogenesis.
AT5G48150	PHYTOCHROME A SIGNALTRANSDUCTION 1 (PAT1)	Member of GRAS gene family. Semi-dominant mutant has a reduced response to far-red light and appears to act early in the phytochrome A signaling pathway.
AT5G49448	AT5G49448	
AT5G51670		Protein of unknown function (DUF668)
AT5G52900		unknown protein
AT5G54490	PINOID-BINDING PROTEIN 1 (PBP1)	Encodes a PINOID (PID) binding protein containing putative EF-hand calcium-binding motifs. The interaction is dependent on the presence of calcium. mRNA expression is up-regulated by auxin. Not a phosphorylation target of PID, likely acts upstream of PID to regulate the activity of this protein in response to changes in calcium levels.
AT5G54500	FLAVODOXIN-LIKEQUINONE REDUCTASE 1 (FQR1)	Encodes a flavin mononucleotide-binding flavodoxin-like quinone reductase that is a primary auxin-response gene.
AT5G54510	DWARF IN LIGHT 1 (DFL1)	Encodes an IAA-amido synthase that conjugates Ala, Asp, Phe, and Trp to auxin. Lines overexpressing this gene accumulate IAA-ASP and are hypersensitive to several auxins. Identified as a dominant mutation that displays shorter hypocotyls in light grown plants when compared to wild type siblings. Protein is similar to auxin inducible gene from pea (GH3).
AT5G57100		Nucleotide/sugar transporter family protein
AT5G57520	ZINC FINGER PROTEIN 2(ZFP2)	Encodes a zinc finger protein containing only a single zinc finger.
AT5G62280		Protein of unknown function (DUF1442)
AT5G64250		Aldolase-type TIM barrel family protein
AT5G65390	ARABINOGALACTANPROTEIN 7 (AGP7)	arabinogalactan protein 7 (AGP7)
AT5G67430		Acyl-CoA N-acyltransferases (NAT) superfamily protein

5.2 *CAMEL-CANAR receptor kinase module targets PIN-dependent transport during auxin canalization*

Table S3. 4 **Overview of the IP-MS results for 35S::CANAR-eGFP**

Shows an overview of the putative interactors after MaxQuant and Perseus statistical analysis. The list is sorted based on the RATIO (highlighted in pale green) of 35S::CANAR-eGFP vs Col-0 WT control. P-values are calculated based on the three replicates of 35S::CANAR-eGFP vs Col-0 WT control using a

two-sided t-test (highlighted in pale green). Yellow highlight indicates bait, green indicates GFP and orange indicates selected proteins in this analysis.

Included as well is a “stickiness” value for all proteins in the list in Tab1. Based on all IP experiments performed in our hands, first the average ratio of all respective proteins was given and next, calculate the percentage of experiments this respective protein has been detected. Sticky proteins will thus get a high score, while other more specific proteins might have very low values or no value at all (not detected before in any other experiment).

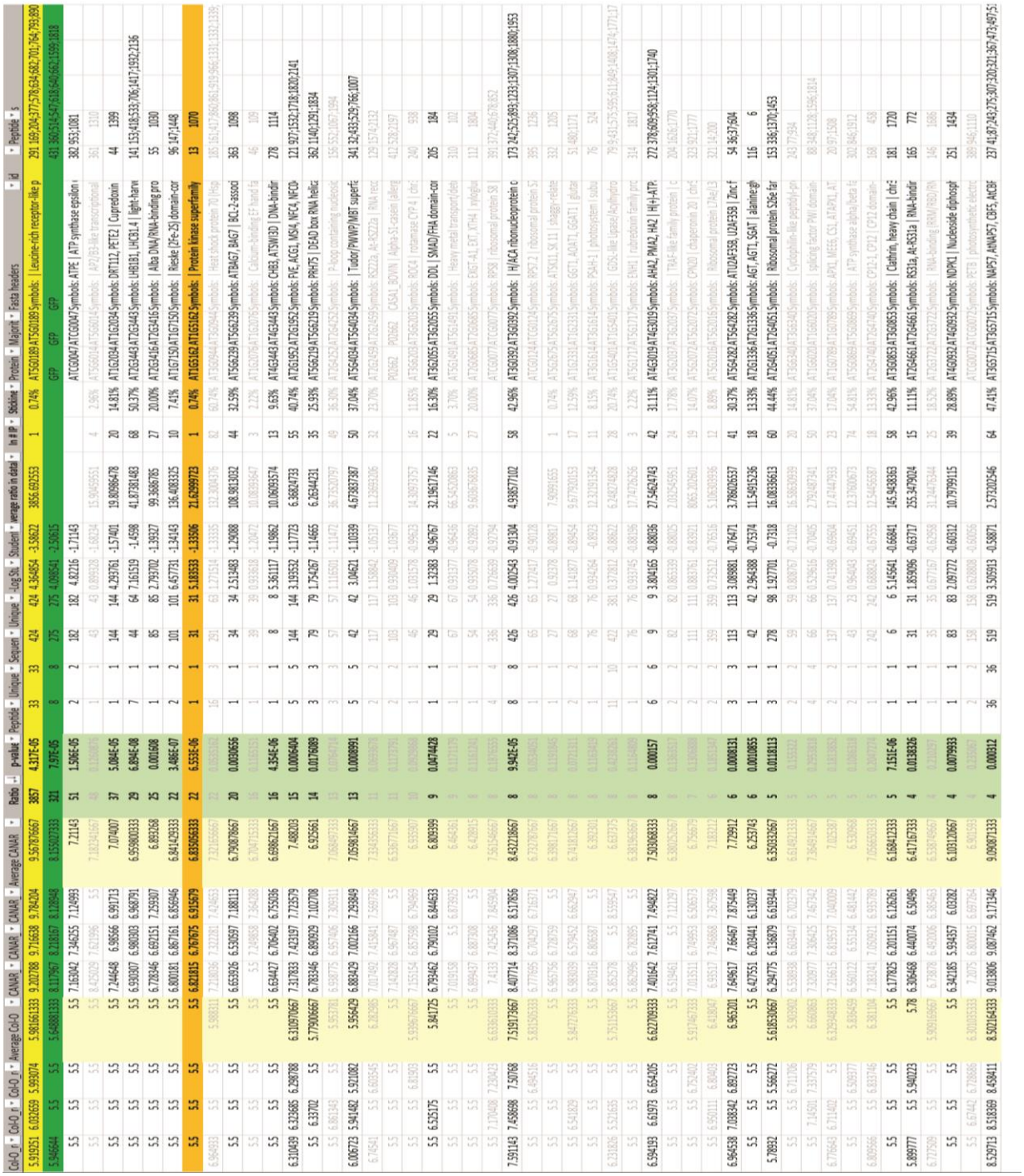

AT5G01890	CANAR				
	overview detected peptides	ATNVLIDAAGEAK	LDAFSLSGHIGR	SCLSVHPK	
		CDVYGFGILVLEVVTGK	LGLVCGSQVPSNRPEMEEVVK	SLDFSHNFLQGDIPDGLGGLYDLR	
		EGLEEGRVEECVDPR	LLASALDR	SLDLSENYFSGNLPDSMK	
		FSIILGIAR	LSGQIPAK	SLGSCSSIR	
		GGFGVVYK	LSSWNSEDYDPCNWVGCTCDPATNR	SQEEFER	
		GLAFLHSSNITHYNMK	LTVSGLIK	TSLQDGRPVAVK	
		GNFPAEEAIPVIK	LVMFSGEVDVFDTTGADALLNK	TSLQDGRPVAVKK	
		HDAAAALALSVGETFSCSPSKDQEFGK	LVMFSGEVDVFDTTGADALLNKDSELGR	VEECVDPR	
		HLHGDESVCLTWR	NSFTGDVLK	VQSALGYTAPEFACR	
		IPDGFFEQCGSLR	NWFSGDVPSDIGR	VSDFGLAR	
		KLTVSGLIK	RPVEYAEDDVVVLCETVR	WMFTGNSESSSLSR	
	overview full protein with detected peptides	MFNGAVSLLFLFLAVVSARADPTFNDDVLGLIVFKAGLDDPLSKLSSWNSEDYDPCNWVGCTCDPATNRVSELRLDAFSLSGHIGRGLLRLQFLHTLVLSNNNLTGTL NPEFPHLGSLQVVDFSGNNLSGRIPDGFFEQCGSLRSVSLANNKLTGSIPVSLSYCSTLTHLNLSSNQLSGRLPRDIWFLKSLKSLDFSHNFLQGDIPDGLGGLYDLRHINL SRNWFSGDVPSDIGRCSSLKSLDLSENYFSGNLPDSMKSLGSCSSIRLRGNSLIGEIPDWIGDIATLEILDLSANNFTGTVPFSLGNLEFLKDLNLSANMLAGELPQTLSN CSNLISIDVSKNSFTGDVLKWMFTGNSESSSLSRFSLHKRSGNDTIMPIVGFLQGLRVLDLSSNGFTGELPSNIWILTSLLQLNMSTNSLFGSIPTGIGGLKVAEILDLSSNL LNGTLPSEIGGAVSLKQLHLHRNRLSGQIPAKISNCSALNTINLSENELSGAIPGSIGSLSNLEYIDLSRNNLSGSLPKEIEKLSHLLTFNISHNNITGELPAGGFFNTIPLSAV TGNPSLCGSVVNRSCLSVHPKPIVLNPNSSNPTNGPALTGQIRKSVLSISALIAIGAAAVIAIGVVAVTLLNVHARSSVSRHDAAAALALSVGETFSCSPSKDQEFGKLVM FSGEVDVFDTTGADALLNKDSELGRGGFGVVYKTSLQDGRPVAVKKLTVSGLIKSQEEFEREMRKLGKLRHKNVVEIKGYYWTQSLQLLIHEFVSGGSLYRHLHGDESV CLTWRQRFSIILGIARGLAFLHSSNITHYNMKATNVLIDAAGEAKVSDFGLARLLASALDRCVLSGKVQSALGYTAPEFACRTVKITDRCDVYGFGILVLEVVTGKRPVE YAEDDVVVLCETVREGLEEGRVEECVDPRLRGNFPAEEAIPVIKLGLVCGSQVPSNRPEMEEVVKILELIQCPSHDLE
	GFP				
	overview detected peptides	EDGNILGHK	GGHVVEGLAGELEQLR		
		FEGDTLVNR	GIDFKEDGNILGHK		
		FICTTGK	SAMPEGYVQER		
		GEELFTGVVPILVELDGDVNGHK	TIFFKDDGNYK		
	overview full protein with detected peptides	MDEKTTGWRGGHVVEGLAGELEQLRARLEHHPQGQREPLEVLFQGPLEVLFQGPENLYFQGAIPGTTENLYFQGELKTAALGQHDEAMVSKGEELFTGVVPILVEL DGDVNGHKFSVSGEGEGDATYGKLTLKFICTTGKLPVPWPTLVTTLTYGVQCFSRYPDHMKQHDFFKSAMPEGYVQERTIFFKDDGNYKTRAEVKFEGDTLVNRIEL KGIDFKEDGNILGHKLEYNYNSHNVYIMADKQKNGIKVNFKIRHNIEDGSVQLADHYQQNTPIGDGPVLLPDNHYLSTQSALSKDPNEKRDHMVLLEFVTAAGITLG MDELYK			
AT1G05700	CAMEL				
	overview detected peptides	LADFGLSR			
	overview full protein with detected peptides	MTEATGLRRFFSKFICCDADDSTIEYEPYVYIPANSYSYAEVTKITNKFNRVHGKGGFGVVYRGVLNKQQVAVKMLNRASIYNIVQFTKEVHDFVKVRHKNLVSLIGYC DDGEHLALIYEFVANGDLNDQLSGKFGNVPSWETRLKIIIGVAQGLEYLHSELRILHRYVKPTNILLGENFEAKLADFGLSRSSPTNPDIQASNKIYVKPGRDPYLHHQYF NSNRLNQTSDIYSFGIVMLEMITNQPVVDNKRESPHISKWVDLKVAKGDTLEIVDLRLNNDFERDSVRKAMDIACSCAARAHNRPSMSQVVELNECLALEMARSN GRTGETTQTQ			

Table S3. 5 Overview of the IP-MS results for 35S::CAMEL-eGFP

Putative interactors after MaxQuant and Perseus statistical analysis. The list is sorted based on the RATIO (highlighted in pale green) of 35S::CAMEL-eGFP vs Col-0 WT control. P-values are calculated based on the three replicates of 35S::CAMEL-eGFP vs Col-0 WT control using a two-sided t-test (highlighted in pale green). Yellow highlight indicates bait, green indicates GFP and orange indicates selected proteins in this analysis.

Included as well is a “stickiness” value for all proteins in the list in Tab1. Based on all IP experiments performed in our hands, first the average ratio of all respective proteins was given and next, calculate the percentage of experiments this respective protein has been detected. Sticky proteins will thus get a high score, while other more specific proteins might have very low values or no value at all (not detected before in any other experiment).

Col-O_r	Col-O_r	Col-O_r	Average Col-C	CAMEL_	CAMEL_	CAMEL_	Average CAMEI	Ratio	p-value	Peptide	Unique	Sequen	Unique	-Log Stu	Student	Average ratio i	In # IPs	Stickiness	Protein	Majorit	Fasta headers	id	Peptides
4.9	4.9	4.9	4.9	8.959676	9.011443	9.058312	9.009810333	**12877**	**1.384E-08**	10	10	186	186	7.858771	-4.10981	83.75	2	1.48%	AT1G3036	AT1G3036	Symbols: ERD4 | Early-responsive to dehydration s	95	48;55;274;385;759;913;1892;1964;2290;2548
4.9	4.9	4.9	4.9	8.938399	8.99408	9.079109	9.003862667	**12702**	**5.923E-08**	10	5	474	263	7.227466	-4.10386	190.1354489	57	42.22%	AT2G4596	AT2G4596	Symbols: PIP1B, TMP-A, ATHH2, PIP1;2 | plasma me	298	88;268;453;591;898;1491;1769;1770;1772;1811
4.9	4.9	4.9	4.9	8.801218	8.820956	8.930867	8.851013667	**8933**	**6.51E-08**	11	3	549	147	7.186419	-3.95101	207.6515682	28	20.74%	AT3G1163	AT3G1163	Symbols: | Thioredoxin superfamily protein | chr3	342	169;186;531;857;858;1394;1873;2060;2186;2187;2646
4.9	4.9	4.9	4.9	8.783989	8.845557	8.805929	8.811825	**8163**	**2.699E-09**	9	4	455	252	8.56879	-3.91183	51.91900493	46	34.07%	AT3G6143	AT3G6143	Symbols: PIP1A, ATPIP1, PIP1, PIP1;1 | plasma mem	451	88;150;589;898;1491;1769;1770;1771;1812
4.9	4.9	4.9	4.9	8.845303	8.626258	8.51484	8.662133667	**5783**	**2.647E-06**	4	4	253	253	5.577204	-3.76213	20.93567189	59	43.70%	AT1G3133	AT1G3133	Symbols: PSAF | photosystem I subunit F | chr1:11	99	542;1229;1480;2590
4.9	4.9	4.9	4.9	8.512737	8.438638	8.528827	8.493400667	**3921**	**2.14E-08**	23	4	276	53	7.669581	-3.5934	27.54624743	42	31.11%	AT4G3019	AT4G3019	Symbols: AHA2, PMA2, HA2 | H(+)-ATPase 2 | chr4:	536	16;39;482;524;641;642;772;824;852;950;980;997;1196;1222;1444;1524;1561;2016;2099;2179;2322;2341;
4.9	4.9	4.9	4.9	8.492523	8.490787	8.386463	8.456591	**3602**	**5.667E-08**	14	3	601	104	7.246647	-3.55659	57.50952734	77	57.04%	AT1G1344	AT1G1344	Symbols: GAPC-2, GAPC2 | glyceraldehyde-3-phosp	55	23;310;324;684;840;1474;1606;1607;1848;2259;2409;2450;2503;2563
4.9	4.9	5.969844	5.256614667	8.744598	8.626309	8.848774	8.739893667	**3043**	**0.0006547**	8	5	402	199	3.183947	-3.48328	61.56415642	27	20.00%	AT1G0162	AT1G0162	Symbols: PIP1C, TMP-B, PIP1;3 | plasma membrane	0	88;590;793;898;1491;1774;1775;1776
4.9	4.9	4.9	4.9	8.365993	8.347486	8.340623	8.351367333	**2827**	**1.393E-10**	6	3	53	265	9.855932	-3.45137	62.0376867	38	28.15%	AT4G0043	AT4G0043	Symbols: TMP-C, PIP1;4, PIP1E | plasma membrane	465	88;592;794;898;1491;1773
4.9	4.9	4.9	4.9	8.243757	8.315046	8.457034	8.338612333	**2745**	**6.612E-07**	18	11	245	155	6.179685	-3.43861	58.41092238	20	14.81%	AT5G6267	AT5G6267	Symbols: AHA11, HA11 | H(+)-ATPase 11 | chr5:251	709	39;576;770;825;921;950;976;1049;1196;1311;1444;1524;1736;1941;2100;2147;2177;2536
4.9	4.9	4.9	4.9	8.342956	8.453731	8.144792	8.313826333	**2593**	**2.932E-06**	3	3	76	76	5.532849	-3.41383	10.62114961	2	1.48%	AT2G3901	AT2G3901	Symbols: PIP2E, PIP2;6 | plasma membrane intrinsi	272	332;2000;2161
4.9	4.9	4.9	4.9	8.226703	8.235125	8.220213	8.227347	**2125**	**1.7E-11**	5	5	22	22	10.76966	-3.32735	40.44748019	28	20.74%	AT5G2306	AT5G2306	Symbols: CaS | calcium sensing receptor | chr5:773	629	188;905;2160;2275;2354
4.9	4.9	4.9	4.9	8.281851	8.205367	8.161997	8.216405	**2072**	**7.468E-08**	10	10	156	156	7.126771	-3.3164	44.9376814	69	51.11%	AT5G5603	AT5G5603	Symbols: HSP81-2, ERD8, HSP90.2, AtHsp90.2 | hea	695	43;248;530;644;834;1235;1289;1290;1338;2207
4.9	4.9	4.9	4.9	8.171288	8.217247	8.244895	8.211143333	**2047**	**1.06E-08**	15	13	19	163	7.974822	-3.31114	51.71811792	8	5.93%	AT3G2886	AT3G2886	Symbols: ATMDR1, ATMDR11, PGP19, MDR11, MDR	389	18;87;290;342;756;927;938;1047;1058;1078;1103;1176;1177;1615;2252
4.9	4.9	4.9	4.9	8.253531	8.194847	8.164323	8.204233667	**2015**	**2.362E-08**	3	3	12	12	7.626668	-3.30423	20.12571533	35	25.93%	AT5G1404	AT5G1404	Symbols: PHT3;1 | phosphate transporter 3;1 | chr	606	2287;2356;2457
4.9	4.9	4.9	4.9	8.159025	8.222924	8.174147	8.185365333	**1929**	**7.115E-09**	10	8	242	185	8.147846	-3.28537	4112.408337	3	2.22%	AT1G2308	AT1G2308	Symbols: PIN7 | Auxin efflux carrier family protein	80	93;294;471;581;688;1439;1701;1702;1881;2296
4.9	4.9	4.9	4.9	8.224118	8.198272	8.102811	8.175067	**1884**	**9.651E-08**	2	2	279	279	7.015441	-3.27507	7.915938341	8	5.93%	AT1G7904	AT1G7904	Symbols: PSBR | photosystem II subunit R | chr1:29	192	2117;2586
4.9	4.9	4.9	4.9	7.514813	8.294444	8.691638	8.166965	**1849**	**0.0006988**	4	4	206	206	3.155625	-3.26697				CON__P00	CON__P00	Contaminant	751	1328;1361;1931;1932
4.9	6.285422	6.086324	5.757248667	8.924538	8.928576	8.958693	8.937269	**1514**	**0.0018239**	11	3	597	205	2.739009	-3.18002	219.2364389	22	16.30%	AT5G0629	AT5G0629	Symbols: 2-Cys Prx B, 2CPB | 2-cysteine peroxiredo	588	169;186;531;857;858;1394;1874;1891;2060;2188;2646
4.9	4.9	4.9	4.9	8.084648	8.066176	8.009579	8.053467667	**1424**	**1.578E-08**	5	5	425	425	7.802018	-3.15347	41.97427325	9	6.67%	AT4G3506	AT4G3506	Symbols: HIPP25 | Heavy metal transport/detoxific	556	59;447;1631;2397;2496
4.9	4.9	4.9	4.9	7.919439	8.057323	8.15045	8.042404	**1388**	**1.244E-06**	6	6	316	316	5.905247	-3.1424	0	0	0.00%	AT3G0974	AT3G0974	Symbols: SYP71, ATSYP71 | syntaxin of plants 71 | c	337	2;474;666;1593;1730;2051
4.9	4.9	4.9	4.9	7.946673	8.311181	7.803033	8.020295667	**1319**	**3.26E-05**	4	3	245	159	4.48676	-3.1203	8.757112307	37	27.41%	AT5G0153	AT5G0153	Symbols: LHCB4.1 | light harvesting complex photo	577	876;1688;2103;2277
4.9	4.9	4.9	4.9	8.091878	8.001734	7.947419	8.013677	**1299**	**2.008E-07**	4	4	223	223	6.697229	-3.11368	136.4083325	10	7.41%	AT1G7150	AT1G7150	Symbols: | Rieske (2Fe-2S) domain-containing pro	175	197;1450;1504;1980
4.9	4.9	4.9	4.9	7.89821	8.002468	8.138271	8.012983	**1297**	**1.486E-06**	5	5	105	105	5.828083	-3.11298	2.622449059	3	2.22%	AT1G4848	AT1G4848	Symbols: RKL1 | receptor-like kinase 1 | chr1:1791	117	181;676;855;1779;1799
4.9	4.9	4.9	4.9	7.939389	8.016239	8.042969	7.999532333	**1258**	**6.035E-08**	7	4	352	181	7.219315	-3.09953	115.1075926	23	17.04%	AT3G5342	AT3G5342	Symbols: PIP2A, PIP2, PIP2;1 | plasma membrane ir	426	78;119;138;433;454;1871;1939
4.9	6.728913	4.9	5.509637667	8.716086	8.20828	8.711824	8.545396667	**1086**	**0.0086511**	13	13	121	121	2.062926	-3.03576	87.19144485	1	0.74%	AT1G5987	AT1G5987	Symbols: PEN3, PDR8, ATPDR8, ABCG36, ATABCG36	147	90;91;406;808;1137;1147;1818;1961;2223;2227;2494;2510;258
4.9	4.9	4.9	4.9	7.904499	8.034629	7.808393	7.915840333	**1037**	**1.335E-06**	3	3	226	226	5.874445	-3.01584	1631.792633	18	13.33%	AT3G6147	AT3G6147	Symbols: LHCA2 | photosystem I light harvesting cc	452	1076;2526;2528
4.9	6.773743	4.9	5.524581	8.574887	8.741128	8.303843	8.539952667	**1036**	**0.0091016**	23	4	282	5	2.040883	-3.01537	26.60925227	46	34.07%	AT2G1896	AT2G1896	Symbols: AHA1, PMA, OST2, HA1 | H(+)-ATPase 1 |	218	16;39;451;479;524;641;642;772;823;950;980;997;1196;1222;1339;1444;1524;1561;2101;2179;2322;2341;
4.9	4.9	4.9	4.9	7.904288	7.96662	7.866624	7.912510667	**1029**	**5.262E-08**	4	4	126	126	7.278814	-3.01251	8.354644196	35	25.93%	AT1G4712	AT1G4712	Symbols: RD21, RD21A | Granulin repeat cysteine p	113	244;923;1563;2519
4.9	4.9	4.9	4.9	7.938655	7.956038	7.813654	7.902782333	**1006**	**2.981E-07**	4	4	116	116	6.525705	-3.00278	17.28951758	4	2.96%	AT1G4520	AT1G4520	Symbols: ATTLL1, TLL1 | triacylglycerol lipase-like 1	111	749;960;1489;2359
4.9	4.9	4.9	4.9	7.801966	7.923094	7.940984	7.888681333	**974**	**2.73E-07**	2	2	11	11	6.56388	-2.98868	0	0	0.00%	AT4G3892	AT4G3892	Symbols: AVA-P3, ATVHA-C3, VHA-C3 | vacuolar-typ	68	1905;1906
4.9	4.9	4.9	4.9	7.85909	7.88063	7.906308	7.882009333	**959**	**2.632E-09**	9	8	114	101	8.579663	-2.98201	63.85749004	5	3.70%	AT4G2596	AT4G2596	Symbols: PGP2 | P-glycoprotein 2 | chr4:13177438	522	883;1171;1175;1434;1603;1613;2252;2274;2517
4.9	4.9	4.9	4.9	7.824731	7.845631	7.891877	7.854079667	**900**	**1.22E-08**	2	1	76	45	7.913638	-2.95408	25.79479984	11	8.15%	AT5G6066	AT5G6066	Symbols: PIP2F, PIP2;4 | plasma membrane intrinsi	703	78;373
4.9	4.9	4.9	4.9	7.802192	7.925519	7.82307	7.850260333	**892**	**1.669E-07**	8	8	199	199	6.777673	-2.95026	13.73978638	16	11.85%	AT2G3095	AT2G3095	Symbols: VAR2, FTSH2 | FtsH extracellular protease	247	114;580;914;1164;1433;1890;1965;2319
4.9	4.9	4.9	4.9	7.844092	7.937558	7.732209	7.837953	**867**	**9.971E-07**	7	7	159	159	6.001272	-2.93795	4.396877169	1	0.74%	AT2G2099	AT2G2099	Symbols: SYTA, NTMC2TYPE1.1, ATSYTA, NTMC2T1.	225	239;618;787;1350;1588;1681;2170
4.9	4.9	4.9	4.9	7.90484	7.933087	7.630733	7.822886667	**837**	**7.055E-06**	8	2	61	273	5.151531	-2.92289	40.519939	69	51.11%	AT1G2993	AT1G2993	Symbols: CAB1, AB140, CAB140, LHCB1.3 | chloropl	93	98;564;680;878;1623;2293;2530;2607
4.9	4.9	4.9	4.9	7.845613	7.906879	7.696217	7.816236333	**825**	**1.267E-06**	1	1	9	9	5.897237	-2.91624				ATCG0077	ATCG0077	Symbols: RPS8 | ribosomal protein S8 | chrC:80068	736	1080
4.9	4.9	4.9	4.9	7.813274	7.79214	7.83465	7.813354667	**819**	**1.889E-09**	5	5	142	142	8.723861	-2.91335	0	0	0.00%	AT4G3547	AT4G3547	Symbols: PIRL4 | plant intracellular ras group-relate	560	229;562;1827;1851;1959
4.9	4.9	4.9	4.9	7.728508	7.78085	7.906917	7.805425	**804**	**6.603E-07**	4	4	79	79	6.180262	-2.90542	0	0	0.00%	AT3G5414	AT3G5414	Symbols: ATPTR1, PTR1 | peptide transporter 1 | ch	430	448;694;1465;1956
4.9	4.9	4.9	4.9	7.789842	7.803744	7.818219	7.803935	**802**	**3.8E-10**	4	1	353	73	9.420165	-2.90393	21.84340416	89	65.93%	AT3G1151	AT3G1151	Symbols: | Ribosomal protein S11 family protein |	341	334;1056;2216;2348
4.9	4.9	4.9	4.9	7.753253	7.784282	7.753361	7.763632	**731**	**1.014E-09**	4	4	147	147	8.993981	-2.86363	7.734962415	18	13.33%	AT1G1284	AT1G1284	Symbols: DET3, ATVHA-C | vacuolar ATP synthase s	51	340;649;1006;1146
4.9	4.9	4.9	4.9	7.800855	7.604107	7.863394	7.756118667	**718**	**3.341E-06**	5	5	103	103	5.476059	-2.85612	4112.408337	3	2.22%	AT2G0142	AT2G0142	Symbols: PIN4, ATPIN4 | Auxin efflux carrier family	202	584;1374;1538;1700;1703
7.485054	7.817764	7.929153	7.743990333	10.53612	10.69532	10.53372	10.58838667	**699**	**3.845E-05**	11	11	707	707	4.415102	-2.8444				GFP	GFP	GFP	776	67;358;490;674;692;735;778;991;1319;1837;2156
4.9	4.9	4.9	4.9	7.793434	7.771918	7.666593	7.743981667	**698**	**2.161E-07**	3	3	15	15	6.66542	-2.84398	10.15381369	1	0.74%	AT4G2289	AT4G2289	Symbols: PGR5-LIKE A | PGR5-LIKE A | chr4:120071	509	299;1041;2157
4.9	4.9	4.9	4.9	7.761409	7.80742	7.644439	7.737756	**688**	**5.115E-07**	2	2	179	179	6.291189	-2.83776	198.7773073	6	4.44%	AT3G6126	AT3G6126	Symbols: | Remorin family protein | chr3:2267540	450	146;1135
4.9	5.876062	6.071882	5.615981333	7.750354	8.666696	8.91401	8.443686667	**673**	**0.005051**	3	3	101	101	2.296626	-2.82771	225.0482346	16	11.85%	AT4G2340	AT4G2340	Symbols: PIP1D, PIP1;5 | plasma membrane intrinsi	511	452;588;1768
4.9	4.9	4.9	4.9	7.737232	7.768682	7.67303	7.726314667	**670**	**5.898E-08**	18	2	306	52	7.229295	-2.82631	732.3501164	44	32.59%	AT1G7992	AT1G7992	Symbols: | Heat shock protein 70 (Hsp 70) family p	196	142;206;424;425;469;511;664;693;773;832;910;1051;1549;1589;1817;2199;2404;262
4.9	4.9	4.9	4.9	7.700929	7.725299	7.742332	7.722853333	**665**	**1.969E-09**	4	4	65	65	8.705814	-2.82285	0	0	0.00%	AT3G5155	AT3G5155	Symbols: FER | Malectin/receptor-like protein kina	416	1660;2010;2211;2618
4.9	4.9	4.9	4.9	7.762904	7.550265	7.840658	7.717942333	**658**	**5.365E-06**	2	2	72	72	5.270412	-2.81794	155.038384	36	26.67%	AT2G3875	AT2G3875	Symbols: ANNAT4 | annexin 4 | chr2:16196582-161	269	288;1099
4.9	4.9	4.9	4.9	7.595684	7.699465	7.768786	7.687978333	**614**	**6.343E-07**	2	2	56	56	6.197699	-2.78798	0	0	0.00%	AT1G1126	AT1G1126	Symbols: STP1, ATSTP1 | sugar transporter 1 | chr1	45	922;1659
4.9	7.1211	4.9	5.640366667	8.453685	8.552048	8.249174	8.418302333	**600**	**0.0203825**	7	7	347	347	1.690742	-2.77794	31.09970161	11	8.15%	AT3G0129	AT3G0129	Symbols: | SPFH/Band 7/PHB domain-containing m	306	153;416;1424;1440;2007;2063;2405
8.098401	8.059033	8.136562	8.097998667	10.88327	10.85784	10.84702	10.86271	**582**	**3.899E-08**	29	29	502	502	7.409024	-2.76471	21.62999723	1	0.74%	AT1G0570	AT1G0570	Symbols: | Leucine-rich repeat transmembrane pr	20	323;510;650;701;798;860;1334;1378;1420;1466;1527;1553;1682;1847;1876;1914;1958;1977;2044;2047;2
4.9	4.9	4.9	4.9	7.596487	7.606016	7.784189	7.662230667	**578**	**1.426E-06**	3	3	179	179	5.845806	-2.76223	4.22309968	1	0.74%	AT2G4582	AT2G4582	Symbols: | Remorin family protein | chr2:1886314	297	594;1084;1142
4.9	4.9	4.9	4.9	7.722272	7.640899	7.610766	7.657979	**573**	**1.274E-07**	2	2	102	102	6.894726	-2.75798	26.8509919	10	7.41%	AT2G3718	AT2G3718	Symbols: RD28, PIP2;3, PIP2C | Aquaporin-like supe	257	434;450
4.9	4.9	4.9	4.9	7.642534	7.652691	7.636729	7.643984667	**555**	**5.01E-11**	4	4	132	132	10.30012	-2.74398	25.8595381	5	3.70%	AT4G3525	AT4G3525	Symbols: | NAD(P)-binding Rossmann-fold superfa	559	271;1269;2308;2645
4.9	4.9	4.9	4.9	7.596036	7.652894	7.682443	7.643791	**554**	**4.373E-08**	3	3	289	289	7.359214	-2.74379	10.3399796	7	5.19%	AT4G3001	AT4G3001	Symbols: | unknown protein;FUNCTIONS IN: mole	535	853;982;2037
4.9	4.9	4.9	4.9	7.74101	7.698935	7.486033	7.641992667	**552**	**4.095E-06**	8	3	326	9	5.387763	-2.74199	594.4703151	58	42.96%	AT2G3688	AT2G3688	Symbols: MAT3 | methionine adenosyltransferase	255	321;744;1283;1494;1555;2109;2369;2601
4.9	4.9	4.9	4.9	7.722609	7.590307	7.601354	7.63809	**547**	**3.438E-07**	1	1	72	72	6.463699	-2.73809	0	0	0.00%	AT3G1624	AT3G1624	Symbols: DELTA-TIP, TIP2;1, DELTA-TIP1, AQP1, ATT	357	100
4.9	4.9	4.9	4.9	7.526959	7.689815	7.685903	7.634225667	**542**	**8.868E-07**	5	5	272	272	6.052182	-2.73423	2.498579923	1	0.74%	AT2G4514	AT2G4514	Symbols: PVA12 | plant VAP homolog 12 | chr2:186	293	446;703;1625;1970;2023
4.9	4.9	4.9	4.9	7.724128	7.599654	7.513244	7.612342	**516**	**1.551E-06**	4	4	141	141	5.809504	-2.71234	33.81328798	13	9.63%	AT3G4678	AT3G4678	Symbols: PTAC16 | plastid transcriptionally active 1	405	1382;1782;1953;2508
4.9	4.9	4.9	4.9	7.724645	7.61343	7.4974	7.611825	**515**	**2.047E-06**	7	7	65	65	5.688844	-2.71182	2683.310771	12	8.89%	AT4G0251	AT4G0251	Symbols: TOC159, TOC86, PPI2, TOC160, ATTOC159	470	462;561;636;716;1336;1927;1996
4.9	4.9	4.9	4.9	7.643887	7.538461	7.641474	7.607940667	**510**	**1.625E-07**	4	4	358	358	6.789219	-2.70794	27.38620062	13	9.63%	AT5G5450	AT5G5450	Symbols: FQR1 | flavodoxin-like quinone reductase	692	765;814;1777;1864
4.9	4.9	4.9	4.9	7.607208	7.565871	7.621114	7.598064333	**499**	**8.574E-09**	2	2	149	149	8.066827	-2.69806	0	0	0.00%	AT5G5101	AT5G5101	Symbols: | Rubredoxin-like superfamily protein | c	685	315;1397
4.9	4.9	4.9	4.9	7.757851	7.601332	7.423966	7.594383	**495**	**9.767E-06**	7	3	30	127	5.010235	-2.69438	65.70266272	62	45.93%	AT4G1496	AT4G1496	Symbols: TUA6 | Tubulin/FtsZ family protein | chr4	16	80;286;669;1083;1259;1708;2266
4.9	4.9	4.9	4.9	7.460387	7.627059	7.682001	7.589815667	**490**	**2.25E-06**	2	2	39	39	5.647847	-2.68982	3.33129705	2	1.48%	AT4G1637	AT4G1637	Symbols: ATOPT3, OPT3 | oligopeptide transporter	496	1110;2212
4.9	4.9	4.9	4.9	7.715427	7.652391	7.376997	7.581605	**480**	**1.339E-05**	1	1	29	29	4.873134	-2.6816	0	0	0.00%	AT5G1096	AT5G1096	Symbols: | Polynucleotidyl transferase, ribonuclea	599	2612
4.9	4.9	4.9	4.9	7.62127	7.57446	7.546247	7.580659	**479**	**2.661E-08**	4	4	105	105	7.574977	-2.68066	3.665453081	2	1.48%	AT5G5252	AT5G5252	Symbols: OVA6, PRORS1 | Class II aaRS and biotin s	687	76;445;879;2175
4.9	4.9	4.9	4.9	7.387621	7.653897	7.69086	7.577459333	**476**	**9.636E-06**	3	3	78	78	5.016091	-2.67746	0	0	0.00%	AT3G1883	AT3G1883	Symbols: ATPLT5, PMT5, ATPMT5 | polyol/monosac	368	944;2229;2273
4.9	4.9	4.9	4.9	7.467475	7.64657	7.612275	7.57544	**474**	**1.059E-06**	2	2	91	91	5.974899	-2.67544	46.74851933	10	7.41%	AT1G0475	AT1G0475	Symbols: VAMP7B, VAMP721, ATVAMP721, AT VAM	15	867;1994
4.9	4.9	4.9	4.9	7.485934	7.532066	7.682804	7.566934667	**464**	**1.476E-06**	5	5	84	84	5.830863	-2.66693	12.87984531	2	1.48%	AT5G5711	AT5G5711	Symbols: ACA8, AT-ACA8 | autoinhibited Ca2+ -ATP	696	105;1537;1857;2078;2244
4.9	4.9	4.9	4.9	7.573336	7.529148	7.592577	7.565020333	**462**	**1.478E-08**	5	5	92	92	7.830351	-2.66502	0	0	0.00%	AT4G0885	AT4G0885	Symbols: | Leucine-rich repeat receptor-like prote	478	365;1157;1318;1379;1387
4.9	4.9	4.9	4.9	7.687217	7.591566	7.400469	7.559750667	**457**	**6.012E-06**	3	3	206	206	5.220976	-2.65975	4.99358712	58	42.96%	AT1G6743	AT1G6743	Symbols: | Ribosomal protein L22p/L17e family pr	86	587;1120;2604
4.9	4.9	4.9	4.9	7.71152	7.367114	7.595496	7.558043333	**455**	**1.247E-05**	5	4	128	116	4.904075	-2.65804	2.635621646	1	0.74%	AT1G5150	AT1G5150	Symbols: CER5, D3, ABCG12, WBC12, ATWBC12 | AI	125	289;621;1365;1612;2279
4.9	4.9	4.9	4.9	7.523239	7.500237	7.641236	7.554904	**452**	**4.386E-07**	14	3	627	13	6.357939	-2.6549	493.0721311	90	66.67%	AT3G0412	AT3G0412	Symbols: GAPC, GAPC-1, GAPC1 | glyceraldehyde-3-	317	23;112;310;324;684;840;1474;1605;1848;2259;2408;2450;2503;2563
4.9	4.9	4.9	4.9	7.564038	7.459453	7.564145	7.529212	**426**	**1.856E-07**	2	2	6	6	6.73137	-2.62921	0	0	0.00%	AT4G0110	AT4G0110	Symbols: ADNT1 | adenine nucleotide transporter	467	1455;2106
4.9	6.669298	6.594337	6.054545	8.62842	8.731412	8.675971	8.678601	**421**	**0.0105259**	13	13	337	337	1.977742	-2.62406	20.35045366	51	37.78%	AT1G7890	AT1G7890	Symbols: VHA-A | vacuolar ATP synthase subunit A	191	494;742;1144;1162;1257;1264;1305;1454;2080;2247;2390;2629;2632
4.9	4.9	4.9	4.9	7.510397	7.539841	7.509229	7.519822333	**417**	**1.281E-09**	11	2	444	112	8.89238	-2.61982	101.5013758	87	64.44%	AT3G1392	AT3G1392	Symbols: EIF4A1, RH4, TIF4A1 | eukaryotic translati	348	97;359;831;845;854;1136;1317;1388;1498;1696;2367
4.9	4.9	4.9	4.9	7.575581	7.59405	7.338297	7.502642667	**401**	**5.973E-06**	8	6	139	103	5.223838	-2.60264	6.644329095	14	10.37%	AT1G7857	AT1G7857	Symbols: RHM1, ROL1, ATRHM1 | rhamnose biosyn	189	166;500;654;740;870;1511;1694;1973
4.9	4.9	4.9	4.9	7.526559	7.568636	7.40929	7.501495	**399**	**6.753E-07**	4	4	58	58	6.170526	-2.60149	53.38563377	9	6.67%	AT3G2375	AT3G2375	Symbols: | Leucine-rich repeat protein kinase fami	378	126;702;1270;2291
4.9	4.9	4.9	4.9	7.462143	7.454708	7.575581	7.497477333	**396**	**3.079E-07**	5	5	257	257	6.511532	-2.59748	7.053303892	8	5.93%	AT3G2871	AT3G2871	Symbols: | ATPase, V0/A0 complex, subunit C/D | c	388	92;253;1482;1523;1587
4.9	4.9	4.9	4.9	7.147769	7.562102	7.774794	7.494888333	**393**	**0.000147**	2	2	36	36	3.832543	-2.59489	6038.4681	8	5.93%	AT4G1242	AT4G1242	Symbols: SKU5 | Cupredoxin superfamily protein |	487	208;1693
4.9	4.9	4.9	4.9	7.432408	7.44604	7.583924	7.487457333	**387**	**7.325E-07**	4	4	114	114	6.135201	-2.58746	0	0	0.00%	AT3G2181	AT3G2181	Symbols: | Zinc finger C-x8-C-x5-C-x3-H type famil	375	103;326;1131;2089
4.9	4.9	4.9	4.9	7.573811	7.42794	7.451725	7.484492	**384**	**5.594E-07**	7	6	102	87	6.252289	-2.58449	21.72692924	34	25.19%	AT4G2419	AT4G2419	Symbols: SHD, AtHsp90.7, AtHsp90-7 | Chaperone p	513	570;663;1035;1116;1260;1262;1904
4.9	4.9	4.9	4.9	7.396827	7.469203	7.543758	7.469929333	**371**	**4.445E-07**	4	4	232	232	6.352165	-2.56993	0	0	0.00%	AT1G1020	AT1G1020	Symbols: WLIM1 | GATA type zinc finger transcripti	39	869;1077;1678;2475
4.9	4.9	4.9	4.9	7.39354	7.387354	7.602266	7.461053333	**364**	**3.453E-06**	2	2	13	13	5.461791	-2.56105	10.70242223	40	29.63%	AT5G5984	AT5G5984	Symbols: | Ras-related small GTP-binding family pr	403	1152;1576
6.202216	6.177074	4.9	5.759763333	8.595959	7.717912	8.645137	8.319669333	**363**	**0.0081818**	10	8	255	20	2.087152	-2.55991	3.087166847	2	1.48%	AT1G7094	AT1G7094	Symbols: PIN3, ATPIN3 | Auxin efflux carrier family	174	243;442;689;1276;1439;1508;1704;1869;2138;2296

AT1G05700	CAMEL			
	overview detected peptides			
		DDTTGINYVSDSSFVETGVSK	MTNNFGQVLGK	SVNSAPQTSPMAK
		EFDISINGVTVAAGFSPK	NCYTLIPIQGK	TSNILLNEK
		EVVYLSQSENIFVCLGNK	PITMTLENSDPNVR	TVIKESQTK
		FLGNDNTTYDSPNGALFFSR	SDIYSFGVVLLEMITGK	VHVSDWVISILR
		GGFGTVYHGFYDNLQVAVK	SFHTESR	VVELALSSVSQNVSDR
		GLNECLQR	SHVSTLVAGTPGYLDPLCFETNGLNEK	VVELALSSVSQNVSDRPNMPHIVR
		LGENPGLCTEISCR	SLMGSPVR	YDDDVYDR
		LLSETSAQGFK	SNTGSFSLR	YLQTNTFFLNPESQSK
		LQIALDAAQGLEYLHCGCKPPIVHR	STLPPIVNALEIYVANSFSQSLTNQEDGDAVTSLK	YQHTLSWR
		LVIPLVASFAALFILLLLSGVFWR	STNDVNNVIDSK	
	overview full protein with detected peptides	MEEFRFLYLIYSAAFALCLVVSVLAQDQSGFISIDCGIPSGSSYKDDTTGINYVSDSSFVETGVSKSIPFTAQRQLQNLRSFPEGSRNCYTLIPIQGKGKKYLIRASF MYGNYDGENGSPEFDLFLGGNIWDTVLLSNGSSIVSKEVVYLSQSENIFVCLGNKGKGTPFISTLELRFLGNDNTTYDSPNGALFFSRRWDLRSLMGSPVRYD DDVYDRIWIPRNFGYCREINTSLPVTSDNNSYSLSSLVMSTAMTPINTTRPITMTLENSDPNVRYFVYMHFAEVEDLSLKPNQTREFDISINGVTVAAGFSPKY LQTNTFFLNPESQSKIAFSLVRTPKSTLPPIVNALEIYVANSFSQSLTNQEDGDAVTSLKTSYKVKKNWHGDPCLPNDYIWEGLNCSYDSLTPPRITSLNLSSSGL TGHISSSFSNLTMIQELDLSNNGLTGDIPEFLSKLKFLRVLNLENNTLTGSVPSELLERSNTGSFSLRLGENPGLCTEISCRKSNSKKLVIPLVASFAALFILLLLSGVF WRIRNRRNKSVNSAPQTSPMAKSENKLLFTFADVIKMTNNFGQVLGKGGFGTVYHGFYDNLQVAVKLLSETSAQGFKEFRSEVEVLVRVHHVNLTALIGYF HEGDQMGLIYEFMANGNMADHLAGKYQHTLSWRQRLQIALDAAQGLEYLHCGCKPPIVHRDVKTSNILLNEKNRAKLADFGLSRSFHTESRSHVSTLVAGT PGYLDPLCFETNGLNEKSDIYSFGVVLLEMITGKTVIKESQTKRVHVSDWVISILRSTNDVNNVIDSKMAKDFDVNSVWKVVELALSSVSQNVSDRPNMPHI VRGLNECLQREESNKNY		
	GFP			
	overview detected peptides			
		AEVKFEGDTLVNR	GEELFTGVVPILVELDGDVNGHK	
		DHMVLLEFVTAAGITLGMDELYK	HNIEDGSVQLADHYQQNTPIGDGPVLLPDNHYLSTQSALSK	
		EDGNILGHK	LEYNYNSHNVYIMADK	
		FEGDTLVNR	SAMPEGYVQER	
		FICTTGK	TIFFKDDGNYK	
		FSVSGEGEGDATYGK		
	overview full protein with detected peptides	MDEKTTGWRGGHVVEGLAGELEQLRARLEHHPQGQREPLEVLFQGPLEVLFQGPENLYFQGAIPGTTENLYFQGELKTAALGQHDEAMVSKGEELFTGVV PILVELDGDVNGHKFSVSGEGEGDATYGKLTLKFICTTGKLPVPWPTLVTTLTYGVQCFSRYPDHMKQHDFFKSAMPEGYVQERTIFFKDDGNYKTRAEVKF EGDTLVNRIELKGIDFKEDGNILGHKLEYNYNSHNVYIMADKQKNGIKVNFKIRHNIEDGSVQLADHYQQNTPIGDGPVLLPDNHYLSTQSALSKDPNEKRD HMVLLEFVTAAGITLGMDELYK		
AT1G70940	PIN3			
	overview detected peptides			
		AVAHPASGDFGGEQQFSFAGK	MLVPDQSHNGETK	
		DVNTNQQTTLPTGGK	PSNLTGAEIYSLSTTPR	
		FGYYPGGGAGSYPAPNPEFSSTTTSTANK	SFCGPNMTPR	
		LAPNSTAALQSK	TGLGGAEASQR	
		LSNFGPADMYSVQSSR	VAIVQAALPQGIVPFVFAK	
	overview full protein with detected peptides	MISWHDLYTVLTAVIPLYVAMILAYGSVRWWKIFSPDQCSGINRFVAIFAVPLLSFHFISTNNPYAMNLRFIAADTLQKIIMLSLLVLWANFTRSGSLEWSITIF SLSTLPNTLVMGIPLLIAMYGEYSGSLMVQIVVLQCIIWYTLLLFLFEFRGAKMLIMEQFPETAASIVSFKVESDVVSLDGHDFLETDAEIGDDGKLHVTVRKSN ASRRSFCGPNMTPRPSNLTGAEIYSLSTTPRGSNFNHSDFYNMMGFPGGRLSNFGPADMYSVQSSRGPTPRPSNFEENCAMASSPRFGYYPGGGAGSYPAP NPEFSSTTTSTANKSVNKNPKDVNTNQQTTLPTGGKSNSHDAKELHMFVWSSNGSPVSDRAGLNVFGGAPDNDQGGRSDQGAKEIRMLVPDQSHNGET KAVAHPASGDFGGEQQFSFAGKEEEAERPKDAENGLNKLAPNSTAALQSKTGLGGAEASQRKNMPPASVMTRLILIMVWRKLIRNPNTYSSLIGLIWALVA FRWHVAMPKIIQQSISILSDAGLGMAMFSLGLFMALQPKLIACGNSVATFAMAVRFLTGPAVMAVAAIAIGLRGDLLRVAIVQAALPQGIVPFVFAKEYNVH PAILSTGVIFGMLIALPITLVYYILLGL		
AT2G01420	PIN4			
	overview detected peptides			
		ENQQQLQEK		
		LLIMEQFPETGASIVSFK		
		MVVSDQPR		
		PSNFEENNAVK		
		PSNLTGAEIYSLSSTPR		
	overview full protein with detected peptides	MITWHDLYTVLTAVVPLYVAMILAYGSVQWWKIFSPDQCSGINRFVAIFAVPLLSFHFISTNDPYAMNFRFVAADTLQKIIMLVLLALWANLTKNGSLEWMI TIFSLSTLPNTLVMGIPLLIAMYGTYAGSLMVQVVVLQCIIWYTLLLFLFEYRGAKLLIMEQFPETGASIVSFKVESDVVSLDGHDFLETDAEIGNDGKLHVTVR KSNASRRSLMMTPRPSNLTGAEIYSLSSTPRGSNFNHSDFYSVMGFPGGRLSNFGPADLYSVQSSRGPTPRPSNFEENNAVKYGFYNNTNSSVPAAGSYPAP NPEFSTGTGVSTKPNKIPKENQQQLQEKDSKASHDAKELHMFVWSSSASPVSDVFGGGAGDNVATEQSEQGAKEIRMVVSDQPRKSNARGGGDDIGGLD SGEGEREIEKATAGLNKMGSNSTAELEAAGGDGGGNNGTHMPPTSVMTRLILIMVWRKLIRNPNTYSSLIGLIWALVAYRWHVAMPKILQQSISILSDAGLG MAMFSLGLFMALQPKIIACGNSVATFAMAVRFITGPAIMAVAGIAIGLHGDLLRIAIVQAALPQGIVPFVFAKEYNVHPTILSTGVIFGMLIALPITLVYYILLGL		
AT1G23080	PIN7			
	overview detected peptides			
		AGLQVDNGANEQVGK	LSNFGPADMYSVQSSR	
		CNSTAELNPK	PSNFEESCAMASSPR	
		EAIETGETVPVK	PSNLTGAEIYSLNTTPR	
		ENHHHVGK	SFYGGGGTNMTPR	
		FGYYPGGAPGSYPAPNPEFSTGNK	VAIVQAALPQGIVPFVFAK	
	overview full protein with detected peptides	MITWHDLYTVLTAVIPLYVAMILAYGSVRWWKIFSPDQCSGINRFVAIFAVPLLSFHFISSNNPYAMNLRFIAADTLQKLIMLTLLIWANFTRSGSLEWSITIFS LSTLPNTLVMGIPLLIAMYGEYSGSLMVQIVVLQCIIWYTLLLFLFEYRGAKILIMEQFPETGASIVSFKVESDVVSLDGHDFLETDAQIGDDGKLHVTVRKSNA SRRSFYGGGGTNMTPRPSNLTGAEIYSLNTTPRGSNFNHSDFYSMMGFPGGRLSNFGPADMYSVQSSRGPTPRPSNFEESCAMASSPRFGYYPGGAPGSYP APNPEFSTGNKTGSKAPKENHHHVGKSNSNDAKELHMFVWGSNGSPVSDRAGLQVDNGANEQVGKSDQGGAKEIRMLISDHTQNGENKAGPMNGDY GGEEESERVKEVPNGLHKLRCNSTAELNPKEAIETGETVPVKHMPPASVMTRLILIMVWRKLIRNPNTYSSLIGLIWALVAFRWDVAMPKIIQQSISILSDAGL GMAMFSLGLFMALQPKLIACGNSTATFAMAVRFFTGPAVMAVAAMAIGLRGDLLRVAIVQAALPQGIVPFVFAKEYNVHPAILSTGVIFGMLIALPITLVYYI LLGL		

5.3 *Publications*

PLOS GENETICS

RESEARCH ARTICLE

WRKY23 is a component of the transcriptional network mediating auxin feedback on PIN polarity

Tomáš Prát[1☯], Jakub Hajný[1,2☯], Wim Grunewald[3], Mina Vasileva[1], Gergely Molnár[1], Ricardo Tejos[3,4], Markus Schmid[5,6], Michael Sauer[7], Jiří Friml[1]*

1 Institute of Science and Technology (IST), Klosterneuburg, Austria, **2** Laboratory of Growth Regulators, Palacký University, Olomouc, Czech Republic, **3** Department of Plant Biotechnology and Bioinformatics, Ghent University and Center for Plant Systems Biology, VIB, Ghent, Belgium, **4** Facultad de Recursos Naturales Renovables, Universidad Arturo Prat, Iquique, Chile, **5** Department of Molecular Biology, Max Planck Institute for Developmental Biology, Tübingen, Germany, **6** Department of Plant Physiology, Umeå Plant Science Centre, Umeå University, Umeå, Sweden, **7** Department of Plant Physiology, University of Potsdam, Potsdam, Germany

☯ These authors contributed equally to this work.
* jiri.friml@ist.ac.at

Citation: Prát T, Hajný J, Grunewald W, Vasileva M, Molnár G, Tejos R, et al. (2018) WRKY23 is a component of the transcriptional network mediating auxin feedback on PIN polarity. PLoS Genet 14(1): e1007177. https://doi.org/10.1371/journal.pgen.1007177

Editor: Lucia Strader, Washington University in St. Louis, UNITED STATES

Received: November 16, 2016

Accepted: December 29, 2017

Published: January 29, 2018

Data Availability Statement: Raw microarray data from this article can be found in the EMBL ArrayExpress repository under accession number E-MEXP-3283. All other relevant data are within the paper and its Supporting Information files.

Funding: This work was supported by the European Research Council (project ERC-2011-StG-20101109-PSDP). WG was a postdoctoral fellow of the Research Foundation Flanders. The funders had no role in study design, data collection

Abstract

Auxin is unique among plant hormones due to its directional transport that is mediated by the polarly distributed PIN auxin transporters at the plasma membrane. The canalization hypothesis proposes that the auxin feedback on its polar flow is a crucial, plant-specific mechanism mediating multiple self-organizing developmental processes. Here, we used the auxin effect on the PIN polar localization in *Arabidopsis thaliana* roots as a proxy for the auxin feedback on the PIN polarity during canalization. We performed microarray experiments to find regulators of this process that act downstream of auxin. We identified genes that were transcriptionally regulated by auxin in an AXR3/IAA17- and ARF7/ARF19-dependent manner. Besides the known components of the PIN polarity, such as PID and PIP5K kinases, a number of potential new regulators were detected, among which the WRKY23 transcription factor, which was characterized in more detail. Gain- and loss-of-function mutants confirmed a role for WRKY23 in mediating the auxin effect on the PIN polarity. Accordingly, processes requiring auxin-mediated PIN polarity rearrangements, such as vascular tissue development during leaf venation, showed a higher *WRKY23* expression and required the WRKY23 activity. Our results provide initial insights into the auxin transcriptional network acting upstream of PIN polarization and, potentially, canalization-mediated plant development.

Author summary

The plant hormone auxin belongs to the major plant-specific developmental regulators. It mediates or modifies almost all aspects of plant life. One of the fascinating features of the auxin action is its directional movement between cells, whose direction can be regulated

and analysis, decision to publish, or preparation of the manuscript.

Competing interests: The authors have declared that no competing interests exist.

by auxin signaling itself. This plant-specific feedback regulation has been proposed decades ago and allows for the self-organizing formation of distinct auxin channels shown to be crucial for processes, such as the regular pattern formation of leaf venation, organ formation, and regeneration of plant tissues. Despite the prominent importance of this so called auxin canalization process, the insight into the underlying molecular mechanism is very limited. Here, we identified a number of genes that are transcriptionally regulated and act downstream of the auxin signaling to mediate the auxin feedback on the polarized auxin transport. One of them is the *WRKY23* transcription factor that has previously been unsuspected to play a role in this process. Our work provides the first insights into the transcriptional regulation of the auxin canalization and opens multiple avenues to further study this crucial process.

Introduction

The phytohormone auxin plays a key role in many aspects of a plant's life cycle. A unique attribute of auxin is its polarized, intercellular movement that depends, among other components, on the polarly localized PIN-FORMED (PIN) auxin exporters [1–3]. The so-called canalization hypothesis proposes that auxin acts also as a cue in the establishment of new polarity axes during the polarization of tissues by the formation of self-organizing patterns due to the formation of narrow auxin transport channels driven by the polarized auxin carriers from an initially broad domain of auxin-transporting cells [4–6]. Canalization has been implied to mediate multiple key plant developmental processes, including formation of new vasculature [7], regeneration after wounding [8, 9], and competitive control of apical dominance [10–12]. Whereas the molecular details of canalization are largely unknown, the key constituents are *(i)* the feedback regulation of the auxin transport directionality by auxin and *(ii)* the gradual concentrating and narrowing of auxin channels [4]. The auxin feedback on the transport directionality can be realized by the auxin impact on the PIN polarity [8] and might be related to an auxin effect on clathrin-mediated internalization of PIN proteins [13, 14], but the connection is still unclear [15]. Presumably, this feedback regulation of the PIN repolarization also plays a role in the establishment of the embryonic apical-basal axis [16, 17], during organogenesis [18], and termination of shoot bending responses [19].

Auxin feedback on the PIN polarity can be experimentally approximated by PIN polarity rearrangements after auxin treatment of *Arabidopsis thaliana* roots. Under standard conditions, PIN1 is localized at the basal (root-ward) sides of endodermal and pericycle cells and cells of the vascular tissue [20], whereas PIN2 exhibits a basal polarity in the young cortex cells, but an apical (shoot-ward) polarity in epidermal cells [21, 22]. After treatment with auxin, PIN1 changes from predominantly basal to also inner-lateral in endodermal and pericycle cells, whereas PIN2 undergoes a localization shift from the basal to also outer-lateral side of cortex cells [8]. The exact molecular mechanism and biological significance of this effect is unclear, but it has so far successfully served as easy, experimentally tractable proxy for auxin feed-back on PIN polarity [8]. It depends on the transcriptional SCF^{TIR1}-Aux/IAA-ARF auxin signalling pathway [23]. In brief, upon auxin binding to the TIR1/AFB receptor family, transcriptional repressors and co-receptors of the Aux/IAA class are degraded, in turn releasing auxin response transcription activators of the ARF family [24, 25].

In a heat-shock (HS)-inducible *HS::axr3-1* line expressing a mutated, nondegradable version of the IAA17 transcriptional repressor [25, 26], as well as in the *arf7 arf19* double mutant defective for these two functionally redundant transcriptional activators expressed in primary

roots [27], auxin is no longer effective in mediating PIN polarity rearrangements in the root meristem [8]. These results suggest that transcriptional auxin signalling regulates the cellular abundance of so far unknown regulators, which, in turn, modify subcellular sorting or trafficking pathways and other polarity determinants, ultimately leading to changes in the polar PIN distribution.

In this work, we carried out an expression profiling experiment in *Arabidopsis* roots to identify potential regulators of the PIN polarity that are transcriptionally regulated by auxin signalling. We identified several novel regulators and characterized in more detail the transcription factor WRKY23 and its role in auxin-mediated PIN polarization, thus providing initial insights into a molecular mechanism of the auxin feedback on the directional auxin flow–one of the key prerequisites of canalization.

Results

Microarray-based identification of components mediating auxin impact on PIN polarity

The rationale behind the microarray approach was to search for genes that were (*i*) regulated by auxin in roots under conditions when auxin changes PIN polarity and (*ii*) their auxin regulation is mediated by the IAA17 (AXR3) transcriptional repressor. First, to look for auxin-induced genes, we matched data from NAA-treated and untreated heat-shocked wild type (WT) Columbia-0 (Col-0) control seedlings and found 523 auxin-induced genes, with a minimum of two-fold difference. As in the *HS*::*axr3-1* line under the same conditions auxin fails to induce PIN polarity changes (Fig 1A and 1B) [8], we compared heat-shocked and auxin-treated Col-0 seedlings to similarly handled *HS*::*axr3-1* seedlings, expressing the auxin-resistant version of IAA17 (AXR3) and we identified 667 genes (Fig 1C). The overlap of this set with the 523 auxin-induced genes yielded 245 genes induced by auxin and regulated downstream of IAA17 (S1 Table), including *PATELLIN2* and *PATELLIN6* that encode phosphatidylinositol transfer proteins, concomitantly characterized to be crucial for the regulation of embryo and seedling patterning in *Arabidopsis* [28]. Further comparison with published microarray data on *arf7 arf19* mutant seedlings [29], which are also ineffective in rearranging the PIN polarity [8], yielded a final list of 125 genes (S2 Table), of which some had previously been found to be involved in PIN polarity regulation, including the AGC3 kinase PINOID (PID). and its homologs WAG1 and WAG2 are known to phosphorylate PIN proteins [30], contributing to the control of their polar distribution [31–33]. Nevertheless, overexpression of *PID* was shown to be dominant over the auxin-induced PIN lateralization [8]. Another identified candidate with a known role in the PIN polar distribution was the phosphatidylinositol-4-phosphate 5 kinase PIP5K1. This protein, together with its close homolog PIP5K2, is enriched on basal and apical membrane domains and they are required for PIN trafficking [34, 35] and localization [36, 37]. Other candidates for polarity determinants include several previously known players in auxin-mediated plant development, such as RUL1, a leucine-rich repeat receptor-like kinase regulating cambium formation, a process linked to PIN polarity control [38].

Auxin-dependent PIN lateralization in the root meristem requires a rather prolonged auxin treatment [8], hinting at the involvement of a whole cascade of transcriptional processes. Therefore, we looked for additional auxin-induced transcription factor (TF) genes, which, based on their analogous behaviour in similar experiments and on their known functions, would be potential candidates for having a role in auxin-mediated development. The list of candidates contains *e.g. MINI ZINC FINGER1 (MIF1)*, affecting auxin responses during ectopic meristem formation [39], but also *WRKY23*. *WRKY* genes belong to a plant-specific

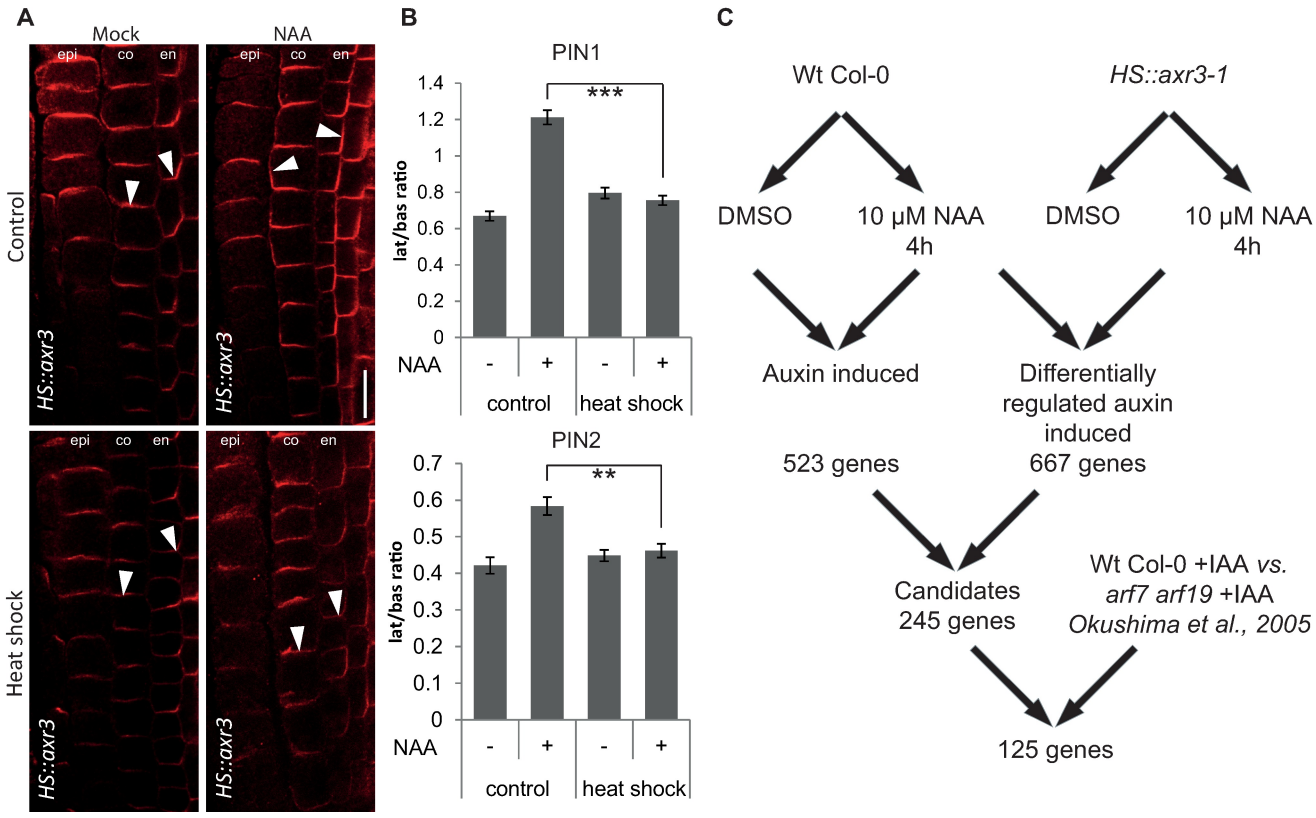

Fig 1. Putative transcriptional components of the auxin-mediated PIN polarization. (A) Simultaneous immunolocalization of PIN1 and PIN2 in *HS*::*axr3-1* plants. Heat shock-induced overexpression of *axr3-1* abolishes lateral PIN relocation after auxin (4 h, 10 μM NAA) treatment, confirming dependence on the SCF^{TIR1}-Aux/IAA-ARF signalling pathway. Arrowheads highlight representative examples of PIN localization in the respective tissues and treatments (PIN1 in endodermis and PIN2 in cortex). Bar = 10 μm. epi, epidermis; co, cortex; en, endodermis. (B) Quantitative evaluation of (A), confirming reduced auxin-dependent relocation of PIN1 (top) and PIN2 (bottom) in the induced *HS*::*axr3-1* line. Graph shows mean ratio of lateral-to-basal signal intensity of PIN1 in endodermal and PIN2 in cortex cells. Error bars indicate standard error. A One-Way ANOVA test compared marked sets of data. (** $p<0.01$; *** $p<0.0001$; $n>35$ cells corresponding to a minimum of 10 roots per treatment and experiment were imaged under comparable conditions). Experiments were carried out at least 3 times; one representative experiment is presented. (C) Scheme of the microarray experiment and analysis strategy.

https://doi.org/10.1371/journal.pgen.1007177.g001

family of 72 TFs in *Arabidopsis*, typically associated with plant defense processes and plant-pathogen interactions [40]. These genes were named by a shared sequence motif of 60 amino acids containing a conserved domain of seven invariant amino acids (WRKYGQK) [41]. The WRKYGQK motif provides a high binding preference and contacts a 6-bp DNA sequence element–the W-box (/TTGACT/C) contained in target gene promoters [40, 42]. Distinct WRKY TFs have distinct selective binding preferences to certain W-box variants [43]. The role of WRKY23 has been established in plant defence processes during plant-nematode interactions, but also in auxin transport regulation by flavonol biosynthesis that affects root and embryo development. In *Arabidopsis* embryos, the *WRKY23* expression attenuates both auxin-dependent and auxin-independent signalling pathways toward stem cell specification [44–46]. In addition, *WRKY23* is unique within its gene family, because none of the other *WRKY* genes in these experimental conditions was responsive to auxin and, thus, present in the gene selection (S2 Table). In this work, we focused on one of the transcription factors fulfilling our selection criteria, and investigated the role of WRKY23-dependent transcriptional regulation in auxin-dependent PIN repolarization.

WRKY23 expression is regulated by auxin signalling

First, we confirmed and analysed the auxin regulation of *WRKY23* expression. Promoters of auxin-inducible genes typically contain tandem-localized auxin response elements (AuxREs) that are recognised by auxin response factors (ARFs) [47, 48]. ARFs dimerize to act as molecular callipers and provide specificity to the auxin-dependent gene regulation by measuring the distance of AuxREs in the element pair at the promoter [48]. The length of the intergenic region between the 3'-UTR of the previous gene *UPBEAT* (*UPB*; *At2g47270*) and the 5'-UTR of *WRKY23* (*At2g47260*) is 4.5 kbp. The predicted 2.4-kbp *WRKY23* promoter by the AGRIS tool [49] contains 10 AuxRE and AuxRE-like sites and the extended promoter of 3.2 kbp used for native promoter fusion construct [44] contains two additional AuxRE sites (Fig 2A). Such a density of auxin-regulatory sequences in the promoter makes direct regulation by ARF-dependent auxin signalling a plausible scenario.

In accordance with these results, we found that *WRKY23* is auxin inducible in a dose- and time-dependent manner. When we treated *Arabidopsis* seedlings with 100 nM NAA for 4 h, the *WRKY23* transcription increased 2-fold, and 1 μM NAA led to a 6-fold increase (Fig 2B). Time response experiments at the consensus concentration of 10 μM NAA used in PIN lateralization experiments [8] revealed that the *WRKY23* transcription starts to increase approximately after 1.5 h of auxin treatment with a stronger increase after between 2 and 4 h (Fig 2C). This relatively slow auxin-mediated transcriptional regulation of *WRKY23* is well within the time frame for the auxin-mediated PIN lateralization that also occurs strongly only after 4 h [8]. The dependence on the auxin signalling was further supported by the compromised *WRKY23* auxin inducibility in the *HS*::*axr3-1* and *arf7 arf19* mutants (Fig 2D and 2E). These results show that the *WRKY23* transcription depends on the SCF^{TIR1}-Aux/IAA-ARF auxin signalling pathway and confirm *WRKY23* as a candidate regulator of auxin-mediated PIN polarization.

A transgenic line harbouring the *uidA* reporter gene (or GUS-coding gene) under the control of a 3.2-kb upstream sequence from *WRKY23* (*WRKY23*::*GUS*), whose expression pattern has previously been confirmed by in situ hybridization [44, 45], revealed that auxin induces the ectopic expression of *WRKY23* in root tissues, partly overlapping with root regions, in which the PIN lateralization can be observed (S1G and S1H Fig). Without auxin treatment, the expression pattern of *WRKY23* partially overlaps with the *DR5* auxin response reporter (S1G and S1I Fig) and auxin distribution as revealed by anti-IAA immunolocalization [44, 45, 50]. Previously, *WRKY23* has been shown to be expressed in all apical cells of an octant stage embryo and at heart stage to be detected in both the root and the shoot stem cell niches (S1D and S1E Fig) [46], possibly indicating that *WRKY23* has—besides its role in root development—also a function in shoot development. We found *WRKY23*::*GUS* expression in pollen grains (S1C Fig), the shoot apical meristem (SAM) (S1A Fig and Fig 2F), as well as at the hydathodes of cotyledons (S1F Fig), coinciding with known auxin response maxima [51]. Sectioning the SAM revealed specific *WRKY23* expression in the L1, L2, and L3 layers (S1A Fig). *WRKY23* promoter activity was prominently associated with the vascular tissues of flowers, cotyledons, and leaves (S1B and S1F Fig and Fig 2G). Notably, the *WRKY23* expression mirrored the pattern of developing leave vasculature with the highest expression in cells adjacent to the differentiated xylem (Fig 2G) and were detected in a venation-like pattern even before any morphological changes typical for the differentiated vasculature were visible (Fig 2F and 2G). In the previous, external auxin source-mediated canalization experiments in pea stems, the PIN channels were preceding the formation of vasculature and later the differentiated xylem formed adjacent to the PIN channels [11]. Thus, the WRKY23 expression pattern in

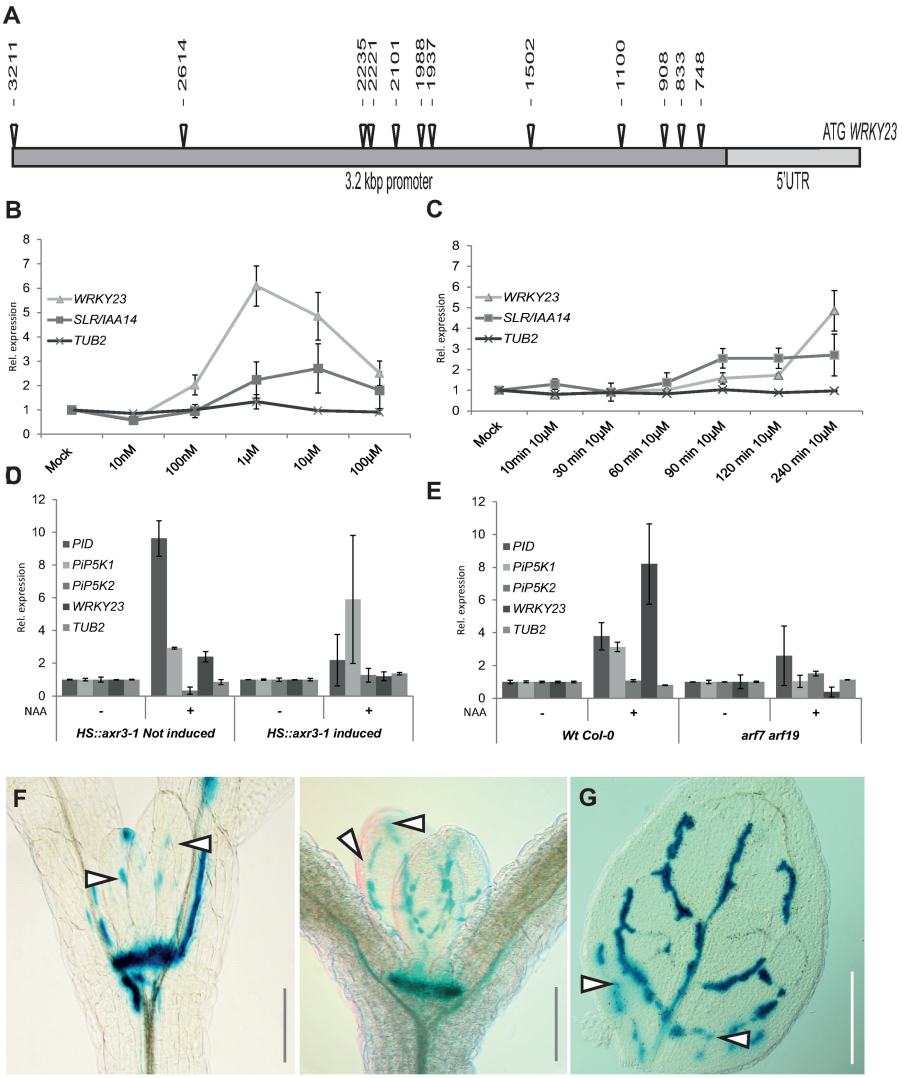

Fig 2. WRKY23 acts downstream of the Aux/IAA—ARF auxin pathway and marks developing vasculature. (A) Schematic depiction of WRKY23 promoter; AuxRE and AuxRE-like response elements are shown as triangles (B and C) *WRKY23* transcript levels depend on auxin dose and treatment time. qRT-PCR analysis of *WRKY23* expression after a 4 h treatment with different concentrations of NAA (B) and after different treatment times with 10 μM NAA (C). *TUB2* and *SLR/IAA14* are shown as negative and positive controls, respectively. Values represent relative fold change of expression. Error bars represent standard deviation (see Materials and Methods for detailed description). (D and E) *WRKY23* expression depends on the SCF^{TIR1}-Aux/IAA-ARF signalling pathway. qRT-PCR confirmation of the microarray experiment showing the expression of *WRKY23* and genes previously connected to PIN polarity in *HS::arx3-1* (D), and in *arf7 arf19* double mutant plants (E). Values represent relative fold change. Error bars indicate standard deviation (see Materials and Methods for detailed description). (F, G) Expression of *WRKY23::GUS* in the shoot apical meristem (SAM) and in the presumptive leaf vasculature (G). Besides strong activity in the SAM, GUS staining overlaps with, and partly precedes, the appearance of differentiating vascular strands in young leaves. Two representative plants in consecutive developmental stages are shown. Patchy expression of *WRKY23::GUS* in the vasculature of young developing true leaves (G). Arrowheads in F and G depict areas with GUS activity presumably coinciding with future vascular strands that are not morphologically discernible yet.

https://doi.org/10.1371/journal.pgen.1007177.g002

Arabidopsis largely overlaps with presumptive PIN channels being consistent with a role of WRKY23 in venation patterning of leaves–a process regulated by the polarized auxin transport [51, 52].

In summary, the presence of auxin-responsive elements in the promoter, the auxin-inducibility of the *WRKY23* expression together with its dependence on AXR3, ARF7 and ARF19 activities indicate that the *WRKY23* transcription is regulated by Aux/IAA- and ARF-dependent auxin signalling. In addition, the association of the *WRKY23* expression with developing vasculature is consistent with a possible involvement of WRKY23 in the auxin-mediated PIN polarization process.

WRKY23 gain-of-function leads to PIN1 and PIN2 lateralization

Next, we tested whether an altered *WRKY23* expression or activity affected the auxin regulation of the PIN1 and PIN2 protein localization. A strong constitutive overexpression of *WRKY23* was obtained by means of a GAL4-VP16-*UAS* transactivation system (*RPS5A>>WRKY23*) [45, 46, 53]. The *35S* promoter-driven WRKY23 line (*35S::WRKY23*) as well as also *35S* promoter-driven dexamethasone-glucocorticoid (DEX/GR) receptor system (*35S::WRKY23-GR*) were used for constitutive overexpression, eventually, with inducible nuclear localization [45, 46]. Constitutive overexpression of *WRKY23* had an impact on the PIN2 but not PIN1 polarity. It caused the PIN2 lateralization in root cortex cells, to some extent mimicking the application of auxin (Fig 3A and 3B). Subsequent treatment with NAA further increased lateralization of PIN2 in cortex cells and caused increased lateralization of PIN1 as compared to wild type (Fig 3A and 3B and S2C and S2D Fig). An inducible *WRKY23* gain-of-function line had a similar effect: seedlings of a *35S::WRKY23-GR* line treated with DEX to induce WRKY23-GR translocation to the nucleus, resulted in PIN2 but not PIN1 lateralization in the cortex cells. Again, additional NAA treatment had an additive effect on PIN2 lateralization and caused a stronger PIN1 lateralization than as seen in the wild type (S3C and S3D Fig and S2C and S2D Fig).

Thus, both constitutive and inducible *WRKY23* gain-of-function consistently led to PIN2 lateralization and increased the auxin-mediated PIN1 and PIN2 lateralization.

Repression of WRKY23 activity abolishes the auxin effect on the PIN2 polarization

In complementary experiments, we tested the downregulation effect of the WRKY23 function. The large WRKY family of homologous proteins has an extensive functional redundancy among individual members [54]. As the functional compensation of *wrky23* loss-of-function by other members was likely, given the large size of the *WRKY* gene family, we used a dominant-negative approach with the chimeric repressor silencing technology [55]. This technology is based on a translational fusion of an activating TF with the repressor domain SRDX, thus inhibiting the expression of target genes. The transactivation activity of WRKY23 had previously been verified in a tobacco transient expression assay, in which the activating or repressing potential of the TF fused to GAL4 had been checked in the presence of a *UAS::Luciferase* construct [45].

Plants expressing *WRKY23-SRDX* under both the native and constitutive promoters showed a clear auxin insensitivity in PIN2 lateralization, namely the auxin treatment did not lead to lateralization when compared to the controls (S3A and S3B Fig). Notably, PIN1 lateralization did not change visibly after NAA treatment (S2C and S2D Fig).

wrky23 partial loss-of-function mutants are defective in auxin impact on the PIN polarity

To investigate intrafamily redundancy and to assess specifically the role of WRKY23 on the auxin effect on the PIN polarity, we isolated two T-DNA insertional mutants in the *WRKY23*

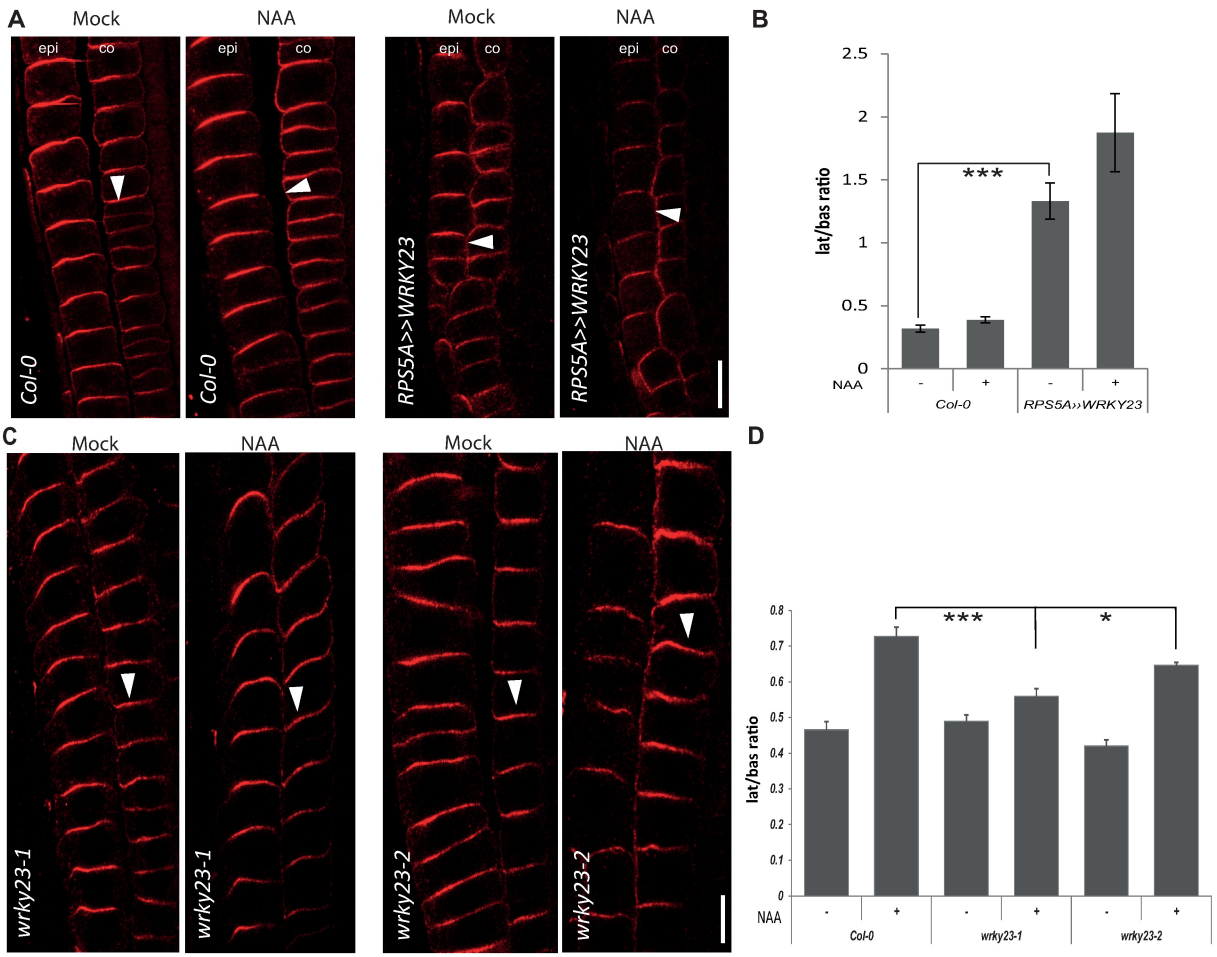

Fig 3. WRKY23 is required for auxin-mediated PIN lateralization in the root. (A) Immunolocalization analysis of PIN2 without or after NAA (4 h, 10 μM) treatment in WT Col-0 and *RPS5A>>WRKY23*. Arrowheads highlight PIN2 polarity. epi, epidermis; co, cortex. (B) Quantitative evaluation of (A) showing mean ratio of PIN2 lateral-to-basal signal intensity in cortex cells. Note that PIN2 lateralization in *RPS5A>>WRKY23* roots is increased even without auxin that still remains effective. Error bars indicate standard error. A One-Way ANOVA test compared marked sets of data (*** $p<0.0001$; $n>35$ cells corresponding to a minimum of 10 roots per treatment and experiment were imaged under comparable conditions). (C) Immunolocalization analysis of PIN2 without or with NAA treatment in WT Col-0 and *wrky23* mutants. Arrowheads highlight representative examples of PIN2 polarity in the. epi, epidermis; co, cortex. (D) Quantitative evaluation of the experiment in (C) showing mean ratio of PIN2 lateral-to-basal signal intensity in endodermal. Error bars indicate standard error. A One-Way ANOVA test compared marked sets of data (* $p<0.05$; *** $p<0.001$; $n>100$ cells corresponding to a minimum of 10 roots per treatment and experiment were imaged under comparable conditions). Experiments were carried out 3 times; one representative experiment is presented).

https://doi.org/10.1371/journal.pgen.1007177.g003

locus, designated *wrky23-1* and *wrky23-2* (Fig 4A). The quantitative reverse transcription-polymerase chain reaction (qRT-PCR) analysis revealed that both alleles are knock-downs, *wrky23-1* having more downregulated expression (Fig 4B).

Similarly to the *WRKY23-SRDX* lines, both *wrky23* mutant alleles showed a reduced PIN2 lateralization response to auxin treatment and, additionally, also reduced PIN1 lateralization. Specifically, following the NAA treatment, the PIN1 and PIN2 lateralization in root endodermal cells was diminished in the *wrky23-2* weaker knock-down and, even more so, in the stronger *wrky23-1* allele (S2A and S2B Fig and Fig 3C and 3D). The observed opposite effects of WRKY23 gain- and loss-of-function on the PIN lateralization suggested that WRKY23 plays an important role in the auxin-mediated PIN polarity rearrangements.

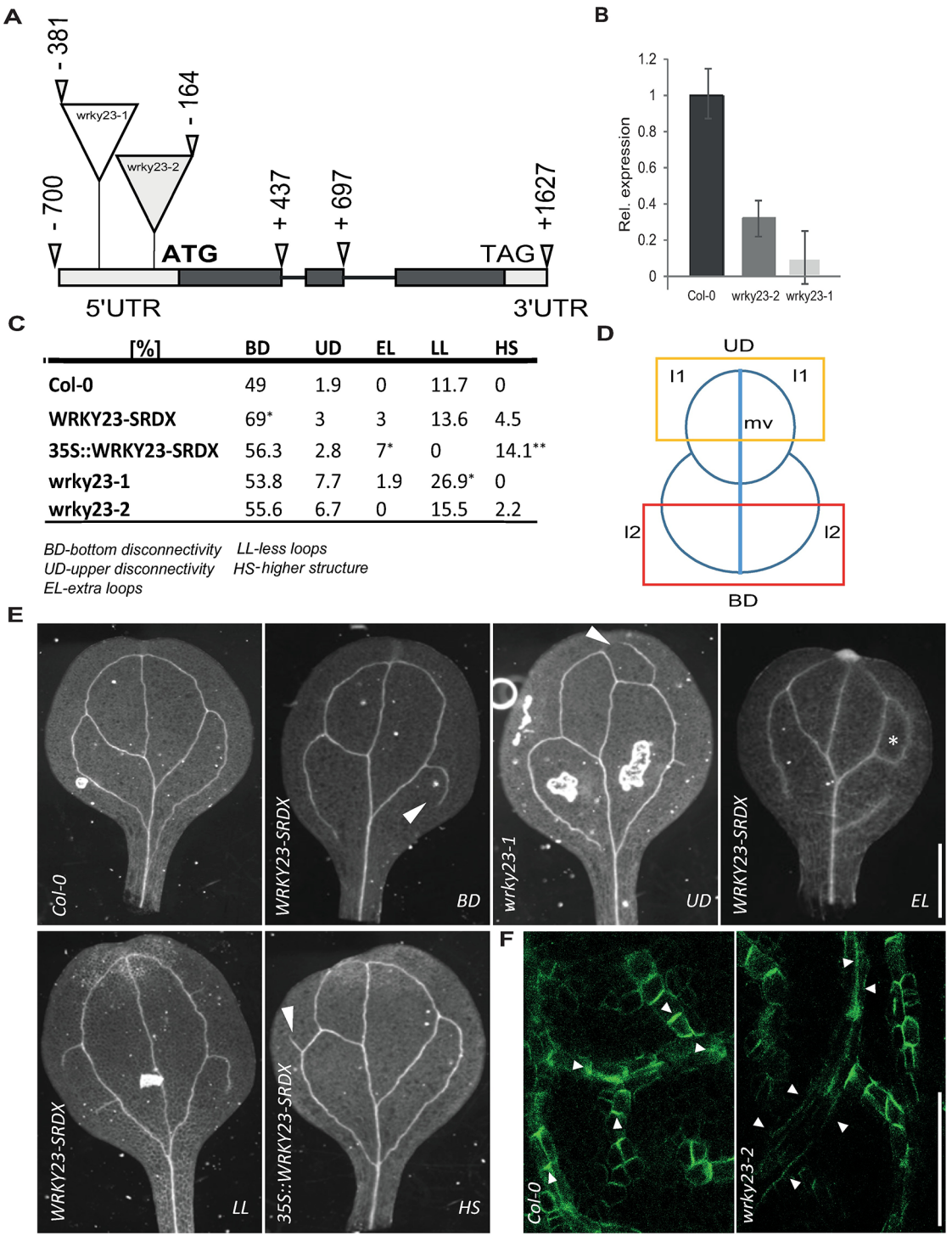

Fig 4. Isolation and characterization of *wrky23* mutants. (A) Schematic representation of the *WRKY23* locus. Exons are represented by boxes, while introns are shown as lines. Coding regions are filled with dark grey. Exact locations of the T-DNA insertions are depicted. (B) qRT-PCR analysis of *WRKY23* expression in the isolated mutant lines. Relative expression values are normalized to the level detected in WT Col-0. See Materials and Methods for more details. (C) Evaluation of cotyledon vasculature defects in *WRKY23-SRDX*, *35S::WRKY23-SRDX* and *wrky23* mutants. A One-Way ANOVA test compared marked sets of data (* $p<0.05$; *** $p<0.001$; $n>50$ cotyledons). (D) Schematic representation of cotyledon vasculature pattern. l1, first loop; l2, second loop; mv, midvein. Yellow and red box delineate UD and BD zone of evaluating. (E) Representative images of analysed vasculature defects. (F) Representative images of immunolocalization analysis of PIN1 in developing young first leaves. In the WT, PIN1 shows typical polarization, whereas in *wrky23-2* mutant this polarization is abolished. At least 50 leaves per genotype were analysed.

https://doi.org/10.1371/journal.pgen.1007177.g004

WRKY23 plays a role in PIN polarization during venation patterning

The importance of a tight PIN polarity regulation for directional auxin fluxes and plant growth and development has been demonstrated previously [2, 3]. Therefore, we analysed the phenotypes related to PIN polarity or auxin transport in transgenic lines with an altered expression or activity of *WRKY23*. *35S*::*WRKY23* overexpressing plants show growth retardation and root meristem patterning defects [45]. Also, dominant negative lines showed severe defects in lateral root organogenesis [45]. Both *WRKY23-SRDX* and *35S*::*WRKY23* lines had shorter roots than those of Col-0 (S4A Fig) and *WRKY23-SRDX* showed defects in gravitropism, similar to those observed in the auxin transport mutant *pin2/eir1* [56, 57]. Notably, native promoter-driven *WRKY23-SRDX* displayed a significant increase in lateral root density (S4B Fig). Notably, none of these phenotypical defects, including root meristem disorganization, root growth inhibition, and lateral root development alteration, were observed in the *wrky23* mutant alleles (S4A and S4B Fig), suggesting that these more pleiotropic defects are not related to the WRKY23 action specifically, but they could reflect a broader role of the *WRKY* gene family in plant development.

The canalization hypothesis proposed that the leaf venation pattern depends on the auxin feedback on the PIN polarity [58]. We analysed several features of vascular defects in cotyledons.–bottom disconnectivity of l2 vein loops (BD), upper disconnectivity of l1 vein loops (UD), extra loops (EL), less loops (LL) and appearance of higher order structures (HS) (Fig 4C–4E). In plants expressing *WRKY23*::*WRKY23-SRDX* and *35S*::*WRKY23-SRDX*, we observed vasculature patterning defects manifested by increased incidence in BD, HS and EL On the other hand, both *wrky23-1* and *wrky23-2* mutant alleles showed more defects in UD and LL (Fig 4C).

Next, we tested the PIN1 polarity during vascular tissue development by means of anti-PIN1 antibody staining on young first leaves. In the WT leaves, the staining revealed a pronounced PIN1 polarization along the basipetal (rootward) direction (S4C Fig). In the *35S*::*WRKY23* and *WRKY23-SRDX* lines, the typical PIN1 polarity was partly or completely abolished in some veins or their parts (S4C Fig). Similar PIN1 polarity defects were also found in *wrky23-1* and *wrky23-2* lines (Fig 4F and S4C Fig). The venation defects might be interpreted in terms of defective canalization (as suggested by the PIN1 polarity defects), although the venation defects differ somewhat from defects induced by auxin transport inhibition [51, 52]. This observation indicates that interference with the PIN polarization does not have the same consequence as inhibition of PIN auxin transport activity.

In summary, our genetic analysis revealed that from the numerous functions of the WRKY family in the regulation of plant development [45, 46], WRKY23 is more specifically involved in auxin-mediated PIN polarity rearrangements and leave venation patterning.

Discussion

Classical experiments have led to the formulation of the so-called canalization hypothesis that proposes an auxin feedback on the auxin transport and consequent formation of auxin channels as a central element of multiple self-organizing developmental processes; in particular formation and regeneration of vasculature [7]. In canalization, the auxin transport through an initially homogeneous tissue follows a self-organizing pattern, leading from initially broad fields of auxin-transporting cells to eventually a narrow transport channel, consequently establishing the position of future vascular veins [6]. This hypothesis [4, 5] is further supported by successful modelling efforts based on the concerted cellular polarization via a feedback mechanism, by which auxin influences the directionality of its own flow by polarity rearrangement of auxin carriers [6, 15, 59–62]. Most of these models rely on hypothetical propositions, such as

auxin flux sensors or direct cell-to-cell communication, giving testimony of our lack of understanding how canalization works mechanistically. However, the auxin impact on the PIN polarization has been experimentally demonstrated in different contexts and this effect has been shown to rely on the transcriptional gene expression activation through auxin signalling [8, 9, 11, 19].

Our transcriptional profiling experiments on auxin-dependent PIN rearrangements in *Arabidopsis* roots provide insight into the transcriptional reprogramming during auxin-mediated PIN polarity rearrangements and identify potential downstream molecular components in this process, including established PIN polarity regulators, such as PID, PIP5K, and PATELLINS [28, 30, 37, 63], validating the soundness of the experimental concept. Among a number of novel components awaiting further characterization, we also found the transcriptional activator *WRKY23*.

WRKY23 is an auxin-responsive gene. The local upregulation of the *WRKY23* expression following the auxin application is consistent with a possible involvement in the PIN repolarization process. The *WRKY23* transcription is induced by auxin in a dose- and time-dependent manner and it is reminiscent of the expression pattern of the *DR5rev* auxin signalling reporter. Notably, *WRKY* genes are traditionally known to be involved in defensive processes in plants. More and more, this limited functional spectrum has been broadened by studies uncovering the involvement of these TFs in developmental and physiological processes other than plant defense [45, 46, 64, 65]. In the case of *WRKY23*, besides a role in plant-nematode interaction with subsequent activation of auxin responses, participation in auxin transport through flavonol synthesis in the root as well as a function in a *mp/bdl*-dependent pathway in embryo development have been demonstrated [44–46].

We show that *WRKY23* is a crucial factor required for auxin-mediated PIN polarity rearrangements, because gain-of-function and dominant-negative *WRKY23* lines as well as *wrky23* mutants were strongly affected in this process. These defects at the cellular level revealed by the exogenous auxin application appears to be developmentally relevant, because *wrky23* mutants are defective also in the PIN1 polarization process during vascular tissue formation of leaf venation and consequently in vascular tissue formation. Notably, increased PIN2 but not PIN1 lateralization in the *WRKY23* overexpression lines and PIN2 but not PIN1 insensitivity to auxin treatment in *WRKY23-SRDX* lines indicate a partly diverging mechanism controlling PIN1 and PIN2 relocation. This is consistent with reported differences in PIN1 and PIN2 trafficking mechanisms [66].

Our results also suggest that *WRKY23* is a critical player in auxin feedback on PIN polar localization. As a TF, *WRKY23* is probably not directly involved in regulating localization of transmembrane proteins, such as PIN proteins. Instead, this work opens avenues for future studies revealing the *WRKY23*-dependent transcriptional network. The identification of WRKY23 and its role in the auxin feedback on the PIN polarity along with other established PIN polarity regulators proves that our transcriptomics dataset can be mined in the future to identify additional regulators. Ultimately, it will provide insights into the molecular mechanism of this key aspect of the canalization-dependent regulation of plant development.

Materials and methods

Plant material and growth conditions

All *Arabidopsis thaliana* (L.) Heynh. lines were in Columbia-0 (Col-0) background. The insertional mutants *wrky23-1* (SALK_003943) and *wrky23-2* (SALK_38289) were obtained from NASC and genotyped with the primers listed in S3 Table. The *arf7 arf19* double mutant and the *HS*::*axr3-1* transgenic line have been described previously [26, 29] as well as the *DR5*::*GUS*

[18] and *PIN1-GFP* [67]. For *RPS5A>>WRKY23* analyses, the F1 generation of a *RPS5A*::*GAL4VP16* [53] × *UAS*::*WRKY23* [45] cross was analysed and compared with the F1 generations from the *UAS*::*WRKY23* × WT Col-0 and *RPS5A*::*GAL4VP16* × WT Col-0 crosses. *WRKY23*::*GUS*, *35S*::*WRKY23-GR*,*35S*::*WRKY23*, *WRKY23*::*WRKY23-SRDX*, and *35S*::*WRKY23-SRDX* have been described previously [44, 45]. Seeds were surface-sterilized overnight by chlorine gas, sown on solid *Arabidopsis* medium (AM+; half-strength MS basal salts, 1% [w/v] sucrose, and 0.8% [w/v] phytoagar, pH 5.7), and stratified at 4˚C for at least 2 days prior to transfer to a growth room with a 16-h light/8-h dark regime at 21˚C. The seedlings were grown vertically for 4 or 6 days, depending on the assay.

Arabidopsis seedlings were treated with auxin or chemicals in liquid AM+ at 21˚C in a growth room with the following concentrations and times: for α-naphthaleneacetic acid (NAA; Sigma-Aldrich) at 10 μM for 4 h; dexamethasone (DEX; Sigma-Aldrich) 10 μM for 24 h. Mock treatments were done with equivalent amounts of DMSO.

Microarray analysis

Wild type Col-0 and *HS*::*axr3-1* seeds were grown vertically on AM+ plates for 5 days. We applied a 40 min heat shock at 37˚C to the seedlings, followed by a 1.5-h recovery at normal growth temperature. Subsequently, the seedlings were transferred to liquid AM+ and treated with 10 μM NAA or DMSO for 4 h. Afterward, the lower third of 100–130 roots from each treatment was cut off, frozen in liquid N_2. RNA was extracted with the RNAeasy mini kit (Qiagen). Probes were prepared and hybridized to the *Arabidopsis* ATH1–121501 gene expression array (Affymetrix) as described [68]. Expression data for Col-0, *HS*::*axr3-1*, both NAA and mock treated, had been deposited under the ArrayExpress number E-MEXP-3283. Expression profiling data for *arf7 arf19* (ArrayExpress: E-GEOD-627) have been published previously [29]. Raw data were pairwise analyzed with the logit-t algorithm [69] with a cutoff of $p = 0.05$.

RNA extraction, cDNA synthesis, and quantitative RT-PCR and analysis

RNA extraction, cDNA synthesis, and quantitative (q)RT-PCR were done as described [37]. Selected candidate gene transcript levels were quantified with qRT-PCR with specific primer pairs, designed with Primer-BLAST (http://www.ncbi.nlm.nih.gov/tools/primer-blast/). Transcript levels were normalized to *GAMMA-TUBULIN 2* (*TUB2*; *AT5G05620*), which was constitutively expressed and auxin independent across samples. All PCRs were run in three biological replicates per three technical repeats. The data were processed with a qRT-PCR analysis software (Frederik Coppens, Ghent University-VIB, Ghent, Belgium). Primers used in this study are listed in the S3 Table.

Whole-mount *in situ* immunolocalization, microscopy, and quantitative PIN relocalization analysis

PIN immunolocalizations of primary roots and young leaves were carried out as described [70]. The antibodies were used as follows: anti-PIN1, 1:1000 [13] and anti-PIN2, 1:1000 [71]. For primary roots, the secondary goat anti-rabbit antibody coupled to Cy3 (Sigma-Aldrich) was diluted 1:600. For young leaves, the secondary goat anti-rabbit antibody coupled to Alexa Fluor 488 (Sigma-Aldrich) was diluted 1:600. For confocal microscopy, a Zeiss LSM 700 confocal microscope was used. The PIN relocalization was quantitative analysed as described [8], at least 3 experiments were performed for each observation. Note that the absolute levels of the PIN lateralization index may vary between individual experiments (depending on the anti-PIN signal strength), but the relative differences are always consistent.

Phenotypic analysis

All measurements were done with ImageJ (http://rsb.info.nih.gov/ij). For the root length analysis 6-day-old seedlings were scanned and root lengths were measured. For the lateral roots analysis 10-day-old seedlings were scanned and lateral root density was calculated from ratio number of LR/root length.

Histological analyses and microscopy

To detect β-glucuronidase (GUS) activity, seedlings were incubated in reaction buffer containing 0.1 M sodium phosphate buffer (pH 7), 1 mM ferricyanide, 1 mM ferrocyanide, 0.1% Triton X-100, and 1 mg/ml X-Gluc for 2 h in the dark at 37˚C. Afterward, chlorophyll was removed by destaining in 70% ethanol and seedlings were cleared.

Tissues (seedlings and cotyledons) were cleared in a solution containing 4% HCl and 20% methanol for 15 min at 65˚C, followed by a 15-min incubation in 7% NaOH and 70% ethanol at room temperature. Next, seedlings were rehydrated by successive incubations in 70%, 50%, 25%, and 10% ethanol for 5 min, followed by incubation in a solution containing 25% glycerol and 5% ethanol. Finally, seedlings were mounted in 50% glycerol and monitored by differential interference contrast microscopy DIC (Olympus BX53) or a stereomicroscope (Olympus SZX16).

Supporting information

S1 Fig. Pattern of *GUS* expression in *WRKY23*::*GUS* plants. (A) SAM section showing specific *WRKY23* expression in the L1, L2, and L3 layers. (B) *WRKY23* expression in the pistil vasculature. (C) Anther showing *WRKY23*::*GUS* activity in pollen (inset). (D) GUS staining of *WRKY23*::*GUS* embryos showing promoter activity in all apical cells of an early globular embryo. (E) GUS activity in the SAM and RAM of an early torpedo stage embryo. (F) Cotyledon showing GUS staining at the hydathode (h) and in the vasculature. (G-J) *WRKY23* promoter activation by auxin treatment. G and H: Expression pattern of *WRKY23*::*GUS* in the root changes following 6 h of auxin treatment. GUS staining becomes generally stronger and additionally expressed in the meristematic and transition zones of the root tip/arrowhead). I and J: *DR5*::*GUS* activity under the same experimental conditions as in (G-H).
(PDF)

S2 Fig. Polarity of PIN1 in *WRKY23* transgenic lines. (A and B) Immunolocalization of PIN1 in *wrky23* mutants and *arf7/19* lines revealing reduced lateralization of PIN1. Arrowheads highlight PIN1 polarity. en, endodermis; per, pericycle. Graph shows mean ratio of lateral-to-basal signal intensity of PIN1 in endodermal cells. Error bars indicate standard error. A One-Way ANOVA test compared marked sets of data (*** $p<0.0001$; $n>60$ cells corresponding to a minimum of 10 roots per treatment and per experiment imaged under comparable conditions). Experiments were carried out at least 3 times; one representative experiment is shown. (C) Immunolocalization of PIN1 in dominant-negative *WRKY23-SRDX* plants driven by native promoter and overexpression lines - *35S*::*WRKY23*, *35S*::*WRKY23-GR*. WT Col-0 was used as a control. Arrowheads highlight PIN1 polarity in endodermal cells. en, endodermis; per, pericycle. Bar = 10 μm. (D) Quantitative evaluation of (C) showing mean ratio of lateral-to-basal signal intensity of PIN1 in cortex cells. Error bars indicate standard error. A One-Way ANOVA test compared marked sets of data (*** $p<0.0001$; $n>60$ cells corresponding to a minimum of 10 roots per treatment and per experiment were imaged under comparable conditions). Experiments were carried out at least 3 times; one representative

experiment is shown.
(PDF)

S3 Fig. Polarity of PIN2 in *WRKY23* transgenic lines. (A) Immunolocalization of PIN2 in dominant-negative *WRKY23-SRDX* plants driven by native and constitutive promoter. WT Col-0 was used as a control (see Fig 3A and quantification in S3B). Arrowheads highlight PIN2 polarity in cortex cells. epi, epidermis; co, cortex. Bar = 10 μm. (B) Quantitative evaluation of (A) showing mean ratio of lateral-to-basal signal intensity of PIN2 in cortex cells. Error bars indicate standard error. A One-Way ANOVA test compared marked sets of data (*** $p<0.0001$; $n>70$ cells corresponding to a minimum of 10 roots per treatment and per experiment were imaged under comparable conditions). Experiments were carried out at least 3 times; one representative experiment is shown.
(C) Immunolocalization of PIN2 in DEX-inducible *35S*::*WRKY23-GR* plants treated with DEX and/or NAA. WT Col-0 was used as control (see quantification in S3D). Arrowheads highlight PIN2 polarity in cortex cells. epi, epidermis; co, cortex. Bar = 10 μm. (D) Graph showing mean ratio of lateral-to-basal signal intensity of PIN2 in cortex cells. Induced *35S*::*WRKY23-GR* roots show slightly more PIN2 lateralization without auxin that is apparently more effective to increase PIN2 lateralization in this line than the controls. Error bars indicate standard error. A One-Way ANOVA test compared marked sets of data (*** $p<0.0001$, * $p<0.05$; $n>35$ cells corresponding to a minimum of 10 roots per treatment and per experiment were imaged under comparable conditions). Experiments were carried out at least 3 times; one representative experiment is shown.
(PDF)

S4 Fig. Phenotype defects in WRKY23 transgenic lines and *wrky23* mutants. (A) Primary root length of 6-day-old transgenic lines and *wrky23* mutants. Central lines show median values; box limits indicate the 25th and 75th percentiles as determined by the R software; whiskers extend 1.5 times the interquartile range from the 25th and 75th percentiles. Significance was determined by two-tailed equal T-test between Col-0 and other lines; (*** $p<0.001$); n>60 roots per line. (B) Lateral root density in plants with impaired WRKY23 function. WRKY-SRDX denotes *WRKY23*::*WRKY23-SRDX*.Box plot properties and statistical analysis are as in (A). n>80 roots per line. (C) Immunolocalization analysis of PIN1 in developing true leaves. In the WT, PIN1 shows typical polarization towards the leaf base, whereas in WRKY23 transgenic lines and *wrky23* mutants this polarization of some branches is abolished. Arrowheads highlights defective PIN1 polarization in vasculature. At least 50 leaves per genotype were analysed. (D) Quantitative evaluation of (C) showing percentage of abolished PIN1 polarity. At least 50 branches per genotype were analysed.
(PDF)

S1 Table. Candidate genes from the microarray experiment. (A) Venn diagram representing gene overlay of microarray experiments. Dataset of auxin-regulated genes in WT Col-0 seedlings was overlaid with a second set of genes acquired from the comparison of auxin-treated WT Col-0 and heat-shock—induced auxin-treated *HS*::*axr3-1* lines. Overlap of these genes yielded a list of 245. (B) List of the 245 genes. Gene model descriptions are depicted as they appear in the TAIR database.
(PDF)

S2 Table. Narrowed-down list of candidate genes from the microarray experiments. (A) Venn diagram representing gene overlay of microarray experiments. Datasets of genes differentially regulated in *HS*::*axr3-1* compared to auxin-regulated genes in WT Col-0 were overlaid with a third set of genes that are no longer auxin regulated in the *arf7 arf19* background [29].

Overlap of all three microarrays gave 125 genes. (B) List of the 125 overlapping genes containing putative polarity regulators. Gene model descriptions are depicted as they appear in the TAIR database.
(PDF)

S3 Table. List of PCR primers used.
(PDF)

Acknowledgments

We thank D. Weigel for support with microarray analysis; F. Coppens for assistance with the qRT-PCR analysis and M. De Cock and M. Abas for help in preparing the manuscript. We gratefully acknowledge the Nottingham Arabidopsis Stock Center (NASC) for providing mutant lines. This work was supported by the European Research Council (project ERC-2011-StG 20101109-PSDP). WG was a postdoctoral fellow of the Research Foundation Flanders.

Author Contributions

Conceptualization: Tomáš Prát, Wim Grunewald, Michael Sauer, Jiří Friml.

Data curation: Tomáš Prát, Jakub Hajný, Wim Grunewald, Mina Vasileva, Gergely Molnár, Ricardo Tejos, Markus Schmid, Michael Sauer, Jiří Friml.

Formal analysis: Tomáš Prát, Jakub Hajný, Wim Grunewald, Gergely Molnár, Ricardo Tejos, Michael Sauer, Jiří Friml.

Investigation: Tomáš Prát, Jakub Hajný, Wim Grunewald, Mina Vasileva, Gergely Molnár, Ricardo Tejos, Markus Schmid, Michael Sauer, Jiří Friml.

Methodology: Tomáš Prát, Jakub Hajný, Wim Grunewald, Michael Sauer, Jiří Friml.

Writing – original draft: Tomáš Prát, Gergely Molnár, Michael Sauer, Jiří Friml.

References

1. Petrášek J, Mravec J, Bouchard R, Blakeslee JJ, Abas M, Seifertová D, et al. PIN proteins perform a rate-limiting function in cellular auxin efflux. Science. 2006; 312: 914–918. https://doi.org/10.1126/science.1123542 PMID: 16601150
2. Wiśniewska J, Xu J, Seifertová D, Brewer PB, Růžička K, Blilou I, et al. Polar PIN localization directs auxin flow in plants. Science. 2006; 312: 883. https://doi.org/10.1126/science.1121356 PMID: 16601151
3. Adamowski M, Friml J. PIN-dependent auxin transport: action, regulation, and evolution. Plant Cell. 2015; 27: 20–32. https://doi.org/10.1105/tpc.114.134874 PMID: 25604445
4. Sachs T. The induction of transport channels by auxin. Planta. 1975; 127: 201–206. https://doi.org/10.1007/BF00380716 PMID: 24430469
5. Sachs T. Cellular interactions in tissue and organ development. Symp Soc Exp Biol. 1986; 40: 181–210. PMID: 3544302
6. Bennett T, Hines G, Leyser O. Canalization: what the flux? Trends Genet. 2014; 30: 41–48. https://doi.org/10.1016/j.tig.2013.11.001 PMID: 24296041
7. Berleth T, Sachs T. Plant morphogenesis: long-distance coordination and local patterning. Curr Opin Plant Biol. 2001; 4: 57–62. PMID: 11163169
8. Sauer M, Balla J, Luschnig C, Wiśniewska J, Reinöhl V, Friml J, Benková E. Canalization of auxin flow by Aux/IAA-ARF-dependent feedback regulation of PIN polarity. Genes Dev. 2006; 20: 2902–2911. https://doi.org/10.1101/gad.390806 PMID: 17043314
9. Mazur E, Benková E, Friml J. Vascular cambium regeneration and vessel formation in wounded inflorescence stems of Arabidopsis. Sci Rep. 2016; 6: 33754. https://doi.org/10.1038/srep33754 PMID: 27649687

10. Booker J, Chatfield S, Leyser O. Auxin acts in xylem-associated or medullary cells to mediate apical dominance. Plant Cell. 2003; 15: 495–507. https://doi.org/10.1105/tpc.007542 PMID: 12566587

11. Balla J, Kalousek P, Reinöhl V, Friml J, Procházka S. Competitive canalization of PIN-dependent auxin flow from axillary buds controls pea bud outgrowth. Plant J. 2011; 65: 571–577. https://doi.org/10.1111/j.1365-313X.2010.04443.x PMID: 21219506

12. Bennett T, Hines G, van Rongen M, Waldie T, Sawchuk MG, Scarpella E, Ljung K, Leyser O. Connective auxin transport in the shoot facilitates communication between shoot apices. PLoS Biol. 2016; 14: e1002446. https://doi.org/10.1371/journal.pbio.1002446 PMID: 27119525

13. Paciorek T, Zažímalová E, Ruthardt N, Petrášek J, Stierhof Y-D, Kleine-Vehn J, et al. Auxin inhibits endocytosis and promotes its own efflux from cells. Nature. 2005; 435: 1251–1256. https://doi.org/10.1038/nature03633 PMID: 15988527

14. Robert S, Kleine-Vehn J, Barbez E, Sauer M, Paciorek T, Baster P, et al. ABP1 mediates auxin inhibition of clathrin-dependent endocytosis in *Arabidopsis*. Cell. 2010; 143: 111–121. https://doi.org/10.1016/j.cell.2010.09.027 PMID: 20887896

15. Wabnik K, Kleine-Vehn J, Balla J, Sauer M, Naramoto S, Reinöhl V, et al. Emergence of tissue polarization from synergy of intracellular and extracellular auxin signaling. Mol Syst Biol. 2010; 6: 447. https://doi.org/10.1038/msb.2010.103 PMID: 21179019

16. Robert HS, Grones P, Stepanova AN, Robles LM, Lokerse AS, Alonso JM, et al. Local auxin sources orient the apical-basal axis in Arabidopsis embryos. Curr Biol. 2013; 23: 2506–2512. https://doi.org/10.1016/j.cub.2013.09.039 PMID: 24291089

17. Wabnik K, Robert HS, Smith RS, Friml J. Modeling framework for the establishment of the apical-basal embryonic axis in plants. Curr Biol. 2013; 23: 2513–2518. https://doi.org/10.1016/j.cub.2013.10.038 PMID: 24291090

18. Benková E, Michniewicz M, Sauer M, Teichmann T, Seifertová D, Jürgens G, Friml J. Local, efflux-dependent auxin gradients as a common module for plant organ formation. Cell. 2003; 115: 591–602. PMID: 14651850

19. Rakusová H, Abbas M, Han H, Song S, Robert HS, Friml J. Termination of shoot gravitropic responses by auxin feedback on PIN3 polarity. Curr Biol. 2016; 26: 3026–3032. https://doi.org/10.1016/j.cub.2016.08.067 PMID: 27773568

20. Friml J, Benková E, Blilou I, Wiśniewska J, Hamann T, Ljung K, et al. AtPIN4 mediates sink-driven auxin gradients and root patterning in *Arabidopsis*. Cell. 2002; 108: 661–673. PMID: 11893337

21. Müller A, Guan C, Gälweiler L, Tänzler P, Huijser P, Marchant A, et al. *AtPIN2* defines a locus of *Arabidopsis* for root gravitropism control. EMBO J. 1998; 17: 6903–6911. https://doi.org/10.1093/emboj/17.23.6903 PMID: 9843496

22. Kleine-Vehn J, Leitner J, Zwiewka M, Sauer M, Abas L, Luschnig C, Friml J. Differential degradation of PIN2 auxin efflux carrier by retromer-dependent vacuolar targeting. Proc Natl Acad Sci USA. 2008; 105: 17812–17817. https://doi.org/10.1073/pnas.0808073105 PMID: 19004783

23. Chapman EJ, Estelle M. Mechanism of auxin-regulated gene expression in plants. Annu Rev Genet. 2009; 43: 265–285. https://doi.org/10.1146/annurev-genet-102108-134148 PMID: 19686081

24. Grones P, Friml J. Auxin transporters and binding proteins at a glance. J Cell Sci. 2015; 128: 1–7. https://doi.org/10.1242/jcs.159418 PMID: 25556248

25. Salehin M, Bagchi R, Estelle M. $SCF^{TIR1/AFB}$-based auxin perception: mechanism and role in plant growth and development. Plant Cell. 2015; 27: 9–19. https://doi.org/10.1105/tpc.114.133744 PMID: 25604443

26. Knox K, Grierson CS, Leyser O. *AXR3* and *SHY2* interact to regulate root hair development. Development. 2003; 130: 5769–5777. https://doi.org/10.1242/dev.00659 PMID: 14534134

27. Wilmoth JC, Wang S, Tiwari SB, Joshi AD, Hagen G, Guilfoyle TJ, et al. NPH4/ARF7 and ARF19 promote leaf expansion and auxin-induced lateral root formation. Plant J. 2005; 43: 118–130. https://doi.org/10.1111/j.1365-313X.2005.02432.x PMID: 15960621

28. Tejos R, Rodriguez-Furlán C, Adamowski M, Sauer M, Norambuena L, Friml J. PATELLINS are regulators of auxin-mediated PIN1 relocation and plant development in *Arabidopsis thaliana*. J Cell Sci. 2017; in press (https://doi.org/10.1242/jcs.204198) PMID: 28687624

29. Okushima Y, Overvoorde PJ, Arima K, Alonso JM, Chan A, Chang C, et al. Functional genomic analysis of the *AUXIN RESPONSE FACTOR* gene family members in *Arabidopsis thaliana*: unique and overlapping functions of *ARF7* and *ARF19*. Plant Cell. 2005; 17: 444–463. https://doi.org/10.1105/tpc.104.028316 PMID: 15659631

30. Michniewicz M, Zago MK, Abas L, Weijers D, Schweighofer A, Meskiene I, et al. Antagonistic regulation of PIN phosphorylation by PP2A and PINOID directs auxin flux. Cell. 2007; 130: 1044–1056. https://doi.org/10.1016/j.cell.2007.07.033 PMID: 17889649

31. Friml J, Yang X, Michniewicz M, Weijers D, Quint A, Tietz O, et al. A PINOID-dependent binary switch in apical-basal PIN polar targeting directs auxin efflux. Science. 2004; 306: 862–865. https://doi.org/10.1126/science.1100618 PMID: 15514156

32. Huang F, Kemel Zago M, Abas L, van Marion A, Galván-Ampudia CS, Offringa R. Phosphorylation of conserved PIN motifs directs *Arabidopsis* PIN1 polarity and auxin transport. Plant Cell. 2010; 22: 1129–1142. https://doi.org/10.1105/tpc.109.072678 PMID: 20407025

33. Zhang J, Nodzyński T, Pěnčik A, Rolčik J, Friml J. PIN phosphorylation is sufficient to mediate PIN polarity and direct auxin transport. Proc Natl Acad Sci USA. 2010; 107: 918–922. https://doi.org/10.1073/pnas.0909460107 PMID: 20080776

34. Mei Y, Jia W-J, Chu Y-J, Xue H-W. *Arabidopsis* phosphatidylinositol monophosphate 5-kinase 2 is involved in root gravitropism through regulation of polar auxin transport by affecting the cycling of PIN proteins. Cell Res. 2012; 22: 581–597. https://doi.org/10.1038/cr.2011.150 PMID: 21894193

35. Ugalde J-M, Rodriguez-Furlán C, De Rycke R, Norambuena L, Friml J, León G, Tejos R. Phosphatidylinositol 4-phosphate 5-kinases 1 and 2 are involved in the regulation of vacuole morphology during *Arabidopsis thaliana* pollen development. Plant Sci. 2016; 250: 10–19. https://doi.org/10.1016/j.plantsci.2016.05.014 PMID: 27457979

36. Ischebeck T, Werner S, Krishnamoorthy P, Lerche J, Meijón M, Stenzel I, et al. Phosphatidylinositol 4,5-bisphosphate influences PIN polarization by controlling clathrin-mediated membrane trafficking in *Arabidopsis*. Plant Cell. 2013; 25: 4894–4911. https://doi.org/10.1105/tpc.113.116582 PMID: 24326589

37. Tejos R, Sauer M, Vanneste S, Palacios-Gomez M, Li H, Heilmann M, et al. Bipolar plasma membrane distribution of phosphoinositides and their requirement for auxin-mediated cell polarity and patterning in *Arabidopsis*. Plant Cell. 2014; 26: 2114–2128. https://doi.org/10.1105/tpc.114.126185 PMID: 24876254

38. Agusti J, Lichtenberger R, Schwarz M, Nehlin L, Greb T. Characterization of transcriptome remodeling during cambium formation identifies *MOL1* and *RUL1* as opposing regulators of secondary growth. PLoS Genet. 2011; 7: e1001312. https://doi.org/10.1371/journal.pgen.1001312 PMID: 21379334

39. Hu W, Feng B, Ma H. Ectopic expression of the Arabidopsis *MINI ZINC FINGER1* and *MIF3* genes induces shoot meristems on leaf margins. Plant Mol Biol. 2011; 76: 57–68. https://doi.org/10.1007/s11103-011-9768-y PMID: 21455630

40. Eulgem T, Somssich IE. Networks of WRKY transcription factors in defense signaling. Curr Opin Plant Biol. 2007; 10: 366–371. https://doi.org/10.1016/j.pbi.2007.04.020 PMID: 17644023

41. Eulgem T, Rushton PJ, Robatzek S, Somssich IE. The WRKY superfamily of plant transcription factors. Trends Plant Sci. 2000; 5: 199–206. PMID: 10785665

42. Ülker B, Somssich IE. WRKY transcription factors: from DNA binding towards biological function. Curr Opin Plant Biol. 2004; 7: 491–498. https://doi.org/10.1016/j.pbi.2004.07.012 PMID: 15337090

43. Ciolkowski I, Wanke D, Birkenbihl RP, Somssich IE. Studies on DNA-binding selectivity of WRKY transcription factors lend structural clues into WRKY-domain function. Plant Mol Biol. 2008; 68: 81–92. https://doi.org/10.1007/s11103-008-9353-1 PMID: 18523729

44. Grunewald W, Karimi M, Wieczorek K, Van de Cappelle E, Wischnitzki E, Grundler F, et al. A role for AtWRKY23 in feeding site establishment of plant-parasitic nematodes. Plant Physiol. 2008; 148: 358–368. https://doi.org/10.1104/pp.108.119131 PMID: 18599655

45. Grunewald W, De Smet I, Lewis DR, Löfke C, Jansen L, Goeminne G, et al. Transcription factor WRKY23 assists auxin distribution patterns during *Arabidopsis* root development through local control on flavonol biosynthesis. Proc Natl Acad Sci USA. 2012; 109: 1554–1559. https://doi.org/10.1073/pnas.1121134109 PMID: 22307611

46. Grunewald W, De Smet I, De Rybel B, Robert HS, van de Cotte B, Willemsen V, et al. Tightly controlled WRKY23 expression mediates Arabidopsis embryo development. EMBO Rep. 2013; 14: 1136–1142. https://doi.org/10.1038/embor.2013.169 PMID: 24157946

47. Ulmasov T, Hagen G, Guilfoyle TJ. ARF1, a transcription factor that binds to auxin response elements. Science. 1997; 276: 1865–1868. PMID: 9188533

48. Boer DR, Freire-Rios A, van den Berg WAM, Saaki T, Manfield IW, Kepinski S, et al. Structural basis for DNA binding specificity by the auxin-dependent ARF transcription factors. Cell. 2014; 156: 577–589. https://doi.org/10.1016/j.cell.2013.12.027 PMID: 24485461

49. Yilmaz A, Mejia-Guerra MK, Kurz K, Liang X, Welch L, Grotewold E. AGRIS: the Arabidopsis Gene Regulatory Information Server, an update. Nucleic Acids Res. 2011; 39: D1118–D1122. https://doi.org/10.1093/nar/gkq1120 PMID: 21059685

50. Friml J, Vieten A, Sauer M, Weijers D, Schwarz H, Hamann T, et al. Efflux-dependent auxin gradients establish the apical—basal axis of *Arabidopsis*. Nature. 2003; 426: 147–153. https://doi.org/10.1038/nature02085 PMID: 14614497

51. Scarpella E, Marcos D, Friml J, Berleth T. Control of leaf vascular patterning by polar auxin transport. Genes Dev. 2006; 20: 1015–1027. https://doi.org/10.1101/gad.1402406 PMID: 16618807

52. Mattsson J, Ckurshumova W, Berleth T. Auxin signaling in Arabidopsis leaf vascular development. Plant Physiol. 2003; 131: 1327–1339. https://doi.org/10.1104/pp.013623 PMID: 12644682

53. Aida M, Beis D, Heidstra R, Willemsen V, Blilou I, Galinha C, et al. The *PLETHORA* genes mediate patterning of the *Arabidopsis* root stem cell niche. Cell. 2004; 119: 109–120. https://doi.org/10.1016/j.cell.2004.09.018 PMID: 15454085

54. Schluttenhofer C, Yuan L. Regulation of specialized metabolism by WRKY transcription factors. Plant Physiol. 2015; 167: 295–306. https://doi.org/10.1104/pp.114.251769 PMID: 25501946

55. Hiratsu K, Matsui K, Koyama T, Ohme-Takagi M. Dominant repression of target genes by chimeric repressors that include the EAR motif, a repression domain, in *Arabidopsis*. Plant J. 2003; 34: 733–739. PMID: 12787253

56. Luschnig C, Gaxiola RA, Grisafi P, Fink GR. EIR1, a root-specific protein involved in auxin transport, is required for gravitropism in *Arabidopsis thaliana*. Genes Dev. 1998; 12: 2175–2187. PMID: 9679062

57. Baster P, Robert S, Kleine-Vehn J, Vanneste S, Kania U, Grunewald W, De Rybel B, Beeckman T, Friml J. $SCF^{TIR1/AFB}$-auxin signalling regulates PIN vacuolar trafficking and auxin fluxes during root gravitropism. EMBO J. 2013; 32: 260–274. https://doi.org/10.1038/emboj.2012.310 PMID: 23211744

58. Sawchuk MG, Scarpella E. Polarity, continuity, and alignment in plant vascular strands. J Integr Plant Biol 2013; 55: 824–834. https://doi.org/10.1111/jipb.12086 PMID: 23773763

59. Rolland-Lagan A-G, Prusinkiewicz P. Reviewing models of auxin canalization in the context of leaf vein pattern formation in Arabidopsis. Plant J. 2005; 44: 854–865. https://doi.org/10.1111/j.1365-313X.2005.02581.x PMID: 16297075

60. Smith RS, Guyomarc'h S, Mandel T, Reinhardt D, Kuhlemeier C, Prusinkiewicz P. A plausible model of phyllotaxis. Proc Natl Acad Sci USA. 2006; 103: 1301–1306. https://doi.org/10.1073/pnas.0510457103 PMID: 16432192

61. Wabnik K, Kleine-Vehn J, Govaerts W, Friml J. Prototype cell-to-cell auxin transport mechanism by intracellular auxin compartmentalization. Trends Plant Sci. 2011; 16: 468–475. https://doi.org/10.1016/j.tplants.2011.05.002 PMID: 21665516

62. Cieslak M, Runions A, Prusinkiewicz P. Auxin-driven patterning with unidirectional fluxes. J Exp Bot. 2015; 66: 5083–5102. https://doi.org/10.1093/jxb/erv262 PMID: 26116915

63. Stenzel I, Ischebeck T, König S, Hołubowska A, Sporysz M, Hause B, Heilmann I. The type B phosphatidylinositol-4-phosphate 5-kinase 3 is essential for root hair formation in *Arabidopsis thaliana*. Plant Cell. 2008; 20: 124–141. https://doi.org/10.1105/tpc.107.052852 PMID: 18178770

64. Bakshi M, Oelmüller R. WRKY transcription factors: Jack of many trades in plants. Plant Signal Behav. 2014; 9: e27700. https://doi.org/10.4161/psb.27700 PMID: 24492469

65. Guan Y, Meng X, Khanna R, LaMontagne E, Liu Y, Zhang S. Phosphorylation of a WRKY transcription factor by MAPKs is required for pollen development and function in *Arabidopsis*. PLoS Genet. 2014; 10: e1004384. https://doi.org/10.1371/journal.pgen.1004384 PMID: 24830428

66. Kleine-Vehn J., et al. Cellular and molecular requirements for polar PIN targeting and transcytosis in plants. Mol Plant. 2008; 6:1056–66.

67. Xu J., et al. A molecular framework for plant regeneration. Science. 2006; 311: 385–388. https://doi.org/10.1126/science.1121790 PMID: 16424342

68. Leal Valentim F, van Mourik S, Posé D, Kim MC, Schmid M, van Ham RCHJ, et al. A quantitative and dynamic model of the Arabidopsis flowering time gene regulatory network. PLoS ONE. 2015; 10: e0116973. https://doi.org/10.1371/journal.pone.0116973 PMID: 25719734

69. Lemon WJ, Liyanarachchi S, You M. A high performance test of differential gene expression for oligonucleotide arrays. Genome Biol. 2003; 4: R67. https://doi.org/10.1186/gb-2003-4-10-r67 PMID: 14519202

70. Sauer M, Friml J. Immunolocalization of proteins in plants. Methods Mol Biol. 2010; 655: 253–263. https://doi.org/10.1007/978-1-60761-765-5_17 PMID: 20734266

71. Abas L, Benjamins R, Malenica N, Paciorek T, Wiśniewska J, Moulinier-Anzola JC, Sieberer T, Friml J, Luschnig C. Intracellular trafficking and proteolysis of the *Arabidopsis* auxin-efflux facilitator PIN2 are involved in root gravitropism. Nat Cell Biol. 2006; 8: 249–256 https://doi.org/10.1038/ncb1369 PMID: 16489343

SCIENTIFIC REPORTS

OPEN

PID/WAG-mediated phosphorylation of the *Arabidopsis* PIN3 auxin transporter mediates polarity switches during gravitropism

Received: 9 March 2017
Accepted: 14 June 2018
Published online: 06 July 2018

Peter Grones[1], Melinda Abas[1,3], Jakub Hajný[1,2], Angharad Jones[4], Sascha Waidmann[3], Jürgen Kleine-Vehn[3] & Jiří Friml[1]

Intercellular distribution of the plant hormone auxin largely depends on the polar subcellular distribution of the plasma membrane PIN-FORMED (PIN) auxin transporters. PIN polarity switches in response to different developmental and environmental signals have been shown to redirect auxin fluxes mediating certain developmental responses. PIN phosphorylation at different sites and by different kinases is crucial for PIN function. Here we investigate the role of PIN phosphorylation during gravitropic response. Loss- and gain-of-function mutants in PINOID and related kinases but not in D6PK kinase as well as mutations mimicking constitutive dephosphorylated or phosphorylated status of two clusters of predicted phosphorylation sites partially disrupted PIN3 phosphorylation and caused defects in gravitropic bending in roots and hypocotyls. In particular, they impacted PIN3 polarity rearrangements in response to gravity and during feed-back regulation by auxin itself. Thus PIN phosphorylation, besides regulating transport activity and apical-basal targeting, is also important for the rapid polarity switches in response to environmental and endogenous signals.

The plant hormone auxin, indole-3-acetic acid (IAA), controls plant growth and development by modulating fundamental cellular processes such as cell division, expansion, and differentiation[1]. Intercellular auxin transport and metabolism are responsible for changes in cellular auxin concentration[2–4], which leads to different auxin responses[5–7]. In recent years, detailed characterization of auxin transport proteins and their regulators has broadened our knowledge of polar auxin transport, auxin gradient formation and mechanisms of differential growth and organogenesis[8,9]. The most prominent auxin transporters are AUX1/LIKE AUX1 auxin importers[10,11], P-glycoproteins of the ATP-binding cassette transporter family of auxin exporters[12], and polarly localized PIN auxin exporters[4,13]. Although all of these proteins are involved in passing auxin across the plasma membrane out of or into the cell, it seems that PIN auxin efflux carriers[14] are predominant in mediating the directionality of the intercellular auxin flow by virtue of their polar subcellular localization in auxin-transporting cells[15,16].

One of the major regulatory mechanisms of PIN polar targeting is phosphorylation. Several studies demonstrated that serine/threonine protein kinases from the AGCVIII kinase family phosphorylate the hydrophilic loop of PIN proteins, which correlates with the change in PIN polar localization[16–21]. Three of these kinases, PINOID (PID), WAG1 and WAG2[22–24] play a crucial role. They are at least partially functionally redundant[18,24,25]. Overexpression of these kinases leads to a basal-to-apical (rootward-to-shootward) shift in PIN polarity that causes disruption of the auxin maxima and to the collapse of the root meristem and agravitropic root growth[22,23]. On the other hand, *pid, wag1, wag2* single or multiple mutants show more preferential basal PIN localization causing deprivation of auxin from the shoot meristem and a pin-like inflorescence phenotype or more basal

[1]Institute of Science and Technology Austria (IST Austria), Am Campus 1, 3400, Klosterneuburg, Austria. [2]Laboratory of Growth Regulators, Palacký University, Křížkovského 511/8, 771 47, Olomouc, Czech Republic. [3]Department of Applied Genetics and Cell Biology, University of Natural Resources and Life Sciences (BOKU), Muthgasse 18, 1190, Vienna, Austria. [4]Cardiff School of Biosciences, The Sir Martin Evans Building, Museum Avenue, Cardiff, CF10 3AX, United Kingdom. Correspondence and requests for materials should be addressed to J.F. (email: jiri.friml@ist.ac.at)

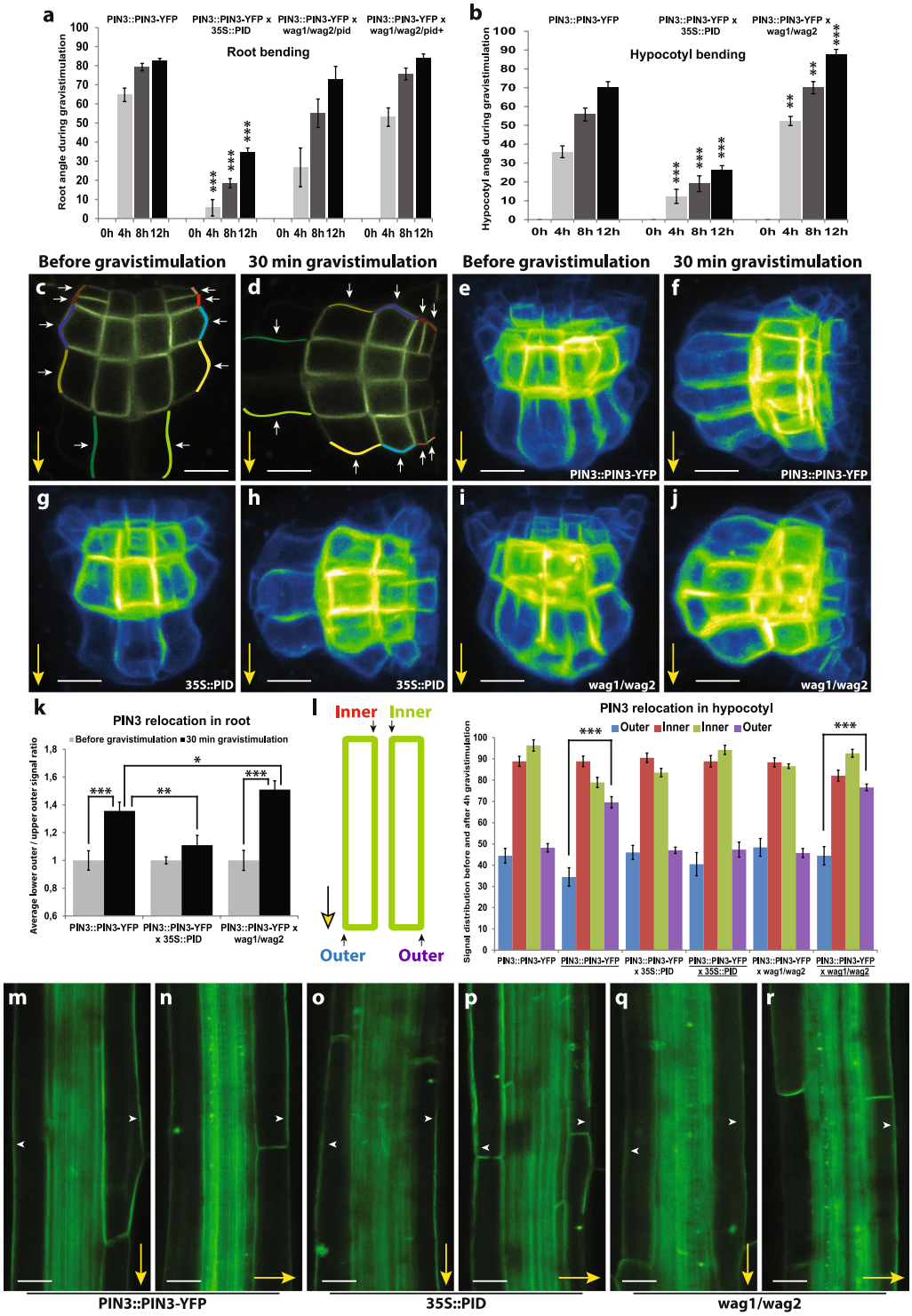

Figure 1. PID kinase is involved in the gravitropism and gravity-induced PIN3 relocation in root and hypocotyl. (**a**) Root bending assay in wild-type, *35S::PID*, *wag1/wag2/pid* and *wag1/wag2* double mutants from the *wag1/wag2/pid+* population after gravistimulation. (**b**) Hypocotyl bending assay in in wild-type, *35S::PID* and *wag1/wag2* backgrounds after gravistimulation. Student's T-tests were calculated for the comparison of each time point with the control (*PIN3::PIN3-YFP*). In hypocotyl, *35S::PID* shows less and *wag1/wag2* more gravitropic bending as compared to the control, while only roots of *35S::PID* exhibited slower bending after gravistimulation. (**c**,**d**) Schemes representing cellular membranes used for quantification of PIN3-YFP protein relocation in root columella cells. Signal intensity ratio before and after gravistimulation was calculated between lower outer (light colors) and upper outer (dark colors). Signal ratio for one root was calculated as an average of signal intensity ratios. (**e–j**) PIN3-YFP relocation in columella before (**e**,**g**,**i**) and after 30 minutes of gravitropic stimulation (**f**,**h**,**j**) in wild type, *35S::PID* and *wag1/wag2*. (**k**) Quantification of gravity-mediated PIN3-YFP relocalization in root. Signal before gravistimulation was normalized to 1. Student's T-tests were calculated

for the comparison of each time point with the control (*s*). *35S::PID* shows less and *wag1/wag2* more gravity-induced PIN3 relocation. (**l**) Scheme representing membranes used for quantification of PIN3-YFP protein relocation in hypocotyl endodermal cells and quantification of gravity-mediated PIN3-YFP relocalization in hypocotyls. Underlined genotypes represent samples after gravistimulation. Student's T-tests were calculated for the comparison of outer membranes signal within each line. *35S::PID* shows less gravity-induced PIN3 relocation in hypocotyl. (**m–r**) PIN3-YFP protein localization in hypocotyl before (m,o,q) and after 4 hours of gravitropic stimulation (n,p,r) in wild type, *35S::PID* and *wag1/wag2*. Experiments were repeated 3 times with 10–15 roots or hypocotyls per sample. Arrowheads indicate localization of the PIN3 protein. Error bars represent SE, (*$p < 0.05$, **$p < 0.01$, ***$p < 0.001$). Yellow arrows indicate gravity vector. Bars = 10 µm.

localization of the otherwise apically localized PIN2 in root epidermis leading to agravitropic root growth[18,23,26]. In accordance with the model that more PID-dependent phosphorylation leads to a preferentially apical PIN localization, phosphomimicking or phosphodead mutations of serine/threonine amino acids within the PIN hydrophilic loop show more apical or basal localization respectively.

Recently, a related subfamily of AGCVIII kinases involved in auxin transport and plant development has been identified. D6 protein kinase (D6PK) localizes to the basal membrane of *Arabidopsis* cells in root and co-localizes with several PIN proteins such as PIN1, PIN2 and PIN4. It was shown that D6PK can interact directly with PIN1 protein and phosphorylate it[27,28].

Changes in polar subcellular localization of PINs seem to be an essential mechanism for redirecting auxin fluxes in response to different environmental stimuli. For example, the apolar distribution of PIN3 becomes polar after gravitropic stimuli, leading to relocalization of PIN3 towards the gravity vector and correlating with changed auxin fluxes[5,29,30]. A similar phenomenon of PIN3 relocation, albeit slower, has been observed during the hypocotyl phototropic response[31]. Recently, a subsequent second re-polarization event during hypocotyl bending has been identified, which is important for resetting the asymmetry in the PIN polar distribution; ultimately leading to the termination of the bending[32]. This second repolarization is likely related to the auxin feed-back on PIN polarity as seen in so called auxin canalization processes of leaf venation and vascular tissue regeneration[33,34]. Although PIN3 and also PIN7[35–37] relocalization events are likely to be involved in redirecting auxin fluxes to create particular growth responses, insight into the underlying mechanism of relocation is still limited.

In this study we examined potential phosphorylation sites in the PIN3 hydrophilic loop and their role in tropic responses. We identified sites that play a role in both PIN3 polarity rearrangements during gravitropic responses, thus demonstrating a crucial role for PIN phosphorylation in polarity switches in response to external signals such as gravity or endogenous signals such as auxin itself.

Results

Importance of phosphorylation for gravity-mediated PIN3 relocation and bending.

Gravistimulation has been shown to induce changes in polar PIN3 localization in roots where PIN3 relocates towards the bottom side of the columella cells after the gravitropic stimulus[5,29,35–37]. PIN phosphorylation by PID has an impact on PIN polarity and auxin transport directionality in different developmental contexts by regulating apical-basal PIN localization[16,17,19]. We tested whether PID contributes to the gravitropic response and also to the gravity-induced relocation of PIN3 in roots and hypocotyls. It is known[18,22] that root bending in PID overexpressing line (*35S::PID*) is defective (Fig. 1a). As analyzed previously[38], *wag1/wag2/pid* triple mutant exhibited slightly slower root bending compared to control, while *wag1/wag2* double mutant from the *wag1/wag2/pid+* segregating population showed no difference in root bending after gravitropic stimuli compared to control (Fig. 1a). On the other hand, during hypocotyl bending, *35S::PID* line showed slower whereas *wag1/wag2* double mutant faster gravitropic response (Fig. 1b).

Overexpression or lack of WAG1/WAG2/PID has been shown to disturb PIN1 and PIN2 localizations[19], which can explain defects in gravitropism. We were interested if gravity-induced PIN3 relocation was also affected, thus we examined PIN3 distribution in root columella cells following gravitropic stimulation. We quantified changes by comparing PIN3-YFP signal intensity on the upper outer and lower outer sides of columella cells (Fig. 1c,d). After 30 minutes of gravistimulation, PIN3 relocates to the new basal cell sides following gravity (Fig. 1e,f,k). In the *35S::PID* overexpression line we observed a significant reduction in this PIN3 polarization (Fig. 1g,h,k). In a similar way, we observed that the *wag1/wag2* double mutant exhibited a more pronounced PIN3-YFP relocation rate after gravitropic stimuli (Fig. 1i–k). Also in the hypocotyl, phosphorylation by PID plays an important role in PIN3 polarization during the tropic response[30,31]. After 120 minutes of gravistimulation we observed relocation of PIN3-YFP to the bottom side of endodermal cells (Fig. 1l–n). Analogously to roots, overexpression of PID in the *35S::PID* line caused a decrease in the relocation rate of PIN3-YFP after gravistimulation (Fig. 1l,o,p) whereas in *wag1/wag2* the PIN3 relocation was more pronounced (Fig. 1l,q,r). Thus, the rates of PIN3 relocalisation in the *PID* overexpressor correlate with the decreased rates of bending observed in these plants.

Further, we tested the potential involvement of PIN phosphorylation by D6PK kinase[28] during the root gravitropic response. After 12 hours of gravitropic treatment we observed no significant differences in any *d6pk* mutants or overexpression lines (Figure S1a), agreeing with previously reported mild gravitropic defects[28]. This argues against an important role of D6PK in root gravitropism, and suggests that the contribution of D6PK for the regulation of PIN activity, either in columella cells for redirection of auxin fluxes, or in epidermis for shootward auxin transport, is not crucial.

Overall these results show that PID/WAG, but not D6PK, play an important role in gravity-mediated PIN3 repolarisation and in gravitropic bending both in roots and shoots. Higher PID expression inhibits PIN3 polarization and gravitropic bending whereas decreased PID/WAG expression leads to increased PIN3 polarization.

a

```
MISWHDLYTVLTAVIPLYVAMILAYGSVRWWKIFSPDQCSGINRFVAIFAVPLLSFHFIS   60
TNNPYAMNLRFIAADTLQKIIMLSLLVLWANFTRSGSLEWSITIFSLSTLPNTLVMGIPL  120
LIAMYGEYSGSLMVQIVVLQCIIWYTLLLFLFEFRGAKMLIMEQFPETAASIVSFKVESD  180
VVSLDGHDFLETDAEIGDDGKLHVTVRKSNASRRSFCGPNMTPRPSNLTGAEIYSLSTTP  240
RGSNFNHSDFYNMMGFPGGRLSNFGPADMYSVQSSRGPTPRPSNFEENCAMASSPRFGYY  300
PGGGAGSYPAPNPEFSSTTTSTANKSVNKNPKDVNTNQQTTLPTGGKSNSHDAKELHMFV  360
WSSNGSPVSDRAGLNVFGGAPDNDQGGRSDQGAKEIRMLVPDQSHNGETKAVAHPASGDF  420
GGEQQFSFAGKEEEAERPKDAENGLNKLAPNSTAALQSKTGLGGAEASQRKNMPPASVMT  480
RLILIMVWRKLIRNPNTYSSLIGLIWALVAFRWHVAMPKIIQQSISILSDAGLGMAMFSL  540
GLFMALQPKLIACGNSVATFAMAVRFLTGPAVMAVAAIAIGLRGDLLRVAIVQAALPQGI  600
VPFVFAKEYNVHPAILSTGVIFGMLIALPITLVYYILLGL                       641
```

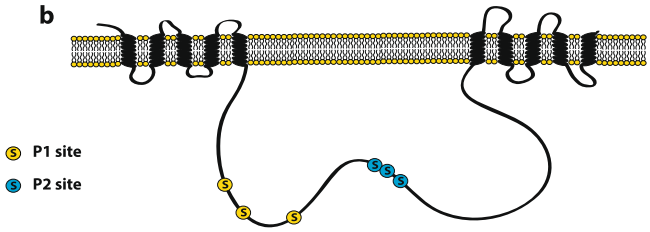

Figure 2. Phosphorylation sites in PIN3. (**a**) Positions of mutated amino acids in the sequence of PIN3 protein. P1 site is marked in yellow and P2 in blue. Transmembrane domains are highlighted in grey. (**b**) Scheme representing positions of mutated residues within PIN3 protein.

Putative phosphorylation residues in the PIN3 hydrophilic loop. Previous studies showed that PID directly phosphorylates the central hydrophilic loop of PIN proteins both *in vitro* and *in vivo*[17,18,28]. Therefore, we investigated the putative phosphorylation sites in the PIN3 loop. Two putative phosphorylation clusters, P1 and P2, both containing three serines (P1: S226, S243, and S283; P2: S316, S317, and S321) (Fig. 2a,b), were chosen. The P1 sites are the previously described conserved TPRxS motif[18,19], whereas the P2 sites are analogous to a described PIN1 phosphorylation site[16,18] that plays an important role during the basal-to-apical PIN1 relocalization[16]. Four different PIN3 mutant constructs were prepared, in which serines were either substituted by alanines (P1A: S226A, S243A, and S283A; P2A: S316A, S317A, and S321A) to mimic the non-phosphorylated state or by aspartic acid to mimic the constitutively phosphorylated status (P1D: S226D, S243D, and S283D; P2D: S316D, S317D, and S321D).

All mutant variants were cloned under the control of the native promoter and introduced into the wild type and *pin3–4* mutant to evaluate their impact on PIN3 function. The transformed plants did not exhibit any strong and obvious developmental defects. Levels of mutated PIN3 transcript in plants were evaluated by qPCR and only lines exhibiting similar expression level as PIN3 in wild type were used for further experiments (Fig. S1b). None of the phosphomutant variants exhibited defects in root length or meristem size, but all of them showed a slight reduction in the hypocotyl length in dark-grown seedlings (Fig. S1c,d,g). In two mutant variants PIN3-YFP-P1D and PIN3-YFP-P2D, the number of emerged lateral roots was slightly lower than that of the wild type (Fig. S1e). Analysis of lateral root stages revealed an increased number of first-stage primordia in PIN3-YFP-P2A and PIN3-YFP-P2D mutant variant (Fig. S1f), whereas the other mutant variants did not reveal any defects during lateral root formation. This suggests some contribution of PIN3 phosphorylation at our chosen sites during root and hypocotyl growth, in particular during the first stages of lateral root development. However, the effects of the chosen phosphomutations on overall development were not very prominent, suggesting that these sites are not important for an overall PIN3 activity, but potentially for some more specific aspects of its function.

***In vivo* phosphorylation of PIN3 mutant variants.** Previous study has shown by mass spectrometry that PIN3 protein is phosphorylated *in vivo* at multiple sites, including the P1 and P2 sites[39]. We evaluated the contribution of the P1 and P2 sites to total phosphorylation of PIN3 by PID kinase. PIN3::PIN3-YFP and all of the mutant constructs were transiently expressed in *N. benthamiana* leaves via *Agrobacterium* infiltration, with or without co-infiltration with PID. Co-expression of PID induced a shift in PIN3-YFP, indicating phosphorylation (Fig. 3a,b). A similar PID-dependent shift was observed when co-expressed with PIN3-YFP-P2A and PIN3-YFP-P2D mutant variants, but not with PIN3-YFP-P1A or PIN3-YFP-P1D mutant variants (Fig. 3a,b; Figure S2a). In fact, even without PID co-expression, the PIN3-YFP-P1A and PIN3-YFP-P1D proteins migrated faster in the SDS-PAGE gel, with less diffusion (sharper bands) compared to the WT or PIN3-YFP-P2A/D mutant variants (Fig. 3c). Since the altered migration and appearance on SDS-PAGE of the PIN3-YFP-P1A and PIN3-YFP-P1D mutant proteins may reflect decreased phosphorylation by endogenous *N. benthamiana* kinases, we ran the same samples on Phostag gels, but no major enhancement of the difference in migration between PIN3-YFP and PIN3-YFP-P1A/D was observed (Fig. 3d). This suggests that the difference in migration is not caused by less endogenous phosphorylation of the P1 site mutant variants. Overall, these results indicated that the PID can still phosphorylate PIN3 when the P2 sites are mutated, while mutations in P1 site largely abolished phosphorylation of PIN3 protein by PID kinase.

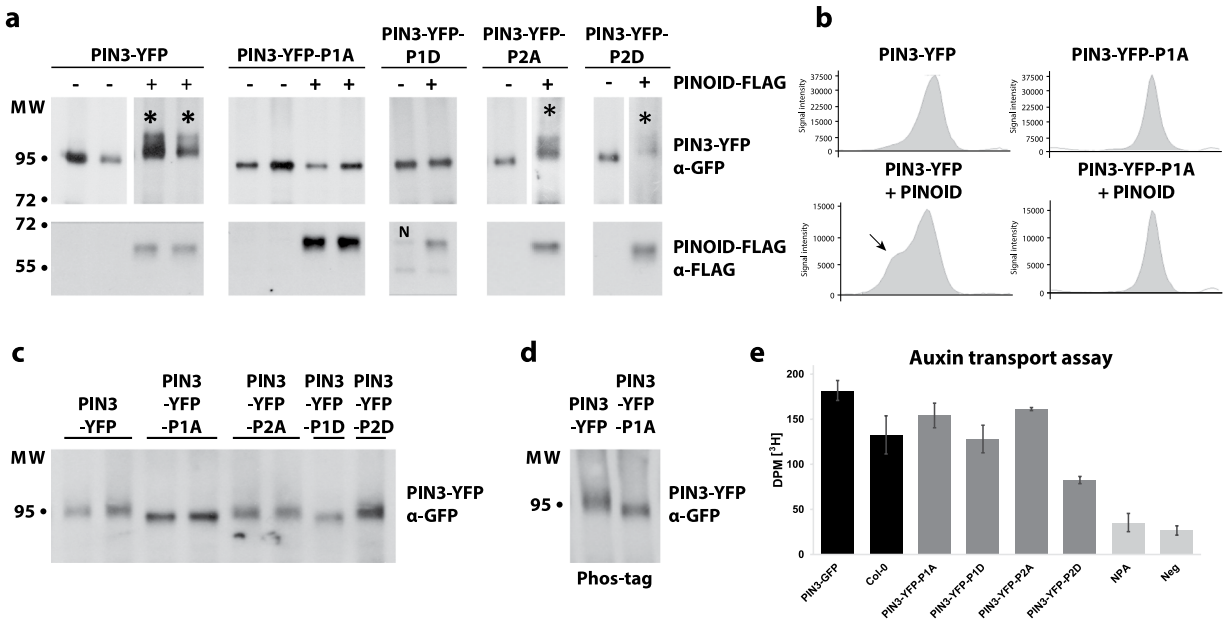

Figure 3. *In vivo* phosphorylation of PIN3-YFP and mutant variants. (**a**) Transiently expressed PIN3-YFP and all mutant variants in *N. benthamiana* with or without co-infiltration with PINOID-FLAG. Total protein was extracted, separated by SDS-PAGE, blotted and probed with anti-GFP and anti-FLAG. Phosphorylation of PIN3-YFP, PIN3-YFP-P2A and PIN3-YFP-P2D by PINOID appears as a distinct smear above the main band (marked with star). Results from one single blot are shown, some lines were exposed longer due to weaker signals. The complete blots and Ponceau stain are shown in Figure S3. N indicates carryover signal from anti-GFP (breakdown product of PIN3-YFP-P1D). (**b**) Lane profiles of the anti-GFP blots for PIN3-YFP and PIN3-YFP-P1A with or without PINOID from (a). Arrow marks additional peak representing phosphorylated protein. (**c**) Faster migration of PIN3-YFP-P1A and PIN3-YFP-P1D in SDS-PAGE compared to WT and PIN3-YFP-P2A/D (**d**) Phostag gel revealed no enhancement in the differences of the migration between PIN3-YFP and PIN3-YFP-P1A. (**e**) Rootward transport of radiolabeled ^{3}H-IAA in decapitated hypocotyls. Neg represents negative control for diffusion in agar. Treatment of 10 μM N-1-naphthylphthalamic acid (NPA), an auxin transport inhibitor, was used as additional negative control. Student's T-test was calculated for the comparison of each line with the control (Col-0). Error bars represent SE.

Next, we evaluated whether mutations in phosphorylation sites might affect auxin transport activity of the PIN3 mutant variants. Etiolated hypocotyls were decapitated and used to measure ^{3}H-IAA transported basipetally into the hypocotyl. We observed altered transport rates in both phosphomimic variants, particularly in PIN3-YFP-P2D compared to the wild type (Fig. 3e). This suggests that the selected phosphorylation sites in PIN3 protein are important for the directional auxin transport in the hypocotyl, notwithstanding that the major contributor of the hypocotyl basipetal/downward transport is believed to be the PIN1 auxin transporter[4].

PIN3 phosphorylation in the root gravitropic responses. We tested the effect of the PIN3 phosphomutant variants on gravitropic response and gravity-induced PIN3 relocalization in roots. All phosphomutant variants introduced in the *pin3-4* background partially rescued the *pin3* mutant phenotype. During the gravitropic response, PIN3-YFP-P1A, PIN3-YFP-P1D and PIN3-YFP-P2A were bending slightly faster (after 4 hours) as compared to the wild-type, but the PIN3-YFP-P2D mutant variant exhibited the least rescue showing defective gravitropic bending comparable to the *pin3-4* mutant (Fig. 4a). Thus the PIN3 phosphomutant variants were not able to completely complement the wild type PIN3 function in root gravitropism.

At the cellular level, all PIN3 phosphomutant variants showed the apolar distribution of the PIN3 protein in columella cells in non-stimulated roots similar to the wild type (Fig. 4c,e,g,i,k). After gravity stimulation (30 min), the PIN3-YFP protein relocated to the new lower sides of columella cells (Fig. 4b–d). Phosphodead PIN3-YFP-P1A and PIN3-YFP-P2A exhibited similar relocation rate to wild type (Fig. 4b,e,f,i,j), whereas phosphomimic PIN3-YFP-P1D and PIN3-YFP-P2D variants exhibited a clear defect in the PIN3 relocation (Fig. 4b,g,h,k,l).

Together, the results suggest the importance of PIN3 phosphorylation in the root gravitropic response, in particular that mimicking constitutive phosphorylation inhibits gravity-induced PIN3 relocation similar to the effects observed in *35S::PID* lines.

PIN3 phosphorylation in the hypocotyl gravitropic response. Next, we tested the effect of the PIN3 phosphomutant variants on the gravitropic response and gravity-induced PIN3 relocalization in hypocotyls. Gravistimulation induces PIN3 polarization towards the new bottom sides of endodermal cells leading to auxin accumulation at the lower side of hypocotyl. This auxin accumulation leads to a second, subsequent PIN3

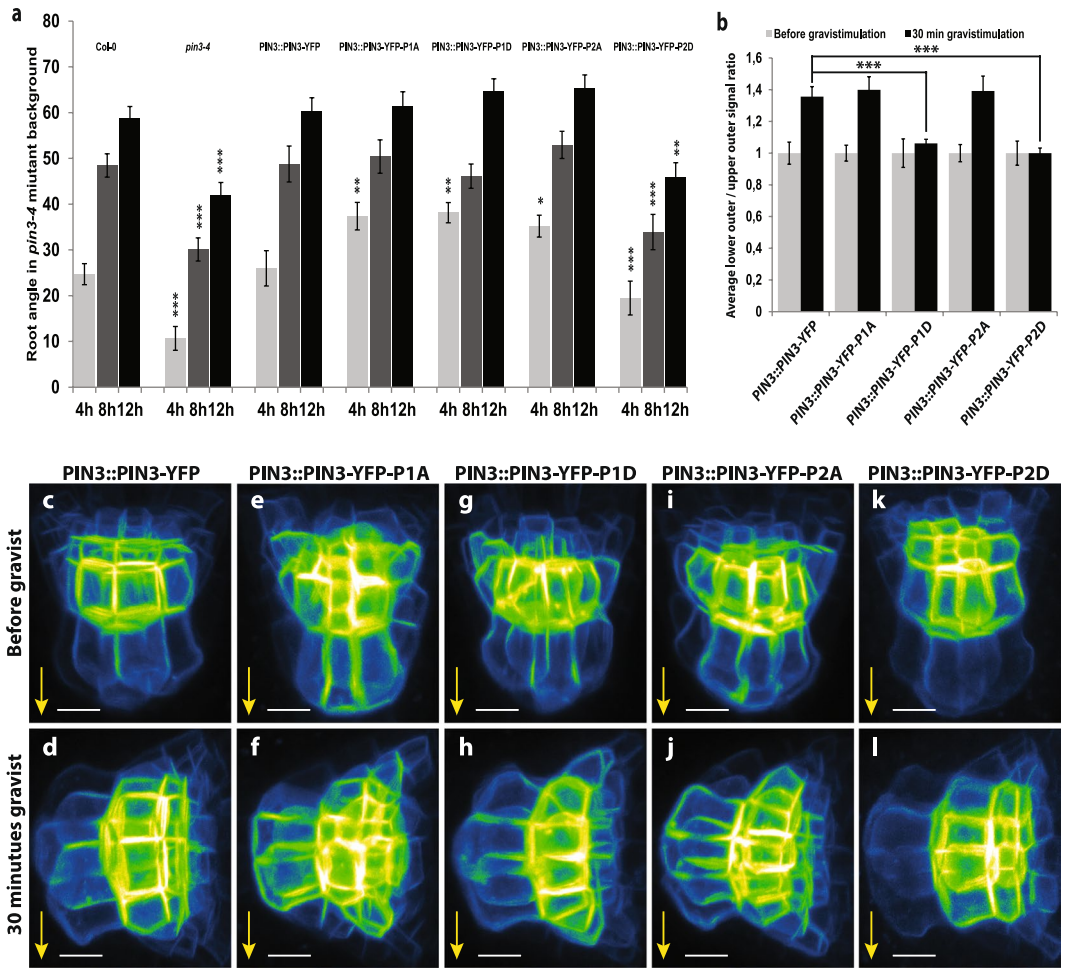

Figure 4. PIN3 phosphorylation is required for PIN3 polarization and root gravitropic response. (**a**) Root bending kinetics of PIN3 mutant variants during gravitropic response. Root curvatures were measured every 4 hours. Student's T-test was calculated for the comparison of each line with the control (Col-0). PIN3-YFP-P2D mutant variant shows slower root bending. (**b**) Quantification of PIN3 polarization in columella cells before and after gravistimulation. Signal before gravistimulation was normalized to 1. Student's T-test was calculated for the comparison of each line with the control (*PIN3::PIN3-YFP*). Both phosphomimic variants, PIN3-P1D and PIN3-P2D, exhibit less gravity-induced PIN3 relocation. (**c–l**) Localization of PIN3-YFP (**c**,**d**), PIN3-YFP-P1A (**e**,**f**), PIN3-YFP-P1D (**g**,**h**), PIN3-YFP-P2A (**i**,**j**), and PIN3-YFP-P2D (**k**,**l**) before (upper row) and after 30 minutes (lower row) of gravitropic stimulation in the wild type background. Values are the average of three biological replicates ($n > 10$ per time point on each replicate). Error bars represent SE, (*$p < 0.05$, **$p < 0.01$, ***$p < 0.001$). Yellow arrows indicate gravity vector. Bars = 10 µm.

polarization, during which PIN3 in cells of the lower hypocotyl sides polarizes back to the upper cell sides, restoring PIN3 expression symmetry and aiding termination of bending[30,32].

Similar to the situation in the root, the line expressing PIN3-YFP-P2D showed a weakest rescue of hypocotyl gravitropism (Fig. 5a). At the cellular level, we observed enhanced signal intensity in the outer lateral membranes of the endodermal cells in the phosphomimicking PIN3-YFP-P1D and PIN3-YFP-P2D lines when compared to the control (Figs 5i, S2b,d,f). After 4 hours gravistimulation, the PIN3-YFP in the cells of the upper hypocotyl side relocates from the outer/upper lateral to the inner/bottom lateral membranes and at the lower hypocotyl side from the inner/upper lateral to the outer/bottom lateral membranes (Fig. 5b,c,i,j). In phosphodead PIN3-YFP-P1A and PIN3-YFP-P2A mutant variants, this gravity induced relocation was comparable to the wild type PIN3-YFP (Figs 5d,f,i,j, S2c,e). On the other hand, similarly as observed in roots, relocation of the PIN3-YFP protein after gravitropic stimuli was less pronounced in phosphomimic PIN3-YFP-P1D and PIN3-YFP-P2D variants (Figs 5e,g,i,j, S2d,f).

Next we tested the auxin effect on PIN3 polar distribution that has been suggested to be important for feed-back regulation of bending termination. Treatments with natural or synthetic auxins can relocate the PIN3 protein in endodermal cells of hypocotyls from the outer lateral to the inner lateral membranes, the so-called "inner-lateralization"[32]. After 4 hours of NAA treatment we observed a reduced PIN3 inner-lateralization for PIN3-YFP-P1D and PIN3-YFP-P2D phosphomimic variants as compared to the phospho-dead variants or control (Fig. 5k,l).

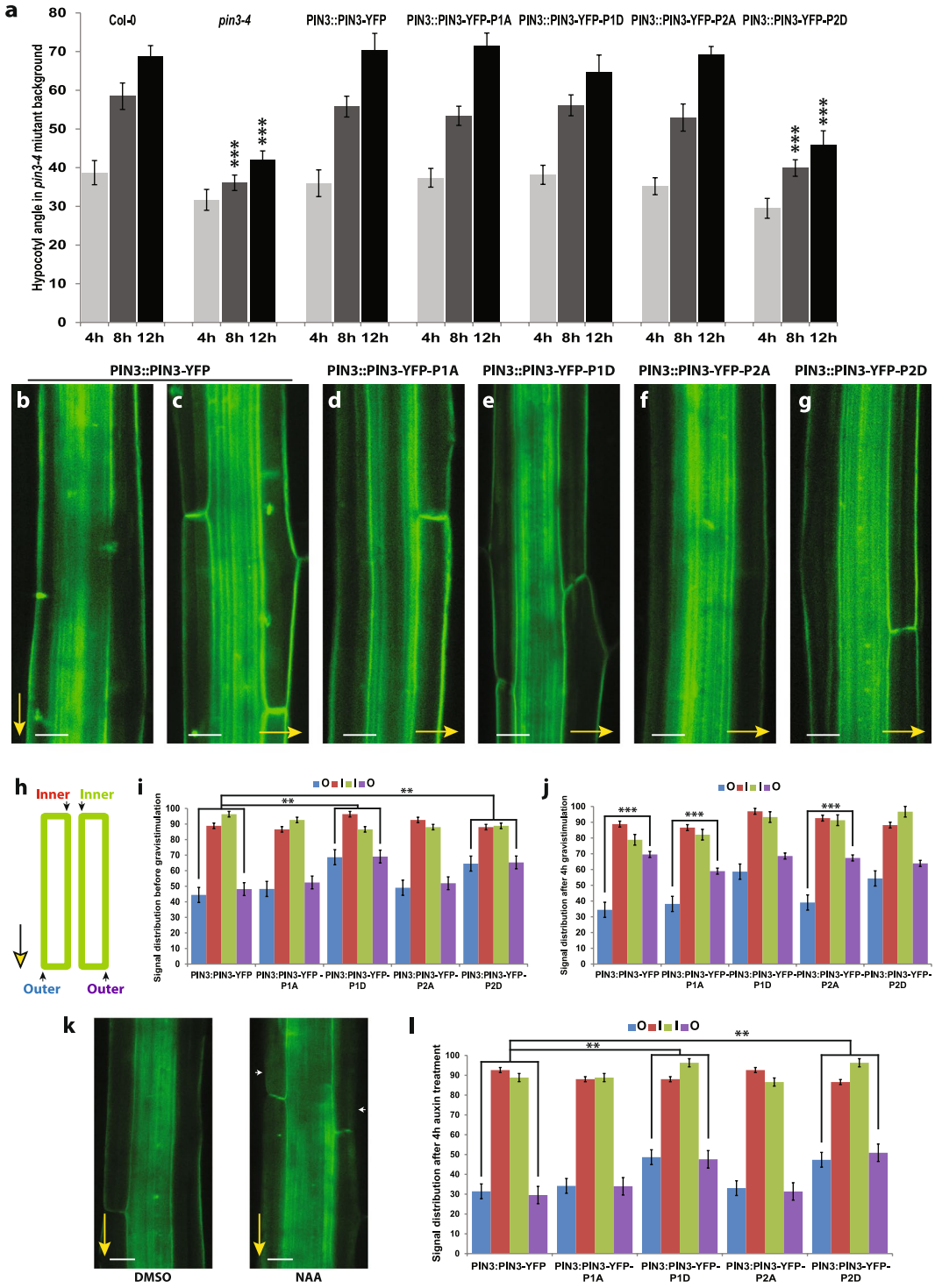

Figure 5. PIN3 phosphorylation is required for PIN3 polarization and hypocotyl gravitropic response. (**a**) Hypocotyl bending kinetics of PIN3 mutant variants during gravitropic response. Curvatures were measured every 4 hours. Student's T-test was calculated for the comparison of each line with the control (Col-0). PIN3-P2D mutant variant shows slower hypocotyl bending. (**b**–**g**) Localization of PIN3-YFP before and after 4 hours of gravistimulation (**b**,**c**) and after gravistimulation in PIN3-YFP-P1A (**d**), PIN3-YFP-P1D (**e**), PIN3-YFP-P2A (**f**), and PIN3-YFP-P2D (**g**). Yellow arrows indicate gravity vector. (**h**) Scheme of quantification showing measured membranes in hypocotyl. (**i**) Quantification of PIN3 signal distribution in hypocotyl endodermal cells. Student's T-test was calculated for the comparison of outer membranes signal within each line. PIN3-P1D and PIN3-P2D exhibit higher signal intensity on outer-lateral membranes. (**j**) Quantitative evaluation of gravity-dependent PIN3 relocation in hypocotyl endodermal cells. Student's T-test was calculated for the comparison of outer membranes signal within each line. Both PIN3-P1D and PIN3-P2D show defective gravity-induced PIN3-YFP relocation. (**k**) Localization of PIN3-YFP before and after 4 hours of 10 μM NAA treatment in wild type. White arrows indicate depletion of PIN3 protein from outer-lateral cell membranes.

(**l**) Quantification of PIN3-YFP signal in endodermal cells of hypocotyl after 4 hours of 10 μM NAA treatment. Student's T-test was calculated for the comparison of each line with the control (*PIN3::PIN3-YFP*). PIN3-P1D and PIN3-P2D exhibit reduced auxin-induced PIN3 inner-lateralization. Error bars represent SE, (**$p < 0.01$, ***$p < 0.001$). Yellow arrows indicate gravity vector. Bars = 10 μm.

These data indicate that in both negative gravitropism of the hypocotyl as well as in positive root gravitropism, PIN3 phosphorylation plays a similar role in gravity-induced relocation and gravitropic response in both above and underground organs. In addition, the hypocotyl experiments revealed a role of PIN3 phosphorylation in auxin-induced relocation.

Discussion

How a directional signal such as gravity is translated within the plant into the directional auxin flow that forms the lateral auxin gradient and thus drives the bending response is conceptually one of the hardest questions in understanding plant tropic responses. The observation that gravistimulation induces changes in the polar localization of PIN auxin transporters, which is consistent with auxin flow being aligned with the gravity vector[5,29,35–37], provides a possible mechanism for gravity-induced redirection of auxin fluxes. PIN phosphorylation by the protein kinase PID has been implicated in both apical/basal PIN polarity and tropic responses[4,9].

Here we have demonstrated that PIN phosphorylation and PID/WAGs kinases activity are involved in the gravity-induced relocation of the PIN3 protein in root columella and hypocotyl endodermal cells. Downregulation of PID/WAGs increases gravity-induced PIN3 relocation and consequently gravitropic bending, whereas upregulation of PID reduces PIN3 relocation and bending. To confirm the role of phosphorylation in this process and to assess which potential phosphorylation sites might be important, we chose two clustered sites, P1 (conserved TPRxS motif[18,19]) and P2 (adapted from[16,18]) that have been shown to be phosphorylated *in vivo*[39–41], and prepared different phosphorylation variants including phosphomimic and phosphodead. Prepared mutant variants in the *pin3-4* mutant background displayed only minor defects in overall development. More specifically, they show defects in the root and hypocotyl gravitropic growth and gravity-induced PIN3 relocation that are in particular observed in the phosphomimic variants. The hypocotyl experiments also revealed a defect in the auxin-mediated PIN3 relocation, again apparent in the phosphomimic variants. These phenotypes of phosphomimic variants correspond with PIN3 relocation and bending phenotypes in root and hypocotyl in *35S::PID* line suggesting that PIN3 phosphorylation at least partly mediated by PID and associated dephosphorylation by phosphatases are required for both gravity-mediated PIN3 relocations and bending.

Our results revealed that the P2 phosphorylation site, which is partially conserved among long PIN proteins[17], is important for the PIN3-mediated gravitropic responses of roots and hypocotyls. The phenotypes of mutations at this site described here by us are not completely analogous to the one already published for PIN1[16]. Our phosphorylation assays revealed additional phosphorylation sites might co-operate with the P2 site during gravitropic responses. As PID/WAG kinases are not strongly expressed in columella cells[18], the P2 sites might be a target of MAPK, which may co-operate with PID during phosphorylation-dependent PIN3-mediated gravitropic responses[16,41].

A similar study about phosphorylation sites in the PIN3 hydrophilic loop has identified a different phosphorylation site, M3 ($_{209}$SNASRRSFCGPNMTPRPS$_{226}$), that is important for subcellular trafficking and PIN3-mediated developmental processes, such as auxin efflux activity, root growth, and root gravitropism[21,42]. Nevertheless, the PIN3-M3 phosphodead mutant variant was demonstrated to be still phosphorylated by PID or WAG1 *in vitro*[21].

In addition to the role of PID kinase in regulating both PIN transport activity and its polar localization, the related D6PK kinase has been also shown to phosphorylate PIN proteins recognizing overlapping residues as PID kinase, but being more specifically involved in regulating PIN activity[27,28]. Nonetheless, the D6PK involvement in root gravitropic responses is unlikely, as various *d6pk* mutant and overexpression lines exhibit at most insignificant gravitropism defects in the root[28]. In addition, the antagonistic component of PID activity, protein phosphatase 6 (PP6) holoenzyme, also targets and regulates PIN subcellular localization[17,43]. In roots, dephosphorylation by PP6 complex led to changes in PIN polarity from apical to basal[44,45], thus the role of phosphatases in controlling PIN polar targeting during gravitropic responses should not be ignored. Given the complexity of the number of putative phosphorylation sites in PIN proteins and different kinases and phosphatases, it seems apparent that multiple overlapping PIN phosphorylation mechanisms will be involved in regulation of different aspects of PIN-dependent auxin transport. Nonetheless, our work provides evidence demonstrating that these phosphorylation processes regulate PIN polarity switches and thus auxin fluxes redirections in response to both environmental and endogenous regulations.

Experimental Procedures. *Plant materials and growth conditions.* The published transgenic and mutant lines were: *PIN3::PIN3-YFP*[46]; *pin3–4* (SALK_005544); *35S::PID-21*[22]; *wag1/wag2/pid*[18]. All seeds were grown on agarose plates containing 1/2 strength Murashige and Skoog medium with 1% sucrose. Seeds were vernalized for 3 days at 4 °C and consequently grown at 18 °C under 16-h-light/8-h-dark photoperiod. For hypocotyl experiments, after stratification the germination was induced by placing the plates in the light for 5–6 hours that were then transferred to darkness and kept at 18 °C for 4 days. For root or hypocotyl gravitropic stimulations, plates with 4-day-old seedlings were turned 90°, scanned at every time point by scanner and the angles were measured by ImageJ. For root length measurements 5 day old seedling were used, for hypocotyl length measurements 4 day old dark grown seedlings. The emerged lateral root assay was performed on 14 day old seedlings and LR primordia were counted with a differential interference contrast microscope BX51 (Olympus). Each experiment was conducted at least in triplicate. For the statistical evaluation, the t-test was done with the Excel statistical package.

PIN3 phosphorylation mutagenesis. The binary vector pK7m42GW containing PIN3::PIN3-YFP sequence[46] was used for transgene construction. Four different DNA fragments (PIN3-P1A, PIN3-P1D, PIN3-P2A, PIN3-P2D) possessing different mutations (Table S1) were synthesized with XhoI and AegI restriction sites on the ends. Via classical cloning all four of these fragments were introduced into the PIN3::PIN3-YFP vector. Transformation of these constructs to *Arabidopsis* was accomplished via *Agrobacterium tumefaciens* (strain PMP90)-mediated infiltration by floral dip. All transformed lines were analyzed and at least 3 independent transgenic lines for each construct with similar expression level were used in this study.

Confocal microscopy. For confocal microscopy, a Zeiss LSM 710 confocal scanning microscope or Zeiss LSM 710 vertical confocal scanning microscope were used. To monitor the gravitropic response, plates were scanned 24 h after gravistimulation. Images were processed in Zeiss ZEN software and ImageJ. Each experiment was performed at least three times.

Quantitative analysis of PIN3 relocalization in root and hypocotyl. All measurements were performed using ImageJ software (National Institutes of Health; http://rsb.info.nih.gov/ij). Quantification of gravity-induced PIN3-YFP relocalization in columella cells was performed on maximal intensity projections of Z-scans of columella cells by measuring the signal intensity at the apical membranes (marked with dark colors) and comparing with signal intensity of basal membranes (marked with light colors) of the cells on the periphery of columella before and after gravistimulation (see scheme in Fig. 1c,d). Signal ratio for one root was calculated as an average of signal intensity ratios. For quantification of the gravity-induced PIN3-YFP relocalization in hypocotyls single plain images from the same focal plane were taken and the rate of PIN3-YFP fluorescence intensity was compared between the outer PM sides of endodermal cells (see scheme in Figs 1l or 5h). The PIN3 relocation is most clearly visible in the upper endodermal cells, since the lower cell signal is influenced by PIN3-YFP signal in stele. Three replicates of 10–15 seedlings with a synchronized germination start were processed. The presented values are the mean of the averages.

***In vivo* phosphorylation of PIN3-YFP and mutant variants.** PIN3-YFP and mutant variants were transiently expressed in *N. benthamiana* by *Agrobacterium* infiltration, with or without co-infiltration with PID. The same *Agrobacterium* lines were used as those used to generate the transgenic *A.thaliana* plants described above. Since these constructs contained the native AtPIN3 promoter, the infiltrated *N. benthamiana* leaves were treated with 1 μM IAA 24 h before harvesting to promote gene expression, as the AtPIN3 promoter is known to be responsive to IAA[47]. For co-infiltration with PID, we used an inducible PID (pINTAM3-PID[23]) or 35S::PID-FLAG[17] cloned into pGREEN. pINTAM3-PID was induced with 1 μM 4OH-tamoxifen (Sigma-Aldrich) and 5 μM beta-estradiol for 24 h before harvesting. All infiltrations were performed with p19 to reduce silencing[48]. Samples were extracted based on Abas & Luschnig[49], with modifications for a quicker extraction in order to detect phosphorylated protein versions. Frozen tissue was ground in liquid nitrogen and collected into extraction buffer containing PhosSTOP (Roche), centrifuged for 3 minutes at 300 g (4 °C) and the supernatant (soluble and membrane fractions) was immediately solubilized with 2% lithium dodecyl sulfate and 10 mM DTE. Samples were centrifuged at 20 000 g for 30 min (4 °C) and the supernatant precipitated by chloroform/methanol[50]. Proteins were separated by SDS-PAGE, blotted and probed with anti-GFP monoclonal mouse antibody (Roche), stripped and probed with anti-FLAG M2 monoclonal mouse antibody (Sigma-Aldrich). As *N. benthamiana* leaves contain a strong non-specific signal from anti-FLAG antibody at about 90 kD, only the lower half of the blot was used for anti-FLAG. For Phos-tag analysis, 25 μM Phos-tag (WAKO) was incorporated into the gel. Phosphorylated bovine casein, ovalbumin, PID and AtPIN1 were used as positive controls for Phos-tag.

Auxin transport assay. Etiolated seedlings were prepared as described above, except plates were kept at 21 °C for 5 days. Etiolated hypocotyls were decapitated to exclude the effect of auxin biosynthesis in cotyledons and a droplet of AM + agar (1.25%) with ^{3}H-IAA (12uL ^{3}H-IAA + 10 mL AM + agar) was applied to the apical part of the hypocotyls. After 6 hours, hypocotyls were collected, homogenized in liquid nitrogen and incubated overnight in Opti-Fluor scintillation cocktail (Perkin Elmer). Amount of transported ^{3}H-IAA was then measured in a scintillation counter (Hidex 300SL) for 300 s with three technical repetitions. Negative control was performed by inserting the droplet above the decapitated hypocotyl to account for any diffusion though the agar. Additional negative control was performed using 10 μM NPA, to inhibit auxin transport.

Quantitative qPCR. Total RNA was extracted with the RNeasy kit (QIAGEN). Poly(dT) cDNA was prepared from total RNA with Superscript III (Invitrogen).Quantitative RT-PCR was done with LightCycler 480 SYBR Green I Master reagents (Roche Diagnostics) and a LightCycler 480 Real-Time PCR System (Roche Diagnostics). Data were analyzed with qBASE v1.3.4[51]. Expression levels were normalized to the non-auxin-responsive genes β-TUBULIN (At5g12250), EEF (At1g30230) and CDKA (At3g48750).

References

1. Mockaitis, K. & Estelle, M. Auxin receptors and plant development: a new signaling paradigm. *Annu. Rev. Cell Dev. Biol.* **24**, 55–80 (2008).
2. Zhao, Y. Auxin Biosynthesis and Its Role in Plant Development. *Annu. Rev. Plant Biol.* **61**, 49–64 (2010).
3. Brumos, J., Alonso, J. M. & Stepanova, A. N. Genetic aspects of auxin biosynthesis and its regulation. *Physiol. Plant.* **151**, 3–12 (2014).
4. Adamowski, M. & Friml, J. PIN-dependent auxin transport: action, regulation, and evolution. *Plant Cell* **27**, 20–32 (2015).
5. Friml, J., Wiśniewska, J., Benková, E., Mendgen, K. & Palme, K. Lateral relocation of auxin efflux regulator PIN3 mediates tropism in Arabidopsis. *Nature* **415**, 806–9 (2002).
6. Vanneste, S. & Friml, J. Auxin: A Trigger for Change in Plant Development. *Cell* **136**, 1005–1016 (2009).
7. Bargmann, B. O. R. *et al.* A map of cell type-specific auxin responses. *Mol. Syst. Biol.* **9**, 688 (2013).

8. Grones, P. & Friml, J. Auxin transporters and binding proteins at a glance. *J. Cell Sci.* **128**, 1–7 (2015).
9. Rakusová, H., Fendrych, M. & Friml, J. Intracellular trafficking and PIN-mediated cell polarity during tropic responses in plants. *Curr. Opin. Plant Biol.* **23**, 116–123 (2015).
10. Bennett, M. J. *et al*. Arabidopsis AUX1 gene: a permease-like regulator of root gravitropism. *Science* **273**, 948–50 (1996).
11. Yang, Y., Hammes, U. Z., Taylor, C. G., Schachtman, D. P. & Nielsen, E. High-affinity auxin transport by the AUX1 influx carrier protein. *Curr. Biol.* **16**, 1123–7 (2006).
12. Geisler, M. *et al*. Cellular efflux of auxin catalyzed by the Arabidopsis MDR/PGP transporter AtPGP1. *Plant J.* **44**, 179–94 (2005).
13. Petrásek, J. *et al*. PIN proteins perform a rate-limiting function in cellular auxin efflux. *Science* **312**, 914–8 (2006).
14. Zourelidou, M. *et al*. Auxin efflux by PIN-FORMED proteins is activated by two different protein kinases, D6 PROTEIN KINASE and PINOID. *Elife* **3** (2014).
15. Wisniewska, J. *et al*. Polar PIN localization directs auxin flow in plants. *Science* **312**, 883 (2006).
16. Zhang, J., Nodzynski, T., Pencík, A., Rolcík, J. & Friml, J. PIN phosphorylation is sufficient to mediate PIN polarity and direct auxin transport. *Proc. Natl. Acad. Sci. USA* **107**, 918–22 (2010).
17. Michniewicz, M. *et al*. Antagonistic regulation of PIN phosphorylation by PP2A and PINOID directs auxin flux. *Cell* **130**, 1044–56 (2007).
18. Dhonukshe, P. *et al*. Plasma membrane-bound AGC3 kinases phosphorylate PIN auxin carriers at TPRXS(N/S) motifs to direct apical PIN recycling. *Development* **137**, 3245–55 (2010).
19. Huang, F. *et al*. Phosphorylation of conserved PIN motifs directs Arabidopsis PIN1 polarity and auxin transport. *Plant Cell* **22**, 1129–42 (2010).
20. Sasayama, D., Ganguly, A., Park, M. & Cho, H.-T. The M3 phosphorylation motif has been functionally conserved for intracellular trafficking of long-looped PIN-FORMEDs in the Arabidopsis root hair cell. *BMC Plant Biol.* **13**, 189 (2013).
21. Ganguly, A., Lee, S.-H. & Cho, H.-T. Functional identification of the phosphorylation sites of Arabidopsis PIN-FORMED3 for its subcellular localization and biological role. *Plant J.* **71**, 810–823 (2012).
22. Benjamins, R., Quint, A., Weijers, D., Hooykaas, P. & Offringa, R. The PINOID protein kinase regulates organ development in Arabidopsis by enhancing polar auxin transport. *Development* **128**, 4057–4067 (2001).
23. Friml, J. *et al*. A PINOID-dependent binary switch in apical-basal PIN polar targeting directs auxin efflux. *Science* **306**, 862–5 (2004).
24. Galván-Ampudia, C. S. & Offringa, R. Plant evolution: AGC kinases tell the auxin tale. *Trends Plant Sci.* **12**, 541–547 (2007).
25. Cheng, Y., Qin, G., Dai, X. & Zhao, Y. NPY genes and AGC kinases define two key steps in auxin-mediated organogenesis in Arabidopsis. *Proc. Natl. Acad. Sci.* **105**, 21017–21022 (2008).
26. Reinhardt, D. *et al*. Regulation of phyllotaxis by polar auxin transport. *Nature* **426**, 255–60 (2003).
27. Barbosa, I. C. R., Zourelidou, M., Willige, B. C., Weller, B. & Schwechheimer, C. D6 PROTEIN KINASE Activates Auxin Transport-Dependent Growth and PIN-FORMED Phosphorylation at the Plasma Membrane. *Dev. Cell* **29**, 674–685 (2014).
28. Zourelidou, M. *et al*. The polarly localized D6 PROTEIN KINASE is required for efficient auxin transport in Arabidopsis thaliana. *Development* **136**, 627–36 (2009).
29. Harrison, B. R. & Masson, P. H. ARL2, ARG1 and PIN3 define a gravity signal transduction pathway in root statocytes. *Plant J.* **53**, 380–92 (2008).
30. Rakusová, H. *et al*. Polarization of PIN3-dependent auxin transport for hypocotyl gravitropic response in Arabidopsis thaliana. *Plant J.* **67**, 817–26 (2011).
31. Ding, Z. *et al*. Light-mediated polarization of the PIN3 auxin transporter for the phototropic response in Arabidopsis. *Nat. Cell Biol.* **13**, 447–52 (2011).
32. Rakusová, H. *et al*. Termination of Shoot Gravitropic Responses by Auxin Feedback on PIN3 Polarity. *Curr. Biol.* **26**, 3026–3032 (2016).
33. Prát, T. *et al*. WRKY23 is a component of the transcriptional network mediating auxin feedback on PIN polarity. *PLOS Genet.* **14**, e1007177 (2018).
34. Mazur, E., Benková, E. & Friml, J. Vascular cambium regeneration and vessel formation in wounded inflorescence stems of Arabidopsis. *Sci. Rep.* **6**, 33754 (2016).
35. Kleine-Vehn, J. *et al*. Gravity-induced PIN transcytosis for polarization of auxin fluxes in gravity-sensing root cells. *Proc. Natl. Acad. Sci. USA* **107**, 22344–9 (2010).
36. Pernisova, M. *et al*. Cytokinins influence root gravitropism via differential regulation of auxin transporter expression and localization in Arabidopsis. *New Phytol.* **212**, 497–509 (2016).
37. Kleine-Vehn, J. *et al*. Cellular and Molecular Requirements for Polar PIN Targeting and Transcytosis in Plants. *Mol. Plant* **1**, 1056–1066 (2008).
38. Santner, A. A. & Watson, J. C. The WAG1 and WAG2 protein kinases negatively regulate root waving in Arabidopsis. *Plant J.* **45**, 752–64 (2006).
39. Xu, S.-L. *et al*. Proteomic analysis reveals O-GlcNAc modification on proteins with key regulatory functions in Arabidopsis. *Proc. Natl. Acad. Sci. USA* **114**, E1536–E1543 (2017).
40. Jia, W. *et al*. Mitogen-Activated Protein Kinase Cascade MKK7-MPK6 Plays Important Roles in Plant Development and Regulates Shoot Branching by Phosphorylating PIN1 in Arabidopsis. *PLoS Biol.* **14**, e1002550 (2016).
41. Dory, M. *et al*. Coevolving MAPK and PID phosphosites indicate an ancient environmental control of PIN auxin transporters in land plants. *FEBS Lett.* **592**, 89–102 (2018).
42. Ki, D., Sasayama, D. & Cho, H.-T. The M3 Phosphorylation Site Is Required for Trafficking and Biological Roles of PIN-FORMED1, 2, and 7 in Arabidopsis. *Front. Plant Sci.* **7**, 1479 (2016).
43. Ballesteros, I. *et al*. Specialized functions of the PP2A subfamily II catalytic subunits PP2A-C3 and PP2A-C4 in the distribution of auxin fluxes and development in Arabidopsis. *Plant J.* **73**, 862–72 (2013).
44. Dai, M. *et al*. A PP6-type phosphatase holoenzyme directly regulates PIN phosphorylation and auxin efflux in Arabidopsis. *Plant Cell* **24**, 2497–514 (2012).
45. Karampelias, M. *et al*. ROTUNDA3 function in plant development by phosphatase 2A-mediated regulation of auxin transporter recycling. *Proc. Natl. Acad. Sci. USA* **113**, 2768–73 (2016).
46. Zadniková, P. *et al*. Role of PIN-mediated auxin efflux in apical hook development of Arabidopsis thaliana. *Development* **137**, 607–617 (2010).
47. Paponov, I. A. *et al*. Comprehensive Transcriptome Analysis of Auxin Responses in Arabidopsis. *Mol. Plant* **1**, 321–337 (2008).
48. Voinnet, O., Rivas, S., Mestre, P. & Baulcombe, D. An enhanced transient expression system in plants based on suppression of gene silencing by the p19 protein of tomato bushy stunt virus. *Plant J.* **33**, 949–56 (2003).
49. Abas, L. & Luschnig, C. Maximum yields of microsomal-type membranes from small amounts of plant material without requiring ultracentrifugation. *Anal. Biochem.* **401**, 217–27 (2010).
50. Wessel, D. & Flügge, U. I. A method for the quantitative recovery of protein in dilute solution in the presence of detergents and lipids. *Anal. Biochem.* **138**, 141–143 (1984).
51. Hellemans, J., Mortier, G., De Paepe, A., Speleman, F. & Vandesompele, J. qBase relative quantification framework and software for management and automated analysis of real-time quantitative PCR data. *Genome Biol.* **8**, R19 (2007).

Acknowledgements

We thank Eva Benková and Remko Offringa who kindly provided us with published *Arabidopsis* lines and Herta Steinkellner for providing *N. benthamiana* plants. We acknowledge the *Arabidopsis* Biological Resource Center and the Nottingham *Arabidopsis* Stock Centre for distributing seeds, and the Department of Applied Genetics and Cell Biology at BOKU Vienna for use of their facilities by M.A. We thank Stefan Kepinski and Suruchi Roychoudhry for valuable comments. The research leading to these results has received funding from the European Research Council under the European Union's Seventh Framework Program/ERC grant agreements n° 282300 and 742985.

Author Contributions

P.G., A.J. and J.F. initiated the work. P.G., A.J. and J.F. designed the experiments. P.G. carried out most of the biological experiments, M.A. designed and performed phosphorylation assays, J.H. performed auxin transport assays and gravitropic response of *d6pk* and *wag1/wag2/pid* mutants, S.W. and J.K.-V. provided plasmid material. P.G., A.J. and J.F. wrote the manuscript with M.A. contributing. All authors approved the final version of this manuscript to be published.

Additional Information

Supplementary information accompanies this paper at https://doi.org/10.1038/s41598-018-28188-1.

Competing Interests: The authors declare no competing interests.

Publisher's note: Springer Nature remains neutral with regard to jurisdictional claims in published maps and institutional affiliations.

Plant Physiology Preview. Published on April 1, 2019, as DOI:10.1104/pp.19.00201

Short title

Pinstatic acid is a modulator of PIN trafficking.

Corresponding author details

Ken-ichiro Hayashi, Ph.D.

Professor, Department of Biochemistry, Okayama University of Science, 1-1 Ridai-cho, Okayama 700-0005, Japan

Title

Pinstatic acid promotes auxin transport by inhibiting PIN internalization

Authors

Akihiro Oochi,[a] Jakub Hajny,[b,h] Kosuke Fukui,[a] Yukio Nakao,[a] Michelle Gallei, [b] Mussa Quareshy,[c] Koji Takahashi,[d,e] Toshinori Kinoshita,[d,e] Sigurd Ramans Harborough,[f] Stefan Kepinski,[f] Hiroyuki Kasahara,[g,i] Richard Napier,[c] Jiří Friml,[b] Ken-ichiro Hayashi[a1]

[a]Department of Biochemistry, Okayama University of Science, Okayama 700-0005, Japan.
[b]Institute of Science and Technology Austria, Klosterneuburg, Austria.
[c]School of Life Sciences, University of Warwick, Coventry, CV4 7AL, United Kingdom
[d]Graduate School of Science, Nagoya University, Chikusa, Nagoya, 464-8602 Japan.
[e]Institute of Transformative Bio-Molecules (WPI-ITbM), Nagoya University, Chikusa, Nagoya, 464-8601, Japan.
[f]Centre for Plant Sciences, Faculty of Biological Sciences, University of Leeds, Leeds LS2 9JT, UK.
[g]Institute of Global Innovation Research, Tokyo University of Agriculture and Technology, Fuchu-shi, Tokyo 183-8509, Japan
[h]Laboratory of Growth Regulators, The Czech Academy of Sciences, Institute of Experimental Botany & Palacký University, Šlechtitelů 27, CZ-78371 Olomouc, Czech Republic
[i]RIKEN Center for Sustainable Resource Science, Yokohama, Kanagawa, 230-0045 Japan

One-sentence summary

Pinstatic acid is an inactive auxin analog for $SCF^{TIR1/AFB}$ core auxin regulatory pathway and positively modulates auxin efflux transport by inhibiting PIN internalization.

Author contribution

A.O. J.H., J.F., Y.N., and K.H. conceived this project and designed research, discussed the data, R.N., S.K., J.F., and K.H. wrote the paper; rapid hypocotyl elongation assay were performed by T.K.,

K.T., ; Endogenous IAA analysis was performed by H.K.; surface plasmon resonance assays were performed by M.Q. and R.N.; pull-down assays were performed by S.R.H. and S.K.; all other experiments were performed by A.O., J.H., M.G., F.K., J.F., Y.N., and K.H..

Funding information

This work was supported in part by the Ministry of Education, Culture, Sports, Science, and Technology through a Grant-in-Aid for Scientific Research (no. JP25114518 to K.H.), BBSRC award BB/L009366/1 to R.N. and S.K. and European Union's Horizon2020 program (ERC grant agreement n° 742985) to J.F.

Corresponding author email

hayashi@dbc.ous.ac.jp

Keywords

Auxin, PIN, polar transport, small molecule, Arabidopsis thaliana, receptor, membrane transport

55 **ABSTRACT**

56 Polar auxin transport plays a pivotal role in plant growth and development. PIN auxin efflux
57 carriers regulate directional auxin movement by establishing local auxin maxima, minima, and
58 gradients that drive multiple developmental processes and responses to environmental signals.
59 Auxin has been proposed to modulate its own transport by regulating subcellular PIN trafficking via
60 processes such as clathrin-mediated PIN endocytosis and constitutive recycling. Here, we further
61 investigated the mechanisms by which auxin affects PIN trafficking by screening auxin analogs and
62 identified pinstatic acid (PISA) as a positive modulator of polar auxin transport in *Arabidopsis*
63 *thaliana*. PISA had an auxin-like effect on hypocotyl elongation and adventitious root formation via
64 positive regulation of auxin transport. PISA did not activate $SCF^{TIR1/AFB}$ signaling and yet induced PIN
65 accumulation at the cell surface by inhibiting PIN internalization from the plasma membrane. This
66 work demonstrates PISA to be a promising chemical tool to dissect the regulatory mechanisms
67 behind subcellular PIN trafficking and auxin transport.

68

69 **INTRODUCTION**

70 The plant hormone auxin is a master regulator of plant growth and development. Indole 3-acetic
71 acid (IAA), the predominant natural auxin, regulates numerous and diverse developmental
72 processes such as establishment of embryo polarity, vascular differentiation, apical dominance and
73 tropic responses to light and gravity (Hayashi, 2012). The auxin responses regulating these diverse
74 developmental events can be modulated at three major steps: auxin metabolism (Korasick et al.,
75 2013; Kasahara, 2016), directional auxin transport (Adamowski and Friml, 2015) and signal
76 transduction (Leyser, 2018).

77 Polar auxin transport plays a crucial role in auxin-regulated development by influencing local
78 auxin maxima and gradients and is mediated principally by three families of membrane proteins, the
79 Auxin1/Like Aux1 (AUX1/LAX) auxin influx carriers, the PIN-FORMED (PIN) auxin efflux facilitators
80 and several members of the ATP-binding cassette group B (ABCB) auxin transporters (Adamowski

and Friml, 2015).

The polar subcellular localization of the auxin efflux machinery determines the directionality of auxin flow. The spatiotemporal regulation of auxin gradients also depends on the cell-specific expression and subcellular localization of plasma membrane (PM)-localized PIN proteins (PIN1 - PIN4 and PIN7), the latter often being responsive to environmental and developmental cues (Adamowski and Friml, 2015). PIN proteins are often asymmetrically distributed within the cell and are constantly recycled between endosomal compartments and the PM. The dynamics of polar localization of PIN proteins regulates the rate and direction of cellular auxin export and this ultimately determines auxin gradients in the tissue. Therefore, the regulatory machinery of the polarity and abundance of PM-localized PIN proteins are crucial for diverse developmental processes and morphogenesis including embryogenesis, initiation of lateral organs, and tropic responses (Robert et al., 2013; Adamowski and Friml, 2015; Rakusova et al., 2015).

The exocytosis and endocytosis of PIN proteins at the PM can be modulated by ADP RIBOSYLATION FACTOR-GUANINE NUCLEOTIDE EXCHANGE FACTORS (ARF-GEFs) including GNOM (Naramoto et al., 2010). PIN proteins are internalized from the PM to the trans-Golgi network / early endosome (TGN/EE) compartments after which PINs can then proceed along the recycling route to the PM (Adamowski and Friml, 2015). An important tool for investigating exocytic protein sorting is Brefeldin A (BFA), which is a reversible inhibitor of ARF-GEFs including GNOM (Geldner et al., 2001; Geldner et al., 2003). BFA treatment leads to accumulation of the endocytosed PINs in artificial intracellular aggregates called BFA bodies, the formation of which can be reversed by washing out the BFA (Geldner et al., 2001).

Clathrin-mediated endocytosis is also involved in the internalization of PIN proteins from the PM (Kitakura et al., 2011; Adamowski et al., 2018) and is modulated by the ROP (Rho guanidine triphosphate hydrolases of plants) family of Rho-like GTPases and their associated RICs (ROP interactive CRIB motif-containing proteins) (Lin et al., 2012; Nagawa et al., 2012). Genetic analysis has revealed that MAB4 (MACCHI-BOU4)/ ENP (ENHANCER OF PID)/NPY1 (NAKED PINS IN

YUCCA-like1), a gene encoding NPH3 (NON-PHOTOTROPIC HYPOCOTYL3)-like proteins and homologous MELs (MAB4/ENP/NPY1-like), regulates PIN abundance at the PM (Furutani et al., 2014). The internalization and trafficking of PIN proteins is dynamically regulated by developmental and environmental cues, such as plant hormones, gravity and light (Ding et al., 2011; Rakusova et al., 2016). Short-term auxin treatments, in particular using synthetic auxin analogs, blocks clathrin-mediated internalization of PIN proteins from the PM and consequently enhances PIN abundance at the PM and increases auxin efflux (Paciorek et al., 2005; Robert et al., 2010). Auxin also induces PIN1 relocalization from basal to the inner lateral PM of root endodermal and pericycle cells (Prat et al., 2018). Similarly, auxin mediates PIN3 relocalization during gravitropic responses to terminate gravitropic bending (Rakusova et al., 2016). Prolonged auxin treatment induces PIN2 vacuolar targeting and degradation, and this is mediated by the $SCF^{TIR1/AFB}$ pathway (Abas et al., 2006; Baster et al., 2013), which presumably also explains the $SCF^{TIR1/AFBs}$-dependent auxin effect on PIN2-GFP accumulation in BFA bodies (Pan et al., 2009). In addition, auxin has been reported to reduce the abundance of photoconvertible PIN2-Dendra at the PM by repressing the translocation of newly synthesized PIN2 to the PM (Jasik et al., 2016). Besides an auxin effect on PIN trafficking, other hormones can influence different aspect of PIN trafficking, including cytokinin (Marhavy et al., 2011), salicylic acid (Du et al., 2013), and gibberellic acid (Salanenka et al., 2018), thus providing a possible entry point for crosstalk of these signaling pathways with the auxin distribution network.

Given these different and sometimes contradictory observations for different PINs resulting from investigations in different cells and using different approaches, the underlying cellular and molecular mechanisms for the targeting and recycling of PIN proteins, and in particular for their regulation by auxin, remain largely unknown.

To develop a useful chemical tool for dissecting the regulatory mechanism of PIN trafficking, we have screened phenylacetic acid (PAA) derivatives for selective modulation of PIN trafficking in *Arabidopsis thaliana*. We identified 4-ethoxyphenylacetic acid, which was designated as PInStatic Acid (PISA) due to its activity on PIN-mediated polar auxin transport. PISA has an auxin-like effect on

hypocotyl elongation and adventitious root formation by positively modulating auxin transport. Similar to conventional auxins, PISA blocks the internalization of PIN proteins from the PM and consequently induces PIN protein accumulation at the PM. PISA is notably different from other known auxin chemical tools, like auxin transport inhibitors 2,3,5 - triiodobenzoic acid (TIBA) and N-1-naphthylphthalamic acid (NPA). Therefore, PISA represents a promising chemical tool for dissecting the complicated regulations of PIN trafficking by auxin.

RESULTS

Pinstatic acid is an inactive PAA analog on TIR1/AFB-Aux/IAA co-receptor complex.

Auxins modulate the expression and degradation of PIN proteins via the $SCF^{TIR1/AFB}$ signaling pathway (Baster et al., 2013; Ren and Gray, 2015). On the other hand, clathrin-mediated endocytosis of PIN is inhibited by auxin via a non-transcriptional pathway (Robert et al., 2010). These positive and negative effects of auxin on PIN trafficking hinder access to the regulatory components in PIN trafficking using conventional genetic approaches. Therefore, we searched for an auxin transport modulator that would make PIN trafficking more amenable to experimentation. To this end, we initially screened PAA derivatives according to the following criteria; (i) The derivative should be inactive within the $SCF^{TIR1/AFB}$ pathway and (ii) derivative treatment should induce auxin-related phenotypes that are different from the phenotypes typical of auxins or auxin transport inhibitors, such as TIBA and NPA.

In the course of screening, we found that 4-ethoxyphenylacetic acid (later denoted PISA) promoted hypocotyl elongation but did not induce auxin-responsive *DR5::GUS* reporter gene expression which is mediated by the $SCF^{TIR1/AFB}$ pathway (Fig. 1A, 1C and 2). Thus, PISA was selected as the most promising candidate from a series of 4-alkyloxy-PAA derivatives and further characterized in detail.

Auxin is biosynthesized by two enzymes, namely TAA1 and YUC in the indole 3-pyruvic acid (IPA) pathway (Kasahara, 2016). The inhibition of this pathway by L-kynurenine (Kyn), a TAA1

159 inhibitor, and yucasin DF, a YUC inhibitor, caused short and curled roots that are typical
160 auxin-deficient phenotypes (Fig. 1B) (He et al., 2011; Tsugafune et al., 2017). A quintuple *yuc 3 5 7 8*
161 *9* mutant showed a similar auxin-deficient root phenotype (Fig. S1A) (Chen et al., 2014). IAA and
162 1-naphthylyacetic acid (NAA) at 50–100 nM recovered these auxin-deficient root defects in root
163 elongation and gravitropism (Fig. 1B and S1A). 3-Ethoxyphenylacetic acid (meta-substituted PISA:
164 mPISA), an analog of PISA (Fig. 1A) that retains weak auxin activity in *DR5::GUS* expression (Fig.
165 1C) also rescued the auxin-deficient curled root phenotype (Fig. 1B). In contrast, PISA did not rescue
166 these root defects caused by auxin deficiency, clearly indicating PISA does not directly act as a
167 typical auxin like IAA or NAA in planta (Fig. 1B and S1A).

168 The tobacco BY-2 cell suspension culture requires auxin for cell proliferation (Winicur et al.,
169 1998). BY-2 cells proliferated in the presence of IAA and NAA (Fig. S1B), but PISA failed to maintain
170 this cell culture (Fig. S1B). The cell morphology of the culture treated with PISA showed swollen cell
171 shapes that are a hallmark of auxin-depletion (Fig. S1C), further suggesting that PISA does not have
172 the effect as an auxin on cell division (Winicur et al., 1998). Auxin-induced rapid cell elongation in
173 etiolated hypocotyls was demonstrated to be mediated by TR1/AFB receptors (Fendrych et al., 2016).
174 However, PISA failed to induce this rapid cell elongation (Fig. S2), suggesting that PISA does not act
175 as a conventional auxin to directly activate the TR1/AFB receptors in the hypocotyl.

176 IAA and the synthetic auxin picloram cause potent induction of auxin-responsive reporter genes
177 such as *DR5* (Fig. 1C). In contrast, PISA did not induce any auxin-responsive *DR5::GUS* and
178 *BA3::GUS* reporter expression, again suggesting that it is inactive as a ligand for the $SCF^{TIR1/AFB}$
179 pathway (Fig. 1C, 1D and S3A). DII-VENUS protein is a translational fusion of the TIR1-interacting
180 domain of Aux/IAA proteins and the fluorescent reporter VENUS (Brunoud et al., 2012). IAA
181 promotes the interaction between DII-VENUS and TIR1 receptor to induce the DII-VENUS
182 degradation and loss of the VENUS signal (Fig. 1E). In contrast, PISA did not induce degradation of
183 DII-VENUS, once again suggesting that PISA does not directly modulate TIR1/AFB-Aux/IAA auxin
184 co-receptor complex formation. Additionally, PISA showed no activity in the yeast auxin-inducible

185 degron (AID) system (Fig. S3B) (Nishimura et al., 2009). In this system, the minichromosome
186 maintenance (MCM) complex is essential for DNA replication in yeast and lines in which MCM is
187 deficient fail to grow (Nishimura et al., 2009). The auxins IAA and NAA, and analog mPISA, all
188 repressed the growth of yeast expressing rice OsTIR1 and Aux/IAA-fused MCM4 protein by
189 promoting the degradation of the fused MCM4 protein (Fig. S3B) (Nishimura et al., 2009). In contrast,
190 PISA did not repress yeast growth in this AID system, indicating again that PISA is not an active
191 ligand for TIR1.

192 These findings were further supported by biochemical assays using Surface Plasmon
193 Resonance (SPR) analysis (Fig. 1F) and a pull-down assay (Fig. S3C) (Lee et al., 2014). IAA
194 promotes assembly of the co-receptor complex of TIR1 and Aux/IAA (domain II) in both assays. In
195 contrast, PISA did not promote the interaction between TIR1 and Aux/IAA in either system (Fig. 1F
196 and S3C). Additionally, the SPR assay also showed that there was no binding of PISA with AFB5 (Fig.
197 S3D), and using the SPR assay to test for anti-auxin activity by mixing 50 μM PISA with 5 μM IAA
198 showed that PISA did not bind and block the TIR1 auxin-binding site (Fig. S3E) whereas the known
199 TIR1/AFB auxin receptor blocker auxinole (Hayashi et al., 2012) reduced the IAA signal dramatically.
200 Thus, in these direct binding assays, PISA does not bind to TIR1/AFB co-receptors. In summary,
201 PISA is completely inactive as a classical auxin that induces the Aux/IAA degradation via TIR1/AFB
202 auxin receptors.

203

204 **PISA promotes hypocotyl elongation by positively modulating polar auxin transport.**

205 PISA promotes hypocotyl elongation in a manner that is typical for auxin effects in Arabidopsis
206 seedlings (Fig. 2A). Since PISA did not activate DR5-monitored auxin response, we carefully
207 examined its effects on auxin-related phenotypes *in planta* in order to address possible modes of
208 PISA action. In light-grown seedlings, PISA at 5–20 μM promoted hypocotyl elongation (Fig. 2A-2D).
209 In contrast, IAA and mPISA inhibited growth at 0.5 and 20 μM, respectively, whereas the
210 AFB5-selective synthetic auxin picloram strongly promoted hypocotyl elongation (Fig. 2D). In the

211 dark, PISA at 2 μM slightly promoted the elongation of etiolated hypocotyls (Fig. 2E and 2F), but did
212 not inhibit their elongation at 20 μM. In contrast, exogenously applied IAA, picloram and mPISA
213 inhibited the elongation of etiolated hypocotyls (Fig. 2F).

214 Having explored a set of physiological responses, we made use of genetic and pharmacological
215 tools to gain insight into the mechanism of PISA action. The auxin signaling mutants *axr1-3* and *tir1-1*
216 *afb2-1* showed high resistance to mPISA (Fig. S4A), implying that mPISA targets auxin signaling in
217 planta (Hayashi, 2012). In contrast, the hypocotyl of *axr1-3* elongated to a similar extent as that of
218 the wild type when treated with PISA (Fig. 3A). Importantly, neither wild type nor *axr1-3* responded to
219 PISA after the inhibition of SCF^{TIR1} auxin signaling by the auxin antagonist auxinole (Fig. 3A and
220 S4B). PISA also failed to promote hypocotyl elongation in the presence of the auxin biosynthesis
221 inhibitor L-kynurenine (Fig. 3A and S4C). These observations indicate that auxin-like effects of PISA
222 on hypocotyl growth require the $SCF^{TIR1/AFB}$ auxin signaling to be activated by endogenous IAA.

223 To examine the effects of PISA on polar auxin transport, seedlings were co-treated with auxin
224 efflux transport inhibitors and PISA. The promotion of elongation by PISA on hypocotyls was blocked
225 by three auxin efflux transport inhibitors, TIBA, BUM (2-[4-(diethylamino)-2-hydroxybenzoyl]benzoic
226 acid) and NPA (Fig. 3B, 3C and S5A) (Fukui and Hayashi, 2018). In addition, treatments with the
227 synthetic auxin picloram and the auxin overproduction line *35S::YUC1* exhibited longer hypocotyls
228 as a high auxin phenotype (Fig. S5B), but in these lines TIBA and NPA did not suppress the
229 elongation (Fig. S5B). The data suggest that PISA could positively modulate polar auxin transport in
230 hypocotyls. To examine further the effects of PISA on basipetal auxin transport, rootward movement
231 of ^{3}H-IAA was analyzed (Fig. 3E). In this assay, NPA reduced the basipetal movement of ^{3}H-IAA in
232 hypocotyls, whereas PISA enhanced it (Fig. 3E). These results collectively show that PISA positively
233 modulates basipetal auxin transport in hypocotyls. Another possible target of PISA could be the
234 regulation of endogenous auxin concentrations, such as via auxin biosynthesis or catabolism.
235 Analysis of endogenous IAA levels in Arabidopsis seedlings showed that they were not affected by
236 PISA treatment (Fig. S6). Together, these results indicate that PISA likely acts by affecting polar

auxin transport.

PISA inhibits root growth by accumulating IAA at the root tip.

PISA inhibited primary root growth in a manner that is similar to conventional auxins. The seedlings were cultured on vertical plates containing PISA for 7 d (Fig. 4A-4C). The auxin signaling mutants, *axr1-3* and *tir1 afb2*, were insensitive to PISA. Additionally, auxin influx transport mutant *aux1-7* was also less sensitive to PISA regarding root growth (Fig. 4C). Taken together with the effects of PISA on auxin transport in the hypocotyl, these results suggest that PISA inhibits primary root growth by modulating auxin transport to affect auxin distribution and maxima. Further, the roots treated with PISA at 100 μM showed severe defects in root cell morphology (Fig. 4B). To examine the effects of PISA on auxin distribution in roots, *DR5::GFP* seedlings were cultured with PISA for 7 d (Fig. 4D). PISA significantly induced GFP expression in the lateral root cap cell, indicating PISA accumulates IAA in the lateral root cap and root growth is inhibited as a consequence. In contrast to auxin signaling mutants, the sensitivity of *pin2* and *pin3 pin7* mutants was comparable to that of the wild type (Fig. 4C). To investigate the short-term effects of PISA, seedlings were treated with PISA for 5 h (Fig. 4E). PISA inhibited root elongation within this 5 h incubation. The *tir1 afb2* mutant was insensitive to PISA, but the *pin2* mutant was more sensitive than the wild type to PISA. Perhaps, in the *pin 2* mutant, the accumulated IAA is not efficiently transported from the lateral root cap. Consistent with root elongation responses (Fig. 4E), PISA induced *DR5::GFP* expression in the lateral root cap after 20 h treatment suggesting enhanced accumulation of endogenous IAA (Fig. 4F). The auxin transport inhibitor TIBA blocks IAA efflux and inhibits root elongation by accumulating IAA (Fig. S5). TIBA highly induced *DR5::GFP* expression near the quiescent center where IAA is biosynthesized (Fig. 4F) (Brumos et al., 2018). Taken together, these results indicate that PISA promotes the auxin transport rate leading to accumulations of IAA at the lateral root cap, resulting in the inhibition of root elongation.

PISA blocked root hair formation by positively modulating auxin transport.

PISA displayed auxin-like activity in its effects on hypocotyl elongation, primary root inhibition and adventitious root formation (Fig. 2). Typical auxin efflux transport inhibitors commonly inhibit the elongation of both primary root and hypocotyl, supporting that PISA is not an inhibitor of auxin efflux transport. The effects of PISA on auxin-related phenotypes can be explained if it works by increasing auxin efflux. To further examine the effects of PISA on auxin efflux transport, the root hair phenotype was analyzed. This process involves the PIN2 proteins, which are localized at the apical side of root epidermal cells and mainly contribute to basipetal (shootward) auxin transport (Abas et al., 2006). The loss of function *pin2*/*eir1* mutant displays impaired root hair formation (Fig. 5A and 5B). The ectopic overexpression of PIN1 in *35S::PIN1* roots also interferes with this shootward auxin transport, and, consequently, *35S::PIN1* seedlings also show defects in root hair formation (Fig. 5A and 5B) (Ganguly et al., 2010), suggesting shootward auxin flow is important for root hair formation (Rigas et al., 2013). In contrast, auxin efflux transport inhibitors TIBA and NPA promote root hair formation (Ganguly et al., 2010), probably by increasing the accumulation of endogenous IAA (Fig. 5C). Importantly, PISA inhibits root hair formation, implying PISA has an opposite effects to auxin efflux inhibitors.

PISA affects adventitious and lateral root formation by positively modulating auxin transport.

PISA induces adventitious root formation at the shoot/root junction as shown in Fig. 2A. Importantly, auxin signaling mutants *slr*/*iaa14* and *arf7 arf19* show severe defects in lateral root formation (Fig. 3D and Table 1) (Okushima et al., 2007). In these mutants, PISA did not promote adventitious root formation at the shoot/root junction and this is consistent with the auxin-like effects of PISA on hypocotyls (Fig. 3D and Table 1). This suggests that adventitious root formation in response to PISA treatment depends on auxin signaling downstream of $SCF^{TIR1/AFB}$. In such a situation, auxin efflux transport inhibitors BUM, NPA and TIBA would reduce polar auxin transport in hypocotyls, resulting in the inhibition of the adventitious root formation and this is indeed what we observed, as shown in

289 Table 1 and Fig. S5A. Taken together, these results suggest that PISA positively modulates the polar
290 auxin transport system, thereby leading to the accumulation of auxin at the shoot/root junction and
291 promoting adventitious root formation.

292 In contrast to the promotion of adventitious roots at the shoot/root junction (Table 1 and Fig. 2A),
293 PISA alone repressed lateral root formation in primary roots (Fig. 6A). In contrast, PISA strongly
294 promoted lateral root numbers when co-incubated with exogenous IAA (Fig. 6B, 6C and S7A). TIBA
295 and NPA did not affect the lateral root number induced by exogenous IAA (Fig. S8A), suggesting that
296 inhibition of auxin efflux does not enhance IAA-induced lateral root formation. This was further
297 investigated using the cell cycle reporter *CYCB1;1::GUS,* which is induced strongly by IAA and NAA
298 in initiating lateral roots. In this assay, PISA enhanced *CYCB1;1::GUS* expression when in the
299 presence of auxins, IAA and NAA (Fig. S7B). Similarly, auxin-induced *DR5::GUS* expression was
300 dramatically enhanced by pretreatments with PISA (12 h) (Fig. 6D). In this experiment, IAA treatment
301 for 6 h at 100 and 500 nM induced *DR5::GUS* expression in elongation zones only (Fig. 6D). This
302 expression pattern was extended along the entire root by the co-incubation of IAA and PISA (Fig.
303 S8B). In contrast, co-treatment with IAA and auxin transport inhibitors (NPA, TIBA, Bz-IAA
304 (5-benzykoxy IAA) and BUM) (Fukui and Hayashi, 2018) activated *DR5::GUS* expression only at the
305 root tips (Fig. 6D). To examine the effects of PISA on basipetal auxin transport, shootward movement
306 of IAA from the root tip was evaluated by *DR5::GUS* assay (Fig. 6E) (Buer and Muday, 2004; Lewis
307 and Muday, 2009). In this shootward auxin transport assay, the *DR5::GUS* seedlings were placed on
308 vertical plates containing PISA and then an agar block containing IAA was placed onto the root tips.
309 The seedlings were then incubated for 10 h. PISA promoted *DR5::GUS* induction derived from root
310 tip IAA (Fig. 6E), suggesting that PISA enhances shootward auxin transport from the root tip. Taken
311 together, these results indicate that PISA increases the net flow of auxin in the roots by positively
312 modulating auxin transport.

313 Other possible targets for PISA are the AUX1/LAX auxin influx transporters. PISA might promote
314 IAA-induced lateral root formation by increasing the uptake of exogenous IAA. To test the effects of

315 PISA on IAA influx transport, seedlings were co-treated with PISA and membrane permeable IAA
316 prodrugs, IAA methyl ester and IAA octyl ester (Fig. S9). These lipophilic IAA esters and NAA (Fig.
317 S7B) can be incorporated into cells by passive diffusion, but not by the AUX1/LAX transporters. PISA
318 enhanced lateral root formation to the same extent with the two IAA esters, NAA and IAA (Fig. S7B
319 and S9), indicating that IAA influx transport is not required for the activity of PISA on lateral root
320 promotion.
321
322 **PISA perturbed asymmetric auxin distribution and gravitropism in root.**
323 Gravistimulation rapidly induces asymmetric auxin distributions in roots and thereby changes the
324 *DR5* reporter expression pattern (Fig.7A). This gravistimulated asymmetric auxin distribution is
325 driven by PIN-mediated shootward auxin movement in the root epidermis (Wisniewska et al., 2006;
326 Baster et al., 2013). After 4 h gravistimulation, the *DR5::GFP* signal increased at the lower side of
327 gravistimulated roots. PISA treatment completely diminished this asymmetric expression of
328 *DR5::GFP* (Fig.7A and 7B) and concomitantly blocked root gravitropic responses (Fig. 7C). These
329 observations show that PISA not only modulates polar auxin transport but specifically affects
330 PIN-mediated asymmetric auxin distribution in gravistimulated roots.
331
332 **PISA blocked the internalization of PIN proteins and promoted their accumulation at the**
333 **plasma membrane.**
334 All the phenotypic effects of PISA can be explained by the positive modulation of auxin transport by
335 PISA. PISA treatment did not affect the expression profiles of *proPIN1::GFP*, *proPIN2::GUS* and
336 *proPIN7::GUS* (Fig. S10), indicating that the primary target of PISA in auxin transport is not the
337 regulation of PIN transcription. To address the mechanism of positive effects of PISA on auxin efflux,
338 we examined the effects of PISA on the recycling of PIN proteins in roots. Brefeldin A (BFA) induces
339 the formation of BFA bodies which incorporate PIN2-GFP protein in *proPIN2::PIN2-GFP* line
340 (Geldner et al., 2003). Auxin (NAA) was shown to inhibit BFA body formation by blocking the

341 endocytosis of PIN2 protein (Fig. 8A) (Paciorek et al., 2005). The negative control compound
342 benzoic acid did not affect BFA body formation (Fig. 8A), but PISA inhibited BFA body formation to
343 the same extent as NAA (Fig. 8A and 8B). Additionally, BFA body formation with both PIN1-GFP
344 fusion and PIN1 native protein was also blocked by NAA and PISA (Fig. S11). These observations
345 suggest that PISA interferes with PIN recycling or vacuolar targeting, and as a consequence
346 promotes the accumulation of PIN proteins at the PM. Since constitutive PIN recycling has been
347 linked to maintenance of its asymmetric, polar distribution, we tested PISA effect on PIN polarity.
348 Indeed, PISA treatment diminished PIN2 polarity at the PM. PIN2 showed pronounced accumulation
349 at the lateral cell sides (Fig. 8C, 8D and S12) and PIN1 showed almost no polarity after treatment
350 with PISA (Fig. S13). Furthermore, PISA at 100 μM disrupted the root architectures and PIN2 polar
351 localization (Fig. S14).

352 This change in the localization of PIN proteins was further investigated using PINOID (PID), a
353 serine threonine kinase of the AGC kinase family which is known to regulate PIN localization on the
354 cellular membranes (Adamowski and Friml, 2015). Overexpression of PID triggers a basal to apical
355 shift in PIN1 localization, thereby perturbing the auxin gradient in the root tip; depleting auxin from
356 the root tip maxima and leading to meristem collapse (Benjamins et al., 2001; Friml et al., 2004).
357 Consistently, PIN1 was localized at apical side in the endodermis of *35S::PID* roots (Fig. 8F).
358 Intriguingly, PISA rescued collapsed root meristems in *35S::PID* roots (Fig. 8E) and the typical apical
359 polarity of PIN1 in *35S::PID* was lost and switched to an apolar pattern in endodermal cells (Fig. 8F).
360 Thus, PISA appears to repress IAA depletion from the *35S::PID* apical meristem by diminishing
361 shootward IAA transport. This is fully consistent with the PISA effect on the polar localization of PIN
362 proteins.

363 To gain further insight into the mechanism by which PISA induces PIN accumulation at the PM,
364 the effects of PISA on PIN2-GFP accumulation were examined in a *tir1 afb1 afb2 afb3* quadruple
365 mutant line (Fig. S15). As in wild-type roots, PIN2-GFP protein was found to be predominantly
366 located at the apical cell sides and not at lateral cell sides despite the severe growth defects in these

roots. PISA promoted the accumulation of PIN2-GFP at lateral cell sides in the quadruple mutant, the same as in the wild-type root. This observation strongly suggests that PISA leads to increases in PIN protein accumulation at the PM without activating the $SCF^{TIR1/AFB}$ pathway.

DISCUSSION

Pinstatic acid is an inert molecule for the TIR1/AFB-Aux/IAA co-receptor complex

In the screening for the auxin transport modulators from the PAA analogs, pinstatic acid (4-ethoxyphenylacetic acid: PISA) was found to be the most promising candidate. PISA does not bind to the $SCF^{TIR1/AFB}$ complex. The classical structure activity relationships of mono-substituted phenylacetic acids demonstrated that 4-substituted PAA is less or inactive as an auxin (Muir et al., 1967). Consistent with these early structure activity relationship studies of PAA derivatives, our results clearly demonstrated that PISA is not a classical auxin directly modulating the $SCF^{TIR1/AFB}$ machinery (Fig. 1). Consistent with this, a docking study using the auxin binding cavity of TIR1 showed that the 4-ethoxy chain in PISA would prevent stable binding of this compound (Fig. S16).

In analogy to PISA, the introduction of alkyloxy chains into IAA and NAA at the 5- or 6-positions diminished their TIR1 binding activity (Tsuda et al., 2011). However, it appears that these alkoxy-IAA and -NAAs are still recognized by PIN efflux proteins to inhibit polar IAA transport in competition with endogenous IAA (Tsuda et al., 2011), suggesting alkoxy-IAAs and alkoxy-NAAs could act as auxin transport inhibitors. On the other hand, PAA is not actively and directionally transported in response to gravitropic stimuli and the distribution of PAA is not inhibited by NPA, suggesting that PAA is distributed by passive diffusion (Sugawara et al., 2015). As for PAA, it seems unlikely that PISA itself would be recognized by PINs in planta.

PISA positively modulates polar auxin transport to induce auxin-like activity.

PISA showed characteristic auxin-like activity on primary root and shoot responses. PISA inhibited primary root elongation and induced adventitious root formation at the shoot / root junction (Fig. 2).

393 The auxin signaling mutants *axr1-3*, *tir1 afb2*, *slr1-1* and *arf7 arf19* were resistant to PISA in primary
394 root inhibition and adventitious root formation, suggesting that some PISA-induced responses might
395 be mediated by the $SCF^{TIR1/AFB}$ signaling pathway (Fig. 4D). However, these responses can also be
396 well explained by the accumulation of endogenous IAA at root tip and the shoot / root junction
397 following elevated IAA efflux. Auxin efflux inhibitors completely repressed adventitious root formation
398 induced by PISA (Table 1), suggesting that IAA movement is required for PISA activity on
399 adventitious root formation. In the primary root, IAA is biosynthesized near the quiescent center (QC)
400 where TAA1 is strongly expressed (Brumos et al., 2018). Auxin efflux inhibitors, TIBA and NPA are
401 considered to have repressed IAA efflux leading to induction of *DR5::GFP* expression near the QC
402 (Fig. 4D) and then results in the inhibition of root elongation (Brumos et al., 2018). In contrast, PISA
403 would promote auxin efflux from the QC to lateral root cap, thereby *DR5::GFP* signal was induced at
404 that place (Fig. 4D). Thus, PISA inhibits root elongation by distinct mechanism of auxin efflux
405 inhibitors.

406 Furthermore, PISA promoted hypocotyl elongation. Auxin efflux transport inhibitors, TIBA,
407 NPA and BUM completely suppressed hypocotyl elongation (Fig. 3B, 3C and S5A). Hypocotyl
408 elongation by synthetic auxin picloram or YUC1 overexpression could not be cancelled by auxin
409 efflux transport inhibitors (Fig. S5B). These evidences suggest that PISA positively modulated auxin
410 transport to show auxin-like activity in the hypocotyl. This was further confirmed by ^{3}H-IAA transport
411 assays in hypocotyl segments (Fig. 3E). Importantly, no auxin analog has been reported to be
412 positive modulator of auxin transport.

413

414 **PISA affects root auxin responses by positively modulating shootward auxin transport.**

415 In contrast to auxin-like effects on primary root growth and shoot elongation, PISA-treated roots
416 showed typical auxin-repressed phenotypes: reduced root hair formation, fewer lateral roots and
417 reduced gravitropic response. Auxin transport inhibitors promoted root hair formation (Fig. 5B) by
418 accumulating endogenous IAA, but blocked lateral root formation and gravitropic responses by

perturbing auxin distribution. The impaired root phenotypes by PISA resemble the root defects in PIN1 overexpressing roots (Rigas et al., 2013), supporting the hypothesis that PISA represses auxin-regulated phenotypes by enhancing auxin efflux. Intriguingly, PISA dramatically enhanced IAA-induced lateral root formation and PISA also promoted IAA-induced *DR5::GUS* expression in entire roots when auxin transport inhibitors did not (Fig. 6B – 6D). Additionally, PISA enhanced shootward auxin movement from the root tip in basipetal auxin transport assays (Fig. 6E). PISA did not increase the endogenous IAA (Fig. S6). Thus, it is unlikely that PISA would elevate endogenous IAA in the shoot by up-regulating *TAA1* and *YUC* expression in the IAA biosynthesis pathway or by inhibiting the IAA inactivation pathway involving GH3 and DAO1 (Korasick et al., 2013). These observations suggest that PISA positively modulates shootward IAA transport in the root.

PISA blocks PIN internalization to accumulate PIN at the plasma membrane in Arabidopsis.

The localization and trafficking of PIN1 and PIN2 proteins have been extensively investigated (Adamowski and Friml, 2015; Rakusova et al., 2015). ROP GTPases-RIC signaling have been shown to inhibit the PIN internalization (Lin et al., 2012; Nagawa et al., 2012), PINOID kinase and D6 Protein Kinase could directly phosphorylate PIN at the PM to regulate the PIN trafficking in a GNOM dependent manner (Adamowski and Friml, 2015). However, the molecular mechanism for the regulation of PIN trafficking, especially PIN internalization, by auxin has been unclear. Our results show that PISA inhibited the formation of BFA bodies containing PIN1 and PIN2 proteins (Fig. 8, and S11). Furthermore, PISA promoted the accumulation of PIN1 and PIN2 proteins at the lateral side of cells. These observations, together with phenotypic data, clearly indicate that by inhibiting PIN internalization PISA would increase PM-localized PIN content, leading to characteristic phenotypes caused by enhanced auxin efflux.

The target of PISA remains an open and intriguing question. PISA is completely inert for transcriptional auxin signaling modulated by SCF $^{TIR1/AFB}$ –Aux/IAA machinery. PISA enhanced PIN2 accumulation at the PM in *tir1 afb1 afb2 afb3* quadruple mutant (Fig. S15) (Pan et al., 2009), implying

TIR1/AFB receptors are not a prerequisite for the inhibition of PIN2 internalization by PISA. Modulation of PIN localization and trafficking are influenced by many regulatory steps (Adamowski and Friml, 2015) and it is likely that auxin could coordinately modulate pathways involving recycling rate, biosynthesis and degradation of PINs in response to environmental and hormonal stimuli.

Many questions still remain as to the mode of action of PISA. It has been reported that auxin reduced formation of BFA bodies by inhibiting delivery of newly synthesized protein rather than by inhibition of PIN internalization (Jasik et al., 2016). On the other hand, PISA inhibited BFA body formation of PIN2-GFP, but enhanced amounts of PIN2-GFP on the PM suggesting that delivery is not impaired and internalization is reduced. Given this, we have no reason to believe that PISA would target the regulatory component of PIN internalization to which endogenous auxin would bind. We anticipate that PISA will become a very useful chemical tool to dissect the regulatory mechanism of auxin transport.

MATERIALS AND METHODS

Plant materials and growth conditions

Arabidopsis (*Arabidopsis thaliana*) ecotype Columbia (Col-0) was used for all experiments. The following transgenic and mutant lines were in the Col-0 ecotype: *axr1-3* [CS3075], *tir1-1 afb2-3* [CS69691], *iaa14*/*slr1-1* (Okushima et al., 2007; Spartz et al., 2012; Chae et al., 2012), *arf7 arf19* (Okushima et al., 2007), *DII-VENUS* (Brunoud et al., 2012), *yuc3 5 7 8 9* (Chen et al., 2014), *proPIN1::PIN1-GFP* (Vieten et al., 2005), *proPIN2::PIN2-GFP* (Vieten et al., 2005), *pin2*/*eir1-1* [CS16706], *35S::PIN1* [CS9375], *35S::PID* (Benjamins et al., 2001), *pPIN2::PIN2-GFP* / *tir1 afb1 afb2 afb3* (Pan et al., 2009). Seeds were surface-sterilized and grown on germination medium (GM; 0.5× Murashige and Skoog salts [Gibco-BRL], 12 g/L sucrose, 1× B5 vitamins, and 0.2 g/L MES containing and 4 g/L agar for horizontal agar plate or 14 g/L agar for vertical agar plates, pH 5.8) containing the indicated hormone and/or chemicals. The length of hypocotyl and lateral root number was measured using ImageJ software.

Chemicals

4-ethoxyphenylacetic acid [CAS Registry Number: 4919-33-9], PISA and 3-ethoxy-phenylacetic acid, mPISA was synthesized from 4-hydroxyphenylacetic acid methyl ester and 3-hydroxyphenylacetic acid methyl ester, respectively. PISA is commercially available from some chemical suppliers (Alfa Aesar, Santa Cruz Biotechnology and, Acros Organics).

Histochemical and Quantitative GUS Measurements

For GUS histochemical analysis, the seedlings were washed with a GUS-staining buffer (100 mM sodium phosphate, pH 7.0, 10 mM EDTA, 0.5 mM $K_4Fe(CN)_6$, 0.5 mM $K_3Fe(CN)_6$, and 0.1% (W/V) Triton X-100) and transferred to the GUS-staining buffer containing 1 mM 5-bromo-4-chloro-3-indolyl-β-d-glucuronide (X-Gluc), the substrate for histochemical staining, and incubated at 37°C until sufficient staining developed. For quantitative measurement, seedlings or the excised roots (n = 15–20) were homogenized in an extraction buffer as described previously (Hayashi et al., 2012). After centrifugation to remove cell debris, GUS activity was measured with 1 mM 4-methyl umbelliferyl-β-d-glucuronide as a fluorogenic substrate at 37°C. The protein concentration was determined by Bradford protein assay (Bio-Rad). The experiments were repeated at least three times with four replications.

DII-VENUS assay

6-d-old DII-VENUS seedlings (Brunoud et al., 2012) were incubated in GM liquid medium containing 10 μM yucasin DF for 3 h at 24°C. The DII-VENUS seedlings were washed out well with fresh medium and incubated in fresh GM liquid medium for 5 min. Exogenous IAA and PISA was added to this medium and fluorescent images of roots were recorded after 60 min.

Surface plasmon resonance assay

Surface plasmon resonance assays were performed as described previously (Quareshy et al., 2017). 50 μM IAA or PISA were used to assay for the formation of the auxin-induced TIR1 - IAA7 co-receptor complex, or AFB5 - IAA7 complex. For the anti-auxin assay, 5 μM IAA and 50 μM PISA (or control compound) were mixed and the sensorgram assessed for a reduced signal to the IAA.

Exogenous IAA-induced lateral root promotion

For lateral root growth, Arabidopsis seedlings were grown vertically for 5 d in continuous light on GM agar plate. The seedlings were transferred to liquid GM medium containing the indicated concentration of IAA and PISA. The seedlings were cultivated under continuous light for another 3 d at 24°C and then the lateral root numbers were recorded. Three independent experiments were performed.

Gravitropic response assay

6-d-old seedlings were grown vertically on GM agar plates under continuous light at 24°C. The seedlings were then transferred to agar plates containing chemicals and cultured vertically for 2 h. The plates were rotated 90° in the vertical plane, followed by incubation for 16 h in the dark. Photographs of the roots were recorded with a digital camera.

Auxin transport assay

For shoot basipetal transport, 6-d-old Col-0 etiolated seedlings grown on GM agar plates were decapitated to avoid endogenous auxin biosynthesis in cotyledons and a droplet of GM agar (12 g/L agar) with ^{3}H-IAA was applied to apical part of the hypocotyls. The seedlings were preincubated with 20 μM PISA for 1 h on agar plate containing PISA. After 6 h, all roots were removed, hypocotyls were collected, homogenized using grinder and liquid nitrogen and incubated overnight in Opti-Fluor scintillation solution (Perkin Elmer). The amount of ^{3}H-IAA was measured in a scintillation counter (Hidex 300SL) for 300 s with three technical repetitions. The decapitated seedlings were placed on

GM agar plate containing 5 μM NPA to inhibit auxin transport, and then ^{3}H-IAA agar droplet was applied to apical part. The negative control (diffusion) was estimated with seedlings transferred to GM agar containing 5 μM NPA during the ^{3}H-IAA droplets incubation (6 h) to inhibit auxin transport.

The root basipetal transport assay was carried out with slight modifications according to the method of D.R. Lewis (Lewis and Muday, 2009). A narrow strip of aluminum foil was vertically embedded in GM agar plate (20 g/L agar) containing 40 μM PISA. 5-d-old *DR5::GUS* seedlings were placed on the GM agar so that the root tip stepped over the edge of the foil strip. An agar block (10 μM IAA and 40 μM PISA) was placed on the root tip. The aluminum strip blocks the diffusion of IAA into the GM agar plate. The plate was incubated vertically for 10 h and GUS activity was visualized histochemically with X-Gluc.

Asymmetric auxin distribution measurement and PIN immunolocalization analysis

All measurements were performed using ImageJ software (National Institutes of Health; http://rsb.info.nih.gov/ij). Quantification of auxin asymmetry was performed on maximal intensity projection of Z-scans of root tip by measuring ratio of signal intensity of upper/lower half of the root. *DR5rev-GFP* reporter line was imaged before and after gravistimulation. PIN immunolocalizations of primary roots were carried out as described (Sauer et al., 2006; Robert et al., 2010). The antibodies used in this study were as follows: anti-PIN1, 1:1000 and anti-PIN2, 1:1000.

Imaging and Image Analysis

Fluorescence images were recorded with a fluorescence microscope (Olympus; BX-50) and a laser scanning confocal microscope (Olympus; FV-3000). Typically, the seedlings were incubated with half-strength MS medium containing chemicals for the indicated time at 24°C and fluorescence images were then immediately recorded. For quantification of the fluorescent signal in epidermal cell in *proPIN2::PIN2-GFP* and *proPIN1::PIN1-GFP*. The same image acquisition parameters were used for all signal measurements. the regions of the visible BFA bodies in the same number and area of

549 root cell were selected and the BFA body signal area (the area of BFA body / the constant root cell
550 area containing same cell number) were calculated by image J software. To measure signal intensity
551 of PM-localized PIN2-GFP, the mean pixel intensities were obtained from the apical and lateral sides
552 of the individual cells by Image J software. The PM-accumulation of PIN2-GFP was shown as the
553 ratio of intensity (the apical side / the lateral side), 50–60 cells were analyzed for 5–7 seedlings in
554 three independent treatments.
555
556 **Statistical Analysis**
557 Statistically significant differences in the results (**$P < 0.05$ or *$P < 0.01$) are based on Welch's
558 two sample *t*-test by SigmaPlot 14.0. The values of mock-treated and PISA-treated samples (Fig. 2,
559 3, 5, 6, 7, and 8) and the values of wild-type and mutant samples treated with PISA at the same
560 concentration (Fig. 4) were statistically tested. Data are means ± SD of independent replicates.
561 Box-and-whisker plots show a median (centerline), upper/lower quartiles (box limits) and
562 maximum/minimum (whiskers).
563
564 **Accession Numbers**
565 Sequence data from this article can be found in the GenBank/EMBL data libraries under accession
566 numbers: *TIR1* (At3g62980), *AFB2* (At3g26810), *AXR1* (At1g05180), *PIN1* (At1g73590), *PIN2*
567 (At5g57090), *PIN3* (At1g70940), *IAA14* (At4g14550), *AUX1* (At2g38120), and *PID* (At2g34650).
568
569 **Supplemental Data**
570 The following supplemental materials are available.
571 Supplemental Figure S1. Auxin activity in an auxin-deficient Arabidopsis mutant and BY2 tobacco
572 cell culture.
573 Supplemental Figure S2. Effects of PISA on rapid cell expansion in hypocotyl.

Supplemental Figure S3. Effects of PISA on SCF^{TIR1} signaling.

Supplemental Figure S4. Effects of mPISA and PISA on the phenotype related to $SCF^{TIR1/AFB}$ pathway.

Supplemental Figure S5. Auxin transport inhibitors blocked PISA-induced high-auxin phenotype, but did not inhibit the high-auxin phenotypes by picloram and YUC1 overexpression.

Supplemental Figure S6. Effects of PISA on endogenous IAA level.

Supplemental Figure S7. Phenotype of Arabidopsis seedlings co-cultured with PISA and auxins.

Supplemental Figure S8. Effects of PISA and auxin transport inhibitors on auxin response in root.

Supplemental Figure S9. PISA promoted the lateral root formation induced by membrane permeable IAA precursors.

Supplemental Figure S10. PISA did not affect the expression of *PIN1::GUS*, *PIN2::GUS* and *PIN7::GUS* reporter expression.

Supplemental Figure S11. Effect of PISA on the BFA body formation of PIN1.

Supplemental Figure S12. Effect of PISA on the internalization of PIN2-GFP.

Supplemental Figure S13. Effect of PISA on the internalization of PIN1.

Supplemental Figure S14. Effect of PISA on the internalization of PIN2 at high concentration.

Supplemental Figure S15. Effects of PISA on PIN2 membrane localization in *tir1 afb 1 afb 2 afb3* mutant.

Supplemental Figure S16. Molecular docking study of PAA, mPISA and PISA with TIR1.

ACKNOWLEDGEMENTS

We thank Dr. H. Fukaki (University of Kobe), Dr. R. Offringa (Leiden University), Dr. Jianwei Pan (Zhejiang Normal University) and Dr. M. Estelle (University of California at San Diego) for providing mutants and transgenic line seeds. The research leading to these results has received funding from JSPS KAKENHI (Grant Number JP25114518) to K.H. and European Union's Horizon2020 program (ERC grant agreement n° 742985) to J.F.

600

Table 1. Effect of PISA on adventitious root formation at shoot/root junction

	WT (Col)	*arf7 arf19*	*slr1*/*iaa14*	TIBA (5 μM)	NPA (5 μM)
mock	1.57±0.65 [a)]	0	0	0	0
PISA (20 μM)	3.21±0.70	0	0	0	0
PISA (50 μM)	5.07±1.03	0	0	0	0

a) adventitious root number at shoot/root junction for each 6-d old seedlings

601

602

603

604

FIGURE LEGENDS

Figure 1. Evaluation of PISA for an auxin-like effect in the $SCF^{TIR1/AFB}$ pathway.

A, The structures of auxins and pinstatic acid (PISA). B, Effects of PISA on auxin-deficient root phenotypes. Arabidopsis plants were cultured for 5 d on vertical agar plate containing chemicals with or without auxin biosynthesis inhibitors, yucasin DF and Kyn. The values in parentheses represent the concentration of chemicals (μM). Bar represents 5 mm. C, Effects of alkyloxy-PAA on auxin-responsive *DR5::GUS* expression. 5-d-old *DR5::GUS* seedlings were incubated with chemicals for 6 h. Methoxy (C1) to pentoxy (C5) PAA derivatives including mPISA and PISA were assessed at 50 μM. D, Quantitative analysis of GUS enzyme activity in the *DR5::GUS* line treated with IAA and PISA. Values are the means ± S.D. (n=9). E, *DII-VENUS* seedlings were incubated with 10 μM yucasin DF for 3 h and then washed with medium. The seedling was incubated with PISA and IAA for another 60 min. Bar represents 500 μm. F, Surface Plasmon Resonance analysis of the auxin-induced interaction between TIR1 and IAA7 degron peptide. The sensorgram shows the effect of 50 μM IAA (green) and 50 μM PISA (blue) on TIR1-DII peptide association and dissociation. The bars show the relative response of PISA to IAA (100%).

Figure 2. Effects of PISA on hypocotyl elongation and adventitious root formation.

A, Arabidopsis seedlings cultured for 7 d with PISA. The values in parentheses represent the concentration of chemicals (μM). Bar represents 5 mm. B, 13-d-old plants grown with PISA. C, Time course of hypocotyl length of seedlings cultured with PISA (closed square: 10 μM and closed triangle: 20 μM). Values are the means ± S.D. (n=15–20). D, Hypocotyl lengths of seedlings cultured for 7 d with PISA and auxins. The hypocotyl length (mm) of the mock-treated seedlings is indicated. Box-and-whisker plots show a median (centerline), upper/lower quartiles (box limits) and maximum/minimum (whiskers). (n=30–38). Statistical significance assessed by Welch's two sample *t*-test. Asterisks indicate significant differences (**p<0.05, *p<0.01). E, Etiolated seedlings cultured for 5 d in dark with PISA and auxins. F, Hypocotyl lengths of etiolated seedling cultured for 3 d in dark with PISA and auxins. Statistical significance assessed by Welch's two sample *t*-test. Asterisks indicate significant differences (n=50–72, **p<0.05, *p<0.01). G, Adventitious root production induced by PISA. Arabidopsis seedlings were cultured for 7 d with PISA and the adventitious root number at shoot and root junction was counted. Asterisks indicate significant differences (n=30, **p<0.05, *p<0.01).

Figure 3. Auxin signaling and transport inhibitors repress PISA-induced hypocotyl phenotypes and PISA promotes basipetal auxin transport in the hypocotyl.

A, The hypocotyl length of Arabidopsis wild-type (WT) and *axr1-3* mutant seedlings cultured for 7 d with chemicals. Relative hypocotyl length is shown as the percentage of that in mock-treated plants (100%). The actual length (mm) of mock-treated hypocotyls are indicated (n=40–48). B, Seedlings

cultured for 7 d with PISA and auxin transport inhibitor, TIBA. C, Hypocotyl length in seedlings cultured with or without TIBA and PISA. Relative hypocotyl length is shown as the percentage of that in mock-treated plants (100%). The actual length (mm) of mock-treated hypocotyls are indicated as box-and-whisker plots (n=40–45). Statistical significance assessed by Welch's two sample *t*-test. Asterisks indicate significant differences (**p<0.05, *p<0.01). D, Seedlings of WT, *arf7 arf19* and *slr1*/*iaa14* mutants cultured for 7 d with or without PISA. The values in parentheses represents the concentration of chemicals (μM). Bar represents 5 mm. E, Rootward transport of radiolabeled ^{3}H-IAA in decapitated hypocotyls. NPA, an auxin transport inhibitor, was used as the negative control. (*p<0.01, n=9).

Figure 4. The effects of PISA on root elongation and auxin distribution in the root tip.
A, Wild-type seedlings cultured for 7 d with PISA. Bar represents 5 mm. B, Wild-type root cultured with 100 μM PISA . Root was counterstained with propidium iodide. Bar represents 100 μm. C, The primary root length of Arabidopsis wild-type (WT) and auxin mutants (*axr1-3, tir1 afb2, pin3 pin7, pin2*/*eir1-1* and *aux1-7*) cultured for 7 d on vertical plate containing PISA. Relative root length is shown as the percentage of that in mock-treated plants (100%). The actual length (mm) of mock-treated roots is indicated. Statistical significance was assessed by Welch's two sample *t*-test between WT and mutants. Asterisks indicate significant differences (n=32-40, **p<0.05, *p<0.01). D, The GFP expression of *DR5::GFP* in roots cultured vertically with PISA for 7 d. Arrows indicate quiescent center (yellow) and lateral root cap (white). Bar represents 100 μm. E, The primary root growth of Arabidopsis WT and auxin mutants over 5 h on vertical plates containing PISA. The actual length (mm) of mock-treated roots is indicated, which were set to 100%. Asterisks indicate significant differences (n=14–17, *p<0.01). F, The GFP expression of *DR5::GFP* cultured vertically with PISA and TIBA for 20 h. The values in parentheses represents the concentration of chemicals (μM). Bar represents 100 μm.

Figure 5. PISA inhibits root hair formation.
A, Root hairs of *pin2*/*eir1, 35S::PIN1* and wild-type (WT) plants treated with PISA. 5-d-old seedlings were cultured for 2 d on vertical agar plates with or without PISA. The values in parentheses represent the concentration of chemicals (μM). B, The root hair length and density of *pin2*/*eir1, 35S::PIN1* and WT plants treated with PISA. The length and density of root hairs within the 2–4 mm region from root tip were measured. Values are the means ± S.D. Asterisks indicate significant differences (n=8–11, *p<0.01). C, The root hair formation of WT seedlings grown with auxins and auxin transport inhibitors. The values in parentheses represent the concentration of chemicals (μM). Bar represents 1 mm.

Figure 6. Effects of PISA on IAA-induced lateral root formation and shootward IAA transport.
A, Effects of PISA on the lateral root formation. Arabidopsis seedlings were cultured for 6 d with PISA.

The number of lateral roots were counted and the density of lateral roots are shown as box-and-whisker plots (n=14–16). B and C, Effects of PISA on IAA-induced lateral root formation. 5-d-old seedlings were cultured for additional 3 d with PISA in the presence of IAA. The density of lateral roots are shown as box-and-whisker plots (B, n=14–16) and representative images are shown (C). Bar represents 5 mm. D, Effects of PISA on IAA-induced *DR5::GUS* expression. 5-d-old *DR5::GUS* seedlings were incubated for 12 h in liquid GM medium with or without PISA or auxin transport inhibitors. IAA was added to the GM medium and the seedlings were further incubated for additional 6 h. The IAA-induced GUS activity was visualized by X-Gluc. Bar represents 1 mm. E, Effects of PISA on shootward IAA transport. An agar block containing IAA was applied to *DR5::GUS* root tips (yellow ring) and the seedlings were incubated on vertical plates containing 40 μM PISA for 10 h. Arrows show the IAA-induced GUS activity. Bar represents 1 mm. Statistical significance assessed by Welch's two sample *t*-test. Asterisks indicate significant differences (*p<0.01). The values in parentheses represent the concentration of chemicals (μM).

Figure 7. PISA inhibits auxin distribution and root gravitropism.

A, Effect of PISA on auxin asymmetric distribution. 4-d-old *DR5::GFP* seedlings were transferred to 20 μM PISA and control medium for 1 h. After 1 h seedlings were gravistimulated for 4 h and imaged. PISA pretreatment abolished auxin asymmetric distribution and seedlings did not respond to gravity stimuli. B, Quantitative evaluation of A, showing a mean ratio of the signal intensity of the upper/lower half of the root. (*p<0.01). C, Effect of PISA on root gravitropic response. Five-d-old wild-type seedlings were placed on vertical GM agar plates containing PISA and then cultured for 3 h in the dark. The plates were further incubated for 16 h after rotating plates at 135° angle against vertical direction. The arrows indicate the vector of gravity before (1) and after (2) the initiation of gravistimulation. The angles were grouped into 30° classes and plotted as circular histograms.

Figure 8. Effects of PISA on PIN internalization from the plasma membrane.

A and B, Effect of PISA on the BFA body formation of PIN2-GFP. 5-d-old *proPIN2::PIN2-GFP* seedlings were incubated for 30 min in liquid GM medium containing PISA and NAA and then BFA was added to the medium. Seedlings were then incubated for additional 60 min. BFA induced PIN2-GFP-marked BFA bodies. The area of BFA body was measured and the area in BFA-treated seedlings (n=25–40, *p<0.01) was adjusted to 100%. The value of the area is shown the means ± S.D. in B. Bar represents 50 μm. C and D, Effect of PISA on the internalization of PIN2-GFP. 5-d-old *proPIN2::PIN2-GFP* seedlings were incubated for 12 h with PISA. The fluorescence intensity of the apical and lateral sides of cells in the root (n=18–20, *p<0.01) were quantified and the fluorescent signal rate (apical side / lateral side) is shown as the means ± S.D. in D. The values in parentheses represent the concentration of chemicals (μM). Bar represents 50 μm. E, Effects of PISA on a collapse of the primary root meristem. 5-d-old root tips of WT and *35S::PID* plants grown vertically on agar plates containing PISA. Bar represents 500 μm. F, Effects of PISA on PIN1 localization in the

endodermis of WT and *35S::PID* roots. Immunolocalization of PIN1 after treatment with PISA for 4 h. Bar represents 10 µm.

LITERATURE CITED

Abas L, Benjamins R, Malenica N, Paciorek T, Wisniewska J, Moulinier-Anzola JC, Sieberer T, Friml J, Luschnig C (2006) Intracellular trafficking and proteolysis of the Arabidopsis auxin-efflux facilitator PIN2 are involved in root gravitropism. Nat Cell Biol **8:** 249-256

Adamowski M, Friml J (2015) PIN-dependent auxin transport: action, regulation, and evolution. Plant Cell **27:** 20-32

Adamowski M, Narasimhan M, Kania U, Glanc M, De Jaeger G, Friml J (2018) A Functional Study of AUXILIN-LIKE1 and 2, Two Putative Clathrin Uncoating Factors in Arabidopsis. Plant Cell **30:** 700-716

Baster P, Robert S, Kleine-Vehn J, Vanneste S, Kania U, Grunewald W, De Rybel B, Beeckman T, Friml J (2013) SCF(TIR1/AFB)-auxin signalling regulates PIN vacuolar trafficking and auxin fluxes during root gravitropism. EMBO J **32:** 260-274

Benjamins R, Quint A, Weijers D, Hooykaas P, Offringa R (2001) The PINOID protein kinase regulates organ development in Arabidopsis by enhancing polar auxin transport. Development **128:** 4057-4067

Brumos J, Robles LM, Yun J, Vu TC, Jackson S, Alonso JM, Stepanova AN (2018) Local Auxin Biosynthesis Is a Key Regulator of Plant Development. Dev Cell **47:** 306-318 e305

Brunoud G, Wells DM, Oliva M, Larrieu A, Mirabet V, Burrow AH, Beeckman T, Kepinski S, Traas J, Bennett MJ, Vernoux T (2012) A novel sensor to map auxin response and distribution at high spatio-temporal resolution. Nature **482:** 103-106

Buer CS, Muday GK (2004) The transparent testa4 mutation prevents flavonoid synthesis and alters auxin transport and the response of Arabidopsis roots to gravity and light. Plant Cell **16:** 1191-1205

Chae K, Isaacs CG, Reeves PH, Maloney GS, Muday GK, Nagpal P, Reed JW (2012) Arabidopsis SMALL AUXIN UP RNA63 promotes hypocotyl and stamen filament elongation. Plant J **71:** 684-697

Chen Q, Dai X, De-Paoli H, Cheng Y, Takebayashi Y, Kasahara H, Kamiya Y, Zhao Y (2014) Auxin overproduction in shoots cannot rescue auxin deficiencies in Arabidopsis roots. Plant Cell Physiol **55:** 1072-1079

Ding Z, Galvan-Ampudia CS, Demarsy E, Langowski L, Kleine-Vehn J, Fan Y, Morita MT, Tasaka M, Fankhauser C, Offringa R, Friml J (2011) Light-mediated polarization of the PIN3 auxin transporter for the phototropic response in Arabidopsis. Nat Cell Biol **13:** 447-452

Du Y, Tejos R, Beck M, Himschoot E, Li H, Robatzek S, Vanneste S, Friml J (2013) Salicylic acid interferes with clathrin-mediated endocytic protein trafficking. Proc Natl Acad Sci U S A **110:** 7946-7951

Fendrych M, Leung J, Friml J (2016) TIR1/AFB-Aux/IAA auxin perception mediates rapid cell wall acidification and growth of Arabidopsis hypocotyls. Elife **5**

Friml J, Yang X, Michniewicz M, Weijers D, Quint A, Tietz O, Benjamins R, Ouwerkerk PB, Ljung K,

Sandberg G, Hooykaas PJ, Palme K, Offringa R (2004) A PINOID-dependent binary switch in apical-basal PIN polar targeting directs auxin efflux. Science **306:** 862-865

Fukui K, Hayashi KI (2018) Manipulation and Sensing of auxin metabolism, transport and signaling. Plant Cell Physiol

Furutani M, Nakano Y, Tasaka M (2014) MAB4-induced auxin sink generates local auxin gradients in Arabidopsis organ formation. Proc Natl Acad Sci U S A **111:** 1198-1203

Ganguly A, Lee SH, Cho M, Lee OR, Yoo H, Cho HT (2010) Differential auxin-transporting activities of PIN-FORMED proteins in Arabidopsis root hair cells. Plant Physiol **153:** 1046-1061

Geldner N, Anders N, Wolters H, Keicher J, Kornberger W, Muller P, Delbarre A, Ueda T, Nakano A, Jurgens G (2003) The Arabidopsis GNOM ARF-GEF mediates endosomal recycling, auxin transport, and auxin-dependent plant growth. Cell **112:** 219-230

Geldner N, Friml J, Stierhof YD, Jurgens G, Palme K (2001) Auxin transport inhibitors block PIN1 cycling and vesicle trafficking. Nature **413:** 425-428

Hayashi K (2012) The interaction and integration of auxin signaling components. Plant Cell Physiol **53:** 965-975

Hayashi K, Neve J, Hirose M, Kuboki A, Shimada Y, Kepinski S, Nozaki H (2012) Rational design of an auxin antagonist of the SCF(TIR1) auxin receptor complex. ACS Chem Biol **7:** 590-598

He W, Brumos J, Li H, Ji Y, Ke M, Gong X, Zeng Q, Li W, Zhang X, An F, Wen X, Li P, Chu J, Sun X, Yan C, Yan N, Xie DY, Raikhel N, Yang Z, Stepanova AN, Alonso JM, Guo H (2011) A small-molecule screen identifies L-kynurenine as a competitive inhibitor of TAA1/TAR activity in ethylene-directed auxin biosynthesis and root growth in Arabidopsis. Plant Cell **23:** 3944-3960

Jasik J, Bokor B, Stuchlik S, Micieta K, Turna J, Schmelzer E (2016) Effects of Auxins on PIN-FORMED2 (PIN2) Dynamics Are Not Mediated by Inhibiting PIN2 Endocytosis. Plant Physiol **172:** 1019-1031

Kasahara H (2016) Current aspects of auxin biosynthesis in plants. Biosci Biotechnol Biochem **80:** 34-42

Kitakura S, Vanneste S, Robert S, Lofke C, Teichmann T, Tanaka H, Friml J (2011) Clathrin mediates endocytosis and polar distribution of PIN auxin transporters in Arabidopsis. Plant Cell **23:** 1920-1931

Korasick DA, Enders TA, Strader LC (2013) Auxin biosynthesis and storage forms. J Exp Bot **64:** 2541-2555

Lee S, Sundaram S, Armitage L, Evans JP, Hawkes T, Kepinski S, Ferro N, Napier RM (2014) Defining binding efficiency and specificity of auxins for SCF(TIR1/AFB)-Aux/IAA co-receptor complex formation. ACS Chem Biol **9:** 673-682

Lewis DR, Muday GK (2009) Measurement of auxin transport in Arabidopsis thaliana. Nat Protoc **4:** 437-451

Leyser O (2018) Auxin Signaling. Plant Physiol **176:** 465-479

Lin D, Nagawa S, Chen J, Cao L, Chen X, Xu T, Li H, Dhonukshe P, Yamamuro C, Friml J, Scheres B, Fu Y, Yang Z (2012) A ROP GTPase-dependent auxin signaling pathway regulates the subcellular distribution of PIN2 in Arabidopsis roots. Curr Biol **22:** 1319-1325

Marhavy P, Bielach A, Abas L, Abuzeineh A, Duclercq J, Tanaka H, Parezova M, Petrasek J, Friml J, Kleine-Vehn J, Benkova E (2011) Cytokinin modulates endocytic trafficking of PIN1 auxin efflux carrier to control plant organogenesis. Dev Cell **21:** 796-804

Muir RM, Fujita T, Hansch C (1967) Structure-activity relationship in the auxin activity of mono-substituted phenylacetic acids. Plant Physiol **42:** 1519-1526

Nagawa S, Xu T, Lin D, Dhonukshe P, Zhang X, Friml J, Scheres B, Fu Y, Yang Z (2012) ROP GTPase-dependent actin microfilaments promote PIN1 polarization by localized inhibition of clathrin-dependent endocytosis. PLoS Biol **10:** e1001299

Naramoto S, Kleine-Vehn J, Robert S, Fujimoto M, Dainobu T, Paciorek T, Ueda T, Nakano A, Van Montagu MC, Fukuda H, Friml J (2010) ADP-ribosylation factor machinery mediates endocytosis in plant cells. Proc Natl Acad Sci U S A **107:** 21890-21895

Nishimura K, Fukagawa T, Takisawa H, Kakimoto T, Kanemaki M (2009) An auxin-based degron system for the rapid depletion of proteins in nonplant cells. Nat Methods **6:** 917-922

Okushima Y, Fukaki H, Onoda M, Theologis A, Tasaka M (2007) ARF7 and ARF19 regulate lateral root formation via direct activation of LBD/ASL genes in Arabidopsis. Plant Cell **19:** 118-130

Paciorek T, Zazimalova E, Ruthardt N, Petrasek J, Stierhof YD, Kleine-Vehn J, Morris DA, Emans N, Jurgens G, Geldner N, Friml J (2005) Auxin inhibits endocytosis and promotes its own efflux from cells. Nature **435:** 1251-1256

Pan J, Fujioka S, Peng J, Chen J, Li G, Chen R (2009) The E3 ubiquitin ligase SCFTIR1/AFB and membrane sterols play key roles in auxin regulation of endocytosis, recycling, and plasma membrane accumulation of the auxin efflux transporter PIN2 in Arabidopsis thaliana. Plant Cell **21:** 568-580

Prat T, Hajny J, Grunewald W, Vasileva M, Molnar G, Tejos R, Schmid M, Sauer M, Friml J (2018) WRKY23 is a component of the transcriptional network mediating auxin feedback on PIN polarity. PLoS Genet **14:** e1007177

Quareshy M, Uzunova V, Prusinska JM, Napier RM (2017) Assaying Auxin Receptor Activity Using SPR Assays with F-Box Proteins and Aux/IAA Degrons. Methods Mol Biol **1497:** 159-191

Rakusova H, Abbas M, Han H, Song S, Robert HS, Friml J (2016) Termination of Shoot Gravitropic Responses by Auxin Feedback on PIN3 Polarity. Curr Biol **26:** 3026-3032

Rakusova H, Fendrych M, Friml J (2015) Intracellular trafficking and PIN-mediated cell polarity during tropic responses in plants. Curr Opin Plant Biol **23:** 116-123

Ren H, Gray WM (2015) SAUR Proteins as Effectors of Hormonal and Environmental Signals in Plant Growth. Mol Plant **8:** 1153-1164

Rigas S, Ditengou FA, Ljung K, Daras G, Tietz O, Palme K, Hatzopoulos P (2013) Root gravitropism and root hair development constitute coupled developmental responses regulated by auxin homeostasis in the Arabidopsis root apex. New Phytol **197:** 1130-1141

Robert HS, Grones P, Stepanova AN, Robles LM, Lokerse AS, Alonso JM, Weijers D, Friml J (2013) Local auxin sources orient the apical-basal axis in Arabidopsis embryos. Curr Biol **23:** 2506-2512

Robert S, Kleine-Vehn J, Barbez E, Sauer M, Paciorek T, Baster P, Vanneste S, Zhang J, Simon S, Covanova M, Hayashi K, Dhonukshe P, Yang Z, Bednarek SY, Jones AM, Luschnig C, Aniento F, Zazimalova E, Friml J (2010) ABP1 mediates auxin inhibition of clathrin-dependent endocytosis in Arabidopsis. Cell **143:** 111-121

Salanenka Y, Verstraeten I, Lofke C, Tabata K, Naramoto S, Glanc M, Friml J (2018) Gibberellin DELLA signaling targets the retromer complex to redirect protein trafficking to the plasma membrane. Proc Natl Acad Sci U S A **115:** 3716-3721

Sauer M, Paciorek T, Benkova E, Friml J (2006) Immunocytochemical techniques for whole-mount in situ protein localization in plants. Nat Protoc **1:** 98-103

Spartz AK, Lee SH, Wenger JP, Gonzalez N, Itoh H, Inze D, Peer WA, Murphy AS, Overvoorde PJ, Gray WM (2012) The SAUR19 subfamily of SMALL AUXIN UP RNA genes promote cell expansion. Plant J **70:** 978-990

Sugawara S, Mashiguchi K, Tanaka K, Hishiyama S, Sakai T, Hanada K, Kinoshita-Tsujimura K, Yu H, Dai X, Takebayashi Y, Takeda-Kamiya N, Kakimoto T, Kawaide H, Natsume M, Estelle M, Zhao Y, Hayashi K, Kamiya Y, Kasahara H (2015) Distinct Characteristics of Indole-3-Acetic Acid and Phenylacetic Acid, Two Common Auxins in Plants. Plant Cell Physiol **56:** 1641-1654

Tsuda E, Yang H, Nishimura T, Uehara Y, Sakai T, Furutani M, Koshiba T, Hirose M, Nozaki H, Murphy AS, Hayashi K (2011) Alkoxy-auxins are selective inhibitors of auxin transport mediated by PIN, ABCB, and AUX1 transporters. J Biol Chem **286:** 2354-2364

Tsugafune S, Mashiguchi K, Fukui K, Takebayashi Y, Nishimura T, Sakai T, Shimada Y, Kasahara H, Koshiba T, Hayashi KI (2017) Yucasin DF, a potent and persistent inhibitor of auxin biosynthesis in plants. Sci Rep **7:** 13992

Vieten A, Vanneste S, Wisniewska J, Benkova E, Benjamins R, Beeckman T, Luschnig C, Friml J (2005) Functional redundancy of PIN proteins is accompanied by auxin-dependent cross-regulation of PIN expression. Development **132:** 4521-4531

Winicur ZM, Zhang GF, Staehelin LA (1998) Auxin deprivation induces synchronous Golgi differentiation in suspension-cultured tobacco BY-2 cells. Plant Physiol **117:** 501-513

Wisniewska J, Xu J, Seifertova D, Brewer PB, Ruzicka K, Blilou I, Rouquie D, Benkova E, Scheres B, Friml J (2006) Polar PIN localization directs auxin flow in plants. Science **312:** 883

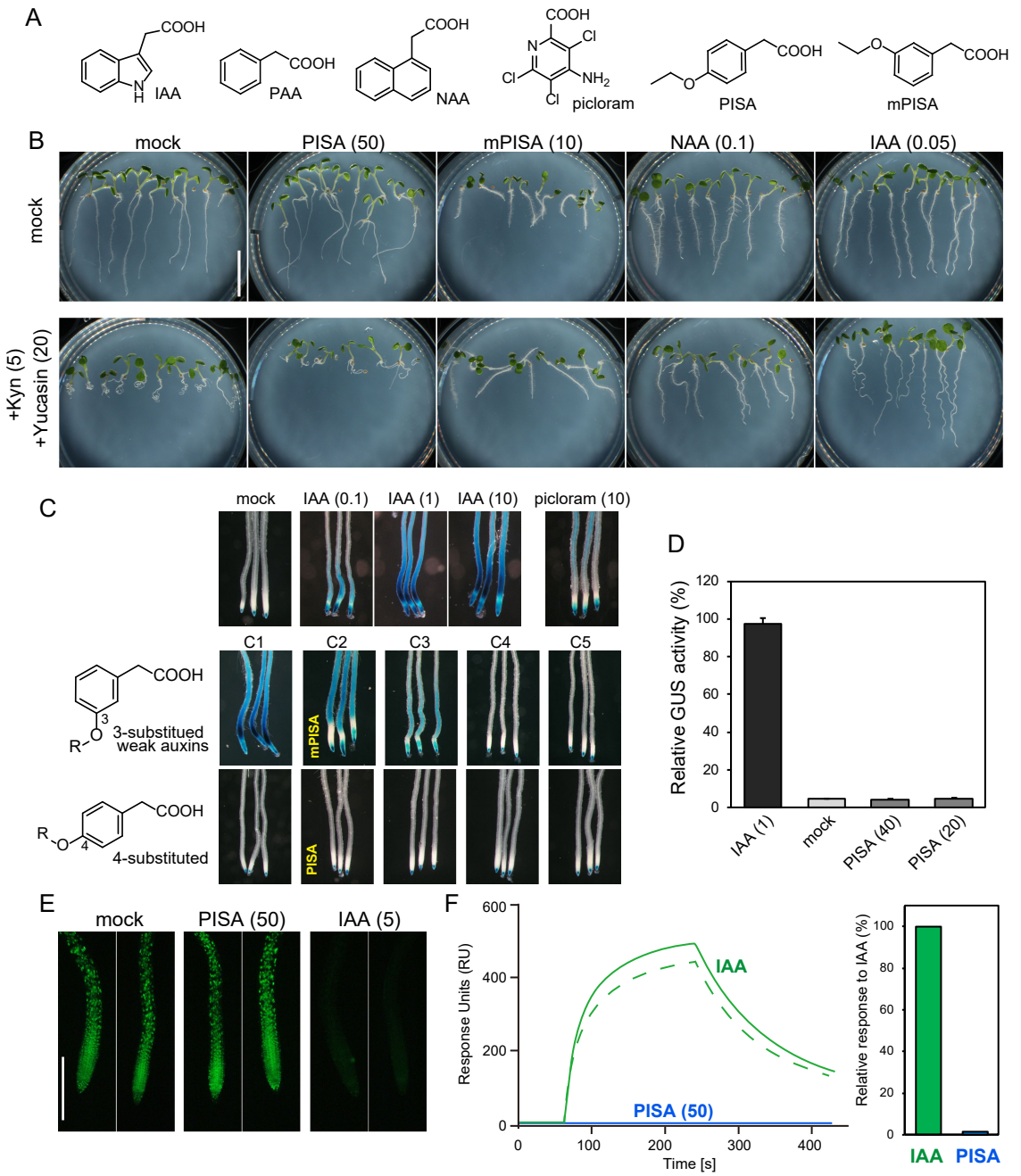

Figure 1. Evaluation of PISA for an auxin-like effect in the SCF$^{TIR1/AFB}$ pathway.
A, The structures of auxins and pinstatic acid (PISA). B, Effects of PISA on auxin-deficient root phenotypes. Arabidopsis plants were cultured for 5 d on vertical agar plate containing chemicals with or without auxin biosynthesis inhibitors, yucasin DF and Kyn. The values in parentheses represent the concentration of chemicals (μM). Bar represents 5 mm. C, Effects of alkyloxy-PAA on auxin-responsive *DR5::GUS* expression. 5-d-old *DR5::GUS* seedlings were incubated with chemicals for 6 h. Methoxy (C1) to pentoxy (C5) PAA derivatives including mPISA and PISA were assessed at 50 μM. D, Quantitative analysis of GUS enzyme activity in the *DR5::GUS* line treated with IAA and PISA. Values are the means ± S.D. (n=9). E, DII-VENUS seedlings were incubated with 10 μM yucasin DF for 3 h and then washed with medium. The seedling was incubated with PISA and IAA for another 60 min. Bar represents 500 μm. F, Surface Plasmon Resonance analysis of the auxin-induced interaction between TIR1 and IAA7 degron peptide. The sensorgram shows the effect of 50 μM IAA (green) and 50 μM PISA (blue) on TIR1-DII peptide association and dissociation. The bars show the relative response of PISA to IAA (100%).

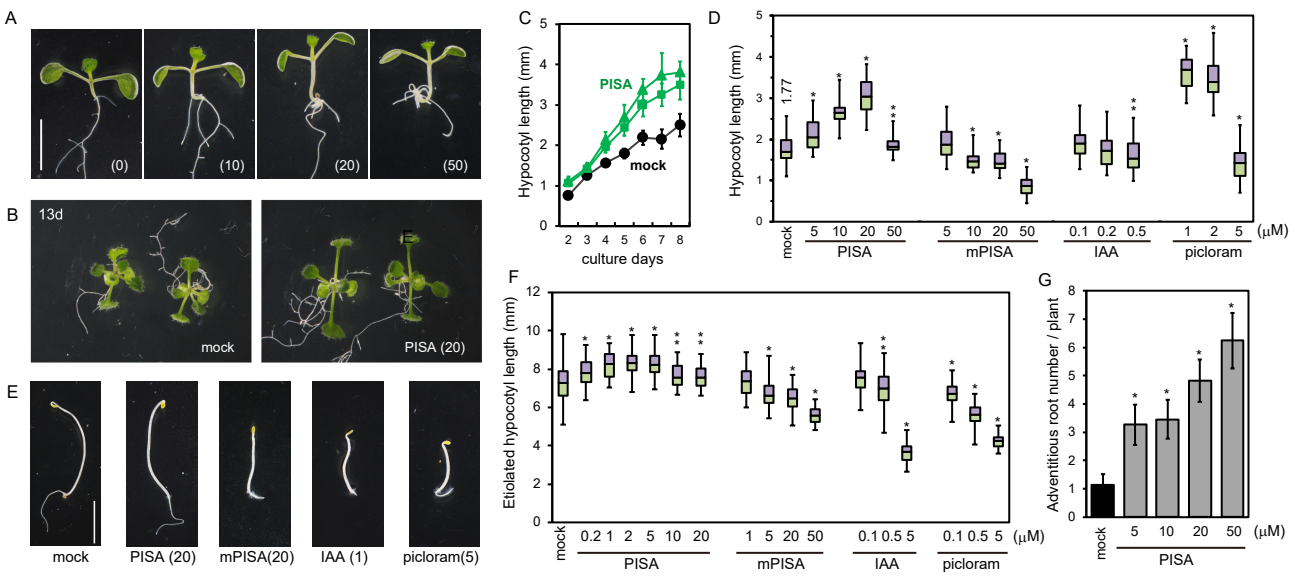

Figure 2. Effects of PISA on hypocotyl elongation and adventitious root formation.
A, Arabidopsis seedlings cultured for 7 d with PISA. The values in parentheses represent the concentration of chemicals (μM). Bar represents 5 mm. B, 13-d-old plants grown with PISA. C, Time course of hypocotyl length of seedlings cultured with PISA (closed square: 10 μM and closed triangle: 20 μM). Values are the means ± S.D. (n=15–20). D, Hypocotyl lengths of seedlings cultured for 7 d with PISA and auxins. The hypocotyl length (mm) of the mock-treated seedlings is indicated. Box-and-whisker plots show a median (centerline), upper/lower quartiles (box limits) and maximum/minimum (whiskers). (n=30–38). Statistical significance assessed by Welch' s two sample t-test. Asterisks indicate significant differences (**p<0.05, *p<0.01). E, Etiolated seedlings cultured for 5 d in dark with PISA and auxins. F, Hypocotyl lengths of etiolated seedling cultured for 3 d in dark with PISA and auxins. Statistical significance assessed by Welch' s two sample *t*-test. Asterisks indicate significant differences (n=50–72, **p<0.05, *p<0.01). G, Adventitious root production induced by PISA. Arabidopsis seedlings were cultured for 7 d with PISA and the adventitious root number at shoot and root junction was counted. Asterisks indicate significant differences (n=30, **p<0.05, *p<0.01).

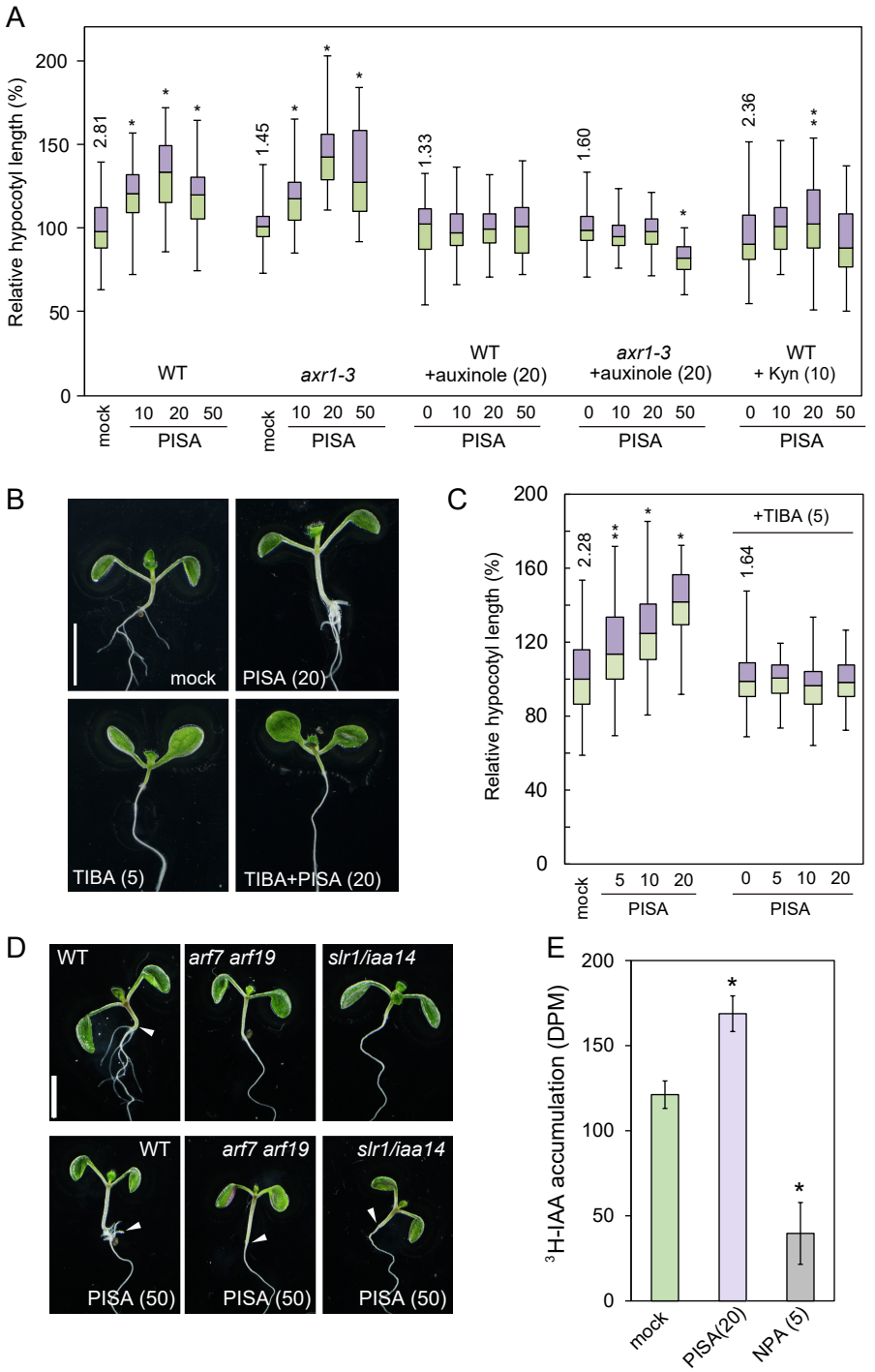

Figure 3. Auxin signaling and transport inhibitors repress PISA-induced hypocotyl phenotypes and PISA promotes basipetal auxin transport in the hypocotyl.

A, The hypocotyl length of Arabidopsis wild-type (WT) and *axr1-3* mutant seedlings cultured for 7 d with chemicals. Relative hypocotyl length is shown as the percentage of that in mock-treated plants (100%). The actual length (mm) of mock-treated hypocotyls are indicated (n=40–48). B, Seedlings cultured for 7 d with PISA and auxin transport inhibitor, TIBA. C, Hypocotyl length in seedlings cultured with or without TIBA and PISA. Relative hypocotyl length is shown as the percentage of that in mock-treated plants (100%). The actual length (mm) of mock-treated hypocotyls are indicated as box-and-whisker plots (n=40–45). Statistical significance assessed by Welch' s two sample *t*-test. Asterisks indicate significant differences (**p<0.05, *p<0.01). D, Seedlings of WT, *arf7 arf19* and *slr1/iaa14* mutants cultured for 7 d with or without PISA. The values in parentheses represents the concentration of chemicals (μM). Bar represents 5 mm. E, Rootward transport of radiolabeled ^{3}H-IAA in decapitated hypocotyls. NPA, an auxin transport inhibitor, was used as the negative control. (*p<0.01, n=9).

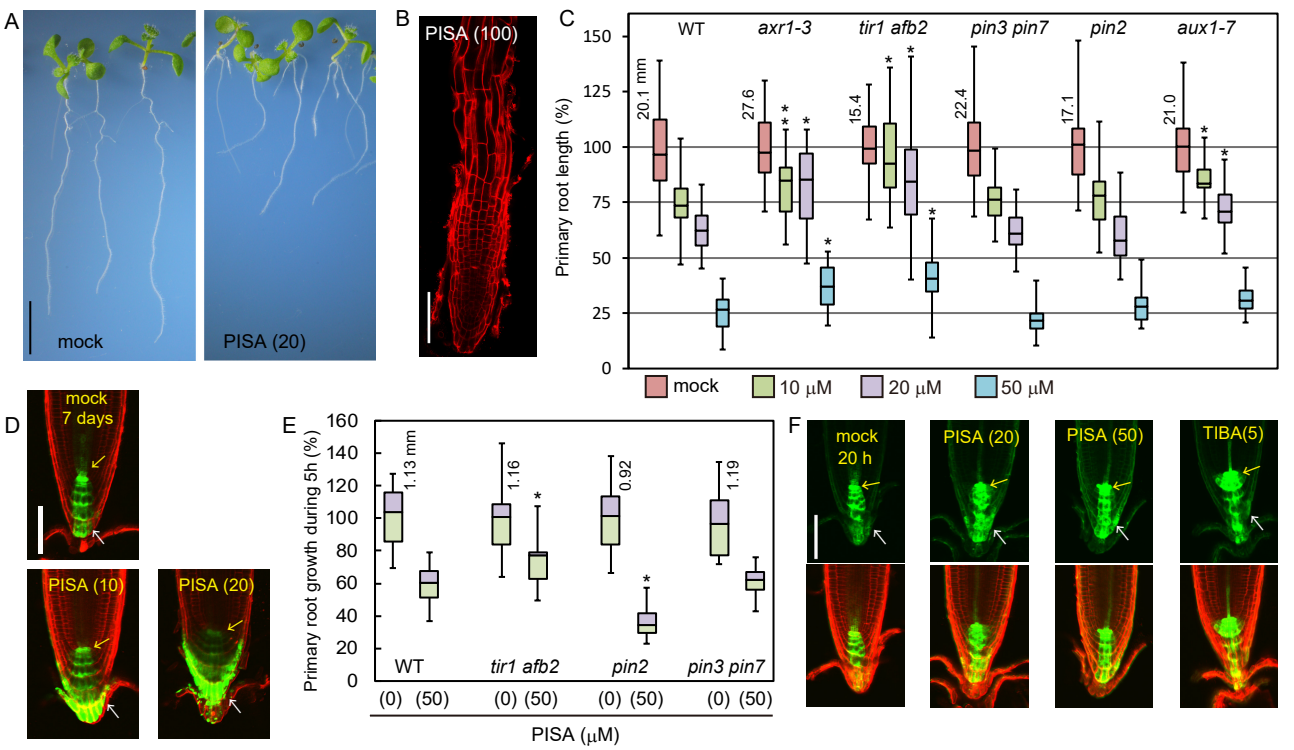

Figure 4. The effects of PISA on root elongation and auxin distribution in the root tip. A, Wild-type seedlings cultured for 7 d with PISA. Bar represents 5 mm. B, Wild-type root cultured with 100 μM PISA . Root was counterstained with propidium iodide. Bar represents 100 μm. C, The primary root length of Arabidopsis wild-type (WT) and auxin mutants (*axr1-3*, *tir1 afb2*, *pin3 pin7*, *pin2/eir1-1* and *aux1-7*) cultured for 7 d on vertical plate containing PISA. Relative root length is shown as the percentage of that in mock-treated plants (100%). The actual length (mm) of mock-treated roots is indicated. Statistical significance was assessed by Welch' s two sample *t*-test between WT and mutants. Asterisks indicate significant differences (n=32-40, **p<0.05, *p<0.01). D, The GFP expression of *DR5::GFP* in roots cultured vertically with PISA for 7 d. Arrows indicate quiescent center (yellow) and lateral root cap (white). Bar represents 100 μm. E, The primary root growth of Arabidopsis WT and auxin mutants over 5 h on vertical plates containing PISA. The actual length (mm) of mock-treated roots is indicated, which were set to 100%. Asterisks indicate significant differences (n=14–17, *p<0.01). F, The GFP expression of *DR5::GFP* cultured vertically with PISA and TIBA for 20 h. The values in parentheses represents the concentration of chemicals (μM). Bar represents 100 μm.

.

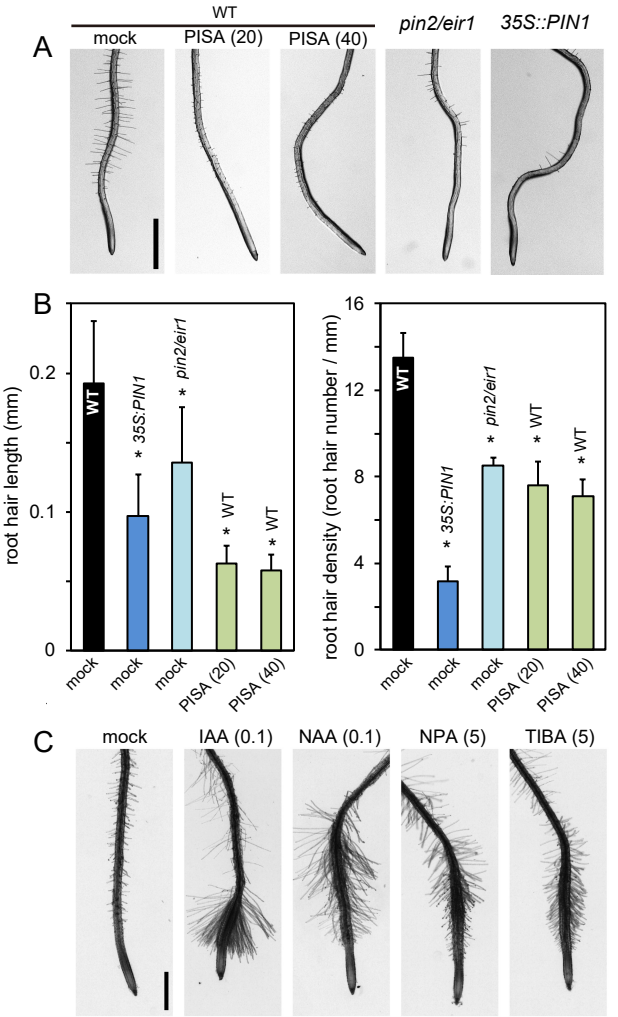

Figure 5. PISA inhibits root hair formation.
A, Root hairs of *pin2/eir1*, *35S::PIN1* and wild-type (WT) plants treated with PISA. 5-d-old seedlings were cultured for 2 d on vertical agar plates with or without PISA. The values in parentheses represent the concentration of chemicals (μM). B, The root hair length and density of *pin2/eir1*, *35S::PIN1* and WT plants treated with PISA. The length and density of root hairs within the 2–4 mm region from root tip were measured. Values are the means ± S.D. Asterisks indicate significant differences (n=8–11, *p<0.01). C, The root hair formation of WT seedlings grown with auxins and auxin transport inhibitors. The values in parentheses represent the concentration of chemicals (μM). Bar represents 1 mm.

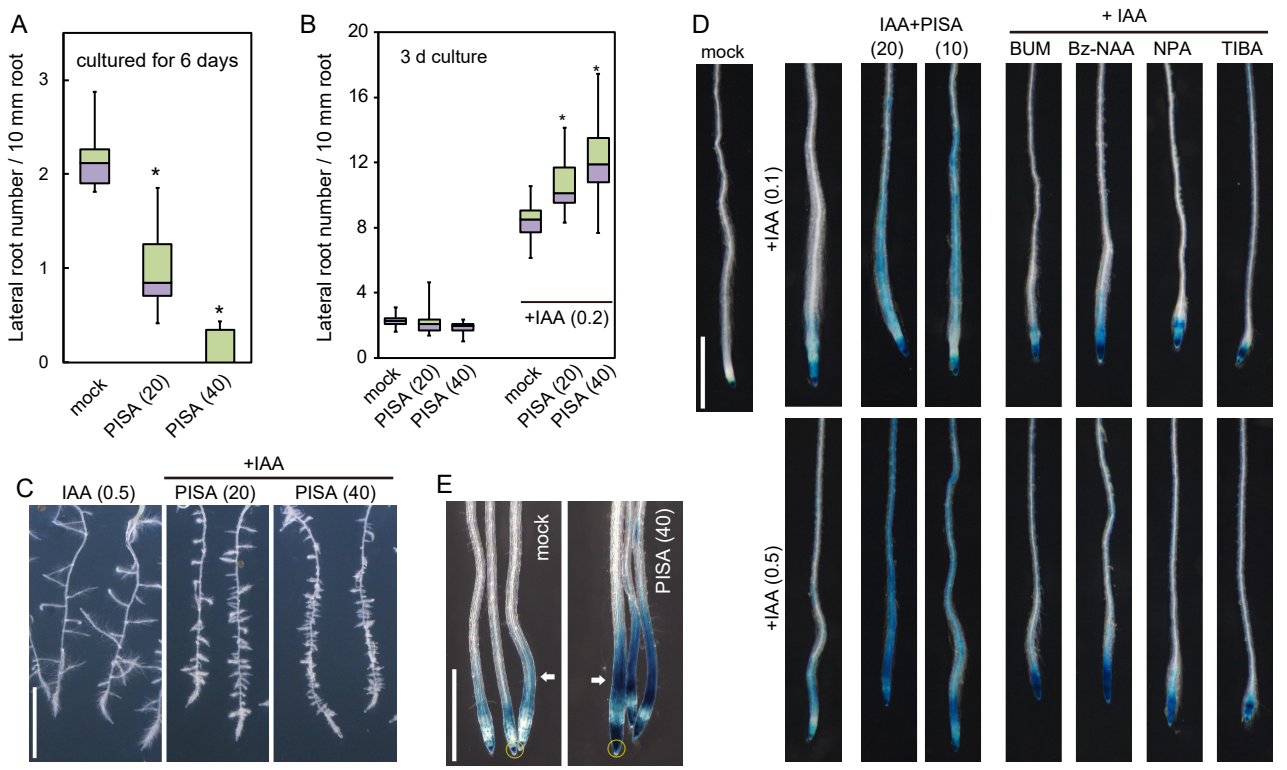

Figure 6. Effects of PISA on IAA-induced lateral root formation and shootward IAA transport.

A, Effects of PISA on the lateral root formation. Arabidopsis seedlings were cultured for 6 d with PISA. The number of lateral roots were counted and the density of lateral roots are shown as box-and-whisker plots (n=14–16). B and C, Effects of PISA on IAA-induced lateral root formation. 5-d-old seedlings were cultured for additional 3 d with PISA in the presence of IAA. The density of lateral roots are shown as box-and-whisker plots (B, n=14–16) and representative images are shown (C). Bar represents 5 mm. D, Effects of PISA on IAA-induced *DR5::GUS* expression. 5-d-old *DR5::GUS* seedlings were incubated for 12 h in liquid GM medium with or without PISA or auxin transport inhibitors. IAA was added to the GM medium and the seedlings were further incubated for additional 6 h. The IAA-induced GUS activity was visualized by X-Gluc. Bar represents 1 mm. E, Effects of PISA on shootward IAA transport. An agar block containing IAA was applied to *DR5::GUS* root tips (yellow ring) and the seedlings were incubated on vertical plates containing 40 μM PISA for 10 h. Arrows show the IAA-induced GUS activity. Bar represents 1 mm. Statistical significance assessed by Welch's two sample *t*-test. Asterisks indicate significant differences (*p<0.01). The values in parentheses represent the concentration of chemicals (μM).

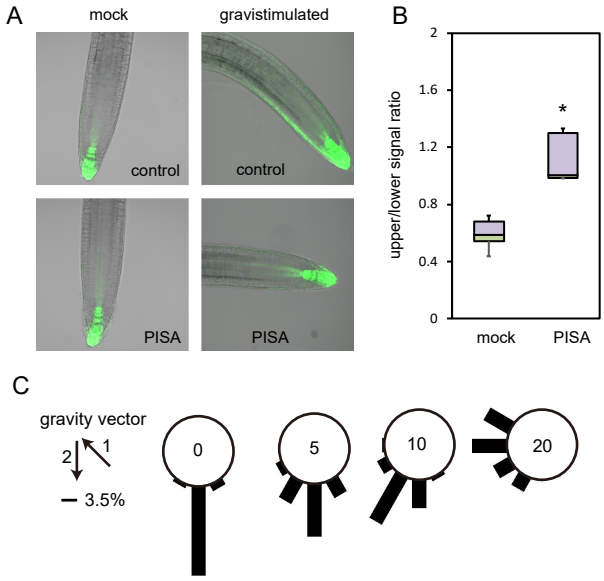

Figure 7. PISA inhibits auxin distribution and root gravitropism.
A, Effect of PISA on auxin asymmetric distribution. 4-d-old *DR5::GFP* seedlings were transferred to 20 μM PISA and control medium for 1 h. After 1 h seedlings were gravistimulated for 4 h and imaged. PISA pretreatment abolished auxin asymmetric distribution and seedlings did not respond to gravity stimuli. B, Quantitative evaluation of A, showing a mean ratio of the signal intensity of the upper/lower half of the root. (*p<0.01). C, Effect of PISA on root gravitropic response. Five-d-old wild-type seedlings were placed on vertical GM agar plates containing PISA and then cultured for 3 h in the dark. The plates were further incubated for 16 h after rotating plates at 135° angle against vertical direction. The arrows indicate the vector of gravity before (1) and after (2) the initiation of gravistimulation. The angles were grouped into 30° classes and plotted as circular histograms.

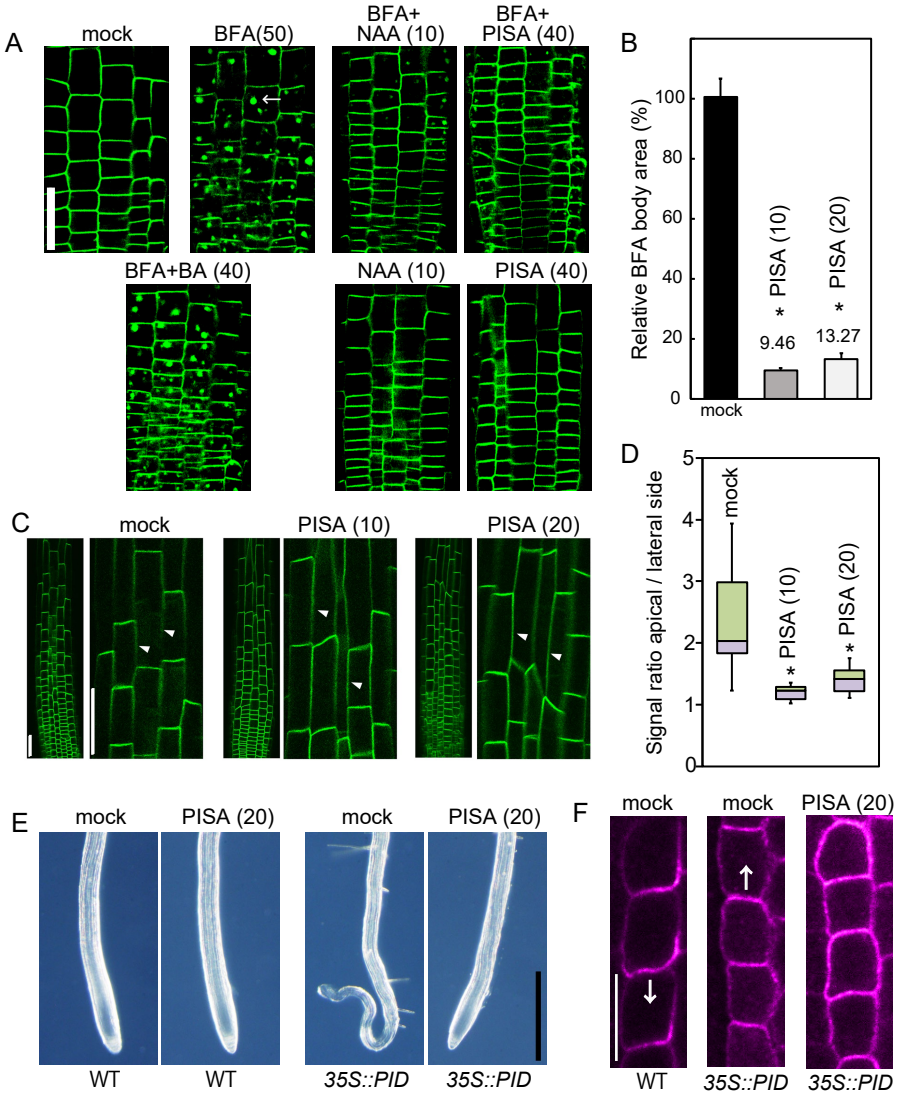

Figure 8. Effects of PISA on PIN internalization from the plasma membrane.
A and B, Effect of PISA on the BFA body formation of PIN2-GFP. 5-d-old *proPIN2::PIN2-GFP* seedlings were incubated for 30 min in liquid GM medium containing PISA and NAA and then BFA was added to the medium. Seedlings were then incubated for additional 60 min. BFA induced PIN2-GFP-marked BFA bodies. The area of BFA body was measured and the area in BFA-treated seedlings (n=25–40, *p<0.01) was adjusted to 100%. The value of the area is shown as the means ± S.D. in B. Bar represents 50 μm. C and D, Effect of PISA on the internalization of PIN2-GFP. 5-d-old *proPIN2::PIN2-GFP* seedlings were incubated for 12 h with PISA. The fluorescence intensity of the apical and lateral sides of cells in the root (n=18–20, *p<0.01) were quantified and the fluorescent signal rate (apical side / lateral side) is shown as the means ± S.D. in D. The values in parentheses represent the concentration of chemicals (μM). Bar represents 50 μm. E, Effects of PISA on a collapse of the primary root meristem. 5-d-old root tips of WT and *35S::PID* plants grown vertically on agar plates containing PISA. Bar represents 500 μm. F, Effects of PISA on PIN1 localization in the endodermis of WT and *35S::PID* roots. Immunolocalization of PIN1 after treatment with PISA for 4 h. Bar represents 10 μm.

Table 1

Effect of PISA on adventitious root formation at shoot/root junction

	WT (Col)	*arf7 arf19*	*slr1/iaa14*	TIBA (5)	NPA (5)
mock	1.57∓0.65 [a)]	0	0	0	0
PISA (20)	3.21∓0.70	0	0	0	0
PISA (50)	5.07∓1.03	0	0	0	0

a) adventitious root number at shoot/root junction for each 6-d old seedlings

Parsed Citations

Abas L, Benjamins R, Malenica N, Paciorek T, Wisniewska J, Moulinier-Anzola JC, Sieberer T, Friml J, Luschnig C (2006) Intracellular trafficking and proteolysis of the Arabidopsis auxin-efflux facilitator PIN2 are involved in root gravitropism. Nat Cell Biol 8: 249-256
Pubmed: Author and Title
Google Scholar: Author Only Title Only Author and Title

Adamowski M, Friml J (2015) PIN-dependent auxin transport: action, regulation, and evolution. Plant Cell 27: 20-32
Pubmed: Author and Title
Google Scholar: Author Only Title Only Author and Title

Adamowski M, Narasimhan M, Kania U, Glanc M, De Jaeger G, Friml J (2018) A Functional Study of AUXILIN-LIKE1 and 2, Two Putative Clathrin Uncoating Factors in Arabidopsis. Plant Cell 30: 700-716
Pubmed: Author and Title
Google Scholar: Author Only Title Only Author and Title

Baster P, Robert S, Kleine-Vehn J, Vanneste S, Kania U, Grunewald W, De Rybel B, Beeckman T, Friml J (2013) SCF(TIR1/AFB)-auxin signalling regulates PIN vacuolar trafficking and auxin fluxes during root gravitropism. EMBO J 32: 260-274
Pubmed: Author and Title
Google Scholar: Author Only Title Only Author and Title

Benjamins R, Quint A, Weijers D, Hooykaas P, Offringa R (2001) The PINOID protein kinase regulates organ development in Arabidopsis by enhancing polar auxin transport. Development 128: 4057-4067
Pubmed: Author and Title
Google Scholar: Author Only Title Only Author and Title

Brumos J, Robles LM, Yun J, Vu TC, Jackson S, Alonso JM, Stepanova AN (2018) Local Auxin Biosynthesis Is a Key Regulator of Plant Development. Dev Cell 47: 306-318 e305
Pubmed: Author and Title
Google Scholar: Author Only Title Only Author and Title

Brunoud G, Wells DM, Oliva M, Larrieu A, Mirabet V, Burrow AH, Beeckman T, Kepinski S, Traas J, Bennett MJ, Vernoux T (2012) A novel sensor to map auxin response and distribution at high spatio-temporal resolution. Nature 482: 103-106
Pubmed: Author and Title
Google Scholar: Author Only Title Only Author and Title

Buer CS, Muday GK (2004) The transparent testa4 mutation prevents flavonoid synthesis and alters auxin transport and the response of Arabidopsis roots to gravity and light. Plant Cell 16: 1191-1205
Pubmed: Author and Title
Google Scholar: Author Only Title Only Author and Title

Chae K, Isaacs CG, Reeves PH, Maloney GS, Muday GK, Nagpal P, Reed JW (2012) Arabidopsis SMALL AUXIN UP RNA63 promotes hypocotyl and stamen filament elongation. Plant J 71: 684-697
Pubmed: Author and Title
Google Scholar: Author Only Title Only Author and Title

Chen Q, Dai X, De-Paoli H, Cheng Y, Takebayashi Y, Kasahara H, Kamiya Y, Zhao Y (2014) Auxin overproduction in shoots cannot rescue auxin deficiencies in Arabidopsis roots. Plant Cell Physiol 55: 1072-1079
Pubmed: Author and Title
Google Scholar: Author Only Title Only Author and Title

Ding Z, Galvan-Ampudia CS, Demarsy E, Langowski L, Kleine-Vehn J, Fan Y, Morita MT, Tasaka M, Fankhauser C, Offringa R, Friml J (2011) Light-mediated polarization of the PIN3 auxin transporter for the phototropic response in Arabidopsis. Nat Cell Biol 13: 447-452
Pubmed: Author and Title
Google Scholar: Author Only Title Only Author and Title

Du Y, Tejos R, Beck M, Himschoot E, Li H, Robatzek S, Vanneste S, Friml J (2013) Salicylic acid interferes with clathrin-mediated endocytic protein trafficking. Proc Natl Acad Sci U S A 110: 7946-7951
Pubmed: Author and Title
Google Scholar: Author Only Title Only Author and Title

Fendrych M, Leung J, Friml J (2016) TIR1/AFB-Aux/IAA auxin perception mediates rapid cell wall acidification and growth of Arabidopsis hypocotyls. Elife 5
Pubmed: Author and Title
Google Scholar: Author Only Title Only Author and Title

Friml J, Yang X, Michniewicz M, Weijers D, Quint A, Tietz O, Benjamins R, Ouwerkerk PB, Ljung K, Sandberg G, Hooykaas PJ, Palme K, Offringa R (2004) A PINOID-dependent binary switch in apical-basal PIN polar targeting directs auxin efflux. Science 306: 862-865
Pubmed: Author and Title
Google Scholar: Author Only Title Only Author and Title

Fukui K, Hayashi KI (2018) Manipulation and Sensing of auxin metabolism, transport and signaling. Plant Cell Physiol
Pubmed: Author and Title
Google Scholar: Author Only Title Only Author and Title

Furutani M, Nakano Y, Tasaka M (2014) MAB4-induced auxin sink generates local auxin gradients in Arabidopsis organ formation. Proc Natl Acad Sci U S A 111: 1198-1203
Pubmed: Author and Title
Google Scholar: Author Only Title Only Author and Title

Ganguly A, Lee SH, Cho M, Lee OR, Yoo H, Cho HT (2010) Differential auxin-transporting activities of PIN-FORMED proteins in Arabidopsis root hair cells. Plant Physiol 153: 1046-1061
Pubmed: Author and Title
Google Scholar: Author Only Title Only Author and Title

Geldner N, Anders N, Wolters H, Keicher J, Kornberger W, Muller P, Delbarre A, Ueda T, Nakano A, Jurgens G (2003) The Arabidopsis GNOM ARF-GEF mediates endosomal recycling, auxin transport, and auxin-dependent plant growth. Cell 112: 219-230
Pubmed: Author and Title
Google Scholar: Author Only Title Only Author and Title

Geldner N, Friml J, Stierhof YD, Jurgens G, Palme K (2001) Auxin transport inhibitors block PIN1 cycling and vesicle trafficking. Nature 413: 425-428
Pubmed: Author and Title
Google Scholar: Author Only Title Only Author and Title

Hayashi K (2012) The interaction and integration of auxin signaling components. Plant Cell Physiol 53: 965-975
Pubmed: Author and Title
Google Scholar: Author Only Title Only Author and Title

Hayashi K, Neve J, Hirose M, Kuboki A, Shimada Y, Kepinski S, Nozaki H (2012) Rational design of an auxin antagonist of the SCF(TIR1) auxin receptor complex. ACS Chem Biol 7: 590-598
Pubmed: Author and Title
Google Scholar: Author Only Title Only Author and Title

He W, Brumos J, Li H, Ji Y, Ke M, Gong X, Zeng Q, Li W, Zhang X, An F, Wen X, Li P, Chu J, Sun X, Yan C, Yan N, Xie DY, Raikhel N, Yang Z, Stepanova AN, Alonso JM, Guo H (2011) A small-molecule screen identifies L-kynurenine as a competitive inhibitor of TAA1/TAR activity in ethylene-directed auxin biosynthesis and root growth in Arabidopsis. Plant Cell 23: 3944-3960
Pubmed: Author and Title
Google Scholar: Author Only Title Only Author and Title

Jasik J, Bokor B, Stuchlik S, Micieta K, Turna J, Schmelzer E (2016) Effects of Auxins on PIN-FORMED2 (PIN2) Dynamics Are Not Mediated by Inhibiting PIN2 Endocytosis. Plant Physiol 172: 1019-1031
Pubmed: Author and Title
Google Scholar: Author Only Title Only Author and Title

Kasahara H (2016) Current aspects of auxin biosynthesis in plants. Biosci Biotechnol Biochem 80: 34-42
Pubmed: Author and Title
Google Scholar: Author Only Title Only Author and Title

Kitakura S, Vanneste S, Robert S, Lofke C, Teichmann T, Tanaka H, Friml J (2011) Clathrin mediates endocytosis and polar distribution of PIN auxin transporters in Arabidopsis. Plant Cell 23: 1920-1931
Pubmed: Author and Title
Google Scholar: Author Only Title Only Author and Title

Korasick DA, Enders TA, Strader LC (2013) Auxin biosynthesis and storage forms. J Exp Bot 64: 2541-2555
Pubmed: Author and Title
Google Scholar: Author Only Title Only Author and Title

Lee S, Sundaram S, Armitage L, Evans JP, Hawkes T, Kepinski S, Ferro N, Napier RM (2014) Defining binding efficiency and specificity of auxins for SCF(TIR1/AFB)-Aux/IAA co-receptor complex formation. ACS Chem Biol 9: 673-682
Pubmed: Author and Title
Google Scholar: Author Only Title Only Author and Title

Lewis DR, Muday GK (2009) Measurement of auxin transport in Arabidopsis thaliana. Nat Protoc 4: 437-451
Pubmed: Author and Title
Google Scholar: Author Only Title Only Author and Title

Leyser O (2018) Auxin Signaling. Plant Physiol 176: 465-479
Pubmed: Author and Title
Google Scholar: Author Only Title Only Author and Title

Lin D, Nagawa S, Chen J, Cao L, Chen X, Xu T, Li H, Dhonukshe P, Yamamuro C, Friml J, Scheres B, Fu Y, Yang Z (2012) A ROP GTPase-dependent auxin signaling pathway regulates the subcellular distribution of PIN2 in Arabidopsis roots. Curr Biol 22: 1319-1325
Pubmed: Author and Title
Google Scholar: Author Only Title Only Author and Title

Marhavy P, Bielach A, Abas L, Abuzeineh A, Duclercq J, Tanaka H, Parezova M, Petrasek J, Friml J, Kleine-Vehn J, Benkova E (2011) Cytokinin modulates endocytic trafficking of PIN1 auxin efflux carrier to control plant organogenesis. Dev Cell 21: 796-804
Pubmed: Author and Title

Google Scholar: Author Only Title Only Author and Title

Muir RM, Fujita T, Hansch C (1967) Structure-activity relationship in the auxin activity of mono-substituted phenylacetic acids. Plant Physiol 42: 1519-1526
Pubmed: Author and Title
Google Scholar: Author Only Title Only Author and Title

Nagawa S, Xu T, Lin D, Dhonukshe P, Zhang X, Friml J, Scheres B, Fu Y, Yang Z (2012) ROP GTPase-dependent actin microfilaments promote PIN1 polarization by localized inhibition of clathrin-dependent endocytosis. PLoS Biol 10: e1001299
Pubmed: Author and Title
Google Scholar: Author Only Title Only Author and Title

Naramoto S, Kleine-Vehn J, Robert S, Fujimoto M, Dainobu T, Paciorek T, Ueda T, Nakano A, Van Montagu MC, Fukuda H, Friml J (2010) ADP-ribosylation factor machinery mediates endocytosis in plant cells. Proc Natl Acad Sci U S A 107: 21890-21895
Pubmed: Author and Title
Google Scholar: Author Only Title Only Author and Title

Nishimura K, Fukagawa T, Takisawa H, Kakimoto T, Kanemaki M (2009) An auxin-based degron system for the rapid depletion of proteins in nonplant cells. Nat Methods 6: 917-922
Pubmed: Author and Title
Google Scholar: Author Only Title Only Author and Title

Okushima Y, Fukaki H, Onoda M, Theologis A, Tasaka M (2007) ARF7 and ARF19 regulate lateral root formation via direct activation of LBD/ASL genes in Arabidopsis. Plant Cell 19: 118-130
Pubmed: Author and Title
Google Scholar: Author Only Title Only Author and Title

Paciorek T, Zazimalova E, Ruthardt N, Petrasek J, Stierhof YD, Kleine-Vehn J, Morris DA, Emans N, Jurgens G, Geldner N, Friml J (2005) Auxin inhibits endocytosis and promotes its own efflux from cells. Nature 435: 1251-1256
Pubmed: Author and Title
Google Scholar: Author Only Title Only Author and Title

Pan J, Fujioka S, Peng J, Chen J, Li G, Chen R (2009) The E3 ubiquitin ligase SCFTIR1/AFB and membrane sterols play key roles in auxin regulation of endocytosis, recycling, and plasma membrane accumulation of the auxin efflux transporter PIN2 in Arabidopsis thaliana. Plant Cell 21: 568-580
Pubmed: Author and Title
Google Scholar: Author Only Title Only Author and Title

Prat T, Hajny J, Grunewald W, Vasileva M, Molnar G, Tejos R, Schmid M, Sauer M, Friml J (2018) WRKY23 is a component of the transcriptional network mediating auxin feedback on PIN polarity. PLoS Genet 14: e1007177
Pubmed: Author and Title
Google Scholar: Author Only Title Only Author and Title

Quareshy M, Uzunova V, Prusinska JM, Napier RM (2017) Assaying Auxin Receptor Activity Using SPR Assays with F-Box Proteins and Aux/IAA Degrons. Methods Mol Biol 1497: 159-191
Pubmed: Author and Title
Google Scholar: Author Only Title Only Author and Title

Rakusova H, Abbas M, Han H, Song S, Robert HS, Friml J (2016) Termination of Shoot Gravitropic Responses by Auxin Feedback on PIN3 Polarity. Curr Biol 26: 3026-3032
Pubmed: Author and Title
Google Scholar: Author Only Title Only Author and Title

Rakusova H, Fendrych M, Friml J (2015) Intracellular trafficking and PIN-mediated cell polarity during tropic responses in plants. Curr Opin Plant Biol 23: 116-123
Pubmed: Author and Title
Google Scholar: Author Only Title Only Author and Title

Ren H, Gray WM (2015) SAUR Proteins as Effectors of Hormonal and Environmental Signals in Plant Growth. Mol Plant 8: 1153-1164
Pubmed: Author and Title
Google Scholar: Author Only Title Only Author and Title

Rigas S, Ditengou FA, Ljung K, Daras G, Tietz O, Palme K, Hatzopoulos P (2013) Root gravitropism and root hair development constitute coupled developmental responses regulated by auxin homeostasis in the Arabidopsis root apex. New Phytol 197: 1130-1141
Pubmed: Author and Title
Google Scholar: Author Only Title Only Author and Title

Robert HS, Grones P, Stepanova AN, Robles LM, Lokerse AS, Alonso JM, Weijers D, Friml J (2013) Local auxin sources orient the apical-basal axis in Arabidopsis embryos. Curr Biol 23: 2506-2512
Pubmed: Author and Title
Google Scholar: Author Only Title Only Author and Title

Robert S, Kleine-Vehn J, Barbez E, Sauer M, Paciorek T, Baster P, Vanneste S, Zhang J, Simon S, Covanova M, Hayashi K, Dhonukshe P, Yang Z, Bednarek SY, Jones AM, Luschnig C, Aniento F, Zazimalova E, Friml J (2010) ABP1 mediates auxin inhibition of clathrin-dependent endocytosis in Arabidopsis. Cell 143: 111-121

Pubmed: Author and Title
Google Scholar: Author Only Title Only Author and Title

Salanenka Y, Verstraeten I, Lofke C, Tabata K, Naramoto S, Glanc M, Friml J (2018) Gibberellin DELLA signaling targets the retromer complex to redirect protein trafficking to the plasma membrane. Proc Natl Acad Sci U S A 115: 3716-3721
Pubmed: Author and Title
Google Scholar: Author Only Title Only Author and Title

Sauer M, Paciorek T, Benkova E, Friml J (2006) Immunocytochemical techniques for whole-mount in situ protein localization in plants. Nat Protoc 1: 98-103
Pubmed: Author and Title
Google Scholar: Author Only Title Only Author and Title

Spartz AK, Lee SH, Wenger JP, Gonzalez N, Itoh H, Inze D, Peer WA, Murphy AS, Overvoorde PJ, Gray WM (2012) The SAUR19 subfamily of SMALL AUXIN UP RNA genes promote cell expansion. Plant J 70: 978-990
Pubmed: Author and Title
Google Scholar: Author Only Title Only Author and Title

Sugawara S, Mashiguchi K, Tanaka K, Hishiyama S, Sakai T, Hanada K, Kinoshita-Tsujimura K, Yu H, Dai X, Takebayashi Y, Takeda-Kamiya N, Kakimoto T, Kawaide H, Natsume M, Estelle M, Zhao Y, Hayashi K, Kamiya Y, Kasahara H (2015) Distinct Characteristics of Indole-3-Acetic Acid and Phenylacetic Acid, Two Common Auxins in Plants. Plant Cell Physiol 56: 1641-1654
Pubmed: Author and Title
Google Scholar: Author Only Title Only Author and Title

Tsuda E, Yang H, Nishimura T, Uehara Y, Sakai T, Furutani M, Koshiba T, Hirose M, Nozaki H, Murphy AS, Hayashi K (2011) Alkoxy-auxins are selective inhibitors of auxin transport mediated by PIN, ABCB, and AUX1 transporters. J Biol Chem 286: 2354-2364
Pubmed: Author and Title
Google Scholar: Author Only Title Only Author and Title

Tsugafune S, Mashiguchi K, Fukui K, Takebayashi Y, Nishimura T, Sakai T, Shimada Y, Kasahara H, Koshiba T, Hayashi KI (2017) Yucasin DF, a potent and persistent inhibitor of auxin biosynthesis in plants. Sci Rep 7: 13992
Pubmed: Author and Title
Google Scholar: Author Only Title Only Author and Title

Vieten A, Vanneste S, Wisniewska J, Benkova E, Benjamins R, Beeckman T, Luschnig C, Friml J (2005) Functional redundancy of PIN proteins is accompanied by auxin-dependent cross-regulation of PIN expression. Development 132: 4521-4531
Pubmed: Author and Title
Google Scholar: Author Only Title Only Author and Title

Winicur ZM, Zhang GF, Staehelin LA (1998) Auxin deprivation induces synchronous Golgi differentiation in suspension-cultured tobacco BY-2 cells. Plant Physiol 117: 501-513
Pubmed: Author and Title
Google Scholar: Author Only Title Only Author and Title

Wisniewska J, Xu J, Seifertova D, Brewer PB, Ruzicka K, Blilou I, Rouquie D, Benkova E, Scheres B, Friml J (2006) Polar PIN localization directs auxin flow in plants. Science 312: 883
Pubmed: Author and Title
Google Scholar: Author Only Title Only Author and Title

New Phytologist

Research

Auxin canalization and vascular tissue formation by TIR1/AFB-mediated auxin signaling in Arabidopsis

Ewa Mazur[1,2], Ivan Kulik[3], Jakub Hajný[3,4] and Jiří Friml[3]

[1]University of Silesia in Katowice, Faculty of Natural Sciences, Institute of Biology, Biotechnology and Environmental Protection, Katowice, Poland; [2]Mendel Centre for Plant Genomics and Proteomics, Central European Institute of Technology (CEITEC), Masaryk University, CZ-62-500, Brno, Czech Republic; [3]Institute of Science and Technology (IST), 3400, Klosterneuburg, Austria; [4]Laboratory of Growth Regulators and Department of Chemical Biology and Genetics, Centre of Region Haná for Biotechnological and Agricultural Research, Faculty of Science, Palacký University and Institute of Experimental Botany ASCR, Šlechtitelů 27 783 71, Olomouc, Czech Republic

Authors for correspondence:
Ewa Mazur
Tel: +48 32 2009447
Email: *ewa.mazur@us.edu.pl*

Ivan Kulik
Tel: +45 91 113704
Email: *ivan.kulik@sund.ku.dk*

Received: *16 September 2019*
Accepted: *10 January 2020*

New Phytologist (2020) **226:** 1375–1383
doi: 10.1111/nph.16446

Key words: *Arabidopsis thaliana*, auxin, auxin canalization, cell polarity, PIN1, TIR1/AFB.

Summary

- Plant survival depends on vascular tissues, which originate in a self-organizing manner as strands of cells co-directionally transporting the plant hormone auxin. The latter phenomenon (also known as auxin canalization) is classically hypothesized to be regulated by auxin itself via the effect of this hormone on the polarity of its own intercellular transport. Correlative observations supported this concept, but molecular insights remain limited.
- In the current study, we established an experimental system based on the model *Arabidopsis thaliana*, which exhibits auxin transport channels and formation of vasculature strands in response to local auxin application.
- Our methodology permits the genetic analysis of auxin canalization under controllable experimental conditions. By utilizing this opportunity, we confirmed the dependence of auxin canalization on a PIN-dependent auxin transport and nuclear, TIR1/AFB-mediated auxin signaling. We also show that leaf venation and auxin-mediated PIN repolarization in the root require TIR1/AFB signaling.
- Further studies based on this experimental system are likely to yield better understanding of the mechanisms underlying auxin transport polarization in other developmental contexts.

Introduction

Plants possess superb abilities to adapt their development to the changing environment. One of them is their capacity to form organized vasculature, which occurs under normal (e.g. leaf venation or when nascent organs connect to the pre-existing vascular network) and traumatic (e.g. re-connection of broken vascular strands after wounding) conditions. The latter example occurs frequently within the ontogeny of higher plants (due to grazing or other types of mechanical stress) and is therefore paramount to their survival. This developmentally fascinating process of vasculature formation involves not only (de)differentiation of multiple cell types, but also coordinated cell polarization ultimately leading to the directional transport of compounds through cellular strands (channels).

It has been proposed that vascular strand formation is regulated by auxin via a putative feedback interaction between its cellular perception and intercellular polar transport (Sachs, 1975, 1981; Uggla *et al.*, 1996, 1998; Tuominen *et al.*, 2000; Sauer *et al.*, 2006; Robert *et al.*, 2013). It is known that vasculature formation is indeed spatially associated with the activation of TIR1/AFB signaling (Lavy *et al.*, 2016) and accumulation of polarly distributed PIN-FORMED (PIN) auxin efflux proteins (Adamowski & Friml, 2015) in the co-directionally polarized strands of vascular progenitors (auxin canalization; Sauer *et al.*, 2006; Zhang *et al.*, 2010; Balla *et al.*, 2011; Mazur *et al.*, 2016; Prat *et al.*, 2018). Observations of a similar correlation between auxin signaling and auxin transport polarization have also been made during embryonic apical–basal axis establishment (Robert *et al.*, 2013), shoot and root organogenesis (Benkova *et al.*, 2003; Heisler *et al.*, 2005; Bhatia *et al.*, 2016) as well as unexpected process such as the termination of shoot gravitropic response (Rakusova *et al.*, 2016).

The classical, 'gold standard' cell biological studies on auxin canalization were based on local auxin application onto the tissues of different plant species (Raven, 1975; Sachs, 1975, 1981), including pea (*Pisum sativum*) stems (Sauer *et al.*, 2006; Balla *et al.*, 2011). In this setup, auxin-transporting channels (and subsequently vascular strands) developed from the application site and connected it to the pre-existing vasculature of a plant. While these observations indicated that auxin canalization occurs via self-organization rather than pre-patterning, further implementation of the classical methodology has been hampered by the difficulty of transgenesis in the corresponding plant species.

Previous reports (Berleth *et al.*, 2000; Dettmer *et al.*, 2009; Bennett *et al.*, 2014) suggested that auxin canalization also

underlies physiological processes such as vasculature regeneration after wounding (Sauer *et al.*, 2006; Mazur *et al.*, 2016), leaf venation (Scarpella *et al.*, 2006; Cano-Delgado *et al.*, 2010; Sawchuk & Scarpella, 2013) and auxin-mediated PIN lateralization in the root (Prat *et al.*, 2018). In particular, it has been shown that leaf vein specification is the result of directional auxin transport mediated by polarized PIN expression demarcating the position of future vascular patterning. From primary broader PIN1 expression domains, the narrow PIN1-marked routes of auxin transport emerged as polarized groups of cells differentiating into vascular connections in leaves (Scarpella *et al.*, 2006; Wenzel *et al.*, 2007). Thus, studies utilizing the classical experimental model based on local auxin application are likely to yield knowledge not only on auxin canalization in the context of its exogenous application but also in other, more physiological roles.

Which components of auxin perception are involved in its feedback on auxin transport has not been rigorously addressed, but the well-characterized signaling pathway involving TRANSPORT INHIBITOR RESPONSE1 (TIR1)/AUXIN SIGNALING F-BOX (AFB) proteins as auxin receptors and the downstream Aux/IAA and auxin response factor (ARF) transcriptional regulators are likely to be implicated (Dharmasiri & Estelle, 2004; Hayashi *et al*, 2012). Although the molecular mechanisms are not entirely clear, it was shown that downstream processes in leaf vascular patterning are controlled by the auxin response transcription factor MONOPTEROS (MP) through an auxin response element in the *AtHB8* gene promoter. *AtHB8* seems to be required to constrict cell fate acquisition to gradually narrower areas, leading to the establishment of procambial cell identity during vein development (Donner *et al.*, 2009). Nonetheless, a demonstration that TIR1/AFB nuclear auxin signaling is required for the auxin feedback on auxin transport polarization during canalization, thus regulating processes such as leaf venation and wounding-induced vasculature regeneration, has not been provided.

Here, we established an experimental system, in which auxin canalization and vasculature formation can be induced by local auxin application. This makes the setup more direct and controllable compared to our previous approach, which involved vasculature regeneration around the wound (Mazur *et al.*, 2016). We use this system in conjunction with genetic, pharmacological and cell biological methods to demonstrate the requirement of TIR1/AFB signaling for auxin canalization and also show its importance for the regeneration of vascular strands and leaf venation.

Materials and Methods

Plant material and plant growth conditions

Wild-type Col-0 (NASC, The Nottingham Arabidopsis Stock Centre; http://www.arabidopsis.info/BasicForm) and reporter lines *DR5rev::GFP* (Friml *et al.*, 2003) and *pPIN1::PIN1:GFP* (Benkova *et al.*, 2003) produced in the Col-0 background were used as controls. *pin1-1*, *tir1-1*, *tir1-1 afb2 afb3*, *arf7-394 arf19-1* and *HS::axr3-1* have been previously described (Knox *et al.*, 2003; Sauer *et al.*, 2006; Lavy & Estelle, 2016; Fendrych *et al*, 2016). *tir1-1 afb1 afb3* was produced by us for this study. All mutants and transgenic lines used in this study are in the *Arabidopsis thaliana* ecotype Columbia (Col-0) background. Plants were germinated in pots with soil and vermiculite mixture (1 : 1, v : v). Seedlings with two pairs of true leaves were individually planted and grown in pots with soaked peaty rings in a growth chamber under long-day light conditions at 20°C. Plants with inflorescence stems 10 cm tall were chosen for the experiments.

Local auxin application and vasculature regeneration experiments in Arabidopsis stems

Young plants with inflorescence stems having primary tissue architecture (vascular bundles separated by interfascicular parenchyma sectors) were chosen for the following two-step experiments, according to the protocol of Mazur *et al.* (2016). First, the flowering parts of the stems were removed by using a sharp razor blade. The resulting stems (7 cm tall after dissection) were attached to a polypropylene tube to stiffen them and placed under a lead ball (2.5 g). The weight was applied for 6 d to produce a closed ring of cambium on the stem circumference (Mazur *et al.*, 2014). Next, the samples were incised transversally above the leaf rosette, and a droplet of lanoline paste with auxin (IAA; Sigma-Aldrich, cat. no. 15148-2G) or auxin plus inhibitors (NPA (*N*-1-naphtylphthalamic acid), Sigma; PEO-IAA (α-(phenyl ethyl-2-one)-indole-3-acetic-acid; auxinole, Sigma)) was locally applied below the cut. The incision was made in the transverse plane to disturb the longitudinal continuum of cambium and polar, basipetal transport of endogenous auxin. We were thus certain that the analyzed changes are the results of the externally applied auxin only. The applied compounds were replaced during the experiments every 2 d with a fresh droplet. For local application, 10 μM water solutions of all compounds mixed with a droplet of lanolin paste were used. Stock solutions of auxin and inhibitors (NPA, auxinole, PEO-IAA) were dissolved in dimethyl sulfoxide (cat. no. D5879-500ML; Sigma). Experiments were conducted twice for each line, with at least 10 plants analyzed in each run. Finally, the samples were collected, manually sectioned and mounted in a 50% glycerol aqueous solution onto imaging glass.

Leaf and cotyledon clearing

To reveal their vasculature, leaves/cotyledons of 8-d-old plants were treated with the following: 70% ethanol (overnight at 4°C); 4% HCl + 20% methanol (12 min at 65°C); 7% NaOH + 60% ethanol (15 min at room temperature); HCl (10 min at room temperature); seedlings were rehydrated by successive incubations in 60/40/20/10% in ethanol for 10 min; and 5% ethanol + 25% glycerol (a few days at 4°C until the air bubbles within the tissue had disappeared).

Verification of transgenic line identity

The mutations in the genomes of the mutant plant lines used in this work were verified by PCR. Namely, genomic DNA was

extracted from mechanically ground leaves of 3-wk-old plants and used as a template in PCR with wild type- and mutation-specific primers. The presence of the *tir1-1* point mutation was tested via *tir1* amplicon digestion with *Mbo*I endonuclease. Since regular PCR results were inconclusive for *afb1* and *afb3* insertional mutations in the *tir1afb1afb3* mutant, reverse transcription PCR was used instead, with cDNA from total leaf RNA preparation used as a template.

Imaging and image analysis

Samples of wounded stems were analyzed via a stereomicroscope (Nikon MSZ1500) equipped with a charge-coupled device (CCD) camera DS-Fi1. The green fluorescent protein (GFP) reporter lines were analyzed using Zeiss Observer.Z1 and Olympus Fluoview FV1000 confocal laser-scanning microscopes. GFP fluorescence was excited by an argon-ion laser light of 488 nm, detected at 510 nm. Acquired images were processed with ZEN 2012 Light Edition and FLUOVIEW software. Transmitted light observations were made via an Olympus BX43 microscope equipped with Olympus SC30 camera. Figures were created with CORELDRAW X6.

Quantification and statistical analysis

All calculations and graphs were made with Microsoft Office EXCEL software. Unpaired Student's *t*-tests ($P < 0.05$) and one-way ANOVA were used to compare sets of data ($P < 0.0001$). Error bars in the graphs indicate standard errors.

Results

Vasculature regeneration after wounding requires TIR1/AFB signaling

Previously (Mazur *et al.*, 2016), we showed that stem vasculature regeneration after wounding was associated with the activation of nuclear auxin signaling and induction of PIN1 auxin transport channels. In the present work, we wanted to test if this regeneration was dependent on the latter two factors.

To this end, we wounded inflorescence stems of Col-0 as well as triple *tir1afb1afb3* and *tir1afb2afb3* mutants and assessed the extent of vasculature regeneration in them 6 d after wounding (DAW; Fig. 1a,b). Double ARF (*arf7arf19*) mutants were analyzed as well, because these particular ARFs have been shown previously to be required for auxin signaling and auxin-mediated rearrangements of polar PIN1 distribution in roots (Okushima *et al.*, 2005; Sauer *et al.*, 2006). While two modes of vascular strand formation, namely passing around the wound and through the callus forming within the wound (both composed of elongated cells with stripes of secondary cell wall features) were present in the majority of sectioned Col-0 stems, only the vasculature passing through callus was visible in all *tir1afb* triple mutant samples (Fig. 1c–f). All *arf7arf19* mutant samples lacked callus formation after injury and did not regenerate vasculature around the wound (Fig. 1g).

In addition to these constitutive mutants, we analyzed *HS::axr3-1* plants, in which the expression of a dominant negative form of the IAA17/AXR3 transcriptional repressor can be induced by thermal stress (Knox *et al.*, 2003; Hayashi, 2012). After the stems were wounded, *HS::axr3-1* induction was conducted by incubating the plants at 37°C for 1 h every day, which strongly inhibited vasculature regeneration and callus formation. In particular, no vasculature formed around the wound in 70% (14/20) of samples 6 DAW. In the remaining 30% of stems (6/20), groups of cells with denser cell walls were present above the wound 6 DAW (Supporting Information Fig. S1). They were never elongated or arranged into well-defined strands and lacked the signs of secondary cell wall patterning.

To study the importance of PIN1, the same experiments were conducted on *pin1-1* knockout plants. The results were similar, with no vasculature passing through callus or around the wound visible 6 DAW in all samples (Fig. 1h).

Thus, our analysis of vasculature regeneration after wounding in constitutive and inducible mutants revealed that while PIN1-mediated auxin transport and TIR1/AFB auxin perception are required for vasculature regeneration around the wound, vasculature can still regenerate through callus when either one of these two processes is suppressed.

Local auxin application induces TIR1/AFB- and PIN1-dependent vascular strand development in Arabidopsis

Having observed a failure of *tir1/afb* mutants to regenerate vasculature after wounding, we wanted to test if this was due to the direct involvement of TIR1/AFB auxin perception in auxin canalization rather than in other regeneration-associated processes. For this, we complemented our wounding protocol with local auxin application. This is a classical experimental setup, which allows us to induce formation of auxin channels specifically by auxin treatment. In particular, although wounding is required in these experiments to stop the normal flow of auxin, its canalization is not induced unless the injury is accompanied by local auxin application below the cut site (Fig. 2a,b).

Application of natural auxin (IAA) dissolved in lanolin wax (100 nM) onto the surface of wounded Col-0 inflorescence stems led to the formation of thick vasculature (appearing as black strands extending downwards from the periphery into the deeper regions of the tissue) 6 d after auxin application (DAA) in almost 80% (32/40) of samples (Fig. 2c).

To test if this phenomenon depended on TIR1/AFB signaling and PIN1-mediated auxin transport, we treated wounded Col-0 stems with local co-application of auxin and inhibitors of either TIR1/AFB signaling (auxinole, PEO-IAA) or auxin transport (NPA) in the same drop of wax (Hayashi *et al.*, 2012). No vascular strands developed around the auxin application site 6 DAA under such experimental conditions (Fig. 2d–g). Local application of auxin onto the stems of *tir1afb1afb3*, *arf7arf19* and *pin1-1* mutants yielded similar results (Fig. 2h–k).

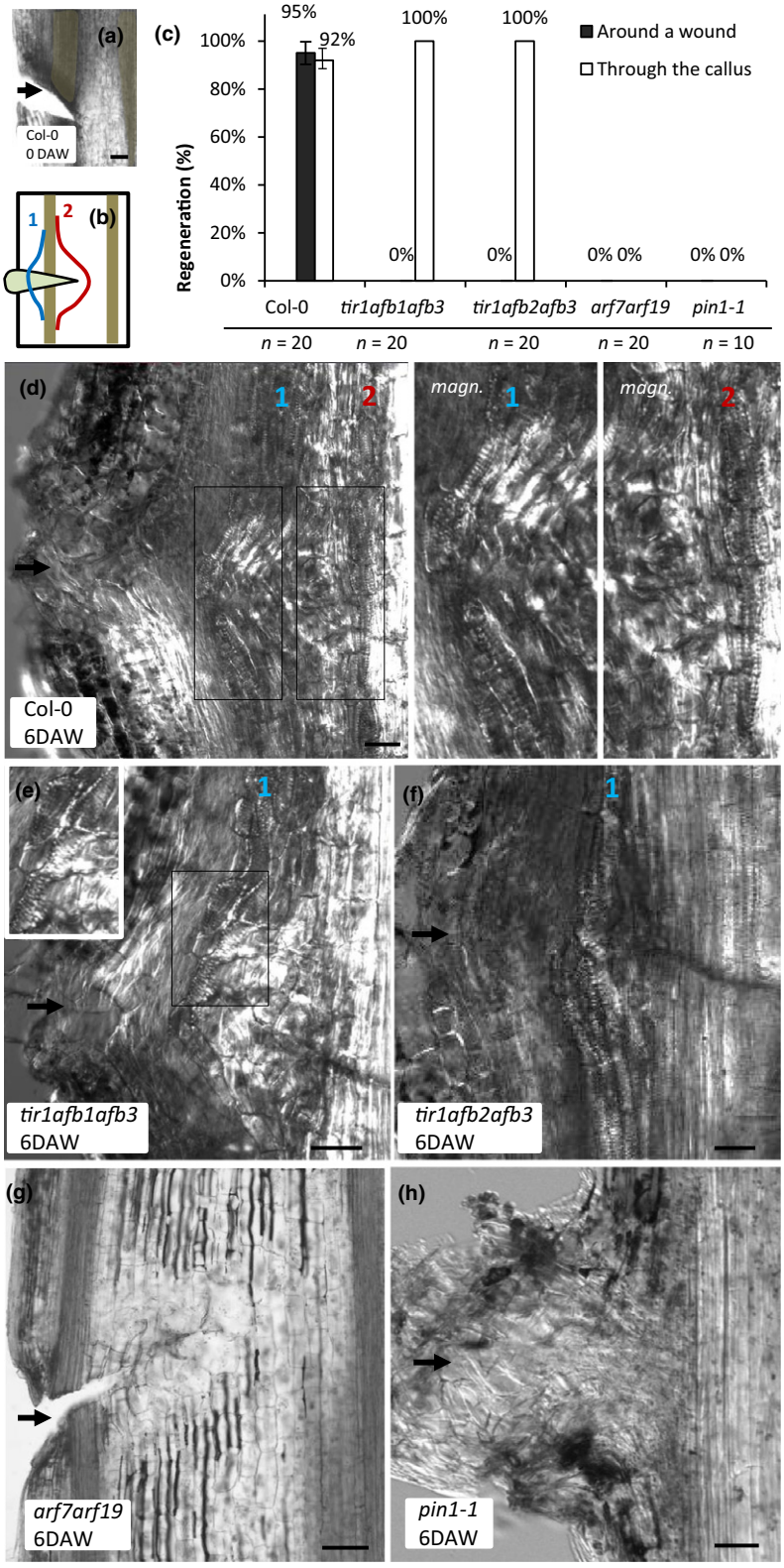

Fig. 1 Vasculature regeneration after wounding in *tir1/afb*, *arf7arf19* and *pin1-1* mutants of Arabidopsis. (a) Longitudinal section through a Col-0 inflorescence stem 8 h after wounding before callus formation. Black arrow indicates the approximate location of the wound. (b) Schematic depiction of vasculature regeneration after wounding in Arabidopsis inflorescence stem. Two brown vascular strands are shown similar to (a). The left one is broken due to wounding. The wound is filled with callus (light brown). (c) Frequencies of vasculature regeneration after wounding in stems of different genotypes. Error bars indicate SE. (d–h) Examples of wounded *Col-0*, *tir1afb1afb3*, *tir1afb2afb3*, *arf7arf19* and *pin1-1* inflorescence stems 6 d after wounding (DAW). Black arrows show the approximate locations of wounding sites. White rectangles specify which parts of the images are magnified to make the secondary cell wall features of regenerated vascular cells more apparent. Blue ('1') and red ('2') numbers mark the regenerated vascular strands passing through callus and around the wound, respectively. Bars, 50 μm (a, d–h). See also Supporting Information Fig. S1.

Thus, via a combination of genetic and pharmacological approaches, we show that TIR1/AFB signaling and PIN1-dependent auxin transport are required for vascular strands development in response to local auxin application in Arabidopsis inflorescence stems.

Local auxin application induces TIR1/AFB- and PIN1-dependent auxin canalization in Arabidopsis

To validate that vascular strand formation in response to local auxin application represents auxin canalization, we visualized

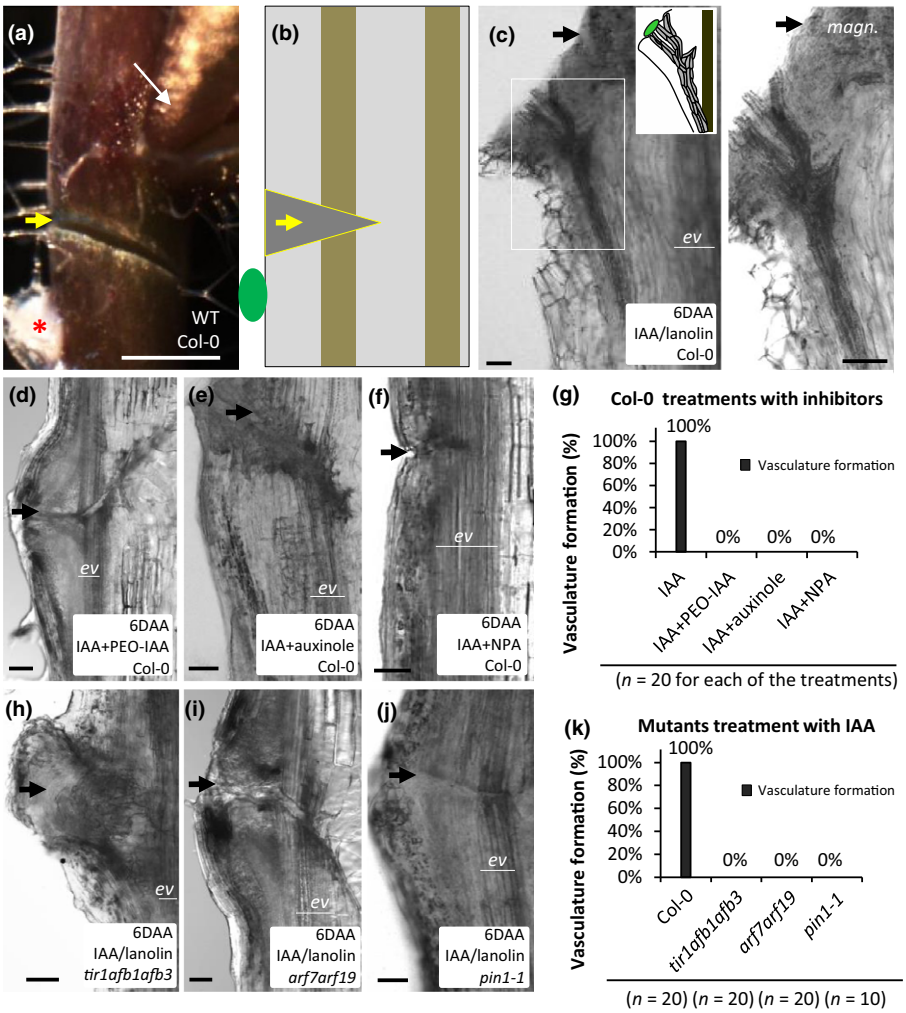

Fig. 2 Vascular strands formation in response to local auxin application onto Arabidopsis stems. (a) Fragment of a wounded Col-0 inflorescence stem. Auxin (with or without various inhibitors) was locally applied in a droplet of lanolin paste below the wound (red asterisk). Axillary buds above the wound were not removed in the experiments (narrow white arrow). (b) Schematic representation of (a) on a longitudinal section. Compounds are applied in a droplet of lanolin paste below the wound (green oval). The droplet is removed from the sample before sectioning for technical reasons and therefore cannot be located on the actual images. The vascular strand is broken by a transverse cut. (c–f) Examples of longitudinal sections of Col-0 stems 6 d after local application (DAA) of IAA alone or its co-application with PEO-IAA, auxinole or NPA. (h–j) Examples of longitudinal sections of *tir1afb1afb3*, *arf7arf19* and *pin1-1* stems 6 d after local application of IAA. (g, k) Frequencies of vascular strands formation under the studied experimental conditions. Thick arrows (yellow or black) indicate the approximate location of wounds. The bottom fragments of broken vascular strands (pre-existing vasculature) are labeled 'ev'. Bars: (a) 1mm; (c–f, h–j) 50 µm.

auxin response and polar auxin transport in the established experimental system via the genetic markers *DR5rev::GFP* (Friml *et al.*, 2003) and p*PIN1::PIN1-GFP* (Benkova *et al.*, 2003), respectively.

Local auxin application resulted in DR5 activation at the application site 8 h after auxin application (HAA; Fig. 3a). GFP-positive cells were arranged in a strand, similar to the vasculature in Fig. 2(c). At 4 DAA, a wide field of bright GFP fluorescence (Fig. S2a) and a narrow channel of cells expressing PIN1-GFP (Fig. 3b) were observed between the organ periphery and the pre-existing stem vasculature. Much weaker induction of DR5rev::GFP and PIN1-GFP expression was visible 4 and 6 DAA near the application site, when the stems were locally co-treated with IAA and TIR1/AFB inhibitors or NPA (Fig. 3c–i; Fig. S2b,c). In particular, green cells did not form defined strands under these experimental conditions and instead were found at the periphery of the organ.

Thus, these data show that local auxin application onto Arabidopsis inflorescence stems induces formation of PIN1-positive, high-auxin response channels from the exogenous source towards the pre-existing stem vasculature, which is blocked by pharmacological inhibition of either auxin perception or its directional transport.

TIR1/AFB signaling is required for proper leaf venation and auxin-induced PIN1 lateralization in the root

To complement our wounding and local auxin application observations with less invasive experiments, we analyzed other, spontaneously occurring auxin canalization-related physiological processes.

First, we looked at leaf venation, because it requires PIN-dependent auxin transport and is accompanied by the formation of DR5/PIN1-positive channels (Scarpella *et al.*, 2006; Sawchuk & Scarpella, 2013), similar to the case of auxin canalization from the exogenous source. We observed that two triple mutants defective in TIR1/AFB-mediated auxin perception (*tir1afb1afb3* and *tir1afb2afb3*) exhibited strong leaf venation defects in cotyledons (Fig. 4a) and primary leaves (Fig. S4). The strong abnormalities included apical disconnections between the central and lateral veins in cotyledons and the lack of one or both lateral veins in leaves (Fig. 4b). Thus, the analysis of leaf/cotyledon vasculature in *tir1/afb* mutants evidently shows that although vasculature can form, its intricate, organized pattern during leaf venation strongly depends on TIR1/AFB auxin perception.

To obtain some glimpses into which cellular processes during canalization are targeted by TIR1/AFB signaling, we analyzed

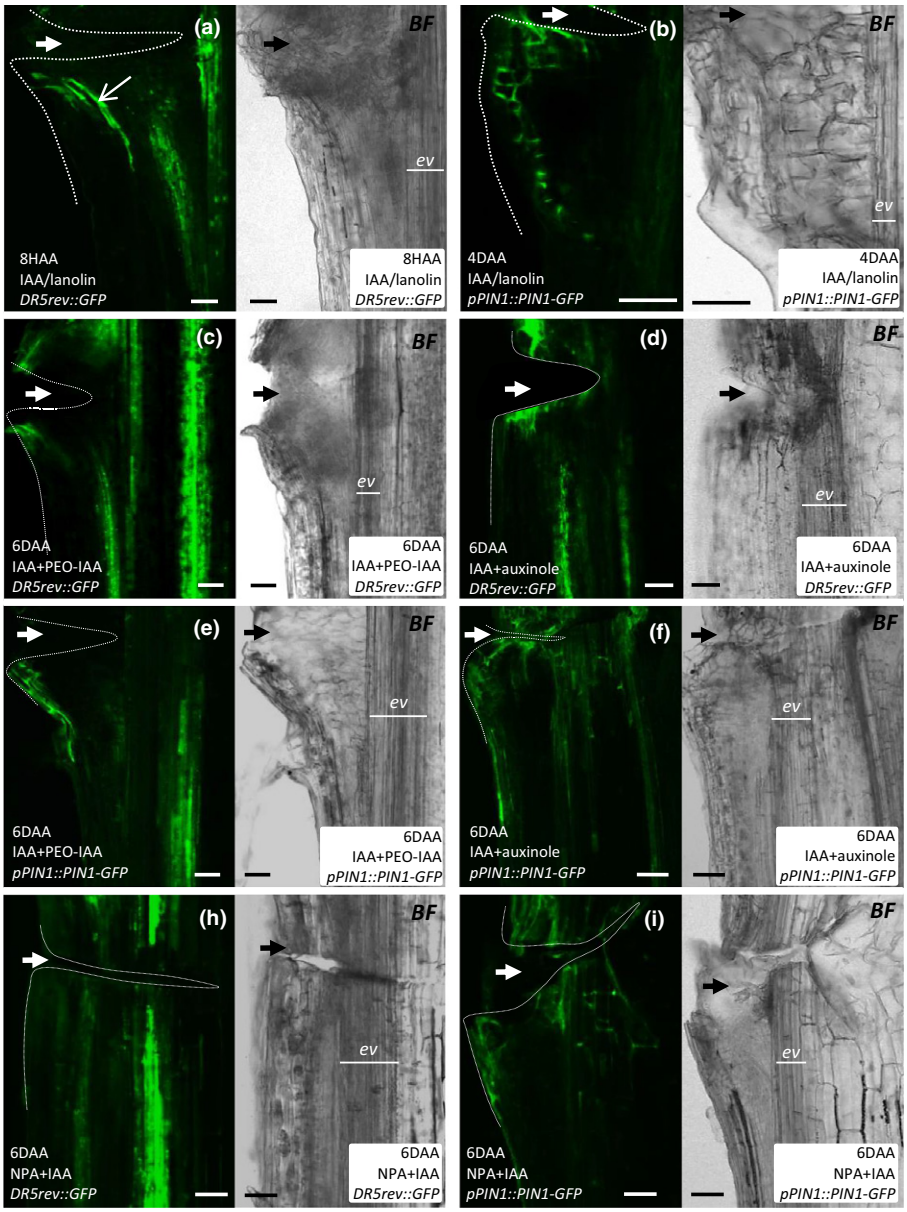

Fig. 3 Requirement of TIR1/AFB auxin perception and PIN-mediated auxin transport in auxin canalization induced by local auxin application onto Arabidopsis stems. (a–i) Examples of longitudinal sections through *DR5rev::GFP* and *pPIN1::PIN1-GFP* stems obtained after local application of IAA alone or along with PEO-IAA, auxinole or NPA. Each section was imaged in green and bright field channels. Dotted lines indicate the wounded stem regions. Thick arrows (white or black) indicate the approximate location of wounds. Bars, 50 μm. See also Supporting Information Fig. S2.

PIN1 re-localization in the root tip cells occurring in response to a relatively short (4 h) auxin treatment (Sauer *et al.*, 2006; Prat *et al.*, 2018). This phenomenon has an unclear physiological significance but provides a simple assessment of auxin's effect on PIN polarity – one of the key prerequisites of canalization. Notably, it also asseses this effect without any obvious accompanying morphological changes or cell fate re-specification processes occurring during vasculature formation. Normally in this case, the intracellular localization of PIN1 shifts from a predominantly basal position to the inner lateral side of endodermal and pericycle cells. However, we found the roots of *tir1afb2afb3* plants to be much less responsive to auxin in terms of this PIN1 lateralization (Fig. S3a,b), which is consistent with similar, previously published observations in *axr3* and *arf7arf19* mutants (Sauer *et al.*, 2006).

In summary, these observations demonstrate that TIR1/AFB signaling is important for auxin canalization not only under more invasive experimental conditions, such as wounding and local auxin application, but also in an undisturbed, physiological process involving vasculature formation such as leaf venation. The TIR1/AFB signaling may act on auxin-mediated PIN1 repolarization, as suggested by defects in this process in the roots of mutants defective in this auxin signaling pathway.

Discussion

The vascular tissue network crucially aids plants to thrive in almost all land habitats. The mechanism of its formation is intriguing not only due to the importance of vasculature for plant life altogether, but also due to its reiterative nature and developmental flexibility (it can be induced in many contexts, such as during generation of nascent organs or regeneration after wounding). These properties of vasculature formation are explained by a self-organizing nature of auxin canalization –

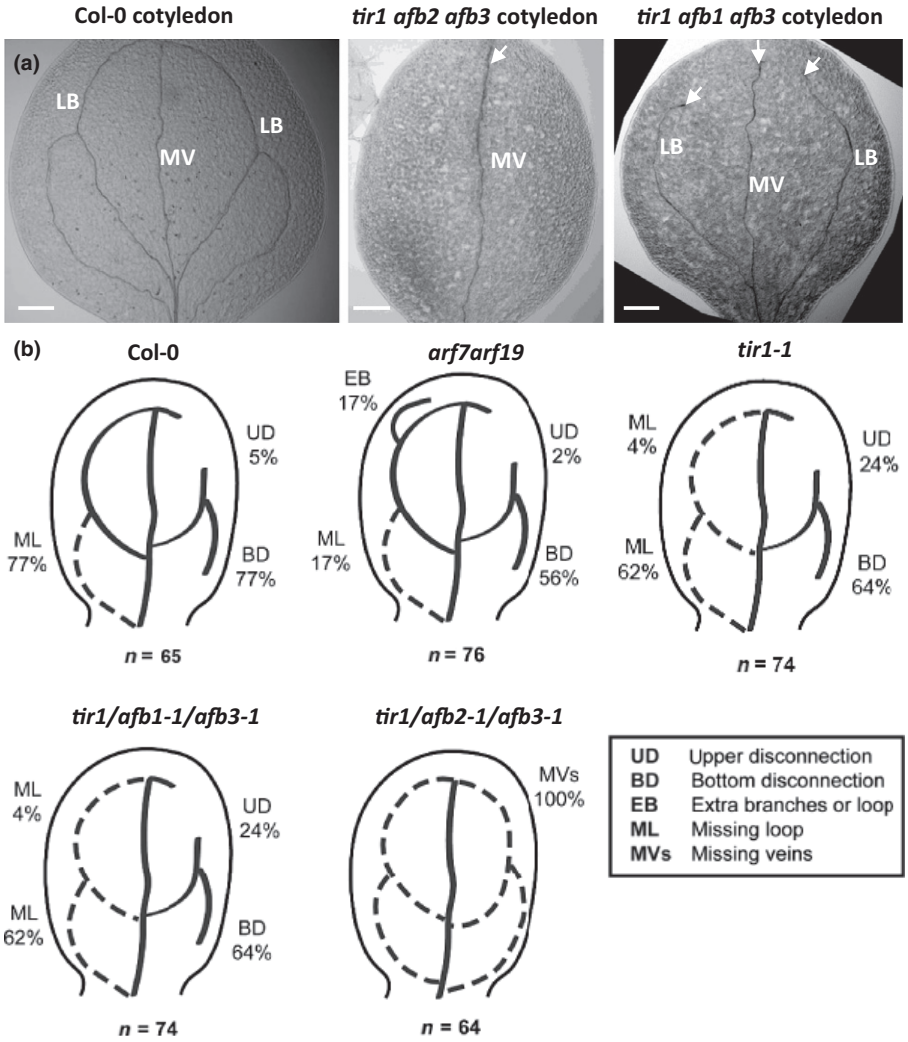

Fig. 4 Cotyledon venation in TIR1/AFB mutants of Arabidopsis. (a) Vasculature defects in Col-0, *tir1afb2afb3* and *tir1afb1afb3* cotyledons. Arrowheads highlight vasculature defects of the lateral branches (LB) and the middle vein (MV). (b) Schemes demonstrating the types and frequencies of venation abnormalities observed. Bars, 200 μm (a). See also Supporting Information Figs S3 and S4.

an organized establishment of auxin transport channels from localized auxin sources. The most evident manifestation of auxin canalization can be observed in classical experiments involving the induction of a canalized auxin flow away from the site of its local application (Sachs, 1975, 1981; Berleth & Sachs, 2001; Sauer *et al.*, 2006; Balla *et al.*, 2011; Sawchuk & Scarpella, 2013; Bennett *et al.*, 2014; Adamowski & Friml, 2015; Cieslak *et al.*, 2015; Mazur *et al.*, 2016). This process is known to involve intracellular polarization of PIN auxin transporters, which is coordinated between individual vasculature progenitors in a way that ultimately generates auxin-transporting channels. Details of the molecular and cell biological mechanisms of this coordinated polarization are missing, however. The classical canalization hypothesis proposes the existence of a positive feedback interaction between auxin perception and the regulation of its intercellular transport direction as determined by the cellular PIN polarities (Vieten *et al.*, 2005; Adamowski & Friml, 2015).

In the past, verification of this idea was difficult because of the limitations of transgenesis in the species where local auxin application experiments were possible. In the present study, we demonstrate that the classical methodology can be successfully applied to the classical genetic model *A. thaliana* with the available large collection of mutants and marker lines. The local auxin application experimental setup has several significant advantages over that previously used to study canalization, such as vasculature regeneration after wounding, as it allows us to: exclude the potential confounding factors associated with stem wounding (because the induction of auxin canalization is achieved by auxin application per se); control the dosage of the inductive stimulus (auxin concentration and duration of its supplementation); and test the inductive potential of various auxin analogs and/or complement the induction of auxin canalization with the effects of other bioactive compounds (e.g. inhibitors).

In addition, we show that auxin canalization under the improved experimental setup depends strictly on PIN1-mediated transport and TIR1/AFB signaling, providing a necessary demonstration of their presumed involvement. The fact that TIR1/AFB signaling is also required for proper progression of auxin canalization-related processes under more physiological conditions, such as vasculature regeneration after wounding, leaf venation and PIN1 lateralization in the root, suggests that the results derived

from the proposed methodology are likely to be not idiosyncratic but of general relevance.

That being said, it would be interesting to test if other cases of vasculature development, such as those occurring during graft transplantation (Melnyk *et al.*, 2015) and organ regeneration from cell culture (Kareem *et al.*, 2015), share this requirement. Furthermore, our experimental system may be used to characterize the role of those auxin signaling components, which have been reported to be important for leaf venation (Donner *et al.*, 2009), under simpler and more controllable auxin canalization conditions.

At the same time, the suggested methodology has certain limitations. In particular, it provides no dynamic, live information, as the samples, due to their thickness and opacity, need to be mechanically sectioned to allow microscopy. For the same reason, it is not trivial to characterize the complete 3D distribution of vasculature and fluorescent reporters, although a more refined method of sectioning compared to that used in this research should alleviate this restriction.

With the present work, we hope to re-ignite the classical studies of auxin canalization using modern transgenesis and imaging techniques. In particular, hypotheses on the interaction between auxin perception and its polar transport could be tested via local auxin application in particular mutants. For example, various cellular processes such as endocytosis protein recycling or degradation may be genetically and pharmacologically manipulated to probe their role in auxin canalization (Wabnik *et al.*, 2010; Grones *et al.*, 2015). Although not perfect, we think that the suggested methodology would help towards the understanding of how individual plant cells communicate with one another to achieve coordinated tissue polarization and how the auxin-transporting channels activate the downstream developmental programs of vasculature differentiation.

Acknowledgements

We thank Mark Estelle, José M. Alonso and the Arabidopsis Stock Centre for providing seeds. We acknowledge the core facility CELLIM of CEITEC supported by the MEYS CR (LM2015062 Czech-BioImaging) and Plant Sciences Core Facility of CEITEC Masaryk University for help in generating essential data. This project received funding from the European Research Council (ERC) under the European Union's Horizon 2020 research and innovation program (grant agreement no. 742985) and the Czech Science Foundation GAČR (GA13-40637S and GA18-26981S) to JF. JH is the recipient of a DOC Fellowship of the Austrian Academy of Sciences at the Institute of Science and Technology. The authors declare no competing interests.

Author contributions

EM, IK, JH and JF designed and conducted experiments and analyzed the data. EM and JF wrote the manuscript, with the assistance of IK.

ORCID

Jiří Friml https://orcid.org/0000-0002-8302-7596
Jakub Hajný https://orcid.org/0000-0003-2140-7195
Ivan Kulik https://orcid.org/0000-0001-9033-1839
Ewa Mazur https://orcid.org/0000-0003-0252-1427

References

Adamowski M, Friml J. 2015. PIN-dependent auxin transport: action, regulation and evolution. *The Plant Cell* **27**: 20–32.

Balla J, Kalousek P, Reinohl V, Friml J, Prochazka S. 2011. Competitive canalization of PIN-dependent auxin flow from axillary buds controls pea bud outgrowth. *The Plant Journal* **65**: 571–577.

Benkova E, Michniewicz M, Sauer M, Teichmann T, Seifertova D, Jürgens G, Friml J. 2003. Local, efflux-dependent auxin gradients as a common module for plant organ formation. *Cell* **115**: 591–602.

Bennett T, Hines G, Leyser O. 2014. Canalization: what the flux? *Trends in Genetics* **30**: 41–48.

Berleth T, Mattsson J, Hardtke CS. 2000. Vascular continuity and auxin signals. *Trends in Plant Science* **5**: 387–393.

Berleth T, Sachs T. 2001. Plant morphogenesis: long-distance coordination and local patterning. *Current Opinion in Plant Biology* **4**: 57–62.

Bhatia N, Bozorg B, Larsson A, Ohno C, Jönsson H, Heisler MG. 2016. Auxin acts through MONOPTEROS to regulate plant cell polarity and pattern phyllotaxis. *Current Biology* **26**: 3202–3208.

Cano-Delgado A, Lee JY, Demura T. 2010. Regulatory mechanisms for specification and patterning of plant vascular tissues. *Annual Review of Cell Developmental Biology* **26**: 605–637.

Cieslak M, Runions A, Prusinkiewicz P. 2015. Auxin-driven patterning with unidirectional fluxes. *Journal of Experimental Botany* **66**: 5083–5102.

Dettmer J, Elo A, Helariutta Y. 2009. Hormone interactions during vascular development. *Plant Molecular Biology* **69**: 347–360.

Dharmasiri N, Estelle M. 2004. Auxin signaling and regulated protein degradation. *Trends in Plant Science* **9**: 302–308.

Donner TJ, Sherr I, Scarpella E. 2009. Regulation of preprocambial cell state acquisition by auxin signaling in *Arabidopsis* leaves. *Development* **136**: 3235–3246.

Fendrych M, Leung J, Friml J. 2016. TIR1/AFB-Aux/IAA auxin perception mediates rapid cell wall acidification and growth of Arabidopsis hypocotyls. *eLife* **5**: e19048.

Friml J, Vieten A, Sauer M, Weijers D, Schwarz H, Hamann T, Offringa R, Jürgens G. 2003. Efflux-dependent auxin gradients establish the apical–basal axis of *Arabidopsis*. *Nature* **426**: 147–153.

Grones P, Chen X, Simon S, Kaufmann WA, De Rycke R, Nodzynski T, Zazimalova E, Friml J. 2015. Auxin-binding pocket of ABP1 is crucial for its gain-of-function cellular and developmental roles. *Journal of Experimental Botany* **66**: 5055–5065.

Hayashi KI. 2012. The interaction and integration of auxin signaling components. *Plant Cell Physiology* **53**: 965–975.

Hayashi KI, Neve J, Hirose M, Kuboki A, Shimada Y, Kepinski S, Nozaki H. 2012. Rational design of an auxin antagonist of the SCF^{TIR1} auxin receptor complex. *ACS Chemical Biology* **7**: 590–598.

Heisler MG, Ohno C, Das P, Sieber P, Reddy GV, Long JA, Meyerowitz EM. 2005. Patterns of auxin transport and gene expression during primordium development revealed by live imaging of the *Arabidopsis* inflorescence meristem. *Current Biology* **15**: 1899–1911.

Kareem A, Durgaprasad K, Sugimoto K, Du Y, Pulianmackal AJ, Trivedi ZB, Abhayadev PV, Pinon V, Meyerowitz EM, Scheres B *et al.* 2015. *PLETHORA* genes control regeneration by a two-step mechanism. *Current Biology* **25**: 1017–1030.

Knox K, Grierson CS, Leyser O. 2003. *AXR3* and *SHY2* interact to regulate root hair development. *Development* **130**: 5769–5777.

Lavy M, Estelle M. 2016. Mechanisms of auxin signaling. *Development* **143**: 3226–3229.

Lavy M, Prigge MJ, Tao S, Shain S, Kuo A, Kirchsteiger K, Estelle M. 2016. Constitutive auxin response in *Physcomistrella* reveals complex interactions between Aux/IAA and ARF proteins. *eLife* **5**: e13325.

Mazur E, Benkova E, Friml J. 2016. Vascular cambium regeneration and vessel formation in wounded inflorescence stems of Arabidopsis. *Scientific Reports* **6**: e33754.

Mazur E, Kurczyńska EU, Friml J. 2014. Cellular events during interfascicular cambium ontogenesis in inflorescence stems of *Arabidopsis*. *Protoplasma* **251**: 1125–1139.

Melnyk CW, Schuster C, Leyser O, Meyerowitz EM. 2015. A developmental framework for graft formation and vascular reconnection in *Arabidopsis thaliana*. *Current Biology* **25**: 1306–1318.

Okushima Y, Overvoorde PJ, Arima K, Alonso JM, Chan A, Chang C, Ecker JR, Hughes B, Lui A, Nguyen D *et al.* 2005. Functional genomic analysis of the *AUXIN RESPONSE FACTOR* gene family members in *Arabidopsis thaliana*: unique and overlapping functions of *ARF7* and *ARF19*. *The Plant Cell* **17**: 444–463.

Prat T, Hajny J, Grunewald W, Vasileva M, Molnar G, Tejos R, Schmid M, Sauer M, Friml J. 2018. *WRKY23* is a component of the transcriptional network mediating auxin feedback on PIN polarity. *PLoS Genetics* **14**: e1007177.

Rakusova H, Abbas M, Han H, Song S, Robert HS, Friml J. 2016. Termination of shoot gravitropic responses by auxin feedback on PIN3 polarity. *Current Biology* **26**: 3026–3032.

Raven JA. 1975. Transport of indoleacetic acid in plant cells in relation to pH and electrical potential gradients and its significance for polar IAA transport. *New Phytologist* **74**: 163–172.

Robert HS, Grones P, Stepanova AN, Robles LM, Lokerse AS, Alonso J, Weijers D, Friml J. 2013. Local auxin sources orient the apical–basal axis in Arabidopsis embryos. *Current Biology* **23**: 2506–2512.

Sachs T. 1975. The induction of transport channels by auxin. *Planta* **127**: 201–206.

Sachs T. 1981. The control of the patterned differentiation of vascular tissues. *Advances in Botanical Research* **9**: 151–262.

Sauer M, Balla J, Luschnig C, Wiśniewska J, Reinöhl V, Friml J, Benkova E. 2006. Canalization of auxin flow by Aux/IAA-ARF-dependent feedback regulation of PIN polarity. *Genes Development* **20**: 2902–2911.

Sawchuk MG, Scarpella E. 2013. Polarity, continuity, and alignment in plant vascular strands. *Journal of Integrative Plant Biology* **55**: 824–834.

Scarpella E, Marcos D, Friml J, Berleth T. 2006. Control of leaf vascular patterning by polar auxin transport. *Genes Development* **20**: 1015–1027.

Tuominen H, Puech L, Regan S, Fink S, Olsson O, Sundberg B. 2000. Cambial-region-specific expression of *the Agrobacterium iaa* genes in transgenic aspen visualized by a linked *uidA* reporter gene. *Plant Physiology* **123**: 531–542.

Uggla C, Mellerowicz EJ, Sundberg B. 1998. Indole-3-acetic acid controls cambial growth in Scots pine by positional signaling. *Plant Physiology* **117**: 113–121.

Uggla C, Moritz T, Sandberg G, Sundberg B. 1996. Auxin as a positional signal in pattern formation in plants. *Proceedings of the National Academy of Sciences, USA* **93**: 9282–9286.

Vieten A, Vanneste S, Wiśniewska J, Benkova E, Benjamins R, Beeckman T, Luschnig C, Friml J. 2005. Functional redundancy of PIN1 proteins is accompanied by auxin dependent cross-regulation of PIN expression. *Development* **132**: 4521–4531.

Wabnik K, Kleine-Vehn J, Balla J, Sauer M, Naramoto S, Reinöhl V, Merks RM, Govaerts W, Friml J. 2010. Emergence of tissue polarization from synergy of intracellular and extracellular auxin signaling. *Molecular Systems Biology* **6**: 447.

Wenzel CI, Schuetz M, Yu Q, Mattsson J. 2007. Dynamics of *MONOPTEROS* and PIN-FORMED1 expression during leaf vein pattern formation in *Arabidopsis thaliana*. *The Plant Journal* **49**: 387–398.

Zhang J, Nodzynski T, Pencik A, Rolcik J, Friml J. 2010. PIN phosphorylation is sufficient to mediate polarity and direct auxin transport. *Proceedings of the National Academy of Sciences, USA* **12**: 918–922.

Supporting Information

Additional Supporting Information may be found online in the Supporting Information section at the end of the article.

Fig. S1 Defects in vasculature regeneration in wounded *HS::axr3-1* Arabidopsis mutant.

Fig. S2 *DR5rev::GFP* and *pPIN::PIN1-GFP* fluorescence distribution at additional time points after local compound application.

Fig. S3 PIN1 lateralization in the roots of *Col-0*, *HS::axr3-1*, *arf7arf19* and *tir1afb2afb3* genotypes in response to NAA treatment.

Fig. S4 Abnormal venation in primary leaf of *tir1afb2afb3* Arabidopsis mutant.

Please note: Wiley Blackwell are not responsible for the content or functionality of any Supporting Information supplied by the authors. Any queries (other than missing material) should be directed to the *New Phytologist* Central Office.

Article

Current Biology

Salicylic Acid Targets Protein Phosphatase 2A to Attenuate Growth in Plants

Graphical Abstract

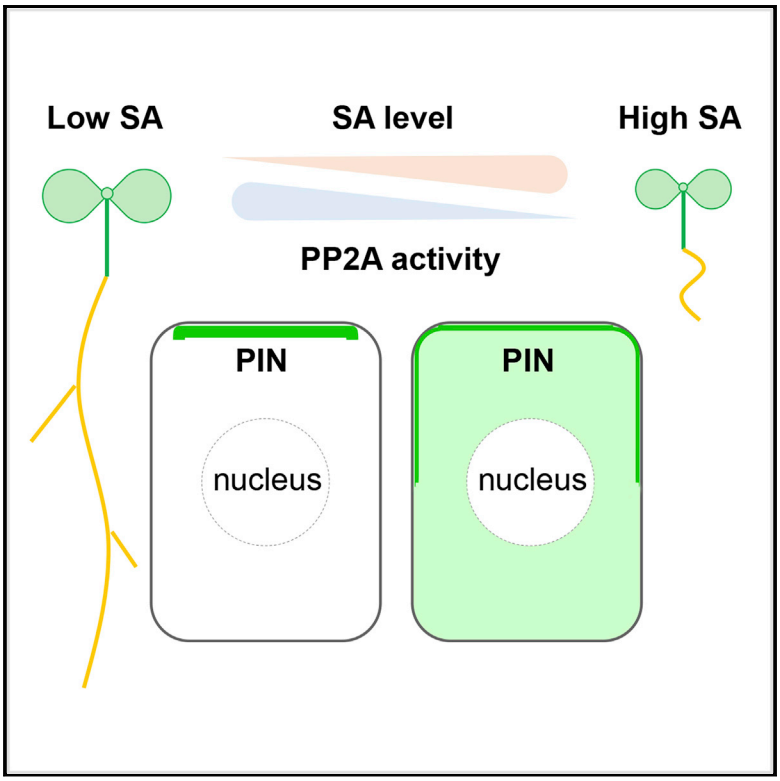

Highlights

- SA modulates root development independently of NPR1-mediated canonical signaling
- SA attenuates growth through crosstalk with the auxin transport network
- SA upregulates the phosphorylation status of PIN auxin efflux carriers through PP2A
- SA directly targets A subunits of PP2A, inhibiting the activity of the complex

Authors

Shutang Tan, Melinda Abas, Inge Verstraeten, ..., Ondřej Novák, Jiří Pospíšil, Jiří Friml

Correspondence

jiri.friml@ist.ac.at

In Brief

Besides the canonical role in immunity, the defense hormone salicylic acid also shapes plant growth and development. Tan et al. show that salicylic acid regulates *Arabidopsis* growth through directly binding to A subunits of the PP2A enzyme and thereby modulating its activity.

Tan et al., 2020, Current Biology *30*, 381–395
February 3, 2020
https://doi.org/10.1016/j.cub.2019.11.058

CellPress

Current Biology
Article

Salicylic Acid Targets Protein Phosphatase 2A to Attenuate Growth in Plants

Shutang Tan,[1] Melinda Abas,[1,2] Inge Verstraeten,[1] Matouš Glanc,[1,3] Gergely Molnár,[1,2] Jakub Hajný,[1,4] Pavel Lasák,[4] Ivan Petřík,[4] Eugenia Russinova,[6,7] Jan Petrášek,[3,8] Ondřej Novák,[4] Jiří Pospíšil,[4,5] and Jiří Friml[1,9,*]
[1]Institute of Science and Technology Austria (IST Austria), Am Campus 1, 3400 Klosterneuburg, Austria
[2]Department of Applied Genetics and Cell Biology, University of Natural Resources and Life Sciences (BOKU), Muthgasse 18, 1190 Vienna, Austria
[3]Department of Experimental Plant Biology, Faculty of Science, Charles University, Viničná 5, 128 44 Prague 2, Czech Republic
[4]Laboratory of Growth Regulators, The Czech Academy of Sciences, Institute of Experimental Botany & Palacký University, Faculty of Science, Šlechtitelů 27, 783 71 Olomouc, Czech Republic
[5]Department of Organic Chemistry, Faculty of Science, Palacký University, tř. 17. listopadu 1192/12, CZ-771 46 Olomouc, Czech Republic
[6]Department of Plant Biotechnology and Bioinformatics, Ghent University, 9052 Ghent, Belgium
[7]Center for Plant Systems Biology, VIB, 9052 Ghent, Belgium
[8]Institute of Experimental Botany, The Czech Academy of Sciences, Rozvojová 263, 165 02 Prague 6, Czech Republic
[9]Lead Contact
*Correspondence: jiri.friml@ist.ac.at
https://doi.org/10.1016/j.cub.2019.11.058

SUMMARY

Plants, like other multicellular organisms, survive through a delicate balance between growth and defense against pathogens. Salicylic acid (SA) is a major defense signal in plants, and the perception mechanism as well as downstream signaling activating the immune response are known. Here, we identify a parallel SA signaling that mediates growth attenuation. SA directly binds to A subunits of protein phosphatase 2A (PP2A), inhibiting activity of this complex. Among PP2A targets, the PIN2 auxin transporter is hyperphosphorylated in response to SA, leading to changed activity of this important growth regulator. Accordingly, auxin transport and auxin-mediated root development, including growth, gravitropic response, and lateral root organogenesis, are inhibited. This study reveals how SA, besides activating immunity, concomitantly attenuates growth through crosstalk with the auxin distribution network. Further analysis of this dual role of SA and characterization of additional SA-regulated PP2A targets will provide further insights into mechanisms maintaining a balance between growth and defense.

INTRODUCTION

Life of multicellular organisms is a permanent trade-off to allocate resources between growth and defense against pathogens. Salicylic acid (SA) is a classical plant hormone traditionally connected with plant immunity, and its levels increase in response to pathogen attack [1]. SA functions as an endogenous signal mediating local and systemic defense responses against pathogens by upregulating the production of pathogenesis-related (PR) proteins. The best characterized components of the SA immunity pathway are the NPR (NONEXPRESSOR OF PR GENES) proteins that include four close isoforms, NPR1–NPR4 [2–4]. Following increase in SA levels, NPR1 translocates from cytoplasm into nucleus [5–7], thereby allowing binding to the downstream transcription factors and regulation of the expression of downstream genes [8]. NPR1, together with NPR3/NPR4, were shown to be bona fide SA receptors for the immune pathway [7, 9, 10]. NPR1 functions as a transcriptional activator, whereas NPR3 and NPR4 are transcriptional repressors, all working independently and harmoniously to regulate the expression of downstream genes [7].

Much less understood is the role of SA beyond plant immunity, in particular in modulating plant growth and development. SA has been implicated in the regulation of photosynthesis, respiration, flowering, senescence, seed germination, and growth. Nevertheless, whether SA signaling for these functions depends on the NPR-mediated pathway or other, so far molecularly uncharacterized mechanism(s) remains unclear [8, 11–15]. Biochemical approaches have identified numerous potential SA binding proteins (SABPs), but their potential roles in SA physiological functions remain unclear [16–19].

SA, similarly to other endogenous signals in plants, executes its effect in concert with other plant hormones. In particular, the SA-auxin signaling crosstalk has been proposed to be important for SA roles in balancing plant defense and development [15]. This notion was strengthened by the observation that SA affects the constitutive subcellular dynamics of PIN (PIN FORMED) auxin transporters [14, 20], which are important regulators of many developmental processes [21]. Nonetheless, the physiological relevance of this SA regulation or the underlying signaling mechanism remains elusive.

Here, we demonstrate an alternative SA signaling mechanism, by which SA, in addition to activating plant immunity, attenuates root growth through regulating PIN-dependent auxin distribution network.

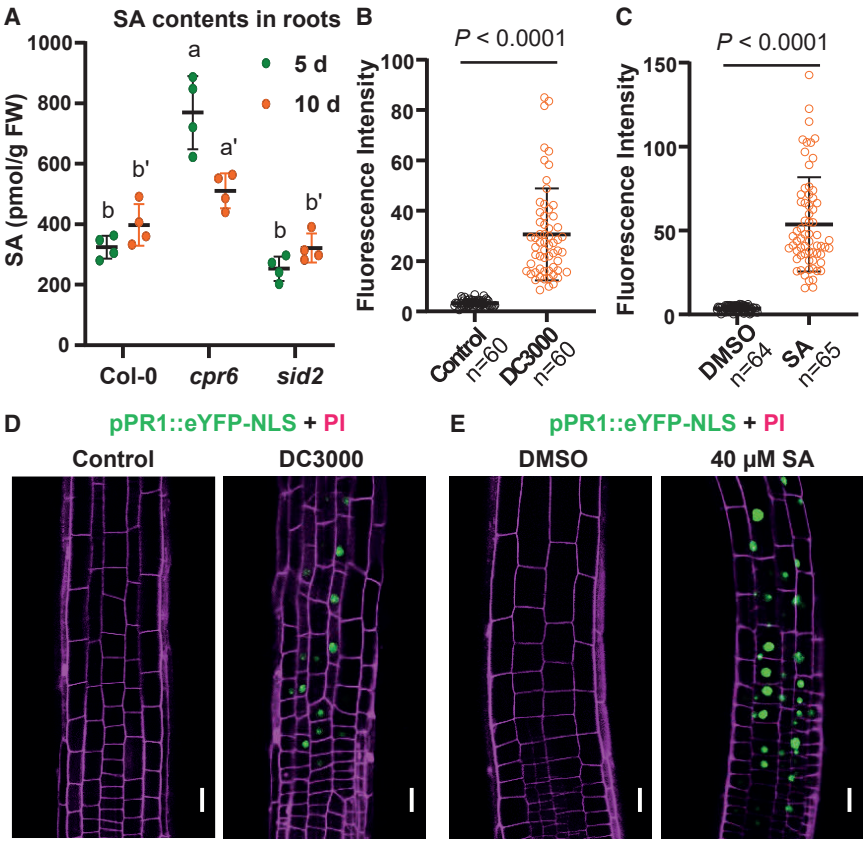

Figure 1. Pathogen-Induced SA Response in Roots, Revealed by the *pPR1::eYFP-NLS* Reporter

(A) SA contents in the roots of 5- or 10-day-old seedlings of Col-0, *cpr6*, and *sid2* (*sid2-3*) measured by LC/MS-MS. n = 4 replicates, with multiple seedlings for each. Dots represent individual values, and lines indicate mean ± SD. Different letters represent significant difference; $p < 0.05$; by one-way ANOVA with a Tukey multiple comparison test.

(B–E) Induced *pPR1::eYFP-NLS* expression by *P. syringae* DC3000 (B and D) or SA (C and E) in roots.

(B and D) 5-day-old *pPR1::eYFP-NLS* seedlings were treated with *P. syringae* DC3000 (optical density 600 [OD_{600}] = 0.01, ~5 × 10^6 colony-forming units [CFUs]/mL) or with resuspension buffer (control) for 48 h and were then imaged by confocal laser scanning microscope (CLSM).

(C and E) For SA treatment, 5-day-old *pPR1::eYFP-NLS* seedlings were transferred to plates with DMSO or 40 μM SA for 24 h and were then imaged by CLSM. Scale bars, 10 μm. For quantification, the average GFP florescence of 5–10 representative cells from 10 seedlings for each treatment was measured by Fiji. The data points were shown as dot plots. Dots represent individual values, and lines indicate mean ± SD. p values were calculated by a two-tailed t test.

See also Figure S1.

RESULTS

SA Regulates Root Growth Independently of Canonical NPR Receptors

The majority of SA physiology studies have focused on adult-stage shoots and so far it remains unclear whether there are significant levels of SA in the root. Therefore, we examined the SA contents by liquid chromatography-tandem mass spectrometry (LC-MS/MS) first. SA production is typically highly elevated after pathogen attack [22], and thus, the basal SA levels in the roots were relatively low but detectable (Figure 1A). There was a small decrease in the SA-biosynthesis-deficient mutant, *sid2-3* [1], and a corresponding increase in the SA overproduction mutant, *cpr6* [23]. Moreover, using *pPR1::eYFP-NLS* reporter line for the NPR1 pathway [24], we detected an induced *PR1* expression in both shoots (Figures S1A–S1D) and roots (Figures 1B–1E) following treatment with either a plant pathogen, *Pseudomonas syringe* DC3000 (Figures 1B and 1D), or SA (Figures 1C and 1E), confirming that pathogen- or SA-mediated activation of NPR1 pathway occurs also in roots.

Given detectable levels of SA in roots and previous indications about a physiological role of SA in roots [14, 25], we examined the effect of exogenously applied SA on root growth. Compared to the control conditions, seedlings growing on 20 or 40 μM SA exhibited shorter (Figures 2A and 2B) and partially agravitropic roots (Figures 2C–2H), as well as fewer lateral roots (Figure 2I). Two inactive SA isomers, 3-hydroxybenzoic acid (3-OH-BA) and 4-hydroxybenzoic acid (4-OH-BA) [26], did not show any obvious effects at comparable concentrations (Figures S1E–S1J). These observations show that SA impacts root development at concentrations equal to or below those established in shoots [7] and its activity is specific to its active structure.

Next, we addressed the requirement of the SA receptors, NPR1/NPR3/NPR4, which are well established in the immune response, for the observed root response [2–4, 7, 10]. NPR1 is a central regulator of the canonical immune pathway, and the downstream transcriptional responses are completely blocked by *npr1* deficiency [3]. Unexpectedly, the well-characterized corresponding mutants *npr1*, *npr3,4* double, and *npr1,3,4* triple mutants did not show a decreased sensitivity to SA in terms of root elongation, gravitropic growth, and lateral root formation (Figures 2B–2I and S1K–S1R). It is noteworthy that the *npr1,3,4* triple mutant exhibited even a pronounced SA-hypersensitive phenotype (Figures S1K–S1R), which might come from downregulation of multiple genes involved in auxin biosynthesis, transport, or signaling.

In conclusion, SA regulates multiple aspects of root development by a signaling mechanism not requiring the established NPR receptors.

SA Regulates PIN-Dependent Auxin Transport and PIN2 Phosphorylation

The root phenotypes generated by SA treatment are reminiscent of defective auxin homeostasis because auxin and its distribution have been shown to regulate primary root growth, gravitropic bending, and lateral root formation [21, 27]. To test the

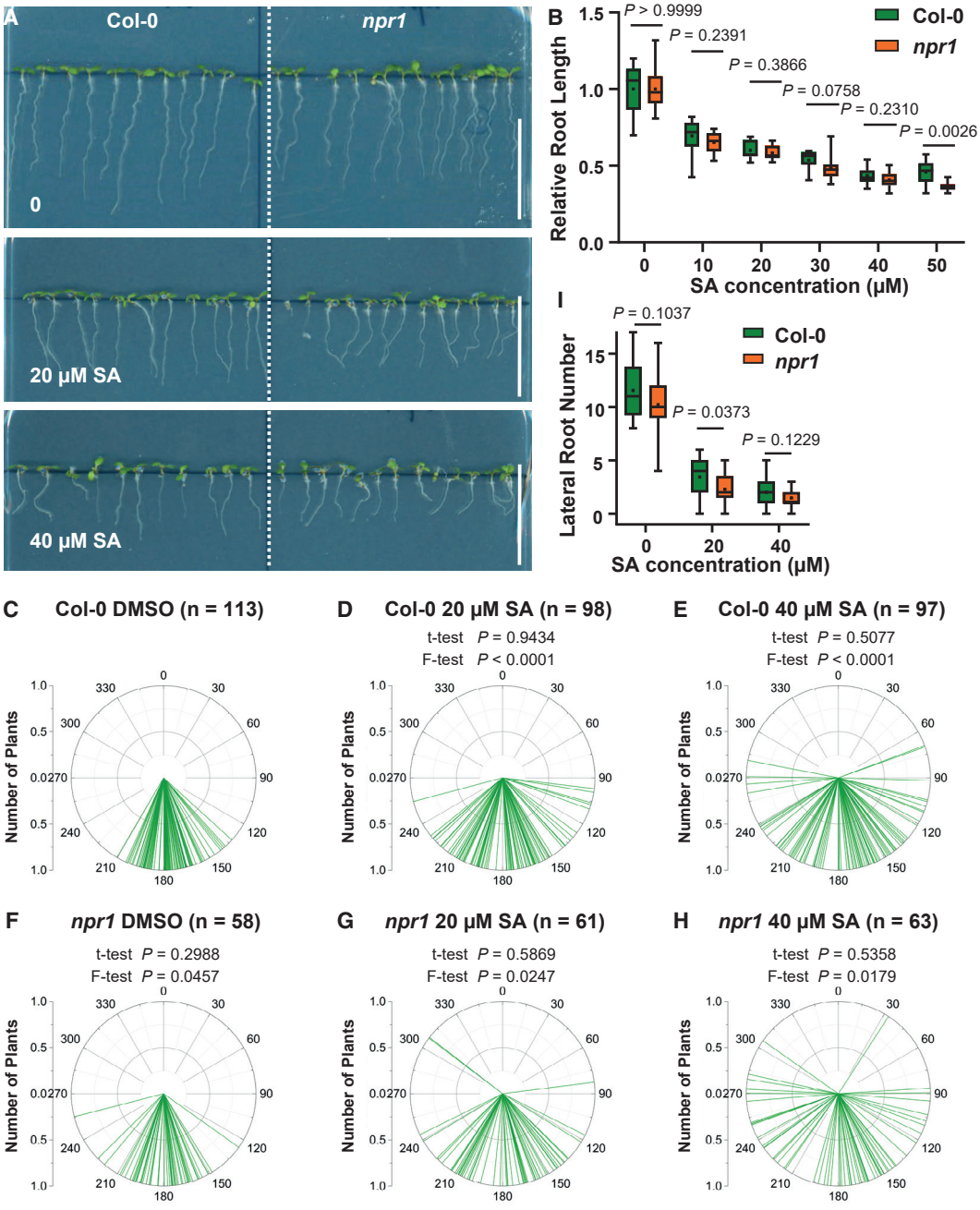

Figure 2. SA Regulates Root Growth and Development in a *NPR1*-Independent Manner

(A) Representative images showing the morphological changes of Col-0 and *npr1* under SA treatment. DMSO is the solvent control. Scale bars, 2 cm.

(B) SA inhibited the primary root elongation in a *NPR1*-independent manner. Root length of 7-day-old Col-0 and *npr1* seedlings grown on MS plates with different concentrations of SA was measured. Relative length was calculated by dividing the values with the root length at SA = 0. Boxplots show the first and third quartiles, with whiskers indicating maximum and minimum, the line for median, and the black dot for mean. n = 11–28; p values were calculated by a two-tailed t test for indicated pairs of Col-0 and *npr1* at a certain concentration of SA.

(C–H) SA interfered with root gravitropism independently of *NPR1*. Root tip angles of 7-day-old Col-0 (C–E) and *npr1* (F–H) seedlings were measured and shown as polar bar charts. Two-tailed t tests were performed to indicate the difference of mean value, and F-tests indicate the difference of variances. For Col-0, SA treatments were compared with the DMSO control, and the *npr1* groups were compared with Col-0 under the same SA treatment, respectively.

(I) Inhibition of lateral root formation by SA does not involve *NPR1*. The number of emerged lateral roots for 10-day-old plants was counted. n = 20–25. p values were calculated by a two-tailed t test.

See also Figure S1.

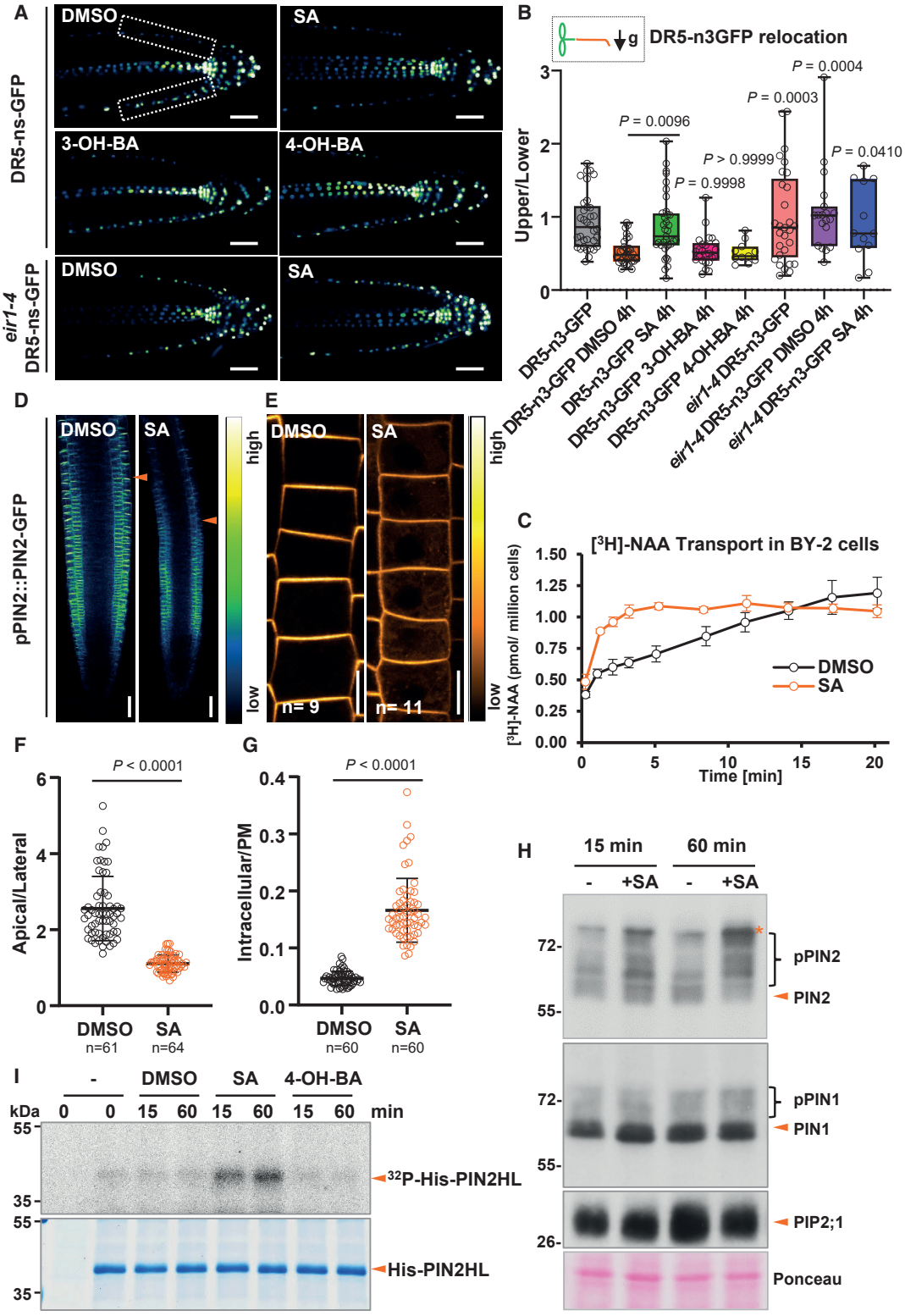

Figure 3. SA Regulates Auxin Transport via Modulating PIN2 Phosphorylation

(A) SA inhibited the relocation of DR5-n3GFP. 5-day-old *DR5v2* and *eir1-4 DR5v2* seedlings were transferred to different plates with DMSO, 40 μM SA, 40 μM 3-OH-BA, or 40 μM 4-OH-BA, respectively, and then turned 90 degrees for gravistimulation. After 4 h, the roots were imaged by CLSM. The GFP channel (DR5-n3GFP) was shown. Scale bars, 10 μm.

(legend continued on next page)

potential effect of SA on auxin response and distribution, we used an auxin-responsive marker DR5-n3GFP (the GFP channel of DR5v2) [28], which monitors auxin response in plant tissues, including the gravity-induced auxin translocation to the lower root side [28]. After 4-h gravistimulation by 90° reorientation, the seedlings treated with SA, unlike the DMSO-treated controls, failed to show a pronounced DR5-n3GFP asymmetry with the stronger signal at the lower root side, in line with the SA-induced gravitropism defect (Figures 3A, 3B, and S2A), as observed before [14]. This suggests that SA interferes with auxin distribution either at the level of transport [21] or local auxin biosynthesis [29]. Recently, SA has been proposed to increase auxin levels in root tips [30]. Nonetheless, this upregulation of iIndole-3-acetic acid (IAA) biosynthesis cannot explain the auxin-related phenotypes described here, such as agravitropic root growth and the reduced lateral root number, because increased auxin levels have rather opposite effects. It is likely that increased IAA biosynthesis after SA treatment is rather the consequence, but not the cause, of the auxin transport regulations by SA, presumably due to a feedback regulatory mechanism.

To test a possible effect of SA on auxin transport, we measured the basipetal (rootward) auxin transport in etiolated hypocotyls, which revealed that SA can inhibit the rootward transport of [^{3}H]-IAA, similar to widely used PIN-dependent auxin transport inhibitors NPA (1-N-naphthylphthalamic acid) and TIBA (2,3,5-triiodobenzoic acid) (Figure S2B). With tobacco BY-2 cultured cells [31], we tested the effect of SA on transport of different auxin analogs, [^{3}H]-NAA and [^{3}H]-2,4-D. SA treatment increased the cellular accumulation of [^{3}H]-NAA (Figure 3C), but not of [^{3}H]-2,4-D or [^{3}H]-BA (Figures S2C and S2D). Despite possible effect on auxin metabolism, this selective effect of SA on accumulation of NAA, which is a good substrate of PIN auxin exporters [32], strongly suggests a regulatory role of SA in PIN-dependent auxin transport. Overall, these observations show that SA, exhibiting distinct activities for different tissues, directly or indirectly regulates auxin transport.

To investigate the mechanism underlying the role of SA in regulating root growth and development, we focus on the root gravitropic phenotype. PIN2 and AUX1 auxin transporters play a prominent role in shootward auxin transport in the root and thus in the auxin redistribution during the gravitropic response [33–37]. Therefore, we analyzed the response of *eir1-4* [36] loss-of-function mutant, which exhibits strongly agravitropic roots. After SA treatment, *eir1-4* showed a slight SA hypersensitivity in primary root elongation but no further enhancement of the gravitropic defect at 40 μM SA (Figures S2E–S2J). These observations suggest that SA acts in the gravitropic response through the auxin efflux carrier PIN2. Using the *eir1-4 DR5-n3-GFP* cross, we could not see gravity-induced DR5-n3-GFP asymmetry and SA treatment had no additional effect (Figures 3A and 3B). Furthermore, we examined the SA effect on the localization of these proteins using *pAUX1::AUX1-YFP* and *pPIN2::PIN2-GFP* marker lines. Whereas we observed no obvious effect of SA treatment on AUX1-YFP except a slight decrease in the overall intensity (Figures S2K–S2M), PIN2-GFP incidence in the plasma membrane of the root epidermis cells upon SA treatment was visibly decreased with higher intracellular signal and less pronounced polar distribution as compared to the control (Figures 3D–3G).

Reversible phosphorylation plays an important role in regulating PIN polarity, subcellular dynamics, and activity. PIN proteins can be phosphorylated by multiple kinases, most prominently PID (PINOID)/WAGs (WAVY ROOT GROWTHs), D6PK/D6PKLs, and PAX (PROTEIN KINASE ASSOCIATED WITH BRX), and dephosphorylated by various phosphatases, including protein phosphatase 2A (PP2A), PP1, and PP6 [38–40]. We examined the PIN2 phosphorylation status by western blot. When roots were extracted with a protocol [36, 41] specifically modified to preserve phosphorylation, PIN2 appeared as a smear of bands (Figure 3H). Phosphatase treatment shifted the slower migrating bands toward the faster migrating band at the base of the smear (Figure S3A), indicating that the upper parts of the smear comprise phosphorylated species. We found that

(B) The ratio of fluorescence between the upper side and the lower side was measured, as shown in (A). n = 34, 30, 35, 24, 11, 29, 19, and 12, respectively. p values are calculated by a two-tailed t test, comparing different datasets with the DR5-n3-GFP DMSO control (t = 4 h), as shown with the horizontal line in the case of DR5-n3-GFP SA 4 h.

(C) SA treatment increased the accumulation of [^{3}H]-NAA in tobacco BY-2 cells, suggesting a decrease in auxin export. DMSO and 200 μM SA were added to the cell culture and then the radioactivity inside of cells was measured at indicated time points after the addition of [^{3}H]-NAA to the DMSO- and SA-treated cell cultures. n = 3.

(D–G) SA treatment impaired the polar localization and promoted the internalization of PIN2-GFP in root epidermis (D and E). *pPIN2::PIN2-GFP* seedlings were grown on plates with DMSO and 40 μM SA for 4 days and were then imaged by CLSM. Scale bars, 20 μm (D) and 10 μm (E), respectively. Arrowheads in (D) indicate the beginning of root transition zone.

(F) The intensity ratio of apical/lateral was measured by Fiji to assess PIN2 polarity.

(G) Quantification of the PIN2-GFP intensity ratio of intracellular/PM.

(F and G) Dots represent individual values, and lines indicate mean ± SD. p values are calculated by a two-tailed t test.

(H) SA treatment enhanced the phosphorylation of PIN2. Roots of 7-day seedlings were treated with DMSO or 40 μM SA for 15 min and 60 min and then analyzed by western blot with an anti-PIN2 antibody (upper panel). Phosphorylation of the multiple phosphorylation sites in PIN2 causes slower migrating species. The more highly phosphorylated, the slower the migration. The same membrane was stripped and detected by anti-PIN1 (second panel) and anti-PIP2;1 (third panel) antibodies, sequentially. The molecular weight (MW) of PIN2 and PIN1 is 69 and 67 kDa, respectively. For unknown reasons, PIN2 runs faster than expected, perhaps due to incomplete denaturing when heated only at 50°C. The shifted bands indicate the phosphorylated PIN proteins. Bottom panel: Ponceau staining is shown. Asterisk indicates partial contribution by a non-specific band (see also in Figure 4A).

(I) SA treatment increased the phosphorylation of His-PIN2-HL in plant extracts. Roots of 7-day seedlings were treated with DMSO or 40 μM SA for 15 min and 60 min, respectively, and then were subject to protein extraction. Crude plant extracts were incubated with recombinant His-PIN2-HL for 60 min with ^{32}P-ATP and $MgCl_2$. The first lane was without His-PIN2-HL as negative control. Reaction samples were analyzed by SDS-PAGE and the subsequent autoradiography. Upper panel: autoradiography is shown; lower panel: Coomassie Brilliant Blue (CBB) staining is shown.

See also Figures S2 and S3.

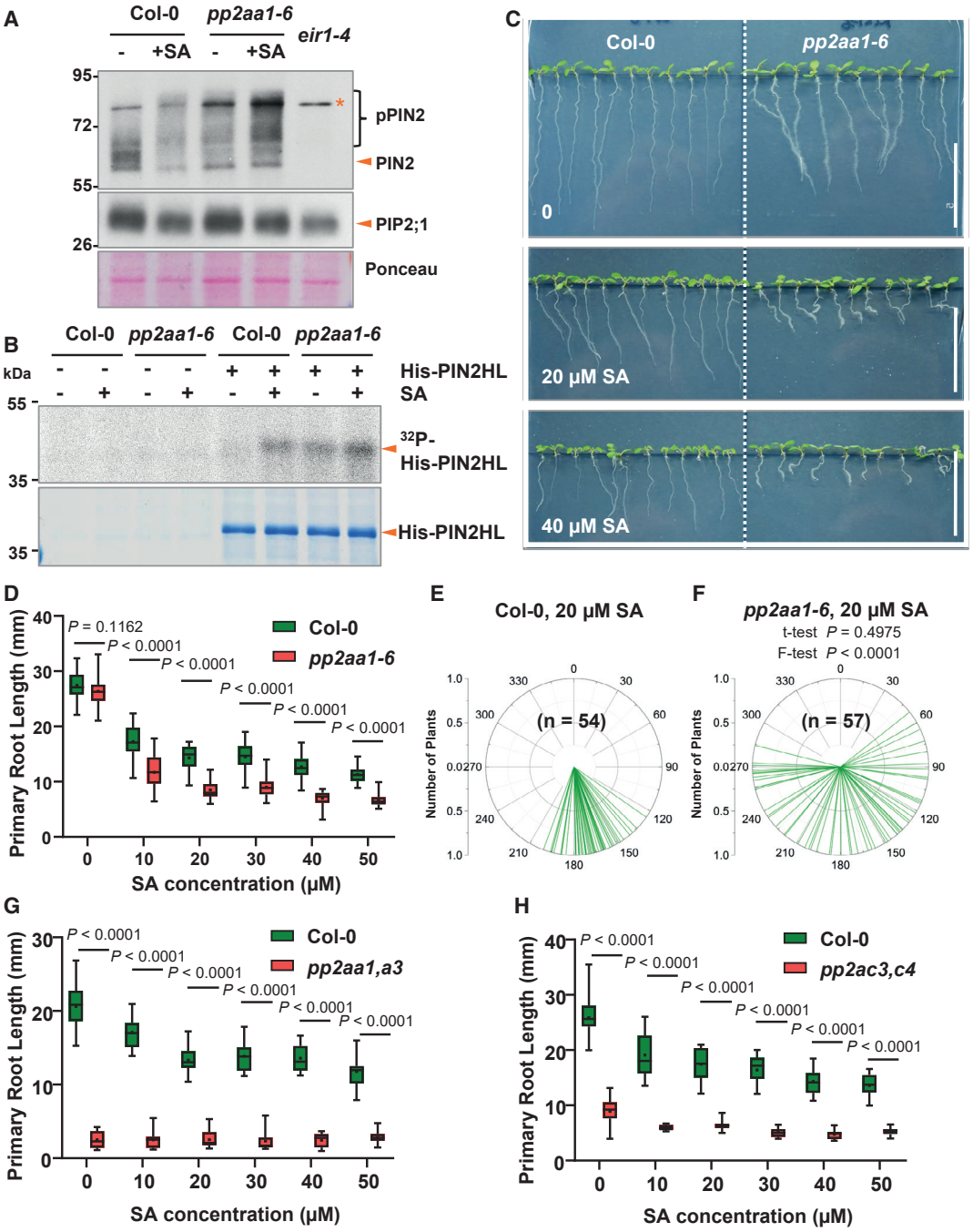

Figure 4. SA Functions through PP2A in Regulating Root Development

(A) SA treatment promoted the phosphorylation of PIN2 in Col-0 to a similar degree as that in *pp2aa1-6*. Roots of 7-day-old Col-0 and *pp2aa1-6* seedlings were treated with DMSO or 40 μM SA for 60 min and were then sampled for protein isolation and western blot. The shifted bands indicate the phosphorylated PIN proteins (upper panel). Asterisk indicates a non-specific band that contributes partially to the signal. The same membrane was stripped and probed with a PIP2;1 antibody to indicate the loading (upper panel). Ponceau staining is shown in the bottom panel.

(B) Phosphorylation with ^{32}P-ATP revealed that SA treatment increased the phosphorylation of His-PIN2-HL in Col-0, whereas this increase was attenuated in *pp2aa1-6*. Upper panel: autoradiography is shown; lower panel: CBB is shown.

(C) Representative images revealing the hypersensitivity of *pp2aa1-6* to SA. Col-0 and *pp2aa1-6* seedlings were grown on plates with SA. Scale bars, 2 cm.

(D) *pp2aa1-6* was hypersensitive to SA in root growth inhibition. Col-0 and *pp2aa1-6* seedlings grew on plates with SA for 7 days and then the primary root length was measured. n = 11–28. p values were calculated by a two-tailed t test for indicated pairs of Col-0 and *pp2aa1-6* at a certain concentration of SA.

(E and F) *pp2aa1-6* was hypersensitive to SA in terms of interfering with root gravitropism. Col-0 (E) and *pp2aa1-6* (F) seedlings grew on plates containing different concentrations of SA for 7 days, and the root tip angles were measured by ImageJ and shown as polar bar charts. p values were calculated by a two-tailed t test in (E) and (F) and indicate differences of variances by a further F-test in (F).

(legend continued on next page)

SA treatment led to a more pronounced shift of PIN2 protein mobility to slower migrating species than seen in control, indicating an increase in phosphorylation status. This occurred as rapidly as after 15 min and more pronounced after 60 min (Figures 3H and S3A). To confirm the SA effect on the change of PIN2 phosphorylation, we expressed and purified the PIN2 hydrophilic loop with His tag (His-PIN2HL) and incubated it with the protein extract from seedlings treated with SA or the inactive isomers in a ^{32}P-ATP phosphorylation reaction (Figure 3I). There was more phosphorylation of the His-PIN2HL with SA. This confirmed that SA treatment led to an increase in PIN2 phosphorylation level, either through stimulating phosphorylation or suppressing dephosphorylation.

Taken together, the physiological, microscopic, and biochemical observations collectively suggest that SA regulates PIN-dependent auxin transport, presumably by changing the phosphorylation status and thus the cellular localization and the activity of PIN proteins. Such mechanism would explain the observed physiological SA effects on root development.

PP2A Is Required for SA Regulation of PIN2 Phosphorylation and Root Development

To gain insight into the mechanism by which SA modulates PIN phosphorylation and root development, we focused on the potential regulators of PIN phosphorylation. Of those, the A subunit of PP2A (PP2AA1/RCN1, ROOTS CURL IN NPA1), an established regulator of PIN phosphorylation and auxin transport [42, 43], came to our attention, as it also appeared in a high-throughput proteomics study as potentially associated with SA binding [44].

We first tested whether PP2AA1 is involved in SA-induced increase of PIN phosphorylation status. Western blot showed that SA treatment could increase the phosphorylation level of PIN2 in wild-type (WT), whereas in PP2AA1 loss-of-function mutant, *pp2aa1* (also known as *pp2aa1-6 and rcn1-6*), there was already a higher level of PIN2 phosphorylation, consistent with PP2AA1 involvement in PIN2 dephosphorylation (Figures 4A and S3B). This phosphorylation was still increased further by SA treatment (Figure 4A), suggesting that the other PP2AA homologs can play a role in the absence of PP2AA1. Accordingly, the ^{32}P-ATP phosphorylation reaction using purified His-PIN2HL incubated with the protein extracts from SA-treated WT and *pp2aa1* seedlings (Figure 4B) confirmed at least partial PP2AA1 requirement for the SA effect on PIN2 phosphorylation.

In line with this, *pp2aa1* mutants (*pp2aa1-6* and *pp2aa1-1*) roots showed hypersensitivity to SA in terms of primary root growth and gravitropic bending (Figures 4C–4F and S3C–S3I). In addition, SA treatment at higher concentrations (50 μM) often led to a slight swelling in WT root tips, whereas in *pp2aa1*, a much stronger root tip swelling was observed even at a lower SA concentration (20 μM; Figure S3C).

PP2A is a heterotrimeric complex composed of A, B, and C subunits with three homologs for the PP2A A subunits, PP2AA1/RCN1, PP2AA2, and PP2AA3 [45]. Notably, overexpression of *PP2AA1* (*35S::myc-PP2AA1*) alone did not lead to obvious changes in SA sensitivity (Figures S3J–S3L), suggesting importance of the whole heterotrimeric PP2A holoenzyme integrity. Single mutants of *pp2aa2* and *pp2aa3* did not show any visible difference in SA sensitivity compared to WT (Figures S4A–S4C). The double mutant of *pp2aa1 pp2aa2-3* (*pp2aa1,a2*) showed a much stronger response to SA than WT or *pp2aa1/rcn1* single mutant (Figures 4D and S4D). The *pp2aa1,a3* double mutant had severe defects in growth and development with a short primary root already without any treatment (Figures S4E–S4H) [43, 45], which is reminiscent to WT treated by higher concentration of SA, and subsequent SA treatment could not further enhance this phenotype (Figure 4G). Similar results were observed for the *pp2ac3,c4* double mutant of the catalytic C subunits [46]. The roots of *pp2ac3,c4* were short without any treatment, and higher exogenous SA treatment did again not further enhance this phenotype (Figure 4H). The mutant in the regulatory subunit, *fass/tonneau2* (*ton2*), has been reported to show a similar phenotype as *pp2aa1,a3* [46]. However, *fass* [46], the double knockout mutant *pp2aa1-1 pp2aa2-1* [43, 45], and triple *pp2aa1-1 pp2aa2-1 pp2aa3-1* [43, 45] were too sick to perform meaningful SA sensitivity assays. It has been well described that these mutants exhibited severe growth defects, with swelling root morphology [45, 46], which are similar to seedlings treated with SA. Thus, loss-of-function mutants in all PP2A subunits perturbed plant sensitivity to SA in terms of root growth. Importantly, phenotypes of the stronger higher order mutants could be phenocopied by SA treatment. The SA-overproducing *cpr6* mutants show a severe dwarf phenotype [8] and increased SA levels in roots (Figure 1A) but no obvious changes in root development (Figure 5A). On the other hand, the *pp2aa1-6 cpr6* double mutant had shorter roots and increased sensitivity to SA (Figures 5A and 5B) as well as exhibited a much more severe dwarf phenotype than *cpr6* alone (Figures 5C and 5D). This provides a genetic confirmation that PP2A is involved in the SA-mediated developmental regulation.

In summary, these biochemical and genetic analyses suggest that the PP2A complex is involved in SA regulation of PIN (de) phosphorylation and root growth.

SA Inhibits PP2A Activity

To further confirm whether SA is an endogenous regulator of PP2A, we tested the sensitivity of *pp2aa1-1* to a known PP2A inhibitor, cantharidin, that binds the C subunits in both animals and plants [45, 47–49]. When grown on media with cantharidin, WT seedlings exhibited shorter, agravitropic roots and root tip swelling as observed for SA treatment, and notably, *pp2aa1* mutants were hypersensitive to cantharidin (Figures S4I and

(G) The *pp2aa1, a3* double mutant exhibited decreased sensitivity to SA. Col-0 and *pp2aa1, a3* seedlings grew on plates with SA for 7 days and then the primary root length was measured. n = 11–25. p values were calculated by a two-tailed t test for indicated pairs of Col-0 and *pp2aa1, a3* at the given concentration of SA.
(H) The *pp2ac3, c4* double mutant exhibited decreased sensitivity to SA. Col-0 and *pp2ac3, c4* seedlings grew on plates with SA for 7 days and then the primary root length was measured. n = 10–21. p values were calculated by a two-tailed t test for indicated pairs of Col-0 and *pp2ac3, c4* at the given concentration of SA.
See also Figures S3 and S4.

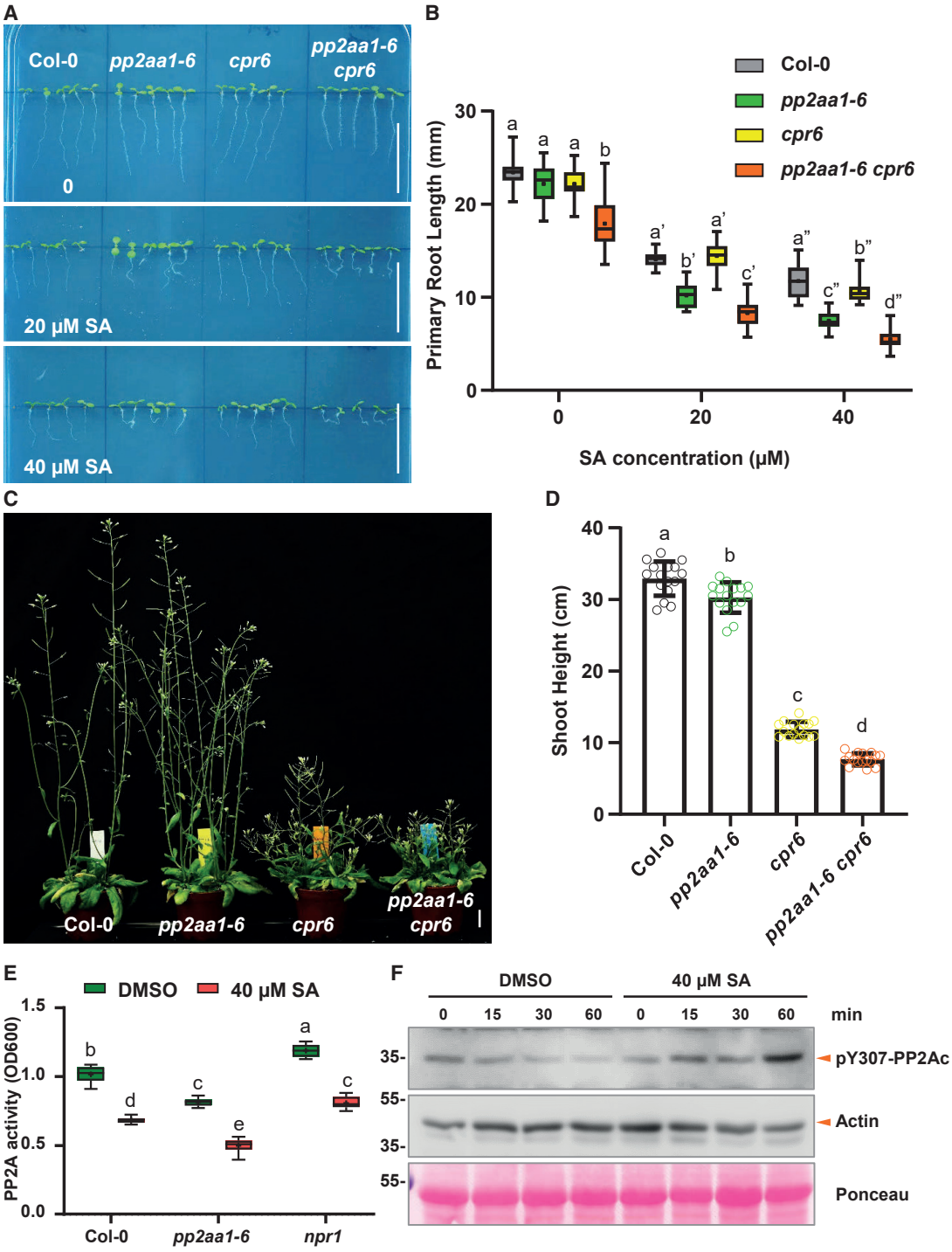

Figure 5. Genetic Analysis of *pp2aa1-6* and *cpr6* Mutations, and SA Inhibits PP2A Activity *In Planta*

(A) Representative images showing the enhanced sensitivity of *pp2aa1-6* to SA. Col-0, *pp2aa1-6*, *cpr6*, and *pp2aa1-6 cpr6* seedlings were grown on plates with different concentrations of SA for 7 days. Scale bars, 2 cm.

(B) The root growth analysis revealed that the *cpr6* mutation decreased the primary root length and increased the SA sensitivity of *pp2aa1-6*. n = 16. Different letters represent significant difference; $p < 0.05$; by one-way ANOVA with a Tukey multiple comparison test.

(C and D) The *pp2aa1-6* mutation enhances the stunted shoot phenotype of *cpr6*. Col-0, *pp2aa1-6*, *cpr6*, and *pp2aa1-6 cpr6* plants were grown for 38 days, and representative plants are shown (C). Scale bar, 2 cm.

(D) The height of plants was measured and shown as dot plots. Dots represent individual values, and lines indicate mean ± SD. n = 16. Different letters represent significant difference; $p < 0.05$; by one-way ANOVA with a Tukey multiple comparison test.

(legend continued on next page)

S4J) as they were to SA. The identical physiological effects of SA to an established PP2A inhibitor and similarities between the SA effects and stronger loss-of-function phenotypes of the PP2A complex indicated that SA may act as an endogenous inhibitor of PP2A.

Therefore, we analyzed PP2A activity in the protein extracts of *Arabidopsis* seedlings using the established colorimetric method with phospho-Ser/Thr peptides as PP2A substrates [50]. This revealed that the *pp2aa1* mutant had lower PP2A activity than WT [48] and that SA treatment decreased PP2A activity in WT (Figure 5E). Notably, the *npr1* mutant defective in an established SA receptor still showed high sensitivity to SA in the PP2A activity assay (Figure 5E). Next, we established an independent method to assess the PP2A activity. In mammalian cells, phosphorylation at Tyr307 (pY307) of the catalytic subunit PP2Ac is used as a measure of PP2A activity and can be detected by a phospho-Tyr307 (pY307)-PP2Ac antibody [51]. Alignment of the five *Arabidopsis* PP2AC subunits with the human and mice homologs indicated that the antigen motif recognized by this antibody is highly conserved across different homologs (Figure S4K), which makes it feasible to use the same antibody to evaluate the PP2A activity *in planta*. The phosphorylation status of PP2ACs, monitored by this method, was robust and stable under control treatments, whereas treating seedlings with SA led to an increased PP2AC phosphorylation (Figure 5F) indicative of decreased PP2A activity.

Taken together, our physiological and biochemical observations show that SA inhibits PP2A activity, indicating that the PP2A complex could be a direct target of SA.

SA Binds to the A Subunits of PP2A

Next, we addressed a mechanism by which SA inhibits PP2A activity. The finding that established SA receptors from the NPR family are not required for this SA effect on root growth and on PP2A activity supported a possibility that SA targets PP2A directly.

To test for a direct SA binding to PP2A, we first used the drug affinity responsive target stability (DARTS) method based on the fact that ligand binding to its protein target typically causes a conformational change, which affects the exposure of protease recognition sites and thus influences protein stability in the presence of the ligand [52]. DARTS using extracts of *pPP2AA1::PP2AA1-GFP* seedlings revealed that SA treatment led to an obvious protection of PP2AA1-GFP against Pronase (mixture of proteases) degradation, but 4-OH-BA did not (Figures 6A, S5A, and S5B). This suggests that SA targets PP2AA1 *in planta*. Notably, although SA concentration as high as 500 μM still showed pronounced protective effects toward PP2AA1-GFP, the 50 μM SA was more effective (Figure 6A). This suggests a more complicated regulatory effect of SA on PP2AA1-GFP stability for the high concentrations.

Differential scanning calorimetry (DSC) is a method to detect thermostability of a protein by measuring the heat release during denaturing [53]. We expressed and purified from *E. coli* His-PP2AA1 (Figures S5C–S5F) and used the recombinant protein for DSC. We detected a denaturing temperature (Tm) of His-PP2AA1 at 48.01°C, but following SA treatment, the Tm shifted to 45.03°C (Figure 6B), suggesting that SA treatment changed PP2AA1 stability, which might be due to conformational changes. A further control with the inactive SA isomer, 4-OH-BA, did not show any effect on PP2AA1 thermostability, confirming this specific activity of SA (Figure S5G). Usually ligand binding stabilizes the target protein [54], but in some well characterized cases, such as receptors for the plant hormone strigolactone, ligand binding caused the destabilization of the protein, which is similar to what we observed for SA and PP2AA1 [55]. Thus, DSC also supports the hypothesis of direct SA binding to PP2AA1.

To further confirm SA binding to PP2AA1 and to measure the binding affinity, we employed the surface plasmon resonance (SPR) method [56]. We first designed a SA analog with a linker, SA-f, which can be immobilized on the SPR sensory chip. A set of SA derivatives have been synthesized with modifications at the meta- and para- positions in the benzoic ring and then we first tested their bioactivity in terms of PIN2-GFP endocytic trafficking as an output of NPR-receptors-independent SA activity [14], as well as the physiological effects on root morphology that we describe here. These tests indicated that modifications at the meta- position did not affect this SA bioactivity (Figure S5H), thus identifying C-10 moiety as being most promising for further modification (Figures S6A, S6B, and S6D–S6F). For the second round, we added a -$(CH_2)_6$-O- linker at the meta-position, SA-1∼3 (Figure S5H), with different groups at the end of the linker to mimic the matrix of sensor chips. SA-2 and SA-3 still kept the activity on PIN2-GFP trafficking (Figures S6C and S7A–S7C) and root development similar to non-modified SA (Figures S6C, S6D, and S7A–S7C). Finally, we synthesized SA-f, with an NH_2- group for immobilization on the SPR sensor chips. Then, we used recombinant His-PP2AA1 and His-PP2AA3 proteins and measured their binding affinity to immobilized SA (Figures S5C–S5F). Indeed, we detected a concentration-dependent binding of His-PP2AA1 to immobilized SA. Plotted with the steady-state binding with different concentrations of the protein, we obtained a K_D of 3.623 μM (Figures 6D and S7D). Performing the same experiment for His-PP2AA3, we also detected binding with an even smaller K_D value of 1.916 μM (Figures 6E and S7E). In a different, single-cycle SPR experimental setup, including 0.1% BSA in the SPR flow to prevent unspecific binding, a similar K_D value (2.374 μM) for PP2AA1 was obtained (Figures S7F and S7G).

(E) SA treatment decreased the total PP2A activity *in planta*. Col-0, *pp2aa1-6*, and *npr1* seedlings were grown on plates containing DMSO or 40 μM SA for 5 days and then sampled for protein isolation and PP2A activity measurement. n = 6. Different letters represent significant difference; $p < 0.05$; by one-way ANOVA with a Tukey multiple comparison test.

(F) SA treatment increased the phosphorylation of the PP2A catalytic subunits (PP2Ac), suggesting the decrease in PP2A activity. 7-day-old Col-0 seedlings were treated with DMSO or 40 μM SA for 0, 15 min, 30 min, and 60 min respectively, and were then collected for protein extraction and the subsequent western blot. A pY307-PP2Ac antibody was used, 1:1,000 (upper panel). The anti-actin blot (medium panel; 1:2,000) and Ponceau staining (bottom panel) indicate the loading amounts.

See also Figure S4.

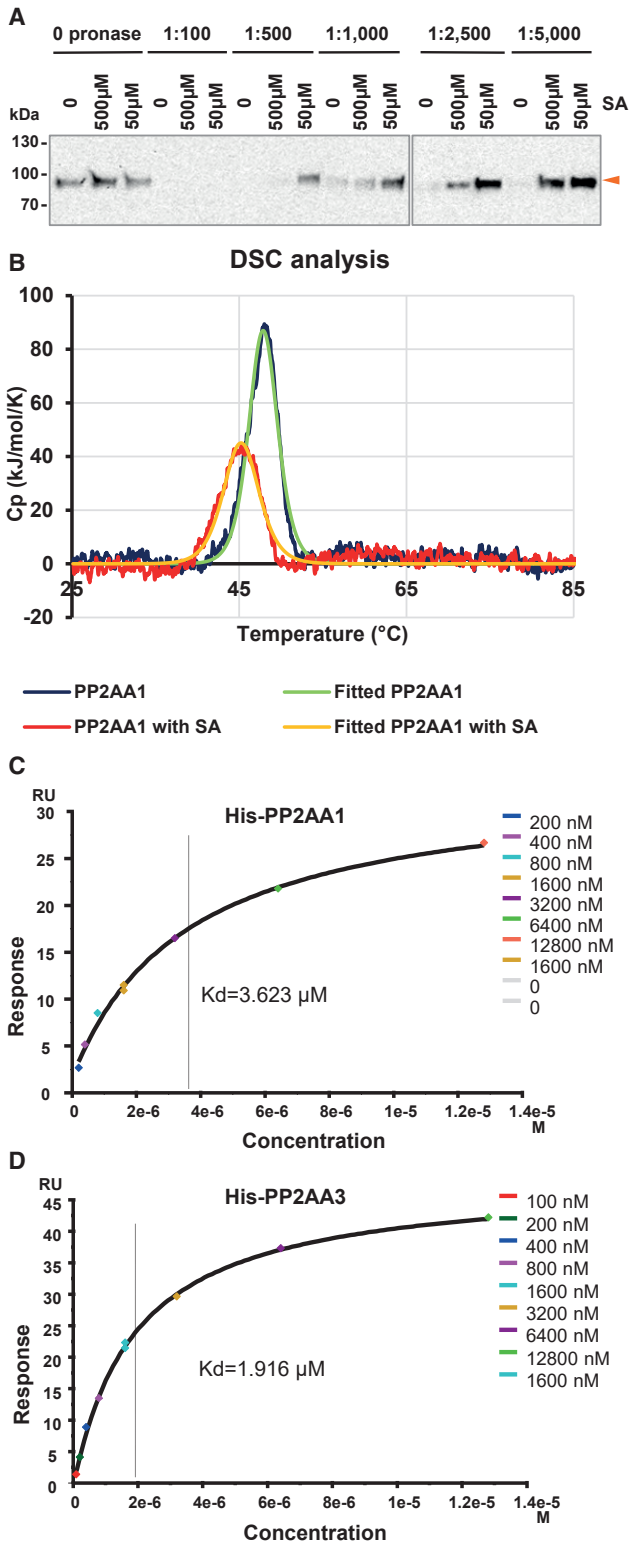

Figure 6. SA Binds to the A Subunit of PP2A

(A) DARTS assay suggests that PP2AA1 is potential target of SA. *pPP2AA1::PP2AA1-GFP* seedlings were used for the protein isolation. Samples were treated with DMSO (mock) and SA and digested by different concentrations of Pronase. Samples were further analyzed by western blot with an anti-GFP antibody.

Thus, all these methodically distinct approaches have confirmed a direct binding of SA to A subunits of PP2A at concentrations well matching the SA physiological activity. The binding of SA to PP2AAs is in line with observations on SA regulating PP2A activity, downstream PIN2 (de)phosphorylation, and auxin-mediated root development.

DISCUSSION

Balancing allocation of resources between growth and defense against pathogens is a common challenge in multicellular organisms [57]. It has been long proposed that, except for the canonical roles as stress hormones, both SA and jasmonic acid (JA) also regulate plant growth and development [12, 15]. Meanwhile, another phytohormone, auxin, well recognized as an essential signaling molecule for growth and development and seemingly involved in almost every aspect of plant life, was proposed to also participate in plant defense against pathogens [11, 15, 58]. Here, we revealed a dual role for the plant hormone SA, which by two parallel perception and signaling mechanisms concomitantly activates immunity and represses growth.

SA is a well-established defense signal of plants; its levels rapidly rise following pathogen attack, and it acts via the NPR-type receptors on transcription of defense genes (Figure 7A) [1]. Here, we identify a parallel signaling pathway that leads to regulation of growth. Both *in vivo* and *in vitro* experiments show that SA specifically binds to the A subunit of the PP2A complex and inhibits its activity. PP2A is a protein phosphatase important for many cellular processes through dephosphorylating various protein substrates [43, 45, 48]. Prominent among its substrates are PIN auxin transporters that play key roles in many developmental processes, and multiple aspects of PIN activity, localization, and subcellular dynamics are mediated by different phosphorylation states [27, 39]. In line with our observation that SA inhibits PP2A activity, increased SA levels lead to an increase in PIN phosphorylation and thus to a change in subcellular PIN distribution and decrease in auxin export activity (Figure 7B). This leads to attenuation of auxin-mediated growth as manifested by a decrease in primary root elongation, inhibition of gravitropic response, and repression of lateral root organogenesis. Identification of SA as direct regulator of PP2A highlights a role for this phosphatase complex as a molecular hub for the trade-off between immune response and

(B) DSC analysis suggesting the potential binding of SA to recombinant His-PP2AA1. 5 μM of purified His-PP2AA1 protein was analyzed by DSC with or without 50 μM SA. Tm = 48.01°C and 45.03°C for His-PP2AA1+DMSO and His-PP2AA1+SA, respectively.

(C) SPR analysis of the His-PP2AA1 and SA interaction. An active synthetic SA analog (SA-f) was immobilized on a CM-5 sensor chip, and different concentrations of His-PP2AA1 were applied. The binding curve was plotted by values at the steady state, for which the sensorgram is shown is Figure S7D. A K_D value of 3.623 μM was detected.

(D) SPR assay reveals the binding of His-PP2AA3 to SA. The same sensor chip as above was used, and different concentrations of His-PP2AA3 were applied. The binding curve was plotted by values at the steady state, with the data points shown in the sensorgram in Figure S7E. A K_D value of 1.916 μM was detected.

See also Figures S5, S6, and S7.

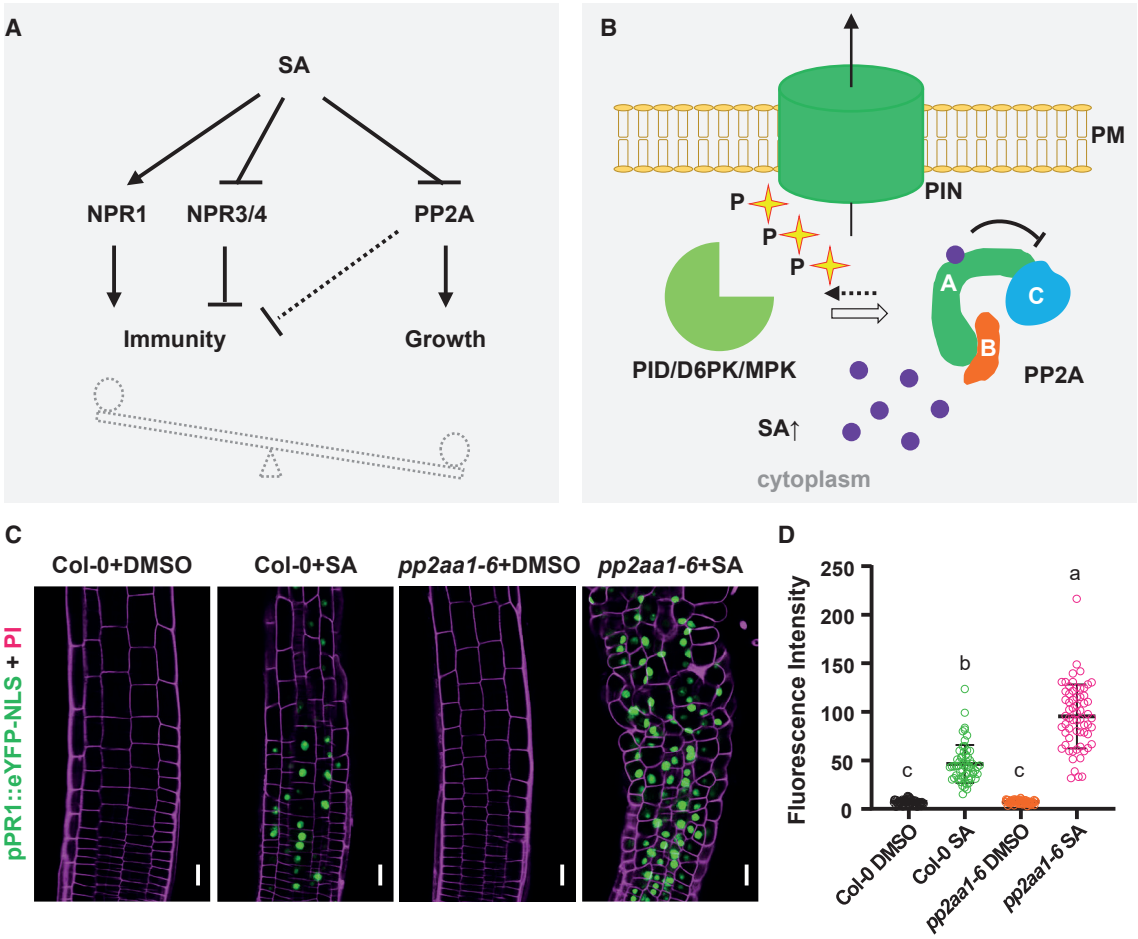

Figure 7. Model for the Parallel SA Action in Immunity and Growth Regulation

(A) SA plays a key role in the growth-immunity transition following pathogen attack: on one hand, SA activates the immune response, through stimulating NPR1 and repressing NPR3/4, all together increasing the expression of downstream defense genes; on the other hand, SA inhibits growth via suppressing PP2A activity and the subsequent dephosphorylation of substrates.

(B) The auxin efflux carrier PIN2 is phosphorylated by different kinases, including PINOID/WAGs, D6PK/D6PKLs, and MAPKs, and dephosphorylated by PP2A. Following pathogen attack, the SA levels increase. SA binds to the A subunits of PP2A and thereafter represses its dephosphorylation activity toward PIN proteins, which leads to hyperphosphorylation of PIN, thereby a decrease in PIN activity ultimately resulting in a decrease in auxin export and attenuation of growth.

(C and D) Induced stronger expression of *pPR1::eYFP-NLS* by SA was detected in *pp2aa1-6*.

(C) *pPR1::eYFP-NLS* seedlings were constantly grown on plates with DMSO or 40 μM SA for 5 days from germination and were then imaged by CLSM. Scale bars, 10 μm.

(D) For quantification, the average GFP florescence of 5–10 representative cells from 10 seedlings for each treatment was measured by Fiji. The data points were showed as dot plots, and lines indicate mean ± SD. Different letters represent significant difference; $p < 0.05$; by one-way ANOVA with a Tukey multiple comparison test.

growth. It is noteworthy that SA does not completely inhibit the PP2A activity, perhaps because PP2AAs are solely the scaffold proteins for the PP2A holoenzyme. This regulatory mode may present a mechanism to fine-tune PP2A activity under different conditions. Notably, we demonstrate that this hyperphosphorylation by PP2A inhibition leads to mislocalization of PIN2, suggesting more kinases, other than PID, involved in apical versus basal PIN targeting [43]. Phosphorylation by mitogen-activated protein kinase (MAPK) gives rise to a decreased PIN polarity and plasma membrane (PM) targeting [59]; thus, it would be interesting to investigate whether PP2A also antagonizes with MAPK in directing PIN localization.

Our previous study revealed that SA interferes with the internalization of PIN proteins, which depends on the clathrin-mediated endocytosis pathway [14]. It has been also reported that *pp2a* mutants, including *pp2aa1*, show decreased PIN internalization [60, 61]. Our proposed SA-PP2A model further clarifies the molecular mechanism underlying the SA effect on PIN trafficking [14]. A recent study shows that SA has an impact on the root meristem patterning via auxin distribution through both upregulating auxin biosynthesis and interfering with transport [30]. Though elevated auxin levels do not typically lead to agravitropic root growth and therefore are likely a result of a regulatory feedback from the blocked auxin transport, it would

still be interesting to test whether PP2A is also involved in this SA effect. Likewise, the observed developmental abnormalities in SA-treated root columella cells [30] were also reported in PP2A mutants [48], further supporting our hypothesis that this SA-PP2A pathway plays more roles in plant growth and development. Here, this study focuses on the SA action on root development, especially PIN2-mediated gravitropism. It is likely that more PP2A substrates, other PIN proteins, or even non-PIN substrates are also involved in these effects.

Previous studies uncovered that plant pathogens interfere with the auxin pathway at the level of the signaling. For example, flagellin of pathogen can induce a microRNA (miRNA) to negatively regulate the expression of auxin receptors, TRANSPORT INHIBITOR RESISTANT1 (TIR1)/ AUXIN SINGNALING F BOX (AFB) [58]. Moreover, SA also stabilizes the negative regulators of auxin signaling pathway, AUXIN/IAA (AUX/IAA) [8], or interferes with auxin biosynthesis [11]. Notably, the *npr1* mutation suppresses the immune response, but not the growth attenuation phenotype of *snc2-1D*, which shows constitutive defense response [62]. Recently, a gain-of-function mutation of *NPR4*, *npr4-4D*, was identified to work together with *npr1-1* and additively to regulate immune response as well as the growth pathway [7]. In view of these observations, we conclude that SA regulates plant growth and development through multiple mechanisms, many of which involve auxin. Generally, it remains unclear whether these other SA effects are mediated by the canonical, NPR1-mediated pathway or require here identified SA-PP2A signaling module.

Notably, by investigating the NPR1-mediated immune response with *pPR1::eYFP-NLS*, we found that *pp2aa1* mutation leads to an increased SA sensitivity (Figures 7C and 7D). It has been reported that bacterial type-III effector proteins could target PP2A to facilitate infection and that multiple *pp2a* loss-of-function mutants, including *pp2aa1*, exhibit elevated response to pathogen attack [63]. Together with our findings, we hypothesize that PP2A, as an essential regulator for multiple pathways, might play a central role in coordinating plant immune response with attenuation of growth and development.

Previous studies demonstrated that NPR1/NPR3/NPR4 are genuine SA receptors, mediating the downstream transcriptional response. NPR proteins share sequence similarity with the mammalian master regulator in the inflammatory response, nuclear factor κB (NF-κB), and specifically its subunit, inhibitor protein I-κB (IκB) [3, 4]. IκB is phosphorylated by an IκB kinase (IKK) complex, whose activity is directly inhibited by salicylates, the active breakdown compound of the common anti-inflammatory drug Aspirin (2-acetoxybenzoic acid), thus providing mechanism of their well-known anti-inflammatory effects [64]. These interesting analogies between plant and mammalian pathogen defense mechanisms, both at the sequence level of involved regulators as well as at structural level of the involved ligands, point to possible evolutionary conservation between these otherwise seemingly unrelated pathogen defense strategies. Given the fact that PP2A regulates the dephosphorylation of numerous substrates, it would be interesting to investigate whether the SA-PP2A signaling module is a part of this evolutionary conserved mechanism and also regulates the NPR-mediated immunity in plants or NF-κB-controlled inflammatory response in mammals.

STAR★METHODS

Detailed methods are provided in the online version of this paper and include the following:

- KEY RESOURCES TABLE
- LEAD CONTACT AND MATERIALS AVAILABILITY
- EXPERIMENTAL MODEL AND SUBJECT DETAILS
  - Plant Materials and Growth Conditions
- METHOD DETAILS
  - Pseudomonas syringae treatment of *Arabidopsis* seedlings
  - Pharmacological treatments
  - Free SA measurement by liquid chromatography-tandem mass spectrometry (LC-MS/MS)
  - Auxin transport in hypocotyls and tobacco BY-2 cells
  - Imaging with Confocal Laser Scanning Microscopy (CLSM)
  - Image analysis and morphological analysis
  - Molecular cloning
  - PP2A activity assay
  - Protein extraction and immunoblot
  - PIN2 phosphorylation assays
  - PIN2-HL phosphorylation assay with [γ-^{32}P]-ATP
  - Drug Affinity Responsive Target Stability (DARTS) assay
  - Recombinant protein expression and purification
  - Differential Scanning Calorimetry (DSC) analysis
  - Chemical synthesis of SA derivatives
  - SPR analysis
  - Accession Numbers
- QUANTIFICATION AND STATISTICAL ANALYSIS
- DATA AND CODE AVAILABILITY

SUPPLEMENTAL INFORMATION

Supplemental Information can be found online at https://doi.org/10.1016/j.cub.2019.11.058.

ACKNOWLEDGMENTS

We thank Shigeyuki Betsuyaku (University of Tsukuba), Alison Delong (Brown University), Xinnian Dong (Duke University), Dolf Weijers (Wageningen University), Yuelin Zhang (UBC), and Martine Pastuglia (Institut Jean-Pierre Bourgin) for sharing published materials; Jana Riederer for help with cantharidin physiological analysis; David Domjan for help with cloning pET28a-PIN2HL; Qing Lu for help with DARTS; Hana Kozubíková for technical support on SA derivative synthesis; Zuzana Vondráková for technical support with tobacco cells; Lucia Strader (Washington University), Bert De Rybel (Ghent University), Bartel Vanholme (Ghent University), and Lukas Mach (BOKU) for helpful discussions; and bioimaging and life science facilities of IST Austria for continuous support. We gratefully acknowledge the Nottingham Arabidopsis Stock Center (NASC) for providing T-DNA insertional mutants. The DSC and SPR instruments were provided by the EQ-BOKU VIBT GmbH and the BOKU Core Facility for Biomolecular and Cellular Analysis, with help of Irene Schaffner. The research leading to these results has received funding from the European Union's Horizon 2020 program (ERC grant agreement no. 742985 to J.F.) and the People Programme (Marie Curie Actions) of the European Union's Seventh Framework Programme (FP7/2007-2013) under REA grant agreement no. 291734. S.T. was supported by a European Molecular Biology Organization (EMBO) long-term postdoctoral fellowship (ALTF 723-2015). O.N. was supported by the Ministry of Education, Youth and Sports of the Czech Republic (European Regional Development Fund-Project "Centre for Experimental Plant Biology" no.

CZ.02.1.01/0.0/0.0/16_019/0000738). J. Pospíšil was supported by European Regional Development Fund Project "Centre for Experimental Plant Biology" (no. CZ.02.1.01/0.0/0.0/16_019/0000738). J. Petrášek was supported by EU Operational Programme Prague-Competitiveness (no. CZ.2.16/3.1.00/21519).

AUTHOR CONTRIBUTIONS

S.T. and J.F. designed research and analyzed data. S.T., M.A., I.V., M.G., G.M., and J.H. performed experiments. I.P. and O.N. provided the SA analyses. P.L. and J. Pospíšil synthesized the SA derivatives. E.R. contributed to the DARTS assay. J. Petrášek contributed to auxin transport assays with BY-2 cells. S.T. and J.F. wrote the manuscript with input from other authors, and all authors revised it.

DECLARATION OF INTERESTS

The authors declare no competing interests.

Received: July 9, 2019
Revised: October 22, 2019
Accepted: November 19, 2019
Published: January 16, 2020

REFERENCES

1. Wildermuth, M.C., Dewdney, J., Wu, G., and Ausubel, F.M. (2001). Isochorismate synthase is required to synthesize salicylic acid for plant defence. Nature *414*, 562–565.
2. Cao, H., Bowling, S.A., Gordon, A.S., and Dong, X. (1994). Characterization of an *Arabidopsis* mutant that is nonresponsive to inducers of systemic acquired resistance. Plant Cell *6*, 1583–1592.
3. Cao, H., Glazebrook, J., Clarke, J.D., Volko, S., and Dong, X. (1997). The *Arabidopsis NPR1* gene that controls systemic acquired resistance encodes a novel protein containing ankyrin repeats. Cell *88*, 57–63.
4. Ryals, J., Weymann, K., Lawton, K., Friedrich, L., Ellis, D., Steiner, H.Y., Johnson, J., Delaney, T.P., Jesse, T., Vos, P., and Uknes, S. (1997). The *Arabidopsis* NIM1 protein shows homology to the mammalian transcription factor inhibitor I kappa B. Plant Cell *9*, 425–439.
5. Mou, Z., Fan, W., and Dong, X. (2003). Inducers of plant systemic acquired resistance regulate NPR1 function through redox changes. Cell *113*, 935–944.
6. Spoel, S.H., Mou, Z., Tada, Y., Spivey, N.W., Genschik, P., and Dong, X. (2009). Proteasome-mediated turnover of the transcription coactivator NPR1 plays dual roles in regulating plant immunity. Cell *137*, 860–872.
7. Ding, Y., Sun, T., Ao, K., Peng, Y., Zhang, Y., Li, X., and Zhang, Y. (2018). Opposite roles of salicylic Acid receptors NPR1 and NPR3/NPR4 in transcriptional regulation of plant immunity. Cell *173*, 1454–1467.e15.
8. Wang, D., Pajerowska-Mukhtar, K., Culler, A.H., and Dong, X. (2007). Salicylic acid inhibits pathogen growth in plants through repression of the auxin signaling pathway. Curr. Biol. *17*, 1784–1790.
9. Fu, Z.Q., Yan, S., Saleh, A., Wang, W., Ruble, J., Oka, N., Mohan, R., Spoel, S.H., Tada, Y., Zheng, N., and Dong, X. (2012). NPR3 and NPR4 are receptors for the immune signal salicylic acid in plants. Nature *486*, 228–232.
10. Wu, Y., Zhang, D., Chu, J.Y., Boyle, P., Wang, Y., Brindle, I.D., De Luca, V., and Després, C. (2012). The *Arabidopsis* NPR1 protein is a receptor for the plant defense hormone salicylic acid. Cell Rep. *1*, 639–647.
11. Yuan, H.M., Liu, W.C., and Lu, Y.T. (2017). CATALASE2 coordinates SA-mediated repression of both auxin accumulation and JA biosynthesis in plant defenses. Cell Host Microbe *21*, 143–155.
12. Rivas-San Vicente, M., and Plasencia, J. (2011). Salicylic acid beyond defence: its role in plant growth and development. J. Exp. Bot. *62*, 3321–3338.
13. Zhang, X., Dai, Y., Xiong, Y., DeFraia, C., Li, J., Dong, X., and Mou, Z. (2007). Overexpression of *Arabidopsis MAP kinase kinase 7* leads to activation of plant basal and systemic acquired resistance. Plant J. *52*, 1066–1079.
14. Du, Y., Tejos, R., Beck, M., Himschoot, E., Li, H., Robatzek, S., Vanneste, S., and Friml, J. (2013). Salicylic acid interferes with clathrin-mediated endocytic protein trafficking. Proc. Natl. Acad. Sci. USA *110*, 7946–7951.
15. Kazan, K., and Manners, J.M. (2009). Linking development to defense: auxin in plant-pathogen interactions. Trends Plant Sci. *14*, 373–382.
16. Klessig, D.F., Tian, M., and Choi, H.W. (2016). Multiple targets of salicylic acid and its derivatives in plants and animals. Front. Immunol. *7*, 206.
17. Slaymaker, D.H., Navarre, D.A., Clark, D., del Pozo, O., Martin, G.B., and Klessig, D.F. (2002). The tobacco salicylic acid-binding protein 3 (SABP3) is the chloroplast carbonic anhydrase, which exhibits antioxidant activity and plays a role in the hypersensitive defense response. Proc. Natl. Acad. Sci. USA *99*, 11640–11645.
18. Choi, H.W., Manohar, M., Manosalva, P., Tian, M., Moreau, M., and Klessig, D.F. (2016). Activation of plant innate immunity by extracellular High Mobility Group Box 3 and its inhibition by salicylic acid. PLoS Pathog. *12*, e1005518.
19. Manohar, M., Wang, D., Manosalva, P.M., Choi, H.W., Kombrink, E., and Klessig, D.F. (2017). Members of the abscisic acid co-receptor PP2C protein family mediate salicylic acid-abscisic acid crosstalk. Plant Direct *1*, e00020.
20. Wang, C., Hu, T., Yan, X., Meng, T., Wang, Y., Wang, Q., Zhang, X., Gu, Y., Sánchez-Rodríguez, C., Gadeyne, A., et al. (2016). Differential regulation of clathrin and its adaptor proteins during membrane recruitment for endocytosis. Plant Physiol. *171*, 215–229.
21. Adamowski, M., and Friml, J. (2015). PIN-dependent auxin transport: action, regulation, and evolution. Plant Cell *27*, 20–32.
22. Lebeis, S.L., Paredes, S.H., Lundberg, D.S., Breakfield, N., Gehring, J., McDonald, M., Malfatti, S., Glavina del Rio, T., Jones, C.D., Tringe, S.G., and Dangl, J.L. (2015). PLANT MICROBIOME. Salicylic acid modulates colonization of the root microbiome by specific bacterial taxa. Science *349*, 860–864.
23. Clarke, J.D., Liu, Y., Klessig, D.F., and Dong, X. (1998). Uncoupling *PR* gene expression from NPR1 and bacterial resistance: characterization of the dominant *Arabidopsis cpr6-1* mutant. Plant Cell *10*, 557–569.
24. Betsuyaku, S., Katou, S., Takebayashi, Y., Sakakibara, H., Nomura, N., and Fukuda, H. (2018). Salicylic acid and Jasmonic acid pathways are activated in spatially different domains around the infection site during effector-triggered immunity in *Arabidopsis thaliana*. Plant Cell Physiol. *59*, 8–16.
25. Zhao, X., Wang, J., Yuan, J., Wang, X.L., Zhao, Q.P., Kong, P.T., and Zhang, X. (2015). NITRIC OXIDE-ASSOCIATED PROTEIN1 (AtNOA1) is essential for salicylic acid-induced root waving in *Arabidopsis thaliana*. New Phytol. *207*, 211–224.
26. Conrath, U., Chen, Z., Ricigliano, J.R., and Klessig, D.F. (1995). Two inducers of plant defense responses, 2,6-dichloroisonicotinec acid and salicylic acid, inhibit catalase activity in tobacco. Proc. Natl. Acad. Sci. USA *92*, 7143–7147.
27. Naramoto, S. (2017). Polar transport in plants mediated by membrane transporters: focus on mechanisms of polar auxin transport. Curr. Opin. Plant Biol. *40*, 8–14.
28. Liao, C.-Y., Smet, W., Brunoud, G., Yoshida, S., Vernoux, T., and Weijers, D. (2015). Reporters for sensitive and quantitative measurement of auxin response. Nat. Methods *12*, 207–210, 2, 210.
29. Brumos, J., Robles, L.M., Yun, J., Vu, T.C., Jackson, S., Alonso, J.M., and Stepanova, A.N. (2018). Local auxin biosynthesis is a key regulator of plant development. Dev. Cell *47*, 306–318.e5.
30. Pasternak, T., Groot, E.P., Kazantsev, F.V., Teale, W., Omelyanchuk, N., Kovrizhnykh, V., Palme, K., and Mironova, V.V. (2019). Salicylic acid affects root meristem patterning via auxin distribution in a concentration-dependent manner. Plant Physiol. *180*, 1725–1739.

31. Petrásek, J., Elčkner, M., Morris, D.A., and Zazímalová, E. (2002). Auxin efflux carrier activity and auxin accumulation regulate cell division and polarity in tobacco cells. Planta *216*, 302–308.

32. Petrásek, J., Mravec, J., Bouchard, R., Blakeslee, J.J., Abas, M., Seifertová, D., Wiśniewska, J., Tadele, Z., Kubeš, M., Covanová, M., et al. (2006). PIN proteins perform a rate-limiting function in cellular auxin efflux. Science *312*, 914–918.

33. Bennett, M.J., Marchant, A., Green, H.G., May, S.T., Ward, S.P., Millner, P.A., Walker, A.R., Schulz, B., and Feldmann, K.A. (1996). *Arabidopsis AUX1* gene: a permease-like regulator of root gravitropism. Science *273*, 948–950.

34. Swarup, R., Friml, J., Marchant, A., Ljung, K., Sandberg, G., Palme, K., and Bennett, M. (2001). Localization of the auxin permease AUX1 suggests two functionally distinct hormone transport pathways operate in the *Arabidopsis* root apex. Genes Dev. *15*, 2648–2653.

35. Luschnig, C., Gaxiola, R.A., Grisafi, P., and Fink, G.R. (1998). EIR1, a root-specific protein involved in auxin transport, is required for gravitropism in *Arabidopsis thaliana*. Genes Dev. *12*, 2175–2187.

36. Abas, L., Benjamins, R., Malenica, N., Paciorek, T., Wiśniewska, J., Moulinier-Anzola, J.C., Sieberer, T., Friml, J., and Luschnig, C. (2006). Intracellular trafficking and proteolysis of the *Arabidopsis* auxin-efflux facilitator PIN2 are involved in root gravitropism. Nat. Cell Biol. *8*, 249–256.

37. Baster, P., Robert, S., Kleine-Vehn, J., Vanneste, S., Kania, U., Grunewald, W., De Rybel, B., Beeckman, T., and Friml, J. (2013). SCF(TIR1/AFB)-auxin signalling regulates PIN vacuolar trafficking and auxin fluxes during root gravitropism. EMBO J. *32*, 260–274.

38. Habets, M.E.J., and Offringa, R. (2014). PIN-driven polar auxin transport in plant developmental plasticity: a key target for environmental and endogenous signals. New Phytol. *203*, 362–377.

39. Armengot, L., Marquès-Bueno, M.M., and Jaillais, Y. (2016). Regulation of polar auxin transport by protein and lipid kinases. J. Exp. Bot. *67*, 4015–4037.

40. Marhava, P., Bassukas, A.E.L., Zourelidou, M., Kolb, M., Moret, B., Fastner, A., Schulze, W.X., Cattaneo, P., Hammes, U.Z., Schwechheimer, C., and Hardtke, C.S. (2018). A molecular rheostat adjusts auxin flux to promote root protophloem differentiation. Nature *558*, 297–300.

41. Abas, L., and Luschnig, C. (2010). Maximum yields of microsomal-type membranes from small amounts of plant material without requiring ultracentrifugation. Anal. Biochem. *401*, 217–227.

42. Garbers, C., DeLong, A., Deruére, J., Bernasconi, P., and Söll, D. (1996). A mutation in protein phosphatase 2A regulatory subunit A affects auxin transport in *Arabidopsis*. EMBO J. *15*, 2115–2124.

43. Michniewicz, M., Zago, M.K., Abas, L., Weijers, D., Schweighofer, A., Meskiene, I., Heisler, M.G., Ohno, C., Zhang, J., Huang, F., et al. (2007). Antagonistic regulation of PIN phosphorylation by PP2A and PINOID directs auxin flux. Cell *130*, 1044–1056.

44. Manohar, M., Tian, M., Moreau, M., Park, S.-W., Choi, H.W., Fei, Z., Friso, G., Asif, M., Manosalva, P., von Dahl, C.C., et al. (2015). Identification of multiple salicylic acid-binding proteins using two high throughput screens. Front. Plant Sci. *5*, 777.

45. Zhou, H.-W., Nussbaumer, C., Chao, Y., and DeLong, A. (2004). Disparate roles for the regulatory A subunit isoforms in *Arabidopsis* protein phosphatase 2A. Plant Cell *16*, 709–722.

46. Spinner, L., Gadeyne, A., Belcram, K., Goussot, M., Moison, M., Duroc, Y., Eeckhout, D., De Winne, N., Schaefer, E., Van De Slijke, E., et al. (2013). A protein phosphatase 2A complex spatially controls plant cell division. Nat. Commun. *4*, 1863.

47. Li, Y.M., and Casida, J.E. (1992). Cantharidin-binding protein: identification as protein phosphatase 2A. Proc. Natl. Acad. Sci. USA *89*, 11867–11870.

48. Yue, K., Sandal, P., Williams, E.L., Murphy, E., Stes, E., Nikonorova, N., Ramakrishna, P., Czyzewicz, N., Montero-Morales, L., Kumpf, R., et al. (2016). PP2A-3 interacts with ACR4 and regulates formative cell division in the *Arabidopsis* root. Proc. Natl. Acad. Sci. USA *113*, 1447–1452.

49. Blakeslee, J.J., Zhou, H.-W., Heath, J.T., Skottke, K.R., Barrios, J.A.R., Liu, S.-Y., and DeLong, A. (2008). Specificity of RCN1-mediated protein phosphatase 2A regulation in meristem organization and stress response in roots. Plant Physiol. *146*, 539–553.

50. Ekman, P., and Jäger, O. (1993). Quantification of subnanomolar amounts of phosphate bound to seryl and threonyl residues in phosphoproteins using alkaline hydrolysis and malachite green. Anal. Biochem. *214*, 138–141.

51. Bos, C.L., Kodach, L.L., van den Brink, G.R., Diks, S.H., van Santen, M.M., Richel, D.J., Peppelenbosch, M.P., and Hardwick, J.C.H. (2006). Effect of aspirin on the Wnt/β-catenin pathway is mediated via protein phosphatase 2A. Oncogene *25*, 6447–6456.

52. Lomenick, B., Hao, R., Jonai, N., Chin, R.M., Aghajan, M., Warburton, S., Wang, J., Wu, R.P., Gomez, F., Loo, J.A., et al. (2009). Target identification using drug affinity responsive target stability (DARTS). Proc. Natl. Acad. Sci. USA *106*, 21984–21989.

53. Gill, P., Moghadam, T.T., and Ranjbar, B. (2010). Differential scanning calorimetry techniques: applications in biology and nanoscience. J. Biomol. Tech. *21*, 167–193.

54. Niesen, F.H., Berglund, H., and Vedadi, M. (2007). The use of differential scanning fluorimetry to detect ligand interactions that promote protein stability. Nat. Protoc. *2*, 2212–2221.

55. Hamiaux, C., Drummond, R.S.M., Janssen, B.J., Ledger, S.E., Cooney, J.M., Newcomb, R.D., and Snowden, K.C. (2012). DAD2 is an α/β hydrolase likely to be involved in the perception of the plant branching hormone, strigolactone. Curr. Biol. *22*, 2032–2036.

56. Karlsson, R., Michaelsson, A., and Mattsson, L. (1991). Kinetic analysis of monoclonal antibody-antigen interactions with a new biosensor based analytical system. J. Immunol. Methods *145*, 229–240.

57. Belkhadir, Y., Yang, L., Hetzel, J., Dangl, J.L., and Chory, J. (2014). The growth-defense pivot: crisis management in plants mediated by LRR-RK surface receptors. Trends Biochem. Sci. *39*, 447–456.

58. Navarro, L., Dunoyer, P., Jay, F., Arnold, B., Dharmasiri, N., Estelle, M., Voinnet, O., and Jones, J.D.G. (2006). A plant miRNA contributes to antibacterial resistance by repressing auxin signaling. Science *312*, 436–439.

59. Jia, W., Li, B., Li, S., Liang, Y., Wu, X., Ma, M., Wang, J., Gao, J., Cai, Y., Zhang, Y., et al. (2016). Mitogen-activated protein kinase cascade MKK7-MPK6 plays important roles in plant development and regulates shoot branching by phosphorylating PIN1 in *Arabidopsis*. PLoS Biol. *14*, e1002550.

60. Kleine-Vehn, J., Huang, F., Naramoto, S., Zhang, J., Michniewicz, M., Offringa, R., and Friml, J. (2009). PIN auxin efflux carrier polarity is regulated by PINOID kinase-mediated recruitment into GNOM-independent trafficking in *Arabidopsis*. Plant Cell *21*, 3839–3849.

61. Karampelias, M., Neyt, P., De Groeve, S., Aesaert, S., Coussens, G., Rolčík, J., Bruno, L., De Winne, N., Van Minnebruggen, A., Van Montagu, M., et al. (2016). ROTUNDA3 function in plant development by phosphatase 2A-mediated regulation of auxin transporter recycling. Proc. Natl. Acad. Sci. USA *113*, 2768–2773.

62. Zhang, Y., Yang, Y., Fang, B., Gannon, P., Ding, P., Li, X., and Zhang, Y. (2010). *Arabidopsis snc2-1D* activates receptor-like protein-mediated immunity transduced through WRKY70. Plant Cell *22*, 3153–3163.

63. Jin, L., Ham, J.H., Hage, R., Zhao, W., Soto-Hernández, J., Lee, S.Y., Paek, S.M., Kim, M.G., Boone, C., Coplin, D.L., and Mackey, D. (2016). Direct and indirect targeting of PP2A by conserved bacterial type-III effector proteins. PLoS Pathog. *12*, e1005609.

64. Yin, M.J., Yamamoto, Y., and Gaynor, R.B. (1998). The anti-inflammatory agents aspirin and salicylate inhibit the activity of I(κ)B kinase-β. Nature *396*, 77–80.

65. Suga, S., Imagawa, S., and Maeshima, M. (2001). Specificity of the accumulation of mRNAs and proteins of the plasma membrane and tonoplast aquaporins in radish organs. Planta *212*, 294–304.

66. Fischer, U., Ikeda, Y., Ljung, K., Serralbo, O., Singh, M., Heidstra, R., Palme, K., Scheres, B., and Grebe, M. (2006). Vectorial information for *Arabidopsis* planar polarity is mediated by combined AUX1, EIN2, and GNOM activity. Curr. Biol. *16*, 2143–2149.

67. Swarup, R., Kargul, J., Marchant, A., Zadik, D., Rahman, A., Mills, R., Yemm, A., May, S., Williams, L., Millner, P., et al. (2004). Structure-function analysis of the presumptive *Arabidopsis* auxin permease AUX1. Plant Cell *16*, 3069–3083.

68. Zhang, Y., Cheng, Y.T., Qu, N., Zhao, Q., Bi, D., and Li, X. (2006). Negative regulation of defense responses in *Arabidopsis* by two *NPR1* paralogs. Plant J. *48*, 647–656.

69. Gross, J., Cho, W.K., Lezhneva, L., Falk, J., Krupinska, K., Shinozaki, K., Seki, M., Herrmann, R.G., and Meurer, J. (2006). A plant locus essential for phylloquinone (vitamin K1) biosynthesis originated from a fusion of four eubacterial genes. J. Biol. Chem. *281*, 17189–17196.

70. Xu, J., and Scheres, B. (2005). Dissection of Arabidopsis ADP-RIBOSYLATION FACTOR 1 function in epidermal cell polarity. Plant Cell *17*, 525–536.

71. Bowling, S.A., Guo, A., Cao, H., Gordon, A.S., Klessig, D.F., and Dong, X. (1994). A mutation in *Arabidopsis* that leads to constitutive expression of systemic acquired resistance. Plant Cell *6*, 1845–1857.

72. Bowling, S.A., Clarke, J.D., Liu, Y., Klessig, D.F., and Dong, X. (1997). The *cpr5* mutant of *Arabidopsis* expresses both NPR1-dependent and NPR1-independent resistance. Plant Cell *9*, 1573–1584.

73. Ishiga, Y., Ishiga, T., Uppalapati, S.R., and Mysore, K.S. (2011). *Arabidopsis* seedling flood-inoculation technique: a rapid and reliable assay for studying plant-bacterial interactions. Plant Methods *7*, 32.

74. Floková, K., Tarkowská, D., Miersch, O., Strnad, M., Wasternack, C., and Novák, O. (2014). UHPLC-MS/MS based target profiling of stress-induced phytohormones. Phytochemistry *105*, 147–157.

75. Lewis, D.R., and Muday, G.K. (2009). Measurement of auxin transport in Arabidopsis thaliana. Nat. Protoc. *4*, 437–451.

76. Schindelin, J., Arganda-Carreras, I., Frise, E., Kaynig, V., Longair, M., Pietzsch, T., Preibisch, S., Rueden, C., Saalfeld, S., Schmid, B., et al. (2012). Fiji: an open-source platform for biological-image analysis. Nat. Methods *9*, 676–682.

77. Kania, U., Nodzyński, T., Lu, Q., Hicks, G.R., Nerinckx, W., Mishev, K., Peurois, F., Cherfils, J., De Rycke, R., Grones, P., et al. (2018). The inhibitor endosidin 4 targets SEC7 domain-type ARF GTPase exchange factors and interferes with subcellular trafficking in eukaryotes. Plant Cell *30*, 2553–2572.

78. Mishev, K., Lu, Q., Denoo, B., Peurois, F., Dejonghe, W., Hullaert, J., De Rycke, R., Boeren, S., Bretou, M., De Munck, S., et al. (2018). Nonselective chemical inhibition of Sec7 domain-containing ARF GTPase exchange factors. Plant Cell *30*, 2573–2593.

79. Kong, X., He, Z., Zhang, Y., Mu, L., Liang, C., Chen, B., Jing, X., and Cammidge, A.N. (2011). A mesogenic triphenylene-perylene-triphenylene triad. Org. Lett. *13*, 764–767.

STAR★METHODS

KEY RESOURCES TABLE

REAGENT or RESOURCE	SOURCE	IDENTIFIER
Antibodies		
Rabbit anti-PIN1	[37]	N/A
Rabbit anti-PIN2	[36]	N/A
Mouse anti-His-tag monoclonal Antibody	Agrisera	Cat# AS11 1771
Mouse anti-myc-tag monoclonal Antibody, clone 4A6	Millipore (Merck)	Cat# 05-724
Phospho-PP2A alpha (Tyr307) Polyclonal Antibody	Thermo Scientific	Cat# PA5-36874; RRID:AB_2553794
Anti-GFP-HRP	Miltenyi Biotec	Cat# 130-091-833; RRID:AB_247003
Monoclonal anti-GFP antibody produced in mouse	Sigma	Cat# G6539; RRID:AB_259941
Anti-PIP2;1	[65]	N/A
Bacterial and Virus Strains		
Escherichia coli DH5α	Lab stock	N/A
E.coli BL21 (DE3)	New England Biolabs	Cat# C2527H
Agrobacterium tumefaciens GV3101	Lab stock	N/A
Pseudomonas syringae pv. tomato DC3000	Armin Djamei lab	N/A
Chemicals, Peptides, and Recombinant Proteins		
brefeldin A	Sigma	Cat# B7651
Propidium Iodide	Sigma	Cat# P3566
PBS Buffer 10 × (1000 mL)	GE Healthcare	Cat# BR100672
PhosSTOP	Sigma/Roche	Cat# 4906837001
cOmplete protease inhibitor cocktail	Sigma/Roche	Cat# 4693124001
Benzoic acid (BA)	Sigma	Cat# 242381
Salicylic Acid (SA)	Sigma	Cat# 247588
3-Hydroxybenzoic acid (3-OH-BA)	Sigma	Cat# H20008
4-Hydroxybenzoic acid (4-OH-BA)	Sigma	Cat# H20059
N-(1-Naphthyl)phthalamidic acid	Sigma	Cat# N12507
2,3,5-Triiodobenzoic acid (TIBA)	Sigma	Cat# T5910
[3H]-IAA (([5-^{3}H]-Indole-3-acetic acid)	American Radiolabeled Chemicals	Cat# ART 0340
[3H]- NAA ([4-^{3}H]-1-Naphthylacetic acid)	American Radiolabeled Chemicals	Cat# ART 0610
[3H]-2,4-D (([5-^{3}H]-2,4-Dichlorophenoxy acetic acid)	American Radiolabeled Chemicals	Cat# ART 0559
Cantharidin	Sigma	Cat# C7632
Imidazole	Sigma	Cat# I5513
FastDigest Hin1II	Thermo Fisher Scientific	Cat# FD1834
FastDigest EcoRI	Thermo Fisher Scientific	Cat# FD0274
FastDigest XhoI	Thermo Fisher Scientific	Cat# FD0694
FastDigest BamHI	Thermo Fisher Scientific	Cat# FD0054
FastDigest SalI	Thermo Fisher Scientific	Cat# FD0644
T4 DNA Ligase Buffer	Thermo Fisher Scientific	Cat# 46300-018
T4 DNA Ligase (1 U/μL)	Thermo Fisher Scientific	Cat# 15224-017
GeneJET Plasmid Miniprep Kit	Thermo Fisher Scientific	Cat# K0503
GeneJET Gel extraction kit	Thermo Fisher Scientific	Cat# K0692
BSA (Bovine Serum Albumin)	Sigma	Cat# A2153
His-PP2AA1	This study	N/A
His-PP2AA3	This study	N/A

(*Continued on next page*)

Continued

REAGENT or RESOURCE	SOURCE	IDENTIFIER
His-PIN2HL	This study	N/A
Critical Commercial Assays		
Bio-Safe Coomassie Stain #1610786	Bio-Rad	Cat# 1610786
Non-Radioactive Phosphatase Assay Systems	Promega	Cat# V2460
HisPur Ni-NTA Resin	Thermo Fisher Scientific	Cat# 88222
γ-[^{32}P]-ATP	PerkinElmer	Cat# NEG502A001MC
Experimental Models: Cell Lines		
Nicotiana tabacum L., cv. Bright Yellow-2 (BY-2)	N/A	N/A
Experimental Models: Organisms/Strains		
Arabidopsis thaliana Col-0	N/A	N/A
A. thaliana Ws-4	NASC	N5390
A. thaliana eir1-4 (pin2-T)	[36]	SALK_091142
A. thaliana aux1-T (aux1)	[66]	SALK_020355
A. thaliana pAUX1::AUX1-YFP	[67]	N/A
A. thaliana pPR1::eYFP-NLS	[24]	N/A
A. thaliana npr1-1	[2]	N/A
A. thaliana npr3-1 npr4-3	[68]	N/A
A. thaliana npr1-1 npr3-1 npr4-3	[68]	N/A
A. thaliana cpr6	[23]	N/A
A. thaliana sid2-3	[69]	SALK_042603
A. thaliana rcn1-1 (rcn1, pp2aa1-1)	[42]	N/A
A. thaliana rcn1-6 (pp2aa1-6)	[49]	SALK_059903
A. thaliana pp2aa2-2	[45]	SALK_037095
A. thaliana pp2aa2-3	[45]	SALK_017541
A. thaliana pp2aa3-2	[45]	SALK_099550
A. thaliana pp2aa1 pp2aa2-3	[45]	N/A
A. thaliana pp2aa1 pp2aa3-1	[45]	N/A
A. thaliana pPIN2::PIN2-GFP	[70]	N/A
A. thaliana pPP2AA1::PP2AA1-GFP	[45]	N/A
A. thaliana DR5v2	[28]	N/A
A. thaliana eir1-4 DR5v2	This study	N/A
A. thaliana pPR1::eYFP-NLS	[24]	N/A
A. thaliana pp2aa1-6 pPR1::eYFP-NLS	This study	N/A
A. thaliana 35S::4 × myc-PP2AA1	This study	N/A
A. thaliana pp2aa1-6 cpr6	This study	N/A
Oligonucleotides		
Primers used in this study, see Table S1	This study	N/A
Recombinant DNA		
Plasmid pET28a-PP2AA1	This study	N/A
Plasmid pET28a-PP2AA3	This study	N/A
Plasmid pET28a-PIN2HL	This study	N/A
Plasmid pEGAD-35S::4 × myc-PP2AA1	This study	N/A
Software and Algorithms		
Arabidopsis Information Resource (TAIR)	http://www.arabidopsis.org/	N/A
ImageJ	https://imagej.nih.gov/ij/	NIH
Fiji	https://fiji.sc/	N/A

(*Continued on next page*)

Continued

REAGENT or RESOURCE	SOURCE	IDENTIFIER
ZEN	https://www.zeiss.com/microscopy/int/products/microscope-software/zen-lite.html	ZEISS
DNA MAN	https://www.lynnon.com/	N/A
ChemSketch	https://www.acdlabs.com/resources/freeware/chemsketch/	N/A

LEAD CONTACT AND MATERIALS AVAILABILITY

Requests for resources and reagents such as plasmids, compounds, mutant and transgenic lines should be directed to and will be fulfilled by the Lead Contact, Jiří Friml (jiri.friml@ist.ac.at).

EXPERIMENTAL MODEL AND SUBJECT DETAILS

Plant Materials and Growth Conditions

Arabidopsis thaliana (L.) mutants or transgenic lines are in Columbia-0 (Col-0) background if not particularly mentioned. The mutants and marker lines *pPIN2::PIN2-GFP* in *eir1-1* [70], *pAUX1::AUX1-YFP* [67], *aux1-T* [66], *eir1-4* (*pin2-T*) [36], *npr1-1* [2, 3], *sid2-3* (*sid2*) [69], *npr3-1 npr4-3* [68], *npr3-2 npr4-2* [68], *npr1-1 npr3-1 npr4-3* [68], *cpr1* [71], *cpr5* [72], *cpr6* [23], *rcn1-1* (*pp2aa1-1*, in Ws) [42], *rcn1-6* (*pp2aa1-6*) [49], *pp2aa2-2* [45], *pp2aa2-3* [45], *pp2aa3-2* [45], *pp2aa1,a2* (*pp2aa1, pp2aa2-3*) [45], *pp2aa1,a3* [45], *pp2aa2,a3* [45], *pPP2AA1::PP2AA1-GFP in Col-0* [45] and *DR5v2* [28] were published previously. The detailed information of plant lines, including mutants and marker lines, used in this study is listed in Key Resources Table. The primers used for genotyping the mutants were listed in Table S1.

For physiological experiments, surface-sterilized seeds were sown on Murashige and Skoog (1/2 MS) medium, supplemented with 1% sucrose, 0.8% phytoagar (pH 5.9), stratified at 4°C for 3 days (d), and then grown vertically in a growth chamber at 21°C with a 16-h-light/8-h-dark photoperiod.

METHOD DETAILS

Pseudomonas syringae treatment of *Arabidopsis* seedlings

P. syringae treatment was performed as reported previously [73]. A single colony of *P. syringae pv. tomato DC3000* (kind gift from Dr. Armin Djamei, IPK- Gatersleben) was cultured in 20 mL King's B (KB) liquid media overnight, to get OD_{600} between 0.4 and 0.6. The DC3000 cells were collected by spinning down at 1600 g, and were then resuspended in infection buffer (0.025% Silwet L-77, and 10 mM $MgCl_2$). The concentration was adjusted to OD_{600} = 0.01 (= ~5 × 10^6 CFU/mL) for treatment. The DC3000 suspension was dispensed into the plates with 5-day-old *pPR1::eYFP-NLS* seedlings and incubated for 3 min at 25°C. Afterward, the suspension was decanted, and seedlings were grown for another 2 days before imaging.

Pharmacological treatments

For long-term growth experiments, seeds were sown on MS plates containing indicated chemicals, including benzoic acid (Sigma, 242381), SA (Sigma, 247588), 3-OH-BA (Sigma, H20008), 4-OH-BA (Sigma, H20059), cantharidin (Sigma, C7632), NPA (Sigma, N12507), and TIBA (Sigma, T5910). After 3-d stratification at 4°C, they were moved to grow in a growth chamber as mentioned in the ''Plant material and growth conditions'' section, for 7 d or 10 d.

For short-term treatment, 4-d-old seedlings were incubated in liquid MS medium containing indicated chemicals for a certain time course as described in the Figure Legends. Detailed information of all chemicals used in this study is listed in Key Resources Table.

Free SA measurement by liquid chromatography-tandem mass spectrometry (LC-MS/MS)

Free SA contents was measured by LC-MS/MS as previously reported [74]. Approximately 10 mg fresh weight (FW) of roots from Col-0, *sid2-3*, and *cpr6* were collected and frozen in liquid nitrogen for LC-MS/MS. SA contents were calculated by the whole amount divided by the fresh weight (pmol/g FW).

Auxin transport in hypocotyls and tobacco BY-2 cells

The basipetal (rootward) transport assay of [^{3}H]-IAA in etiolated hypocotyls was performed according to a previous report [75], with a few modifications. 6-day-old etiolated Col-0 seedlings were placed on MS plates containing indicated chemicals, with 15 seedlings as one biological replicate, and 3 replicates per treatment. The [^{3}H]-IAA (PerkinElmer, ART-0340) droplets were prepared in MS medium with 1.25% agar and 500 μM [^{3}H]-IAA (1.45 μL in 10 mL), supplemented with same concentration of the chemicals as in the respective plate. The seedlings were decapitated and then covered with a [^{3}H]-IAA droplet at the shootward end. After incubation

for 6 hours in the dark, the lower part of the hypocotyls was cut and collected and were then ground completely in liquid nitrogen and homogenized in 1 mL scintillation solution (PerkinElmer, 6013199). The samples were incubated overnight to allow the radioactivity to evenly diffuse into the whole volume of the scintillation cocktail. Finally the radioactivity was measured with a scintillation counter (Hidex 300XL), with each sample counted for 100 s, 3 times. 3 samples with only the scintillation solution were used as background controls.

The transport of [^{3}H]-NAA, [^{3}H]-2,4-D, and [^{3}H]-BA in tobacco BY-2 cells was performed as published previously [32].

Imaging with Confocal Laser Scanning Microscopy (CLSM)

Fluorescence imaging was performed using a Zeiss LSM800 confocal laser scanning microscope (CLSM) with a GaAsP detector (Zeiss, Germany). The manufacturer's default settings (smart mode) were used for imaging GFP (excitation, 488 nm; emission, 495-545 nm)-, and tdTomato (excitation 561 nm; emission, 571-630 nm)-tagged proteins respectively. To image FM4-64-stained cells, a laser line of 543 nm was used for excitation, and an emission light with a wavelength of 600-700 nm was collected. For PI staining, excitation of 561 nm was used and emission signal was collected using a filter of 580- 680 nm. All images were recorded in 8 bit depth, 2 × line averaging. The images were analyzed and visualized with Fiji program [76].

Image analysis and morphological analysis

For root length measurement, photos were taken with a scanner (Epson Perfection V800 Photo) and then the root length was measured with ImageJ. The representative photos were taken by a camera (Sony A600 with a macro lens, 30mm/F3.5).

Molecular cloning

For pET28a-PIN2HL, pET28a-PP2AA1 and pET28a-PP2AA3 constructs, coding regions of *PIN2HL*, *PP2AA1* (primers PP2AA1-1/ PP2AA1-2) and *PP2AA3* (primers PP2AA3-1/ PP2AA3-2) were amplified and subcloned into vector pET28a (Novagen) with EcoRI/ SalI, EcoRI/*Xho*I, and EcoRI/*Xho*I respectively.

All the plasmids were identified by PCR and confirmed by sequencing (LGC). The primers used were listed in Table S1.

PP2A activity assay

The total PP2A activity assay was performed as previously reported with a Ser/Thr protein phosphatase assay kit (Promega, V2460) [48]. Approximately 1g of 7-d-old seedlings were ground in liquid nitrogen. Phosphatase storage buffer (250 mM imidazole, 1 mM EGTA, 0.1% β-mercaptoethanol, and 0.5mg/ml BSA, pH7.2) was added (1/2, volume/weight, hereafter short as v/w) to the frozen tissues and centrifuged to remove cell debris. Endogenous free phosphate was removed with the supplied Sephadex G-25 columns. PP2A phosphatase activity was measured using a molybdate dye-based phosphatase assay kit (Promega, V2460). The reactions were incubated at 37°C for 30 min before being terminated by the molybdate dye and additive mixture. The transparent 96-well plate was read on a Biotek Synergy H1 plate reader at 25°C at 600 nm, with 4 reads per well. The experiment was performed in three independent biological replicates for each treatment.

Protein extraction and immunoblot

To examine the expression level of myc-PP2AA1 in the *35S::myc-PP2AA1* overexpression line, or the phosphorylation level at Tyr307 (Y307) of PP2A C subunits, 100 mg of 7-d-old Col-0 seedlings were frozen in liquid nitrogen, ground totally, and homogenized in plant extraction buffer (20 mM Tris-HCl, pH 7.5, 150 mM NaCl, 0.5% Tween-20, 1 mM EDTA (ethylenediaminetetraacetic acid), 1 mM DTT (1,4-dithiothreitol)) containing a protease inhibitor cocktail (cOmplete, Roche). After addition of an equal volume of 3 × SDS (sodium dodecyl sulfate) loading buffer, the samples were boiled for 5 min, fractionated by 10% SDS-PAGE (sodium dodecyl sulfate-polyacrylamide gel electrophoresis) and transferred to a PVDF membrane by wet blotting. The membrane were incubated with a mouse anti-myc antibody (Millipore) or a mouse pY307-PP2Ac antibody (Millipore) and then with a bovine anti-mouse IgG HRP (horseradish peroxidase)-conjugated secondary antibody (GE Healthcare). HRP activity was detected by the Supersignal Western Detection Reagents (Thermo Scientific) and imaged with a GE Healthcare Amersham 600RGB system.

PIN2 phosphorylation assays

Roots from Col-0 and *pp2aa1-6* were treated with 40 μM SA or DMSO for 15 min, 1 h and 2 h. Untreated roots were also collected at time zero from Col-0, *pp2aa1-6* and *eir1-4* respectively. Protein extraction was performed as previously [41], with modifications for preserving phosphorylation status. The extraction buffer (EB) was: 50 mM Na_2HPO_4 (pH 7.4), 25% w/w sucrose, 7.5% glycerol, 20 mM betaglycerolphosphate, 5 mM Na_2MoO_4, 50 mM NaF, 0.1% casein, 10 mM EDTA (pH 8), 5 mM EGTA (pH 8), 20 mM borate/10 mM Tris-HCl (pH 8.2), 1 mM Na_3VO_4, 10 nM okadaic acid, 1 × PhosStop (Roche). Protease inhibitors (1 mM PMSF (phenylmethanesulfonyl fluoride), 1 mM Pefabloc-SC, 2 μg/mL E64, 0.7 μg/mL pepstatin A, 1 μg/mL aprotinin, and 1 μg/mL leupeptin) and insoluble PVPP (polyvinylpolypyrrolidone) were used. Samples were milled in liquid N_2, extracted with 4 volumes of EB, transferred to PVPP and spun at 500 g (2 min, 4°C). The supernatant was cleared again at 400 g (3 min, 4°C). The supernatant was saved as a total protein fraction, or diluted with 2 volumes of water and spun at 21, 000 g (20 min, 4°C) or 55, 000 g (10 min, 4°C) to obtain a membrane fraction pellet. All samples were solubilized with 0.5% SDS plus 20 mM DTE (Dithioerythritol), and precipitated with chloroform/methanol. Samples (corresponding to 2 or 3 mg original root weight) were denatured by heated only at 50°C to avoid aggregation, and were separated by SDS-PAGE and blotted. Blots were Ponceau stained to confirm loading, probed with rabbit anti-PIN2 [36],

stripped and reprobed with anti-PIN1 [37] or anti-PIP2;1 [65]. HRP activity was detected by the Supersignal Western Detection Reagents (Thermo Scientific) and imaged with Biorad XRS Chemidoc or conventional film.

PIN2-HL phosphorylation assay with [γ-^{32}P]-ATP

The phosphorylation assay of PIN2-HL with [γ-^{32}P]-ATP was performed as previously described [43], with a few modifications. Roots from Col-0 and *pp2aa1-6* (approximately 100 mg) were treated with 40 μM SA or DMSO for 1 h, and harvested for protein extraction. The samples were ground in liquid nitrogen and homogenized in 100 μL protein extraction buffer (20 mM Tris-HCl, pH 7.5, 150 mM NaCl, 0.5% Tween-20, 1 mM DTT, cOmplete protease inhibitor cocktail). 20 μL ($\sim$10 μg) recombinant His-PIN2HL protein was added with 4 μL plant extract, and then the reaction was initiated by adding 10 mM $MgCl_2$ and 2 μL (20 μCi) [γ-^{32}P]-ATP (NEG502A001MC, Perkin-Elmer). After incubation at 25°C for 1h, the reaction was terminated by adding 10 μL SDS loading buffer. The protein samples were separated by SDS-PAGE. The gel was rinsed with deionized H_2O, covered with a thin transparent plastic membrane, and developed with a phosphor plate overnight. The phosphor plate was finally scanned with a Fujifilm FLA 3000 plus DAGE system.

Drug Affinity Responsive Target Stability (DARTS) assay

The DARTS assay to test the binding of SA to PP2AA1-GFP was performed as previously reported [77, 78]. *pPP2AA1::PP2AA1-GFP* seedlings (7d) were used for total protein extraction. After harvesting, the samples were ground in liquid nitrogen, resuspended in protein extraction buffer (25 mM Tris-HCl, pH 7.5; 150 mM NaCl; 0.1% IGEPAL CA-630, Roche cOmplete protease inhibitor cocktail, EDTA free) with a 1:2 (w/v) ratio, and spun down to discard the cell debris. After quantifying the protein concentration (Quick Start Bradford Reagent, Bio-Rad), the cell lysate was aliquoted and incubated with 0, 50 μM or 500 μM SA respectively for 30 min at 25°C, mixing at a low speed. The treated extracts were further aliquoted, and mixed with different concentrations of Pronase (Roche) in Pronase buffer (25 mM Tris-HCl, pH 7.5; 150 mM NaCl). After incubation at 25°C for 30 min, the proteolytic digestion was terminated by adding protease inhibitor cocktail (cOmplete, Roche) and the samples were kept on ice for 10 min. The protein samples were then analyzed by western blot. PP2AA1-GFP was detected by an anti-GFP antibody (JL8, Clontech, 1:2000). HRP activity was detected by the Supersignal Western Detection Reagents (Thermo Scientific) and imaged with a GE Healthcare Amersham 600RGB system.

Recombinant protein expression and purification

Recombinant proteins were expressed in the *E. coli* strain BL21 (DE3) with induction by 0.5 mM IPTG (Isopropyl β-D-1-Thiogalactopyranoside, 16°C, 12 h) and then purified using Ni-NTA His binding resin (Thermo Scientific) according to the manufacturer's manual. The eluted samples were then purified with size exclusion chromatography, with a Superdex 200 increase column, on an ÄKTA pure chromatography system (GE Healthcare). Fractions were collected by 500 μL, and then analyzed by SDS-PAGE, followed by Coomassie brilliant blue (CBB, Bio-Safe Coomassie Stain #1610786 from BioRad) staining to check the protein quality.

Differential Scanning Calorimetry (DSC) analysis

The DSC analysis was performed with a MicroCal PEAQ-DSC Automated instrument (Malvern Panalytical). 5 μM PP2AA1 in 1 × PBS, with or without 50 μM SA, were heated from 25°C to 85°C at a heating rate of 1°C /min, cooled *in situ* and heated again under the same conditions. Data was obtained and analyzed with the provided program.

Chemical synthesis of SA derivatives

General information

All starting materials were used as received from commercial sources (Sigma-Aldrich, Merck, and Lach-Ner) without further purification. 2-(6-bromohexyl)isoindoline-1,3-dione was prepared using published procedure. THF [79] was distilled under argon from sodium benzophenone ketyl. All reactions were performed in round-bottom flasks fitted with rubber septa using the standard laboratory techniques. Reactions sensitive to air and/or moisture were performed under a positive pressure of argon. Analytical thin-layer chromatography (TLC) was performed using aluminum plates pre-coated with silica gel (silica gel 60 F^{254}). TLC plates were visualized by exposure to ultraviolet light and then were stained by submersion in basic potassium permanganate solution or in ethanolic phosphomolybdic acid solution followed by brief heating. Column chromatography was performed on silica gel 60 (40-63 μm). Melting points (mp) were tested on a capillary melting point apparatus. ^{1}H NMR and ^{13}C NMR spectra were recorded on 500 and 125 MHz in $CDCl_3$, CD_3OD, acetone-d_6 and DMSO-d_6; chemical shifts (δ ppm) and coupling constants (Hz) of ^{1}H NMR are reported in a standard fashion with relative to the remaining $CHCl_3$ present in $CDCl_3$ (δH = 7.27 ppm), central line of pentet in CHD_2OD present in CD_3OD (δH = 3.31 ppm), central line of pentet in $CHD_2C(O)CD_3$ present in acetone-d_6 (δH = 2.05 ppm), and central line of pentet in CHD_2SOCD_3 present in DMSO-d_6 (δH = 2.50 ppm). ^{13}C NMR chemical shifts (δ ppm) are reported relative to $CDCl_3$ (δC = 77.23 ppm, central line of triplet), CD_3OD (δC = 49.0 ppm, central line of heptet), $CD_3C(O)CD_3$ (δC = 29.84 ppm, central line of heptet), and DMSO-d_6 (δC = 39.52 ppm, central line of heptet). Proton coupling patterns are represented as singlet (s), doublet (d), doublet of doublet (dd), triplet (t), triplet of triplet (tt), pentet (p), and multiplet (m). HRMS data were obtained using quadrupole/ion trap mass analyzer. Analysis and assignments were made by comparison with literature spectroscopic data or using 2D-COSY, HSQC, HMBC, 2D-NOESY and 1D-NOEdiff experiments. Purity of final compounds was determined using the following protocol: Compound (1 mg) was dissolved in 1 mL of 1% methanol and injected (10 μL) onto a reverse-phased column (Symmetry C18, 5 μm, 150 mm × 2.1 mm; Waters, Milford, MA, USA) incubated at 25°C. Solvent (A) consisted of 15 mM ammonium formate adjusted to pH 4.0. Solvent (B) consisted of

methanol. At flow-rate of 200 μL/min, following binary gradient was used: 0 min, 10% B; 0-24 min. linear gradient to 90% B; 25-34 min. isocratic elution of 90% B; 35-45 min. linear gradient to 10% B. The effluent was introduced then to PDA detector (scanning range 210-700 nm with 1.2 nm resolution) and an electrospray source (source temperature 120°C, desolvation temperature 300°C, capillary voltage 3 kV, cone voltage 20 V). Nitrogen was used as well as cone gas (50 L/h) and desolvation gas (500 L/h). Data acquisition was performed in the full scan mode (50-1000 Da), scan time of 0.5 s. and collision energy of 6 V. Analyses were performed in positive mode (ESI^+) or in negative mode (ESI^-), therefore data were collected as quasi-molecular ions of $[M+H]^+$ and $[M-H]^-$, respectively.

C-10 (5-(allyloxy)-2-hydroxybenzoic acid)

Successively, K_2CO_3 (1.23 g, 8.93 mmol, 1.5 equiv) and allyl bromide (0.643 mL, 7.4 mmol, 1.25 equiv) were added to a solution of methyl 2,5-dihydroxybenzoate (1.0 g, 6.0 mmol, 1.0 equiv) in dry acetone (60 mL) and the resulting mixture was heated up to 60°C. After 5h at 60°C, the reaction mixture was cooled to 25°C (room temperature) and diluted with H_2O (50 mL). The whole mixture was extracted with CH_2Cl_2 (3 × 75 mL). Organic layers were combined and washed with brine (50 mL), dried over $MgSO_4$, filtered and volatiles were removed under reduced pressure. The residue was purified by flash column chromatography (SiO_2; hexane:EtOAc = 20:1 - > 10:1) and yielded 5-O-allylated ester (0.719 g, 58%). ^1H NMR (500 MHz, $CDCl_3$) δ (ppm): 3.95 (s, 3H), 4.52 (dt, *J* = 5.2, 1.8 Hz, 2H), 5.32 (dd, *J* = 10.5, 1.6 Hz, 1H), 5.43 (dd, *J* = 17.2, 1.7 Hz, 1H), 6.06 (ddt, *J* = 17.6, 10.5, 5.3 Hz, 1H), 6.92 (d, *J* = 9.2 Hz, 1H), 7.11 (dd, *J* = 9.2, 3.2 Hz, 1H), 7.32 (d, *J* = 3.2 Hz, 1H), 10.39 (s, 1H); 13C NMR (126 MHz, $CDCl_3$) δ (ppm): 52.3, 69.5, 111.7, 113.1, 117.8, 118.4, 124.6, 133.1, 150.8, 156.1, 170.2; MS (ESI^+), *m/z* (%): 209 $[M+H]^+$ (100); HRMS (ESI^+) *calcd.* for $C_{11}H_{13}O_4$ $[M+H]^+$: 209.0808, found 209.0808. 5-O-allylated ester (0.5 g, 2.4 mmol, 1.0 equiv) was dissolved in dry THF (24 mL) at 25°C. Potassium trimethylsilanolate (TMSOK, 0.924 g, 7.2 mmol, 3.0 equiv) was added and the resulting mixture was stirred at 25°C for 24 h. After this period of time, pH of the reaction mixture was adjusted to 2 with help of 10% aq. HCl. Organic solvents were removed under reduced pressure and additional H_2O (20 mL) was added. The whole mixture was extracted with CH_2Cl_2 (2 × 50 mL) and combined organic layers were washed with brine (30 mL), dried over $MgSO_4$ and evaporated to dryness under reduced pressure. The residue was purified by column chromatography (SiO_2; hexan:EtOAc:AcOH = 2:1:0.1 - > 1:1:0.1) to yield the desired compound C-10 (364 mg, 78%). ^1H NMR (500 MHz, $CDCl_3$) δ (ppm): 4.53 (dt, *J* = 5.3, 1.7 Hz, 2H), 5.32 (dd, *J* = 10.6, 1.5 Hz, 1H), 5.43 (dd, *J* = 17.4, 1.6 Hz, 1H), 6.06 (ddt, *J* = 17.5, 10.6, 5.4 Hz, 1H), 6.96 (d, *J* = 9.2 Hz, 1H), 7.19 (dd, *J* = 9.0, 3.1 Hz, 1H), 7.39 (d, *J* = 3.3 Hz, 1H), 10.03 (s, 1H); ^{13}C NMR (126 MHz, $CDCl_3$) δ (ppm): 69.8, 110.9, 113.8, 118.2, 119.1, 126.6, 133.2, 151.4, 157.1, 174.7; MS (ESI^+), *m/z* (%): 195 $[M+H]^+$; HRMS (ESI^+) *calcd.* for $C_{10}H_{11}O_4$ $[M+H]^+$: 195.0652, found 195.0651.

SA-1 (5-((6-aminohexyl)oxy)-2-hydroxybenzaldehyde hydrochlorid)

SA-3 (0.4 g, 1.09 mmol, 1.0 equiv) was dissolved in THF/H_2O = 2:1 (9.0 mL) and the resulting solution was cooled to 0°C. A solution of $HSO_3(NH_2)$ (0.211 g, 2.2 mmol, 2.0 equiv) in H_2O (2.2 mL) followed by $NaClO_2$ (0.108 g, 1.2 mmol, 1.1 equiv) in H_2O (1.2 mL) was added, and the resulting mixture was stirred at 0°C for 2 h. H_2O (20 mL) was added and the resulting solution was extracted with CH_2Cl_2 (3 × 50 mL). Organic layers were combined and washed with brine (25 mL), dried over Na_2SO_4, filtered and volatiles were removed under reduced pressure to yield carboxylic acid (0.343 g, 82%) sufficiently pure to be used in the next step. ^1H NMR (500 MHz, acetone-d_6) δ (ppm): 1.37 – 1.50 (m, 2H), 1.49 – 1.60 (m, 2H), 1.67 – 1.75 (m, 2H), 1.81 – 1.92 (m, 2H), 3.66 (t, J = 7.1 Hz, 2H), 4.20 (t, *J* = 6.6 Hz, 2H), 7.04 (dd, *J* = 8.9, 3.1 Hz, 1H), 7.11 (d, *J* = 9.0 Hz, 1H), 7.42 (d, *J* = 3.1 Hz, 1H), 7.92 (dd, *J* = 6.0, 3.3 Hz, 2H), 8.20 (dd, *J* = 6.0, 3.3 Hz, 2H); MS (ESI^+), *m/z* (%): 384 $[M+H]^+$; HRMS (ESI^+) *calcd.* for $C_{21}H_{21}NO_6Na$ $[M+Na]^+$: 406.1261, found 406.1262. Carboxylic acid (0.300 g, 0.78 mmol, 1.0 equiv) was dissolved in EtOH (8 mL) and hydrazine hydrate (0.076 mL, 1.56 mmol, 2.0 equiv) was added. The resulting mixture was stirred at 60°C for 6 h. White precipitate formed upon heating was filtered off and the filtrate was concentrated under reduced pressure to yield viscose oil. EtOH (10 mL) and H_2O (10 mL) were added and the pH was adjusted to 2 with help of 2.0 M aq. HCl. Concentration of the resulting mixture under reduced pressure and subsequent co-evaporation of the residue with EtOH (2 × 10 mL) and toluene (2 × 15 mL) yielded desired compound SA-1 (0.052 g, 27%). Mp: > 190°C (dec.); ^1H NMR (500 MHz, CD_3OD) δ (ppm): 1.44 – 1.51 (m, 2H), 1.51 – 1.62 (m, 2H), 1.65 – 1.75 (m, 2H), 1.82 (ddt, *J* = 14.2, 7.9, 4.2 Hz, 2H), 2.94 (t, *J* = 7.6 Hz, 3H), 4.07 (t, *J* = 6.3 Hz, 2H), 6.96 (dd, *J* = 8.9, 3.0 Hz, 1H), 7.00 (d, *J* = 8.9 Hz, 1H), 7.24 (d, *J* = 3.0 Hz, 1H); ^{13}C NMR (126 MHz, CD_3OD) δ (ppm): 26.6, 27.1, 28.5, 30.1, 40.7, 70.8, 116.9, 118.1, 121.3, 122.3, 152.1, 157.8, 168.5; MS (ESI^+), *m/z* (%): 254 $[M-Cl]^+$; HRMS (ESI^+) *calcd.* for $C_{13}H_{20}NO_4$ $[M-Cl]^+$: 254.1387, found 254.1388.

SA-2 (5-((5-(1,3-dioxoisoindolin-2-yl)pentyl)oxy)-2-hydroxybenzaldehyde)

2,5-dihydroxybenzaldehyde (0.5 g, 3.62 mmol, 1.0 equiv) was dissolved in dry DMF (36 mL) and K_2CO_3 (0.6 g, 4.3 mmol, 1.2 equiv) and 2-(6-bromohexyl)isoindoline-1,3-dione (1.07 g, 3.62 mmol, 1.0 equiv) were added. The resulting mixture was heated at 70°C for 4 h. All volatiles were removed under reduced pressure and the residue was dissolved in H_2O (50 mL). The whole mixture was extracted with EtOAc (3 × 50 mL) and combined organic layers were washed with brine (25 mL), dried over Na_2SO_4, filtered and evaporated to dryness. The residue was purified by flash column chromatography (SiO_2; hexane:EtOAc = 4:1- > 2:1) to yield SA-2 (0.627 g, 49%) as a yellowish viscose oil. ^1H NMR (500 MHz, $CDCl_3$) δ(ppm): 1.48 – 1.60 (m, 2H), 1.77 (p, *J* = 7.3 Hz, 2H), 1.82 – 1.93 (m, 2H), 3.73 (dd, *J* = 7.8, 6.5 Hz, 2H), 4.01 (t, *J* = 6.3 Hz, 2H), 6.85 (d, *J* = 9.0 Hz, 1H), 7.08 (dd, *J* = 8.9, 3.2 Hz, 1H), 7.28 (d, *J* = 3.1 Hz, 1H), 7.72 (dd, *J* = 5.5, 3.1 Hz, 2H), 7.85 (dd, *J* = 5.5, 3.1 Hz, 2H), 10.40 (s, 1H); ^{13}C NMR (126 MHz, $CDCl_3$) δ (ppm): 23.5, 28.4, 28.9, 37.9, 68.9, 113.5, 114.4, 123.4, 123.7, 125.4, 132.2, 134.2, 150.8, 155.8, 168.7, 189.9; MS (ESI^+), *m/z* (%): 354 $[M+H]^+$; HRMS (ESI^+) *calcd.* for $C_{20}H_{20}NO_5$ $[M+H]^+$: 354.1336, found 354.1335.

SA-3 (5-((6-(1,3-dioxoisoindolin-2-yl)hexyl)oxy)-2-hydroxybenzaldehyde)

Using the same procedure as for SA-2 synthesis. The residue was purified by flash column chromatography (SiO_2; hexane:EtOAc = 4:1- > 2:1) to yield SA-3 (1.04 g, 78%) as a white solid. Mp = 148-149°C; ^1H NMR (500 MHz, $CDCl_3$) δ (ppm): 1.41 (dd, *J* = 15.3, 7.9 Hz,

2H), 1.46 – 1.56 (m, 2H), 1.70 (dt, *J* = 15.0, 7.6 Hz, 2H), 1.74 – 1.84 (m, 2H), 3.69 (t, *J* = 7.3 Hz, 2H), 3.98 (t, *J* = 6.4 Hz, 2H), 6.83 (d, *J* = 9.2 Hz, 1H), 7.07 (dd, *J* = 8.9, 3.1 Hz, 1H), 7.28 (d, *J* = 3.3 Hz, 1H), 7.70 (dd, *J* = 5.3, 2.9 Hz, 2H), 7.82 (dd, *J* = 5.3, 2.9 Hz, 2H), 7.90 (s, 1H), 10.40 (s, 1H); ^{13}C NMR (126 MHz, $CDCl_3$) δ (ppm): 25.8, 26.7, 28.6, 29.2, 38.0, 69.1, 113.4, 114.4, 123.4, 123.7, 125.4, 132.2, 134.1, 150.9, 155.7, 168.7, 190.0; MS (ESI^+), *m/z* (%): 368 $[M+H]^+$; HRMS (ESI^+) *calcd.* for $C_{21}H_{22}NO_5$ $[M+H]^+$: 368.1492, found 368.1492.

SA-f (5-((5-aminopentyl)oxy)-2-hydroxybenzoic acid)

Methyl 2,5-dihydroxybenzoate (4.1 g, 24.4 mmol, 1.0 equiv) was dissolved in acetone/H_2O = 3.3:1 (190 mL) and K_2CO_3 (13.48 g, 98 mmol, 4 equiv) followed by 1,5-dibromopentane (10.0 mL, 73.4 mmol, 3.0 equiv) were added. The resulting mixture was refluxed for 4h, allowed to cool to 25°C and volatiles were removed under reduced pressure. Residue was extracted with CH_2Cl_2 (540 mL) and the organic layer was washed with H_2O (220 mL), brine (150 mL), dried over $MgSO_4$, filtered and evaporated to dryness yielding crude methyl 5-((5-bromopentyl)oxy)-2-hydroxybenzoate (16.5 g) as a brown oil. Crude ester was dissolved in acetone/H_2O = 3.3:1 (190 mL) and NaN_3 (7.9 g, 121.8 mmol, 5.0 equiv) was added. The resulting mixture was refluxed for 24 h before being allowed to cool to 25°C. Volatile solvents were removed under reduced pressure and the resulting mixture was extracted with CH_2Cl_2 (500 mL). Organic layer was washed with H_2O (150 mL), brine (100 mL), dried over $MgSO_4$, filtered and evaporated under reduced pressure. Resulting crude product was purified by flash column chromatography (SiO_2; hexan:EtOAc = 20:1- > 10:1) and yielded the desired methyl 5-((5-azidopentyl)oxy)-2-hydroxybenzoate (6.8 g, 99%) as a colorless oil. ^{1}H NMR (500 MHz, $CDCl_3$) δ (ppm): 1.40 – 1.53 (m, 2H), 1.60 – 1.67 (m, 2H), 1.81 (dt, *J* = 14.6, 6.5 Hz, 2H), 3.30 (t, *J* = 6.8 Hz, 2H), 3.93 (t, *J* = 6.3 Hz, 2H), 3.96 (s, 3H), 6.92 (d, *J* = 9.0 Hz, 1H), 7.08 (dd, *J* = 9.0, 3.1 Hz, 1H), 7.29 (d, *J* = 3.1 Hz, 1H), 10.37 (s, 1H); ^{13}C NMR (126 MHz, $CDCl_3$) δ (ppm): 23.6, 28.8, 29.0, 51.5, 52.5, 68.5, 112.1, 113.0, 118.7, 124.7, 151.6, 156.2, 170.5; MS (ESI^+), *m/z* (%): 280 $[M+H]^+$; HRMS (ESI^+) *calcd.* for $C_{13}H_{18}N_3O_4$ $[M+H]^+$: 280.1292, found 280.1291. Azide (6.79 g, 24.4 mmol, 1.0 equiv) was dissolved in dry THF (234 mL) and TMSOK (10.4 g, 73.2 mmol, 3 equiv; 90% purity) was added. The resulting mixture was stirred at 25°C for 24 h, cooled to 0°C and the pH of the mixture was adjusted to pH = 2 by 10% aq. HCl. The volume of the resulting mixture was in vacuo reduced to ½ of its original volume, and H_2O (100 mL) was added. The whole mixture was extracted with CH_2Cl_2 (2 × 400 mL) and combined organic layers were washed with H_2O (120 mL), brine (180 mL), dried over $MgSO_4$, and organic solvents were removed under reduced pressure. Crude product was dissolved in CH_2Cl_2 (20 mL) and hexane (60 mL) was added. Two third of the resulting solvent mixture were removed under reduced pressure and the desired 5-((5-azidopentyl)oxy)-2-hydroxybenzoic acid crystalized off the solution upon prolonged standing (24 h) at 25°C in form of white needles (5.89 g, 91%). Mp = 81-82.5°C; ^{1}H NMR (500 MHz, $CDCl_3$) δ (ppm): 1.53 – 1.63 (m, 2H), 1.64 – 1.75 (m, 2H), 1.82 (dq, *J* = 8.0, 6.3 Hz, 2H), 3.33 (t, *J* = 6.9 Hz, 2H), 3.95 (t, *J* = 6.3 Hz, 2H), 6.95 (d, *J* = 9.1 Hz, 1H), 7.15 (dd, *J* = 9.1, 3.1 Hz, 1H), 7.35 (d, *J* = 3.1 Hz, 1H), 10.08 (s, 1H); ^{13}C NMR (126 MHz, $CDCl_3$) δ (ppm): 23.6, 28.9, 29.0, 51.6, 68.6, 110.9, 113.3, 119.0, 126.2, 151.8, 157.0, 173.6; MS (ESI^-), *m/z* (%): 264 $[M-H]^-$; HRMS (ESI^+) *calcd.* for $C_{12}H_{15}N_3O_4Na$ $[M+Na]^+$: 288.0955, found 288.0956. 5-((5-azidopentyl)oxy)-2-hydroxybenzoic acid (0.75 g, 2.83 mmol, 1.0 equiv) was dissolved in EtOAc (14 mL) and 10% of palladium on carbon (3.8 mg, 0.05 equiv) was added. The whole mixture was placed under the hydrogen atmosphere (1.0 atm) and stirred for 24h. The whole mixture was filtered through microfilter (0.5 μm) and the filter was washed with MeOH (2 × 15 mL). Combined filtrates were evaporated under reduced pressure to give 5-((5-aminopentyl)oxy)-2-hydroxybenzoic acid SA-f (0.664 g, 98%) as a viscose oil. ^{1}H NMR (500 MHz, DMSO-d_6) δ (ppm): 1.42 (p, *J* = 7.7 Hz, 2H), 1.57 (p, *J* = 7.6 Hz, 2H), 1.64 (p, *J* = 7.3, 6.8 Hz, 2H), 2.78 (t, *J* = 7.4 Hz, 2H), 3.80 (t, *J* = 6.2 Hz, 2H), 6.69 (d, *J* = 8.8 Hz, 1H), 6.86 (dd, *J* = 8.8, 3.1 Hz, 1H), 7.36 (d, *J* = 3.2 Hz, 1H); ^{13}C NMR (126 MHz, DMSO-d_6) δ (ppm): 22.6, 26.8, 28.3, 38.8, 67.7, 114.4, 116.3, 119.5, 120.2, 149.4, 156.4, 171.5; MS (ESI^-), *m/z* (%): 238 $[M-H]^-$; HRMS (ESI^+) *calcd.* for $C_{12}H_{15}N_3O_4Na$ $[M+Na]^+$: 262.1050, found 262.1050. Purity 98+% (LC-MS), R_t = 11.93 min.

SPR analysis

SPR analysis of SA binding to His-PP2AA1 or His-PP2AA3 was performed with a Biacore T200 instrument (GE Healthcare). A synthesized active SA analog, SA-f, was immobilized on a CM5 sensor chip (GE Healthcare) first: the carboxyl group of the CM5 sensor chip was activated using a mixture of 1-ethyl-3-(3-dimethyl aminopropyl) carbodiimide hydrochloride (EDC) and N-hydroxy-succinimide (NHS) for 7 min at a flow rate of 5 μL/min. After activation, 1 mM of SA-f dissolved in 0.1 M borate buffer (pH 10) was passed over for a period of 3 min at 5 μL/min for immobilization. Then excess reactive groups were inactivated by flowing ethanolamine hydrochloride-NaOH pH 8.5 for 7 min, at 5 μL/min. 1 × PBS buffer (GE Healthcare) was used as running buffer in all assays. To test SA binding of His-PP2AA1 or His-PP2AA3, proteins were diluted in 1 × PBS buffer, and then flowed through the flow cell of sensor chip with SA-f immobilized or through the reference cell. The binding signal was generated by subtracting the signal of reference cell from that generated with the SA-f flow cell. The flow cells were regenerated with flowing 250 mM NaOH solution. Details about the chemical synthesis of SA derivatives are described in the Supplemental Information.

Accession Numbers

Sequence data from this article can be found in the *Arabidopsis* Genome Initiative or GenBank/EMBL databases under the following accession numbers: PIN1 (AT1G73590), PIN2 (AT5G57090), NPR1 (AT1G64280), NPR2 (AT4G26120), NPR3 (AT5G45110), NPR4 (AT4G19660), PINOID (AT2G34650), PP2AA1 (AT1G25490), PP2AA2 (AT3G25800), PP2AA3 (AT1G13320), PP2AC3 (AT3G58500), and PP2AC4 (AT2G42500).

QUANTIFICATION AND STATISTICAL ANALYSIS

For measurement of primary root length and root tip angles, photos were analyzed with ImageJ (https://imagej.nih.gov/ij/download.html). Fluorescence intensity of marker lines were quantified by Fiji (https://fiji.sc/).

Most data plotting and statistics were performed with Graphpad Prism8. A two-tailed t test was used for comparing two datasets. One-way ANOVA with a Tukey multiple comparison test was performed to evaluate the differences of multiple datasets. For root gravitropic responses, polar bar charts were generated by Origin 8.0, and both two-tailed t test and F-test were used to evaluate the mean value and variances respectively.

DATA AND CODE AVAILABILITY

This study did not generate/analyze datasets/code.

Plant Science 303 (2021) 110750

Contents lists available at ScienceDirect

Plant Science

journal homepage: www.elsevier.com/locate/plantsci

Developmental roles of Auxin Binding Protein 1 in *Arabidopsis thaliana*

Zuzana Gelová [a], Michelle Gallei [a], Markéta Pernisová [b,c], Géraldine Brunoud [b], Xixi Zhang [a,d], Matouš Glanc [a,e], Lanxin Li [a], Jaroslav Michalko [a], Zlata Pavlovičová [a], Inge Verstraeten [a], Huibin Han [a], Jakub Hajný [a,f], Robert Hauschild [a], Milada Čovanová [g], Marta Zwiewka [h], Lukas Hoermayer [a], Matyáš Fendrych [a], Tongda Xu [i], Teva Vernoux [b], Jiří Friml [a,*]

[a] *Institute of Science and Technology (IST), Am Campus 1, 3400 Klosterneuburg, Austria*
[b] *Laboratoire Reproduction et Développement des Plantes, Univ Lyon, ENS de Lyon, UCB Lyon 1, CNRS, INRA, 69342 Lyon, France*
[c] *Functional Genomics and Proteomics, National Centre for Biomolecular Research, Faculty of Science, Masaryk University, Kamenice 5, 62500 Brno, Czech Republic*
[d] *Department of Applied Genetics and Cell Biology, University of Natural Resources and Life Sciences (BOKU), Muthgasse 18, 1190 Vienna, Austria*
[e] *Department of Experimental Plant Biology, Faculty of Science, Charles University, Viničná 5, 12844 Prague, Czech Republic*
[f] *Laboratory of Growth Regulators, The Czech Academy of Sciences, Institute of Experimental Botany & Palacký University, Šlechtitelů 27, 78371 Olomouc, Czech Republic*
[g] *The Czech Academy of Sciences, Institute of Experimental Botany, Rozvojová 263, 165 02 Praha 6, Czech Republic*
[h] *Mendel Centre for Plant Genomics and Proteomics, Central European Institute of Technology (CEITEC), Masaryk University, Kamenice 5, 625 00 Brno, Czech Republic*
[i] *FAFU-Joint Centre, Horticulture and Metabolic Biology Centre, Haixia Institute of Science and Technology, Fujian Agriculture and Forestry University, Fuzhou, 350002 Fujian, People's Republic of China*

ARTICLE INFO

Keywords:
AUXIN BINDING PROTEIN 1 (ABP1)
Auxin
Plant development
Auxin signaling

ABSTRACT

Auxin is a major plant growth regulator, but current models on auxin perception and signaling cannot explain the whole plethora of auxin effects, in particular those associated with rapid responses. A possible candidate for a component of additional auxin perception mechanisms is the *AUXIN BINDING PROTEIN 1 (ABP1)*, whose function *in planta* remains unclear.

Here we combined expression analysis with gain- and loss-of-function approaches to analyze the role of *ABP1* in plant development. *ABP1* shows a broad expression largely overlapping with, but not regulated by, transcriptional auxin response activity. Furthermore, *ABP1* activity is not essential for the transcriptional auxin signaling. Genetic *in planta* analysis revealed that *abp1* loss-of-function mutants show largely normal development with minor defects in bolting. On the other hand, *ABP1* gain-of-function alleles show a broad range of growth and developmental defects, including root and hypocotyl growth and bending, lateral root and leaf development, bolting, as well as response to heat stress. At the cellular level, *ABP1* gain-of-function leads to impaired auxin effect on PIN polar distribution and affects BFA-sensitive PIN intracellular aggregation.

The gain-of-function analysis suggests a broad, but still mechanistically unclear involvement of *ABP1* in plant development, possibly masked in *abp1* loss-of-function mutants by a functional redundancy.

1. Introduction

The phytohormone auxin is a major coordinator of plant growth that governs a multitude of developmental processes. Its versatility is related to its differential distribution within plant tissues and the ability of cellular auxin concentrations determine various cell fate decisions. The establishment of these morphogenic auxin gradients and local auxin maxima is achieved by a combination of local auxin biosynthesis [1] and synergetic, directional cell-to-cell polar auxin transport [2].

Auxin concentration affects cellular processes, mainly through a modulation of transcription. A broad range of auxin-responsive transcriptional regulators remodel the transcriptome of cells through tissue specific expression and thus trigger complex developmental changes [3]. On this transcriptional level, auxin controls processes such as embryogenesis, vascular tissues formation and organogenesis of the shoot apex or maintenance of the root apical meristem [4].

Nevertheless, some cellular auxin effects occur too fast to be a result of transcriptome remodeling and/or they were shown not to require

* Corresponding author.
E-mail address: jiri.friml@ist.ac.at (J. Friml).

https://doi.org/10.1016/j.plantsci.2020.110750
Received 1 September 2020; Accepted 5 November 2020
Available online 13 November 2020

functional transcription or *de novo* protein synthesis. Auxin triggers rapid hyperpolarization of the plasma membrane leading to protoplast swelling [5,6], induces calcium ion and proton fluxes across the plasma membrane and therefore alkalizes the apoplast [7,8], and inhibits clathrin-mediated endocytic trafficking processes [9,10].

The auxin signal is transduced via several mechanisms [11,12]. The canonical pathway is mediated by a nuclear-localized co-receptor complex comprising the TRANSPORT INHIBITOR RESISTANT1/AUXIN SIGNALING F-BOX (TIR1/AFB) F-box proteins and the AUXIN/INDOLE-3-ACETIC ACID (Aux/IAA) transcriptional repressors. Here, auxin promotes the interaction of TIR1/AFBs with Aux/IAAs that results in ubiquitin-dependent degradation of the Aux/IAA proteins. Aux/IAA proteins act as transcriptional repressors of AUXIN RESPONSE FACTORs (ARFs) transcription factors and thus their degradation activates auxin-responsive transcription [13].

Notably, recent findings suggest that TIR1/AFB signaling mediates both rapid transcriptional as well as even faster non-transcriptional auxin effects on growth. In shoots, auxin via the TIR1/AFB pathway induces fast apoplast acidification and growth promotion by a rapid transcriptional regulation of *SMALL AUXIN UPREGULATED (SAUR)* genes [14,15]. In contrast, auxin-mediated growth inhibition in roots occurs within 30 s and does not require *de novo* protein synthesis but is still strictly dependent on the TIR1/AFB pathway [16]. Furthermore, the auxin-mediated fast depolarization of the plasma membrane and Ca^{2+} uptake were demonstrably linked with the TIR1/AFB signaling pathway [17].

Recently, two additional non-canonical auxin-sensing mechanisms were described. Auxin has been shown to bind directly to the atypical ARF ARF3/ETTIN to modulate chromatin states and interaction with other transcriptional regulators during gynoecium development [18,19]. The other mechanism involves TRANSMEMBRANE KINASE 1 (TMK1), a member of the plasma membrane-localized TMK receptor-like kinase family [20]. It was shown that auxin triggers cleavage of TMK1's intracellular kinase domain and its consequent translocation to the nucleus. There, the TMK1 kinase domain binds, phosphorylates and thus stabilizes two non-canonical Aux/IAAs, IAA32 and IAA34. Via this alternative transcriptional pathway, auxin regulates apical hook development [21]. TMK1 also regulates lateral root organogenesis and auxin biosynthesis by other cellular mechanisms [22,23]. Importantly, while the canonical TIR1/AFB receptors sense auxin predominantly in the nucleus, the TMKs located in the plasma membrane may perceive auxin from the apoplast by an unknown perception mechanism.

The accumulating developmental roles of TMKs in conjunction with their plasma membrane localization stir up a decades-lasting debate on the existence of a cell-surface auxin receptor. In the past, the best candidate appeared to be AUXIN BINDING PROTEIN 1 (ABP1). This evolutionally conserved 22-kDa glycoprotein [24,25] has been shown to bind auxin at apoplastic pH 5.5 [26–28] and although it predominantly localizes to the endoplasmic reticulum (ER), a small fraction has been proposed to reside in the apoplast [29]. ABP1 has been proposed to be mainly associated with rapid non-transcriptional auxin-mediated processes, but the genetic analysis has been hampered by the lack of viable loss-of-function mutants. It has also remained unclear how apoplastic ABP1 could transduce the auxin signal into the cell and therefore the requirement of a plasma membrane-localized docking partner was hypothesized. Later, ABP1 was found to interact with TMK1 in an auxin-dependent manner. It was proposed that ABP1 and TMK1 form an auxin-sensing complex at the plasma membrane that activates downstream cellular processes via small GTPases ROP2 and ROP6 and their effector proteins RIC1 and RIC4 [30–32]. Based on the phenotypes of *ABP1* gain-of-function mutants, the weak *abp1-5* allele and conditional *abp1* knock-down lines [33] *ABP1* was proposed to play a role in clathrin-mediated endocytosis [10,34,35], growth-correlating microtubule re-orientation [36], cell wall remodeling [37] or interdigitated growth of leaf pavement cells [30,36]. All these proposed roles were called into question by the failure to complement the alleged embryo lethal *abp1* phenotypes, by the coding sequence of *ABP1* [35] and by the identification of new *abp1* knock-out alleles with no obvious morphological phenotypes [38]. These discrepancies were clarified by proofs that the original *abp1* embryo lethal phenotypes were caused by disruption of a neighboring gene rather than *ABP1* itself [39,40]. Furthermore, the *abp1-5* line carries many additional mutations [41] and the conditional knock-down lines, despite independently targeting either ABP1 mRNA or protein [33], also have other targets [42]. Thus, with much of the previously used genetic material called into question and with only superficial phenotype analysis of the more recent, verified knock-out lines [38], the developmental and physiological roles of ABP1 still remain largely unclear.

Here we used the verified gain- and loss-of-function mutant lines in Arabidopsis to (re)evaluate the role of ABP1 in cellular processes, physiological responses and plant development.

2. Materials and methods

2.1. Plant material

Wild-type Col-0 (NASC, The Nottingham Arabidopsis Stock Centre; http://www.arabidopsis.info, N1092) was used as a control line. Previously published *Arabidopsis thaliana* lines were used in this study: *ABP1*$_{i1,2}$*::GUS* [43]; *abp1-C1*, *abp1-TD1* and background Col-0 used for generating *abp1-C1* by CRISPR (in text mentioned as WT for *abp1-C1*) [38]; *DR5rev::GFP* [44]; *35S::ABP1-GFP* [10]. The following *Arabidopsis thaliana* lines were generated in this study: *DR5rev::GFP;abp1-C1* and *DR5rev::GFP;abp1-TD1*. *DR5rev::GFP* was introduced into both *abp1* mutant backgrounds by genetic crossing. The *ABP1::ABP1;abp1-TD1* line was generated by introducing the *ABP1::ABP1* construct into the *abp1-TD1* background and the *ABP1::GFP-ABP1;abp1-C1* line was generated by introducing the *ABP1::GFP-ABP1* construct into the *abp1-C1* background using Agrobacterium-mediated transformation [45]. All transgenic lines and mutants used in this study are listed in Supplemental Table 1. All primers used for genotyping are listed in Supplemental Table 2.

2.2. Vector construction

All plasmids were constructed by the Gateway cloning technology (www.invitrogen.com). Previously generated constructs pDONR221-ABP1cDNA and pDONR221-ABP1cDNA-M2X containing cDNA sequence of *ABP1* [35] were used to construct the final plasmids *35S::ABP1* and *35S::ABP1-M2X* by recombination into the p2GW7 destination vector. *ABP1::ABP1* was constructed as follows: the 3.0 kb promoter, genomic coding region and 0.6 kb of 3' untranslated region for *ABP1* was amplified and inserted into a pDONR-Zeo vector, then inserted into the pGWB401 destination vector. *ABP1::GFP-ABP1* was constructed using a 1585 bp promoter fragment [43] and a N-terminal GFP fusion directly after the N-terminal signal peptide. The GFP insertion was flanked at the 5' end by a PKAPA linker (tested for cleavage using the SignalP-5.0 server) and at the 3' end by a PKPAPKPA linker. The *ABP1* fragments were amplified from genomic DNA using primer pairs 1 and 2 (promoter, signal peptide and 5' linker), 3 and 4 (GFP and 3' linker) and 5 and 6 (gABP1 gene body including 3' UTR). All three fragments were fused in a single overlap PCR reaction and cloned into the pDONR221 entry vector. The resulting construct was cloned into the pKGW,0 destination vector and sequenced. All primers used in this study are listed in Supplemental Table 2. All plasmids used in this study are listed in Supplemental Table 3.

2.3. Growth conditions

Seeds were chlorine gas sterilized or sterilized with 70 % EtOH, sown on plates with ½ Murashige and Skoog (MS) medium supplemented with

1 % (w/v) sucrose and 0.8 % (w/v) Phytoagar (pH 5.9) and stratified for 2 days at 4 °C. For experiments using Arabidopsis seedlings, the seedlings were grown on plates at 21 °C under a long-day photoperiod (16 h light/8 h dark) for the required time period. For experiments performed in soil, *in vitro* grown seedlings were transferred to soil and grown under a long-day photoperiod (16 h light/8 h dark) at 21 °C and 40 % relative humidity for the required time period. The light sources used were Philips GreenPower light emitting diode production modules in a deep red, far red, blue combination with a photon density of 140.4 µmol/m^2/s ± 3 %. For phyllotaxis measurement experiment, plants in soil were cultivated in growth chambers at 22 °C and 40 % relative humidity. Plants were kept under short day conditions (8 h light/16 h dark) for 28 days and then transferred to long day conditions (16 h light/8 h dark). Plants were always grown together within the growth chamber and with randomized positions within each tray in order to minimize the effect of environmental fluctuations. For etiolated growth, the plated and stratified seeds were exposed to light for 8 h and further covered with aluminum foil to cultivate them in the dark at 21 °C for 4 days (the shoot gravity response experiment) or in the dark chamber at 24 °C for 5 days (the etiolated growth experiment).

2.4. Histochemical GUS staining

6-d-old light-grown seedlings or 3-d-old etiolated seedlings of *ABP1$_{i1,2}$::GUS* were stained in 0.1 M sodium phosphate buffer (pH 7.0) containing 0.1 % X-GlcA sodium salt (Duchefa, 7240-90-6), 2 mM K_3[Fe(CN)$_6$], 2 mM K_4[Fe(CN)$_6$] and 0.05 % Triton X-100 for 2 h (light-grown seedlings) or 1 h (etiolated seedlings) at 37 °C. Further, samples were incubated overnight in 80 % (v/v) ethanol at room temperature. Tissue clearing was conducted as previously described [46]. DIC microscopy for analysis of GUS staining was performed using an Olympus BX53 microscope equipped with 10x and 20x air objectives and a DP26 CCD camera. For treatment, 5-d-old seedlings of *ABP1$_{i1,2}$::GUS* were transferred to ½ MS media supplemented with DMSO (mock) for 3.5 h, 25 µM L-Kynurenine (Sigma-Aldrich, 2922-83-0) for 3.5 h and 25 µM L-Kynurenine for 2 h followed by 300 nM IAA (Duchefa, 87-51-4) for 1.5 h. Subsequently, GUS staining and DIC microscopy were performed as described above.

2.5. Quantitative real-time PCR

After treatment with 100 nM IAA, seedlings were sampled in 4 biological replicates at different times (t0, 5 min, 30 min, 1 h, 2 h and 4 h). Total RNA was prepared from max100 mg of shoots/roots of 5-d-old seedlings with the RNeasy Plant Mini Kit (Qiagen, 74904) according to the manufacturers's instructions. cDNA was synthesized from 2 µg of total RNA using the QuantiNova Reverse Transcription Kit (Qiagen, 205410). For the mutant expression analyses, 3 biological replicates of full seedlings were used. All samples were pipetted in 3 technical replicates in a 384 well plate using an automated JANUS Workstation (PerkinElmer). According to the manufacturer's instructions, 5 µL reaction volume contained 2.5 µL Luna® Universal qPCR mastermix (NEB, M3003S). RT-qPCR analyses were performed using the Real-time PCR Roche Lightcycler 480 and the expression of PP2AA3 (At1G13320) or EF1a (At5G60390) was used as a reference [47]. For *ABP1*, 5 different primer pairs were evaluated and one representative graph is included in the manuscript. The primers used for the presented analysis are listed in Supplemental Table 2.

2.6. Confocal laser scanning microscopy and image analysis

Confocal laser scanning microscopy for analysis of fluorescence intensity was performed on a Zeiss LSM800 microscope assisted with Zeiss Zen 2011 software. Images were acquired with 20x/0.8 NA air (DR5 evaluation) or 40x/1.2 NA water immersion objectives (immunostaining).

2.7. DR5-GFP intensity measurement

5-d-old seedlings were transferred from solid ½ MS media to plates supplemented with either DMSO or 1 µM IAA for 3 h and imaged using confocal microscopy. The fluorescence intensity of GFP (excitation wavelength: 488 nm) was measured in ImageJ.

2.8. Microfluidic vRootchip

A microfluidic chip, vRootchip was used to analyze root tip growth in real-time. The manufacturing of the chip, sample preparation procedure, and data analysis of root tip growth was performed as described previously [16] and according to Li and Verstraeten *et* al. (unpublished). vRoot-chip was used with 10 nM IAA treatment in ¼ MS and 0.1 % sucrose. For imaging, the vertical confocal microscopy setup was used as described previously [16,48] and according to Li and Verstraeten et al. (unpublished). The 10 nM IAA solution was supplemented with the cell-impermeable fluorescent dye Tetramethylrhodamine isothiocyanate–Dextran [16].

2.9. Protoplast assay

Protoplasts from 3-d-old Arabidopsis root suspension culture were isolated and transformed as previously described [49]. Plasmids were prepared with an E.Z.N.A. Plasmid Maxi Kit I (Omega Bio-Tek, D6922-02). Protoplasts were co-transfected with 6 µg of *35S::ABP1* or *35S::ABP1-M2X*, 2.5 µg of *DR5::LUC* [50] and 2.5 µg of *35S::Renilla* [51]. As a control, protoplasts co-transfected with *DR5::LUC* and *35S::Renilla* were used. The protoplasts were incubated with either 100 nM NAA (Sigma-Aldrich, 86-87-3) for 16 h or without treatment for 12 h followed by 100 nM NAA for 4 h in the dark at room temperature. The corresponding amount of DMSO was used as mock treatment. Chemiluminescence measurement was performed with the Dual-Luciferase Reporter Assay System kit (Promega, E1910) using a Spectrophotometer BioTek SynergyH1 plate reader and Gen 5 software (both BioTek).

2.10. Root length analysis

Plates with 4- and 7-d-old seedlings were scanned using an Epson Perfection V370 Photo flatbed scanner and the root length was measured using ImageJ.

2.11. Root gravitropic assay

For measurements of root gravitropic curvature kinetics, 4-d-old seedlings were placed on plates with ½ MS and rotated 90° and roots were imaged using a vertically placed flatbed scanner (Epson Perfection V370 Photo). Multiple plates were held in place on the scanner by a custom-made holder. Max. 12 ROIs of the seedlings were automatically imaged with a resolution of 1200 dpi in 10 min time intervals using an AutoIt script for 8 h. In ImageJ, the time-lapse movies of the seedlings were manually cropped and registered (stabilized) using the Fiji plugin "StackReg" in "Rigid body" mode.

2.12. Root growth (RG)-tracker

We developed a custom MATLAB application named RG-tracker (https://research-explorer.app.ist.ac.at/librecat/record/8294) with a graphical user interface that allows entirely automated root growth analysis and tracking of the root tips. Root tips were segmented based on the pixel classification workflow of Ilastik [52], which only requires manual retraining in case the imaging conditions change drastically. For each point in time, the positions of the root tips were determined by segmenting the tip-probability output, performing particle size filtering and calculating the center of mass. The root tips were then tracked over time by solving the linear assignment problem using the Hungarian

algorithm (Munkres). The tracking algorithm can deal with gaps in the root tip detection and both the gap closing and the maximum linking distance can be specified in the GUI. Completed tracks are filtered by minimum track length, duration and maximum growth speed to remove miss-detections and then presented to the user as an overlay of raw data, tip segmentation and tip tracks. At this point the user can exclude additional tracks from further analysis and export the overlay of the tracks and the root time-lapse. The x/y coordinates of each root tip, growth speed, direction of growth, growth angle and root length are then calculated for each point in time and exported for further analysis. All experiment specific parameters such as the segmentation threshold, particle size, and track filters can be saved and together with the segmentation project file form the complete data set to clearly recapitulate the data analysis.

2.13. Lateral root analysis

For the analysis of lateral root primordia, samples of 6-d-old seedling were collected and the tissue was cleared as previously described [46]. To visualize the lateral root primordia DIC microscopy was performed using an Olympus BX53 microscope equipped with a 20x air objective. The lateral root primordia were staged according to Malam and Benfey (1997) [46]. For analysis of emerged lateral roots, 4-d-old seedlings were transferred from ½ MS plates to plates supplemented with 500 nM NAA or DMSO. After 3 days, the plates were scanned using an Epson Perfection V370 Photo flatbed scanner and the pictures were analyzed using ImageJ.

2.14. Etiolated hypocotyl growth

To analyze the growth of etiolated hypocotyls, the seedlings were recorded at 12 h intervals for 120 h in a dark chamber equipped with an infrared light source (880 nm LED; Velleman, Belgium) and a spectrum-enhanced camera (EOS035 Canon Rebel Xti, 400DH) with built-in clear wideband-multicoated filter and standard accessories (Canon) and operated by the EOS utility software. The hypocotyl length was measured using ImageJ.

2.15. Etiolated hypocotyl bending

To determine hypocotyl gravitropism, the 3-d-old dark grown seedlings were rotated 90°. The plates were scanned using an Epson Perfection V370 Photo flatbed scanner and the hypocotyl bending angle was measured after gravity stimulation in 6 h intervals for 24 h using ImageJ.

2.16. Rosette size analysis

Seeds were germinated and grown on horizontally placed plates for 12 days, scanned using an Epson Perfection V370 Photo flatbed scanner and the rosette size was measured manually in ImageJ.

2.17. Vasculature development analysis

10-d-old cotyledons were collected and the tissue was cleared as follows: 2 days incubation in 70 % ethanol with a subsequent incubation in 4 % HCl, 20 % methanol solution at 65 °C for maximum 15 min, followed by an incubation in 7 % NaOH, 60 % ethanol solution at RT for another 15 min. The cotyledons were then re-hydrated in a series of decreasing ethanol concentrations (60 %, 40 %, 20 % and 10 %) for 1 h in each concentration at RT. Before mounting the cotyledons in 50 % glycerol onto microscopy slides they were incubated for 1 h in 25 % glycerol, 5 % ethanol solution at RT. Imaging was done using an Olympus BX53 microscope equipped with a 4x air objective.

2.18. Hypocotyl growth under high temperature

Seeds were germinated and grown on ½ MS plates with or without 10 g/L sucrose under 28 °C, continuous light for 7 days. The plates were scanned using an Epson Perfection V370 Photo flatbed scanner and the hypocotyl length was measured using ImageJ.

2.19. Hyperosmotic stress assay

4-d-old seedlings were transferred on media supplemented with either 200 mM mannitol or 100 mM NaCl for 4 days. The plates were scanned using an Epson Perfection V370 Photo flatbed scanner and the root extension was measured using ImageJ.

2.20. UV laser ablation and periclinal division analysis

3-d-old seedlings were transferred from solid ½ MS medium to plates containing 10 μM propidium iodide (Sigma-Aldrich, 25535-16-4) supplemented with 1 μM NAA or DMSO. The subsequent sample preparation, UV laser ablation, imaging and periclinal cell division analysis was performed as described previously [53].

2.21. Bolting time, leaf number and branch number analysis

Seeds were suspended in 0.1 % agarose and spread out in soil. The number of plants, bolted and with the primary inflorescence stem grown 1 cm, was recorded every day. The number of rosette and cauline leaves was counted when the first flower of each plant bloomed. The rosette branch was referred to the branch directly attached to the rosette, while the cauline branch was defined as the branch on the primary stem. The number of cauline branches and rosette branches were counted 21 days after sowing.

2.22. Phyllotaxis and internode length measurement

Analyses of 25 plants per genotype were performed when the last flowers had appeared. Angles and internode lengths between two subsequent siliques were measured starting from the lowest one. For each individual of each genotype, the variance of the divergence angles was computed, and individual variances of divergence angles were compared between genotypes using a non-parametric Kruskal–Wallis test in R (version 3.5.1, r-project.org), since their values were not normally distributed.

2.23. Immunostaining

Immunostaining was performed with 3 to 4-d–old seedlings as previously described [54]. The primary antibodies used were rabbit anti-PIN1 [9] diluted 1:1000 (v/v) and rabbit anti-PIN2 [55] diluted 1:1000 (v/v). The secondary antibody used was sheep anti-rabbit conjugated with Cy3 (Sigma-Aldrich, C2306) diluted 1:600 (v/v).

2.24. PIN lateralization

3to 4-d-old seedlings were treated either with 10 μM NAA or DMSO as a control for 4 h in liquid ½ MS medium. Subsequently, immunostaining using PIN1 and PIN2 antibodies was performed. Samples were imaged using confocal microscopy. The fluorescence intensity of Cy3 (excitation wavelength: 548 nm) was measured using ImageJ.

2.25. BFA treatment

4-d–old seedlings were incubated in liquid ½ MS medium at a final concentration of 25 μM BFA (Sigma-Aldrich, 20350-15-6) for 1 h. For BFA/NAA treatment the seedlings were pre-treated with 5 μM NAA for 30 min followed by co-treatment with 25 μM BFA and 5 μM NAA for 1 h.

As control, seedlings were incubated in liquid ½ MS medium supplemented with DMSO substituting NAA. Subsequently, immunostaining using PIN1 and PIN2 antibodies was performed. Samples were imaged using confocal microscopy and the fluorescence signal of Cy3 (excitation wavelength: 548 nm) was detected. BFA body formation was scored from 0 (no BFA body formation) to 3 (maximal BFA body formation) for each image, reflecting both the number of cells with BFA bodies as well as size and number of BFA bodies per cell. To avoid cognitive bias, all images were encoded prior to analysis.

2.26. Global transcriptome data analysis

Tissue-specific expression pattern and expression following different perturbations were obtained using Genevestigator (www.genevestigator.com) and were based on the 'AT_AFFY_ATH1-0' dataset.

2.27. Statistical analysis

If not mentioned differently, all data were analyzed using Student's t tests with p-value (*, $P < 0.05$; ** $P < 0.01$; *** $P < 0.001$) in the software Prism v8.3.0 (GraphPad).

2.28. Accession numbers

Sequences data from this article can be found in the GenBank/EMBL libraries under the following accession numbers: ABP1 (AT4G02980); PP2AA3 (At1G13320); EF1a (At5G60390).

3. Results

3.1. ABP1 expression and regulation by auxin

To obtain indications regarding the developmental processes and conditions in which ABP1 might play a role, we analyzed the *ABP1* expression pattern. The analysis of publicly available global transcriptome data in GENEVESTIGATOR® [56] suggested that *ABP1* is expressed constitutively in different tissues during development. *ABP1* transcription appears to be the highest in rosette leaves and roots, whilst lowest in pollen (Fig. S1A-B). In seedlings, *ABP1* is expressed in cotyledons, hypocotyls and root tips as well as in lateral roots. Global transcriptomics data following different perturbations suggested that *ABP1* expression is elevated in response to heat and slightly decreased following biotic stress (Fig. S1C).

To obtain more detailed insight into the *ABP1* expression pattern and confirm the global transcriptome analysis-based notions, we used an *ABP1::GUS* line to report *ABP1* promoter activity *in vivo*. GUS staining of

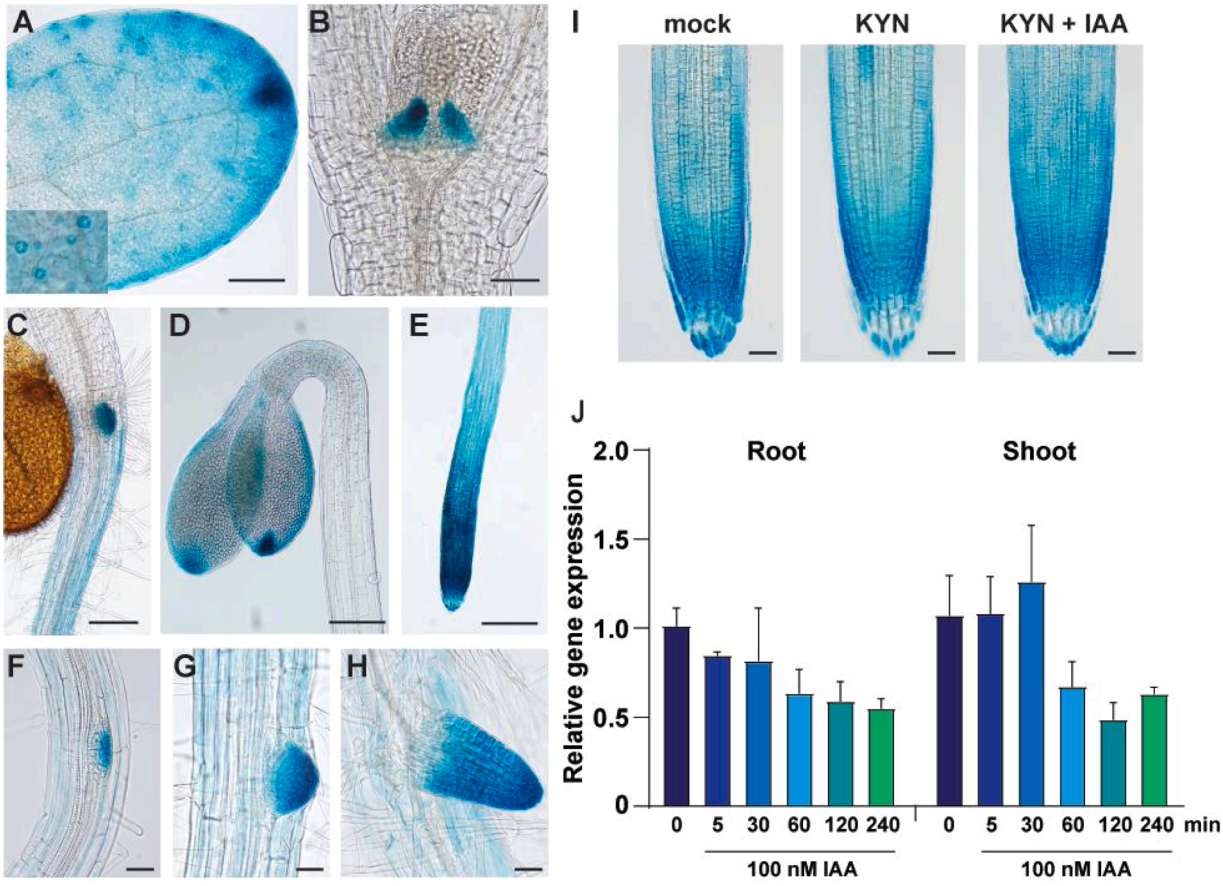

Fig. 1. *ABP1* expression and regulation by auxin.
(A–H) *ABP1::GUS* expression pattern. (A) 6-d-old cotyledon with inset detail of stomata, scale bar =100 μm. (B) shoot with hydathods of 6-d-old seedling, scale bar =50 μm. (C) shoot-root junction of 6-d-old seedling, scale bar =50 μm. (D) apical hook of 3-d-old etiolated seedling, scale bar =100 μm. (E) root tip of 6-d-old seedling, scale bar =100 μm. (F–H) lateral root primordia of 6-d-old seedling in IV, V and emerged stage respectively, scale bar =20 μm.
(I) Representative pictures of *ABP1::GUS* expression pattern in 5-d-old seedlings after treatment with DMSO (mock) for 3.5 h, 25 μM L-Kynurenine for 3.5 h and 25 μM L-Kynurenine for 2 h followed by 300 nM IAA for 1.5 h. For each treatment, at least 15 seedlings were evaluated. The experiment was repeated 2 times with similar results. Scale bar =20 μm.
(J) Quantitative Real-time PCR of *ABP1* expression in roots and shoots of 5-d-old Col-0 seedlings after DMSO (mock), and 5 min, 60 min, 120 min and 240 min of 100 nM IAA treatments. Expression of *ABP1* is normalized on expression of *PP2A* housekeeping gene. Experiment was repeated 3 times with similar result.

6-d-old seedlings confirmed the *ABP1* expression in cotyledons in which we detected stronger *ABP1* promoter activity in hydathodes and stomata (Fig. 1A-B). In both light- and dark-grown hypocotyls, the *ABP1* promoter activity was very low (Fig. 1C–D). Further, we confirmed *ABP1* expression in the primary root, particularly in the root tip (Fig. 1E) and during different stages of lateral root development (Fig. 1F–H). We observed that *ABP1* expression pattern in hydathodes, root tip and lateral roots largely overlaps with that of *DR5* reporters for transcriptional auxin response [43,44,50,57–59].

Therefore, we tested whether auxin regulates *ABP1* promoter activity and transcription. We employed L-Kynurenine, an inhibitor of auxin biosynthesis [60], to decrease auxin levels in the *ABP1::GUS* seedlings. We tested both, the effect of L-Kynurenine treatment alone or with subsequent auxin treatment, to study the effect of exogenously applied auxin. Overall, we detected no obvious changes in GUS reporter activity either after L-Kynurenine or after L-Kynurenine followed by auxin treatments (Fig. 1I).

To additionally verify these observations, we examined the auxin effect on *ABP1* transcription using real-time quantitative PCR (RT-qPCR). We performed RT-qPCR with roots and shoots of 5-d-old wild-type seedlings after auxin treatment. Consistent to what we observed with the *ABP1::GUS* transgenic line, auxin treatment did not strongly affect *ABP1* transcription (Fig. 1J).

These results show that *ABP1* expression overlaps with auxin

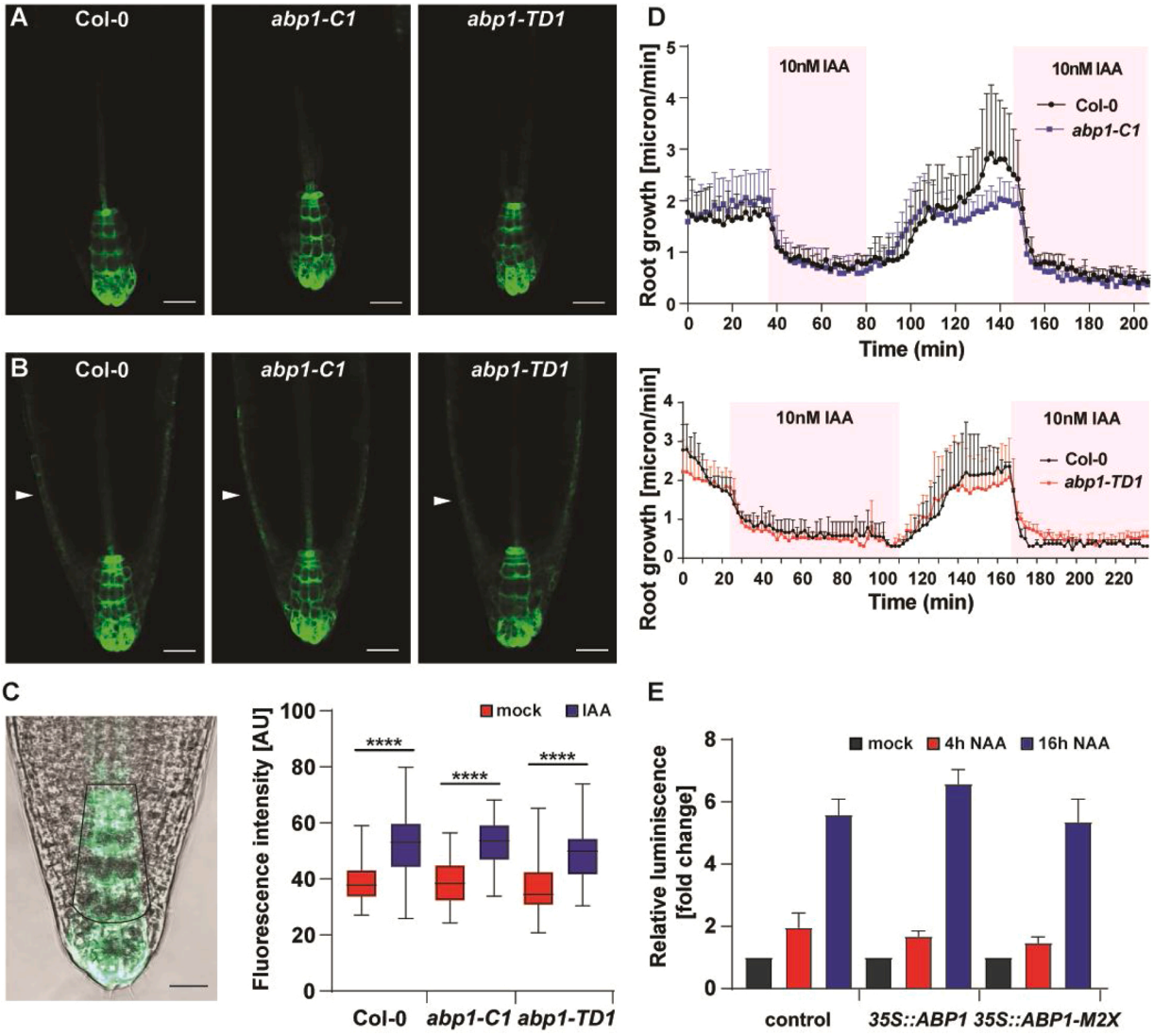

Fig. 2. Involvement of ABP1 in TIR1/AFB-mediated auxin responses.

(A–B) *DR5rev::GFP* expression pattern in 5-d-old seedlings of wild-type Col-0, *abp1-C1* and *abp1-TD1* mutants with DMSO (A) or with 1 μM IAA (B) treatment for 3 h. Arrowheads point to DR5 signal expanded to lateral root cap. Scale bar =30 μm.

(C) Representative picture of *DR5rev::GFP* expression in Col-0 with highlighted region that was quantified. Scale bar =50 μm. Quantification of *DR5rev::GFP* signal in root tips of 5-d-old Col-0, *abp1-C1* and *abp1-TD1* seedlings with DMSO (A) or with 1 μM IAA (B) treatment for 3 h. For each genotype per treatment, at least 15 seedlings were measured. The pooled result of 2 independent experiments is presented. For box plot, box defines the first and third quartiles, and the central lines in the box represent the median. Whiskers, from minimum to maximum. Asterisks indicate significant differences according to Student's t-tests (****, $P < 0.0001$).

(D) Root growth rate of *abp1-C1* (upper graph) and *abp1-TD1* (lower graph) compared to Col-0 measured in the vRootchip with repetitive 10 nM IAA treatment (magenta). n = 5, 6 for Col-0 and *abp1-C1*, respectively. n = 5 for *abp1-TD1*; n = 3,2 for Col-0 from 0−102 min and 102−236 min, respectively. Error bars denote standard deviation. The experiment was repeated 2 times with similar results.

(E) Activity of *DR5::LUC* reporter in response to *ABP1* and *ABP1-M2X* overexpression after mock (DMSO) and 100 nM IAA treatment in protoplasts. The values presented were calculated as a ratio between *DR5::LUC* enzymatic activity and internal control *Renilla::LUC* enzymatic activity and were further normalized on mock treatment values. Error bars denote standard error. The statistical difference was tested by Student's t-test. The experiment was repeated 2 times with similar results.

response maxima during seedling development, but that *ABP1* promoter activity and *ABP1* transcription are not significantly regulated by auxin.

3.2. Involvement of ABP1 in TIR1/AFB-mediated auxin responses

Considering that *ABP1::GUS* expression pattern largely overlaps with that of DR5 reporters for transcriptional auxin response [43,44,50,57–59], we investigated whether *ABP1* function is in any way linked to the transcriptional auxin signaling downstream of TIR1/AFB receptors [12,61]. First, we introduced *DR5rev::GFP* reporter into *abp1* loss-of-function mutants (*abp1-C1* and *abp1-TD1*). In the *abp1* mutant backgrounds, *DR5rev::GFP* expression pattern in the root tip was not visibly altered and showed the typical maximum in the columella cells and quiescent center [57,58,62] (Fig. 2A). After auxin treatment, the *DR5rev::GFP* signals in *abp1* mutants expanded to the lateral root cap and stele to the same extent as in the control (Fig. 2B). Quantification of the DR5 signal without and with auxin treatment in the root tips did not reveal any differences between the control and *abp1* mutants (Fig. 2C). Taken together, these results show that the DR5 auxin response reporter's readout does not depend on a functional *ABP1*.

Recently it was demonstrated, that the TIR1/AFB pathway is required for a rapid non-transcriptional auxin response [16]. We used this experimental system to investigate TIR1/AFB-mediated non--transcriptional auxin effects on root growth in the mutant lines. Evaluation of root growth on the vertical imaging set-up with high spatio-temporal resolution [16,48] revealed a comparable auxin sensitivity of the *abp1-C1* and *abp1-TD1* mutants and the control line in terms of rapid inhibition of root growth (Fig. 2D) suggesting that *abp1* loss-of-function does not affect the TIR1/AFB-mediated non-transcriptional response.

Next, we tested the effect of *ABP1* gain-of-function on TIR1/AFB-mediated transcriptional auxin signaling by performing a transient expression assay in Arabidopsis protoplasts. We derived protoplasts from root cell culture, co-transfected them with *DR5::LUC* reporter together with either *35S::ABP1* or *35S::ABP1-M2X* carrying a mutation in the auxin-binding site [35] and measured the *DR5::LUC* signal with and without auxin. The DR5-driven luciferase activity increased after both short (4 h) and long (16 h) term auxin treatment, however neither *ABP1* nor *ABP1-M2X* overexpression had any significant influence on this induction (Fig. 2E).

These results do not support a strict requirement of *ABP1* function in the canonical, TIR1/AFB-mediated auxin signaling pathway.

3.3. Role of ABP1 in primary root growth and root gravity response

Since *ABP1* is expressed in the primary root and root tip (Fig. 1C, E) and auxin is a major regulator of root growth [16,63–65], we analyzed whether *abp1* loss-of-function or the overexpression influences primary root growth. We used two independent loss-of function mutant lines, *abp1-C1* and *abp1-TD1* and a line expressing *ABP1-GFP* under the control of the ubiquitous 35S promoter (*ABP1-GFP^{OE}*) (Fig. S2). Visually, roots of all tested lines developed normally (Fig. 3A). We measured the root length of 4- and 7-d-old seedlings and found that the root growth of *abp1* mutants was comparable to WT, while roots of *ABP1-GFP^{OE}* were shorter

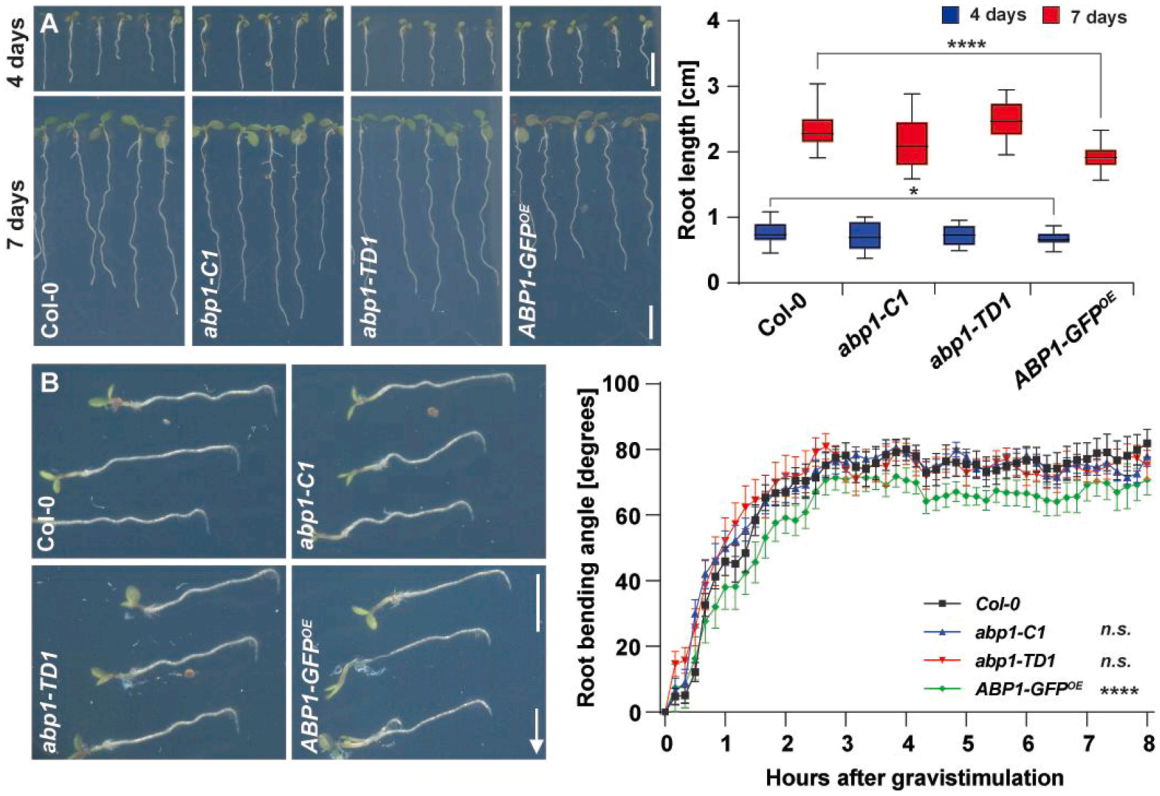

Fig. 3. Role of ABP1 in primary root growth and root gravity response.
(A) Representative images of 4- (upper panel) and 7-d-old (lower panel) Col-0, *abp1-C1*, *abp1-TD1*, and *ABP1-GFP^{OE}* seedlings. Scale bar =5 mm. The boxplot shows the root length of 4- and 7-d-old Col-0, *abp1-C1*, *abp1-TD1*, and *ABP1-GFP^{OE}* seedlings. For each genotype, at least 15 roots were measured. For box plot, box defines the first and third quartiles, and the central lines in the box represent the median. Whiskers, from minimum to maximum. Asterisks indicate significant differences according to Student's t tests (*, $P < 0.05$; ****, $P < 0.0001$). The experiment was repeated 2 times with similar results.
(B) Representative images of 4-d-old Col-0, *abp1-C1*, *abp1-TD1*, and *ABP1-GFP^{OE}* seedlings after 8 h gravistimulation by 90° reorientation. Scale bar =1 cm. Arrow indicates gravity direction. Kinetics of root bending during 8 h of gravity stimulus for Col-0, *abp1-C1*, *abp1-TD1*, and *ABP1-GFP^{OE}*. For each line at least 15 roots were measured. Error bars denote standard deviation. Asterisks indicate significant differences according to Student's t tests (****, $P < 0.0001$). The experiment was repeated 2 times with similar results.

(Fig. 3A).

Asymmetric auxin distribution is involved in gravitropism, an important plant adaptive process manifested by shoot and root bending [66–69]. In order to describe a role of *ABP1* during root bending, we gravistimulated (90° reorientation) roots of 4-d-old *abp1* and *ABP1-GFP*^{OE} seedlings for 8 h and measured the root bending kinetics. We observed that *abp1* mutants showed a normal root gravitropic response while the roots of *ABP1-GFP*^{OE} bent significantly slower (Fig. 3B).

In summary, the *abp1* loss-of-function mutants do not have any impact on either root growth or root bending, whereas gain-of-function leads to slower root growth and root bending.

3.4. Role of ABP1 during lateral root development

As *ABP1* is expressed during lateral root development (Fig. 1F–H), and auxin promotes lateral root initiation and formation [59], we analyzed lateral root development in 6-d-old *abp1* and *ABP1-GFP*^{OE} seedlings. We counted and scored all lateral root primordia stages. The analysis revealed that both *abp1* mutants and *ABP1-GFP*^{OE} developed a comparable number of lateral root primordia (Fig. 4A). In addition, we could not find any differences in the frequency of individual primordial stages (Fig. 4B).

To test the auxin effect on lateral root emergence, we transferred 4-d-old seedlings to media supplemented with auxin and 3 days later we counted the density of emerged lateral roots. We observed that the density of emerged lateral roots was comparable between *abp1* mutants and WT, while *ABP1-GFP*^{OE} developed less lateral roots (Fig. 4C).

Together, the results presented above demonstrate that both *abp1* loss-of-function mutants do not have any impact on lateral root development, but that *ABP1* overexpression leads to impaired auxin-induced lateral root development.

3.5. Role of ABP1 in etiolated growth and shoot gravity response

Auxin is required for a sustained rapid hypocotyl-elongation of

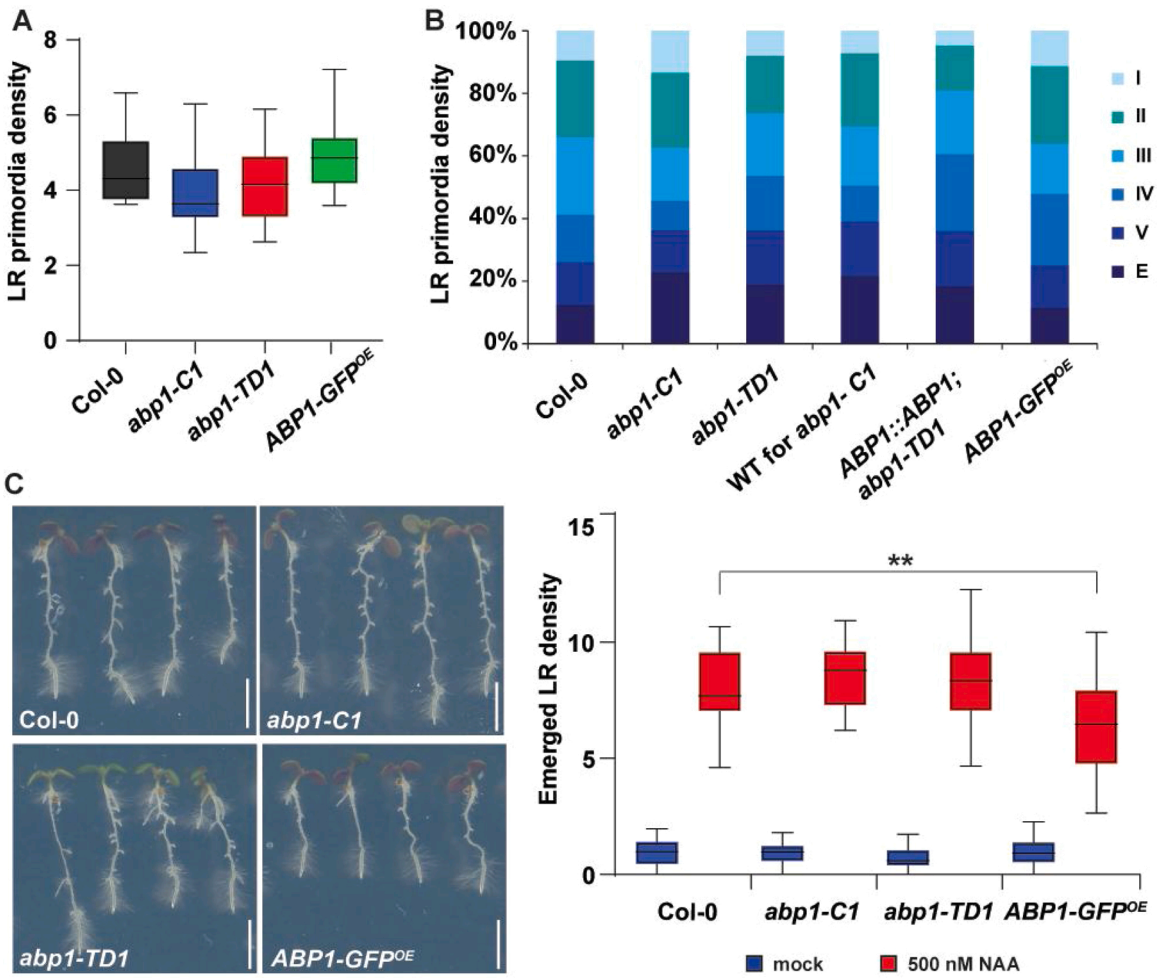

Fig. 4. Role of ABP1 during lateral root development.

(A) Density of lateral root (LR) primordia in 6-d-old Col-0, *abp1-C1*, *abp1-TD1*, and *ABP1-GFP*^{OE} seedlings. For each line, primordia of at least 15 roots were counted. For box plot, box defines the first and third quartiles, and the central lines in the box represent the median. Whiskers, from minimum to maximum. The statistical difference was tested by Student's t-test. The experiment was repeated 2 times with similar results.

(B) Density of individual lateral root primordia stages in 6-d-old Col-0, *abp1-C1*, *abp1-TD1*, WT for *abp1-C1* as control for *abp1-C1*, complemented *abp1-TD1* mutant (*ABP1::ABP1;abp1-TD1*) as control for *abp1-TD1*, and *ABP1-GFP*^{OE} seedlings expressed as percentage. For each line, primordia of at least 15 roots were scored. The experiment was repeated 2 times with the similar results.

(C) Representative pictures of Col-0, *abp1-C1*, *abp1-TD1*, and *ABP1-GFP*^{OE} roots 3 days after 500 nM NAA treatment. Scale bar =5 mm. The box plot shows emerged lateral root density. For each line at least 15 roots were scored. For box plot, box defines the first and third quartiles, and the central lines in the box represent the median. Whiskers, from minimum to maximum. Asterisks indicate significant differences according to Student's t tests (** $P < 0.01$). The experiment was repeated 2 times with similar results.

plants grown in darkness [70–72]. The auxin-induced growth of etiolated hypocotyl segments is not altered in *abp1* loss-of-function mutants [15]. To complement these observations in intact plants, we analyzed growth of etiolated hypocotyls for both *abp1* loss- and gain-of-function lines and measured the hypocotyl length of the dark-grown seedlings every twelve hours (Fig. 5A). Initially, the hypocotyls of all tested lines elongated at the same speed. Later, starting 36 h after germination, etiolated hypocotyls of *ABP1-GFP*^{OE} elongated faster and they were significantly longer than the control 120 h after germination. On the other hand, etiolated hypocotyls of both *abp1* mutant alleles elongated comparably to the controls.

The gravitropic response of the hypocotyl is also regulated by auxin [67–69]. To investigate a possible function of *ABP1* in hypocotyl gravitropism, we gravistimulated 3-d-old etiolated hypocotyls and measured the bending angle after 6, 18 and 24 h. The analysis revealed that the *ABP1-GFP*^{OE} hypocotyls bend significantly less than WT (Fig. 5B). The difference was noticeable already 6 h after gravistimulation. Notably, both *abp1* mutants showed a similar tendency towards slower bending, albeit not significant.

In summary, these observations unveiled that *abp1* loss-of-function alleles do not show defects in etiolated hypocotyl growth and gravitropic responses, whereas gain-of-function of *ABP1* leads to increased elongation and defective gravity-mediated hypocotyl bending.

3.6. Role of ABP1 in leaf development and vasculature formation

In cotyledons, auxin and its directional transport act as a positional cue for vasculature vein formation [73,74] and also regulate leave shape and serration [75]. We analyzed whether ABP1 plays a role in the young rosette growth and development as well as in cotyledon vasculature formation. Macroscopically, neither *abp1* mutants nor *ABP1-GFP*^{OE} showed any defects in cotyledon development (Fig. 6A). We measured the size of young rosettes consisting of both cotyledons and primary leaves. We found that *ABP1-GFP*^{OE} had slightly bigger rosettes (Fig. 6A).

The vasculature of cotyledons typically consists of four formed closed loops (Fig. 6B). We scored the number and the completeness of these loops in *abp1* mutants and *ABP1-GFP*^{OE}. We observed a normal vasculature pattern in both *abp1* mutants, but *ABP1-GFP*^{OE} showed irregularities at higher frequency than WT (Fig. 6B). The most striking difference in *ABP1-GFP*^{OE} were fewer loops (22 % in WT and 46 % in *ABP1-GFP*^{OE}) and loops that were opened at their upper end, which is almost never seen in WT (2 % in WT and 6.5 % in *ABP1-GFP*^{OE}).

The results show that, whilts *abp1* loss-of-function has no impact on leaves growth and venation, *ABP1* gain-of-function affects vasculature formation.

3.7. Role of ABP1 during stress

Abiotic stresses, such as salinity and osmotic stress, induce changes in turgor pressure and in polar auxin transport [76–78] and thus lead to root growth inhibition. On the other hand, an increase of auxin biosynthesis results in higher salt tolerance [79,80]. The regulation of *ABP1* transcription by various stresses such as heat (Fig. S1) prompted us to test the requirement of *ABP1* to adapt to stress.

We challenged *abp1* mutants with osmotic stress using mannitol or sodium chloride treatments to assess the involvement of *ABP1* in stress

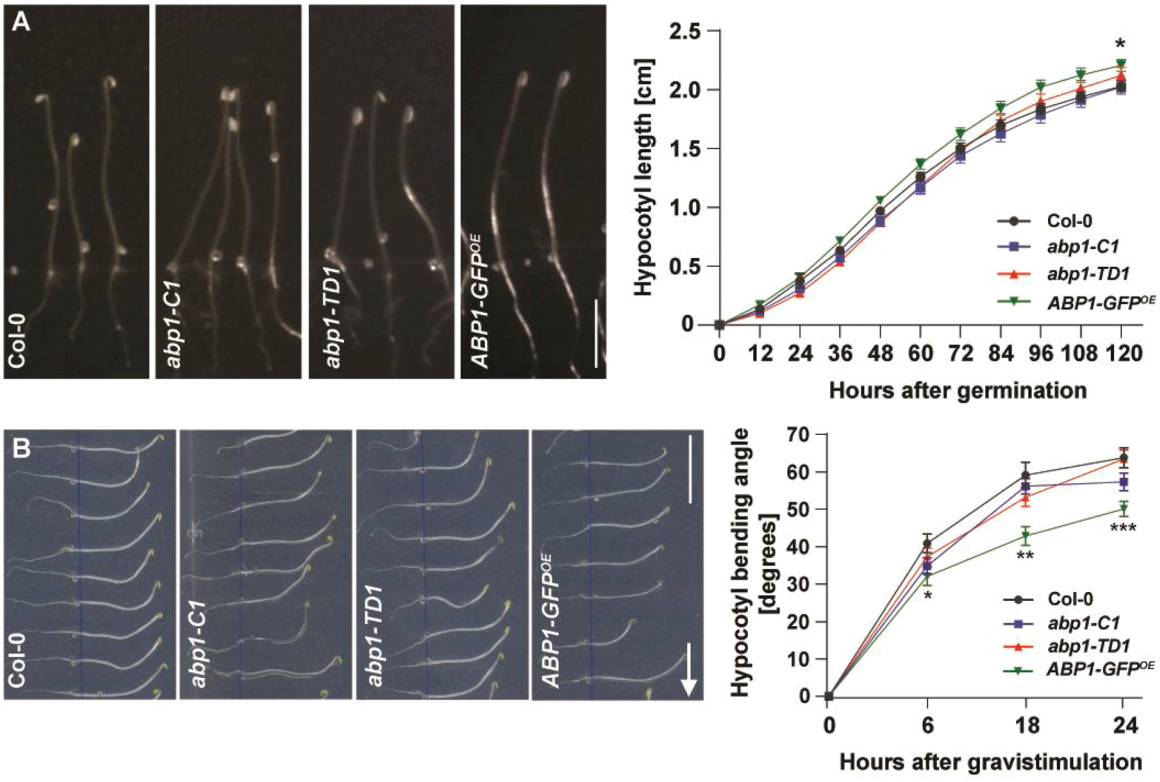

Fig. 5. Role of ABP1 in etiolated growth and shoot gravity response.
(A) Representative images of 3-d-old etiolated hypocotyls of Col-0, *abp1-C1*, *abp1-TD1*, and *ABP1-GFP*^{OE}. Scale bar =1 cm. Elongation rate of Col-0, *abp1-C1*, *abp1-TD1*, and *ABP1-GFP*^{OE} etiolated hypocotyls. For each line at least 10 hypocotyls were measured. Error bars denote standard error. The experiment was repeated for 2 times with similar results. Asterisks indicate significant differences according to Student's t tests (*, $P < 0.05$).
(B) Representative images of 24 h gravity stimulated etiolated hypocotyls of Col-0, *abp1-C1*, *abp1-TD1*, and *ABP1-GFP*^{OE}. Scale bar =1 cm. Arrow indicates gravity direction. Kinetics of hypocotyl bending of Col-0, *abp1-C1*, *abp1-TD1* and *ABP1-GFP*^{OE} during 24 h of gravity stimulation. For each line at least 10 hypocotyls were measured. Error bars denote standard error. Asterisks indicate significant differences according to Student's t tests (*, $P < 0.05$; ** $P < 0.01$; *** $P < 0.001$). The experiment was repeated 3 times with similar results.

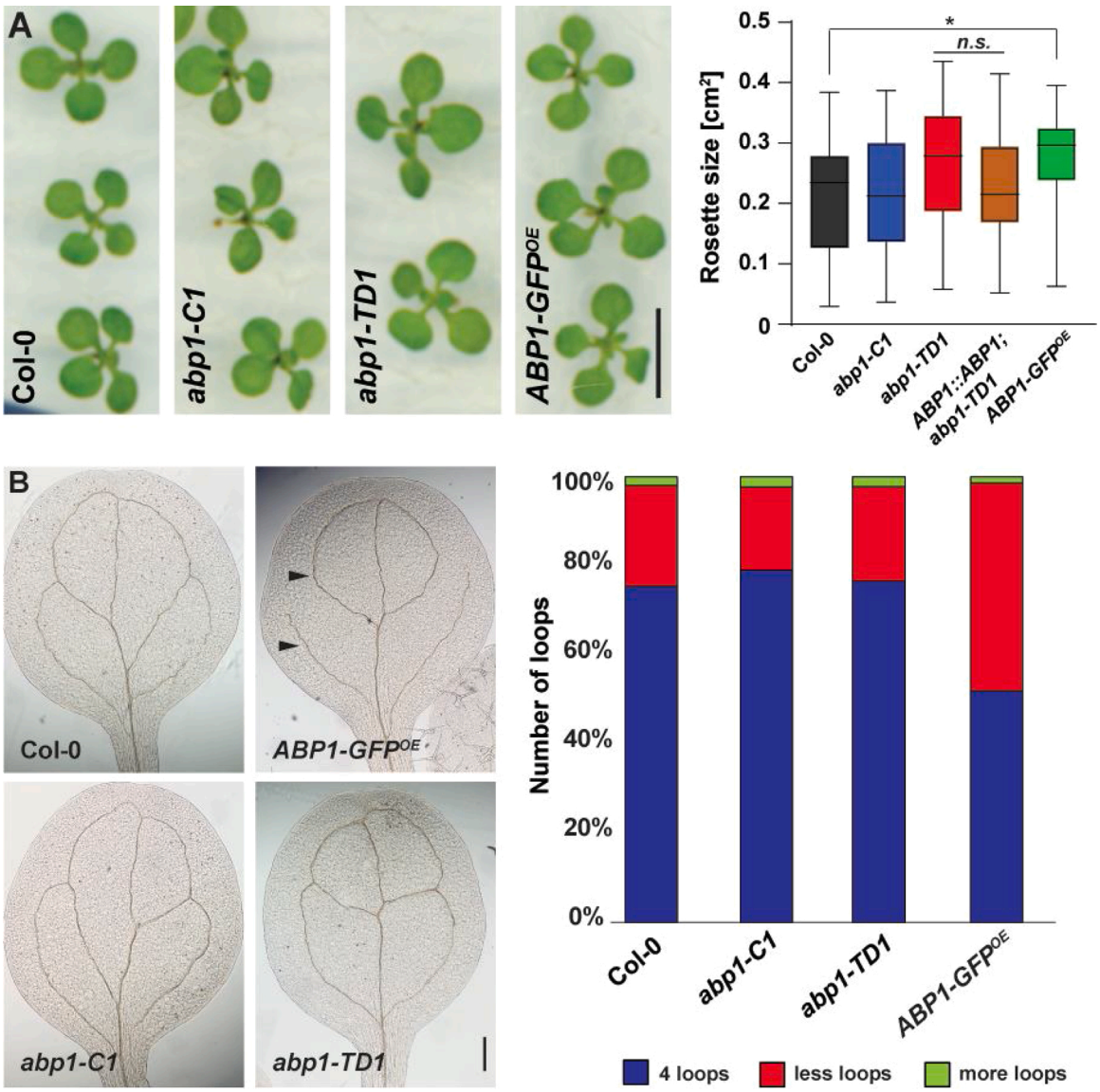

Fig. 6. Role of ABP1 in leaf development and vasculature formation.

(A) Representative images of the rosettes of 12-d-old of Col-0, *abp1-C1*, *abp1-TD1* and *ABP1-GFP^{OE}* seedlings. Scale bar =5 mm. The boxplot shows the size of the rosettes for Col-0, *abp1-C1*, *abp1-TD1*, complemented *abp1-TD1* mutant (*ABP1::ABP1;abp1-TD1*) as control for *abp1-TD1*, and *ABP1-GFP^{OE}*. For each genotype and experiment, more than 19 rosettes from 12-d-old seedlings were measured. For box plot, box defines the first and third quartiles, and the central lines in the box represent the median. Whiskers, from minimum to maximum. Asterisks indicate significant differences according to Student's *t*-tests (*, $P < 0.05$). The experiment was repeated 2 times with the similar result.

(B) Representative pictures of cotyledons venation pattern of 10-d-old Col-0, *abp1-C1*, *abp1-TD1* and *ABP1-GFP^{OE}* seedlings. Scale bar =200 μm. Arrowheads point to typical vasculature defects in *ABP1-GFP^{OE}*. Quantification of number of loops in 10-d-old cotyledons of Col-0, *abp1-C1*, *abp1-TD1* and *ABP1-GFP^{OE}* is presented as percentage. For each line at least 20 cotyledon leaves were scored. The experiment was repeated 2 times with similar results.

responses. Overall, following the treatments, root growth and lateral root formation of WT and *abp1* mutants were inhibited (Fig. 7A–C). In addition, no obvious differences in root growth inhibition were observed after mannitol or sodium chloride treatment between the tested lines (Fig. 7B–C).

High temperature promotes auxin biosynthesis, thereby leading to rapid hypocotyl growth [70]. To address a potential role of *ABP1* in auxin-mediated rapid hypocotyl growth in response to high temperature and the presence of sugar, we characterized hypocotyl elongation of *abp1* and *ABP1-GFP^{OE}* seedlings grown under high temperature (28 °C), on media supplemented with or without sucrose. When grown in high temperature (28 °C) on the medium with sucrose, *ABP1-GFP^{OE}* exhibited longer hypocotyls compared to WT, whereas the hypocotyl length of *abp1* mutants was comparable to that of WT plants (Fig. 7D). At high temperature (28 °C), but in absence, of sucrose the hypocotyl elongation of *ABP1-GFP^{OE}* line was less inhibited than in WT (Fig. 7E).

To test whether *ABP1* plays a role in wound healing responses, we performed a targeted cell ablation in the root tips of *abp1-TD1* and *ABP1-GFP^{OE}* lines [53,81]. After cell ablation, the numbers of initiating periclinal cell divisions in *abp1-TD1* and *ABP1-GFP^{OE}* were similar to that in WT (Fig. S3).

Taken together, the results show that the root growth of *abp1* loss-of-function mutants is not influenced differently by salt stress and high temperature. *ABP1* gain-of-function seedlings show increased hypocotyl growth when grown at high temperature.

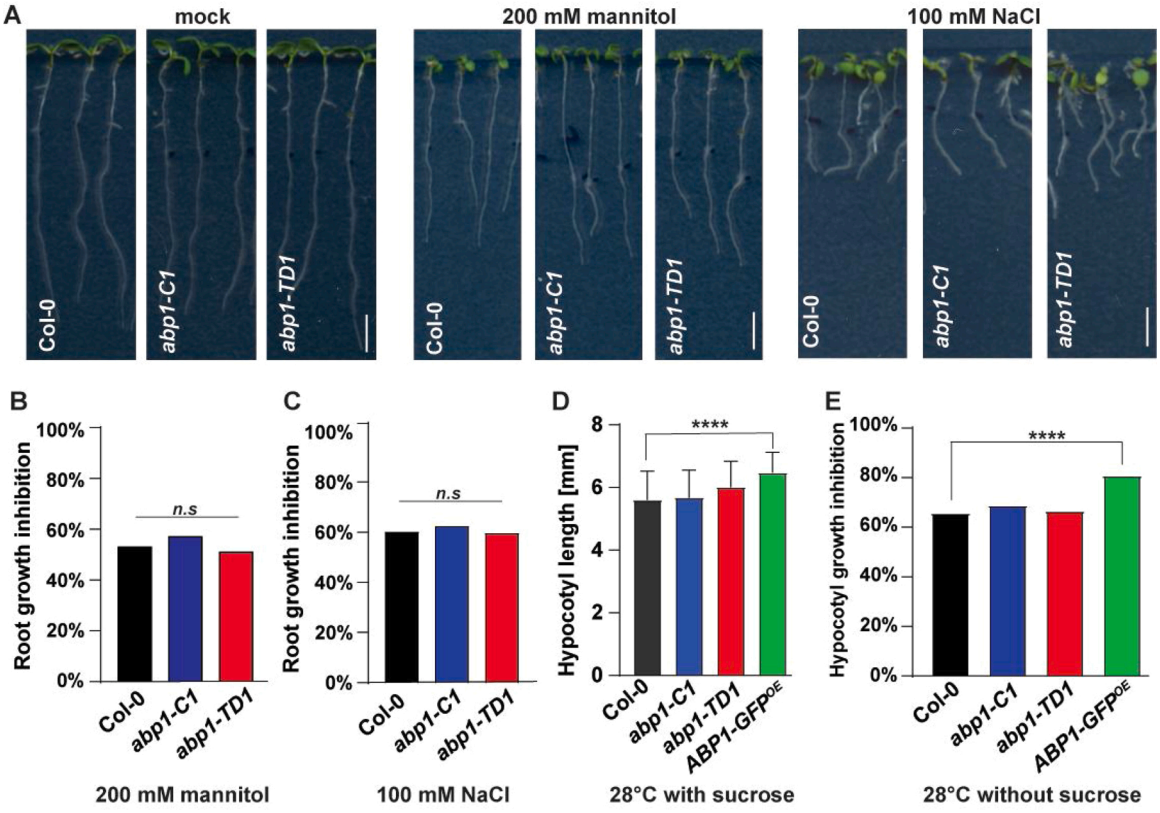

Fig. 7. Role of ABP1 during stress.

(A) Representative images of 8-d-old Col-0, *abp1-C1, abp1-TD1* and *ABP1-GFP*^{OE} seedlings grown for 4 days on control media or on media supplemented with either 200 mM mannitol or 100 mM NaCl. Scale bar =5 mm.

(B–C) Quantification of the root growth inhibition of Col-0, *abp1-C1* and *abp1-TD1* seedlings after treatment with 200 mM mannitol (B) or 100 mM NaCl (C). For each genotype, at least 10 roots were measured per experiment. The experiment was repeated 3 times with the similar results and the pooled values are presented. The statistical significance was tested by Wilcoxon test.

(D) Quantification of the hypocotyl length of 7-d-old Col-0, *abp1-C1, abp1-TD1* and *ABP1-GFP*^{OE} seedlings grown under continuous light, higher temperature (28 °C). For each genotype and experiment, at least 25 hypocotyls were analyzed. Error bars denote standard error. Asterisks indicate significant differences according to Student's t tests (****, $P < 0.0001$). The experiment was repeated 3 times with the similar results.

(E) Quantification of the hypocotyl growth inhibition sucrose of Col-0, *abp1-C1, abp1-TD1* and *ABP1-GFP*^{OE} seedlings grown under continuous light, higher temperature (28 °C) and in absence of sucrose. For each genotype, at least 10 roots were measured per experiment. Asterisks indicate significant differences according to Student's t tests (****, $P < 0.0001$). The experiment was repeated 3 times with the similar results and the pooled values are presented.

3.8. Role of ABP1 in rosette leaves and inflorescence development

The establishment of auxin maxima in the shoot apical meristem (SAM) and directed basipetal polar auxin transport are crucial for overall shoot development [59,82–86]. *ABP1* is expressed in both SAM and rosette leaves (Fig. S1B), therefore we investigated its possible function in shoot development.

First, we characterized leaf development. Visually, the size and shape of rosette leaves in *abp1* mutants and *ABP1-GFP*^{OE} plants were comparable to that of WT plants. We quantified the rosette leaves number at the stage when the first flower of each individual plant bloomed. We observed that the *apb1-TD1* mutant developed slightly more, whereas the *ABP1-GFP*^{OE} line developed significantly less rosette leaves in comparison to WT (Fig. 8A). However, the results for the *abp1-TD1* mutant line were variable between the experimental repetitions. We found no difference in the number of cauline leaves for any of the analyzed lines (Fig. S4A).

Further, we studied the function of *ABP1* during bolting. We measured the length of the first internode of *abp1* mutants and *ABP1-GFP*^{OE} and we recorded the timing to reach 1 cm. Compared to WT, both *abp1* mutants and *ABP1-GFP*^{OE} line bolt earlier, at 21st and 22nd day after sowing versus 23rd day in WT (Fig. 8B).

To determine whether *ABP1* is involved in phyllotaxis establishment, we measured the sequence of divergence angles between siliques in *abp1* mutants. Visually, *abp1* mutants developed normal inflorescence stems (Fig. 8C). WT plants typically exhibit a spiral phyllotaxis that leads to a distribution of the consecutive organs on the stem with a divergence angle close to 137.5° [87]. Our analysis revealed that the distribution of divergence angles in *abp1* mutants was not altered (Fig. 8D–F). We also analyzed the internode length between the siliques and counted the number of rosette and cauline branches of *abp1* mutant and *ABP1-GFP*^{OE} plants. However, we did not detect any differences (Fig. S4B-D).

The results show that overexpression of *ABP1* affects the number of rosette leaves and that both *ABP1* loss- and gain-of-function accelerate bolting.

3.9. Role of ABP1 in auxin-mediated PIN polarization and BFA-visualized PIN trafficking

The formation of organized vasculature requires coordinated cell polarization. The canalization hypothesis proposes that auxin acts as a polarizing cue in this process [88] and that auxin feed-back on PIN polarity, together with constitutive PIN endocytic trafficking are important features in this process [54,89,90]. Since overexpression of *ABP1* results in defects in vascular tissue formation (Fig. 6B), we tested whether *abp1* loss- or gain-of-function alleles show defects in these

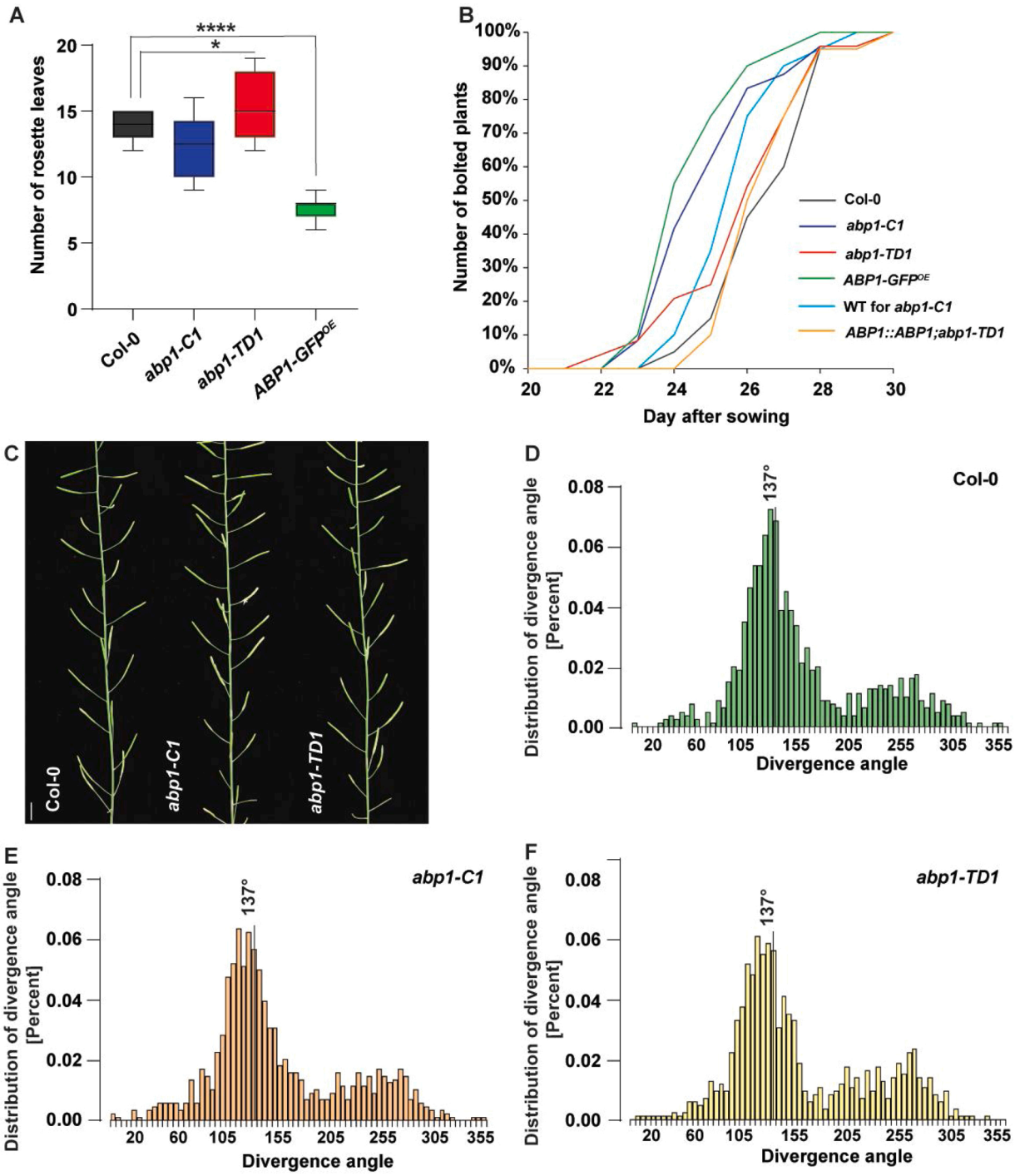

Fig. 8. Role of ABP1 in rosette leaves and inflorescence development.

(A) Boxplot showing the number of rosette leaves of Col-0, *abp1-C1*, *abp1-TD1* and *ABP1-GFP*^{OE} plants. For each genotype per experiment, at least 10 rosettes were scored when the first flower bloomed on each single plant. For box plot, box defines the first and third quartiles, and the central lines in the box represent the median. Whiskers, from minimum to maximum. Asterisks indicate significant differences according to Student's t tests (*, $P < 0.05$; ****, $P < 0.0001$). The experiment was repeated 3 times with the similar result.

(B) Quantification of bolting time of Col-0, *abp1-C1*, *abp1-TD1*, *ABP1-GFP*^{OE}, WT for *abp1-C1*, and *ABP1::ABP1;abp1-TD1*. The graph shows number of plants with inflorescence stem ≥ 1 cm for the given day in percentage. For each genotype per experiment, at least 20 plants were scored. The experiment was at this given setup repeated 2 times with the similar result, and additionally 2 times for Col-0, *abp1-C1*, *abp1-TD1*, *ABP1-GFP*^{OE} with the similar result.

(C) Representative pictures of the inflorescence stem of Col-0, *abp1-C1*, and *abp1-TD1*. Scale bar =1 cm.

(D–F) Distribution of divergence angles between the siliques in Col-0, *abp1-C1*, and *abp1-TD1*. For each genotype divergence angles of 25 individual plants were measured.

processes. To evaluate the effect of auxin on PIN polarity, we analyzed the repolarization of PIN1 from the basal to the inner lateral side in root endodermis cells and the repolarization of PIN2 from the basal to the outer lateral side in root cortex cells [54] following auxin treatment in *abp1* mutants and *ABP1-GFP*^{OE}. Anti-PIN1 and anti-PIN2 immunolocalization revealed that PIN1 and PIN2 repolarization was not altered in *abp1* mutants, while overexpression of ABP1 led to reduced or no repolarization of PIN1 and PIN2 respectively (Fig. 9A–B).

Further, we used the trafficking inhibitor Brefeldin A (BFA) to indirectly visualize PIN intracellular trafficking [91]. BFA treatment results in PIN internal aggregation manifested as BFA-body formation and this effect is decreased when BFA is used together with auxin [9]. The anti-PIN1 immunostaining in roots after BFA treatment showed that the intracellular aggregation of PIN1 was similar to that of WT in both *abp1* mutants (Fig. 9C) and [92]. In *ABP1-GFP*^{OE} we observed repeatedly that BFA affected PIN1 intracellular aggregation more severely (BFA bodies were more pronounced) (Fig. 9C). Anti-PIN1 immunostaining after auxin and BFA co-treatment confirmed that auxin inhibited BFA-body formation. Comparison of the *abp1* mutants with the corresponding complemented lines did not reveal any consistent changes in the auxin effect on BFA-induced PIN1 aggregation, whereas *ABP1-GFP*^{OE} showed again slightly more BFA-induced PIN1 aggregation even in presence of auxin (Fig. 9C). The analysis of the BFA effect on PIN2 intracellular aggregation revealed no consistent and reproducible differences in BFA-body formation between WT, *abp1* mutants and *ABP1-GFP*^{OE} (Fig. 9D). Accordingly, auxin and BFA co-treatment led to a comparable and variable decrease of PIN2 intracellular aggregation in WT, *abp1* mutants and *ABP1-GFP*^{OE} (Fig. 9D).

Taken together, the *ABP1* overexpression interferes with auxin-induced PIN repolarization and slightly affects BFA-induced, constitutive PIN1 but not PIN2 trafficking, while mutation in *ABP1* does not show altered auxin feed-back on PIN polarity or constitutive PIN recycling.

4. Discussion

ABP1 has been identified in maize decades ago based on its potential ability to bind auxin [93,94]. Nonetheless, the developmental roles and cellular functions of ABP1 remain unclear due to problems with some of the genetic material [35,39,40,42] and due to the lack of obvious developmental defects after superficial analyzes of the verified knock-out lines [38].

Here, we assessed the function of ABP1 in various developmental processes and (re)evaluated its role in cellular processes related to trafficking and polar distribution of PIN auxin transporters.

4.1. ABP1 is not essential for or regulated by TIR1/AFB-mediated auxin responses

ABP1 promoter activity has been reported to overlap, to some extent, with that of the transcriptional DR5 auxin reporter during early seedling development [43]. Our analysis revealed a similar overlap in hydathodes, root tips and lateral root primordia as well as in older seedlings. The activity of the *ABP1* promoter at places with high auxin response suggested either that auxin might regulate the transcription of *ABP1* or that ABP1 is somehow linked to TIR1/AFB-mediated transcriptional auxin signaling.

Indeed, *ABP1* was previously identified among early auxin-regulated genes. *ABP1* transcription was upregulated by auxin in a dose dependent manner within 30 min in 19-d-old WT seedlings [95]. Our observations in 5-d-old WT roots and shoots did not reveal any changes in *ABP1* expression following auxin treatment. These contradictory findings suggest that a potential auxin effect on *ABP1* transcription could be tissue- and/or developmental stage-dependent.

Also, the connection between *ABP1* and TIR1/AFB-mediated auxin signaling was previously investigated. Downregulation of the *ABP1* activity was shown to affect transcription of auxin-responsive genes [33,95,96], to regulate Aux/IAA homeostasis and thus negatively impact on the SCF$^{TIR1/AFB}$ pathway [97]. However, these observations are inconclusive due to the potential off-targets in the conditional knock-down lines [42] and the inactivation of *ABP1* did not have any significant effects on the DR5 auxin response reporter activity [33]. In the verified *abp1* knock-out lines it was reported that auxin-regulated gene expression is unchanged [38] and our analysis in these lines and following *ABP1* overexpression in protoplasts did also not reveal any changes in DR5 reporter activity. Furthermore, *abp1* knock-out lines also showed normal TIR1/AFB-mediated non-transcriptional auxin effect on root growth. Overall, these observations suggest that *ABP1* is not directly involved in the TIR1/AFB-mediated auxin response.

4.2. ABP1 loss-of-function mutants show minor defects in development

The initial analysis of CRISPR and T-DNA insertion *abp1* knock-out mutants did not reveal any obvious defects during development under normal conditions leading to a conclusion that *ABP1* is not required for Arabidopsis development [38]. We analyzed different auxin-related phenotypes of the corresponding *abp1* knock-out mutants in more detail. We observed that both *abp1* alleles exhibited normal root growth, etiolated hypocotyl, root and shoot gravitropic responses, lateral root and leaf development, including venation and phyllotaxis. Notably, both *abp1* mutant alleles bolted earlier compared to the control lines. Accelerated bolting in *abp1* mutants might be caused by changes in auxin levels caused by either impaired biosynthesis, auxin transport or eventually a change in auxin sensitivity. Nonetheless, it is unclear why such changes are not reflected also in other developmental processes regulated by auxin.

4.3. ABP1 gain-of-function lines show a plethora of auxin-related phenotypes

ABP1 overexpression has been shown previously to cause several postembryonic developmental defects [5,10,35,98,99]. Similarly, our analysis of a stable line expressing *35S::ABP1-GFP* revealed that *ABP1* gain-of-function leads to developmental changes. Seedlings overexpressing *ABP1* have reduced root length, impaired auxin-induced lateral root development, enhanced elongation of both high temperature- and dark-grown hypocotyls, reduced root and shoot gravitropic response, defective vasculature development, increased size of young rosettes but decreased number of rosettes leaves. Additionally, similar to the *abp1* mutants, *ABP1* overexpressors also bolted earlier. At the cellular level, we confirmed the previous observations [10,35] that the *ABP1* gain-of-function affects the BFA-sensitive PIN endocytic trafficking and newly showed that they also impair auxin effects on PIN polar distribution in root cells.

All aforementioned processes, which were found defective in *ABP1* gain-of-function mutants are linked to auxin regulation. It is therefore conceivable that, in line with the importance of the auxin binding pocket for the *ABP1* function [35], *ABP1* plays so far a mechanistically unclear role in auxin perception and signaling.

4.4. Potential role and functional mechanism of Arabidopsis ABP1

Arabidopsis *ABP1* was identified based on the orthology with *ABP1* previously found in maize [98,100]. Auxin-binding properties of maize ABP1 are well characterized. Several biochemical studies along with the structural analysis of the ABP1-auxin co-crystal revealed that maize ABP1 binds auxin with the highest affinity at apoplastic pH 5.5, while binding at pH 7.2 corresponding to the ER lumen where the majority of protein is localized, is much lower [26–29,94,101]. In contrast, the auxin-binding properties of Arabidopsis ABP1 have not been characterized yet. Based on the high homology with the maize protein, it is assumed that Arabidopsis ABP1 binds auxin in a similar manner. This

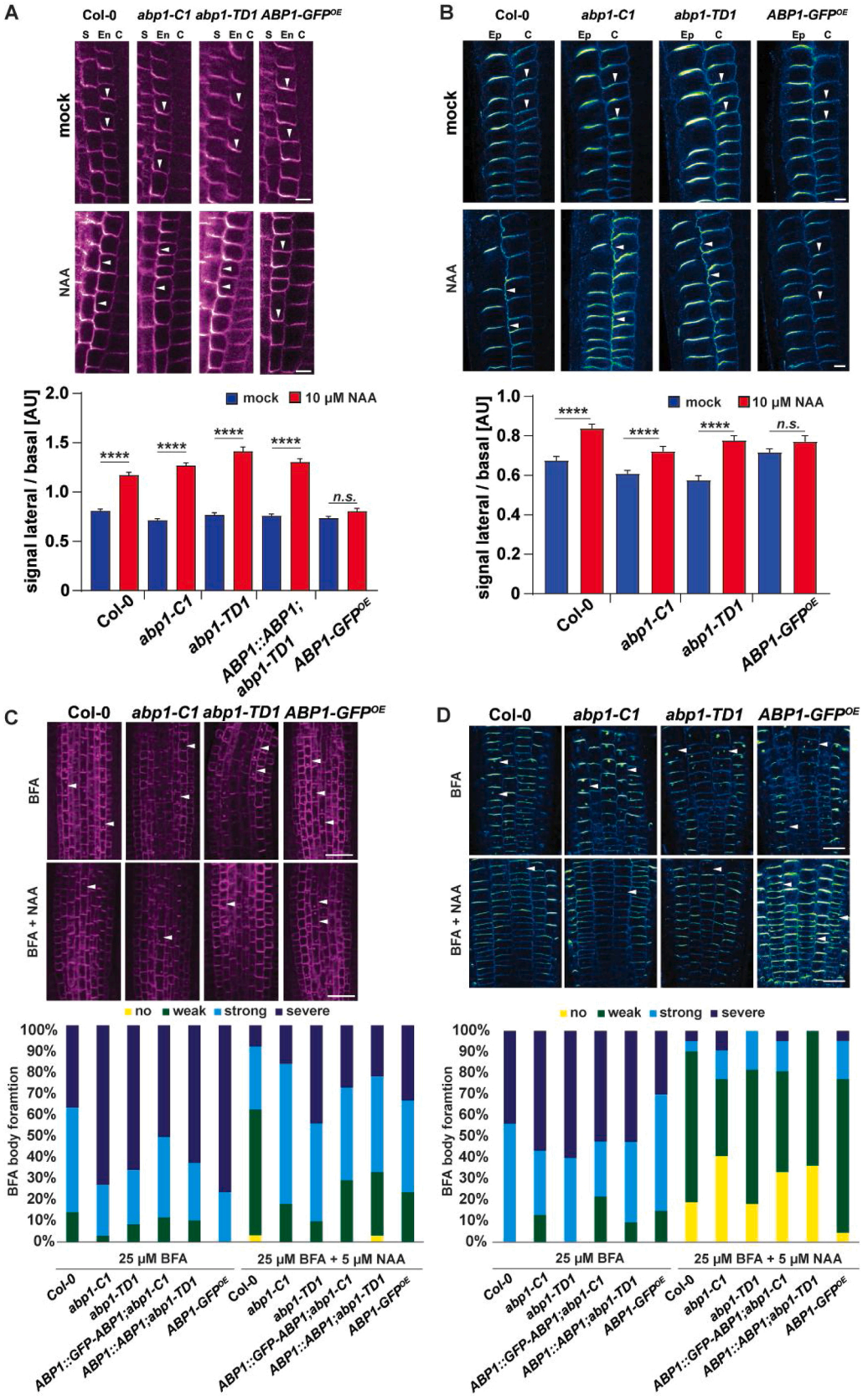

Fig. 9. Role of ABP1 in auxin-mediated PIN polarization and BFA-visualized PIN trafficking.

(A) Representative pictures of PIN1 immunolocalization in root meristem of 4-d-old Col-0, *abp1-C1*, *abp1-TD1* and *ABP1-GFP*^{OE} after mock (upper panel) and 4 h 10μM NAA treatment (lower panel). Scale bar =5 μm. The letters indicate an appropriate cell file - S (stele), En (endodermis), C (cortex). Arrow heads point to basal/lateral PIN1 localization in endodermis. The quantitative evaluation shows mean ratio of PIN1 lateral-to-basal signal intensity ratio in endodermis cells of Col-0, *abp1-C1*, *abp1-TD1*, *ABP1::ABP1;abp1-TD1* and *ABP1-GFP*^{OE}. Error bars denote standard error. Asterisks indicate significant differences according to Student's t tests (****, $P < 0.0001$). The experiment was repeated 3 times, one representative experiment is presented.

(B) Representative pictures of PIN2 immunolocalization in root meristem of 4-d-old Col-0, *abp1-C1*, *abp1-TD1* and *ABP1-GFP*^{OE} after mock (upper panel) and 4 h 10μM NAA treatment (lower panel). Scale bar =5 μm. The letters indicate an appropriate cell file – Ep (epidermis), C (cortex). Arrow heads point to basal/lateral PIN2 localization in cortex. The quantitative evaluation shows mean ratio of PIN2 lateral-to-basal signal intensity ratio in cortex cells of Col-0, *abp1-C1*, *abp1-TD1* and *ABP1-GFP*^{OE}. Error bars denote standard error. Asterisks indicate significant differences according to Student's t tests (****, $P < 0.0001$). The experiment was repeated 3 times, one representative experiment is presented.

(C) Representative pictures of PIN1 immunolocalization in primary root stele of 4-d-old Col-0, *abp1-C1*, *abp1-TD1* and *ABP1-GFP*^{OE} after 1 h 25 μM BFA treatment (upper panel) and after 30 min 5 μM NAA pre-treatment followed by 1 h 25 μM BFA and 5 μM NAA co-treatment (lower panel). Arrow heads point to affected cells. Scale bar =20 μm. The quantitative evaluation shows the scoring of an overall count of formed BFA bodies in Col-0, *abp1-C1*, *abp1-TD1*, *ABP1::GFP-ABP1;abp1-C1*, *ABP1::ABP1;abp1-TD1* and *ABP1-GFP*^{OE}. At least 8 roots were scored for each genotype and experiment. The pooled result of 3 independent experiments is presented.

(D) Representative pictures of PIN2 immunolocalization in primary root epidermis of 4-d-old Col-0, *abp1-C1*, *abp1-TD1* and *ABP1-GFP*^{OE} after 1 h 25 μM BFA treatment (upper panel) and after 30 min 5 μM NAA pre-treatment followed by 1 h 25 μM BFA and 5 μM NAA co-treatment (lower panel). Arrow heads point to affected cells. Scale bar =20 μm. The quantitative evaluation shows the scoring of an overall count of formed BFA bodies in Col-0, *abp1-C1*,

abp1-TD1, *ABP1::GFP-ABP1;abp1-C1*, *ABP1::ABP1;abp1-TD1* and *ABP1-GFP*^{OE}. At least 8 roots were scored for each genotype and experiment. The pooled result of 3 independent experiments is presented.

statement is supported by the finding that the auxin-binding pocket of Arabidopsis ABP1 is important for its gain-of-function cellular and developmental roles [35].

The ABP1 binding optimum at pH 5.5 would imply that ABP1 is functional in the apoplast, further supported by auxin-dependent interaction between ABP1 and the plasma membrane-localized receptor-like kinase TMK1 [30,31]. TMK1 belongs to a four-member TMK receptor-like kinase family, that function redundantly and multiple mutants show severe reduction in organ size and substantial growth retardation [20]. Both TMK1 and TMK4 play roles in auxin-mediated developmental processes and in the control of local auxin biosynthesis [22,23,30]. Importantly, TMK1 mediates auxin signaling that regulates differential growth of the apical hook [21]. However, the mechanism of how TMK1 perceives auxin remains elusive.

The function of ABP1 as a part of the auxin perception machinery contributing towards TMK-based downstream signaling, is a tempting hypothesis consistent with a rather broad spectrum of auxin-related growth defects. But it is not supported by the rather mild phenotypic defects in the *abp1* loss-of-function mutants, especially considering that *ABP1* is a single copy gene in Arabidopsis [100]. On the other hand, *ABP1* is evolutionary conserved and ubiquitous in vascular plants [102], suggesting that it has an important and conserved function. Structurally ABP1 belongs to an ancient group of germin and germin-like proteins that have a highly conserved tertiary structure despite low similarity in primary sequence among the members [28,103]. Therefore, it is possible that some other proteins from the germin family are functionally redundant with ABP1, thus masking the effect of the *abp1* mutation. Nonetheless, to identify and characterize functional homologues within this large family will be a challenging task. An alternative explanation for the weak developmental defects in *abp1* loss-of-function mutants is that *ABP1* plays an important role in specific processes that provide competitive advantage in nature but are not easily manifested under laboratory conditions.

5. Conclusions

In conclusion, our detailed phenotypic analysis of both *ABP1* gain- and loss-of-function lines provides new insights into the developmental role of *ABP1*. Despite the overlap of *ABP1* expression pattern with auxin response maxima during seedling development, none of our observations supports a direct involvement of *ABP1* in the TIR1/AFB-mediated transcriptional auxin response. *abp1* knock-out mutants show only mild phenotypic defects, whereas *ABP1* overexpression generates a broad range of potentially auxin-related phenotypes. The previously described strong and related defects in conditional *abp1* knock-down lines let us hypothesize that the discrepancy between the effects of loss- and gain-of-function is due to the action of unknown germin family proteins that are functionally redundant with ABP1.

Author contribution

Z.G., Mi.Ga., M.P., X.Z., Ma.Gl., L.L., J.M., I.V., H.H., J.H., M.Č., M. Z., L.H., M.F., T.V. and J.F. designed and conducted experiments and analyzed data. G.B. and Z.P. helped with performing experiments. R.H. and I.V. developed RG-tracker. Z.G., L.H. and T.X. contributed with the generation of the genetic material. Z.G., X.Z., Mi.Ga. and J.F. wrote the manuscript.

Declaration of Competing Interest

The authors report no declarations of interest.

Acknowledgments

We would like to acknowledge Bioimaging and Life Science Facilities at IST Austria for continuous support and also the Plant Sciences Core Facility of CEITEC Masaryk University for their support with obtaining a part of the scientific data. We gratefully acknowledge Lindy Abas for help with *ABP1::GFP-ABP1* construct design. This project has received funding from the European Research Council (ERC) under the European Union's Horizon 2020 research and innovation program [grant agreement no. 742985] and Austrian Science Fund (FWF) [I 3630-B25] to J. F.; DOC Fellowship of the Austrian Academy of Sciences to L.L.; the European Structural and Investment Funds, Operational Programme Research, Development and Education - Project „MSCAfellow@MUNI" [CZ.02.2.69/0.0/0.0/17_050/0008496] to M.P.. This project was also supported by the Czech Science Foundation [GA 20-20860Y] to M.Z and MEYS CR [project no.CZ.02.1.01/0.0/0.0/16_019/0000738] to M. Č.

Appendix A. Supplementary data

Supplementary material related to this article can be found, in the online version, at doi:https://doi.org/10.1016/j.plantsci.2020.110750.

References

[1] J. Brumos, L.M. Robles, J. Yun, T.C. Vu, S. Jackson, J.M. Alonso, A.N. Stepanova, Local auxin biosynthesis is a key regulator of plant development, Dev. Cell 47 (2018) 306–318, https://doi.org/10.1016/j.devcel.2018.09.022, e5.
[2] M. Adamowski, J. Friml, PIN-dependent auxin transport: action, regulation, and evolution, Plant Cell 27 (2015) 20–32, https://doi.org/10.1105/tpc.114.134874.
[3] B.O. Bargmann, S. Vanneste, G. Krouk, T. Nawy, I. Efroni, E. Shani, G. Choe, J. Friml, D.C. Bergmann, M. Estelle, K.D. Birnbaum, I.D.B. Inte, A Map of Cell Type-specific Auxin Responses, 2013, pp. 1–13, https://doi.org/10.1038/msb.2013.40.
[4] D. Weijers, D. Wagner, Transcriptional responses to the auxin hormone, Annu. Rev. Plant Biol. 67 (2016) 539–574, https://doi.org/10.1146/annurev-arplant-043015-112122.
[5] B. Steffens, C. Feckler, K. Palme, M. Christian, M. Böttger, H. Lüthen, The auxin signal for protoplast swelling is perceived by extracellular ABP1, Plant J. 27 (2001) 591–599, https://doi.org/10.1046/j.1365-313X.2001.01103.x.
[6] R.I. Dahlke, S. Fraas, K.K. Ullrich, K. Heinemann, M. Romeiks, T. Rickmeyer, G. Klebe, K. Palme, H. Lüthen, B. Steffens, Protoplast swelling and hypocotyl growth depend on different auxin signaling pathways, Plant Physiol. 175 (2017) 982–994, https://doi.org/10.1104/pp.17.00733.
[7] G.B. Monshausen, N.D. Miller, A.S. Murphy, S. Gilroy, Dynamics of auxin-dependent Ca 2+ and pH signaling in root growth revealed by integrating high-resolution imaging with automated computer vision-based analysis, Plant J. 65 (2011) 309–318, https://doi.org/10.1111/j.1365-313X.2010.04423.x.
[8] H.W. Shih, C.L. Depew, N.D. Miller, G.B. Monshausen, The cyclic nucleotide-gated channel CNGC14 regulates root gravitropism in arabidopsis thaliana, Curr. Biol. 25 (2015) 3119–3125, https://doi.org/10.1016/j.cub.2015.10.025.
[9] T. Paciorek, E. Zazímalová, N. Ruthardt, J. Petrásek, Y.-D. Stierhof, J. Kleine-Vehn, D.A. Morris, N. Emans, G. Jürgens, N. Geldner, J. Friml, Auxin inhibits endocytosis and promotes its own efflux from cells, Nature 435 (2005) 1251–1256, https://doi.org/10.1038/nature03633.
[10] S. Robert, J. Kleine-Vehn, E. Barbez, M. Sauer, T. Paciorek, P. Baster, S. Vanneste, J. Zhang, S. Simon, M. Čovanová, K. Hayashi, P. Dhonukshe, Z. Yang, S. Y. Bednarek, A.M. Jones, C. Luschnig, F. Aniento, E. Zažímalová, J. Friml, ABP1 mediates auxin inhibition of clathrin-dependent endocytosis in arabidopsis, Cell 143 (2010) 111–121, https://doi.org/10.1016/j.cell.2010.09.027.
[11] M. Kubeš, R. Napier, Non-canonical auxin signalling: fast and curious, J. Exp. Bot. 70 (2019) 2609–2614, https://doi.org/10.1093/jxb/erz111.
[12] M. Gallei, C. Luschnig, J. Friml, Auxin signalling in growth: schrödinger's cat out of the bag, Curr. Opin. Plant Biol. 53 (2020) 43–49, https://doi.org/10.1016/j.pbi.2019.10.003.

[13] O. Leyser, Auxin signaling, Plant Physiol. 176 (2018) 465–479, https://doi.org/10.1104/pp.17.00765.

[14] A.K. Spartz, S.H. Lee, J.P. Wenger, N. Gonzalez, H. Itoh, D. Inzé, W.A. Peer, A. S. Murphy, P.J. Overvoorde, W.M. Gray, The SAUR19 subfamily of SMALL AUXIN UP RNA genes promote cell expansion, Plant J. 70 (2012) 978–990, https://doi.org/10.1111/j.1365-313X.2012.04946.x.

[15] M. Fendrych, J. Leung, J. Friml, Tir1/AFB-Aux/IAA auxin perception mediates rapid cell wall acidification and growth of Arabidopsis hypocotyls, Elife 5 (2016) 1–18, https://doi.org/10.7554/eLife.19048.

[16] M. Fendrych, M. Akhmanova, J. Merrin, M. Glanc, S. Hagihara, K. Takahashi, N. Uchida, K.U. Torii, J. Friml, Rapid and reversible root growth inhibition by TIR1 auxin signalling, Nat. Plants 4 (2018) 453–459, https://doi.org/10.1038/s41477-018-0190-1.

[17] J. Dindas, S. Scherzer, M.R.G. Roelfsema, K. Von Meyer, H.M. Müller, K.A.S. Al-Rasheid, K. Palme, P. Dietrich, D. Becker, M.J. Bennett, R. Hedrich, AUX1-mediated root hair auxin influx governs SCFTIR1/AFB-type Ca2+ signaling, Nat. Commun. 9 (2018), https://doi.org/10.1038/s41467-018-03582-5.

[18] S. Simonini, J. Deb, L. Moubayidin, P. Stephenson, M. Valluru, A. Freire-Rios, K. Sorefan, D. Weijers, J. Friml, L. Østergaard, A noncanonical auxin-sensing mechanism is required for organ morphogenesis in arabidopsis, Genes Dev. 30 (2016) 2286–2296, https://doi.org/10.1101/gad.285361.116.

[19] A. Kuhn, S.R. Harborough, H.M. McLaughlin, B. Natarajan, I. Verstraeten, J. Friml, S. Kepinski, L. Østergaard, Direct ETTIN-auxin interaction controls chromatin states in gynoecium development, Elife 9 (2020) 1–18, https://doi.org/10.7554/eLife.51787.

[20] N. Dai, W. Wang, S.E. Patterson, A.B. Bleecker, The TMK subfamily of receptor-like kinases in Arabidopsis display an essential role in growth and a reduced sensitivity to auxin, PLoS One 8 (2013) 1–12, https://doi.org/10.1371/journal.pone.0060990.

[21] M. Cao, R. Chen, P. Li, Y. Yu, R. Zheng, D. Ge, W. Zheng, X. Wang, Y. Gu, Z. Gelová, J. Friml, H. Zhang, R. Liu, J. He, T. Xu, TMK1-mediated auxin signalling regulates differential growth of the apical hook, Nature 568 (2019) 240–243, https://doi.org/10.1038/s41586-019-1069-7.

[22] R. Huang, R. Zheng, J. He, Z. Zhou, J. Wang, Y. Xiong, T. Xu, Noncanonical auxin signaling regulates cell division pattern during lateral root development, Proc. Natl. Acad. Sci. U. S. A. 116 (2019) 21285–21290, https://doi.org/10.1073/pnas.1910916116.

[23] Q. Wang, G. Qin, M. Cao, R. Chen, Y. He, L. Yang, Z. Zeng, Y. Yu, Y. Gu, W. Xing, W.A. Tao, T. Xu, A phosphorylation-based switch controls TAA1-mediated auxin biosynthesis in plants, Nat. Commun. 11 (2020), https://doi.org/10.1038/s41467-020-14395-w.

[24] N. Leblanc, C. Roux, J.M. Pradier, C. Perrot-Rechenmann, Characterization of two cDNAs encoding auxin-binding proteins in Nicotiana tabacum, Plant Mol. Biol. 33 (1997) 679–689, https://doi.org/10.1023/a:1005757815212.

[25] S. Watanabe, S. Shimomura, Cloning and expression of two genes encoding auxin-binding proteins from tobacco, Plant Mol. Biol. 36 (1998) 63–74, https://doi.org/10.1023/A:1005999821066.

[26] H. Tian, D. Klambt, A.M. Jones, Auxin-binding protein 1 does not bind auxin within the endoplasmic reticulum despite this being the predominant subcellular location for this hormone receptor, J. Biol. Chem. 270 (1995) 26962–26969, https://doi.org/10.1074/jbc.270.45.26962.

[27] N. Leblanc, K. David, J. Grosclaude, J.M. Pradier, H. Barbier-Brygoo, S. Labiau, C. Perrot-Rechenmann, A novel immunological approach establishes that the auxin-binding protein, Nt-abp1, is an element involved in auxin signaling at the plasma membrane, J. Biol. Chem. 274 (1999) 28314–28320, https://doi.org/10.1074/jbc.274.40.28314.

[28] E.J. Woo, J. Marshall, J. Bauly, J.G. Chen, M. Venis, R.M. Napier, R. W. Pickersgill, Crystal structure of auxin-binding protein 1 in complex with auxin, EMBO J. 21 (2002) 2877–2885, https://doi.org/10.1093/emboj/cdf291.

[29] A.M. Jones, E.M. Herman, KDEL-containing auxin-binding protein is secreted to the plasma membrane and cell wall, Plant Physiol. 101 (1993) 595–606, https://doi.org/10.1104/pp.101.2.595.

[30] T. Xu, M. Wen, S. Nagawa, Y. Fu, J.-G. Chen, M.-J. Wu, C. Perrot-Rechenmann, J. Friml, A.M. Jones, Z. Yang, Cell surface- and rho GTPase-based auxin signaling controls cellular interdigitation in Arabidopsis, Cell 143 (2010) 99–110, https://doi.org/10.1016/j.cell.2010.09.003.

[31] T. Xu, N. Dai, J. Chen, S. Nagawa, M. Cao, H. Li, Z. Zhou, X. Chen, R. De Rycke, H. Rakusová, W. Wang, A.M. Jones, J. Friml, S.E. Patterson, A.B. Bleecker, Z. Yang, Cell surface ABP1-TMK auxin-sensing complex activates ROP GTPase signaling, Science 343 (2014) 1025–1028, https://doi.org/10.1126/science.1245125.

[32] P. Grones, J. Friml, Auxin transporters and binding proteins at a glance, J. Cell. Sci. 128 (2015) 1–7, https://doi.org/10.1242/jcs.159418.

[33] A. Tromas, N. Braun, P. Muller, T. Khodus, I.A. Paponov, K. Palme, K. Ljung, J. Y. Lee, P. Benfey, J.A.H. Murray, B. Scheres, C. Perrot-Rechenmann, The AUXIN BINDING PROTEIN 1 is required for differential Auxin responses mediating root growth, PLoS One 4 (2009) 1–11, https://doi.org/10.1371/journal.pone.0006648.

[34] X. Chen, S. Naramoto, S. Robert, R. Tejos, C. Löfke, D. Lin, Z. Yang, J. Friml, ABP1 and ROP6 GTPase signaling regulate clathrin-mediated endocytosis in Arabidopsis roots, Curr. Biol. 22 (2012) 1326–1332, https://doi.org/10.1016/j.cub.2012.05.020.

[35] P. Grones, X. Chen, S. Simon, W.A. Kaufmann, R. De Rycke, T. Nodzyński, E. Zažímalová, J. Friml, Auxin-binding pocket of ABP1 is crucial for its gain-of-function cellular and developmental roles, J. Exp. Bot. 66 (2015) 5055–5065, https://doi.org/10.1093/jxb/erv177.

[36] X. Chen, L. Grandont, H. Li, R. Hauschild, S. Paque, A. Abuzeineh, H. Rakusová, E. Benkova, C. Perrot-Rechenmann, J. Friml, Inhibition of cell expansion by rapid ABP1-mediated auxin effect on microtubules, Nature 516 (2014) 90–93, https://doi.org/10.1038/nature13889.

[37] S. Paque, G. Mouille, L. Grandont, D. Alabadí, C. Gaertner, A. Goyallon, P. Muller, C. Primard-Brisset, R. Sormani, M.A. Blázquez, C. Perrot-Rechenmann, AUXIN BINDING PROTEIN1 links cellwall remodeling, auxin signaling, and cell expansion in Arabidopsis, Plant Cell 26 (2014) 280–295, https://doi.org/10.1105/tpc.113.120048.

[38] Y. Gao, Y. Zhang, D. Zhang, X. Dai, M. Estelle, Y. Zhao, Auxin binding protein 1 (ABP1) is not required for either auxin signaling or Arabidopsis development, Proc. Natl. Acad. Sci. U. S. A. 112 (2015) 2275–2280, https://doi.org/10.1073/pnas.1500365112.

[39] J. Michalko, M. Dravecká, T. Bollenbach, J. Friml, Embryo-lethal phenotypes in early abp1 mutants are due to disruption of the neighboring BSM gene [version 1; referees: 3 approved], F1000Research 4 (2015), https://doi.org/10.12688/f1000research.7143.1.

[40] X. Dai, Y. Zhang, D. Zhang, J. Chen, X. Gao, M. Estelle, Y. Zhao, Embryonic lethality of Arabidopsis abp1-1 is caused by deletion of the adjacent BSM gene, Nat. Plants 1 (2015) 3–6, https://doi.org/10.1038/nplants.2015.183.

[41] T.A. Enders, S. Oh, Z. Yang, B.L. Montgomery, L.C. Strader, Genome sequencing of arabidopsis abp1-5 reveals second-site mutations that may affect phenotypes, Plant Cell 27 (2015) 1820–1826, https://doi.org/10.1105/tpc.15.00214.

[42] J. Michalko, M. Glanc, C. Perrot-Rechenmann, J. Friml, Strong morphological defects in conditional Arabidopsis abp1 knock-down mutants generated in absence of functional ABP1 protein, F1000Research 5 (2016) 86, https://doi.org/10.12688/f1000research.7654.1.

[43] M. Klode, R.I. Dahlke, M. Sauter, B. Steffens, Expression and subcellular localization of Arabidopsis thaliana auxin-binding protein 1 (ABP1), J. Plant Growth Regul. 30 (2011) 416–424, https://doi.org/10.1007/s00344-011-9203-2.

[44] J. Friml, A. Vieten, M. Sauer, D. Weijers, H. Schwarz, T. Hamann, R. Offringa, G. Jürgens, Efflux-dependent auxin gradients establish the apical-basal axis of Arabidopsis, Nature 426 (2003) 147–153, https://doi.org/10.1038/nature02085.

[45] S.J. Clough, A.F. Bent, Floral dip: a simplified method for Agrobacterium -mediated transformation of Arabidopsis thaliana, Plant J. 16 (1998) 735–743, https://doi.org/10.1046/j.1365-313x.1998.00343.x.

[46] J.E. Malamy, P.N. Benfey, Organization and cell differentiation in lateral roots of Arabidopsis thaliana, Development 124 (1997) 33–44.

[47] T. Czechowski, M. Stitt, T. Altmann, M.K. Udvardi, W.-R. Scheible, Genome-Wide Identification and Testing of Superior Reference Genes for Transcript Normalization in Arabidopsis, Plant Physiol. 139 (2005) 5 LP–17, https://doi.org/10.1104/pp.105.063743.

[48] D. von Wangenheim, R. Hauschild, M. Fendrych, V. Barone, E. Benková, J. Friml, Live tracking of moving samples in confocal microscopy for vertically grown roots, Elife 6 (2017), https://doi.org/10.7554/eLife.26792.

[49] J. Mathur, C. Koncz, Callus culture and regeneration, Methods Mol. Biol. 82 (1998) 31–34, https://doi.org/10.1385/0-89603-391-0:31.

[50] T. Ulmasov, J. Murfett, G. Hagen, T.J. Guilfoyle, Creation of a highly active synthetic AuxRE, Society 9 (1997) 1963–1971, https://doi.org/10.1105/tpc.9.11.1963.

[51] C. Després, C. Chubak, A. Rochon, R. Clark, T. Bethune, D. Desveaux, P.R. Fobert, The Arabidopsis NPR1 disease resistance protein is a novel cofactor that confers redox regulation of DNA binding activity to the basic domain/leucine zipper transcription factor TGA1, Plant Cell 15 (2003) 2181–2191, https://doi.org/10.1105/tpc.012849.

[52] S. Berg, D. Kutra, T. Kroeger, C.N. Straehle, B.X. Kausler, C. Haubold, M. Schiegg, J. Ales, T. Beier, M. Rudy, K. Eren, J.I. Cervantes, B. Xu, F. Beuttenmueller, A. Wolny, C. Zhang, U. Koethe, F.A. Hamprecht, A. Kreshuk, Ilastik: interactive machine learning for (Bio)image analysis, Nat. Methods 16 (2019) 1226–1232, https://doi.org/10.1038/s41592-019-0582-9.

[53] L. Hoermayer, J.C. Montesinos, P. Marhava, E. Benková, S. Yoshida, J. Friml, Wounding-induced changes in cellular pressure and localized auxin signalling spatially coordinate restorative divisions in roots, Proc. Natl. Acad. Sci. (2020), https://doi.org/10.1073/pnas.2003346117, 202003346.

[54] M. Sauer, J. Balla, C. Luschnig, J. Wisniewska, V. Reinöhl, J. Friml, E. Benková, Canalization of auxin flow by Aux/IAA-ARF-dependent feedback regulation of PIN polarity, Genes Dev. 20 (2006) 2902–2911, https://doi.org/10.1101/gad.390806.

[55] L. Abas, R. Benjamins, N. Malenica, T.T. Paciorek, J. Wiśniewska, J.C. Moulinier-Anzola, T. Sieberer, J. Friml, C. Luschnig, Intracellular trafficking and proteolysis of the Arabidopsis auxin-efflux facilitator PIN2 are involved in root gravitropism, Nat. Cell Biol. 8 (2006) 249–256, https://doi.org/10.1038/ncb1369.

[56] T. Hruz, O. Laule, G. Szabo, F. Wessendorp, S. Bleuler, L. Oertle, P. Widmayer, W. Gruissem, P. Zimmermann, Genevestigator V3: a reference expression database for the meta-analysis of transcriptomes, Adv. Bioinformatics 2008 (2008) 420747, https://doi.org/10.1155/2008/420747.

[57] S. Sabatini, D. Beis, H. Wolkenfelt, J. Murfett, T. Guilfoyle, J. Malamy, P. Benfey, O. Leyser, N. Bechtold, P. Weisbeek, B. Scheres, An auxin-dependent distal organizer of pattern and polarity in the Arabidopsis root, Cell. 99 (1999) 463–472, https://doi.org/10.1016/s0092-8674(00)81535-4.

[58] J. Friml, E. Benková, I. Blilou, J. Wisniewska, T. Hamann, K. Ljung, S. Woody, G. Sandberg, B. Scheres, G. Jürgens, K. Palme, AtPIN4 mediates sink-driven auxin gradients and root patterning in Arabidopsis, Cell 108 (2002) 661–673, https://doi.org/10.1016/S0092-8674(02)00656-6.

[59] E. Benková, M. Michniewicz, M. Sauer, T. Teichmann, D. Seifertová, G. Jürgens, J. Friml, Local, efflux-dependent auxin gradients as a common module for plant

organ formation, Cell 115 (2003) 591–602, https://doi.org/10.1016/S0092-8674(03)00924-3.
[60] W. He, J. Brumos, H. Li, Y. Ji, M. Ke, X. Gong, Q. Zeng, W. Li, X. Zhang, F. An, X. Wen, P. Li, J. Chu, X. Sun, C. Yan, N. Yan, D.Y. Xie, N. Raikhel, Z. Yang, A. N. Stepanova, J.M. Alonso, H. Guo, A small-molecule screen identifies L-Kynurenine as a competitive inhibitor of TAA1/TAR activity in ethylene-directed auxin biosynthesis and root growth in Arabidopsis, Plant Cell 23 (2011) 3944–3960, https://doi.org/10.1105/tpc.111.089029.
[61] M. Lavy, M. Estelle, Mechanisms of auxin signaling, Development 143 (2016) 3226–3229, https://doi.org/10.1242/dev.131870.
[62] Z. Ding, J. Friml, Auxin regulates distal stem cell differentiation in Arabidopsis roots, Proc. Natl. Acad. Sci. U. S. A. 107 (2010) 12046–12051, https://doi.org/10.1073/pnas.1000672107.
[63] M.L. Evans, H. Ishikawa, M.A. Estelle, Responses of Arabidopsis roots to auxin studied with high temporal resolution: comparison of wild type and auxin-response mutants, Planta 194 (1994) 215–222, https://doi.org/10.1007/BF00196390.
[64] H.M.O. Leyser, F.B. Pickett, S. Dharmasiri, M. Estelle, Mutations in the AXR3 gene of Arabidopsis result in altered auxin response including ectopic expression from the SAUR-AC1 promoter, Plant J. 10 (1996) 403–413, https://doi.org/10.1046/j.1365-313x.1996.10030403.x.
[65] K. Scheitz, H. Lüthen, D. Schenck, Rapid auxin-induced root growth inhibition requires the TIR and AFB auxin receptors, Planta 238 (2013) 1171–1176, https://doi.org/10.1007/s00425-013-1941-x.
[66] C. Luschnig, R.A. Gaxiola, P. Grisafi, G.R. Fink, EIR1, a root-specific protein involved in auxin transport, is required for gravitropism in Arabidopsis thaliana, Genes Dev. 12 (1998) 2175–2187, https://doi.org/10.1101/gad.12.14.2175.
[67] H. Rakusová, M. Fendrych, J. Friml, Intracellular trafficking and PIN-mediated cell polarity during tropic responses in plants, Curr. Opin. Plant Biol. 23 (2015) 116–123, https://doi.org/10.1016/j.pbi.2014.12.002.
[68] S.H. Su, N.M. Gibbs, A.L. Jancewicz, P.H. Masson, Molecular mechanisms of root gravitropism, Curr. Biol. 27 (2017) R964–R972, https://doi.org/10.1016/j.cub.2017.07.015.
[69] H. Han, H. Rakusová, I. Verstraeten, Y. Zhang, J. Friml, SCF TIR1 / AFB auxin signaling for bending termination, Plant Physiol. Prev. 183 (2020) 37–40, https://doi.org/10.1104/pp.20.00212.
[70] W.M. Gray, A. Östin, G. Sandberg, C.P. Romano, M. Estelle, High temperature promotes auxin-mediated hypocotyl elongation in Arabidopsis, Proc. Natl. Acad. Sci. U. S. A. 95 (1998) 7197–7202, https://doi.org/10.1073/pnas.95.12.7197.
[71] A. Peaucelle, R. Wightman, H. Höfte, The control of growth symmetry breaking in the Arabidopsis hypocotyl, Curr. Biol. 25 (2015) 1746–1752, https://doi.org/10.1016/j.cub.2015.05.022.
[72] K. Takahashi, K.I. Hayashi, T. Kinoshita, Auxin activates the plasma membrane H +-ATPase by phosphorylation during hypocotyl elongation in Arabidopsis, Plant Physiol. 159 (2012) 632–641, https://doi.org/10.1104/pp.112.196428.
[73] E. Scarpella, D. Marcos, J. Friml, T. Berleth, Control of leaf vascular patterning by polar auxin transport, Genes Dev. 20 (2006) 1015–1027, https://doi.org/10.1101/gad.1402406.
[74] C. Verna, S.J. Ravichandran, M.G. Sawchuk, N.M. Linh, E. Scarpella, Coordination of tissue cell polarity by auxin transport and signaling, Elife 8 (2019) 1–30, https://doi.org/10.7554/eLife.51061.
[75] A. Hay, M. Barkoulas, M. Tsiantis, ASYMMETRIC LEAVES1 and auxin activities converge to repress BREVIPEDICELLUS expression and promote leaf development in Arabidopsis, Development 133 (2006) 3955–3961, https://doi.org/10.1242/dev.02545.
[76] C.S. Galvan-Ampudia, M.M. Julkowska, E. Darwish, J. Gandullo, R.A. Korver, G. Brunoud, M.A. Haring, T. Munnik, T. Vernoux, C. Testerink, Halotropism is a response of plant roots to avoid a saline environment, Curr. Biol. 23 (2013) 2044–2050, https://doi.org/10.1016/j.cub.2013.08.042.
[77] M. Zwiewka, T. Nodzyński, S. Robert, S. Vanneste, J. Friml, Osmotic stress modulates the balance between exocytosis and clathrin-mediated endocytosis in Arabidopsis thaliana, Mol. Plant 8 (2015) 1175–1187, https://doi.org/10.1016/j.molp.2015.03.007.
[78] W. Liu, R.-J. Li, T.-T. Han, W. Cai, Z.-W. Fu, Y.-T. Lu, Salt stress reduces root meristem size by nitric oxide-mediated modulation of auxin accumulation and signaling in Arabidopsis, Plant Physiol. 168 (2015) 343–356, https://doi.org/10.1104/pp.15.00030.
[79] J.I. Kim, D. Baek, H.C. Park, H.J. Chun, D.-H. Oh, M.K. Lee, J.-Y. Cha, W.-Y. Kim, M.C. Kim, W.S. Chung, H.J. Bohnert, S.Y. Lee, R.A. Bressan, S.-W. Lee, D.-J. Yun, Overexpression of Arabidopsis YUCCA6 in potato results in high-auxin developmental phenotypes and enhanced resistance to water deficit, Mol. Plant 6 (2013) 337–349, https://doi.org/10.1093/mp/sss100.
[80] Q. Ke, Z. Wang, C.Y. Ji, J.C. Jeong, H.-S. Lee, H. Li, B. Xu, X. Deng, S.-S. Kwak, Transgenic poplar expressing Arabidopsis YUCCA6 exhibits auxin-overproduction phenotypes and increased tolerance to abiotic stress, Plant Physiol. Biochem. 94 (2015) 19–27, https://doi.org/10.1016/j.plaphy.2015.05.003.
[81] P. Marhava, L. Hoermayer, S. Yoshida, P. Marhavý, E. Benková, J. Friml, Re-activation of stem cell pathways for pattern restoration in plant wound healing, Cell 177 (2019) 957–969, https://doi.org/10.1016/j.cell.2019.04.015, e13.
[82] T. Vernoux, J. Kronenberger, O. Grandjean, P. Laufs, J. Traas, PIN-FORMED 1 regulates cell fate at the periphery of the shoot apical meristem, Development 127 (2000) 5157–5165.
[83] D. Reinhardt, T. Mandel, C. Kuhlemeier, Auxin regulates the initiation and radial position of plant lateral organs, Plant Cell 12 (2000) 507–518, https://doi.org/10.1105/tpc.12.4.507.
[84] D. Reinhardt, E.R. Pesce, P. Stieger, T. Mandel, K. Baltensperger, M. Bennett, J. Traas, J. Friml, C. Kuhlemeier, Regulation of phyllotaxis by polar auxin transport, Nature. 426 (2003) 255–260, https://doi.org/10.1038/nature02081.
[85] M. Furutani, Y. Nakano, M. Tasaka, MAB4-induced auxin sink generates local auxin gradients in Arabidopsis organ formation, Proc. Nat. Acad. Sci. U. S. A 2013 (2013), https://doi.org/10.1073/pnas.1316109111.
[86] M.G. Heisler, C. Ohno, P. Das, P. Sieber, G.V. Reddy, J.A. Long, E.M. Meyerowitz, Patterns of auxin transport and gene expression during primordium development revealed by live imaging of the Arabidopsis inflorescence meristem, Curr. Biol. 15 (2005) 1899–1911, https://doi.org/10.1016/j.cub.2005.09.052.
[87] F. Besnard, Y. Refahi, V. Morin, B. Marteaux, G. Brunoud, P. Chambrier, F. Rozier, V. Mirabet, J. Legrand, S. Lainé, E. Thévenon, E. Farcot, C. Cellier, P. Das, A. Bishopp, R. Dumas, F. Parcy, Y. Helariutta, A. Boudaoud, C. Godin, J. Traas, Y. Guédon, T. Vernoux, Cytokinin signalling inhibitory fields provide robustness to phyllotaxis, Nature 505 (2014) 417–421, https://doi.org/10.1038/nature12791.
[88] T. Berleth, T. Sachs, Plant morphogenesis: long-distance coordination and local patterning, Curr. Opin. Plant Biol. 4 (2001) 57–62, https://doi.org/10.1016/S1369-5266(00)00136-9.
[89] K. Wabnik, J. Kleine-Vehn, J. Balla, M. Sauer, S. Naramoto, V. Reinöhl, R.M. H. Merks, W. Govaerts, J. Friml, Emergence of tissue polarization from synergy of intracellular and extracellular auxin signaling, Mol. Syst. Biol. 6 (2010), https://doi.org/10.1038/msb.2010.103.
[90] M. Glanc, M. Fendrych, J. Friml, Mechanistic framework for cell-intrinsic re-establishment of PIN2 polarity after cell division, Nat. Plants 4 (2018) 1082–1088, https://doi.org/10.1038/s41477-018-0318-3.
[91] N. Geldner, J. Firml, Y.D. Stierhof, G. Jürgens, K. Palme, Auxin transport inhibitors block PIN1 and vessicle trafficing, Nature 413 (2001) 425–428.
[92] I.A. Paponov, J. Dindas, E. Król, T. Friz, V. Budnyk, W. Teale, M. Paponov, R. Hedrich, K. Palme, Auxin-induced plasma membrane depolarization is regulated by AUXIN transport and not by AUXIN BINDING PROTEIN1, Front. Plant Sci. 9 (2019), https://doi.org/10.3389/fpls.2018.01953.
[93] R. Hertel, K.S. Thomson, V.E.A. Russo, In-vitro auxin binding to particulate cell fractions from corn coleoptiles, Planta 107 (1972) 325–340, https://doi.org/10.1007/BF00386394.
[94] M. Löbler, D. Klämbt, Auxin-binding protein from coleoptile membranes of corn (Zea mays L.). II. Localization of a putative auxin receptor, J. Biol. Chem. 260 (1985) 9854–9859.
[95] Y. Effendi, S. Rietz, U. Fischer, G.F.E. Scherer, The heterozygous abp1/ABP1 insertional mutant has defects in functions requiring polar auxin transport and in regulation of early auxin-regulated genes, Plant J. 65 (2011) 282–294, https://doi.org/10.1111/j.1365-313X.2010.04420.x.
[96] N. Braun, J. Wyrzykowsk, P. Muller, K. David, D. Couch, C. Perrot-Rechenmann, A.J. Fleming, Conditional repression of Auxin Binding Protein1 reveals that it coordinates cell division and cell expansion during postembryonic shoot development in Arabidopsis and tobacco, Plant Cell 20 (2008) 2746–2762, https://doi.org/10.1105/tpc.108.059048.
[97] A. Tromas, S. Paque, V. Stierlé, A.L. Quettier, P. Muller, E. Lechner, P. Genschik, C. Perrot-Rechenmann, Auxin-Binding Protein 1 is a negative regulator of the SCF TIR1/AFB pathway, Nat. Commun. 4 (2013), https://doi.org/10.1038/ncomms3496.
[98] A.M. Jones, Auxin-dependent cell expansion mediated by overexpressed auxin-binding protein 1, Science (80-.) 282 (1998) 1114–1117, https://doi.org/10.1126/science.282.5391.1114.
[99] J.M. Bauly, I.M. Sealy, H. Macdonald, J. Brearley, S. Droge, S. Hillmer, D. G. Robinson, M.A. Venis, M.R. Blatt, C.M. Lazarus, R.M. Napier, Overexpression of auxin-binding protein enhances the sensitivity of guard cells to auxin, Plant Physiol. 124 (2000) 1229–1238, https://doi.org/10.1104/pp.124.3.1229.
[100] K. Palme, T. Hesse, N. Campos, C. Garbers, M.F. Yanofsky, J. Schell, Molecular analysis of an auxin binding protein gene located on chromosome 4 of arabidopsis, Plant Cell 4 (1992) 193–201, https://doi.org/10.1105/tpc.4.2.193.
[101] W. Diekmann, M.A. Venis, D.G. Robinson, Auxins induce clustering of the auxin-binding protein at the surface of maize coleoptile protoplasts, Proc. Natl. Acad. Sci. U. S. A. 92 (1995) 3425–3429, https://doi.org/10.1073/pnas.92.8.3425.
[102] R.M. Napier, K.M. David, C. Perrot-Rechenmann, A short history of auxin-binding proteins, Plant Mol. Biol. 49 (2002) 339–348.
[103] J.M. Dunwell, J.G. Gibbings, T. Mahmood, S.M. Saqlan Naqvi, Germin and germin-like proteins: evolution, structure, and function, Crit. Rev. Plant Sci. 27 (2008) 342–375, https://doi.org/10.1080/07352680802333938.